Functionalized Ru(II) polypyridines and phthalocyanines: Potential dyes for dye-sensitized solar cells (DSSCs)

By

ADELOYE Adewale Olufunsho

Department of Chemistry

Faculty of Science and Agriculture

University of Fort Hare, Alice

South Africa.

January 2011

Functionalized Ru(II) polypyridines and phthalocyanines: Potential dyes for dye-sensitized solar cells (DSSCs)

By

ADELOYE Adewale Olufunsho

B.Sc. Hons. (Chemistry) Ado-Ekiti, M.Sc. (Pharmaceutical Chemistry), M.Phil. (Chemistry) Ife

Being a thesis Submitted to the Faculty of Science & Agriculture in fulfillment of the requirements for the award of

DOCTOR OF PHILOSOPHY IN CHEMISTRY

of the University of Fort Hare

South Africa

Supervisor: Dr P. A. Ajibade

January 2011

CERTIFICATION

This is to certify that this thesis is a record of original research carried out by ADELOYE, ADEWALE OLUFUNSHO under my supervision at the Department of Chemistry, Faculty of Science and Agriculture, University of Fort Hare, South Africa.

---------- ----------

Date Supervisor:

P. A. Ajibade

B.Sc. (Hons), M.Sc. (Ibadan), PhD (UZ),

MRSC (London).

ACKNOWLEDGEMENTS

I would like to appreciate and thank Dr. P. A. Ajibade, greatly for the invitation extended to me to embark on this research work in his laboratory, and for all his immense contributions throughout the programme.

The sponsorship of this research work by the South African National Energy Research Institute (SANERI) and provision of bursary is gratefully acknowledged. The provision of grant holder bursary by Govan Mbeki Research Centre is highly appreciated.

I thank the Department of Chemistry for the provision of space and laboratory to carry out this research work and the University of Fort Hare, for providing a conducive environment. I also appreciate the study leave granted by the Obafemi Awolowo University, Ile-Ife, Nigeria.

It is very pleasing to me to thank and appreciate both the academic and non-academic members of staff in the Department of Chemistry, University of Fort Hare, Alice, my colleagues in the laboratory and beyond for their friendship, contributions and supports during the programme.

When I checked the lab notebook for the experimental section page by page, I recalled the past three years I devoted to my projects. I am excited and encouraged with the achievement in this period of time; however, with sadness and sentiment lingered at the same time. I cannot find a suitable word to express this kind of mixed feelings. The time I spent in University of Fort Hare, Alice, South Africa is filled with

good memories. There is happiness and sadness here, sweetness and bitterness; there is laughter here, and tears as well.

With time flying, I would like to thank and appreciate Mr Isaac Akinbulu and Mr Temitope Olomola (both from Rhodes University, Grahamstown, SA) for their unflinching and immense contributions towards the analyses of the electrochemical and NMR spectroscopic experiments. You guys deserved recognitions. I thank Dr. Lukas le Roux and Mr Franscious Cummings (CSIR, SA) for carrying out the experiment and assistance in the interpretation of the solar-to-electrical conversion efficiency experimental results.

I would like to appreciate the good roles and contributions from Prof. A. Okoh, Prof. A. Afolayan and Dr & Prof. (Mrs) Oyedeji while in South Africa. My past teachers: Prof. F.A Ogunbona, Prof. O.O. Bolaji, Prof. T.A. Olugbade, Prof. C. O. Obafemi, Prof. I. A. O. Ojo, and my Mentor: Prof. Abiodun Oguntuga Ogundaini. My thanks also go to my academic colleagues: Dr. S. O. Ogundare, Dr. Jaiyeola, Dr. & Mrs. J. O. Soyelu, Dr & Dr. (Mrs) M. Ogunrombi, Dr (Mrs) Olabanji, Dr Eyitayo Fakunle, Dr & Dr. (Mrs) M. Trzebiatowska-Gusowska, Mr Adekunle Saheed, Mr Winston Doherty, Dr (Mrs) Ogunlusi, Dr (Mrs) Elusiyan, Dr J.O. Soyinka, Dr E. O. Awe, Miss Oluwaseun Fakunle and Mrs Ibukun Osuagwu. I appreciate my spiritual fathers in the Lord: Prophet Adedeji Ayoade and Prophet Akinyoade for their encouragement, prayers and well wishes at all times. May the Lord God bless and reward you.

I would like to specially thank my sweetheart Pharm. (Mrs) E. O. Adeloye, my wonderful son (Aanuoluwapo), and my jewel (Oluwafunsho Temitope). Thank you so

much for keeping the flag flying while I was away from home. I appreciate my loving Parent's in-law: Prof. & Dr. (Mrs) C. O. Fakunle, for their love, support, encouragement and prayers. I appreciate my Brothers Ademola and Adekunle, my sisters Adenike and Oyinade Adeloye and my mum for being there.

Lastly, this journey could have been too much wonderful if my late father Prince Julius Adeiya Adeloye were to be alive. I appreciate you dad for given me directions in life and your constant word to me, quoting: "For record past can't always last and they will not carry you through, the work you've only begun"

DEDICATION

This work is dedicated to THE LORD JEHOVAH GOD, for the mighty things He has done, for His pleasure is not in strong horses, nor His delight in brave soldiers.

I praise His SUPREME greatness.

TABLE OF CONTENTS Page

GLOSSARY OF ABBREVIATIONS

Bpy	2,2'-Bipyridine
Phen	1,10-Phenanthroline
Terpy	2,2':6',2"-Terpyridine
PC	Phthalocyanines
RuPc	Ruthenium Phthalocyanines
DMAA	2,3-Dimethylacrylic acid
MBY	1-Methoxy-1-buten-3-yne
PPh_3	Triphenylphosphine
Pd/C	Palladium carbide
THF	Tetrahydrofuran
DMF	Dimethylformamide
C_{60}	Fullerenes
NMR	Nuclear Magnetic Resonance
MHz	Megahertz
IR	Infrared
^{1}H	proton NMR
^{13}C	Carbon 13 NMR

TLC	Thin Layer Chromatography
R_f	Retention factor
J-value	Coupling constant
ppm	parts per million
HOMO	Highest Occupied Molecular Orbital
LUMO	Lowest Unoccupied Molecular Orbital
Φ	Quantum Yield
L	Ligand
C	Complex
MLCT	Metal-to-Ligand Charge Transfer
MC	Metal Centre
UV-Vis	Ultraviolet-Visible
Et_3N	Triethylamine
λ_{max}	Maximum Absorption Wavelength
λ_{exc}	Excitation Wavelength
λ_{em}	Emission Wavelength
rt	Room Temperature
DMSO	Dimethylsulphoxide
TiO_2	Titanium dioxide
DSSCs	Dye-Sensitized Solar Cells
OLEDs	Organic Light Emitting Diodes
CV	Cyclic Voltammogram

E_{pa}	Positive Anodic Potential
$E_{1/2}$	Half-Wave Cathodic Potential
F	Faraday
c	Concentration
D	Dielectric Constant
t	Time
n	Number of electron (s)
ε	Molar Extinction Coefficient
g	Grams
nm	Nanometres
R_{sh}	Shunt Resistance
R_s	Series Resistance
FF	Fill Factor
J_{sc}	Short Circuit Current
V_{oc}	Open Circuit Potentials
η	Solar Conversion Efficiency

LIST OF TABLES

LIST OF SCHEMES

LIST OF FIGURES

LIST OF APPENDICES

Page

Publications included as part of the thesis

(1) Adewale O. Adeloye and Peter A. Ajibade. Synthesis and Characterization of a Heteroleptic Ru(II) Complex of Phenanthroline Containing Oligo-Anthracenyl Carboxylic Acid Moieties. *Int. J. Mol. Sci.* **2010**, *11*, 3158-3176.

(2) **Adewale O. Adeloye** and Peter A. Ajibade. Synthesis and Characterization of a Ru(II) Complex with Functionalized Phenanthroline Ligands Having Single-Double Linked Anthracenyl and 1-Methoxy-1-buten-3-yne Moieties. *Molecules* **2010**, *15*, 7570-7581.

(3) **Adewale O. Adeloye** and Peter A. Ajibade. Synthesis, characterization and preliminary investigation of the electro redox properties of anthracenyl-functionailzed terpyridyl ligands. *Tetrahedron Lett.* 2011, 52, 274-277.

(4) **Adewale O. Adeloye** and Peter A. Ajibade. Synthesis, characterization and electrochemistry of anthracenyl-functionalized bisterpyridyl Ruthenium(II) complexes –*IJMS* (Submitted).

(5) **Adewale O. Adeloye** and Peter A. Ajibade. A convenient synthesis, electrochemistry and spectroscopic properties of new series of single- and double-decked functionalized anthracenyl ruthenium(II) phthalocyanine complexes. *Dyes and Pigments* (Submitted).

(6) Adewale O. Adeloye and Peter A. Ajibade. Synthesis, characterization and sensitization properties of functionalized anthracenyl-based bipyridyl ruthenium(II) charge transfer complexes (to be submitted).

(7) Adewale O. Adeloye and Peter A. Ajibade. Synthesis, characterization and sensitization properties of functionalized anthracenyl-based phenanthrolyl ruthenium(II) charge transfer complexes (to be submitted).

Conference/Workshop presentations

(1) Peter Ajibade and Adewale Adeloye. Functionalized anthracenyl 2,2'-bipyridyl Ru(II) complexes as dyes for DSSCs. 238 American Chemical Society National Meeting, Washington DC, August 16-20, 2009.

(2) **Adewale O. Adeloye** and Peter A. Ajibade. Ruthenium(II) complexes of anthracenyl functionalized 1,10-phenanthroline: Potential dyes for dye-sensitized solar cells. South African Chemical Institute (SACI) Conference on Inorganic Chemistry (INORG2009) Bloemfontein, South Africa (Sept. 13-17).

(3) **Adewale O. Adeloye.** "Functionalized Ru(II) polypyridine complexes: Potential dyes for dye-sensitized solar cells (DSSCs)". South African Chemical Institute (SACI) Postgraduate Seminar held at the University of Fort Hare, Alice, South Africa (Oct. 23rd, 2009).

(4) **Adewale O. Adeloye.** "Functionalized Anthracenyl-Ru(II) Polypyridyl Complexes as Potential Dyes for DSSCs". SA/Germany Science, Research and Technology Cooperation Agreement held in Rhodes University, Grahamstown, South Africa (Sept. 7-8th, 2010).

(5) **Adewale O. Adeloye**. Synthesis, Photophysical and Electrochemical Investigation of Heteronuclear Ru(II) Polypyridine Complexes containing Anthracene and 2,3-Dimethylacrylic acid Functionalities. (To be presented at 2011 South African Chemical Institute (SACI) Conference at University of Witwaterstrand, South Africa (Jan. 16–21, 2011).

ABSTRACT

This study describes the design, synthesis, characterization and preliminary investigation of the solar-to-electrical energy conversion efficiency of ruthenium(II) functionalized polypyridine and phthalocyanine complexes with extended π-conjugation. Polypyridinyl functionalized with anthracene, 2,3-dimethylacrylic acid and 1-methoxy-1-buten-3-yne were synthesized and characterized by infrared, UV-Vis, photoluminescence, ^{1}H and ^{13}C NMR and elemental analysis. The functionalized polypyridine molecules were used to synthesize various ruthenium(II) homoleptic/heteroleptic and/or heteronuclear complexes and their photophysical and electrochemical properties evaluated.

The preliminary results of the solar-to-electrical conversion efficiencies of some synthesized Ru(II) polypyridyl complexes were presented in chapter 5. It was found out as expected that the ruthenium(II) polypyridine complexes containing either heteronuclear polypyridine ligands or their thiocyanate analogues of the types $[Ru(L_1)_2L_2(PF_6)_2]$, $[RuL_1(L_2)_2(PF_6)_2]$ and $[RuL_1L_2(NCS)_2]$, showed better photophysical properties (red-shifted metal-to-ligand charge-transfer (MLCT) transitions concomitant with enhanced molar extinction coefficients), luminescence and interesting electrochemical redox properties than those containing homonuclear ligand types $[Ru(L_1)_3(PF_6)_2]$. The ruthenium(II) anthracenyl functionalized phthalocyanine complexes which were obtained by electrophilic aromatic substitution reactions in the peripheral positions gave good solubility properties in various organic solvents and also showed interesting near infrared absorption and electroredox characteristics. Cyclic and square wave voltammetries of these complexes revealed

major redox processes and the numbers of electron(s) transfer were determined by chronocoulometry. It was established that a mono- and/or multi-electronic transfer reactions can occur in the various ruthenium(II) complexes. The photophysical properties of some complexes showed them to be better and promising candidates in the design of chemosensors, organic light emitting diodes (OLEDs) and as photosensitizers, while their redox-active natures make them potential mediators in electron-transfer for various photochemical processes. However, due to low surface concentration and/or adsorption of some tested complexes on TiO_2 semiconductor nanocrystalline particle, low currents were generated and the highest solar-to-electrical conversion efficiency recorded in this study was 0.10 %.

CHAPTER ONE

CHAPTER ONE

1.0 INTRODUCTION AND LITERATURE REVIEW

The forecasts for the next 50 years predict that human energy need are likely to double while fossil energy reserves are shrinking. In an attempt to reduce the use of fossil fuels which are limited and heavily contribute to global warming, scientists are looking for other sustainable energy sources to serve our future energy needs. Of these, solar energy is promising because the Earth receives more energy from the sun in one hour than is used by all humanity in the course of an entire year [1]. Much research has gone into producing efficient solar cells, the devices which convert sunlight to electricity through a process called the photovoltaic effect. Solar energy as renewable energy is environmentally friendly, abundant and also free. Therefore, direct photoconversion of solar energy by using photovoltaic technology is increasingly recognized as a viable hi-tech solution to the growing energy challenge [2, 3].

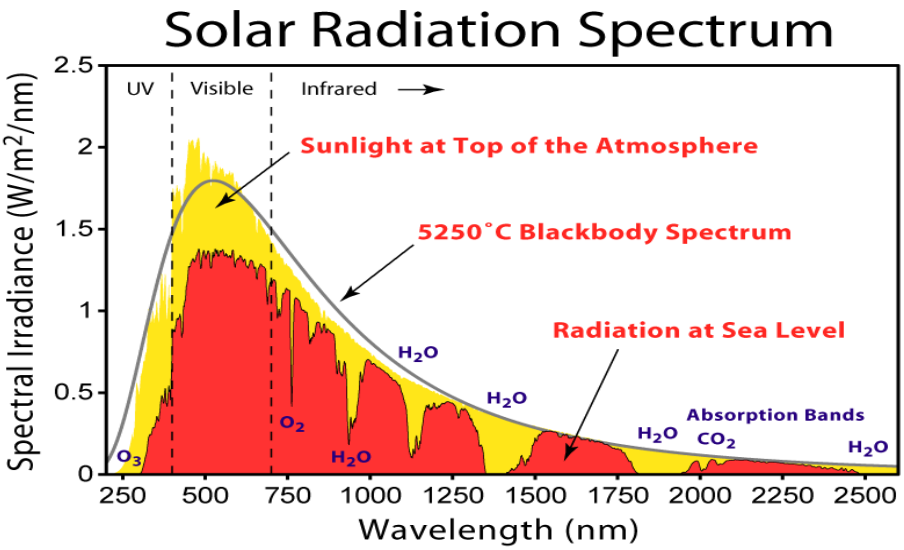

Figure1.1. Schematic picture of the sun irradiation intensity distributed over wavelength [4].

Currently, solar cells are made largely from inorganic semiconductors (e.g. highly purified silicon crystals), similar to those used in computer chips, but these inorganic semiconductors are expensive because they require high purity crystals and need to be fabricated in vacuum. Therefore, researchers are seeking new inexpensive alternatives. Research into organic and organometallic molecules (in the form of both small-molecules and macromolecules), has recently shown great promise. Organic solar cells attract considerable attention due to their unique advantages, such as low cost, lightweight, ease of solution processability and potential use in flexible and large–area devices [5–7].

In general, there are two types of organic solar cells commonly in use, namely, bulk-heterojunction solar cells (BHJSCs) [8] and dye-sensitized solar cells (DSSCs) [5, 9]. The BHJSCs are typically made by sandwiching a thin film of photoactive polymers between two electrodes such as indium tin oxide and aluminium. A typical DSSC consists of two glass plates coated with a transparent conductive oxide layer. The working electrode is covered with a film of a dye-sensitized substance and the counter electrode is coated with a catalyst. Both plates are sandwiched together with the gap between them filled by an electrolyte. Light absorption is carried out by dye molecules in which the absorbed photons cause dye photoexcitation to release an electron rapidly to the semiconductor. The injected electrons then hop through the colloidal TiO_2 particles to reach the collector. Following this, the electron passes through an outer circuit to reach the other transparent conductive oxide layer at the counter electrode, ultimately doing electrical work for the user. Finally, the electron is transferred to the electrolyte where it reduces the oxidant and the reduced form reduces the excited dye to the ground state and completes the circuit. Organo-metallic donor materials are widely

used in DSSCs in which the Grätzel-type cell (Figures 1.2, 1.3) based on cis-dithiocyanato-4,4'-dicarboxylic acid–2,2'-bipyridyl ruthenium(II) complex owes much success to this work [5, 6, 10]. Over the years, a large number of other related dyes have been reported in the literature [8, 11]. In these types of cells, ruthenium(II) dyes have played a prominent role and PCEs as high as 11 % using AM 1.5 conditions have been obtained [9, 10].

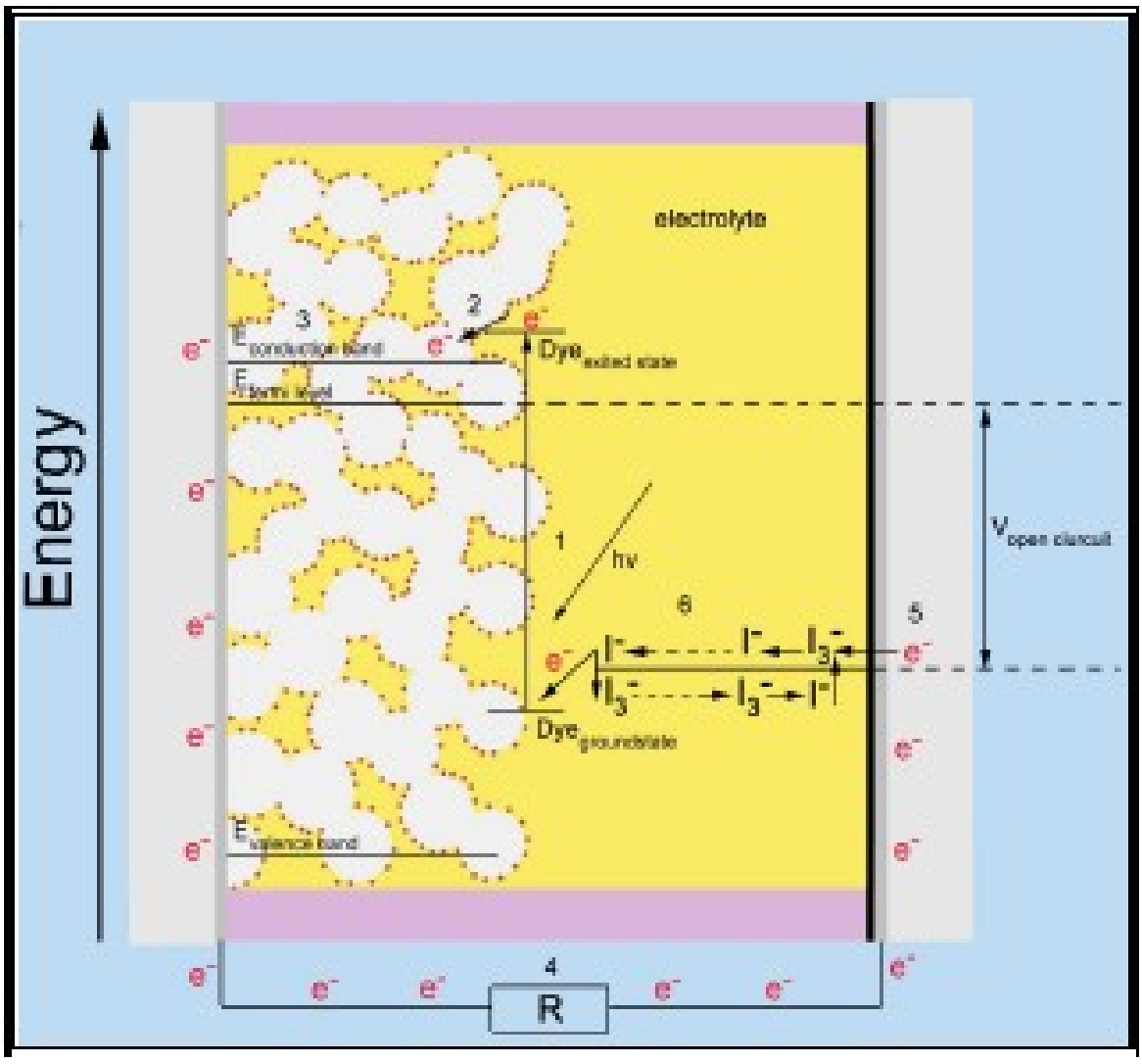

Figure 1.2 Principle of operation and energy level scheme of the dye-sensitized nanocrystalline solar cell.

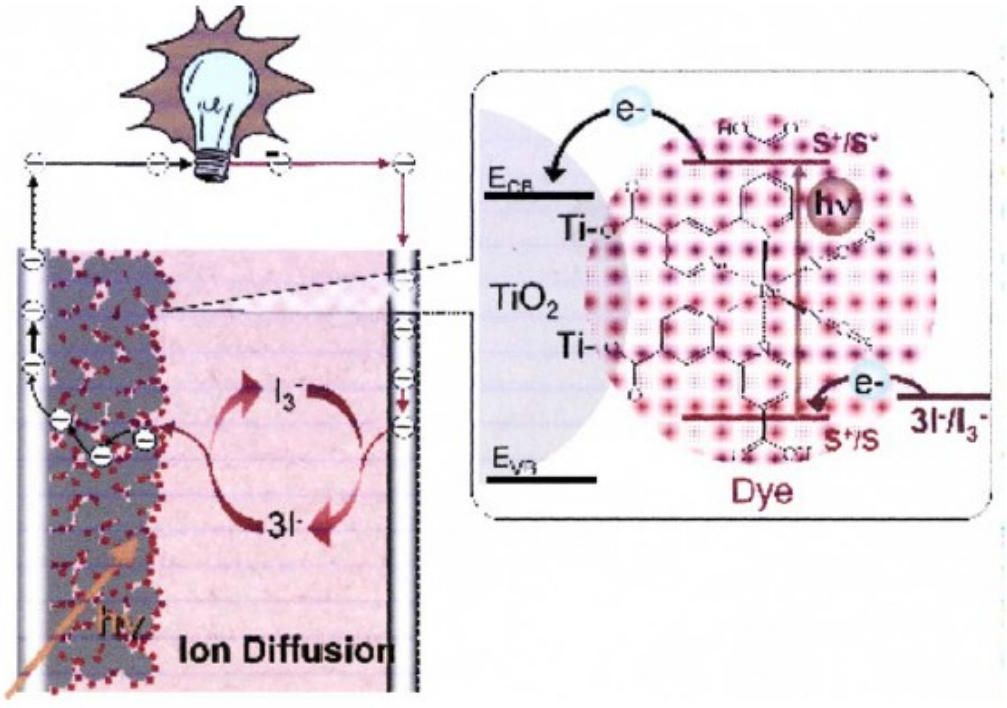

Figure 1.3 Schematic drawing showing the currently used embodiment of the DSC. It employs dye-derivatized TiO_2 nanocrystals as light harvesting units.

As described above, the following steps result in one complete cycle of the DSSC.

(1) Excitation of the sensitizer molecule upon irradiation by light

$$S + h\nu \rightarrow S^*$$

(2) Charge injection into the conduction band of the semiconductor

$$S^* \rightarrow S^+ + e_{cb}^- \text{ (SC)}$$

(3) Regeneration of the sensitizer molecule

$$S^* + Red \rightarrow S + Ox$$

(4) Regeneration of the electrolyte

$$Ox + e^- \rightarrow Red$$

It should be noted that the sensitizer regeneration process does not produce the initial sensitizer environment immediately (10 ns) [12]. Instead, slow (μs to ms) cation transfer follows regeneration to yield the initial sensitizer. That means the oxidized sensitizer may be reduced in ~ 10 ns, but it is not in its equilibrium environment prior to light absorption until slow (μs to ms) cation transfer has taken place [13].

1.1 The Chemistry of 2,2'-Bipyridines and Their Derivatives

Bipyridines (IUPAC), also known as bipyridyls, dipyridyls, and dipyridines, are aromatic nitrogen heterocycles that form complexes with most transition metals. This class of compounds contains six possible regioisomers which include the symmetrical isomers (2,2', 3,3', and 4,4'), and the asymmetrical ones (2,3', 2,4', and 3,4'). The most common of these is the bidentate chelate (bpy = 2,2'-bipyridine) though the 2,3'- and the 3,3'-bipyridines are found to be naturally abundant in certain varieties of tobacco [14-18]. Bipyridine ligands interact with metals via both σ-donating nitrogen atoms and π-accepting molecular orbitals [19]. Bipyridines and its derivatives feature prominently in studies of electron and energy transfer, supramolecular and materials chemistry, and catalysis [20–23].

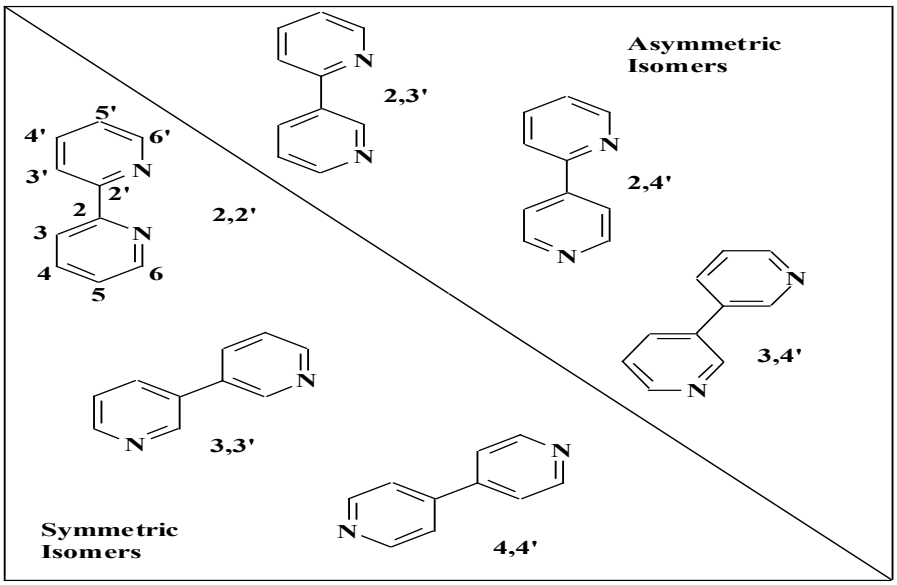

Figure 1.4 Regioisomeric forms of bipyridines

1.1.2 Synthesis of Bipyridine Ring Systems

1.1.2.1 Traditional Methods

2,2'-Bipyridine was first synthesized more than 110 years ago by Fritz Blau, who simply dry-distilled the copper salt of picolinic acid [14]. Since then, the preparation of this parent bidentate ligand has been improved dramatically using different synthetic strategies. Bipyridine (bpy) [24] and symmetrically substituted derivatives [25,26] have traditionally been synthesized by a number of different routes, including the Ullmann reaction, which involves homocoupling of a halopyridine in the presence of M^0 where M = copper or nickel. The process most often used for large-scale industrial manufacturing of bpy is Raney nickel coupling of simple pyridine [27, 28]. While this Ni(0) catalyst can also be used with methyl pyridines (picolines) to form dimethyl-substituted bipyridines, the process is limited to simple, symmetric derivatives. More complex unsymmetrical derivatives have been generated by reaction of pyridinium salts with α,β-unsaturated ketones followed by treatment with ammonium acetate to effect cyclization of the second ring [29] This

preparation, known as the Krö hnke method, is still commonly used to prepare bipyridine derivatives, though, more recent synthetic methods involve cross-coupling of halopyridines with organometallic pyridines and transition metal mediated homocoupling of halopyridines. These methods allow the construction of bipyridine ligands in higher yields and permit the incorporation of a number of functional groups.

1.1.3 Metal-catalyzed Coupling Reactions

1.1.3.1 Homocoupling of halopyridines

The most useful transition metal-mediated halopyridine homocouplings make use of a Ni^0 catalyst [30], most often generated in situ through reduction of a Ni(II) complex. This method provides product in much higher yield than the classic Ullmann reaction and is compatible with many functional groups. For example, the chiral bipyridine (**2**) was generated in 91 % yield via Ni-catalyzed homocoupling of the pyridyl chloride, (**1**) (Scheme 1.1) [31].

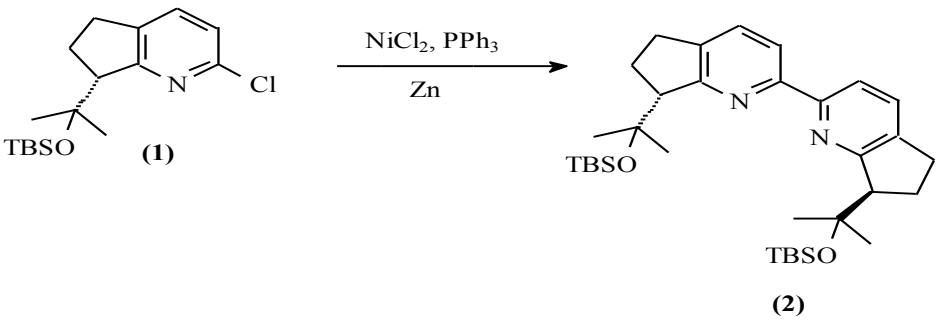

Scheme 1.1 Homocoupling method of bipyridine synthesis

Reactions that employ other catalyst systems for halopyridine homocouplings such as Pd/C [32] and Cu(II) [33] typically afford product in lower yields. This methodology has also been used to generate 3,3'-bipyridine (72 %) [34] and methyl-

substituted 3,3'-bipyridines (84 %) [35]. The 3,4,3',4'-tetramethoxy substituted bipyridine, which is a precursor to the natural tetrahydroxy bipyridine, Orelline, was similarly afforded in 80 % yield through homocoupling of a dimethoxy-substituted iodopyridine [36]. Bipyridines substituted at the 3 and 3' positions exhibit a large steric repulsion between substituents while in the *cis* configuration [37], they bind metals more weakly and form strained nonplanar structures [38]. However, a series of 3,3'-disubstituted bipyridines were coordinated to ruthenium, and it was demonstrated that molecular distortions could be used to advantage in modulating physical properties of the resulting complexes [39].

1.1.3.2 Cross-coupling of halopyridines with pyridyl organometallics

In order to synthesize unsymmetric as well as symmetric bipyridines, methods involving cross-coupling of a halopyridine with an organometallic pyridine have been developed. Typically, halopyridines are coupled with pyridylstannanes (Stille), pyridylborates (Suzuki), or pyridylzinc reagents (Negishi), where the two pyridines may or may not have the same structure to give symmetric and unsymmetrical products, respectively (Scheme 1.2).

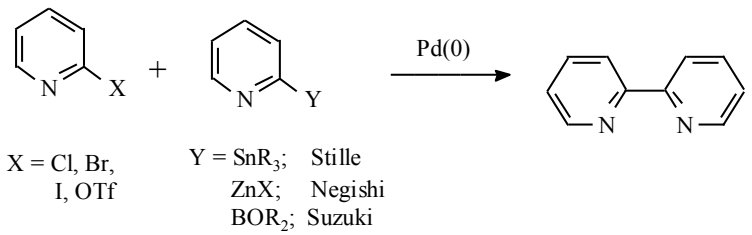

Scheme 1.2 Cross-coupling of halopyridines

For example, 5,5'-dimethyl bipyridine has been prepared in 86 % yield by coupling 2-bromo-5-methylpyridine and the analogous tributylstannane [40]. Many of the functionalities are stable toward Stille reaction conditions, including ester [41]

carboxylate, cyano, and nitro groups. Pyridine N-oxides have also been used as coupling partners in Stille reactions to produce unsubstituted [42] and bromo- and nitro-substituted bipyridine 1-oxides without occurrence of side reactions [43] An analogue of bipyridine, 2-pyridin-2-yl quinoline, was synthesized via coupling of a pyridylstannane with a pyridyl triflate [44] in place of the halopyridine [45].

Halopyridines also serve as viable coupling partners with organozinc reagents in Negishi coupling reactions to give functionalized bipyridines such as 4-bromo-4'-methoxy bipyridine [46]. A pyridyl triflate has been used in place of the halopyridine to generate some products in higher yields. For example, 4-, 5-, and 6-methyl bipyridine were obtained in 93–98 % yield using the appropriate pyridyl triflate [47, 48]. Negishi strategies have also been used to synthesize 2,4'-bipyridine [49] and bipyridine ligands with the solubilizing 4-methoxy-2,6-dimethylphenyl, or ‘‘manisyl’’ group [50].

Boron-substituted pyridine reagents can be used to construct the bipyridine ring system by coupling them with halopyridines in the presence of a Pd(0) catalyst and a base (Suzuki method). Various ligands have been made in this manner in moderate to high yields, including 2,3-bipyridine (85 %) [51] and 3,5-dimethyl bipyridine (60 %) [52]. One valuable feature of the Suzuki method is that it is compatible with stannanes. A pyridyl diethylborane has been coupled to a tributyl tin-functionalized pyridyl bromide [53]. This compatibility is useful for polypyridine syntheses because subsequent Stille coupling of the bipyridyl stannane is possible.

Another synthetic strategy that produces substituted bipyridines in moderate to high yields involves coupling of pyridyl sulfoxides with pyridyl Grignard reagents (Scheme 1.3) [54, 55]. The coupling of a bromopyridine and an aryl bromide with hexamethylditin in the presence of a palladium catalyst has generated various

diarenes in one pot [56]. 2,3'-Bipyridine (Figure 1.4) was synthesized in 59 % yield by a modification of this method that used hexamethylditin to couple pyridyl triflates with aryl bromides [57].

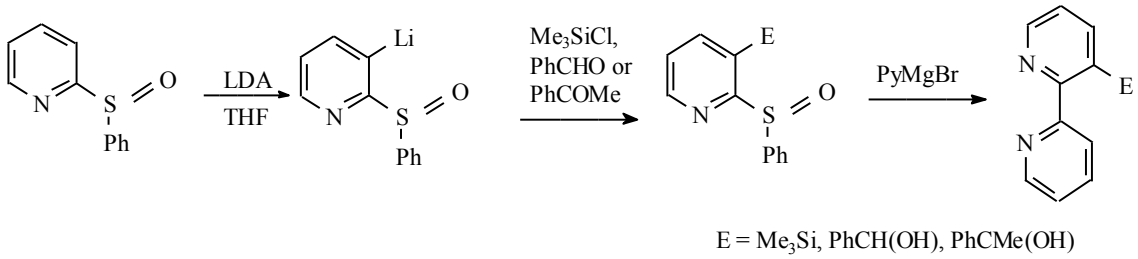

Scheme 1.3 Synthesis of bipyridine using pyridyl sulfoxide with Grignard reagents

1.1.4 Preparation from Acyclic Precursors

1.1.4.1 Krö hnke method

Aside from coupling of two pyridyl reagents, bipyridines can also be constructed from acyclic precursors. As mentioned above, the most common of these cyclization reactions is the Krö hnke method [29]. Recent uses of this methodology include the synthesis of bromo-functionalized methylbipyridines by reaction of an acetylpyridinium iodide salt with methacrolein in formamide (Scheme 1.4) [58].

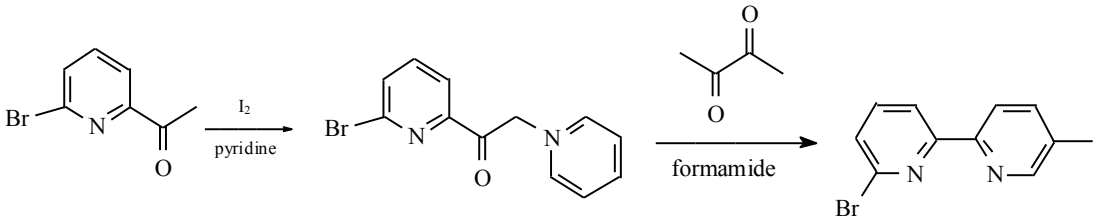

Scheme 1.4 Synthesis of bipyridines from acyclic precursors

A variation by Potts utilizes α-oxoketene dithioacetals in a condensation–cyclization bipyridine synthesis [59, 60]. For example, reaction of the α-oxoketene dithioacetal 3,3-bis(methylthio)-1-(2-pyridinyl)-2-propen-1-one with acetone and potassium *t*-butoxide, followed by treatment of the intermediate 1,5-enedione potassium salt, (**3**), with ammonium acetate produced the unsymmetric 6-methyl-4-(methylthio)-bpy, (**4**) (Scheme 1.5). Desulfurization with nickel boride afforded 6-methyl bipyridine in 72 % yield. Various substituted bpys with alkyl and alkylsulfonyl groups were similarly produced in yields ranging from 37- 94 %.

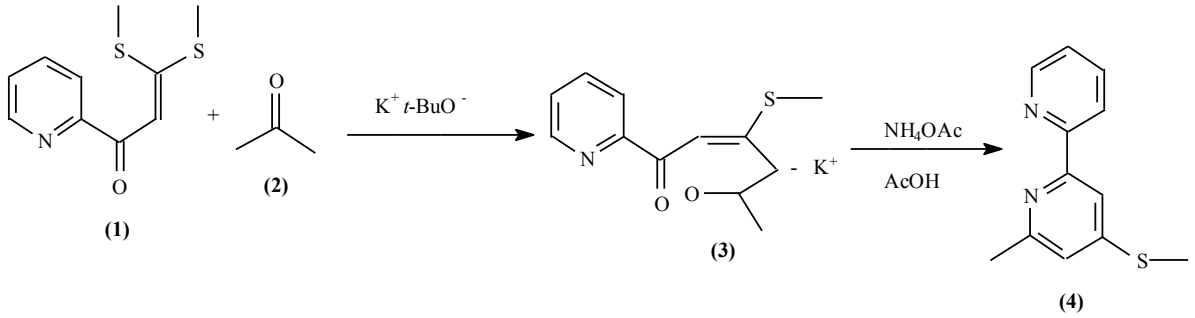

Scheme 1.5 Potts methods of synthesis of bipyridine

1.1.4.2 Cycloaddition methods

Bipyridines have also been synthesized by a number of cycloaddition methods. For example, stannylated bipyridines, (**6**), which can serve as Stille coupling partners for the synthesis of terpyridines and higher oligopyridines, have been generated in 77 % and 83 % yield by a thermally induced [4+2], regioselective cycloaddition between 1,2,4-triazines (**5**) and tributyl(ethynyl)tin derivatives (Scheme 1.6) [61]. As a result of steric interaction of the bulky tributyl tin group with the pyridine ring, less than 5 % of the final product was the 3-substituted isomer.

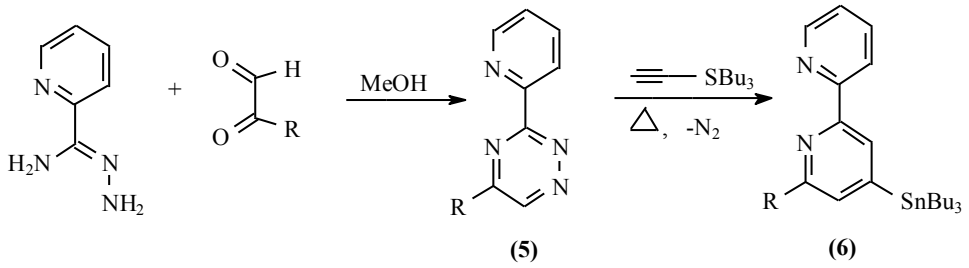

Scheme 1.6 Synthesis of substituted bipyridine via cyclo-addition method

Annelated, 3-substituted bipyridines have been prepared from alkynenitriles and alkynyl substituted pyridines using a Co(I)-catalyzed [2+2+2] cycloaddition strategy [62]. Moreover, 3,3'-disubstituted bipyridines ((**7**) and (**8**)) have been generated from acyclic 5-hexynenitrile and 1,3'-diynes in a single step (Scheme 1.7) [63]. While the isolated yields are moderate (<50 %), this intriguing one-step preparation exhibits very high regioselectivity with respect to formation of the first pyridine ring.

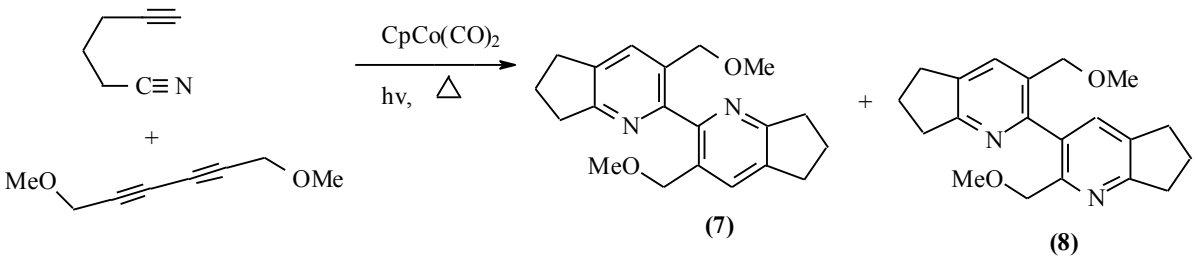

Scheme 1.7 Generation of bipyridine by annelation method

1.1.4.3 Other Synthetic Methods

The ring opening of bitriazolopyridines, (**9**), with the addition of various reagents leads to the formation of 6,6'-disubstituted bpys [64, 65]. Bipyridines substituted with a secondary alcohol, an ester linkage, and a ketone were synthesized using sulfuric acid, acetic acid, and selenium dioxide, respectively (Scheme 1.8) [64].

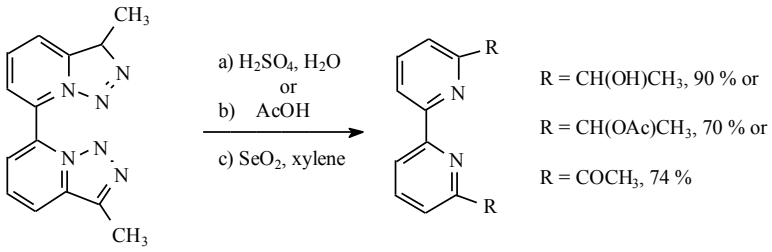

(9)

Scheme 1.8 Synthesis of substituted bipyridine via ring opening of bitriazolopyridine

Over 500 bipyridine derivatives have been synthesized using a solid state ‘‘combinatorial’’ approach or five beta-ketoesters, 10 aldehydes, and 10 enamines through sequential Knoevenagel/Hantzsch condensation reactions [66].

1.2 Reaction of the basic bipyridine ring system

1.2.1 Oxidation and Reduction

Bipyridines may be oxidized to picolinic acid with hot permanganate [14. 67] and reduced to 2,2'-bipiperidine with sodium metal in refluxing alcohols [68] or via hydrogenation [69]. Reaction of bipyridine ligands with peroxides or peracids has generated either 1-or 1,1'-N-oxides (or a mixture of the two). These ylides serve as valuable intermediates in many synthetic schemes because one or more of the nitrogen atoms is ‘‘protected.’’ Removal of the oxide is effected by reagents such as phosphorus trichloride or hydrogen iodide [67, 70].

1.2.2 Substitution

Electrophilic substitution reactions primarily occur *meta*- to the nitrogen atoms, while more common nucleophilic substitutions typically take place at positions ortho and para to nitrogen. For example, methyl lithium and phenyl lithium were

reacted with 4,4'-diBu^t bipyridine to generate 6,6'-dimethyl-4,4'-diBu^t bipyridine and 6,6'-diphenyl-4,4'-diBu^t bipyridine, respectively, in high yield [71].

Bipyridines with halogen substituents are useful coupling agents in oligopyridine [72] syntheses, as well as starting points for numerous other derivatizations. Many halobipyridine derivatives are known, and have been made by a number of different methods. While some procedures are general to a given halogen and ring position, often, specific halogen-substituted isomers require unique preparations. Chlorination of bipyridine N-oxide generates a mixture of the 4- and 6-substituted monochloro bipyridines, which can be resolved with $NiCl_2$ to afford the 6-chloro product in 40 % yield [73]. Other chlorinated bipyridines have also been synthesized, including 4,4'-dichloro (33 %) [74] and 5,5'-dichloro (40 %) [75]. The 4,4'-dibromo bipyridine ligand has been prepared in three steps from bipyridine in 24 % yield by modifications [76, 77], of the classical method of Case [70] while the 5-bromo- and 5,5'-dibromo derivatives were synthesized in moderate yield using direct bromination of bipyridine hydrobromide salts [78]. The 6,6'-dibromo bipyridine ligand was generated in 72 % yield by homocoupling of 2,6-dibromopyridine in the presence of *n*-BuLi, $CuCl_2$, and O_2 [79]. The 5,5'-substituted bisiodo bipyridine has been formed (70 %) by conversion of 5,5'-diamino bipyridine to the diazonium intermediate, followed by reaction with potassium iodide [80]. Other bisiodo bipyridine isomers may be formed using similar transformations involving the diazonium ion or by halogen exchange with a sodium iodide/acetyl chloride mixture [81].

Halobipyridines have also been generated by coupling halopyridyl precursors. For example, 6-bromo bipyridine [82] and 6,6'-dichloro bipyridine [83] were synthesized in 80 % and 66 % yield by coupling 2,6-dibromopyridine and 2-chloro-6-

bromopyridine, respectively, with the appropriate 2-pyridyl sulfoxide. The 6,6'-dichloro bipyridine ligand has also been produced in 53 % yield by Stille cross-coupling of 2-chloro-6-bromopyridine and 2-chloro-6-stannyl pyridine [84]. The 6-substituted cyano bipyridine has been generated in 95 % yield from bipyridine N-oxide by reaction with trimethylsilylcyanide and dimethylcarbamylchloride [85]. This is an improvement on an earlier method that generated 6-cyano bipyridine from the N-oxide in 62 % yield using potassium cyanide and benzoyl chloride [86]. This ligand has been used in electrochemical studies of rhenium complexes with sterically hindered bipyridine derivatives, as well as a precursor in the synthesis of 6-carbothioamide-bpy, which showed antitumor activity against P-388 lymphocytic leukemia in mice [86]. The 6,6'-diamino substituted bipyridine was generated in 52 % from the dibromo bipyridine precursor in three steps: (1) H_2NNH_2; (2) $NaNO_2$, HCl/H_2O; (3) $NaBH_4$, phase transfer reagent [87]. The 5,5'-diamino isomer was synthesized in 60 % by Ni-catalyzed homocoupling of 5-amino-2-chloropyridine [88].

1.3 Functionalized Bipyridines: Synthesis and Uses of common building blocks

1.3.1 Hydrocarbons

Substituted bipyridine derivatives are known to serve as important building blocks for many supramolecular and higher order structures [89]. While most of these bipyridine ligands with nucleophilic and/or electrophilic groups have been known for some time, recent synthetic improvements have made their preparation easier and more efficient [90]. Many functionalized bipyridine ligands can be synthesized from the appropriate alkyl precursors, which are most efficiently constructed using one of the coupling strategies as mentioned in previous Sections.

Bipyridines with aryl substituents have been prepared in high yield by Suzuki coupling methods. For example, 4,4'-di *o*-tolyl- (**10**), 4,4'-di *p*-tolyl- (**11**), and 4,4'-dimesityl-bpy (**12**) were generated by coupling the appropriate boronic acid with 4,4'-dibromo bipyridine (Scheme 1.9) [91].

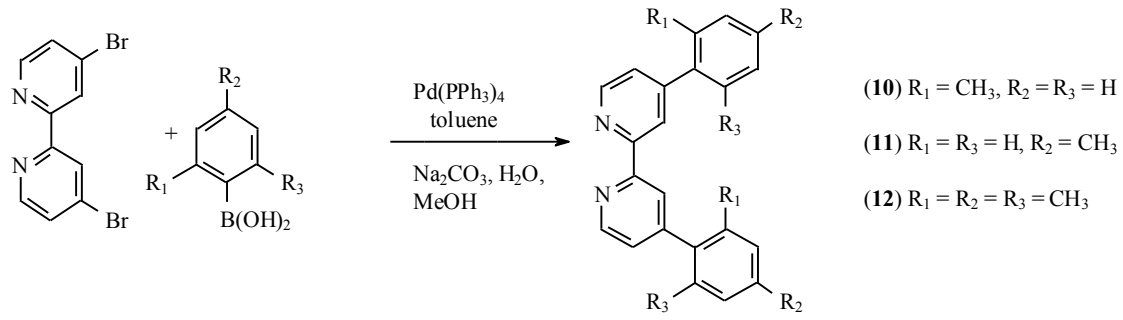

Scheme 1.9 Synthesis of aryl derivated bipyridines using Suzuki coupling method

Intramolecular charge transfer has been observed in bipyridine ligands bearing electron-donating groups (the bipyridine rings serve as the electron acceptor) such as pyrenyl. This ligand was synthesized in 61 % yield by a modified tin coupling of 4-bromo bipyridine with a pentacoordinated monoorganotin, which was generated in situ by combining 1-iodopyrene with bis-[N,N-bis (trimethylsilyl)amino] tin(II) (Scheme 1.10) [92]. These conditions may prove valuable for bipyridine syntheses in general because they are mild than those for typical Stille couplings, and avoid product contamination with organotin reagents.

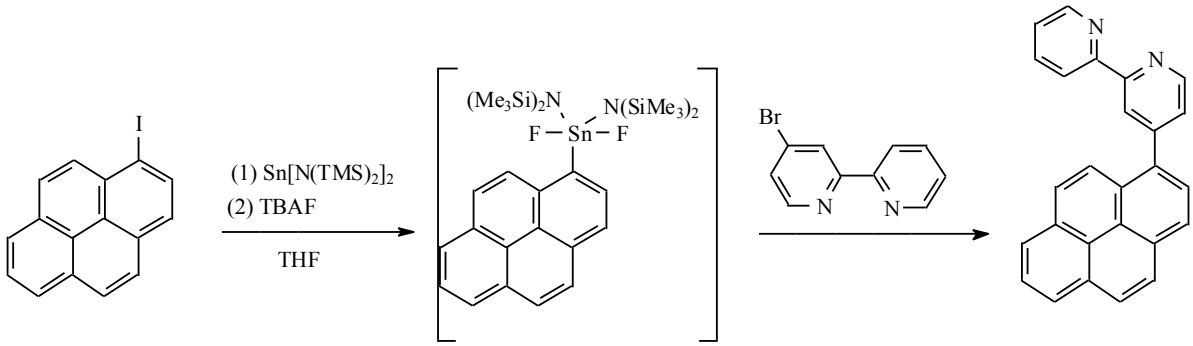

Scheme 1.10 Synthesis of pyrenylbipyridine using organotin catalyst

1.3.2 Acid Derivatives

The most common method for generating bipyridines with carboxylic acid groups is to oxidize methyl precursors. For example 4,4'-dimethyl-bpy can be oxidized with $K_2CrO_7(CrO_3)/H_2SO_4$ [93, 94] or $KMnO_4$ [95, 96] to form the 4,4'-diacid. The ligand 1,10-phenanthroline has been oxidized to generate the 3,3'-diacid [97, 98]. Esterification, reduction to the dialcohol, and partial oxidation or Swern oxidation to the aldehyde are all possible (Scheme 1.11). Both 4-formyl and 4,4'-bis(formyl) bipyridines have alternately been synthesized in high yield from methyl precursors via enamination using Bredereck's reagent followed by subsequent oxidative cleavage with sodium periodate [99].

Another method for synthesizing aldehydes is by reacting 4-aminomethyl-4'-methyl bipyridine with DCC/1-hydroxy- benzotriazole in a DMF/CH_2Cl_2 solvent mixture, followed by deprotection of the 1,3-dioxolane group [100]. Aldehyde-functionalized bipyridines have been bound to silica surfaces to form Fe(II) recognition sites [100].

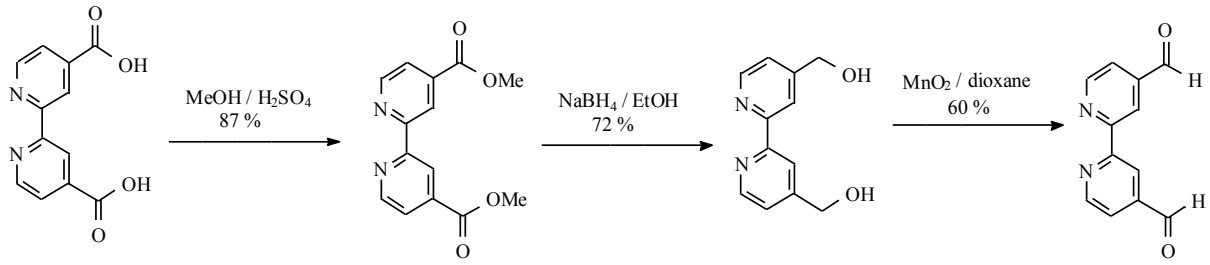

Scheme 1.11 Synthesis of carboxylated bipyridine via alkyl oxidation

Often, the carboxylic acid groups are converted to acyl chlorides with $SOCl_2$ [101, 102] prior to esterification with various alcohols and reaction with other nucleophiles [103]. Both mono-and difunctional ester-substituted bipyridines have been generated in moderate yield by palladium(0) - catalyzed carboalkoxylation of halo-or triflate-substituted precursors in the presence of CO, an alcohol, and a

tertiary amine [104]. Reduction of ester functionalities with $NaBH_4$ has furnished the corresponding alcohols. The 4-and 4,4'-substituted hydroxymethyl bipyridines have also been synthesized from halomethyl precursors, (4-$BrCH_2$ bpy) and (4,4'-bis($BrCH_2$) bpy), respectively, by reaction with NaOAc followed by acetate hydrolysis [105].

The 5,5'-dihydroxymethyl bipyridine ligand has been prepared (55 %) by converting 5,5'-dimethyl bipyridine to the bis N-oxide with hydrogen peroxide, followed by reaction with acetic anhydride in acetic acid [106], then hydrolysis with KCN in ethanol 107].

1.3.3 Unsymmetrical Derivatives

The preparation of unsymmetrical derivatives is often challenging in bipyridine syntheses. The most successful methods involve cross-coupling approaches; however, it is also possible to generate unsymmetric bipyridine derivatives by monofunctionalizing symmetric precursors. For example, certain analogues were formed through monolithiation of 6,6'-bis(hydroxymethyl)-bpy [108] or 4,4'-Me_2bpy followed by reaction with RX, where R contained an acetal group and X is a halogen [109]. Standard organic functional group conversions on the pendant chain, R, to proceed to an aldehyde, an acid, an alcohol, a halogen, and an amine were all compatible with the bipyridine ring system. Some methods for achieving unsymmetric compounds take advantage of the solubility differences between starting materials and products, which allow for the separation of monofunctionalized species from any difunctional by-products that may have formed. For example, reaction of 4,4'-bis(chloromethyl) bipyridine with $CaCO_3$ in refluxing dioxane/water has afforded the hetero-difunctional 4-hydroxymethyl-4'-chloromethyl bipyridine

ligand [110]. The 5,5'-disubstituted ethyl ester can be converted to the monocarbohydrazide by stirring with hydrazine. By manipulating the solvent conditions, the unsymmetric product precipitates out of solution before the second ester group can react (Scheme 1.12) [111].

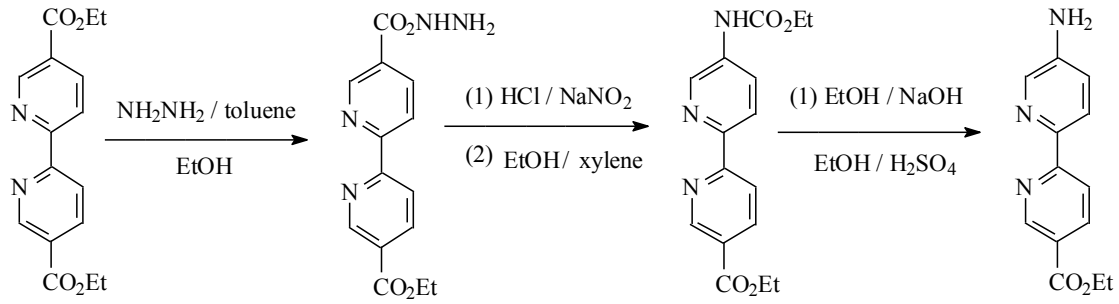

Scheme 1.12 Synthesis of unsymmetric bipyridine derivatives

1.3.4 Multidentate Chelates

Bipyridines have been functionalized with additional coordinating groups to form numerous multidentate structures. Among these systems are bipyridines with additional pyridyl or bipyridyl groups (namely terpyridine and higher order oligopyridines), oxygen chelates (**13**) [112], sulfur groups (**14**) [113, 114] as well as cyclic (**15**) and other higher order (**16**) amines [115].

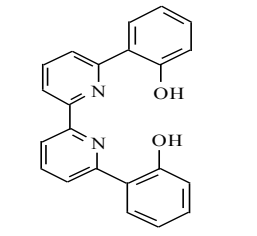
(13)

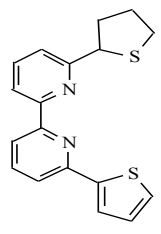
(14)

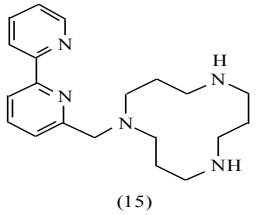
(15)

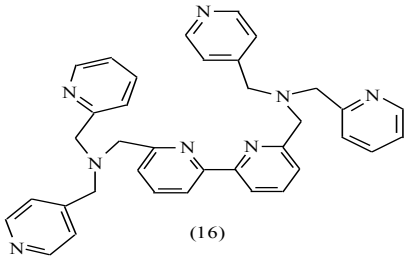
(16)

The ligands 6,6'-bis(2-hydroxyphenyl)-bpy, (**13**), and 6,6'-bis(2"-thienyl)-bpy, (**14**), each have two additional groups that may chelate. Ligand (**13**) has been shown to be tetradentate in some copper complexes, and was prepared from 6,6'-diacetyl bipyridine in 90 % yield [116]. The mono-substituted phenolic bipyridine is also known [117]. The dithienyl substituted bipyridine was synthesized via Negishi coupling of 6,6'-dibromo bipyridine and 2-thienylzinc chloride [114].

1.3.5 Polymers

Bipyridines have been incorporated into polymer chains in three basic ways (**17**-**19**). Macroligands, (**17**), possess a single bipyridine ligand with polymer chains as substituents. Polymers with bipyridines in the backbone (**18**) or as side chains (**19**) are also common.

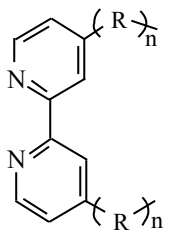

(17)

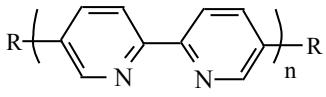

(18)

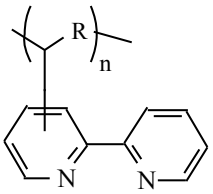

(19)

1.3.6 Macroligands

Polymers with a single bipyridine binding site covalently bound at the centre or end of the chain have been chelated to both discrete metal ions, [118-120] and metal clusters [121]. Variants of poly(oxazoline), polystyrene, poly(methyl methacrylate), poly(ethylene glycol), poly(lactic acid), and poly(caprolactone) are known. These macroligands have been synthesized by polymerizing from bipyridine ligands with initiator functionalities [118] or by coupling reactive bipyridines with end groups of linear polymer chains [122]. Similar macromolecular bipyridine ligands with

large dendritic wedges in the 4 and 4' positions have been bound to Ru(II) centers to generate dendrimers with a photoactive [$Ru(bpy)_3^{2+}$] core [123]. Buckminsterfullerene units have also been incorporated into bipyridine systems by coupling an acyl chloride-functionalized C_{60} molecule with a hydroxy-functionalized bipyridine. Two of these ligands were reacted with $Cu(MeCN)_4(PF_6)$ to generate a metal-centered dimer [124].

1.3.7 Bipyridines in the Main Chain

Various bishalo-functionalized bipyridine ligands have been polymerized through iterative coupling steps to generate polypyridyl structures. Monomers such as 5,5'-dibromo-3,3'-dinitro-bpy [125], and 5,5'-diiodo-bpy [126] as well as many of their alkyl-substituted derivatives [127] are competent for either cross-coupling with stannanes and borates or for Ni(0)-catalyzed homocouplings. The Heck coupling reaction has been employed in the generation of bipyridyl-containing conjugated copolymers [128].

Polycondensation of bipyridine diacid or bipyridine dicarbonyl dichloride ligands with the hydrochlorides of 2,5-diamino-1,4-benzenediol; 4,6-diamino-1,3-benzenediol; 2,5-diamino-1,4-benzenedithiol; and 2,3,5,6-tetraaminopyridine in poly(phosphoric acid) have generated rigid-rod poly(benzobisoxazole)-, poly(benzobisthiazole)-, and poly(benzobisimidazole)-bpy copolymers, respectively [129, 130]. These polymers have high oxidative and thermal stability and exhibit interesting nonlinear optical, conductivity, and luminescence properties [131, 132]. Various polyamides and polyesters have also been produced through condensation methods using bipyridine diacid/diamine [133] and bipyridine diacid chloride/alcohol [134] pairs. Other condensation reactions have generated bpy-phenylene-vinylene

type polymers that can be switched from partially to fully conjugated reaction with metal ions [135].

The 4,4'-bipyridine ligand has been utilized in the synthesis of linear coordination polymers as well as grids and networks through reaction with transition metal ions. These inorganic–organic polymers and frameworks are potential candidates for use in catalysis, molecular recognition, and nonlinear optics [136-141].

The dithienyl substituted ligand, (**14**), can be electrothermally polymerized in MeCN to generate stable *n*-doped materials with high bandgaps [114]. Metallorotaxanes have also been formed using the bpy-thienyl copolymers by coordinating open bipyridine sites with a suitable ruthenium complex [142]. Ruthenium complexes of the form $[RuL_3]^{2+}$ and $[RuL(bpy)_2]^{2+}$ (L= 4,4'-(4-anilinovinyl)-bpy) undergo electrochemical polymerization to form a conducting and an insulating film, respectively. The ligand was generated by coupling the dimethyl bipyridine dianion with *p*-aminobenzaldehyde [143]. Analogous ligands with 3-methoxystyryl-derivatives at either the 4 or 4 and 4' positions of the bipyridine ring were similarly synthesized by coupling *m*-methoxybenzaldehyde with the dimethyl dianion, and their Ru(II) complexes were also polymerized to generate electroactive films [144]. Numerous other polymer chains with bipyridine units in the backbone have been prepared [145, 146].

1.4 Chemistry of Phenanthroline and its Derivatives

1.4.1 *Introduction and Basic Transformations*

Blau and Gerdiessen [14, 147] are credited with the earliest published syntheses of 1,10-phenanthrolines (phen, (**20**)) in the late nineteenth century. While the coloured metal complexes of these compounds had been reported, their utility as colorimetric indicators was not discussed until 1931 [148]. For the next several decades, phenanthroline derivatives served primarily as colourimetric indicators for many transition metals.

Throughout this period, the contributions of G. F. Smith [149-152], F. H. Case [153-155], A. A. Schilt [156], and others toward the chemistry of these complexes resulted in a wealth of synthetic routes for derivatives of (**20**). The flourishing studies of polypyridyl-coordinated metal complexes provided inspiration for preparing unique phenanthrolines with a wealth of pendant photo- and electro-active molecules [19, 151].

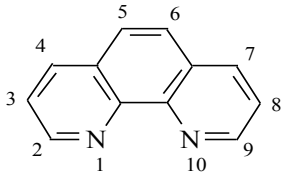

(20)

While many phenanthrolines are available from commercial suppliers, the synthesis of this ligand from its various precursors is often necessary in the preparation of more elaborate structures. The earliest syntheses of (**20**) proceeded by dual Skraup condensation about *o*-phenylenediamine, in a single-pot reaction [14, 147]. The low reported yields of this reaction, along with failed subsequent attempts to improve upon it [162], led to the use of sequential Skraup or Dö bner-Miller condensations, with isolation of the intermediate 8-aminoquinoline (**21**). Reaction of (**21**) with glycerol (**22**) or acrolein (**23**) in the presence of sulphuric or phosphoric acid

and arsenic pentoxide produces (**20**) directly, (Scheme 1.13) [149, 153-155, 162, 163].

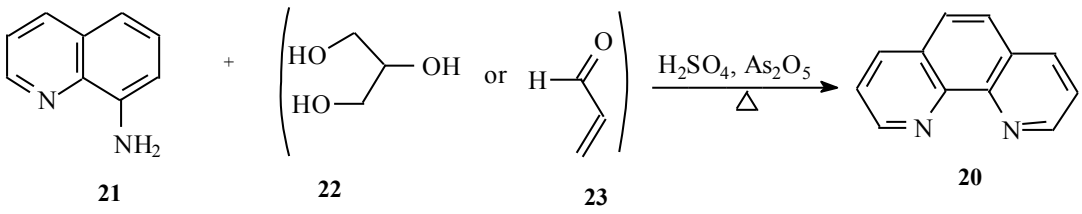

Scheme 1.13 Synthesis of 1,10-phenanthroline using Skraup condensation method

Additionally, phenanthrolines may be prepared from quinolines through Friedlander condensation [164]. Beginning with 8-amino-7-quinoline- carbaldehyde (**24**), the second pyridine ring is closed by coupling with an enolizable ketone, with concomitant loss of water, according to (Scheme 1.14) [165]. This route benefits from higher synthetic yields and the elimination of arsenic pentoxide as an oxidizing agent. Preparation of the starting quinoline (**24**) is often the most difficult step [166]. The efforts of Thummel and co-workers have resulted in several derivatives, including 5,6-dihydro-[**20**] [164, 167] and fused aryl-[**20**] [158, 159].

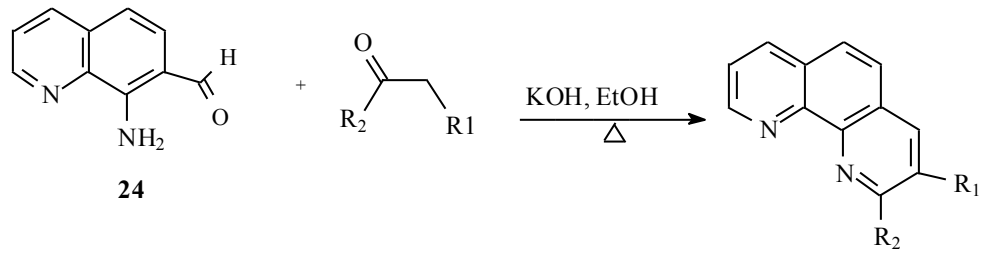

Scheme 1.14 Synthesis of 2,3-disubstituted phenanthroline using Friedlander condensation method

Many of the ring-substituted derivatives of 1,10-phenanthroline have been prepared by the aforementioned coupling reactions, using appropriately substituted precursors [149, 153-155, 170]. Regio-specific aromatic substitution reactions have improved the yields of substituted phenanthrolines, and reduced the dependence on the toxic arsenic compounds employed in the Skraup synthesis. These reactions typically give mixtures of mono- and symmetrically disubstituted phenanthrolines, which must be separated through careful workup.

1.4.2 The Reactivity of 1,10-Phenanthroline and derivatives

As one might anticipate, the ^{1}H NMR chemical shift of 1,10-phenanthroline is slightly different in each symmetry position. For example, the 2 and 9 positions show the highest chemical shifts, while the 3 and 8 positions display the lowest chemical shifts. A general prediction regarding the chemical reactivity of 1,10-phenanthroline is difficult. While the heterocyclic ring system possesses some chemical reactivity similar to pyridine, there are some significant differences. In both molecules, the position *meta* to the nitrogen is electron rich, while the *para* position is electron poor. 4,7-dibromophen (*p*-bromophen), consequently, should display similar chemical reactivity to *p*-bromopyridine, because the electron density of the carbon is poor in both molecules at the position *para* to nitrogen.

In order to make use of the 4,7-positions of 1,10-phenanthroline for substitution purposes, we have to understand more fully the chemical characteristics of all of the positions on the phenanthroline heterocycle. Since 1,10-phenanthroline has similar electron densities at the various carbon positions relative to pyridine, the ^{1}H NMR peaks should also be similar between them. The ^{1}H NMR spectrum of

pyridine has resonances at 7.38, 7.75 and 8.59 ppm. The corresponding resonances for 1,10-phenanthroline occur at 7.26, 7.55, 8.00, and 8.26 [171].

1.4.2.1 Halogenation

Halogenated derivatives of 1,10-phenanthroline are the most common starting reagents for the synthesis of more elaborate structures. Brominated phenanthrolines are convenient substrates for palladium-catalyzed alkynyl and aryl coupling reactions. In bromobenzene [172] or nitrobenzene [173] solutions, bromine adds to 1,10-phenanthroline at the 3- and 8-positions with similar yields (25 %) for both the mono- and di-brominated product. Bromination at the 5- and 6-positions is accomplished in fuming sulphuric acid [174]. Treatment of 1,10-phenanthroline-4,7-dione with $POBr_3$ gives 4,7-dibromo-1,10-phenanthroline [175]. Bromination proceeds with very high yields in oleum at elevated temperatures, producing 5-bromo-1,10-phenanthroline exclusively [174]. The reaction of 1,10-phenanthroline with hypochlorous acid leads to chlorination at the 5- and 6-positions [176]. Oxidative chlorination with phosphorus pentachloride gives the 2,9-dichloro-1,10-phenanthroline, as well as the 2,3,8,9-tetrachloro-1,10-phenanthroline [177]. Chlorinated-1,10-phenanthroline may be converted sequentially through the thiol-1,10-phenanthroline to the sulfonato-1,10-phenanthroline [178]. Several trihalomethyl derivatives, particularly fluorinated phenanthrolines, have also been prepared [179-183].

1.4.2.2 Oxidative Substitutions

Treatment of 1,10-phenanthroline with oleum and nitric acids gives 5-nitro-1,10-phenanthroline (**25**) with yields from 70 to 90 %, depending on reaction

temperature [150]. A side product of this reaction is the 1,10-phenanthroline-5,6-dione (**26**), whose colourless iron(II) complex was of little interest at the time of its discovery. A versatile precursor to many other phenanthrolines, (**26**) is readily prepared by treatment of 1,10-phenanthroline with sulfuric and nitric acids in the presence of bromide [184-186]. Through a dioxime intermediate, 5,6-diamino-1,10-phenanthroline (**27**) is obtained [187]. 5-Amino-1,10-phenanthroline (**28**) may be prepared directly from (**25**) with Sn-HCl reduction [185]. Alternatively, amino-1,10-phenanthroline may be formed by conversion of the corresponding chloro-1,10-phenanthroline with ammonia [188].

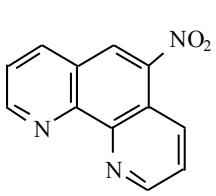

25

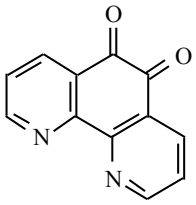

26

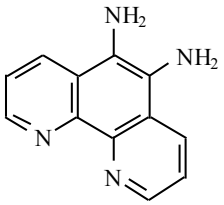

27

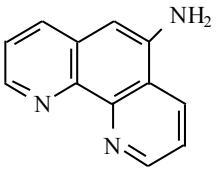

28

Oxidation of 1,10-phenanthroline with commercial bleach (hypochlorite) in the presence of a phase transfer catalyst [189, 190] gives the 1,10-phenanthroline-5,6-epoxide (**29**), which is quite versatile in the preparation of a variety of 5-subsituted-phenanthrolines, including cyano-, hydroxy-, dimethylamino-, aza-18-crown-6-, and methoxy-1,10-phenanthroline [191]. Under acidic conditions, this reaction permits the direct conversion of 1,10-phenanthroline to (**26**) [190, 192].

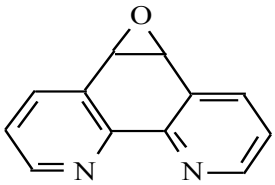

29

Methylated phenanthroline is commonly oxidized to the aldehyde by selenium dioxide in dioxane, and then to the carboxylic acid by treatment with nitric acid [183, 193]. A selenium-free route to the aldehyde has been reported using iodine in DMSO [194].

1.4.2.3 Alkylation and Catalyzed Cross-coupling

The addition of alkyl [195] and aryl [196-198] groups to the 2- and 9-positions of 1,10-phenanthroline proceeds most commonly by using organolithium reagents. Alkyl extension of methylated-1,10-phenanthroline is also achieved by lithiation [199]. Ziessel and co-workers were instrumental in the application of palladium(0)-catalyzed coupling reactions to bromo- and chloro-substituted phenanthrolines, bipyridines, and terpyridines [200, 201]. In all cases, conditions have been established to promote the coupling of various alkynyl moieties to these ligands, making it possible to generate new materials such as rod-like organometallic structures and polymers [172, 201-209]. Aryl coupling using a phenylboronic ester following the coupling reaction of Suzuki [210] has been accomplished as well [208].

1.4.2.4 Molecular Recognition and Phenanthroline-based Ionophores

Consistent with much of the early work regarding 1,10-phenanthroline and its derivatives as colourimetric indicators for transition-metal ions, various phenanthrolines have recently been developed as ion-selective electrochemical sensors, as fluorometric sensors, and as agents for selective ion transport, particularly useful in the detection and transport of Li^+ [211-215]. The recognition event occurs by complexation with either the diimine moiety of 1,10-phenanthroline [211] or with a crown ether-substituted 1,10-phenanthroline [212, 214, 215].

Some of the most successful sensing applications of 1,10-phenanthroline and its derivatives are realized when they are chelated to ruthenium(II) centers. The visible-absorbing metal-to-ligand charge transfer (MLCT) excited states associated with these complexes possess long-lifetime, high quantum yield photoluminescence [157-159]. The long lifetimes associated with these chromophores make them susceptible to collisional quenching reactions, such as electron and energy transfer. In terms of sensing, the orange-to-red MLCT-based emission provides a stable and accurate response (in intensity and lifetime) to dioxygen. Demas and co-workers have thoroughly developed this idea using a variety of ligands, metal centers, and solid support materials [216-220]. The charge transfer photoluminescence in ruthenium(II) diimine complexes is also temperature dependent, providing a luminescence response that can accurately determine temperature in a variety of environments [221-224]. In addition to these simple analytes, many other d_6-metal-chelated 1,10-phenanthroline systems have been developed for response to a variety of specific analytes such as pH, [225, 226], heavy metals, [191, 215] and various metal ions [221].

Developments in the world of anion sensing have generated two new phenanthroline-based structures. Sessler and co-workers have prepared a colourimetric and electrochemical-based fluoride ion sensor from ruthenium(II) and cobalt(III) coordination compounds, each containing 1,10-phenanthroline derivatized with dipyrrolylquinoxaline (DPQ) (**30**) receptor [227]. This ligand was prepared through condensation of (**26**) with the appropriate 1,2-diamino-[DPQ] precursor. A related ligand (**31**) and its corresponding ruthenium(II) (bis)-heteroleptic complex were synthesized by Anzenbacher and co-workers for luminescence lifetime based sensor for cyanide and related ions [228].

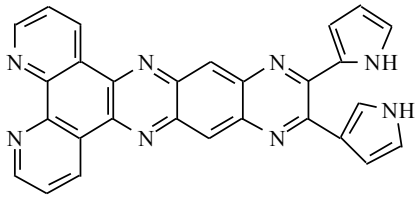

30

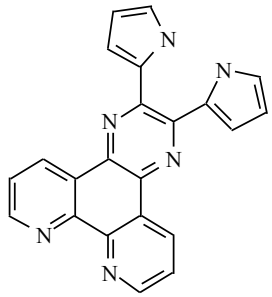

31

1.4.2.5 Chromophore-containing Phenanthrolines

1,10-phenanthroline and its derivatives have been largely unexplored for chromophore attachment unlike the 2,2'-bipyridine and 2,2',6'2"-terpyridine structures since there are a limited number of reactive structures available for synthetic elaboration. C. R. Luman and his group have made use of nucleophilic (**28**) in the preparation of coumarin and naphthalimide-containing ligands, (**32**), (**33**), and (**34**) [229-232]. The introduction of these organic chromophores into ruthenium(II) complexes has led to MLCT compounds possessing large absorption cross-sections and markedly extended room-temperature, excited-state lifetimes. Rodgers and co-workers have also made use of (**28**) as a nucleophile in the preparation of an amide-linked pyrene derivative of 1,10-phenanthroline, (**35**) [233]. $[Ru(bpy)_2(\mathbf{35})]^{2+}$ served as the basis for future studies of excited triplet-state equilibria in ruthenium(II) MLCT chromophores.

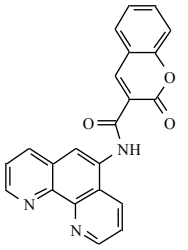

32

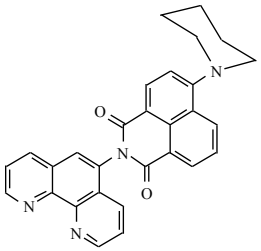

33

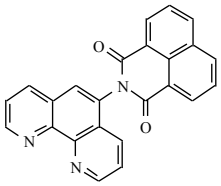

34

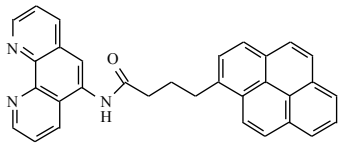

35

Schmehl, Thummel et al. [164] prepared related structures where pyrene was covalently linked to 1,10-phenanthroline through a single C-C bond in the position 2 (**36**) to show the role of intraligand states in the deactivation of MLCT chromophores [234, 235]. Several other chromophoric 2-aryl-1,10-phenanthrolines were also prepared (aryl = phenyl (**37**), 2-naphthyl (**38**), 1-anthracenyl (**39**), using the same condensation strategy [163]. Recently, Thummel's group developed more elaborate structures designed to elucidate the effects of governing the cyclometalation process in complexes of Ru(II) [236]. C. R. Luman and his group also have employed Suzuki coupling to generate 5-pyrenyl-1,10-phenanthroline (**40**) from 5-bromo-1,10-phenanthroline-3-pyreneboronic acid [237, 238]. It was noted that the reactivity of the 2- and 9- positions in 5-bromo-1,10-phenanthroline to strong organic bases such as *n*-BuLi prohibits the formation of 1,10-phenanthroline-5-boronic acid using standard reaction conditions. However, this limitation can likely be circumverted using boronic esters under milder conditions, as described by Sauvage et al. [208].

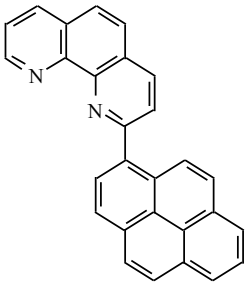

36

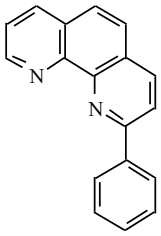

37

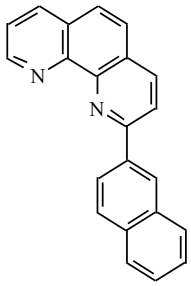

38

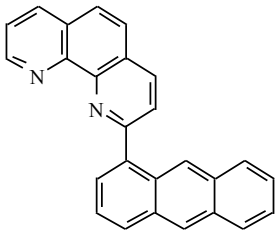

39

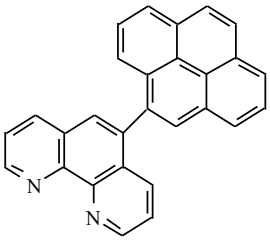

40

1.4.2.6 Electroactive Ligands

The rich coordination chemistry of 1,10-phenanthroline has encouraged the synthesis of new structures that serve as electron acceptors when chelated to appropriate metal complexes. Schanze and Sauer prepared a variety of proline-bridged *p*-benzoquinone derivatives of $[Ru(bpy)_2(phen)]^{2+}$, connected to the metal centre through an amide bond utilizing the carboxy terminus of L-proline [239]. In all cases, the amide linkage to L-proline was generated from the phen-NH_2 group resident on the metal complex. Other ligands exist in which the quinone is conjugated with the phenanthroline rings (**41**), (**42**) [192, 240].

The Hupp group utilized electrochemical oxidation of $[Ru(phen)_3]^{2+}$ in the presence of tertbutyl-4-pyridine, 4-phenylpyridine, or 4,4'-bipyridine to prepare the pyridinium derivatives, (**43**), (**44**), and (**45**), respectively [241]. It is believed that activation of coordinated (1,10-phen) is facilitated by oxidation of ruthenium(II) to

ruthenium(III). Subsequent elimination of an H atom from (1,10-phen) by the substituted pyridines is likely accomplished by spontaneous reduction of ruthenium(III) to ruthenium(II), producing the pyridinium salt.

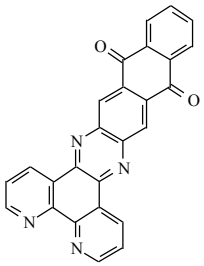

41

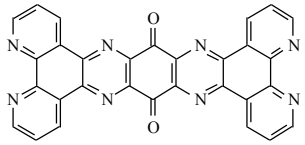

42

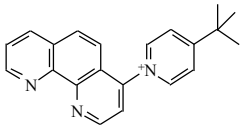

43

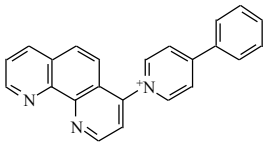

44

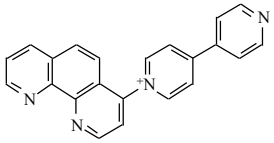

45

1.4.2.7 Polymer Supports for Phenanthrolines

The inclusion of coordination compounds into polymer matrices creates a stable and malleable environment in which the photophysical and electronic properties of these complexes may be studied. The electroactivity of thin-film-modified electrodes shows promise for new photovoltaics, electrochromics, electrocatalysts, and electroanalytical applications. One approach to these systems is to condense a modified ligand onto an existing polymer chain. This route has been successful in modifying polymers with phenanthrolines through ester [242] and sulphonamide [243, 244] linkages via nucleophilic substitution.

Another method uses a ligand co-monomer, such as an acrylimide-substituted phenanthroline (**46**). Masked photopolymerization of a thin film of (**46**) on a conductive glass electrode resulted in an electrochemically modulated film, which acted as a polarization grating [245]. A more elementary route to ligand-

functionalized polymers is by electropolymerization of the ligand at the electrode surface. This has been demonstrated with coordinated complexes of 5-chloro-1,10-phenanthroline [246, 247]. 5-amino-1,10-phenanthroline (**28**), [248] and pyrrole-substituted phenanthrolines (**47**) [249].

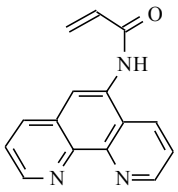

46

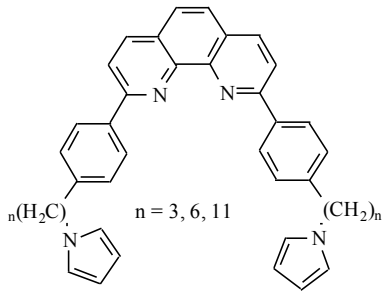

47

1.5 The reactivity of 2,2':6',2''-Terpyridine and Their Derivatives

Terpyridine was isolated for the first time in the early 1930s by Morgan and Burstall [249, 250] who heated pyridine with anhydrous $FeCl_3$ in an autoclave (50 atm) for 36 h to a temperature of about 340 ^{o}C. The parent terpyridine was isolated along with a myriad of other N-containing products. It was subsequently discovered that the addition of Fe(II) ions to a solution of terpyridine compounds gave rise to a purple colour giving the first indication of metal complex formation. Since this pioneering work was performed, the chemistry of terpyridine remained merely a curiosity for nearly 60 years, at which point its unique properties were incorporated into the construction of supramolecular assemblies.

The terpyridine molecule contains three nitrogen atoms and can therefore act as a tridentate ligand [251, 252]. It has been extensively studied as an outstanding complexing ligand for a wide range of transition metal ions. The ever-expanding potential applications are the results of advances in the design and synthesis of tailored terpyridine derivatives. The well-known characteristics of terpyridine metal

complexes are their special redox and photophysical properties, which greatly depend on the electronic influence of the substituents. Therefore, terpyridine complexes may be used in photochemistry for the design of luminescent devices [253] or as sensitizers for light-to-electricity conversion [254, 255]. Ditopic terpyridinyl units may form polymetallic species that can be used to prepare luminescent or electrochemical sensors [256, 257]. In clinical chemistry and biochemistry, functionalized terpyridine have found a wide range of potential applications [258], from colourimetric metal determination [259, 260] to DNA binding agents [261-263] and antitumor research [264-266]. Terpyridines have also been utilized for catalytic purposes [267, 268] and in asymmetric catalysis [269]. Another interesting application regarding novel supramolecular architectures is the formation of “mixed complexes”, where two differently functionalized terpyridine ligands are coordinated to single transition metal ion [270, 272].

1.5.1 Cross-coupling synthesis of terpyridine

Appropriate methodologies for the construction of functionalized terpyridines were based on directed cross-coupling procedures. Traditional examples, such as the cross-coupling of organosulphur compounds [264] or lithiopyridines with $CuCl_2$ [265], have the disadvantage that they generally result in overall poor conditions. Modern Pd(0)- catalyzed coupling reactions combine the desired efficiency and simplicity with controllable substitution possibilities. Suzuki [266], Negishi [267], and Stille couplings [268] are all based on a Pd(0)/Pd(II) catalytic cycle. Particularly, the Stille cross-coupling has become a popular route to terpyridines, because of its, (a) universal building block principle, (b) multi-gram product accessibility and (c) well-directed functionalization at almost every desired position (Scheme 1.15) [269-272].

2,2':6',2"-Terpyridines functionalized at the central and/or terminal pyridine rings, can be obtained utilizing appropriate 2,6-dihalopyridines (**48**) as central building blocks which can be reacted with 2-trialkyl- stannlpyridine (**49**) and Pd(0) catalysts in toluene for at least 24 h.

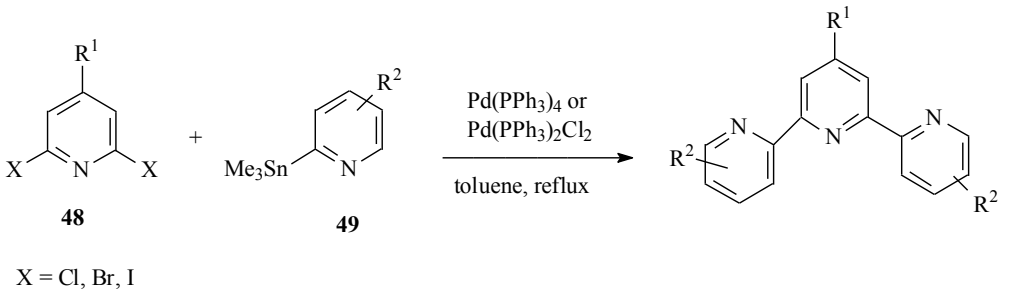

Scheme 1.15 Stille-coupling of 2-trimethylstannylpyridines and 2,6-dihalopyridines

Terpyridine synthesis via the Stille procedure can be conducted by utilizing 2,6-bis(trimethylstannyl)pyridines (**50**) as a central ring, and coupling them with the corresponding 2-bromopyridines (**51**) (Scheme 1.16) [273, 274].

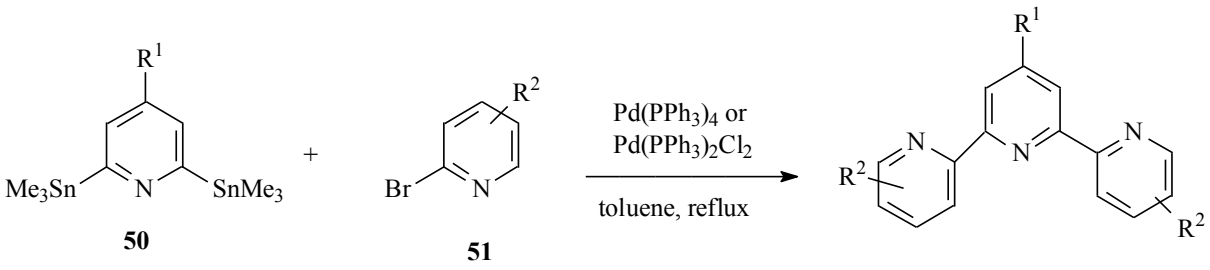

Scheme 1.16: Stille-coupling of bis(trimethylstannyl) pyridines and 2- bromopyridines

Other Pd-catalyzed cross-coupling procedures have not yet been used for the synthesis of terpyridines themselves, but seem to be appropriate methods; for instance, Negishi cross-coupling was used for the synthesis of terpyridine-related compounds [275] and related 2,2'-bipyridines [276] in excellent yields.

1.5.2 Synthesis of 2,2':6',2"-terpyridine derivatives

Terpyridines may be functionalized at both the central and the terminal rings; therefore, the desired groups must be incorporated into the initial substituted starting compounds via ring-assembly or coupling procedures.

1.5.2.1 4'-Aryl-substituted-2,2':6',2"-Terpyridine Derivatives

Substitution at the 4'-position of tpy is unique in that it provides a ligand which still retains the C_2 symmetry of the parent molecule. No such monosubstituted analogue exists for 2,2'-bipyridine (bpy), and thus these 4'-substituted derivatives of tpy have been particularly useful in the construction of well-organized assemblies. The basic ingredient is acetylpyridine (**52**), which provides the two distal rings of tpy, as well as C2', C3', C5' and C6' of the central ring. C4' originates from an aldehyde (**53**) which is generally aromatic. In (Scheme 1.17), an intermediate 1,5-diketone (**54**) condenses with a nitrogen source, often ammonium acetate, to provide the final tpy (**55**).

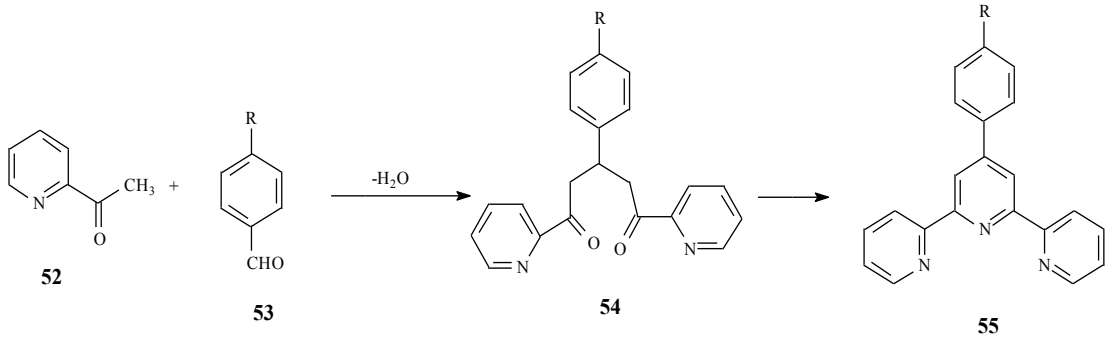

Scheme 1.17: Synthesis of a 4'-substituted tpy by condensation method

1.5.2.2 4'-Substituted-2,2':6',2''-Terpyridinoxyl Derivatives

4'-Terpyridinoxy derivatives represent a dominant substitution pattern because of their convenient accessibility via (a) nucleophilic aromatic substitution of 4'-haloterpyridines by any primary alcohols and analogs or (b) S_N2-type nucleophilic substitution of the alcoholates of 4'-hydroxyterpyridines (the “enol” tautomer of the 4-terpyridine). A large variety of functional terpyridinoxy derivatives have been originated from these methods as represented in (**56**–**60**).

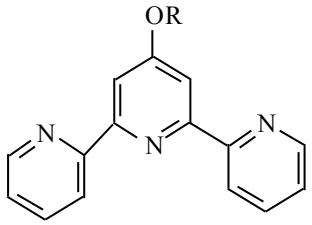

$R = (CH_2)_3OH$, (**56**)

$R = (CH_2)_3NH_2$, (**57**)

$R = (CH_2)_2CO_2H$, (**58**)

$R = (CH_2)_4OBu$, (**59**)

R = —C≡CH, (**60**)

A new approach to terpyridinoxy moieties has taken advantage of the Mitsunobu reaction; for example, terpyridone was reacted with alcohols in the presence of triphenylphosphine and diisopropylazodicarboxylate [277]. This methodology is very mild (*ca*, 2–3 h at 25 ^oC), yet, sensitive or complicated functional groups, such as alkynes or nucleosides can be introduced.

1.5.2.3 6-Substituted terpyridines

Substitutions at the 6- and 6''-positions of tpy are of considerable importance, since these positions are closest to the tridentate coordination site and thus can interact strongly with a bound metal. The 6-tpy substituted amidrazone (**62**) reacts with 1,10-phenanthroline-5,6-dione (**61**) to provide the 1,2,4,8,9-pentaazatri-

phenylene (**63**), which then cycloadds to norbornadiene followed by [4+2] cycloreversion, extruding nitrogen and cyclopentadiene to give the interesting quaterpyridyl derivative (**64**) (Scheme 1.18) [278].

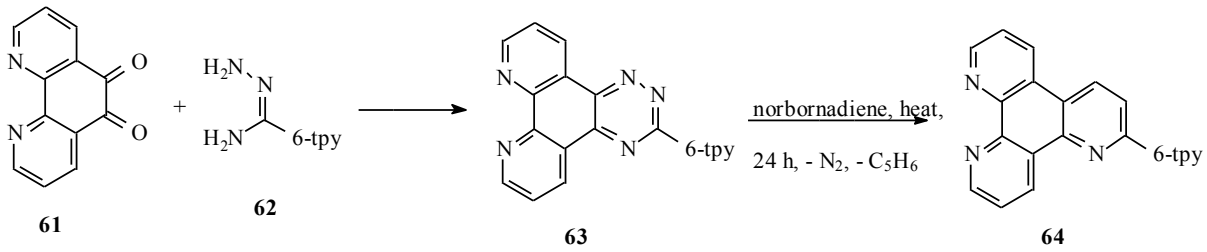

61 **62** **63** **64**

Scheme 1.18 Synthesis of 6-substituted terpyridine derivative via cycloaddition method

1.5.3 Disubstituted terpyridines

1.5.3.1 3,3"-Disubstituted terpyridines

The azidophenylselenation reaction of (**65**) provides a species which can be subsequently cyclised to give the tetrahydropyridine derivative (**66**) as a mixture of stereoisomers (Scheme 1.19). After purification, this species undergoes oxidation to the dicarbomethoxytpy (**67**) in 60 % yield [279].

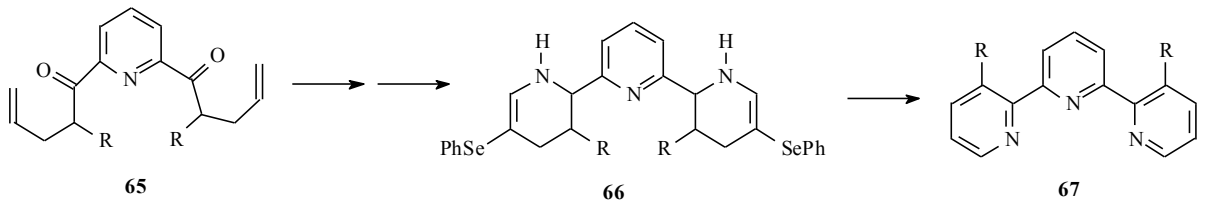

65 **66** **67**

Scheme 1.19 Synthesis of 3,3"-disubstituted functionalized terpyridine

1.5.3.2 4,4"-Disubstituted terpyridines

Treatment of 4-dimethylaminopyridine with BuLi-$Me_2NCH_2CH_2$–OLi affords α-lithiation in good yield. Various electrophiles can then be introduced, including tri-*n*-butylstannane to provide (**68**). Stille coupling with (**69**) affords the disubstituted tpy (**70**) in 50 % yield (Scheme 1.20) [280].

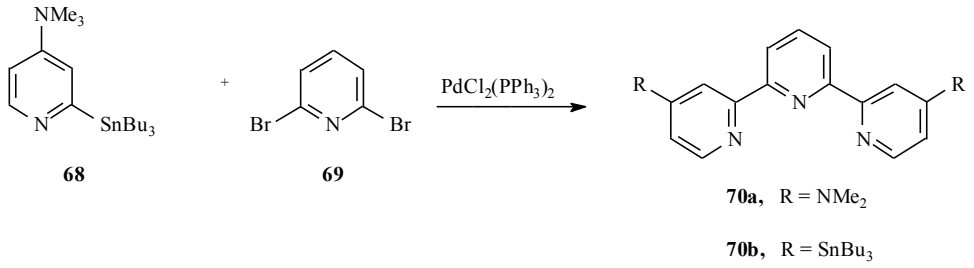

Scheme 1.20 Synthesis of 3,3"-disubstituted terpyridine using Stille coupling method

1.5.3.3 5,5"-Disubstituted terpyridines

Double Stille couplings which employ 2,6-di-(tri-n-butylstannyl)pyridine (**72**) and two equivalents of a 5-substituted-2-bromopyridine lead efficiently to 5,5"-disubstituted tpys. Thus 5-methyl-2-bromopyridine (**71**) reacts with (**72**) to provide (**73**) (Scheme 1.21) [281].

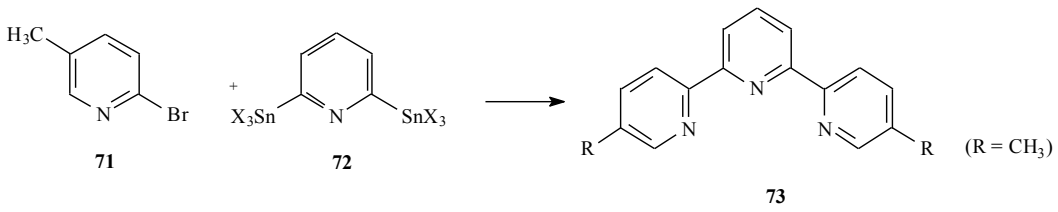

Scheme 1.21 Synthesis of 5,5"-disubstituted terpyridine using Double Stille coupling method

1.5.3.4 6,6"-Disubstituted terpyridines

A simple method for the introduction of phenyl groups at the ortho-positions of tpy involves treatment with phenyllithium at 25 ^{o}C to give a bis-adduct, which can then be hydrolyzed and rearomatized with manganese dioxide to provide a 21 % yield of 6,6"-diphenyltpy [282]. Alternatively, the diketo-intermediate (**75**) will provide a 64 % yield of the same molecule. If (**75**) is first protected as its bisketal, macrocyclization with disodium hexaethylene glycolate, followed by deprotection and central pyridine formation, affords the intriguing crown ether (**76**) (Scheme 1.22) [283]. The dibromotpy (**74**) can be converted through its diester ($CO_2C_4H_9$) and diol (CH_2OH) to the corresponding dialdehyde (CHO) [284].

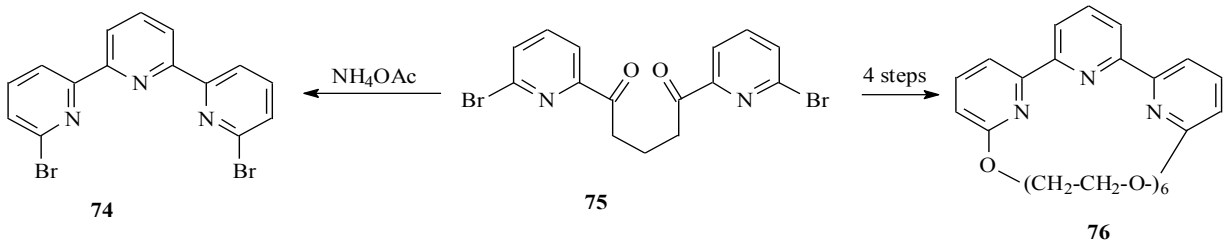

Scheme 1.22 Synthesis of 6,6"-disubstituted terpyridine using Dietrich-Buchecker method

1.5.3.5 3',4'-Disubstituted terpyridines

An interesting condensation has been reported in which a 2-pyridyl-1,3-butanedione (**77a**) reacts with α-aminoacrylonitrile (**78**) to provide 3-cyano-4-(trifluoromethyl)tpy (**79**) in 30 % yield (Scheme 1.23) [285]. The reaction has been used employing a wide variety of partners besides those involving 2-pyridyl. The Hantzsch approach has been used in the reaction of keto-ester (**77b**) with enone (**80**) to provide (**81**), where the 2-furfuryl group may be oxidized under mild conditions to provide the 3',4'-tpy dicarboxylic acid [286].

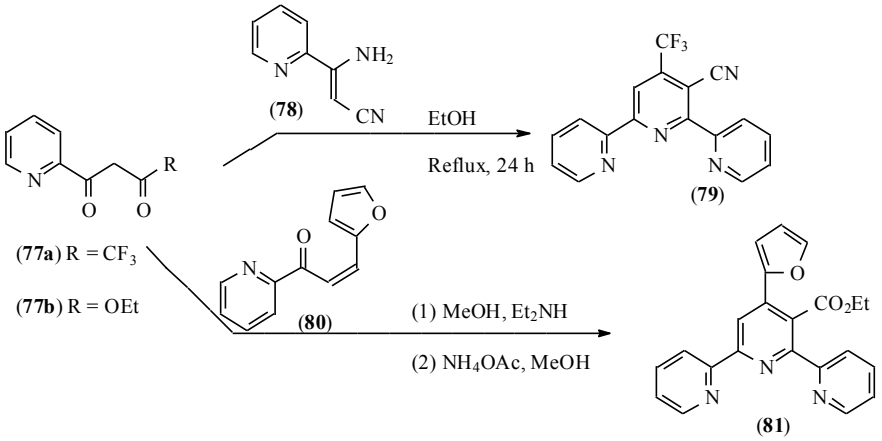

Scheme 1.23 Synthesis of 3',4'-disubstituted terpyridines by Yamaguchi condensation method

1.5.4 Trisubstituted terpyridines

Stille coupling of the 4'-carbomethoxy derivative of (64) with 2-tributylstannyl-6-methylpyridine provides the 6,4',6"-trisubstituted derivative (**82a**) which may be converted with NBS to the bromomethyl species (**82b**) [287]. The dibromo-*p*-tolyl tpy (**82c**) has been prepared and converted into its di-butylester (**82d**) [284]. The reaction of lithium diphenylphosphide with 4'-phenyltpy provides an 84 % yield of the bisdiphenylphosphino species (**82e**) [288]. An analogous tpy with two N-methyl-hydrazinyl substituents (**82f**) has also been reported [289]. Treatment of 4'-nitro-5,5"-dimethyltpy (**83a**) with sodium azide in DMF provides the analogous 4'-azido derivative (**83b**) [290]. Similar monomethyl, disubstituted tpys have also been prepared.

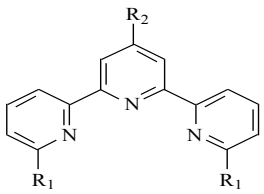

(**82a**) $R_1 = CH_3$, $R_2 = CO_2Et$

(**82b**) $R_1 = CH_2Br$, $R_2 = CO_2Et$

(**82c**) $R_1 = Br$, $R_2 = p$-tolyl

(**82d**) $R_1 = CO_2C_4H_9$, $R_2 = p$-tolyl

(**82e**) $R_1 = PPh_2$, $R_2 = Ph$

(**82f**) $R_1 = N(Me)NH_2$, $R_2 = Ph$

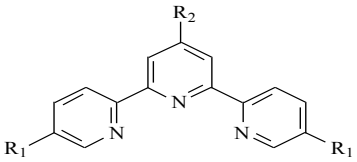

(**83a**) $R_1 = CH_3$, $R_2 = NO_2$

(**83b**) $R_1 = CH_3$, $R_2 = N_3$

1.5.5 Tetrasubstituted terpyridines

The Krö hnke synthesis applied to 2,6-diacetylpyridine affords a variety of 4,4",5,5"-tetrasubstituted tpys which can then be transformed in good yields to (**84a–f**) [291].

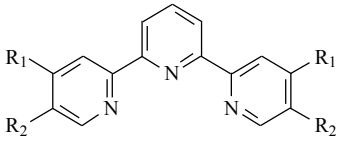

(**84a**) $R_1 = CH_3$, $R_2 = CH_3$

(**84b**) $R_1 = C_6H_5$, $R_2 = CH_3$

(**84c**) $R_1 = CHO$, $R_2 = CH_3$

(**84d**) $R_1 = CH{=}CHN(CH_3)_2$, $R_2 = CH_3$

(**84e**) $R_1 = CH_2OH$, $R_2 = CH_3$

(**84f**) $R_1 = CO_2CH_3$, $R_2 = CH_3$

1.5.6 Fused (Annelated) terpyridines (Benzo-fused)

The Friedländer condensation of 2-aminobenzaldehyde (**86**) with 2,6-diacylpyridines provides diquinolinylpyridines, which are dibenzo-fused analogues of tpy. The diketones (**85a–c**) are derived from dicycloalkenopyridines in two steps and condensed with (**86**) to afford (**87a–c**) (Scheme 1.24) [292]. If 1-amino-2-naphthalenecarbaldehyde is substituted for (**86**), the dinaphtho-fused system (**88**) results [293]. A bisdimethylene-bridged analogue of (**88**) has been prepared from

(**85a**). If one uses 2-aminobenzophenone in place of (**86**), the 2-(4-phenylquinolinyl) derivatives may be prepared, and a series of 2-aminobenzophenones bearing methyl, nitro, cyano, and bromo substituents have provided a series of substituted derivatives [294].

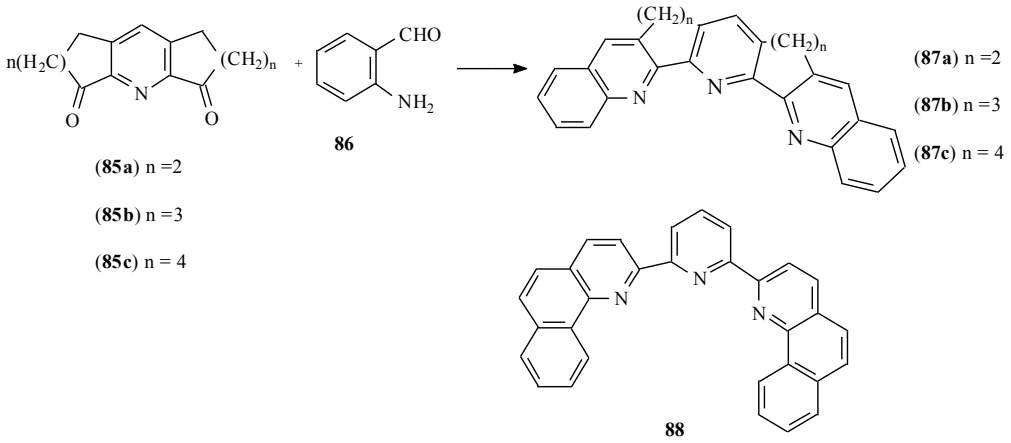

Scheme 1.24 Synthesis of benzo-fused terpyridine derivative by Friedlander condensation method

1.6 The reactivity of Anthracene and its Derivatives

Anthracene (**89**) is a tricyclic aromatic hydrocarbon derived from coal tar. Its molecular formula is $C_{14}H_{10}$ (C_nH_{2n-18}) and molecular weight 178.23. Anthracene melts at 216-218 ^oC and boils at 354 ^oC. It is Insoluble in water but soluble in most organic solvents such as CS_2, ROHs, benzene, chloroform and hydronaphthalenes. Unsubstituted anthracene is a planar geometry. Its oxidation yields anthraquinone, the parent substance of a large class of dyes and pigments. Anthracene is a basic substance for production of anthraquinone dyes, pigments, insecticides, wood preservatives and coating materials. Anthracene is a nucleus for polymer soluble pigments. Anthracene forms reversible photodimer through the 9,10-positions in response to light and provides photochromic applications. Anthracene family

compounds are base materials for colourings. They have useful functions such as light and temperature sensitivity, heat resisitance, conductivity, emittability and corrosion resistance. Specifically, the anthracene moiety absorbs in the blue-green region and in terms of spectral coverage, this absorption enhances the light-harvesting capacity of the complexes. Anthracene's emission spectrum peaks at between 400 and 440 nm [295, 296].

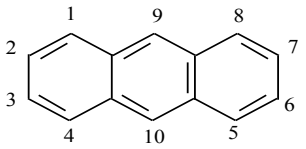

89

Due to π-electron cloud overlaps, anthracene exhibits semiconductor property. Organic semiconductors have some merits of self radiation, flexibility, light weight, easy fabrication and low cost. Anthracene derivatives have been used for the detection of high energy photons, electron, alpha particles and showed both hole and electron transport and hole transfer materials. They have also been investigated as organic electroluminescence materials for the applications in organic solar cells, biosensitizers and display devices, such as OLED (Organic Light Emitting Diode), OTFT (Organic Thin Film Transistor), wearable display and electronic paper.

The reversible bonding and photochromic properties of anthracene are the basis of many potential applications using poly and mono-substituted anthracene derivatives [297-299]. Photochromism is the reversible transformation of a chemical species between two forms by the absorption of electromagnetic radiation, where the two forms have different absorption spectra. Trivially, this can as well be described as a reversible change of colour upon exposure to light.

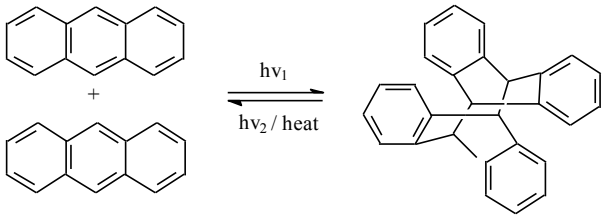

90

Scheme 1.25 Photochromic reactions of anthracene

Photochromism does not have rigorous definition, but is usually used to describe compounds that undergo a reversible photochemical reaction where an absorption band in the visible part of the electromagnetic spectrum changes dramatically in strength or wavelength. The dimer (**90**), (Scheme 1.25) is connected by two covalent bonds resulting from the [4+4] cycloaddition. The dimer reverts to anthracene thermally or with UV irradiation below 300 nm. In many cases, an absorbance band is present in only one form, [300, 301]. Anthracene derivatives form an important class of highly efficient, stable, blue-light emitting materials. It has been suggested that non-planar derivatives of anthracene, due to steric factors may hinder close packing and improve the device performance; hence the EL anthracene derivatives have been designed solely on the basis of this principle. 9,10-dianthrylanthracene (**91**) (OLEDs) properties, for example, has been investigated and result showed that the molecule does not have same molecular parameters as the other substituted ones. The main parameters for hole/electron transport at the molecular level are the “reorganization energies” due to the oxidation and reduction of the molecule and the “electronic splitting” between adjacent molecules [301].

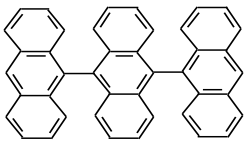

(**91**)

1.7 The Chemistry of Ru(II) polypyridine complexes

Ru(II) polypyridyl complexes due to their favourable photophysical and photochemical properties are commonly used as photosensitizers in many different applications. Other transition metals, such as Os(II), Re(I) and Ir(III) can also be used [302, 303]. In line with the aims and objectives of this research work, this section reviews the photophysical and photochemical properties of ruthenium(II) complexes.

1.7.1 Photochemical and photophysical processes

The first act of any photochemical and photophysical process is the absorption of a photon by a molecule. The excited state that is formed in this way is a high energy, unstable species which must undergo some type of deactivation. Electromagnetic radiation consists of an oscillating electric field and an orthogonal oscillating magnetic field. In dipole transitions the molecule interacts with the electric component of the electromagnetic field. Upon absorption of a photon, one electron is transferred from a lower to a higher quantum state of the molecule. The electronically excited state is obviously energetically unstable, and therefore has to get rid of this extra energy via different decay processes as shown in Figure 1.5. The excited state deactivation can occur via:

(i) disappearance of the original molecule (photochemical reaction),

(ii) emission of light (luminescence),

(iii) degradation of the excess energy into heat (radiationless deactivation),

(iv) some type of interaction with other species present in the solution (quenching process).

Electronic states are characterized by their multiplicity that is singlet states with paired electron spins and triplet states with unpaired electron spins. An excited triplet state is usually lower in energy than its singlet state counterpart. The size of the system, *e.g.* atoms, small or large molecules as well as the surroundings, *e.g.* gas phase, solution or solid state can significantly affect which transitions that can be probed. The description presented here is valid for large molecules in solution.

Absorption occurs from the ground state, which is often a singlet state, therefore here, denoted S_0, to a vibrationally excited level of an electronically excited state, S_n, of the same multiplicity as the ground state. The vibrational population collapses into the lowest vibrational level of S_n, in a process called vibrational relaxation (VR). The excited state can thereafter be deactivated via different processes of emissive or non-emissive character. Internal conversion (IC) can occur, which corresponds to a radiationless transition to vibronically excited states of the ground state S_0. Another important radiationless deactivation process is the intersystem crossing (ISC), which occurs between excited states of different spin multiplicity, *e.g.* from a singlet to a triplet state, or vice versa. From the lowest excited state of a given multiplicity, that is, S_1 and T_1 state respectively, radiative transition can occur.

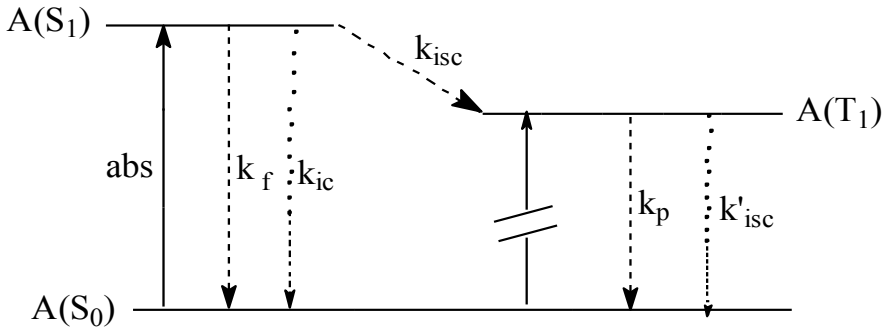

Figure 1.5 Schematic Jablonski diagram showing the various deactivation processes. K_f, K_{ic}, K_{isc}, K_p, and K'_{isc} are the unimolecular rate constants for fluorescence, internal conversion, $S_1 \rightarrow T_1$ intersystem crossing, phosphorescence, and $T_1 \rightarrow S_0$ intersystem crossing, respectively.

1.7.2 Light absorption and light emission sensitizers

The class of chemical reactions that plays the most important role in the connection between chemistry and light is that of electron transfer reactions. Ru(II) polypyridine complexes have given a substantial contribution to recent development of this class of reactions. Ru(II) polypyridine compounds are extensively used not only as primary reactants in electron transfer processes involving light, but also as mediators of potential photochemical and chemiluminescence processes.

1.7.3 Photosensitizer requirements

A good photosensitizer has to fulfill several important general requirements, irrespective of which application it is aimed for. Furthermore, depending on its use, specific prerequisites may apply. Therefore, the properties of the photosensitizers in use are to a large extent compromises between wanted and unwanted properties. In

particular, this section discusses the requirements on photosensitizers aimed for absorption of sunlight to drive further electron transfer reactions

1.7.3.1 Stability

A good photosensitizer must be stable, both in its ground and excited states, as well as in various redox states. In order to function properly, the photosensitizer should also be inert to side reactions, so that it can be used over and over again to promote the desired electron transfer reactions. Obviously it must also be stable towards light-induced decomposition.

1.7.3.2 Absorption properties

A strong absorption, *i.e.* a high molar absorption coefficient, in a suitable spectral region is essential for a good photosensitizer. It is important that the photosensitizer can capture photons efficiently and therefore it must absorb in the region where the sun emits radiation. Around 40 % of the sun intensity on earth falls in the range 300–600 nm, which is also the region where most natural pigments absorb. For transition metal complexes based on Ru(II), Os(II) and Re(I) the desired absorption is normally a metal to ligand charge transfer transition (MLCT transition). In the case of Ru(II) complexes this band is normally observed between 400 and 600 nm [304, 305].

1.7.3.3 Redox properties

A fundamental requirement is that the oxidized or reduced photosensitizer, in its ground state, should be a stable species. Furthermore, both the oxidation and the reduction processes must be fully reversible [304]. For the electron transfer

processes, the relevant thermodynamic parameters are obtained from the oxidation and reduction potentials of the photosensitizer.

1.7.3.4 Geometrical considerations

Ideally, the electron acceptor and donor should be well separated in space in order to reduce unwanted interaction. Therefore, a linear construction of a **D**-**P**-**A** array is preferable. However, a potential problem when covalently attaching electron donor and acceptor moieties to the photosensitizer is the possible formation of different geometrical isomers.

Isomer formation reduces the spatial control of donor and acceptor with respect to each other and may lead to complex kinetics and unwanted fast back electron transfer reactions. This problem is illustrated in Figure 1.5, using Ru(II)-tris-bipyridine and Ru(II)-bis-terpyridine as model compounds. Here, the great advantage of tridentate ligands over bidentate ligands is illustrated clearly by a comparison of the model complexes $[Ru(tpy)_2]^{2+}$ and $[Ru(bpy)_3]^{2+}$. For bis-tridentate complexes substitution in the 4'-position of the central pyridine ring will automatically lead to a linear, or at least a quasi-linear array, where the electron acceptor and donor will be well separated in space. This can be obtained also for the tris-bidentate complexes, as is shown in Figure 1.6, but other isomers will form as well. Thus, from a geometrical point of view, photosensitizers based on tridentate ligands are the most interesting alternatives [302, 307].

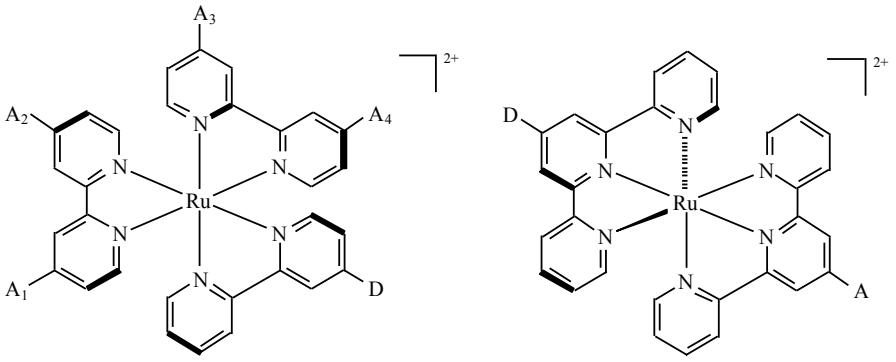

Figure 1.6. Left: Possible geometrical isomers of $[Ru(bpy)_3]^{2+}$ upon substitution of electron donor (**D**) and acceptor motifs (**A**). Right: shows that it is possible to obtain rod-like molecular arrays upon substitution on the central pyridines on $[Ru(tpy)_2]^{2+}$.

1.7.3.5 Excited state properties

The key to a functional photosensitizer is its excited state properties, since the desired reactions occur from the excited state. Most important are the excited state lifetime, the excited state energy, and the emission quantum yield. The excited state lifetime has to be long enough to allow for the desired electron transfer reactions to occur before the sensitizer relaxes back to its ground state. Excited state energy is also very important since it sets the limit for the driving force for further electron transfer reactions. Finally, the emission quantum yield, Φ, should ideally be high. A high emission yield provides the possibility of using the emission properties as probe to measure and understand the photophysical behaviour. The excited state lifetime and the emission quantum yield are related, but the emission quantum yield is not necessarily proportional to the excited state lifetime. Excited state properties are generally very sensitive to the structure of the complex and can be tuned in several ways, including *e.g.* appropriate choice of ligands and substituents [308].

1.7.4 Tuning of the excited state properties of Ru(II) polypyridyl complexes

Design of photosensitizers that can be incorporated into linear rod-like molecular arrays needs consideration of all the requirements as described above. However, in the present section, general strategies to increase the excited state lifetime of the bipyridine, phenanthroline and the geometrically favourable bis-tridentate Ru(II)-polypyridyl complexes will be described. Thereafter the work of this thesis will be presented and discussed, focusing on how to make bi- and tridentate Ru(II)-polypyridyl complexes designed particularly for dye-sensitized solar cells as well as other applications where longer excited state lifetimes are desirable.

1.7.5 Strategies to extend the excited state lifetime

The excited state lifetime is a very important property of a photosensitizer. If the photosensitizer should function properly it must be long enough to provide the desired electron and energy transfer. Many different strategies used at extending the excited state lifetime have proven successful such as the use of electron donating or withdrawing substituents 309-316]. Strong electron withdrawing groups such as SO_2Me attached to the 4'-position of the terpyridine gives room temperature excited state lifetimes of around 30 ns [314]. However electron donating groups will destabilize the metal based HOMO more than they destabilize the ligand-based LUMO and therefore non-radiative decay will be facilitated. Electron withdrawing substituents will instead lower the ^{3}MLCT excited state energy due to a greater stabilization of LUMO as compared to the metal-based HOMO [310].

An increase in the excited state lifetime could also be achieved by the use of bichromophoric systems, with an intrinsically long-lived organic triplet at a somewhat lower energy than the ^{3}MLCT state, serving as an energy reservoir. If this strategy should result in a longer excited state lifetime the electronic coupling between the different chromophores must be minimized so that the individual electronic properties are maintained. This approach often results in very long excited state lifetimes but bi-exponential decays are frequently observed. The gain in emission lifetime is however exactly counterbalanced by a loss in reactivity because the fractional population of the MLCT state is correspondingly small. Thus the yield of photoreaction from the MLCT state would not increase by this approach, as demonstrated by the fact that the MLCT emission yield is as low as in the reference complexes without organic chromophore. Furthermore, the addition of the extra chromophore will also destroy the possible construction of linear rod like molecular arrays [309, 317-326].

1.7.6 A new design strategy to extend the π-system of Ru(II) bi- and tri-dentate complexes

As observed from previous sections, it is not an impossible task to increase the excited state lifetime of Ru(II)-polypyridyl complexes based on polypyridyl ligands. However, if all the requirements described (Section 1.7.3) should be fulfilled and the driving force for further reactions be high enough, a new approach that does not stabilize the ^{3}MLCT state but rather destabilizes the ^{3}MC state has to be developed. Our strategy in tuning the excited state properties of the Ru(II) complexes is based on the new design of bidentate and tridentate polypyridyl ligands by extending the π-system of the ligands using both unsaturated alkylene,

alkynylene and polyaromatic molecules of which the anchoring ligand group carry carboxylic acid functionality which is to serve as linkage to the semiconductor nanocrystalline titanium dioxide in an application such as the dye-sensitized solar cells.

It has been known for a long time [327-329] that in a series of complexes of the same metal ion, one can determine the orbital nature of the lowest excited state by a suitable choice of ligands. The energy of the MC excited states depends on the ligand field strength, which in its turn depend on the σ-donor and π-acceptor properties of the ligands, the steric crowding around the metal (that can preclude a sufficiently close approach between metal and ligand) [330], and the bite angle of the polydentate ligands (which in some cases cannot be optimized because of molecular constraints [331]. The energy of the MLCT excited states depends on the reduction potential of the ligand involved in the MLCT transition, the oxidation potential of the metal in the complex (which is affected by the electron donor and acceptor properties of all the ligands), and by the charge separation caused by the transition. The energy of the LC excited states depends on intrinsic properties of the ligands, such as the HOMO-LUMO energy gap and the singlet-triplet splitting.

1.8 The Chemistry and applications of Ru(II) phthalocyanine complexes

Phthalocyanines are widely used as pigments in textiles, polymers and paints [332]. They exhibit remarkable qualities like light fastness, brightness and stability towards environmental influences. Pc's consist of a planar macrocycle with an 18 π-electron system, which mainly confers this known stability. For many years, these macrocycles have been the target of meticulous investigation [333], particularly

considering their properties as dyes [334, 335]. In recent times, research has been retargeted for applications in materials science [336-340] (Figure 1.7), including phthalocyanines as liquid crystals [341-343], as Langmuir-Blodgett films [344-348], as molecular semiconductors [349], in electrophotographic applications [350-353], in optical-data storage [354-356], in cancer therapy [357-359], in fuel cells [360], in photoelectro-chemical cells [361], in photovoltaic cells [362] in gas sensing devices [363-370], as organic semi-conductors [336-338, 371, 372], as photosensitizers, [373] and in nonlinear optics [374, 375]. Phthalocyanines do not occur in nature, but they are structurally related to porphyrins such as haemoglobin, vitamin B12 and chlorophyll (Figure 1.8).

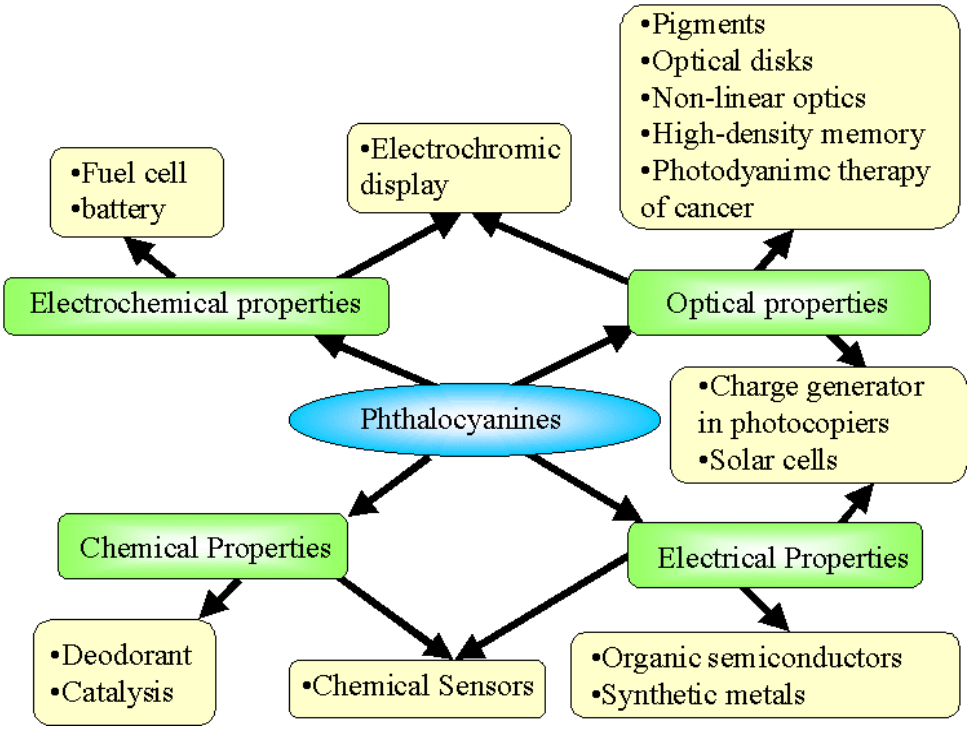

Figure 1.7 Some applications of phthalocyanines.

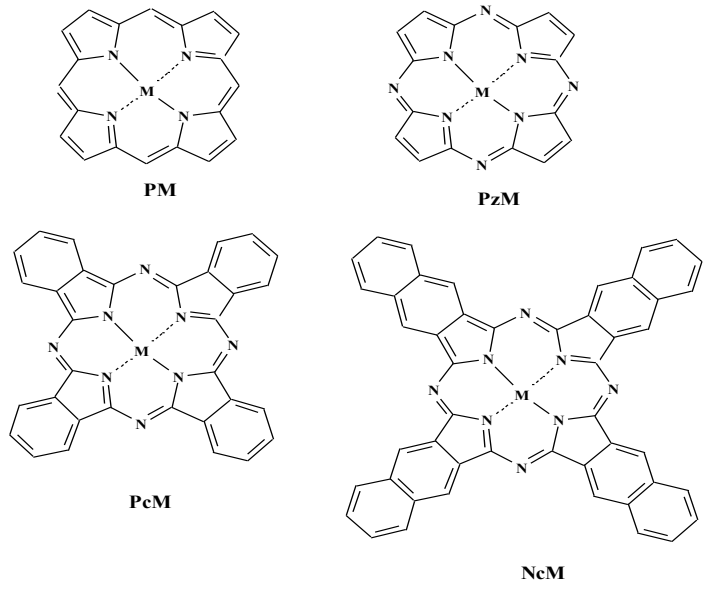

Figure 1.8 Porphine (PM), Porphyrazine (PzM), Phthalocyanine (PcM) and Naphthalocyanine (NcM) complexes.

1.8.1 Absorption spectra of phthalocyanines

Purity and intensity of phthalocyanine's colour arises from an isolated and intense band (Q-band) at the red end of the visible spectrum of light, between 650 and 720 nm approximately. A second band (B-Band) appears between 300 and 400 nm, being generally less intense (Figure 1.9). In the spectra of metal phthalocyanine solutions, the intense Q-band arises from a doubly degenerate π-π*-transition between the A_{1g} (a^2_{1u}) ground state to the first excited singlet state, which has E_u ($a^1_{1u}e^1g$) symmetry. The second allowed π-π*-transition (B-band) is caused by a transition between either an a_{2u} or a b_{2u} orbital to the e_g orbital (LUMO) [376]. In the case of metal free phthalocyanines all states are non-degenerated, due to the reduced D_{2h} molecular symmetry. The Q-band transition is polarized in either the x or y direction, and is therefore splitted in two bands [377].

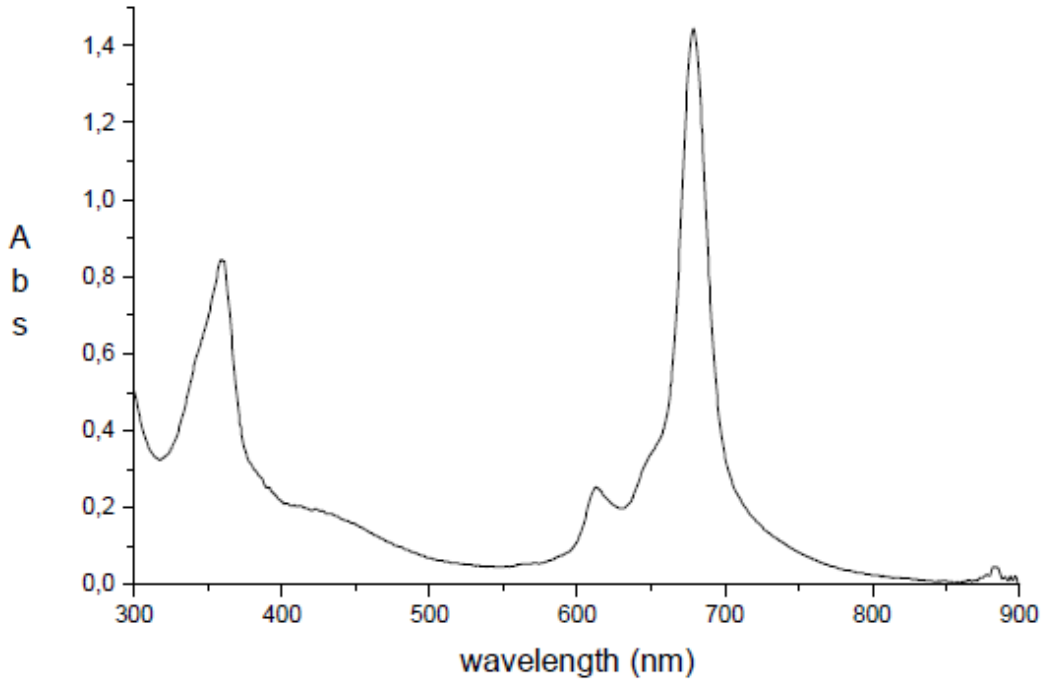

Figure 1.9. UV-Vis Spectrum of a typical metallophthalocyanine [434)

1.8.2 General synthesis of phthalocyanines

In general, the synthesis of phthalocyanines proceeds from a single step reaction, normally denominated cyclotetramerization of benzoic acid or its derivatives, e.g. phthalic anhydride, phthalimide, *o*-cyanobenzamide, phthalonitrile or isoindolinediimine [337, 378], (Figure 1.10). The most used precursor for substituted phthalocyanine synthesis is the substituted phthalonitrile, or in some cases, when the low reactivity of the precursor inhibits the macrocycle formation, isoindolinediimines can be used as well. Nucleophilic hindered bases like 1,8-diazabicylo-[5,4,0]-undec-7-ene (DBU) can be used as powerful catalysts for the cyclotetramerization of phthalonitriles in solution (e.g. pentanol, octanol), with the metal ion as template for the formation of metal phthalocyanines [337].

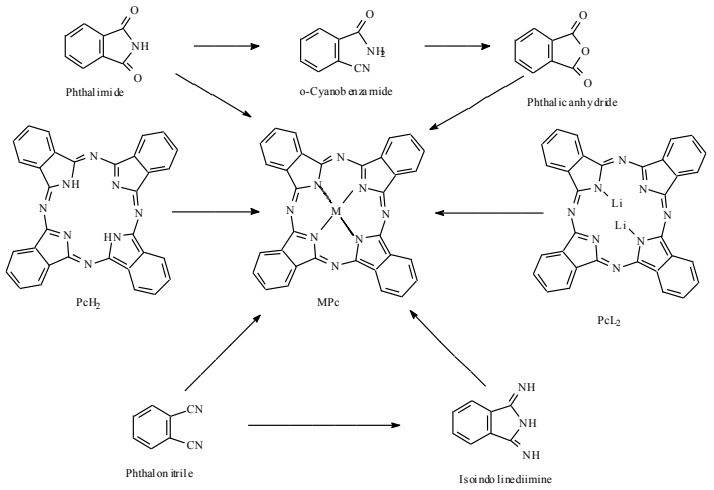

Figure 1.10 General synthetic scheme for phthalocyanines

1.8.3 Solubilization of phthalocyanines

The solubility of phthalocyanines in common organic solvents can be increased by introduction of bulky or long chain substituents in the periphery of macrocycle (peripheral substitution) and/or, in case of possibility, by coordination of the central metal with additional axial ligands (axial substitution) [379-381]. Depending on the position of the substituents in the precursor, different structural isomers are formed during the preparation of phthalocyanines.

Asymmetric precursors, like 3-, 4-, 3,4-, 3,5- substituted phthalonitriles, form a mixture of structural isomers during the tetracyclomerization. As an example, the four isomers of 2,(3)-tetrasubstituted phthalocyanine are shown in Figure 1.10. The single isomers are (C_{4h}) 2,9,16,23-, (D_{2h}) 2,10,16,24-, (C_{2v}) 2,9,17,24- and (C_s) 2,9,16,24-tetrasubstituted complexes.

Symmetrically disubstituted precursors, due to their location, form either the 2,3,9,10,16,17,23,24- [382] or the 1,4,8,11,15,18,22,25- [337], octasubstituted phthalocyanines (Figure 1.11). Also the 1,2,3,4,8,9,10,11,15,16,17,18,22,23,24,25-hexadecasubstituted have been prepared [383]. Substituents enable phthalocyanine

solvation because they increase the distance between the stacked molecules [336, 337]. The peripherally substituted phthalocyanines studied in more detail are the tetra- and octa- substituted ones [336]. Generally, the solubility of tetrasubstituted phthalocyanines is higher than the octasubstituted analogues, mainly due to the fact that the tetrasubstituted phthalocyanines are prepared as a mixture of isomers (Figure 1.10), and therefore, leading to a lower degree of order in the solid state, when compared to the symmetrically octasubstituted phthalocyanines (Figure 1.11): 1,4- and 2,3- octasubstituted phthalocyanines [384].

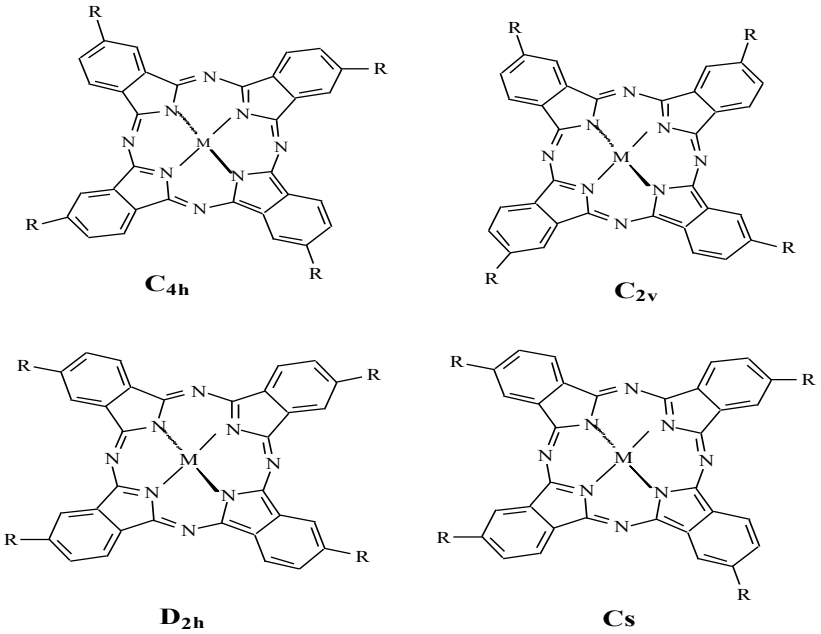

Figure 1.11. Constitutional isomers from 2, (3)-tetrasubstituted phthalocyanines

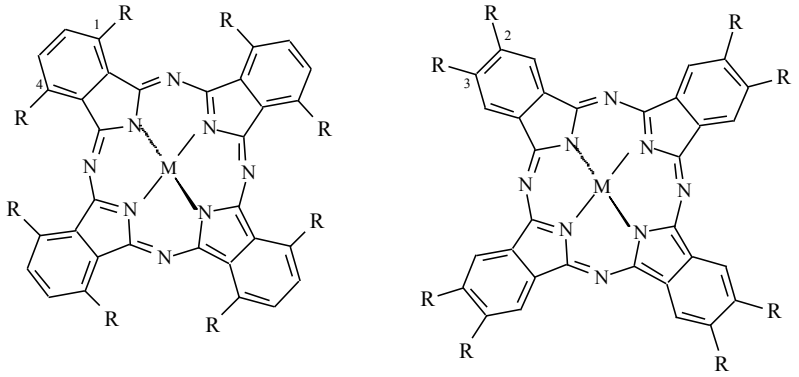

Figure 1.12. 1,4- and 2,3-octasubstituted phthalocyanines

Furthermore, the less symmetrical isomers have a higher dipole moment derived from the more unsymmetrical arrangement of the substituents in the periphery of the macrocycle. This was proven by Hanack *et al.* after complete separation of the four structural isomers for the first time [385, 386].

1.8.4 Expansion of the π-system: benzoannulated phthalocyanines

Preparation of benzoannulated phthalocyanines such as 1,2-naphthalocyanine (Nc), 2,3-naphthalocyanine, anthracenocyanine (Ac) or 9,10 phenanthrenocyanine (Phc), from the corresponding benzoannulated phthalonitriles, is carried out under similar conditions to those of general phthalocyanine synthesis (Figure 1.13). The characteristic properties of these complexes are mainly due to their extended π-electron systems. In the electronic absorption spectra going from 2,3-naphthalocyanine to 2,3-anthracenocyanine, an increasing bathochromic shift of the Q-band compared to phthalocyanines is observed [387]. The HOMO-LUMO energy gap generally decreases in systems with larger π-electron delocalization. This increasingly larger π-electron system enhances intermolecular π-π interactions, favouring stronger aggregation and lower solubility [388].

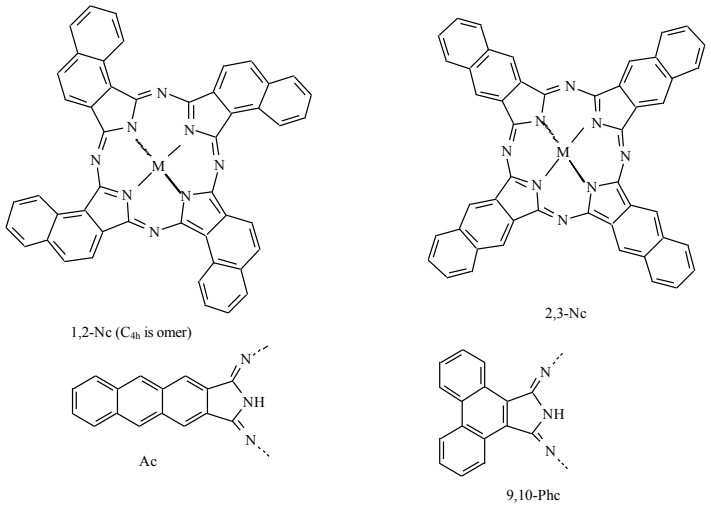

Figure 1.13: Benzoannulated phthalocyanines

1.9 Aims of the work

The aim of this work at first is synthetic, since we plan to synthesize novel ruthenium(II) polypyridyl and phthalocyanine complexes with extended π-conjugation bonds with the purpose of having longer wavelengths at the visible region of absorption and an enhanced molar extinction coefficient to serve as good photosensitizers for the dye-sensitized solar cells. Therefore, the synthetic methodology would be based on a systematic increase in the number of conjugated bonds in the molecules.

Both the ligands and complexes will be characterized by infrared, UV-Vis absorption, luminescence, ^{1}H and ^{13}C NMR, elemental analysis and electrochemistry. The solar to electrical conversion efficiency of some of the complexes will be evaluated.

1.10 Rationale for the current study

For the past two decades, different arrays of dyes have been synthesized for the conversion of solar energy to electricity. The N3 dye (4,4'-dicarboxyl-2,2'-bipyridyl- ruthenium(II)-dithiocyanate), has the highest solar-to-energy conversion efficiency of about 11 % compared to a silicon based photovoltaic cells with 16 % conversion efficiency. The major drawback of N3 dye is in its lack of absorption in the red region of the visible spectrum. The molecular designs of ruthenium polypyridyl complexes as photosensitizers for nanocrystalline TiO_2 solar cells that can absorb visible light of all colours present a challenging task. The most sorted dye is expected to have suitable ground- and excited- state redox properties so that the two key electron-transfer steps (charge injection and regeneration of the dye) occur efficiently. It has been so difficult to fulfill both requirements simultaneously during the designing of a charge transfer (CT) sensitizer.

To overcome these problems, systematic tuning of the LUMO and HOMO energy levels of the Ru(II) polypyridyl complexes are necessary to estimate the optimal threshold wavelength for maximum power conversion of a single-junction converter. In the ruthenium polypyridyl complexes, absorption can be turned to lower energy region by introducing a ligand with a low lying π* molecular orbital, or by destabilization of the metal t_2g orbital with a strong donor ligands. Highly conjugated molecular compounds have also been introduced in the arrays of dyes for the dye sensitized solar cells in order to improve the conversion efficiency, but not one has given efficiency above the N3 dye reported by Grätzel *et al* since 1991 [417]. Organic dyes, such as porphyrins and phthalocyanines with extended π-bond conjugation have been employed as sensitizers, but porphyrins cannot compete with the N3 or black dye sensitizer due to their lack of red light and near IR absorption.

Phthalocyanines do show intense absorption bands in this spectral region. However, problems with aggregation and the unsuitable energetic position of the LUMO level, which is low for electron transfer to the TiO_2 conduction band, have turned out to be intractable so far.

The molecular engineering of ruthenium complexes for DSSC presents a challenging task as several strigent requirements have to be fulfilled by the sensitizers and these are very difficult to be met simultaneously. The ruthenium complex widely used at present as sensitizers absorb strongly in the visible region of the solar spectrum but not in the near IR region where significant amount of solar energy reaches the Earth. The main objective of this study therefore is to contribute to efforts being made to improve photosensitizers to enable the absorption of the PV cell to be more closely matched that of solar energy spectrum in order to improve cell efficiency. The study is based on functionalization of polypyridines and phthalocyanines through the synthesis of novel organic molecules and their corresponding Ru(II) complexes that might be able to absorb in the near IR region of the solar spectrum.

CHAPTER TWO

Part of this chapter has been reported as

(1) Adewale O. Adeloye and Peter A. Ajibade. Synthesis and Characterization of a Heteroleptic Ru(II) Complex of Phenanthroline Containing Oligo-Anthracenyl Carboxylic Acid Moieties. *Int. J. Mol. Sci.* **2010**, *11*, 3158-3176.

(2) Adewale O. Adeloye and Peter A. Ajibade. Synthesis and Characterization of a Ru(II) Complex with Functionalized Phenanthroline Ligands Having Single-Double Linked Anthracenyl and 1-Methoxy-1-buten-3-yne Moieties. *Molecules* **2010**, *15*, 7570-7581.

CHAPTER TWO

SYNTHESIS, CHARACTERIZATION AND ELECTROCHEMISTRY OF Ru(II) COMPLEXES OF FUNCTIONALIZED POLYPYRIDYL

2.0 Reagents and Materials

The commercial available reagents were used as acquired. 2,2'-bipyridine, 1,10-phenanthroline hydrate, 2,2':6',2"-terpyridine, phthalonitrile, 9,10-dibromoanthracene, 2,3-dimethylacrylic acid, 1-methoxy-1-buten-3-yne, 1,8-diazabicycloocta [5.4.0] undec-7-ene (DBU), ammonium thiocyanate (NH_4NCS), ammonium hexafluorophosphate (NH_4PF_6), ruthenium(III) chloride, sodium hydroxide, palladium-carbide, copper(I) chloride, potassium hydroxide were purchased from Aldrich and were used without further purification. Hydrobromic acid, Conc. H_2SO_4, Conc. HNO_3, methanol, ethanol, chloroform, dichloromethane, toluene, ethyl acetate, benzene, acetone, triphenyl phosphine, dimethylsulphoxide, dimethylformamide, and triethylamine (puriss grade) were purchased from Fluka. The following starting reagents: 9-bromo-10-(2,3-DMAA)-anthracene, 9-bromo-10-(2,3-DMAA)-dianthracene, 4-bromo-2,2'-bipyridine, 5-bromo-1,10-phenanthroline, and 4,7-dibromo-1,10-phenanthroline, and Ruthenium(II) dichloro-tetrakis-dimethylsulphoxide [$RuCl_2(dmso)_4$] precursor were synthesized according to standard literature method [256, 404–406, 408].

2.1.0 Instrumentation

The following instruments were used for the analysis and characterization of the ligands and complexes:

2.1.1 IR Spectroscopy

Perkin Elmer System 2000 FT-IR Spectrophotometer and Bruker Tensor 27: solid substances were grounded with KBr and pressed to pellets; liquid compounds were measured directly in Bruker Tensor 27.

2.1.2 UV/Vis Spectroscopy

Recorded in a 10.00 mm path length quartz cell on a Perkin Elmer Lambda 35 using dimethylformamide unless otherwise stated.

2.1.3 ^{1}H and ^{13}C NMR Spectroscopy

Nuclear Magnetic Resonance (NMR) spectra were run on a Bruker EMX 400 MHz spectrometer for ^{1}H and 100 MHz for ^{13}C. The chemical shift values were reported in parts per million (ppm) relative to (TMS) as internal standard. Chemical shifts were also reported with respect to DMSO d_6 at δ_c 40.98 and DMSO d_6 at δ_H 2.50 or $CDCl_3$ at δ_c 77.30 and δ_H 7.24 ppm.

2.1.4 Photoluminescence

Recorded in a 10.00 mm path length quartz cell on a Perkin Elmer Lambda 45 spectrofluorimeter using dimethylformamide (or otherwise stated).

2.1.5 Cyclic and square wave Voltammogram

Autolab potentiostat PGSTAT 302 (EcoChemie, Utrecht, The Netherlands) driven by the general purpose Electrochemical System data processing software (GPES, software version 4.9). Square wave voltammetric analysis was carried out at a frequency of 10 Hz, amplitude = 50 mV and step potential = 5 mV. A conventional three-electrode system was used. The working electrode was a bare glassy carbon electrode (GCE), Ag|AgCl wire and platinum wire were used as the pseudo reference and auxiliary electrodes, respectively. Prior to use, the electrode surface was polished with alumina on a Buehler felt pad and rinsed with excess millipore water. All electrochemical experiments were performed in freshly distilled dry DMF containing $TBABF_4$ as supporting electrolyte.

2.1.6 Melting point

Melting point was determined using a Gallenkamp electrothermal melting point apparatus.

2.1.7 Elemental analysis

Elemental analyses of the compounds were performed on Fisons elemental analyzer.

2.1.8 Thin Layer Chromatography (TLC)

All thin layer chromatography (tlc) analyses were done with aluminium sheet precoated with normal phase silica gel 60 F_{254} (Merck, 0.20 mm thickness) unless otherwise stated. The tlc plates were developed using any of the following solvent systems:

(1)	Solvent system A:	Dichloromethane-Methanol	(9:1)
(2)	Solvent system B:	Dichloromethane-Methanol	(7:3)
(3)	Solvent system C:	Dichloromethane-Benzene	(3:7)
(4)	Solvent system D:	Chloroform-Methanol	(1:1)
(5)	Solvent system E:	Dichloromethane-Ethyl acetate	(4:1)
(6)	Solvent system F:	Diethyl ether-Methanol	(1:1)

Developed tlc plates were viewed under ultraviolet light (254 nm and 366 nm) to monitor reaction synthesis.

2.1.9 Sephadex LH-20 Column Chromatography

Gel filtration was performed using Sephadex LH-20 previously swollen in specified solvent (s) prior to loading of extract onto the column (3.5 cm x 8.5 cm).

2.2 Synthesis of Anthracene derivatives

2.2.1 Synthesis of 9-Bromo-10-(2,3-dimethylacrylic acid)-anthracene

In a 500 mL round bottom flask, 9,10-Dibromoanthracene (6.71 g, 19.8 mmol) and 2,3-dimethylacrylic acid (2 g, 19.8 mmol) were dissolved in benzene /dichloromethane (200 mL, v/v, 1:1) followed by the addition of 1.0 mL volume of Et_3N, KOH (1.1 g, 19.8 mmol) and 0.05 g of palladium carbide as catalyst. After 8 h reflux, the mixture was filtered and concentrated to dryness *in vacuo*. Degassed water (300 mL) was added and the yellow organic solid precipitated at the bottom of the flask was extracted with chloroform. The chloroform extract was then concentrated *in vacuo*, and recrystallized in 50 % Et_2O-EtOH mixture to afford a brilliant yellow solid.

2.2.2 Synthesis of 9-Bromo-10-(2,3-dimethylacrylic acid)-dianthracene

In a 250 mL flask, 9-Bromo-10-(2,3-dimethylacrylic acid)-anthracene (2.5 g, 7.04 mmol) obtained in (Section 2.4.1), and 9,10-Dibromoanthracene (2.37 g, 7.04 mmol) were dissolved in benzene/dichloromethane (200 mL, v/v, 1:1). The reaction was refluxed for 18 h under palladium/carbide cross-catalyzed reaction in a modified method as reported by Yamamoto and co-worker [405]. The reaction was monitored by tlc and a light-green solid product was obtained after recrystallization from Et_2O-EtOH (50 mL, v/v, 1:1) and dried over Na_2SO_4. (Yield = 92 %; Mp = 220–222 ^oC).

2.3.0 Synthesis of 2,2'-bipyridine and phenanthroline derivatives

2.3.1 Synthesis of 4-Bromo-2,2'-bipyridine

To a stirred solution of bipyridine (15 g, 96 mmol), HBr (7.8 g, 5.2 mL) in CH_3OH (60 mL), was added a 47 % aqueous solution of H_2O_2 (3.3 g, 3 mL) slowly over a period of 15 min at room temperature. The mixture was stirred for 20 h whilst monitoring the reaction progress by tlc. After completion, the solvent was removed *in vacuo*, and the residue dissolved in EtOAc (150 mL), washed with brine solution (3 x 100 mL) and dried over anhydrous Na_2SO_4. The product was isolated carefully by column chromatography on silica gel using CH_2Cl_2–EtOAc (200 mL, v/v, 4:1) to give a yellow-red viscous liquid which was allowed to air dry and finally recrystallized from Et_2O–EtOH (50 mL, v/v, 1:1).

2.3.2 Synthesis of 5-Bromo- and 4,7-Dibromo-1,10-phenanthroline

To a 20 g (0.1 mol) of 1,10-phenanthroline hydrate in a 500 mL flask was added 66 mL methanolic solution of HBr (8.2 g, 5.5 mL). Hydrogen peroxide was added slowly in drops for a period of 20 minutes under a vigorous and continuous

stirring at room temperature. After 20 h of stirring, the faint pink solution was concentrated *in vacuo* at 60–70 ^{o}C to remove methanol. The residue was dissolved in water (50 mL), and then extracted with EtOAc (3 x 250 mL). The aqueous and the ethyl acetate fractions were concentrated to dryness. To the ethyl acetate extract, dichloromethane (3 x 200 mL) was added and the insoluble precipitate was filtered and air dried. The dichloromethane soluble extract was concentrated to dryness *in vacuo* and were finally recrystallized in Et_2O (80 mL) to afford 5-bromo-1,10-phenanthroline (white solid) and 4,7-dibromo-1,10-phenanthroline (pale white solid) respectively.

*2.3.3 Synthesis of 4-(2,3-DMAA)-2,2'-bipyridine **(L1)***

4-bromo-2,2'-bpy (1.05 g, 3.38 mmol) of and 2,3-dimethylacrylic acid (DMAA) (0.34 g, 3.38 mmol) were dissolved in MeOH (40 mL) in a 250 mL flask. Et_3N (1.0 mL and palladium-carbide (0.050 g) were added and the mixture was reflux for 8 h at a temperature between 110–120 ^{o}C. The reaction was allowed to cool to room temperature and the solvent removed under reduced pressure. The residue was dissolved in degassed water and then extracted with chloroform. The chloroform extract was concentrated *in vacuo* to obtain a brilliant colourless liquid which solidified after about 48 h at room temperature. The resultant residue was recrystallized in Et_2O (30 mL)

*2.3.4 Synthesis of 4-(9-anthracenyl-10-(2,3-DMAA))-2,2'- bipyridine **(L2)***

4-bromo-2,2'-bpy (1 g, 4.82 mmol) and 9-bromo-10-(2,3-dimethylacrylic acid)-anthracene (1.72 g, 4.82 mmol) were dissolved in benzene-dichloromethane (50 mL,

v/v, 1:1), followed by the addition of Et_3N (1 mL), KOH and palladium-carbide (0.05 g). The reaction was carried out under reflux for 12 h at temperature 110–120 ^oC.

*2.3.5 Synthesis of 5-(2,3-DMAA)-1,10-Phenanthroline **(L3)***

5-bromo-1,10-phenanthroline (1 g, 3.86 mmol) and 2,3-dimethylacrylic acid (0.39 g, 3.86 mmol) were dissolved in MeOH (40 mL) in a 250 mL flask. Et_3N (1.0 mL) and palladium-carbide (0.050 g) were added and the mixture was reflux for 14 h between 110–120 ^oC. The reaction was allowed to cool to room temperature and the solvent removed under reduced pressure. The residue was dissolved in degassed water and the extracted with chloroform. The chloroform extract was concentrated *in vacuo* to obtain a brilliant colourless liquid which solidified after 48 h at room temperature. The resultant residue was recrystallized in Et_2O.

*2.3.6 4,7-Bis(2,3-DMAA)-1,10-Phenanthroline **(L4)***

4,7-dibromo-1,10-phenanthroline (0.15 g, 4.84 mmol) and *trans*-2,3-dimethylacrylic acid (0.97 g, 9.68 mmol) were dissolved in methanol (50 mL) and triethylamine (1.0 mL) and 20 mg palladium carbide were added. The mixture was reflux for 24 h and the resultant red solution was allowed to cool to room temperature and concentrated under reduced pressure to afford red-brownish liquid product. To the crude product, degassed water (50 mL) was added to form a homogenous phase solution, which was then extracted with chloroform. The chloroform extract was concentrated *in vacuo* and then recrystallized in Et_2O.

*2.3.7 5-(9-anthracenyl-10-(2,3-dimethylacrylic acid)-1,10-Phenanthroline **(L5)***

5-bromo-1,10-phenanthroline (1.0 g, 3.86 mmol) and 9-bromo-10-(2,3-dimethylacrylic acid)-anthracene (1.37 g, 3.86 mmol) were dissolved in benzene-dichloromethane (70 mL, v/v, 1:1), followed by the addition of Et_3N (1 mL), KOH and palladium-carbide (0.05 g). The reaction was carried out under reflux for 12 h at temperature 110–120 ^oC. Isolation and purification of the residue was followed as reported in (Section 2.3.4).

*2.3.8 4,7-Bis(9-anthracenyl-10-(2,3-DMAA)-1,10-Phenanthroline **(L6)***

4,7-dibromo-1,10-phenanthroline (0.25 g, 0.74 mmol) and 9-bromo-10-(2,3-dimethylacrylic acid)-anthracene (0.53 g, 1.48 mmol) were dissolved in benzene-dichloromethane (70 mL, v/v, 1:1), followed by the addition of Et_3N (1 mL), KOH and palladium-carbide (0.05 g). The reaction was carried out under reflux for 12 h at temperature 110–120 ^oC.

*2.3.9 4-(9-dianthracenyl-10-(2,3-(DMAA)-7-(9-anthracenyl-10-(2,3-(dimethylacrylic acid)-1,10-phenanthroline **(L7)***

In a 250 mL round bottom flask, 9,10-dibromoanthracene (0.37 g, 1.10 mmol) and 2,3-dimethyl-acrylic acid (0.20 g, 1.10 mmol) were dissolved in benzene/dichloromethane (75 mL, v/v, 1:1) followed by addition of triethylamine (1.0 mL), KOH (0.06 g, 1.10 mmol) and palladium carbide (0.05 g). After 8 h reflux, the mixture was filtered and concentrated to dryness *in vacuo*. Degassed water (30 mL) was added and the yellow organic solid precipitated at the bottom of the flask was extracted with chloroform. The chloroform extract was concentrated *in vacuo*, and recrystallized from a 50 % diethyl ether-ethanol mixture to afford a brilliant yellow

solid **1**. In another reaction, an equivalent molar ratio of the yellow solid product **1** and 9,10-dibromoanthracene were dissolved in benzene/dichloromethane (100 mL, v/v, 1:1) and refluxed at 110–120 ºC for 18 h under palladium/carbide cross-catalyzed reaction conditions using a modified reaction method as reported by Yamamoto and co-workers [405]. A light-green solid product **2** was obtained as a 9-bromo-10-(2,3-dimethylacrylic acid)-dianthracene after recrystallization from diethyl ether. Following a one reaction synthetic process; an equivalent molar ratio of 9-bromo-10-(2,3-dimethylacrylic acid)-dianthracene (0.78 g, 1.48 mmol), 4,7-dibromo-1,10-phenanthroline (0.49 g, 1.48 mmol) were reacted using the same reaction condition afforded product **3** as 4-(9-dianthracenyl-10-(2,3-dimethylacrylic acid)-7-bromo-1,10-phenanthroline. In the final reaction (iii), 9-bromo-10-(2,3-dimethylacrylic acid)-anthracene and product **3** were reacted in benzene/dichloromethane (80 mL, v/v, 1:1) under similar reaction conditions to afford the desired product 4 as **L7**.

*2.3.10 4,7-Bis(9-trianthracenyl-10-(2,3-DMAA)-[1,10] phenanthroline **(L8)***

9-bromo-10-(2,3-dimethylacrylic acid)-dianthracene (0.058 g, 1.10 mmol) and 4,7-bis(9-bromoanthracenyl)-1,10-phenanthroline (0.37 g, 0.50 mmol) were dissolved in ethanol (40 mL) and stirred mechanically for about 25 min. To this solution, triethylamine (1 mL) and palladium/carbide (0.05 g) were added. The mixture was refluxed at 120 °C for 8 h. The crude product was filtered hot, allowed to cool to room temperature and the solvent removed by evaporation under reduced pressure. The pure product L8 was obtained by re-crystallization in 50 % EtOH-Et_2O.

*2.3.11 Attempted synthesis of 4-(1-ethynylphenyl-4-(2,3-DMAA)-2,2'-bipyridine **(L9)***

1-Bromo-4-ethynylbenzene (0.19 g, 1.07 mmol) and 4-Bromo-2,2'-bpy (0.25 g) were dissolved in MeOH (50 mL) and stirred. Et_3N (1.0 mL), KOH (0.6 g, 1.07 mmol) and Pd/C (0.05 g) were added and the mixture was refluxed for 72 h in the dark. To the green solution, equivalent weight of 2,3-dimethylacrylic acid (0.11 g, 1.07 mmol) was added and the solution was further refluxed for 4 h. The resultant solution (green) was allowed to cool to room temperature and filtered. The filtrate was reduced to one-tenth of its volume to afford a red liquid. Degassed water (25 mL) was added and the organic material extracted with dichloromethane (60–70 mL), and recrystallized with Et_2O-EtOH (50 %).

*2.3.12 4,7-Bis(1-methoxy-1-buten-3-yne)-[1,10]-phenanthroline **(L10)***

The synthesis of L10 followed a modified synthetic method as reported by Venkataraman and co-workers [407]. In an argon-filled standard Schlenk tube, palladium-carbide (0.34 mmol, 0.8 %), copper chloride (0.084 g, 0.84 mmol, 2.0%) and triphenylphosphine (1.107 g, 4.22 mmol, 10 %) were added to a thick-walled glass tube and tetrahydrofuran (50 mL) was added to form a green solution. The mixture was stirred vigorously for 10 min prior to addition of triethylamine (7.5 mL), 4,7-dibromo-1,10-phenanthroline (3.5 mmol) and 1-methoxy-1-buten-3-yne (7.0 mmol). The mixture was refluxed under argon at 100–110 ºC for 24 h. After reaction was complete, the crude product was filtered and the red filtrate concentrated *in vacuo* to afford red oil. The red oil was adsorbed onto a silica gel in a column and eluted in *n*-hexane-dichloromethane mixture (50 %, 200 mL).

2.4.0 Synthesis of Ru(II) Homoleptic Complexes Containing Substituted Bipyridine and Phenanthroline Ligands

*2.4.1 Synthesis of Ru(II)-tris-(4-(2,3-dimethylacrylic acid)-2,2'-bipyridyl-bis-hexafluorophosphate complex (**C1**)*

In a 250 mL flask, $[RuCl_2(dmso)_4]$ (0.05 g, 1.03 mmol) was dissolved in *N,N*-dimethylformamide followed by the addition of ligand **L1** (0.08 g, 3.09 mmol). The mixture was refluxed at 120 °C for 5 h in the dark. The solution was allowed to cool to room temperature and filtered to remove unreacted starting material. The filtrate was concentrated to dryness and 40 mL of 0.05 M NaOH solution was added to give dirty brown precipitate which was filtered off. The pH of the resulting solution was adjusted to 3 with 0.5 M HNO_3. The solution was left to stand in the fridge (-2 °C) for 12 h before being filtered and concentrated *in vacuo*. Aqueous solution of NH_4PF_6 was added to precipitate the residue from the bulk, and then filtered. The crude residue product was adsorbed onto Sephadex LH-20 adsorbent in a glass column and eluted using solvent system D (chloroform-methanol, 50 %, 250 mL) [409].

*2.4.2 cis-dithiocyanato-bis-[4(2,3-dimethylacrylic acid)]-2,2'-bipyridyl-ruthenium (II) complex (**C2**)*

Ligand **L1** (0.30 g, 1.02 mmol), $[RuCl_2(dmso)_4]$ (0.25 g, 0.51 mmol) and excess of NH_4NCS (0.75 g, 10.4 mmol, 10 % excess) were added as a mixture in DMF (Scheme 2.14). The synthetic method is as reported for **C1** complex.

*2.4.3 Attempted synthesis of cis-dithiocyanato-bis-4-(1-ethynylphenyl-4-(2,3-dimethyl acrylic acid)-2,2'-bipyridine-ruthenium(II) complex (**C3**)*

The complex was prepared in a similar manner as described for **C2** above. Ligand **L9** (0.20 g, 0.58 mmol), $[RuCl_2(dmso)_4]$ (0.14 g, 0.29 mmol) and excess of NH_4NCS (0.89 g, 11.67 mmmol, 10 % excess) were dissolved in DMF/MeOH (80 mL, 1:1, v/v), and refluxed for 12 h in the dark to afford complex **C3**.

*2.4.4 Tris-4-(9-anthracenyl-(2,3-dimethylacrylic acid)-2,2'-bipyridyl-ruthenium(II)-bis-hexafluorophosphate complex (**C4**)*

The complex was prepared in a similar manner as described for **C1** above. Ligand **L2** (0.22 g, 0.51 mmol), $[RuCl_2(dmso)_4]$ (0.08 g, 0.17 mmol) were added as a mixture in DMF (60 mL). The product was obtained after precipitation from excess aqueous NH_4PF_6.

*2.4.5 cis-dithiocyanato-bis-4-(9-anthracenyl-(2,3-dimethylacrylic acid)-2,2'-bipyridyl-ruthenium(II) complex (**C5**)*

The complex was prepared in a similar manner as described for **C2** above. Ligand **L2** (0.20 g, 0.47 mmol), $[RuCl_2(dmso)_4]$ (0.11 g, 0.24 mmol) and excess of NH_4NCS (0.72 g, 9.40 mmmol, 10 % excess) were dissolved in DMF/MeOH (80 mL, 1:1, v/v), and refluxed for 12 h in the dark . Complex **C5** was obtained after column chromatography and purification of the crude product.

*2.4.6 cis-dithiocyanato-4-(2,3-dimethylacrylic acid)-2,2'-bipyridyl-4-(9-anthracenyl -(2,3-dimethylacrylic acid)-2,2'-bipyridyl-ruthenium(II) complex (**C6**)*

The complex was prepared in a similar manner as described for **C5** above. Ligand **L1** (0.25 g, 0.98 mmol), **L2** (0.42 g, 0.98 mmol), [$RuCl_2(dmso)_4$] (0.24 g, 0.49 mmol) and excess of NH_4NCS (0.75 g, 9.85 mmmol, 10 % excess) were dissolved in DMF/MeOH (80 mL, 1:1, v/v), and refluxed for 12 h in the dark.

*2.4.7 Tris-5-(2,3-dimethylacrylic acid)-1,10-phenanthroline Ru(II) bis-hexafluoro-phosphate complex (**C7**)*

The complex was prepared in a similar manner as described for **C1** above. Ligand **L3** (0.16 g, 0.58 mmol), [$RuCl_2(dmso)_4$] (0.09 g, 0.19 mmol) were dissolved in DMF (60 mL). A red oily product was obtained after column chromatography (Et_2O-MeOH, 50 %), and was precipitated by adding excess of aqueous NH_4PF_6.

*2.4.8 cis-dithiocyanato-bis-5-(2,3-dimethylacrylic acid)-1,10-phenanthroline-ruthenium(II) complex (**C8**)*

The complex was prepared in a similar manner as described for **C2** above. Ligand **L3** (0.50 g, 1.79 mmol), and [$RuCl_2(dmso)_4$] (0.22 g, 0.45 mmol) were dissolved in DMF (60 mL) and reflux for 10 min to allow proper dissolution of reagents before 5 mL aqueous solution of excess of NH_4NCS (0.27 g, 3.59 mmmol, 10 % excess) was added, the mixture was refluxed for 6 h to afford the complex product.

*2.4.9 tris-5-(9-(anthracenyl-(2,3-dimethylacrylic acid)-1,10-phenanthroline ruthenium(II) bis-hexafluorophosphate complex (**C9**)*

The complex was prepared in a similar manner as described for C11 above. Ligand **L5** (0.10 g, 0.22 mmol) and $[RuCl_2(dmso)_4]$ (0.04 g, 0.07 mmol) were dissolved in DMF/MeOH (60 mL, 1:1, v/v) and refluxed. The product was precipitated by adding excess aqueous NH_4PF_6.

*2.4.10 cis-dithiocyanato-bis-5-(9-anthracenyl-(2,3-dimethylacrylic acid)-1,10-phenan throline-ruthenium(II) complex (**C10**)*

The complex was prepared in a similar manner as described for **C2**. A stoichiometric amount of **L5** (0.10 g, 0.22 mmol), $[RuCl_2(dmso)_4]$ (0.05 g, 0.11 mmol) and excess of NH_4NCS (0.17 g, 2.20 mmmol, 10 % excess) were dissolved in DMF/MeOH (80 mL, 1:5, v/v), and refluxed for 12 h in the dark.

2.5.0 Synthesis of Ru(II) Heteronuclear Complexes Containing Substituted Bipyridine and Phenanthroline Ligands

*2.5.1 4-(2,3-dimethylacrylic acid)-2,2'-bipyridyl-5-(2,3-dimethylacrylic acid)-1,10-phenanthroline-ruthenium(II) bis-hexafluorophosphate complex (**C11**)*

The general method of synthesis as reported for **C1** was used in the synthesis of **C11**. In a 250 mL flask, Ligand **L1** (0.21 g, 0.81 mmol), **L3** (0.11 g, 0.41 mmol) and $RuCl_2(dmso)_4$ (0.20 g, 0.41 mmol) were dissolved in MeOH (60 mL). The mixture was refluxed for 6 h. Precipitation was carried out with NH_4PF_6 and the product further recrystallized from Et_2O-EtOH (50 %, 30 mL).

*2.5.2 cis-dithiocyanato-4-(2,3-dimethylacrylic acid)-2,2'-bipyridyl-5-(2,3-dimethyl-acrylic acid)-1,10-phenanthroline-ruthenium(II) complex (**C12**)*

A mixture of **L1** (0.23 g, 0.92 mmol), **L3** (0.26 g, 0.92 mmol), $[RuCl_2(dmso)_4]$ (0.44 g, 0.92 mmol) in DMF (40 mL) was refluxed for 20 min after which excess of NH_4NCS (0.70 g, 10.4 mmmol, 10 % excess) was added. The product was purified by column chromatography in Sephadex LH-20.

*2.5.3 4-(2,3-dimethylacrylic acid)-2,2'-bipyridyl-bis-5-(2,3-dimethyl acrylic acid)-1,10-phenanthroline ruthenium(II) bis-hexafluorophosphate complex (**C13**)*

This complex was prepare as reported for **C11** using a 1:2 equimolar weight of **L1** (0.36 g, 1.40 mmol) and **L3** (0.31 g, 0.07 mmol) with $[RuCl_2(dmso)_4]$ (0.34 g, 0.07 mmol).

*2.5.4 cis-dithiocyanato-5-(9-anthracenyl-(2,3-dimethylacrylic acid)-1,10-phenanthro-line-4-(9-anthracenyl-2,3-dimethylacrylic acid)-2,2-bipyridine ruthenium(II) complex (**C14**)*

A mixture of **L2** (0.12 g, 0.27 mmol), **L5** (0.12 g, 0.27 mmol), $[RuCl_2(dmso)_4]$ (0.43 g, 0.09 mmol) and excess of NH_4NCS (0.41 g, 5.39 mmmol, 10 % excess) were added as a mixture in DMF (40 mL) (Scheme 2.26). The synthetic method is as reported for complex **C12**.

2.6.0 Synthesis of Ru(II) Heteroleptic Complexes Containing 4,7-Disubstituted Phenanthroline Derivatives

*2.6.1 cis-dithiocyanato-4-(9-dianthracenyl-10-(2,3-dimethylacrylic acid)-7-(9-anthracenyl-10-(2,3-dimethylacrylic acid)-1,10-phenanthroline-4,7-bis(1-methoxy-1-buten-3-yne)-1,10-phenanthroline ruthenium(II) complex **(C15)***

In a 250 mL flask, $[RuCl_2(dmso)_4]$ (0.095 g, 0.20 mmol) was dissolved in *N,N* dimethylformamide (40 mL) followed by successive addition of **L7** (0.41 g, 0.59 mmol) and **L10** (0.20 g, 0.59 mmol) and excess aqueous solution of NH_4NCS (0.90 g, 0.01 mmol, 10 % excess) after 10 min of reflux. The reflux was done under argon at 150^oC for 8 h in the dark. After the reaction, the solution was allowed to cool to room temperature and filtered to remove unreacted starting materials. The filtrate was concentrated to dryness and 40 mL of 0.05 M NaOH solution was added to give a dirty brown precipitate which was filtered off. The pH of the resulting solution was adjusted to 3 with 0.5 M HNO_3. The solution was left to stand in the fridge (-2^oC) for 12 h before filtration and concentration *in vacuo*. Water was added to the semisolid to remove excess NH_4NCS. The water insoluble product was collected on sintered glass crucible by suction filtration and washed with diethyl ether and dried in the oven at a moderate temperature. The resulting crude complex was dissolved in methanol and carefully adsorbed on the Sephadex LH 20 column chromatography using solvent system D as mobile phase. The product was further recrystallized in EtOH-Et_2O.

*2.6.2 cis-dithiocyanato-4,7-bis(2,3-dimethylacrylic acid)-1,10-phenanthroline-4,7-bis(9-trianthracenyl-10-(2,3-dimethylacrylic acid)-1,10-phenanthroline ruthenium(II) complex **(C16)***

In a 250 mL flask, $[RuCl_2(dmso)_4]$ (0.05 g, 10.46 mmol) was dissolved in *N,N*-dimethylformamide followed by the successive addition of **L4** (0.04 g, 10.46 mmol) and **L8** (0.15 g, 10.46 mmol) and excess of NH_4NCS (0.07 g, 10.46 mol). The mixture was heated at 120°C for 5 h in the dark. The solution was allowed to cool to room temperature and filtered to remove unreacted starting material. The filtrate was concentrated to dryness and 40 mL of 0.05 M NaOH solution was added to give dirty brown precipitate which was filtered off. The pH of the resulting solution was adjusted to 3 with 0.5 M HNO_3. The solution was left to stand in the fridge (-2°C) for 12 h before being filtered and concentrated *in vacuo*. Water was added to the resulting semisolid to remove excess NH_4NCS. The water insoluble product was collected on sintered glass crucible by suction filtration and washed with distilled water, followed by diethyl ether and dried. The resulting crude complex was purified twice by column chromatography on Sephadex LH 20 using $CHCl_3$-MeOH (1:1) as eluting solvent.

2.7.0 Experimental Results and Physicochemical properties of Ru(II) Complexes of 2,2'-Bipyridyl and 1,10-Phenanthrolyl Derivatives

2.7.1. Characterization of 4-(2,3-dimethylacrylic acid)-2,2'-bipyridine (L1)

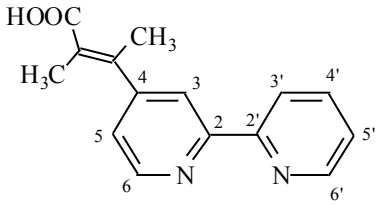

Colour: White crystalline solid.

Melting point: ND

IR (KBr, ν_{cm}^{-1}): 3054, 2927, 2676, 1965, 1690, 1648, 1581, 1559, 1456, 1419, 1346, 1251, 1141, 1089, 1040, 992, 893, 757, 653, 631, 619, 555.

^{1}H NMR (400 MHz, DMSO): δ 8.66 (d, *J* = 4.0 Hz, H–6, 6'), 8.41 (d, *J* = 8.0 Hz, H–3, 3'), 7.86 (dd, *J* = 7.6, 8.0 Hz, H–5, 5'), 7.36 (dd, *J* = 5.2, 7.2 Hz, H–4'), 1.73 (s, CH_3), 1.66 (d, CH_3).

^{13}C NMR (400 MHz, DMSO): δ 169.76, 156.21, 149.98, 137.86, 136.88, 129.74, 124.81, 121.32, 14.81, 12.71.

Percentage yield: 0.90 g, 67 %

2.7.2. Characterization of 4-(9-anthracenyl-10-(2,3-dimethylacrylic acid))-2,2'-bipyridine (L2)

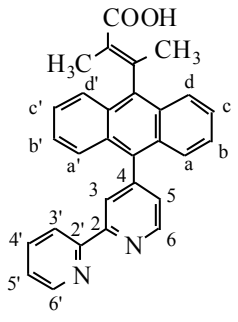

Colour: Yellow crystalline solid.

Melting point: 167–169 ^{o}C

IR (KBr): 3427, 3056, 2926, 1952, 1802, 1690, 1622, 1582, 1558, 1524, 1456, 1437, 1420, 1349, 1304, 1256, 1162, 1149, 1089, 1040, 1028, 995, 926, 747, 676, 654, 619, 605, 578.

^{1}H NMR (400 MHz, DMSO): δ 9.20 (2d, *J* = 1.6, 4.4 Hz, H–6, 6'), 8.57 (dd, *J* = 3.2, 6.8 Hz, H–a, b), 8.26 (d, *J* = 2.0 Hz, H–3, 5), 8.24 (d, *J* = 1.6 Hz, H–4'), 7.62 (dd, *J* = 3.2. 6.8 Hz, H-c, d), 2.17 (s, CH_3), 1.67 (s, CH_3).

^{13}CNMR (400 MHz, DMSO): δ 156.76, 150.31, 146.27, 144.21, 135.94, 131.03, 128.52, 128.25, 127.44, 126.49, 124.21, 123.51, 123.04, 30.90 and 21.92.

Percentage yield: 1.93 g, 71 %

2.7.3. Characterization of 5-(2,3-dimethylacrylic acid)-1,10-phenanthroline (L3)

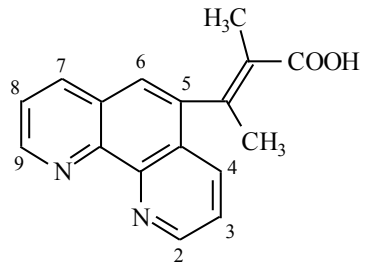

Colour: White-pink crystalline solid.

Melting point: ND

IR (KBr): 3419, 3032, 2929, 1694, 1652, 1619, 1589, 1561, 1506, 1420, 1385, 1343, 1256, 1219, 1140, 1093, 1080, 1037, 1015, 843, 766, 734, 769, 625, 530.

^{1}H NMR (400 MHz, $CDCl_3$): δ 11.32 (br, OH), 8.97 (t, 2H, H–2, 9), 7.92 (t, 2H, H–3, 8), 7.91 (s, 1H, H–6), 7.44 (d, 1H, H–4), 6.82 (d, 1H, H–7), 1.67 (s, CH_3), 1.58 (d, CH_3).

^{13}C NMR (400 MHz, $CDCl_3$): δ 150.39, 150.30, 146.30, 146.21, 138.79, 136.13, 128.81, 128.72, 126.68, 126.59, 123.27, 123.19, 14.74, and 12.14.

Percentage yield: 0.74 g, 53 %

2.7.4. Characterization of 4,7-Bis(2,3-dimethylacrylic acid)-1,10-phenanthroline (L4)

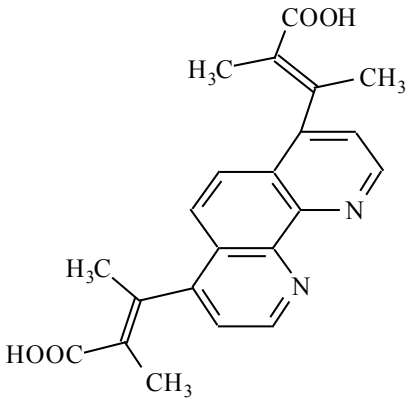

Colour: White creamy solid.

Melting point: 85–86 °C

IR (KBr) v_{max}/cm^{-1}: 3419, 3032, 2929, 1694, 1652, 1619, 1589, 1561, 1506, 1420, 1385, 1343, 1256, 1219, 1140, 1093, 1080, 1037, 1015, 843, 766, 734, 769, 625, 530.

^{1}H NMR (400 MHz, DMSO): δ 9.09 (d, *J* = 3.6 Hz, H-9), 8.55 (br, H-2), 8.43 (d, *J* = 8.0 Hz, H-8), 7.91 (s, H-5, H-6), 7.72 (d, *J* = 4.4 Hz, H-3), 2.54 (s, CH_3), 1.70 (t, CH_3).

^{13}C NMR (400 MHz, DMSO): δ 169.67, 150.74, 146.40, 137.01, 129.30, 127.47, 124.10, 14.90, 12.75.

Electrochemical data: E_{pa}/V = 0.45 V, $E_{1/2}/V$ = -0.23, -0.59 V

Elemental analysis: Found: C 70.56, H 4.99, N 7.23; Calcd for $C_{24}H_{20}N_2O_4$: C 70.20, H 5.36, N, 7.44.

Percentage yield: 0.90 g, 80 %

2.7.5. Characterization of 5-(9-anthracenyl-10-(2,3-dimethylacrylic acid)-1,10-phenanthroline (L5)

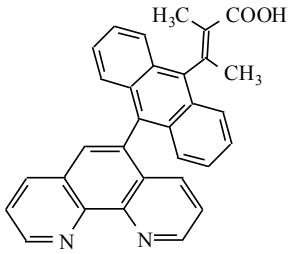

Colour: Yellow crystalline solid.

Melting point: 167−169^{o}C

IR (KBr) v_{max}/cm^{-1}: 3427, 3055, 2979, 2924, 2552, 1966, 1871, 1802, 1579, 1558, 1453, 1417, 1304, 1255, 1140, 1089, 1040, 994, 926, 756, 654, 619, 579.

^{1}H NMR ($CDCl_3$): δ 9.18 (d, *J* = 3.2 Hzj), 8.23 (d, *J* = 7.2 Hz), 7.77 (s), 7.62 (dd, *J* = 4.4, 8.0 Hz), 6.97 (d, *J* = 7.2 Hz), 1.81 (t, CH_3), 1.23 (t, CH_3).

^{13}C NMR ($CDCl_3$): 150.28, 146.19, 139.25, 135.97, 128.61, 126.49, 123.06, 14.42, 11.74.

Percentage yield: 1.40 g, 59 %

2.7.6. Characterization of 4,7-Bis(9-anthracenyl-10-(2,3-dimethylacrylic acid)-1,10-phenanthroline (L6)

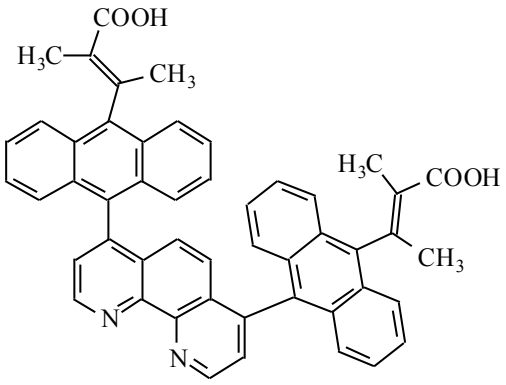

Colour: Yellow crystalline solid.

Melting point: 223–224 ^{o}C

IR (KBr) v_{max}/cm^{-1}: 3413, 3076, 3027, 2928, 2865, 1947, 1929, 1817, 1621, 1522, 1437, 1385, 1349, 1329, 1304, 1256, 1162, 1148, 1027, 960, 926, 838, 746, 675, 604, 578.

^{1}H NMR (DMSO-d_6): δ 9.10 (d, *J* = 4.0 Hz, H-2, 9), 7.98 (d, H-3, 8), 8.36 (s, H-5, 6), 8.48 (dd, *J* = 8.0 Hz, 4H), 7.77 (m, 4H), 2.08 (s, CH_3).

^{13}C NMR (DMSO-d_6): δ 150.82, 146.44, 137.06, 129.34, 127.55, 124.17.

Percentage yield: 0.46 g, 67 %

2.7.7. Characterization of 4-(9-dianthracenyl-10-(2,3-(dimethylacrylic acid)-7-(9-anthracenyl-10-(2,3-(dimethylacrylic acid)-1,10-phenanthroline (L7)

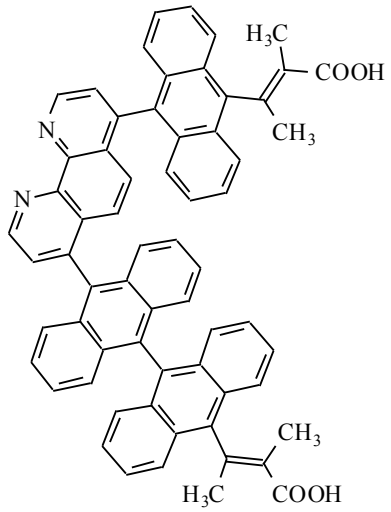

Colour: Yellow-green solid.

Melting point: 203–205 ^{o}C

IR (KBr) v_{max}/cm^{-1}: 3381, 3027, 2925, 1929, 1621, 1587, 1502, 1422, 1346, 1304, 1255, 1217, 1137, 1091, 1026, 925, 853, 778, 746, 675, 623, 578.

^{1}H NMR (DMSO-d_6): δ 9.10 (d, *J* = 4.0 Hz, H-2, 9), 7.98 (d, H-3, 8), 8.36 (s, H-5, 6), 8.48 (dd, *J* = 8.0 Hz, 4H), 7.77 (m, 4H), 2.08 (s, CH_3).

^{13}C NMR (DMSO-d_6) δ 150.38, 150.28, 146.30, 146.21, 138.79, 136.21, 136.13, 128.81, 128.72, 126.68, 126.59, 123.27, 123.19, 14.74, 12.14.

Elemental Analysis: found: C, 84.66; H, 5.15; N, 3.55 requires $C_{64}H_{44}N_2O_4$), calculated: C, 84.93; H, 4.90; N, 3.10.

Percentage yield: 1.00 g, 56 %

2.7.8. Characterization of 4,7-Bis(9-trianthracenyl-10-(2,3-dimethylacrylic acid)-1,10-phenanthroline (L8)

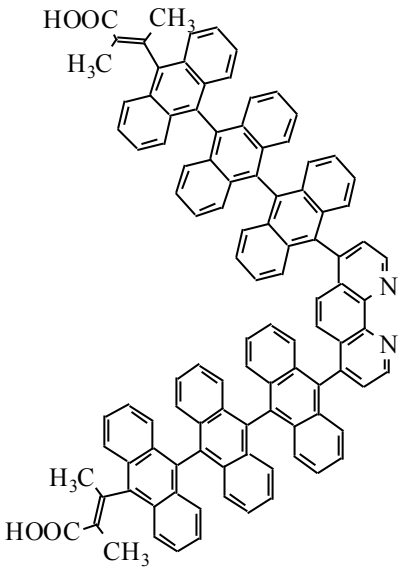

Colour: Orange red solid.

Melting point: 188–190 °C.

IR data (KBr, cm^{-1}): 3381, 3027, 2925, 1817, 1621, 1587, 1522, 1502, 1436, 1422, 1346, 1304, 1255, 1172, 1161, 1137, 1091, 1026, 960, 883, 778, 746, 623, 578.

UV-Vis (λ_{max}/nm ε = M^{-1} cm^{-1}) ($CHCl_3$): 379 (41 000), 359 (42 900), 341 (38 260), 325 (14 750).

^{1}H NMR (400 MHz, $CDCl_3$): δ 9.26 (d, *J* = 4.4 Hz, 2H), 8.40 (s, 2H), 7.67 (d, *J* = 4.4 Hz, 2H), 8.29 (dd, *J* = 3.4, 5.8 Hz, 4H), 7.98 (dd, *J* = 3.2, 6.4 Hz, 4H), 7.77 (dd, *J* = 3.8, 7.0 Hz, 4H), 7.45 (dd, *J* = 3.1, 6.6, 4H), 1.82 (s, CH_3), 1.79 (s, CH_3).

^{13}C NMR (100 MHz, $CDCl_3$): δ; 183.1, 149.9, 144.9, 139.5, 136.7, 134.1, 133.5, 131.6, 128.7, 128.1, 127.2, 126.6, 126.2, 125.3, 123.4, 14.6.

Electrochemical data: E_{pa}/V = 0.48 V, $E_{1/2}$/V -0.38, -0.57, -0.94 V

Elemental Analysis: Found: C 84.80, H 5.01, N 1.85; required $C_{106}H_{68}N_2O_4.4H_2O$: Calculated: C 84.55, H 5.09, N 1.86.

Percentage yield: 0.51 g, 54 %

2.7.9. Characterization of 4-(4-(2,3-dimethylacrylic acid)-phenylethynyl)-2,2'-bipyridine (L9)

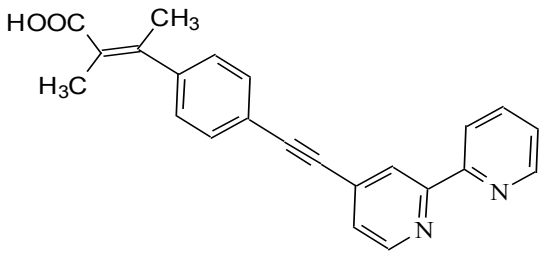

Colour: Red semi-solid.

Melting point: ND.

IR (KBr): 3415, 3060, 2928, 2865, 2039, 1967, 1640, 1618, 1588, 1561, 1504, 1421, 1344, 1216, 1138, 1091, 1010, 851, 767, 736, 622, 523, 481, 409.

^{1}H NMR ($CDCl_3$): δ 10.89 (s, br = OH), 8.73 (d, *J* = 4.0 Hz), 8.38 (d, *J* = 7.6 Hz), 7.85 (dd, *J* = 7.6, 6.0 Hz), 7.34 (dd, *J* = 4.4, 6.0 Hz), 7.01 (d, *J* = 6.8 Hz), 1.80, 1.83 (CH_3).

^{13}C NMR ($CDCl_3$): δ 173.68, 149.08, 137.56, 139.74, 137.17, 128.14, 123.82, 121.44, 14.53, 11.60.

Percentage yield: 0.32 g, 58 %

2.7.10. Characterization of 4,7-Bis(1-methoxy-1-buten-3-yne)-1,10-phenanthroline (L10)

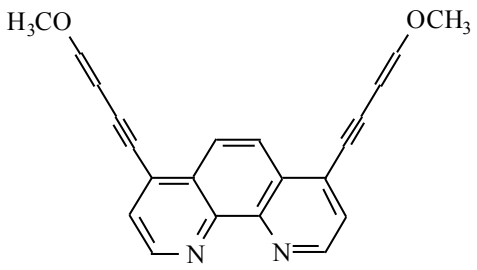

Colour: Red-brown semi-solid.

Melting point: ND

TLC characteristics: R_f = 0.67 (C_6H_{14}-CH_2Cl_2, 1:1, v/v)

IR (KBr): 3478, 3416, 3063, 2931, 2039, 1638, 1619, 1589, 1504, 1421, 1345, 1219, 1091, 852, 738, 696, 624, 541, 496.

^{1}H NMR ($CDCl_3$): δ 9.16 (d, *J* = 3.6 Hz, 2H, H-2, 9), 8.19 (d, *J* = 8.0 Hz, 2H, H-3, 8), 7.72 (s, 2H, H-5, 6), 7.58 (d, *J* = 3.6 Hz, 2H, H_a), 7.30 (d, *J* = 3.6 Hz, 2H, H_b).

^{13}C NMR ($CDCl_3$): δ 150.67, 146.61, 137.56, 137.45, 136.36, 134.20, 132.51, 132.41, 132.37, 129.14, 128.96, 128.93, 128.87, 126.90, 123.45, 101.84, 54.20, 47.66.

Elemental Analysis: Found: C, 77.89; H, 4.52; N, 8.45. Required: $C_{22}H_{16}N_2O_2$ Calculated: C, 77.63; H, 4.74; N, 8.23.

Percentage yield: 1.00 g, 57 %

2.7.11. Characterization of Ru(II)-tris-(4-(2,3-dimethylacrylic acid)-2,2'-bipyridyl-bis-hexafluorophosphate complex (C1)

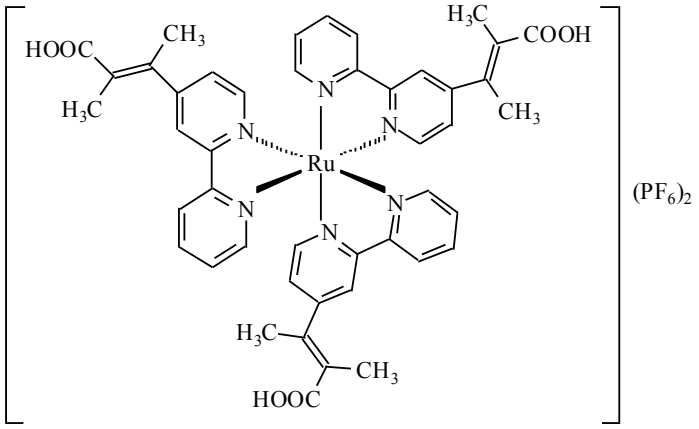

Colour: Dark brown solid

Melting point: 201–204 ^{o}C

IR (KBr) v_{max}/cm^{-1}: 3430, 2926, 2855, 1622, 1607, 1497, 1464, 1446, 1424, 1385, 1314, 1270, 1245, 1162, 1125, 1070, 838, 763, 731, 610, 557, 472, 421.

UV-Vis (λ_{max}/nm, ε = M^{-1} cm^{-1}, DMF): 343 (2059), 447 (3218), 914 (880) and 1015 (1200)

Emission wavelength: ($\lambda_{exc.}$ = 640 nm, λ_{em} = 747 nm).

^{1}H NMR (DMSO-d_6): δ 8.62 (d, *J* = 5.6 Hz, 1H), 8.06 (s, 1H), 7.69 (s, 1H), 7.43 (s, 1H).

^{13}C NMR (DMSO-d_6): δ 157.23, 151.82, 128.52, 125.03

Percentage yield: 0.083 g, 64 %.

2.7.12. Characterization of cis-dithiocyanato-bis-(4-(2,3-dimethylacrylic acid)-2,2'-bipyridyl)-ruthenium (II) complex (C2)

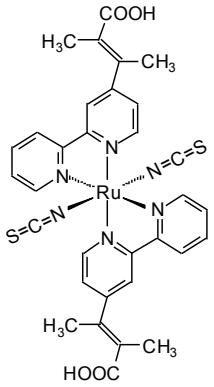

Colour: Dark brown solid

Melting point: > 250 ^{o}C

IR (KBr) v_{max}/cm^{-1}: 3550, 3479, 3237, 2923, 2851, 2106, 1638, 1617, 1460, 1443, 1420, 1309, 1265, 1243, 1155, 1084, 1022, 800, 760, 728, 620, 474, 421.

UV-Vis (λ_{max}/nm, $\varepsilon = M^{-1}\ cm^{-1}$, DMF): 346 (2520), 497 (2055), 665 (1090), 740 (730), 905 (499) and 1015 (740).

Emission wavelength: ($\lambda_{exc.}$ = 640 nm, λ_{em} = 682 nm).

^{1}H NMR (DMSO-d_6): δ 8.45 (dd, 0.8, 1.2 Hz), 7.77 (m), 2.05 (s, CH_3)

^{13}C NMR: NA

Electrochemical Data: Ru^{2+}/Ru^{3+} = +0.90 V; $E_{cathodic}$ = -0.61 V, E_{anodic} = 0.29 V.

Percentage yield: 0.066 g, 51 %.

2.7.13. Partial characterization of cis-dithiocyanato-bis-4-(4-(2,3-dimethyl acrylic acid)-phenyl ethynyl)-2,2'-bipyridine-ruthenium(II) complex (C3)

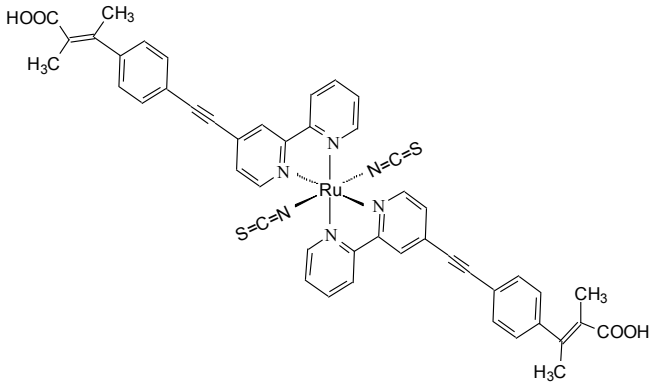

Colour: Green solid

Melting point: 256–258 ^{o}C

IR (KBr) v_{max}/cm^{-1}: 3551, 3476, 3414, 3236, 2928, 2109, 1976, 1721, 1639, 1617, 1497, 1486, 1446, 1385, 1295, 1221, 1157, 1121, 882, 806, 767, 729, 692, 620, 476, 402.

UV-Vis (λ_{max}/nm, ε = M^{-1} cm^{-1}, DMF): 376 (3540), 527 (1590).

Emission wavelength: ($\lambda_{exc.}$ = 640 nm, λ_{em} = 745 nm).

Percentage yield: 0.048 g, 39 %.

2.7.14. Characterization of tris-4-(9-anthracenyl-(2,3-dimethylacrylic acid)-2,2'-bipyridyl-ruthenium(II)-bis-hexafluorophosphate complex (C4)

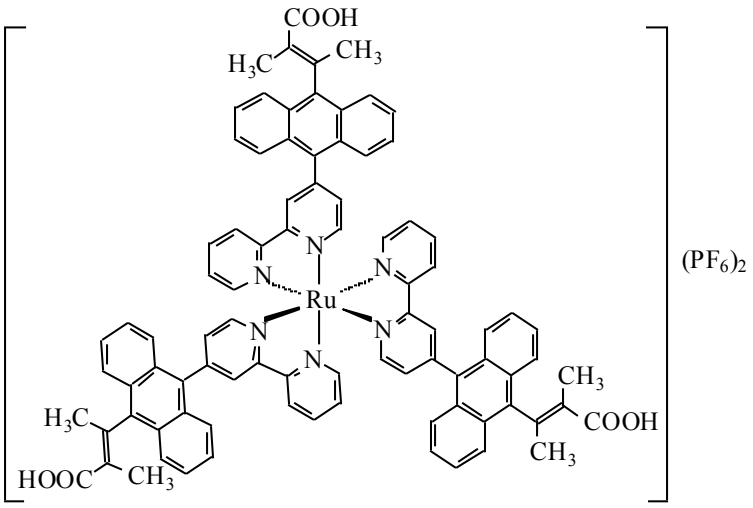

Colour: Orange solid

Melting point: 226–227 ^{o}C

IR (KBr) v_{max}/cm^{-1}: 3430, 3076, 2928, 2865, 1902, 1678, 1622, 1591, 1580, 1437, 1332, 1321, 1304, 1285, 1256, 1206, 1170, 1098, 1028, 969, 937, 926, 809, 747, 694, 622, 604, 579, 387.

UV-Vis (λ_{max}/nm, ε = M^{-1} cm^{-1}, DMF): 358 (4342), 379 (4960), 401(5557), 447 (5770), 907 (1410) and 1011 (1970).

Emission wavelength: ($\lambda_{exc.}$ = 640 nm, λ_{em} = 710 nm).

^{1}H NMR ($CDCl_3$): δ 8.83 (d, *J* = 7.6 Hz), 8.56 (m), 8.17 (s), 7.74 (s), 7.53 (s)

^{13}C NMR ($CDCl_3$): NA

Electrochemical Data: Ru^{2+}/Ru^{3+} = 0.64 V; E_{anodic} = 0.42 V, $E_{cathodic}$ = -0.99 V.

Percentage yield: 0.135 g, 45 %.

2.7.15. Characterization of cis-dithiocyanato-bis-4-(9-anthracenyl-(2,3-dimethyl acrylic acid)-2,2'-bipyridyl-ruthenium(II) complex (C5)

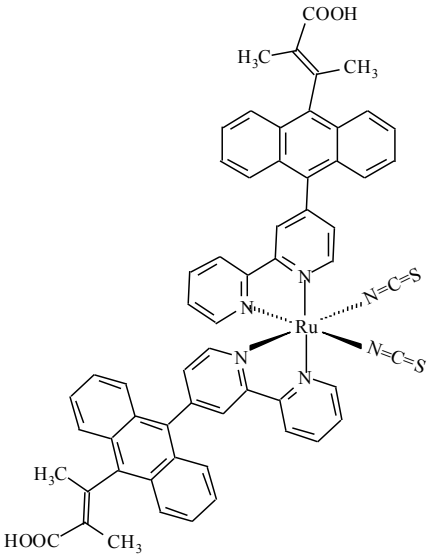

Colour: Dark brown solid

Melting point: 278–281 ^{o}C

IR (KBr) v_{max}/cm^{-1}: 3419, 3077, 3027, 2958, 2925, 2855, 2106, 1621, 1497, 1459, 1437, 1384, 1350, 1304, 1256, 1162, 1088, 1027, 960, 926, 838, 804, 746, 675, 604, 578, 558, 464, 429.

UV-Vis (λ_{max}/nm, ε = M^{-1} cm^{-1}, DMF): 351 (3040), 370 (5790), 390 (9175), 413 (8970), 479 (740), 929 (744), 1037 (664).

Emission wavelength: ($\lambda_{exc.}$ = 640 nm, λ_{em} = 710 nm).

^{1}H NMR (DMSO-d_6): δ 9.89 (d, *J* = 5.2 Hz), 9.17 (d, *J* = 4.4 Hz), 8.82 (s), 8.69 (s), 8.55 (d, *J* = 6.4 Hz), 8.25 (d, *J* = 6.8 Hz), 7.73 (d, *J* = 5.2 Hz), 2.55 (s, CH_3), 2.08 (s, CH_3).

^{13}C NMR ($CDCl_3$): ND

Percentage yield: 0.38 g, 37 %.

2.7.16. Characterization of cis-dithiocyanato-4-(2,3-dimethylacrylic acid)-2,2'-bipyridyl-4-(9-anthracenyl-(2,3-dimethylacrylic acid)-2,2'-bipyridyl ruthenium(II) complex (C6)

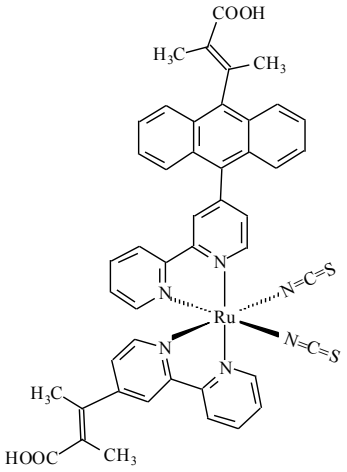

Colour: Dark brown solid

Melting point: > 260 ^{o}C

IR (KBr) v_{max}/cm^{-1}: 3551, 3478, 3414, 3239, 3066, 2922, 2103, 1635, 1617, 1584, 1533, 1459, 1443, 1419, 1309, 1239, 1155, 1089, 1039, 1014, 961, 926, 839, 805, 760, 718, 682, 619, 611, 557, 473, 426, 399.

UV-Vis (λ_{max}/nm, ε = M^{-1} cm^{-1}, DMF): 363 (6435), 379 (6278), 404 (4923), 417 (3827), 512 (4543)

Emission wavelength: ($\lambda_{exc.}$ = 640 nm, λ_{em} = 680 nm).

^{1}H NMR (CD_3OD): δ 8.71 (d, *J* = 7.6 Hz), 8.61 (d, *J* = 6.8 Hz), 8.14 (s), 7.83 (s), 7.73 (s), 7.50 (d, *J* = 1.2 Hz), 2.16 (s, CH_3), 1.29 (s, CH_3).

^{13}C NMR: NA

Cyclic voltammetry Data: Ru^{2+}/Ru^{3+} = 0.47 V; $E_{1/2}$ = -0.62 V, $E_{cathodic}$ = -0.91 V.

Percentage yield: 0.60 g, 36 %.

2.7.17. Characterization of tris-5-(2,3-dimethylacrylic acid)-1,10-phenanthroline ruthenium(II)-bis-hexafluorophosphate complex (C7)

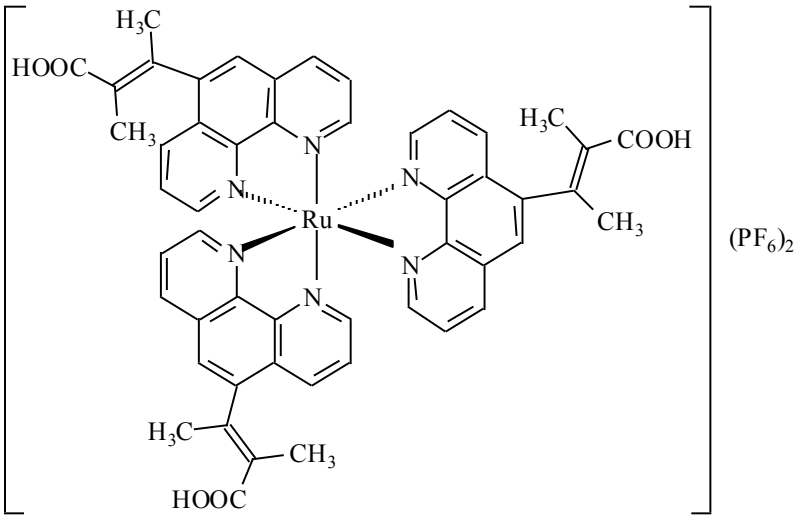

Colour: Orange solid

Melting point: 236–239 ^{o}C

IR (KBr) v_{max}/cm^{-1}: 3551, 3479, 3414, 3238, 2928, 2852, 1637, 1617, 1428, 1412, 1342, 1256, 1206, 1147, 1095, 1018, 927, 839, 775, 747, 722, 620, 557, 529, 474, 407.

UV-Vis (λ_{max}/nm, ε = M^{-1} cm^{-1}, DMF): 421 (12477), 443 (13030)

Emission wavelength: ($\lambda_{exc.}$ = 640 nm, λ_{em} = 715 nm).

^{1}H NMR ($CDCl_3$): δ 8.75 (d, *J* = 8.4 Hz), 8.36 (s), 8.06 (d, *J* = 5.2 Hz), 7.74 (dd, *J* = 5.2, 8.4 Hz), 6.71 (d, *J* = 6.8 Hz), 2.06 (s, CH_3), 1.71 (m, CH_3)

Cyclic voltammetry Data: Ru^{2+}/Ru^{3+} = 0.84 V, $E_{1/2}$ = 0.15 V, 0.47 V.

Percentage yield: 0.13 g, 53 %.

2.7.18. Characterization of cis-dithiocyanato-bis-5-(2,3-dimethylacrylic acid)-1,10-phenanthroline-ruthenium (II) complex (C8)

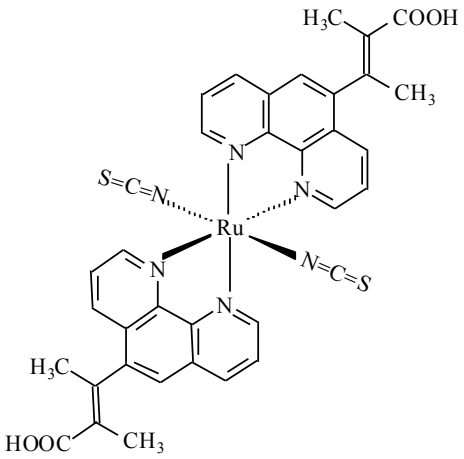

Colour: Orange solid

Melting point: 201–204 ^{o}C

IR (KBr) v_{max}/cm^{-1}: 3423, 3058, 2926, 2856, 2086, 2058, 1978, 1631, 1427, 1384, 1221, 1205, 1147, 1056, 879, 844, 773, 721, 621, 559.

UV-Vis (λ_{max}/nm, ε = M^{-1} cm^{-1} $CHCl_3$-MeOH): 416 (5866), 444 (6323), 907 (511), 960 (590), and 1007 (697).

Emission wavelength: ($\lambda_{exc.}$ = 630 nm, λ_{em} = 700 nm).

^{1}H NMR ($CDCl_3$): δ 8.77 (d, *J* = 8.0 Hz), 8.39 (s), 8.10 (d, *J* = 4.8 Hz), 7.78 (dd, *J* = 5.2, 8.0 Hz), 2.57 (s, CH_3).

^{13}C NMR ($CDCl_3$): δ 153.62, 148.13, 137.69, 131.33, 128.92, 127.17.

Percentage yield: 0.38 g, 38 %.

2.7.19. Characterization of tris-5-(9-(anthracenyl-(2,3-dimethylacrylic acid)-1,10-phenanthroline-ruthenium(II)bis-hexafluorophosphate complex (C9)

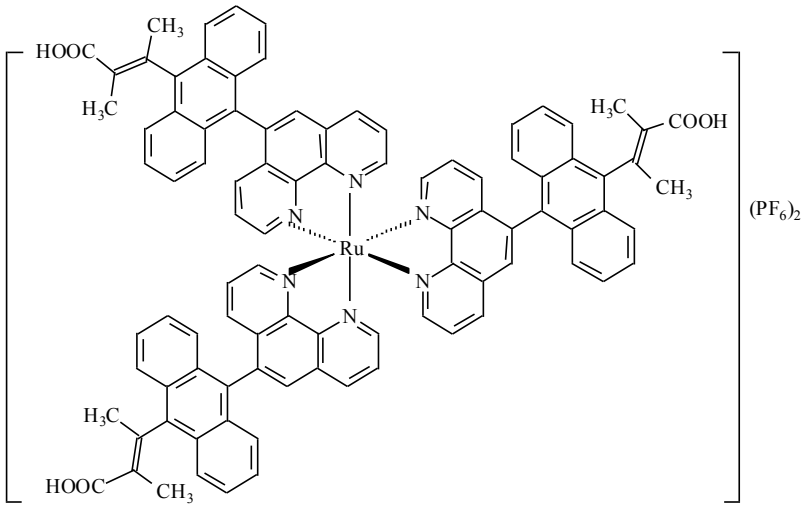

Colour: Dark Orange solid

Melting point: > 300 ^{o}C

IR (KBr) v_{max}/cm^{-1}: 3550, 3474, 3414, 2926, 1638, 1617, 1464, 1447, 1309, 1256, 1162, 1028, 926, 838, 761, 747, 731, 620, 578, 557, 475.

UV-Vis (λ_{max}/nm, ε = M^{-1} cm^{-1} DMF): 343 (9230), 362 (12330), 383 (17096), 405 (18240), 452 (11556).

Emission wavelength: ($\lambda_{exc.}$ = 500 nm, λ_{em} = 676 nm).

^{1}H NMR ($CDCl_3$): δ 8.83 (d, *J* = 8.0 Hz), 8.56 (dd, *J* = 3.2, 6.8 Hz), 8.17 (t), 7.82 (dt, *J* = 3.2, 6.8 Hz), 7.73 (d, *J* = 5.6 Hz), 7.53 (dd, *J* = 6.0, 6.4 Hz).

^{13}C NMR ($CDCl_3$): δ 157.42, 152.07, 138.79, 131.26, 128.75, 125.34, 13.94.

Cyclic voltammetry Data: E_{anodic} = +0.43 V, Ru^{2+}/Ru^{3+} = +0.71 V; $E_{1/2}$ = -0.58 V.

Percentage yield: 0.08 g, 60 %.

2.7.20. Characterization of cis-dithiocyanato-bis-5-(9-anthracenyl-(2,3-dimethyl acrylic acid)-1,10-phenanthroline-ruthenium(II) complex (C10)

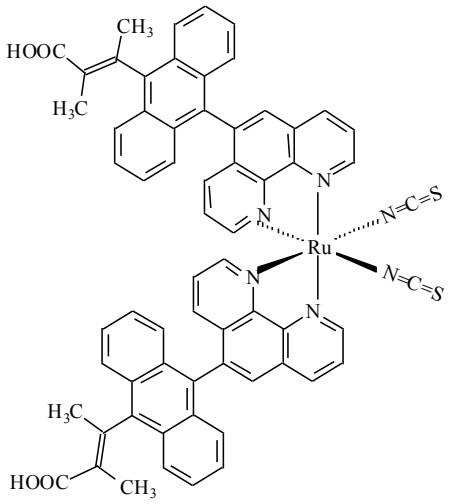

Colour: Dark brown solid

Melting point: > 260^{o}C

IR (KBr) v_{max}/cm^{-1}: 3551, 3479, 3414, 3237, 2928, 2104, 1971, 1638, 1617, 1459, 1438, 1304, 1256, 1156, 1090, 1026, 926, 804, 747, 730, 622, 579, 475, 404.

UV-Vis (λ_{max}/nm, ε = M^{-1} cm^{-1}, DMF): 345 (11578), 363 (17721), 383 (23614), 405 (21232), 505 (6655).

Emission wavelength: ($\lambda_{exc.}$ = 540 nm, λ_{em} = 660 nm).

^{1}H NMR ($CDCl_3$): δ 8.80 (s), 8.59 (dd, *J* = 3.6, 7.2 Hz), 8.45 (d, *J* = 2.0), 8.10 (t), 7.90 (s), 7.63 (dd, *J* = 2.8, 6.8 Hz), 2.17 (s, CH_3), 2.04 (s, CH_3).

^{13}C NMR ($CDCl_3$): Poor Resolution.

Cyclic voltammetry Data: Ru^{2+}/Ru^{3+} = 0.43 V; $E_{cathodic}$ = -0.57 V.

Percentage yield: 0.79 g, 25 %.

2.7.21. Characterization of bis-4-(2,3-dimethylacrylic acid)-2,2'-bipyridyl-5-(2,3-dimethylacrylic acid)-1,10-phenanthroline-ruthenium(II) bis-hexafluoro phosphate complex (C11)

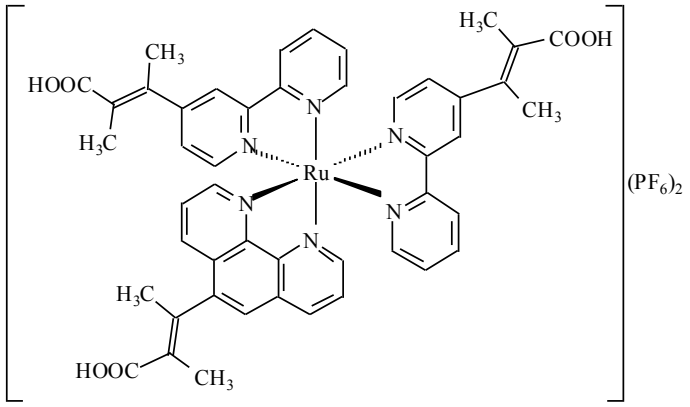

Colour: Reddish-brown solid

Melting point: > 250 ^{o}C

IR (KBr) v_{max}/cm^{-1}: 3551, 3479, 3414, 3237, 2928, 2099, 1638, 1617, 1464, 1447, 1428, 1243, 1095, 838, 760, 731, 721, 620, 557, 478, 404.

UV-Vis (λ_{max}/nm, $\varepsilon = M^{-1}\ dm^{-1}$, DMF): 452 (21160).

Emission wavelength: ($\lambda_{exc.}$ = 640 nm, λ_{em} = 672 nm).

^{1}H NMR (DMSO-d_6): δ 8.84 (d, *J* = 7.6 Hz), 8.39 (s), 8.17 (t), 7.75 (d, *J* = 4.0 Hz), 7.56 (m), 1.73 (s, CH_3), 1.66 (d, CH_3).

^{13}C NMR (DMSO-d_6): δ 169.76, 157.71, 157.44, 157.40, 153.13, 152.30, 152.08, 147.72, 138.79, 138.69, 137.76, 131.35, 128.96, 128.95, 128.76, 128.72, 128.64, 127.33, 127.29, 125.33, 125.24, 14.81, 12.71.

Cyclic voltammetry Data: E_{anodic} = 0.43 V, Ru^{2+}/Ru^{3+} = 0.82 V; $E_{cathodic}$ = -0.59 V.

Percentage yield: 0.28 g, 53 %.

2.7.22. Characterization of cis-dithiocyanato-4-(2,3-dimethylacrylic acid)-2,2'-bipyridyl-5-(2,3-dimethyl acrylic acid)-1,10-phenanthroline-ruthenium(II) complex (C12)

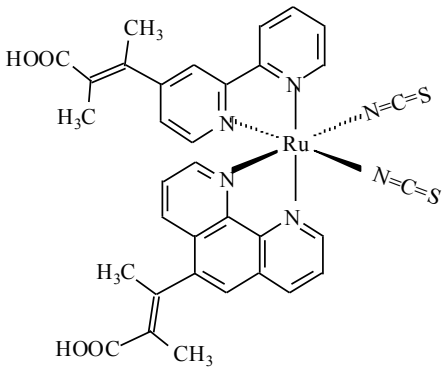

Colour: Dark brown solid

Melting point: > 250 ^{o}C

IR (KBr) v_{max}/cm^{-1}: 3551, 3479, 3414, 3237, 2926, 2101, 1971, 1638, 1617, 1443, 1425, 1093, 1022, 841, 807, 762, 719, 620, 478, 399.

UV-Vis (λ_{max}/nm, ε = M^{-1} cm^{-1}, DMF): 350 (4757), 501 (6970).

Emission wavelength: ($\lambda_{exc.}$ = 650 nm, λ_{em} = 690 nm).

^{1}H NMR ($CDCl_3$): δ 8.81 (s), 8.43 (d, *J* = 7.2 Hz), 8.06 (s), 8.00 (d, *J* = 8.8 Hz), 7.51 (s), 2.17 (s, CH_3), 1.25 (s, CH_3).

^{13}C NMR: Poor Resolution

Cyclic voltammetry Data: Ru^{2+}/Ru^{3+} = 0.45 V; $E_{cathodic}$ = -0.64, -0.80 V.

Percentage yield: 0.37 g, 22 %.

2.7.23. Characterization of 4-(2,3-dimethylacrylic acid)-2,2'-bipyridyl-bis-(5-(2,3-dimethylacrylic acid)-1,10-phenanthroline-ruthenium(II) bis-hexafluoro phosphate complex (C13)

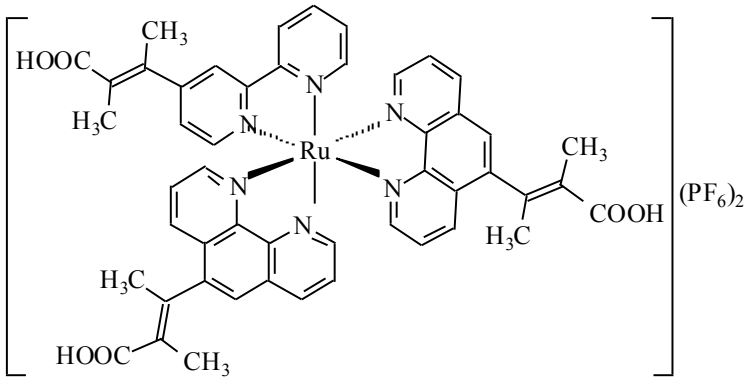

Colour: Deep Orange Red solid

Melting point: 201–203 ^{o}C

IR (KBr) v_{max}/cm^{-1}: 3551, 3478, 3414, 3237, 2926, 1638, 1617, 1497, 1464, 1447, 1429, 1314, 1270, 1244, 1162, 1125, 839, 765, 701, 671, 621, 557, 478, 418.

UV-Vis (λ_{max}/nm, ε = M^{-1} cm^{-1}, DMF): 452 (21160).

Emission wavelength: ($\lambda_{exc.}$ = 650 nm, λ_{em} = 680 nm).

^{1}H NMR (DMSO-d_6): δ 8.80 (d, *J* = 7.6 Hz), 8.14 (t), 7.71 (d, *J* = 5.6 Hz), 7.50 (t), 7.21 (s), 7.09 (s), 6.96 (s), 6.71 (d, *J* = 7.2 Hz), 1.70 (s, CH_3).

^{13}C NMR (DMSO-d_6): δ 169.20, 156.96, 151.62, 138.36, 136.88, 135.92, 14.58, 12.36.

Percentage yield: 0.44 g, 44 %.

2.7.24. Characterization of cis-dithiocyanato-4-(9-anthracenyl-2,3-dimethyl acrylic acid)-2,2-bipyridine-5-(9-anthracenyl-(2,3-dimethyl acrylic acid)-1,10-phenanthroline ruthenium(II) complex (C14)

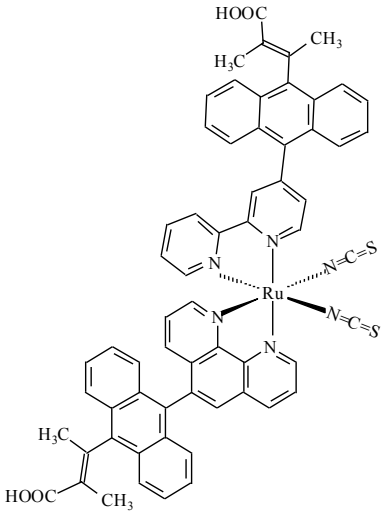

Colour: Brown solid

Melting point: > 260 ^{o}C

IR (KBr) v_{max}/cm^{-1}: 3557, 3478, 3415, 3237, 2926, 2105, 1974, 1639, 1618, 1497, 1461, 1441, 1304, 1257, 1157, 1027, 926, 804, 749, 730, 622, 477.

UV-Vis (λ_{max}/nm, ε = M^{-1} cm^{-1}, DMF): 345 (6945), 363 (10328), 383 (13540), 405 (12365), 420 (4045), 513 (3874)

Emission wavelength: ($\lambda_{exc.}$ = 550 nm, λ_{em} = 683 nm).

^{1}H NMR (DMSO-d$_6$): δ 8.60 (dd, *J* = 2.4, 6.0 Hz), 7.63 (dd, *J* = 2.0, 6.0 Hz), 7.00 (d, 2.4 Hz).

^{13}C NMR (DMSO-d$_6$): δ 168.89, 135.17, 126.31, 123.52, 123.28, 122.71, 9.81, 6.81

Cyclic voltammetry Data: Ru^{2+}/Ru^{3+} = 0.93 V; E_{anodic} = 0.42 V, $E_{cathodic}$ = -0.72 V.

Percentage yield: 0.45 g, 42 %.

2.7.25. Characterization of cis-dithiocyanato-bis-4,7-(1-methoxy-1-buten-3-yne) -1,10-phenanthroline-4-(9-dianthracenyl-10-(2,3-dimethylacrylic acid)-7-(9-anthracenyl-10-(2,3-dimethylacrylic acid)-1,10-phenanthroline ruthenium (II) complex (C15)

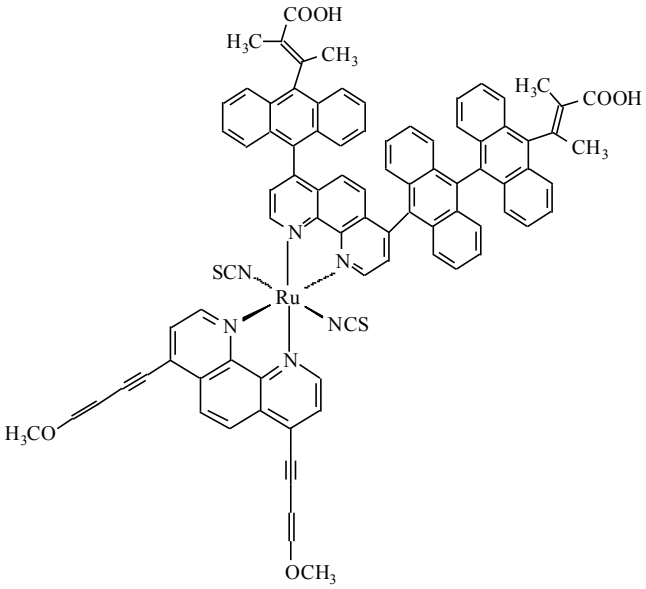

Colour: Dark-brown solid

Melting point: 252–254 ^{o}C

TLC Characteristic: R_f = 0.63 (Solvent system D).

IR (KBr, ν_{cm}^{-1}): 3550, 3472, 3414, 3236, 3052, 2925, 2853, 2107, 1972, 1637, 1618, 1543, 1496, 1435, 1385, 1304, 1256, 1162, 1119, 1094, 1028, 998, 926, 843, 800, 748, 721, 697, 619, 528, 473.

UV-Vis (λ_{max}/nm, ε = M^{-1} cm^{-1}, DMF): 343 (5490), 363 (6957), 384 (9815), 405 (10000), 461 (4140), 915 (1057), 1008 (908).

Emission: $\lambda_{exc.}$ = 550 nm, $\lambda_{em.}$ = 690 nm.

^{1}H NMR (DMSO-d_6): δ 8.53 (d, *J* = 2.8 Hz, 1H), 8.52 (d, *J* = 2.8 Hz, 1H), 8.17 (d, *J* = 2.2 Hz, 4H), 7.79 (dd, *J* = 2.8, 6.8 Hz, 8H), 7.62 (d, *J* = 4.0 Hz, 2H), 7.58 (d, *J* = 11.2 Hz, 2H), 7.56 (d, *J* = 8.0 Hz, 2H), 2.08 (s, CH_3).

Elemental Analysis: Found: C, 72.52; H, 4.46; N, 5.63. Requires: $C_{88}H_{60}N_6O_6S_2Ru$, Calculated: C, 72.26; H, 4.13; N, 5.75, S, 4.38.

Percentage yield: 0.45 g, 28 %

2.7.26. Characterization of cis-dithiocyanato-4,7-bis(2,3-dimethylacrylic acid)-1,10-phenanthroline-4,7-bis(9-trianthracenyl-10-(2,3-dimethyl acrylic acid)-1,10-phenanthroline-ruthenium(II) complex (C16)

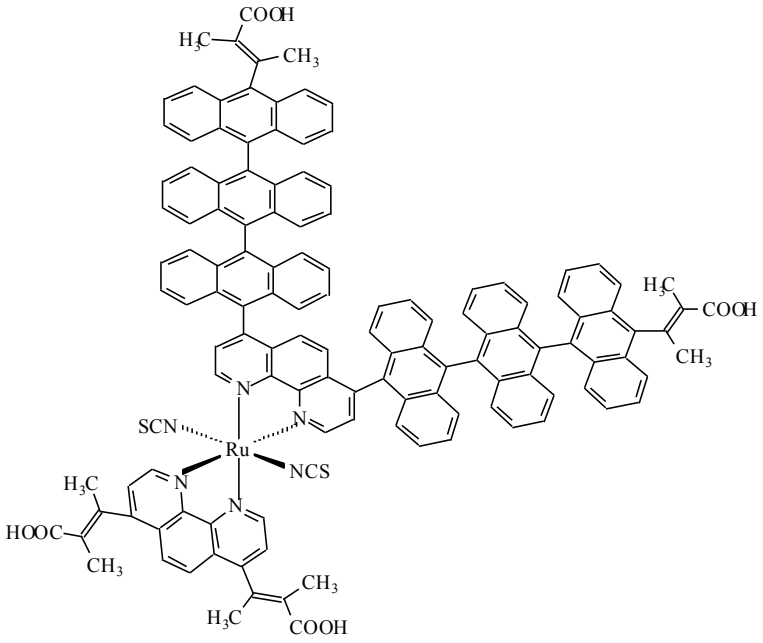

Colour: Dark-brown solid

Melting point: 240–243 °C

IR (KBr) $\nu_{cm\text{-}1}$: 3413, 3070, 2925, 2851, 2087, 1941, 1677, 1591, 1515, 1443, 1384, 1352, 1332, 1169, 1082, 935, 890, 830, 809, 769, 694, 621, 583, 466, 444.

UV-Vis (λ_{max}/nm, ε = M^{-1} cm^{-1}, $CHCl_3$-MeOH): 317 (7566), 342 (7890), 360 (9123), 380 (8134), 446 (2702), 896 (1419), 1003 (1000).

Emission: $\lambda_{exc.}$ = 470 nm, $\lambda_{em.}$ = 745 nm.

^{1}H NMR (400 MHz, DMSO-d_6): δ 9.38 (d, *J* = 14.80 Hz, 1H), 8.99 (d, s, 2H), 8.81 (d, *J* = 2.00 Hz, 2H), 8.70 (dd, *J* = 8.41, 1.87 Hz, 2H), 8.66 (d, *J* = 7.98 Hz, 3H), 8.46 (d, *J* = 8.49 Hz, 3H), 8.30 (d, *J* = 3.61 Hz, 3H), 8.22 (dd, *J* = 5.53, 3.36 Hz, 9H), 7.94 (dd, *J* = 5.47, 3.30 Hz, 14H), 7.88 (d, *J* = 8.66 Hz, 4H), 1.23 (s, CH_3)

^{13}C NMR: δ 183.2, 134.9, 134.1, 133.5, 130.8, 130.4, 129.7, 129.6, 128.9, 128.7, 128.4, 127.3, 126.3, 123.0, 122.6, 122.1, 121.7, 121.4.

Electrochemistry: E_{anodic}/V = 0.17, Ru^{2+}/Ru^{3+} = 0.63 V; $E_{1/2}$/V = -0.27, -0.45, -0.86.

Elemental Analysis: Found: C 77.23, H 4.73, N 4.34; requires: $C_{130}H_{88}N_6S_2O_8Ru$; C 77.02, H 4.38, N 4.15.

Percentage yield: 0.13 g, 42 %

2.8 Discussion of Results: Ligands and Ru(II) Homo and Heteroleptic Complexes Containing Substituted Bipyridine and Phenanthroline Ligands

2.8.1. Synthesis of 2,2'-bipyridyl and 1,10-phenanthrolyl derivatives

Functionalized anthracene, 2,2'-bipyridine and 1,10-phenanthroline derivatives were synthesized as outlined in Schemes 2.1–2.12. The initial aromatic substitution of one of the bromide ion on 9,10-dibromoanthracene with 2,3-dimethylacrylic acid was successful due to the fact that we were able to find a satisfactory solvent system combination (50 %, dichloromethane – benzene), to overcome the poor solubility property of 9,10-dibromoanthracene in common organic solvents (Scheme 2.1). The subsequent dehalogenation procedure was carried out according to a well established procedure under a high temperature, and palladium catalyzed cross-coupling reaction method [405].

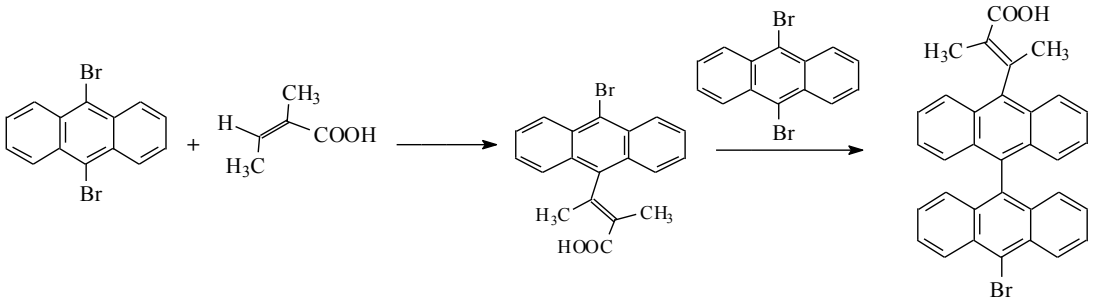

Scheme 2.1 Synthesis of 9-Bromo-10-(2,3-DMAA)-anthracene and 9-Bromo-10-(2,3-DMAA)-dianthracene.

The synthesis of the 2,2'-bipyridine and 1,10-phenanthroline derivatives was carried out by the initial introduction of required bromine functions on the polypyridine under an environmentally benign condition as reported by Vyas and co-

workers [404]. This method affords the 4-bromo-2,2'-bipyridine, 4,7-dibromo-1,10-phenanthroline and 5-bromo-1,10-phenanthroline (Scheme 2.2).

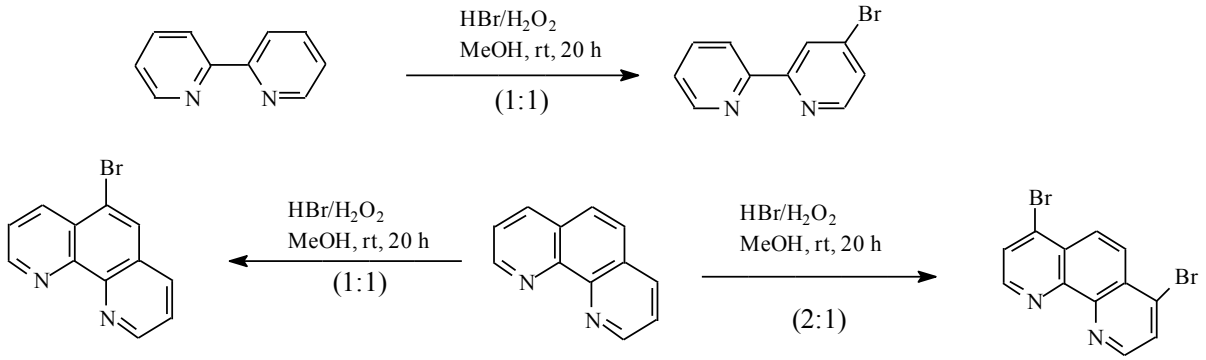

Scheme 2.2: Cold synthesis of bromo-bipyridyl and phenanthroly derivatives

Ligands **L1**, **L3,** and **L4** were obtained by one step nucleophilic aromatic substitution reaction of the bromide group of 4-bromo-2,2'-bipyridine and 4,7-dibromo-, and 5-bromo-1,10- phenanthroline with 2,3-dimethylacrylic acid respectively according to Schemes 2.3. The yield of **L1**, **L3** and **L4** was high and all the ligands have good solubility property in common organic solvents.

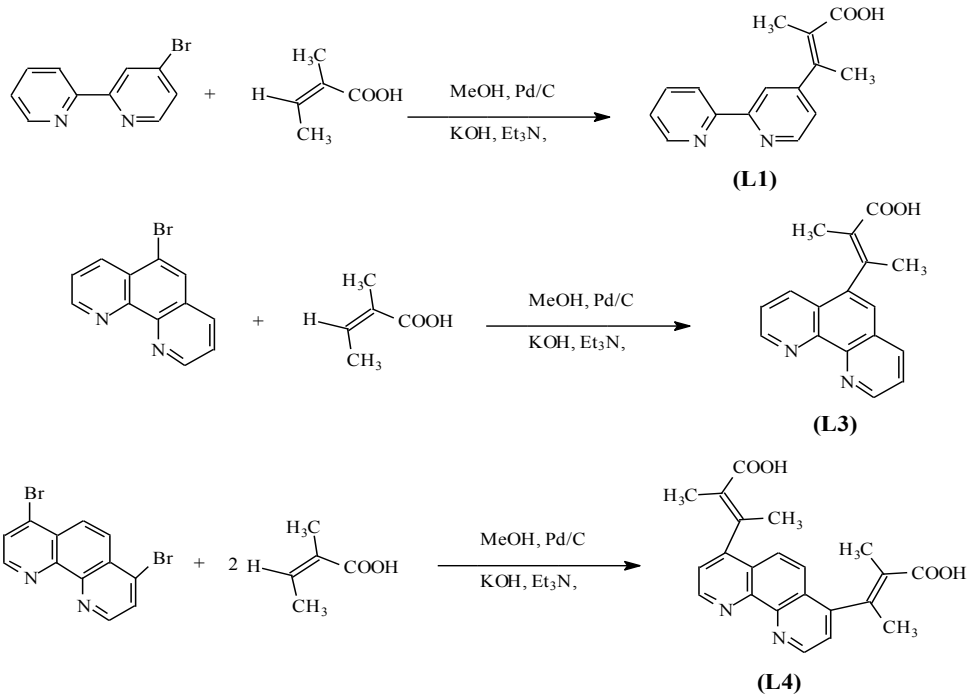

Scheme 2.3: Synthesis of 2,3-dimethylacrylic acid substituted bipyridine and phenanthroline derivatives

The synthesis of **L2**, **L5**, and **L6**, essentially follow two major reaction steps due to the initial synthesis of a 2,3-dimethylacrylic acid functionalized anthracenyl group. Although, the reaction condition was similar to that used for non-anthracenyl containing ligands, however, the use of equivalent volume ratio of dichloromethane–benzene solvent aids in the solubilization of anthracene. It was found out that this reaction can also be reversed by first reacting halogenated polypyridine with 9,10-dibromoanthracene and a subsequent dehydrohalogenation reaction with 2,3-dimethylacrylic acid [405].

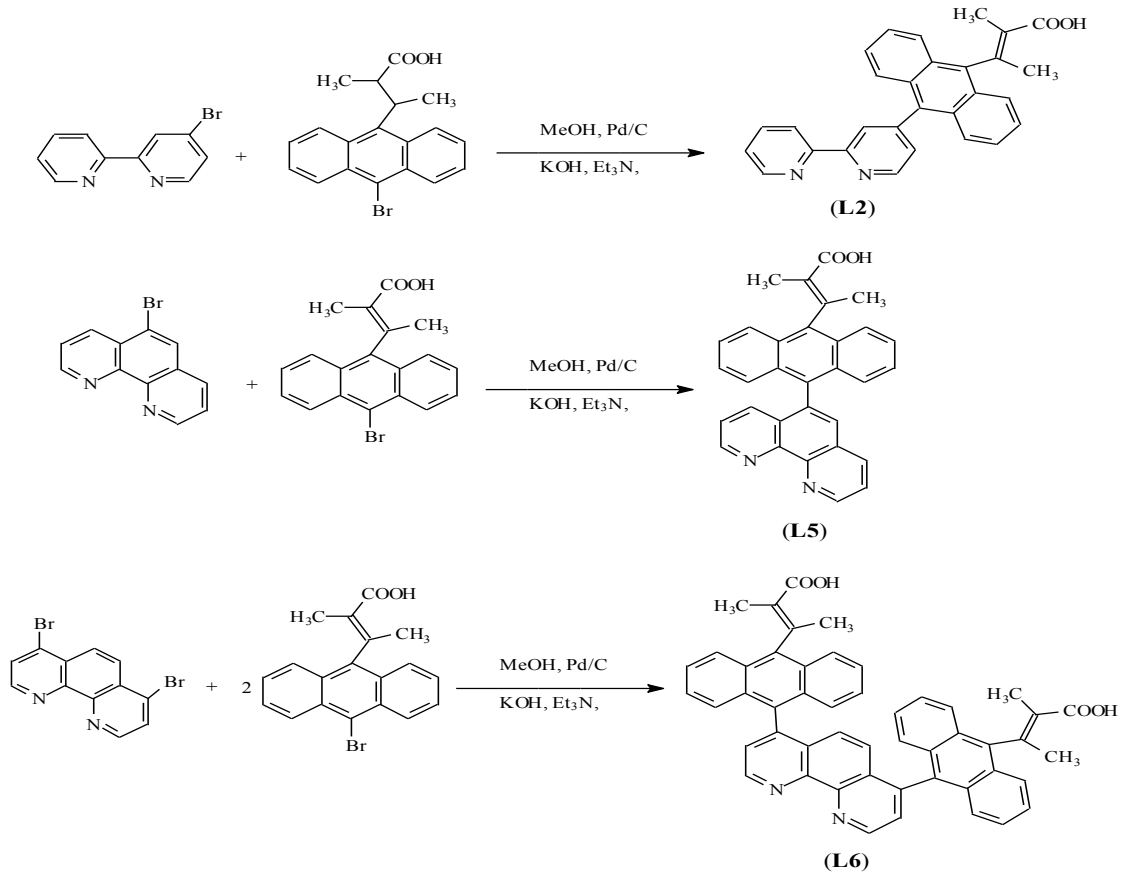

Scheme 2.4: Synthesis of functionalized anthracenyl bipyridine and phenanthroline derivatives

Multi-step reaction procedures were used in the synthesis of **L7** and **L8**. Scheme 2.5 shows the stepwise synthetic pathways; 9,10-Dibromoanthracene, 2,3-

dimethylacrylic acid and 4,7-dibromo-1,10-phenanthroline are the starting materials for **1**, **2**, **3** and **L7** following with slight modifications the well established procedures reported in the literature [256, 404, 405]. 9-Bromo-10-(2,3-dimethylacrylic acid) (**1**) was obtained when 9,10-dibromoanthracene and 2,3-dimethylacrylic acid were refluxed in a benzene/dichloromethane mixture under basic conditions using triethylamine, potassium hydroxide and palladium carbide. Further treatment of **1** with 9,10-dibromoanthracene using the same reaction conditions afforded **2** after recrystallization from diethyl ether. Reaction of **2** with 4,7-dibromo-1,10-phenanthroline in benzene/dichloromethane under palladium catalyzed cross reaction conditions gave **3**. Subsequently, a stoichiometric addition of **1** and **3** under the same reaction conditions as reported previously afford the desired **L7** as a yellowish-green solid. Similar reaction conditions were used in the synthesis of **L8**, such that 4,7-bis(9-bromoanthracenyl)-1,10-phenanthroline was first synthesized by a direct cross-coupling of 4,7-dibromo-1,10-phenanthroline with 9,10-dibromo-anthracene using a stoichiometric ratio (1:2) under palladium catalyzed reaction. The reaction between 4,7-bis(9-bromoanthracenyl)-1,10-phenanthroline and product **2** in (Scheme 2.5) afforded the desired **L8**.

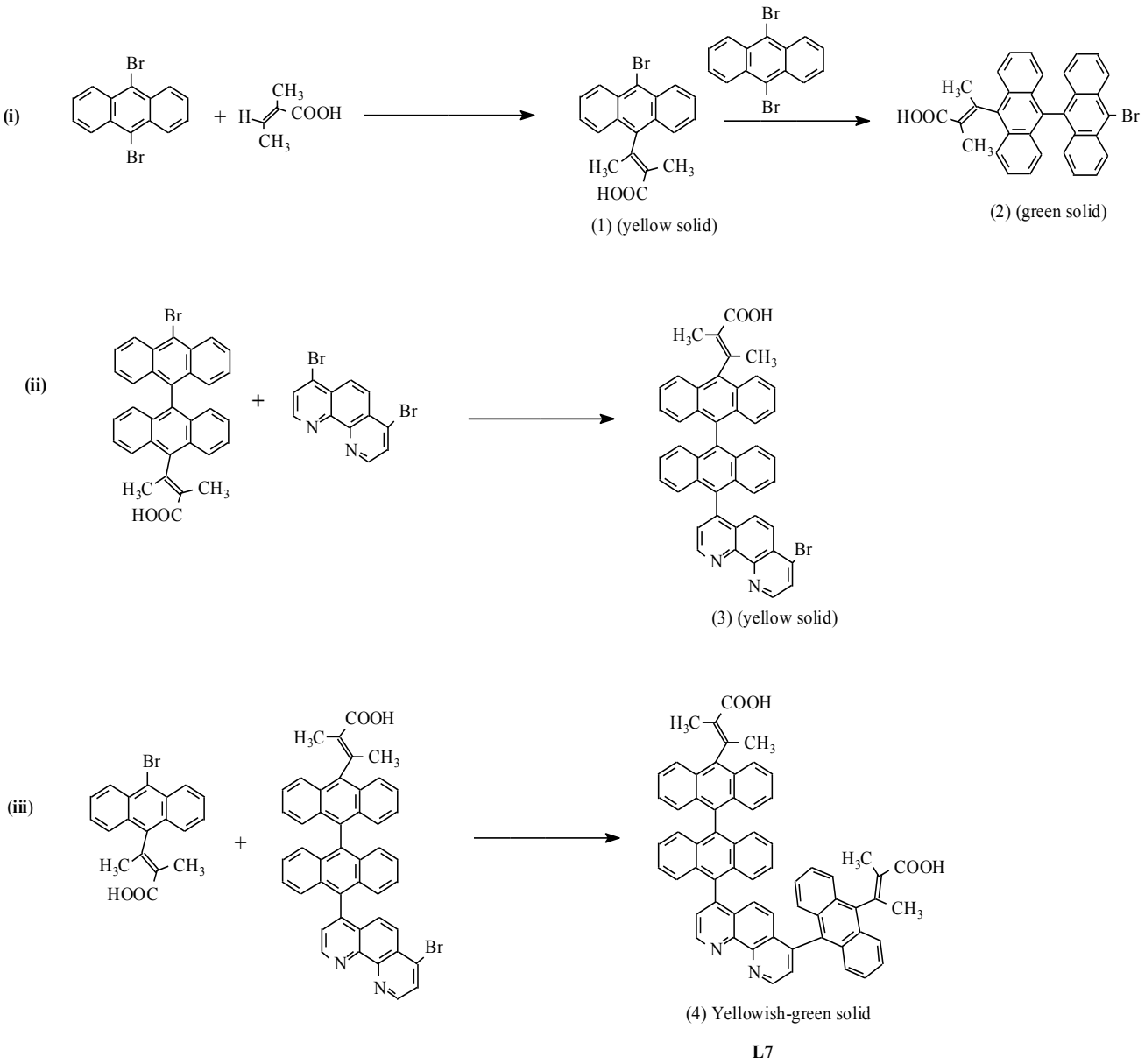

Scheme 2.5: Synthesis of single-double linked-4,7-anthracenyl disubstituted 1,10-phenanthroline.

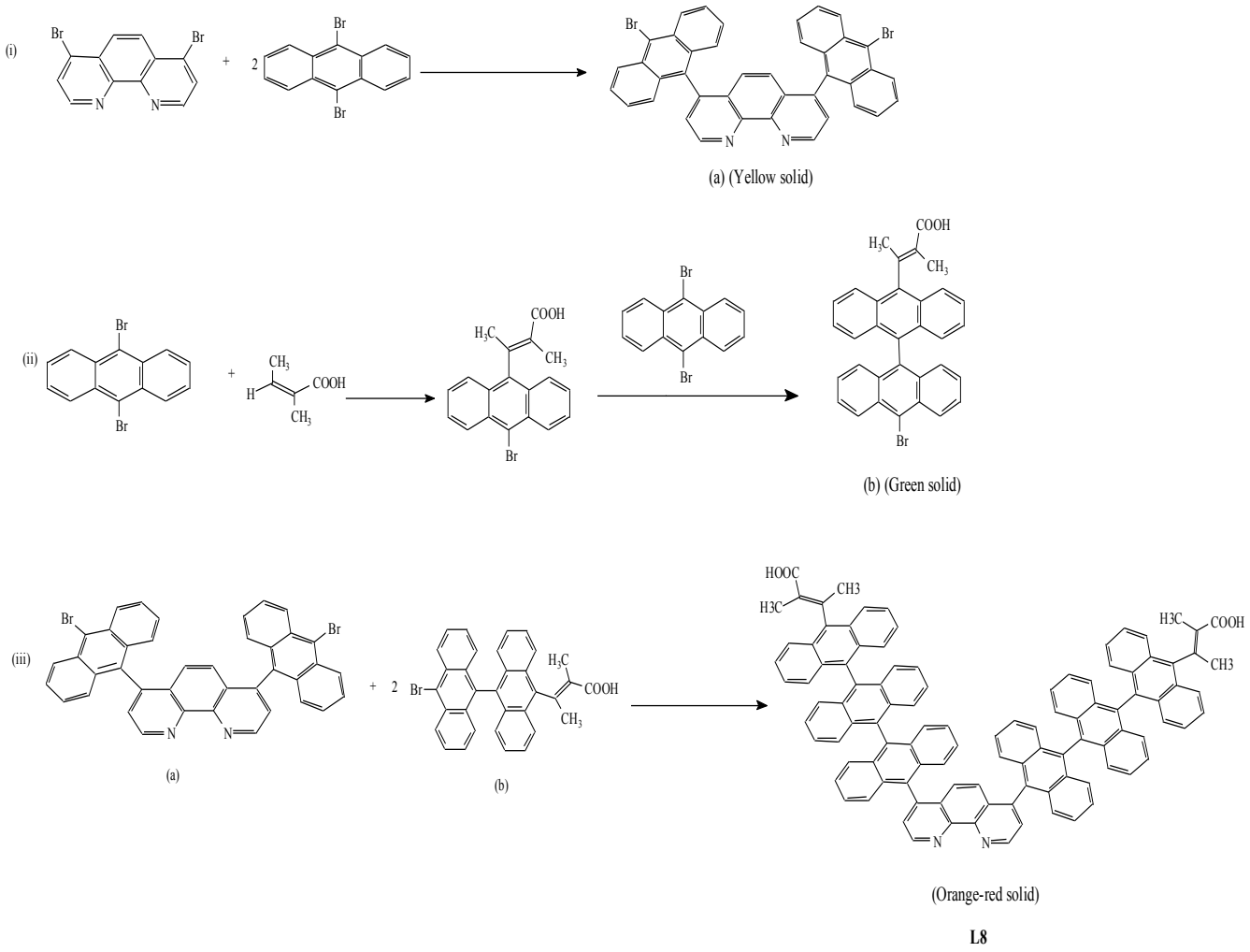

Scheme 2.6: Synthesis of a triple-triple linked 4,7-anthracenyl-disubstituted 1,10-phenanthroline

The synthesis of **L9** was carried out using the same methodology as reported for L1 but was allowed to reflux for a longer period of 72 hours before the introduction of 2,3-dimethylacrylic acid and subsequent purifications to afford a red oil (Scheme 2.7).

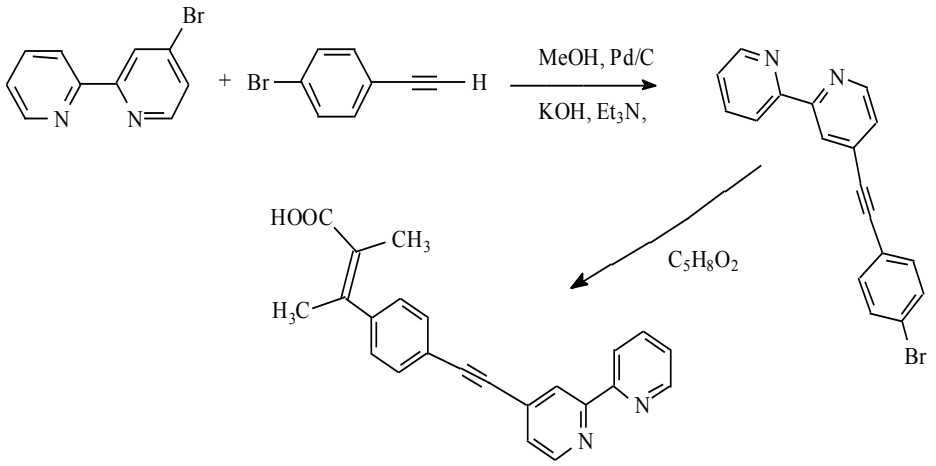

Scheme 2.7: Synthesis of 4-(1-ethynylphenyl-4-(2,3-DMAA)-2,2'-bipyridine

L10 was synthesized following the methodology reported by Venkataraman *et al*. [407]. The reaction was carried out under inert atmosphere such that the labile acetylene group is protected from air oxidation that is common to the normal type of chemical reactions. The product was isolated as a reddish-brown semi-solid.

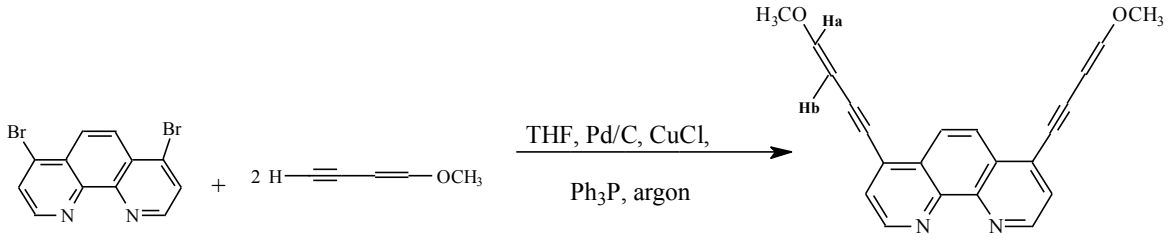

Scheme 2.8: Synthesis of 4,7-Bis(1-methoxy-1-buten-3-yne)-1,10-phenathroline

The synthesis of the metal precursor $[RuCl_2(dmso)_4]$ and all the complexes **C1**–**C16**, was carried out by following the general route shown in scheme 2.9. The first step was the coordination of the DMSO ligand with $RuCl_3(H_2O)$ followed by the sequential substitution of the dmso with synthesized ligands to obtain the intermediary complexes such as: $Ru(L_x)_3Cl_2$, $Ru(L_x)(L_y)_2Cl_2$, $Ru(Ly)_3Cl_2$ and/or $Ru(L_x)_2(L_y)Cl_2$, (where L_x and L_y = substituted 2,2'-bipyridyl or phenanthrolyl derivatives). The final step may involve either the coordination of the –NCS ligand or

the precipitation of the complex with PF_6. A solvent combination such as methanol-dimethylformamide may be required in the synthesis of the heteronuclear complexes to overcome the partial solubility of ligands in dimethylformamide. Except for the synthesis of complexes **C1**, **C4**, **C7**, **C9**, **C11**, and **C13** containing the hexafluorophosphate ions, all other complexes namely **C2**, **C5**, **C6**, **C8**, **C10**, **C12**, **C14**, **C15** and **C16** actually are synthesized in a one pot reaction since all the reagents are added in the solution at the same time, yielding the desired complexes. No isolation of any intermediary compound is required.

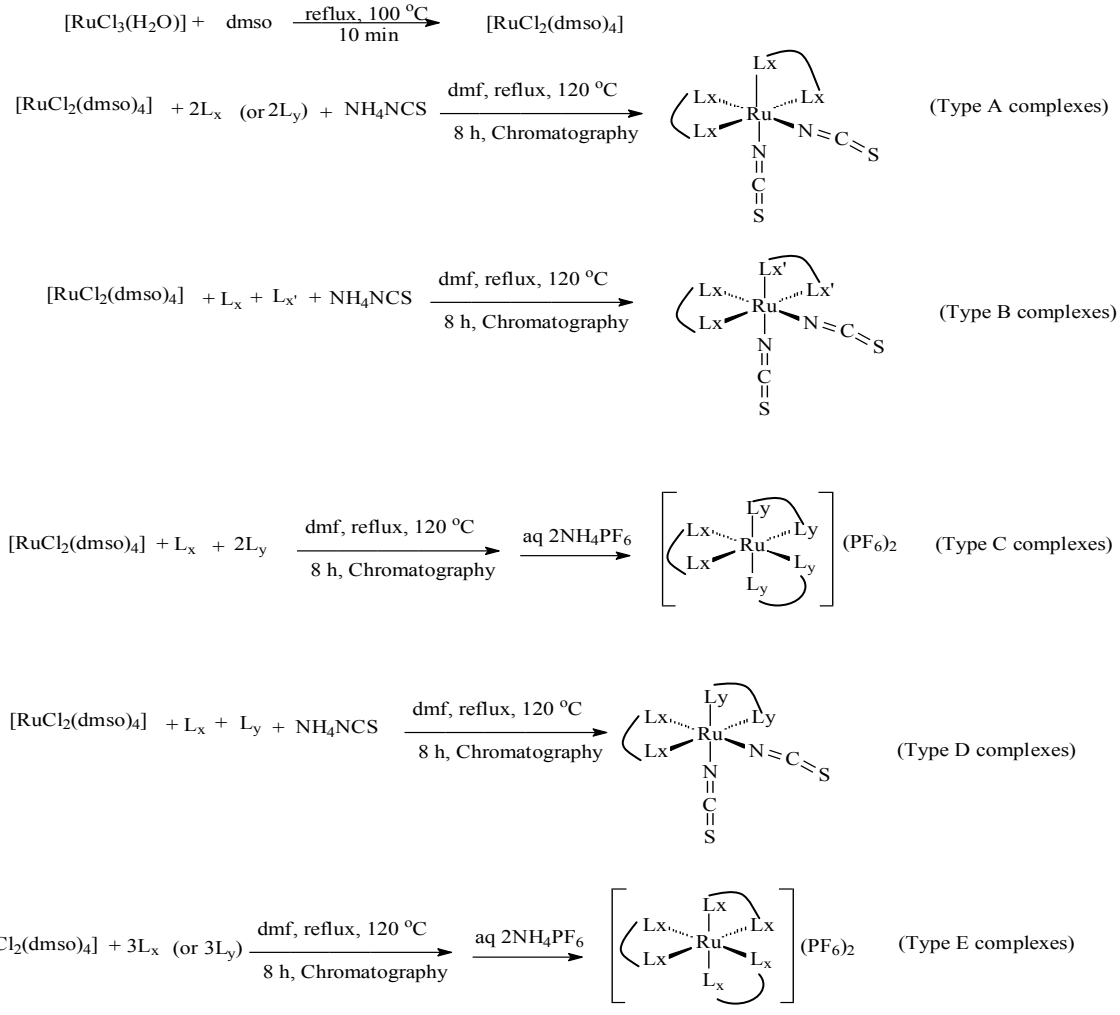

Scheme 2.9 Synthetic profiles for Ru(II) complexes of 2,2'-bipyridyl and 1,10-phenanthrolyl (Ligand combinations).

Due to similarities in the chemical structures, complexes **C1**–**C16** are grouped under following reaction types (A–E) as follows:

Type A reactions: Complexes **C2**, **C3**, **C5**, **C8 and C10**:

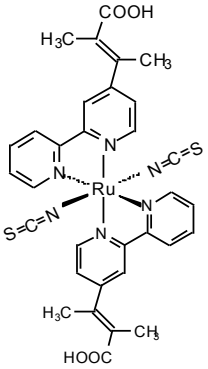

C2

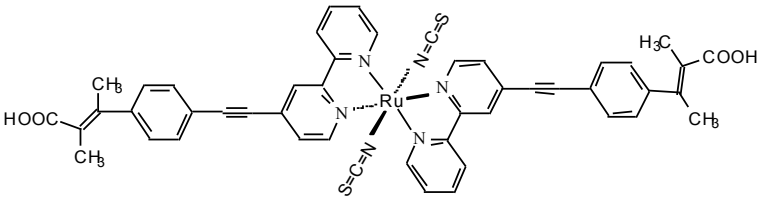

C3

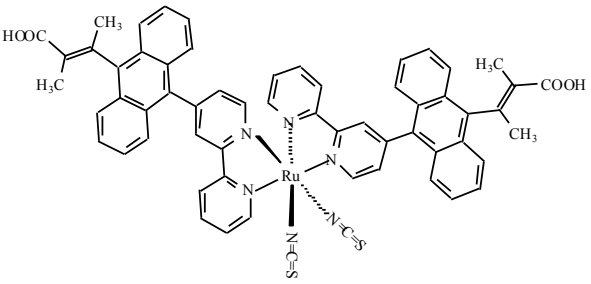

C5

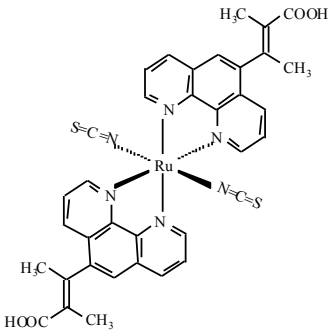

C8

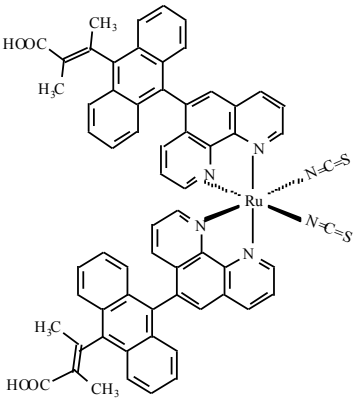

C10

Type B reactions: Complexes **C6**, **C15** and **C16**.

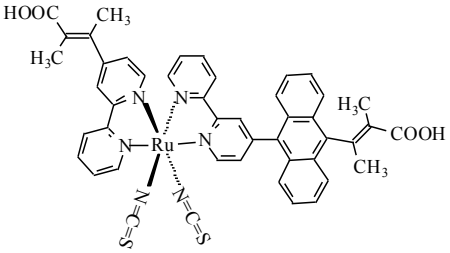

C6

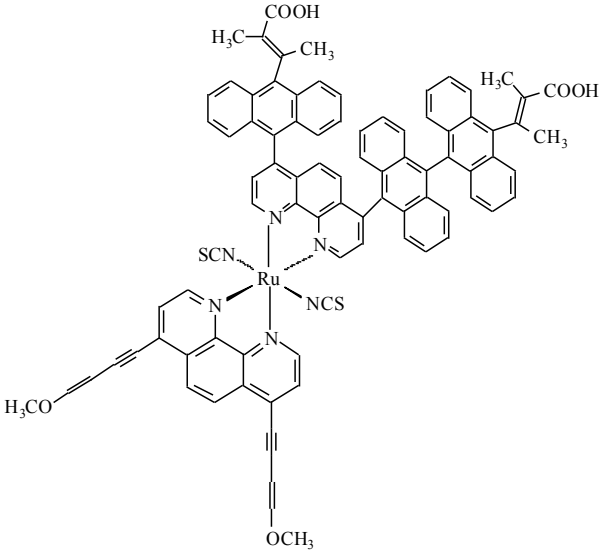

C15

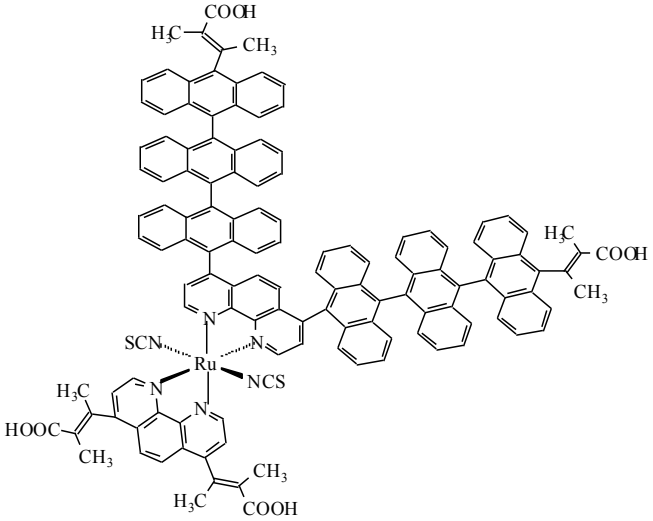

C16

Type C reactions: Complexes **C11** and **C13**

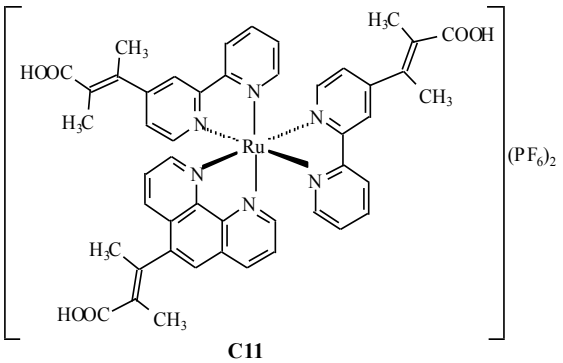

C11

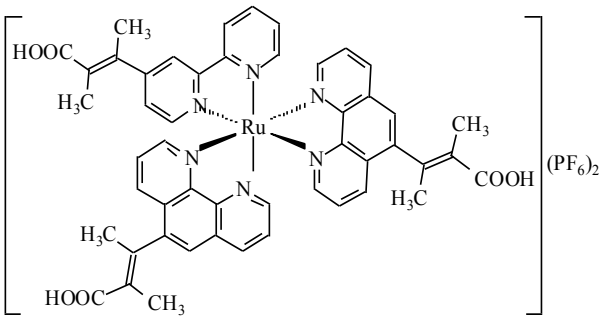

C13

Type D reactions: Complexes **C12** and **C14**

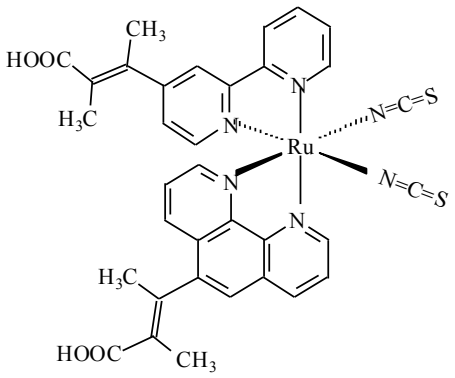

C12

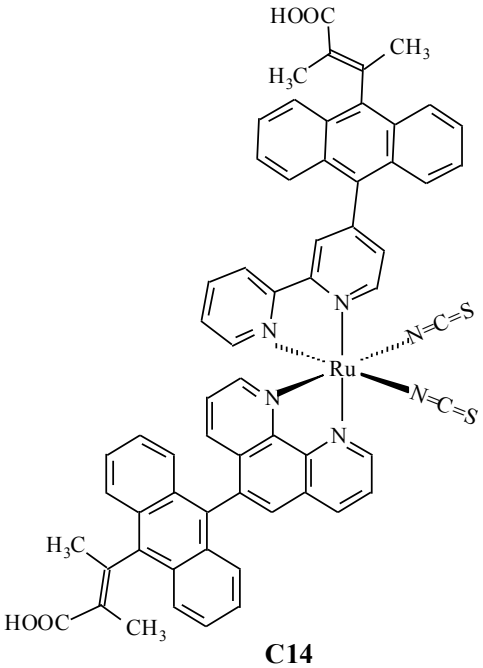

C14

Type E reactions: Complexes **C1**, **C4**, **C7** and **C9**

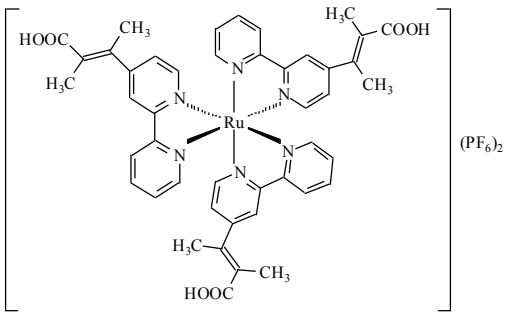

C1

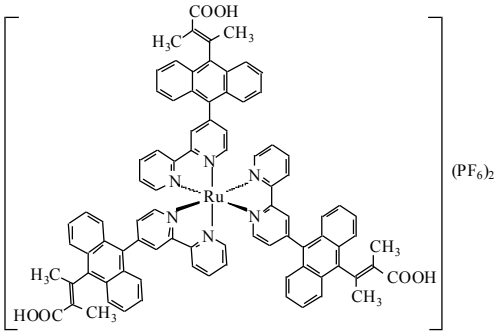

C4

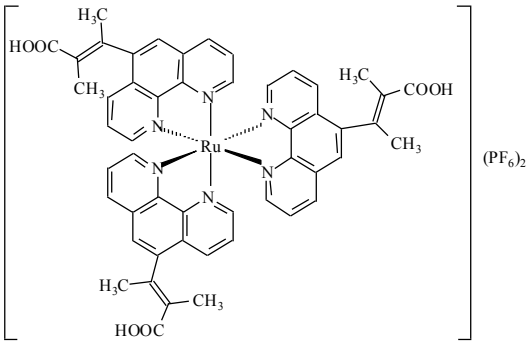

C7

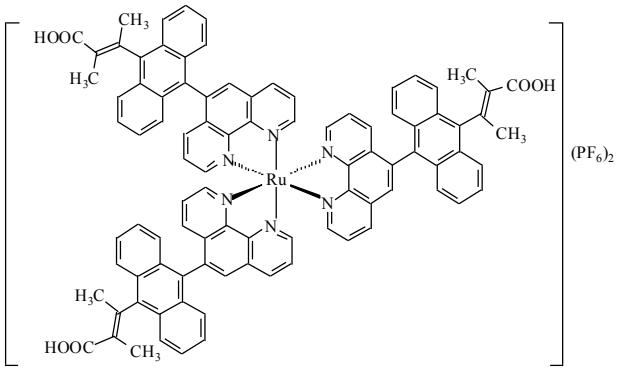

C9

2.8.2 Infrared absorption spectroscopy in relation to complex structures

The FT–IR spectra of the starting materials, the ligands and the complexes showed certain characteristic absorption bands that were compared and assigned on careful comparison. Due to structural similarities among the various ligands, a strong vibrational band between 3427–3419 cm^{-1} was found. This gave indication of the presence of an O–H group possibly from the carboxylic acid moiety in the ligands. This band, however, shifted to higher frequency at 3478 cm^{-1} in ligand **L10** which has only methoxy substituent. The vibrational frequency bands between 3076-3027 cm^{-1} may be due to the presence of α,β-unsaturated carboxylic acid and/or aromatic C–H stretching characteristics of the molecules. The band at 2928 cm^{-1} shows the presence of C–H stretching of methyl groups. In the **L9** and **L10**, the acetylene (C≡C stretching) vibration was found at 2039 cm^{-1}. This band is conspicuously absent in all other ligands. The bands at 1694, 1690, and 1622 cm^{-1} are due to carbonyl stretching and the aromatic C═C stretching band was found in the region of 1621 cm^{-1}. Bands between 1581-1502 cm^{-1} were assigned to the C═N stretching of the polypyridyl groups. The strong bands in the region 1456-1417 cm^{-1} were assigned to C–H deformation of the methyl groups and the presence of ethereal groups (C–O) in the molecules were confirmed with the bands at 1256, 1216 cm^{-1}. At the fingerprint region, the strong peak band at 926 cm^{-1} was conspicuously absent in those ligands containing no anthracenyl functionalities. This band is indicative of the C-C bond linkage between the anthracene and the bipyridine or phenanthroline ligand.

In the FT–IR spectra of the complexes, it was observed that nearly all the complexes showed an upward shift in absorption frequency for the O–H stretching vibration at 3550 cm^{-1}. No major change in frequency was observed in the region

3237-2850 cm^{-1}. The presence of thiocyanate ligand was confirmed with a vibrational band frequency at 2106 cm^{-1} in all the complexes having –NCS group coordination. This peak was absent in all homoleptic and heteronuclear complexes with no thiocyanate substitutions. One major observation noticed in the complexes containing acetylene bonds (**C3** and **C15**) was the absence of the peak at 2039 cm^{-1}.

There appear overlaps of frequency in this region with those of the thiocyanate. This could be explained in terms of the small change in the dipole moment during vibration, monosubstituted acetylenes usually show a weak band [407,410]. The bands at 1677 cm^{-1} and 1284 cm^{-1} in complex **C16** were assigned to the ν(C=O) and ν(C-O) stretching of carboxylic acid groups, respectively. A common absorption frequency band at 1638 cm^{-1} (antisymmetric $–COO^-$ stretch) which tends to overlap with the C=C stretch present in all the complexes except **C16** gave indication that a partial deprotonation of the ν_{asym}(COO) might be expected.

However, C=C and C=N stretching bands of the bipyridyl and phenanthrolyl ligands appear near 1600 cm^{-1} making it difficult to determine if the carboxylated polypyridyl ligands are fully protonated or only partially protonated on this basis. The band around 1384-1400 cm^{-1} was assigned to the carboxylate symmetric ν(-COO-) of the carboxylic acid group. Furthermore, peaks in the region 770 and 730 cm^{-1} demonstrate the existence of four adjacent hydrogen atoms common to the anthracenyl ligands and their corresponding complexes. All vibrational peaks in the region are found relatively weak and broad in the complexes, which may be ascribed to the loss of crystallinity and the broad distribution of the anthracene chain length [410]. The weak absorption frequencies between 466 and 444 cm^{-1}, respectively, show the coordination of nitrogen atoms of the ancillary ligands to ruthenium central metal atom [253].

2.8.3. UV-Vis absorption and Emission spectroscopy

2.8.3.1 UV-Vis absorption and Emission spectra of Type A reaction complexes

The solution electronic spectra of Type A reaction complexes were recorded in 300–1100 nm range in dimethylformamide. The absorption spectra of all the complexes are dominated by metal-to-ligand charge transfer transitions (MLCT). This broad MLCT band appears between 400 and 700 nm. Complex **C2** showed three absorption wavelengths at 351, 506 and 674 nm compared to **C3**, **C5** and **C8** with only two major absorption wavelengths at 376, 536 nm; 367, 529 nm; and 416, 443 nm respectively. In complex **C10**, apart from the broad MLCT band at 507 nm, the vibronic peaks of anthracene molecule were found at 345, 362, 383 and 405 nm (Figure 2.1). These peaks were not well defined in **C5** due to a very low molar extinction coefficient property of the complex. Though, in terms of molar extinction coefficient, **C8** gave the highest value, but with corresponding lowest absorption wavelength among the complexes.

The influence of anthracene was found in the **C10**, the absorption wavelength covered a large area of the visible spectrum concomitant with good molar extinction coefficient. In general, for these types of complexes, we assume that absorption wavelengths in particular may not only be governed by the extension of π-bond conjugation but other characteristics such as the substituent positions on ligand and the ligand types play significant roles.

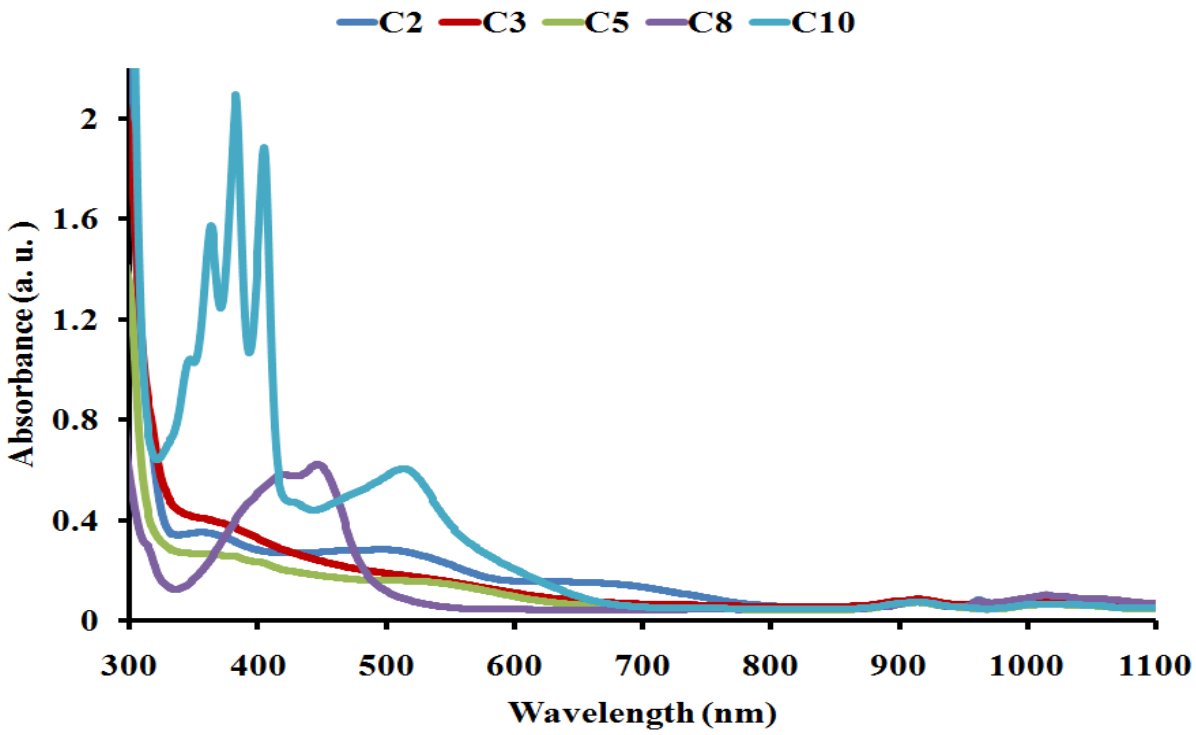

Figure 2.1 Comparison of the UV-Vis absorption spectra of Ru(II) mono–substituted bipyridine and phenanthroline complexes

The emission spectra of the complexes are displayed in Figure 2.2. All the complexes at a concentration of 1.0 x 10^{-4} M solution in DMF show photoluminescence properties at room temperature. The complexes were excited at 450 nm wavelength and the luminescence maxima are located at 683, 745, 709, 701 and 663 nm for complexes **C2**, **C3**, **C5**, **C8** and **C10** respectively. In terms of molecular structure of complexes, complex **C3** having a double–triple bond conjugation displayed the highest emission wavelength at 745 nm. We assumed that the presence of this conjugative bond had a significant effect on the π→π* orbital energy. The emission wavelength of **C5** at 709 was blue-shifted (*ca* = 8 and 16 nm) in **C8** and **C10** respectively, with corresponding decrease in the intensity ratio. This

result shows that functionalized anthracenyl bipyridyl complexes have better photoluminescence properties than those of the phenanthrolyl complexes.

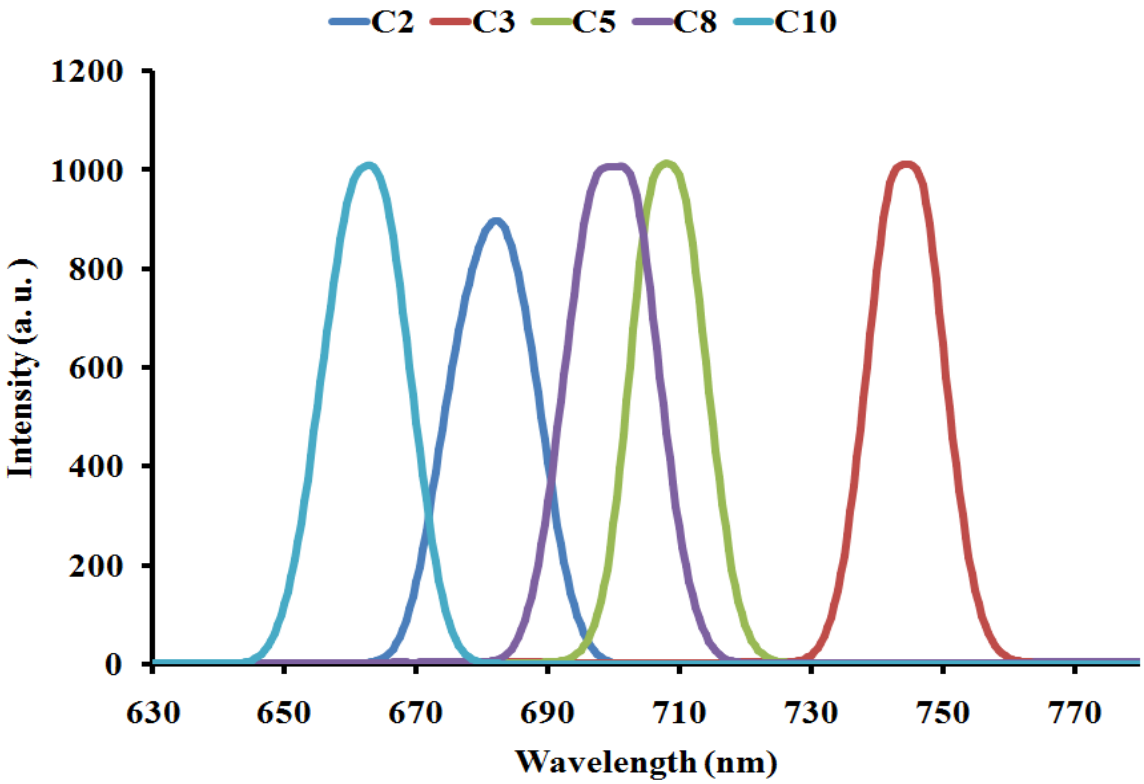

Figure 2.2 Comparison of the Emission spectra of Ru(II) mono–substituted bipyridine and phenanthroline complexes

2.8.3.2. UV-Vis and Emission spectra of Type B reaction complexes

The UV-Vis absorbance and emission spectra of the Type B reaction complexes in dimethylformamide are displayed in Figure 2.3 and 2.4 respectively. In the UV-region, all the complexes (**C6**, **C15** and **C16**) display four distinct vibronic peaks for the intra ligand ($\pi \rightarrow \pi^*$) charge transfer transitions characteristics of anthracene derivatives at 360, 374 and 403 nm for **C6**; 343, 363, 384 and 405 nm for **C15**; 341, 360 and 379 nm for **C16**. The complexes show broad and intense absorption bands between 419 and 600 nm with wavelength maxima at 503, 461 and 443 nm for **C6**, **C15** and **C16** respectively. These absorption bands were due to

the metal–to–ligand charge transfer transition (MLCT) of the complexes. The molar extinction coefficient was found to decrease with corresponding increase in the number of anthracene units in the molecules, such that **C6** with only one anthracenyl unit showed the best molar efficiency value (ε = 4543 $M^{-1}cm^{-1}$) compared to (ε = 4140 and 2702 $M^{-1}cm^{-1}$) for **C15** and **C16** respectively.

In terms of molecular structure, **C15** contained half the value of the number of anthracene units as found in **C16**, however, it could be seen that the influence of a double–triple bond conjugation had a great influence on the molar absorptivity coefficient, thus it could be taken that the distance transfer of electronic energy through anthracene may have been obstructed due to molecular aggregation [406, 413]. In the long wavelength tail of the absorption spectra, small but significantly distinct shoulders at 915 nm (ε = 1057), and 1008 nm (ε = 908) were observed. These absorption features are thought to correspond to the lowest ^{3}MLCT excited states [5].

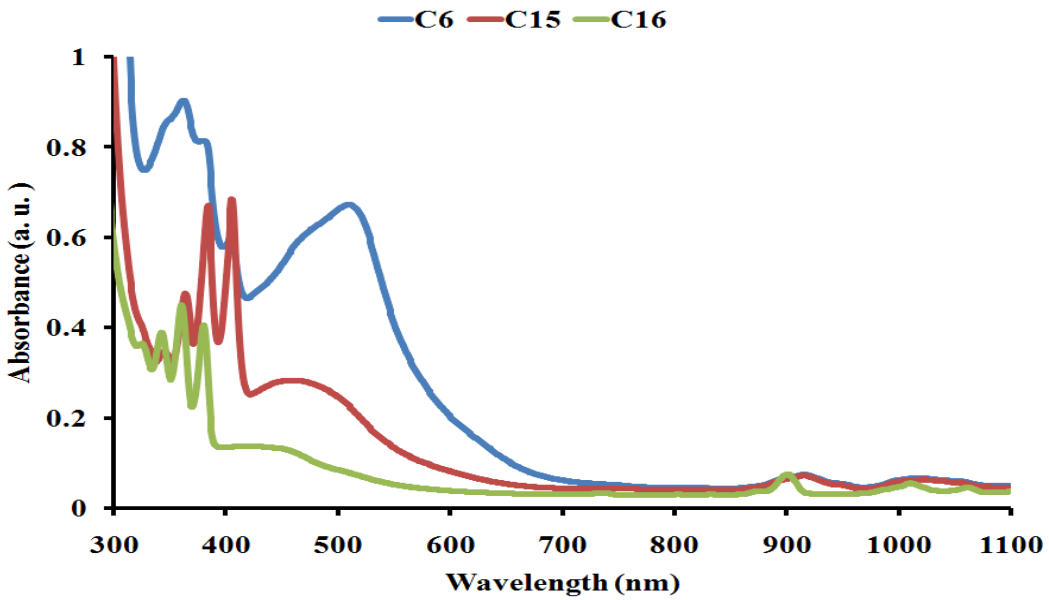

Figure 2.3 Comparison of the UV-Vis absorption spectra of heteroleptic Ru(II) bipyridine and phenanthroline complexes

The emission spectra of complexes **C6**, **C15** and **C16** are displayed in Figure 2.4. Upon excitation into the ^{1}LC and ^{1}MLCT bands (λ_{exc} = 550 nm), the complexes display appreciable luminescence at room temperature. Emission maxima (λ_{max}, nm) for the complexes are found at 673, 690 and 743 nm for **C6**, **C15** and **C16** respectively. The emission intensity was found to decrease with increase in the number of anthracene units in the molecule as this could be related to molecular weight of complexes [406]. It is well known that conjugated functional organic molecules are useful for the study of electron transport at the molecular scale and that the use of fused-ring systems is a powerful and practical approach. It could be seen in the complexes that the choice of ligand has significant effects on the energy ordering of the low energy excited state and, in particular to the orbital nature of the lowest excited state which also influence the positions of the metal centre (MC), ligand centre (LC) as well as the MLCT of the complexes.

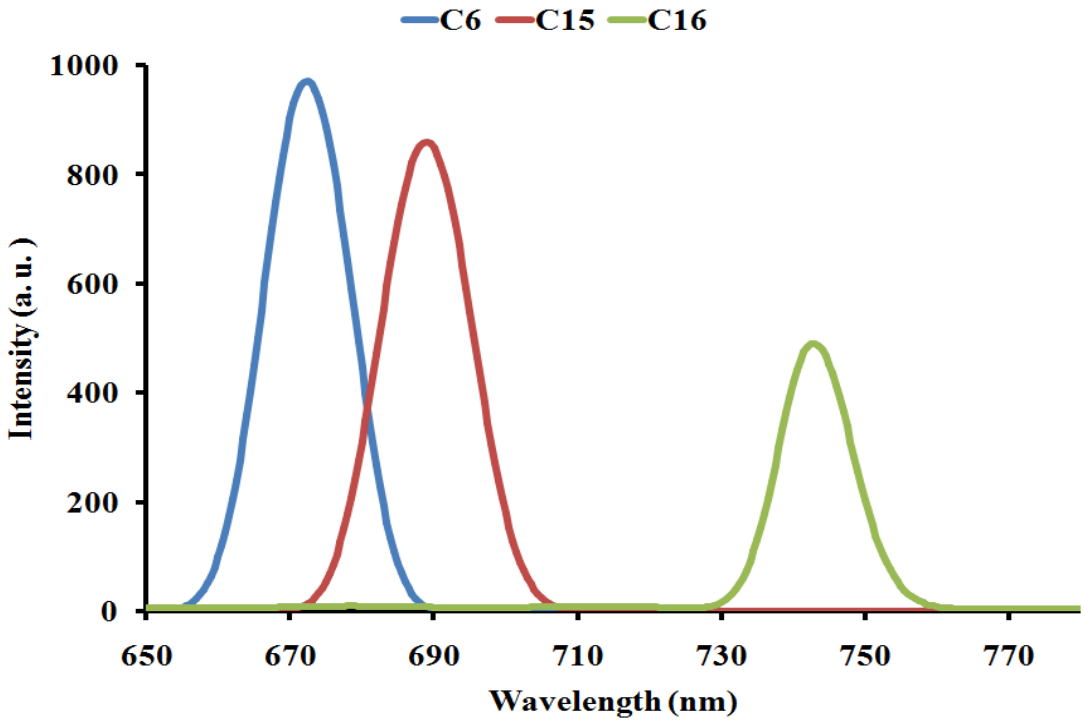

Figure 2.4 Comparison of the Emission spectra of heteroleptic Ru(II) bipyridine and phenanthroline complexes

2.8.3.3. UV-Vis and Emission spectra of Type C reaction complexes

The UV-Vis absorption spectra of **C11** and **C13** are displayed in Figure 2.5. The spectra are found almost overlapping each other and are dominated by the metal–to–ligand charge transfer transitions (MLCT) in the range 400–500 nm. Both complexes showed typical visible absorption wavelength maxima at 451 nm. Based on the molecular structures of the two complexes, much difference could not be found since **C11** was coordinating with two functionalized molecules of bipyridyl and one phenanthroline, vis-a-vis **C13**, coordinating with two phenanthroline and one bipyridyl. The influence of the extension of π-bond conjugation through phenanthroline in **C13** could not be observed. The anchoring ligands in the two complexes are the same.

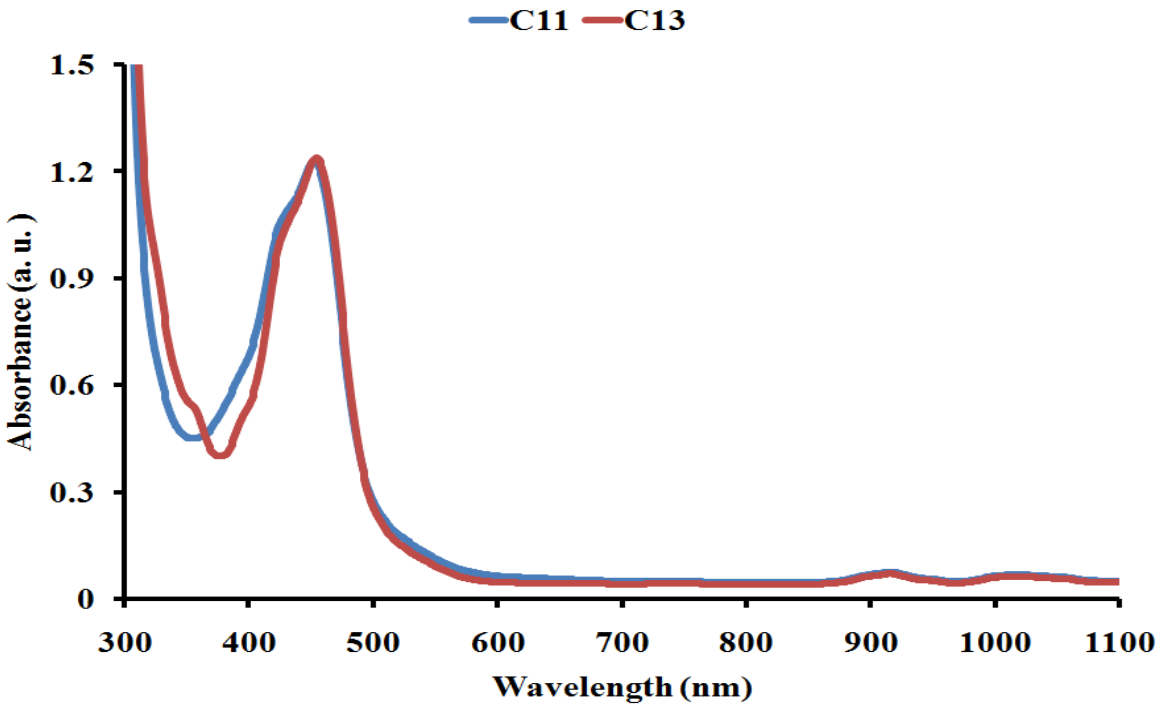

Figure 2.5 Comparison of the UV-Vis absorption spectra of heteronuclear Ru(II) bipyridine and phenanthroline complexes

The two complexes display appreciable photoluminescence properties at room temperature. The emission spectra are displayed in Figure 2.6. Emission of **C11** peaks at 658 nm and attained maxima wavelength at 673 nm. The influence of a small increase in conjugation length was however noticed in **C13**, which peak up at 667 nm and attained maxima wavelength at 682 nm.

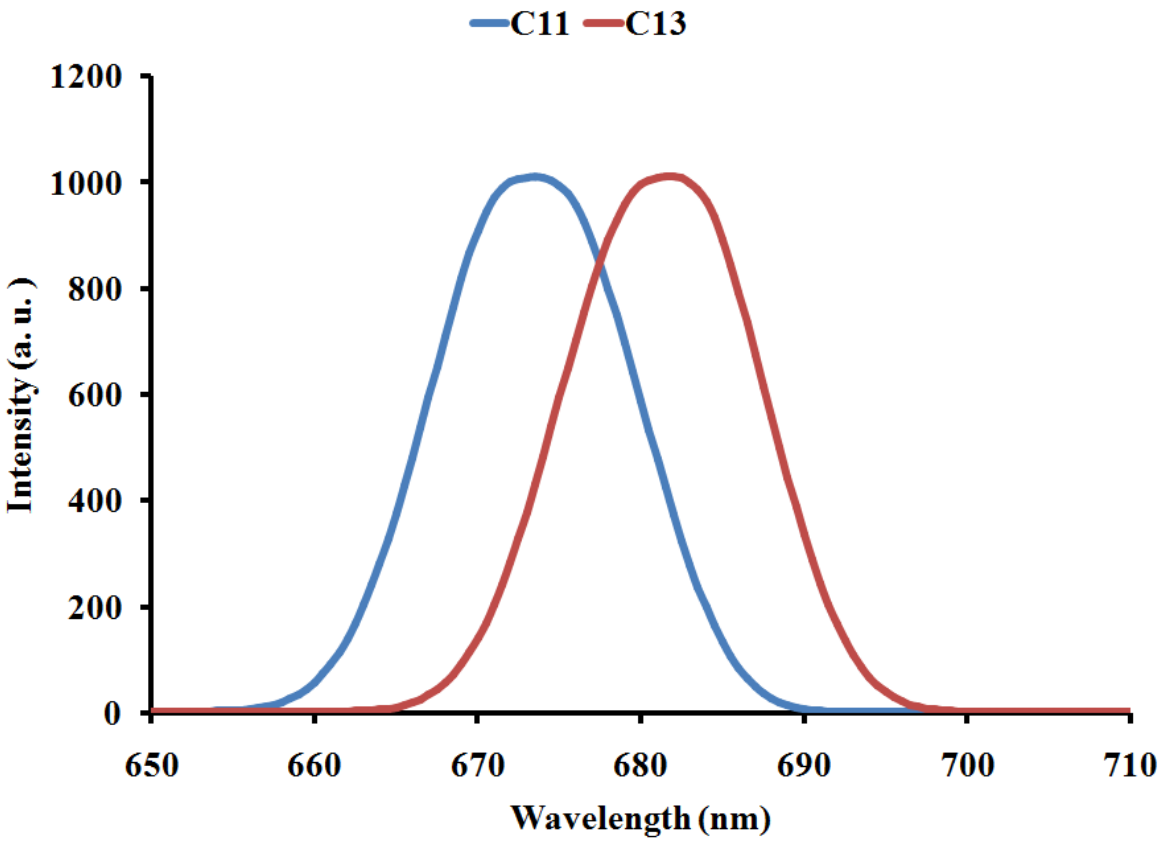

Figure 2.6 Comparison of the Emission spectra of heteronuclear Ru(II) bipyridine and phenanthroline complexes

2.8.3.4. UV-Vis and Emission spectra of Type D reaction complexes

The absorption spectra of both complexes **C12** and **C14** of the type D reaction are displayed in Figure 2.7. The sensitizers show the expected broad and intense MLCT absorption band in the visible region of 400 – 650 nm characteristics of ruthenium(II) polypyridyl complexes which can be assigned from the metal centre

based t_2g orbital to the lowest bipyridyl and phenanthrolyl ligand based π* orbital. For this series, the MLCT transition of **C12** at 502 nm is red-shifted to 507 nm in **C14**. The molar extinction coefficient value at this region for **C12** (ε = 6970 M^{-1} cm^{-1}) is far greater than that recorded for **C14** (ε = 3874 $M^{-1}cm^{-1}$). This we thought could be due to the presence of anthracenyl which displayed its vibronic peaks in the region between 345 – 405 nm. A small but significant absorption peaks at 352 and 421 nm (ε = 4808 and 4045 $M^{-1}cm^{-1}$) for **C12** and **C14** respectively are assigned to the second metal–to–ligand charge transfer transitions (MLCT) based on the premise that two different types of ligands are coordinating to the Ru(II) metal centre.

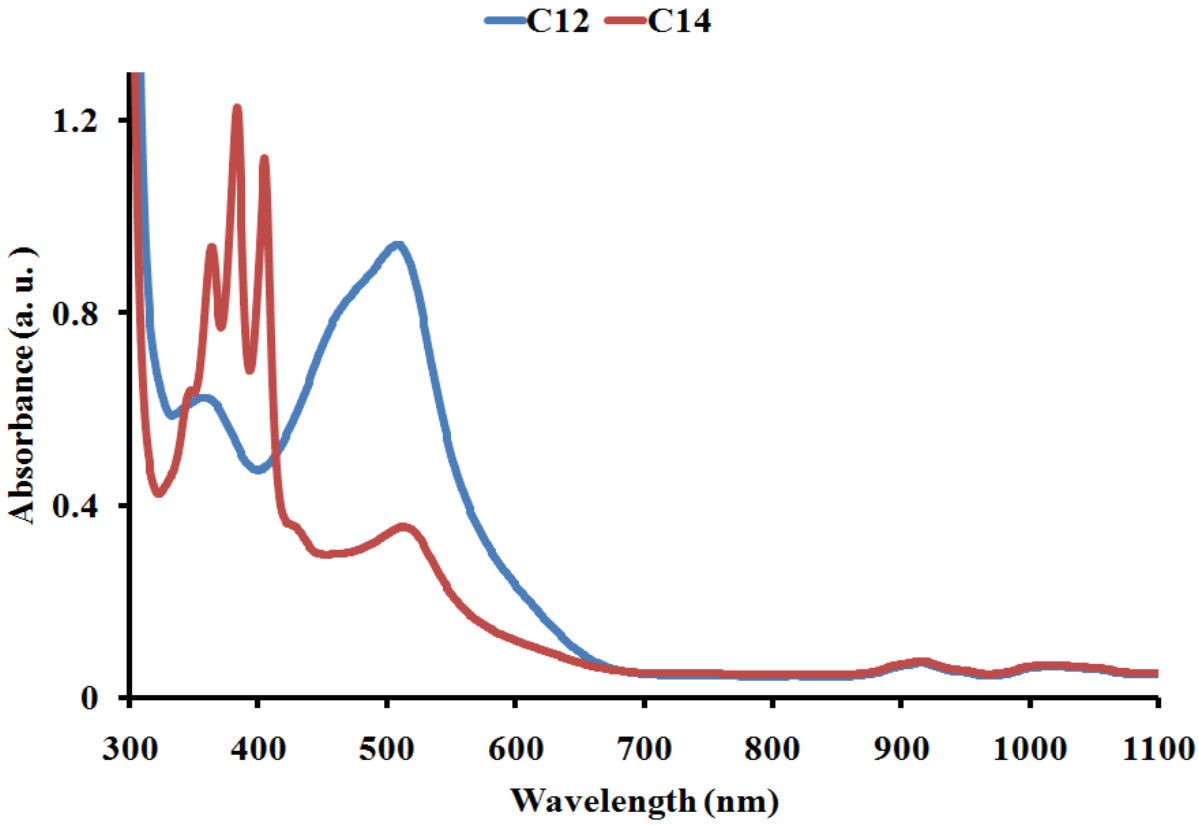

Figure 2.7 Comparison of the UV-Vis absorption spectra of heteronuclear Ru(II) functionalized anthracenyl/(non-anthracenyl) bipyridine and phenanthroline complexes

The two complexes display photoluminescent emission characteristics similar to those reported earlier for **C11** and **C13** above. The λ_{max} for **C12** and **C14** are found respectively at 686 and 683 nm. The spectra are shown in Figure 2.8.

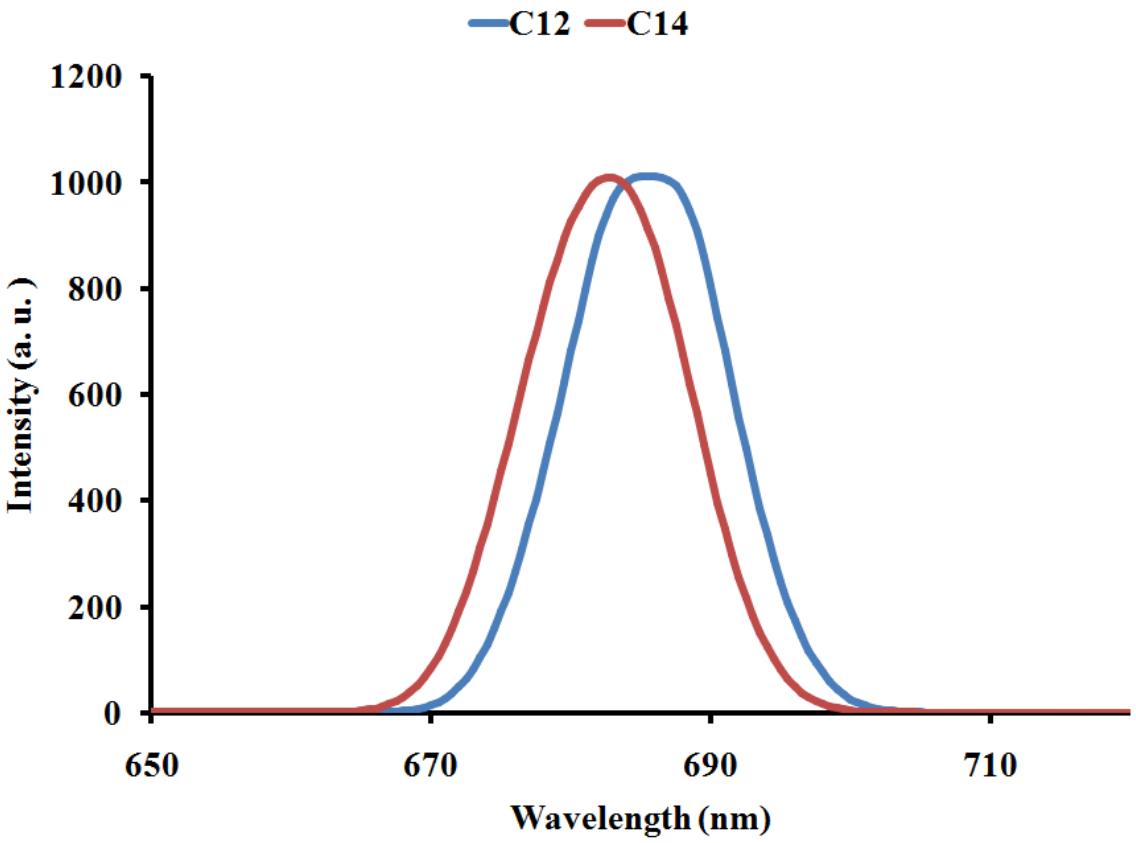

Figure 2.8 Comparison of the Emission spectra of heteronuclear Ru(II) functionalized anthracenyl/(non-anthracenyl) bipyridine and phenanthroline complexes.

2.8.3.5. UV-Vis and Emission spectra of Type E reaction complexes

The Type E reaction complexes are homonuclear ruthenium(II) complexes that are precipitated with ammonium hexafluorophosphate. The UV-Vis spectra are displayed in Figure 2.9 below. At the UV-region, 200-300 nm, contained the π→π* intra ligand absorption for the bipyridyl and phenanthroly ligands. This region is not shown here in the spectra. The near-visible region between 350-405 nm was

occupied by the vibronic absorption peaks for the substituted anthracene. The vibronic peaks were of higher intensity in **C9** for a substituted phenathroline ligand than its counterpart **C4**, containing the bipyridyl ligand. The peaks were not found in both **C1** and **C7** complexes. At the visible region, 410–520 nm, all the complexes show the metal–to–ligand charge transfer transitions (MLCT) characteristics of a Ru(II) complexes. For the bipyridyl ruthenium(II) complexes (**C1** and **C4**), virtually, the wavelength differ by only 1 nm (445 and 446 nm) respectively, but higher molar extinction coefficient is recorded for **C4**. The opposite could be said for the phenanthroline complexes as found in **C7** and **C9**. By comparison, complex **C9** absorption maximum wavelength at 451 nm which is blue-shifted (*ca* = 5 nm) in **C7**.

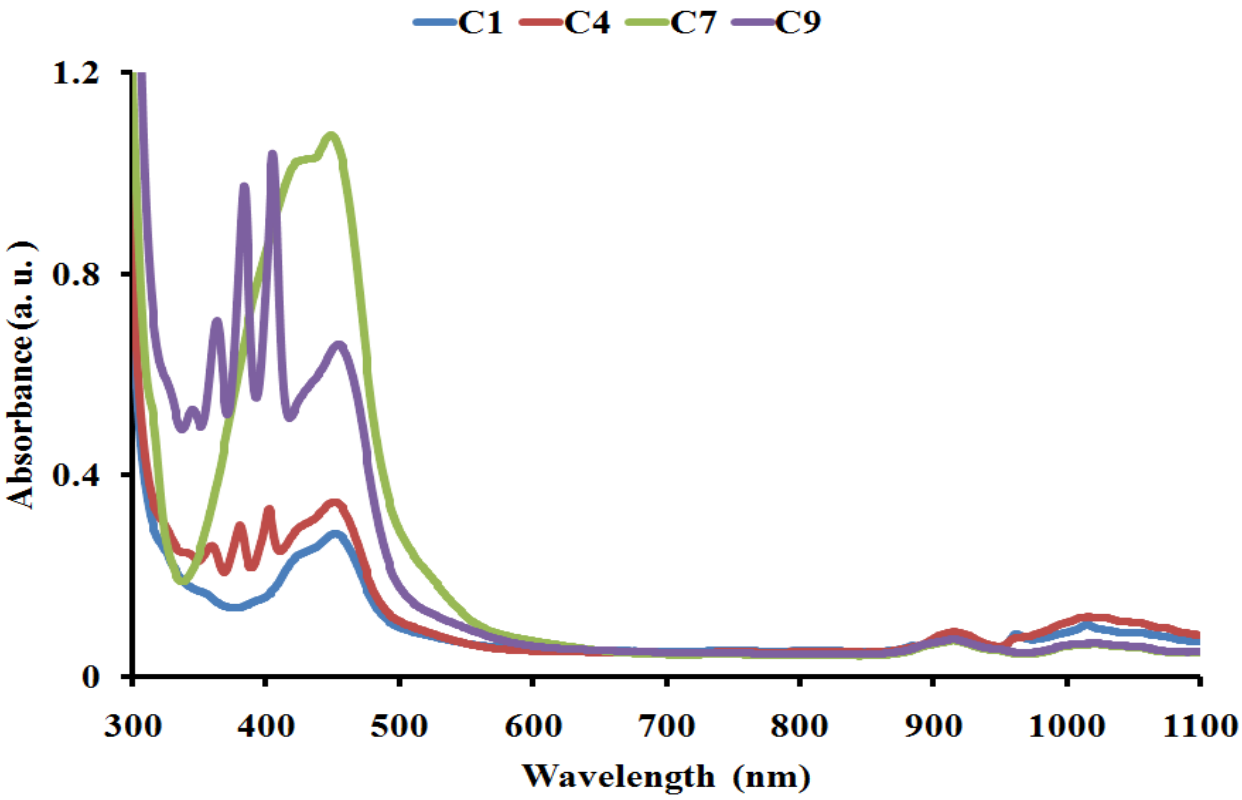

Figure 2.9 Comparison of the UV-Vis absorption spectra of homonuclear Ru(II) functionalized anthracenyl/(non-anthracenyl) bipyridine and phenanthroline complexes

The emission spectra of the complexes **C1**, **C4**, **C7** and **C9** are shown in Figure 2.10. It is observed that all the complexes display good photoluminescence properties. However, the information from the spectra shows that towards the near infrared region, emission of the complexes is governed by the molecular weight. **C1** with least molecular weight (863.94 a.u) gave the highest emission wavelength at 748 nm which is blue-shifted (*ca* = 39, 33 and 72) for **C4**, **C7** and **C9** respectively.

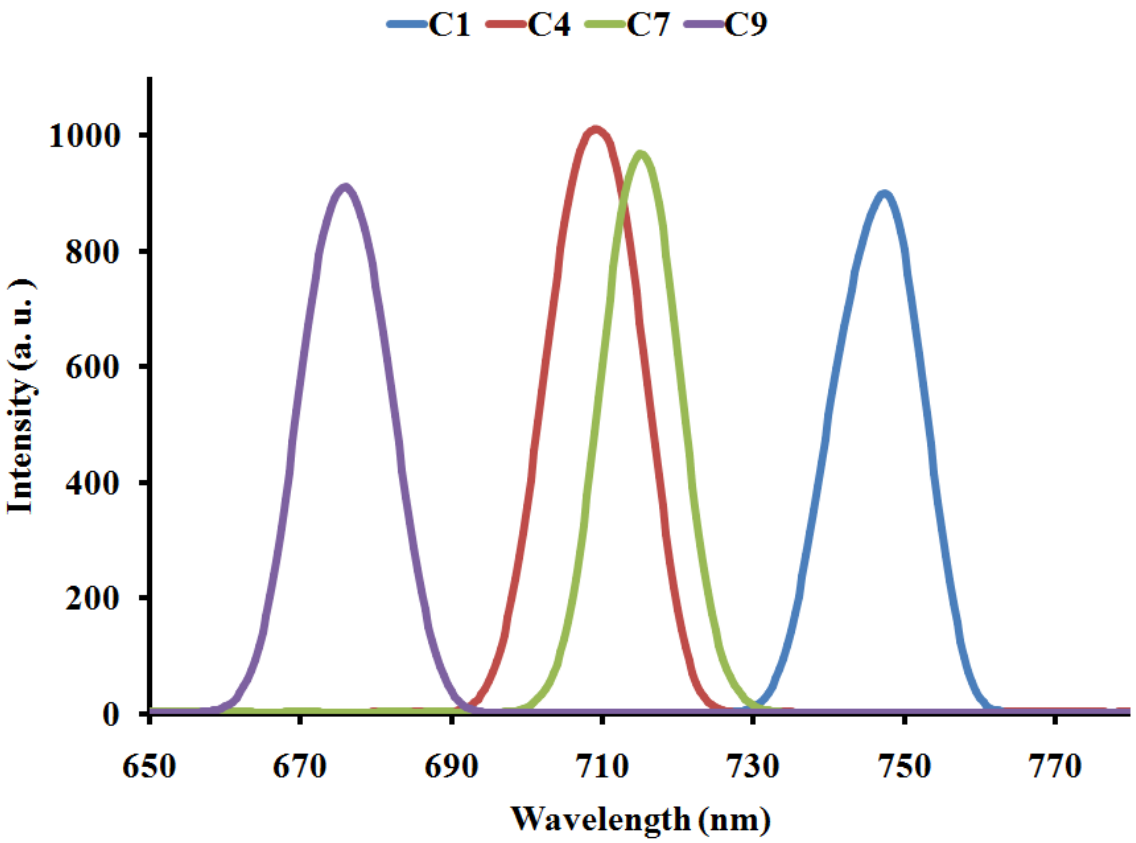

Figure 2.10 Comparison of the Emission spectra of homonuclear Ru(II) functionalized anthracenyl/(non-anthracenyl) bipyridine and phenanthroline complexes.

2.8.4 Nuclear Magnetic Resonance of ligands and complexes

The proton nmr spectrum of **L1** contains six peaks at 8.66 (d, 1H), 8.41 (d, 1H), 7.86 (dd, 1H), 7.36 (1H), 1.73 (s, 3H), 1.66 (d, 3H) ppm. The bipyridine peak positions are very similar to the starting bromo-bipyridine material. The principal difference is due to the inclusion of the methyl resonance at the upfield region of the spectrum. The ^{13}C nmr spectrum gave the anticipated peaks at 169.76, 156.21, 149.98, 137.86, 136.88, 129.74, 124.81, 121.32, 14.81 and 12.71. The bipyridine peaks due to chemical equivalency were observed in the range 156-128 ppm. The peak at 169.76 ppm was assigned to the carbonyl carbon; the two peaks at 124.81 and 121.32 were assigned to the alkenyl carbons, while the methyl groups were found at 14.81 and 12.71 ppm. The proton nmr of **L2** show five signals at the aromatic region at δ 9.20 (d), 8.57 (dd), 8.26 (d), 8.24 (d), 7.62 (dd) were assigned to the bipyridine and anthracene moieties. The two singlet peaks at the aliphatic region were assigned to the methyl groups at δ 2.17 and 1.67 ppm. The ^{13}C spectrum of **L2** was similar to that of **L1** except those additional peaks at 131.03, 128.25, 127.44 and 126.49 ppm that were assigned to the anthracenyl carbons signals (See Appendices 1-5).

Structure of L1 and L2

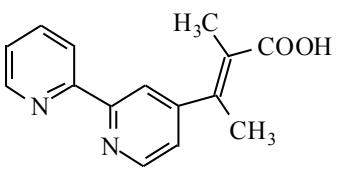

L1

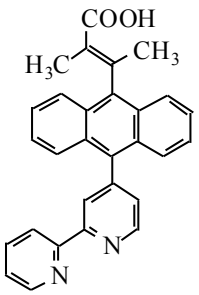

L2

The proton nmr of **L3** is very similar to that obtained for **L1**. The only difference in is the ^{13}C nmr that contained additional carbon peaks of the phenanthroline ligands. The proton nmr spectrum of **L4** showed four doublets and a singlet peak in the aromatic region (δ 9.09–7.72 ppm); these were unambiguously assigned to H-2, H-3, H-8, H-9 and H-5, H-6 respectively. The methyl protons were found as singlet-triplet peaks in the aliphatic region. In **L5**, two doublets, one doublet of doublet and a singlet peak were observed at the aromatic region (δ 9.18–6.97 ppm). These were assigned to H–2, 9; H–4, 7, and H–3, 8 respectively and the singlet peak assigned to H-6. It was difficult to really distinguish the anthracene protons in the spectrum. However, a downfield shift (*ca* = 0.21 ppm) was observed when compared to **L3**. A good proton nmr spectrum could not be obtained for **L6** due to its poor solubility in the solvent. Comparison of **L4**, proton nmr spectrum with that of **L7** and **L8**, two additional doublet of doublet peaks were found at δ 8.48 and 7.77 ppm, and δ 7.99 and 7.45 ppm respectively for the ligands and were unambiguously assigned to the anthracene protons.

The proton nmr spectrum of **L9** showed five major peak signals at the aromatic region. The two doublet peaks at δ 7.01 and 8.38 ppm were assigned to the phenyl ring protons while a doublet peak at δ 8.73 ppm was assigned to the H–2. The two doublets of doublet peaks at δ 7.85 and 7.34 ppm were assigned to the protons in ring B due to chemical equivalency and the H–3 in ring A of the bipyridine ligand respectively. However, we could not categorically confirmed the correctness of structure for **L9** on the premise of the proton nmr data alone due to the absent of alkynyl peaks in the ^{13}C nmr spectrum of the ligand, even though, the infrared spectrum of the ligand shows the vibration frequency characteristic of the alkynyl functional group. In the ^{13}C nmr signals of the ligand, a total of seven peaks were

found in the range of δ 173 –121 ppm corresponding to the presence of carbonyl, bipyridyl, and phenylene functions while at the aliphatic region two prominent peak signals at 14.53 and 11.60 ppm were assigned to the *trans* methyl groups in the molecule.

The proton nmr spectrum of **L10** in chloroform gave four doublet peaks signals and one singlet peak all at the aromatic region. The doublet peaks at δ 9.16, 8.19 were assigned to H–2, 9; H–3, 8; of the 4,7 disubstituted phenanthroline while the doublet peak signals at 7.72 and 7.58 ppm were unequivocally assigned to the two protons of the ethylene carbons of the double-triple bond linked 1-methoxy-1-buten-3-yne substituent. The Carbon 13 nmr spectrum of **L10** showed signals peaks in the range δ 150–123 ppm for the phenanthroline ring, a peak at 101.84 was assigned to the ethynyl peak, while the peaks at 54.20 and 47.66 ppm are due to the OCH_3 group (See Appendices 6–21).

Structure of L3 – L10

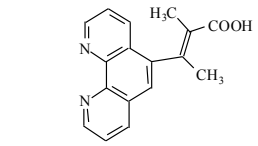

L3

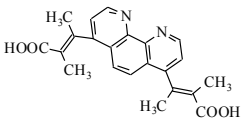

L4

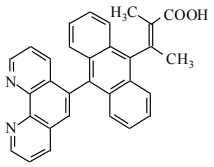

L5

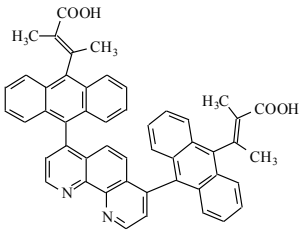

L6

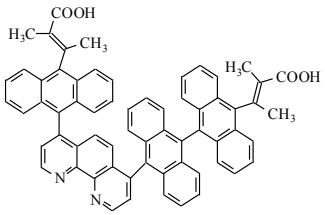

L7

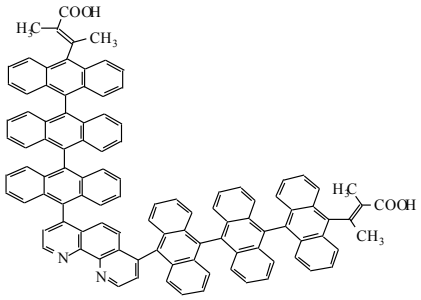

L8

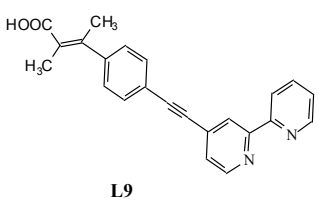

L9

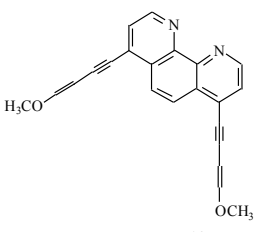

L10

Complex **C1** was purified using Sephadex LH-20 column chromatography and was obtained as a dark-brown solid. The proton nmr spectrum of the complex show only one doublet peak at δ 8.62 ppm and three singlet peaks at 8.06, 7.69 and 7.43 ppm at the aromatic region. When compared to the proton nmr spectrum data of the coordinating ligand **L1**, all proton peaks experience upfield shifts in the chemical shift values, this is attributed to the effect of the lone pair-lone pair electron donor property of the nitrogen atoms of the bipyridyl rings to the ruthenium metal centre. However, unlike in **L1**, the aliphatic region of the spectrum is devoid of the presence of the methyl protons chemical shift to signify the presence of the substituent group of the 2,3-dimethylacrylic acid. This result was further corroborated with the absence of the carbonyl and/or methyl peaks in the ^{13}C nmr spectrum. We tend to adduce the loss of this peaks to the fragmentation of 2,3-dimethylacrylic acid possibly during intense heating and/or column chromatography in Sephadex LH-20 (See Appendices 29, 30).

Structure of complex **C1**

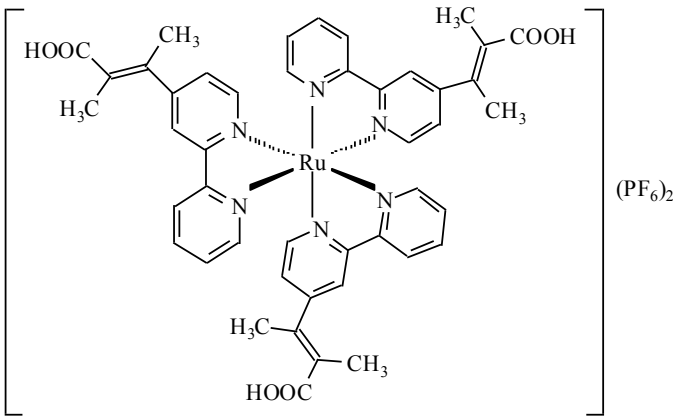

The proton spectrum of **C2** is more complex due to the non-symmetric nature of the participating ligands. At the aliphatic region, the singlet peak at δ 2.05 ppm accounted for the methyl protons present in the complex. Due to the poor solubility of **C4** in various organic solvents, an unsatisfactory proton nmr spectrum was

obtained and it was difficult to assign individual peaks based on the available data (See Appendices 31 and 32).

The proton nmr spectrum of **C5** in dmso-d_6 showed five doublet peaks and two singlet peaks in the aromatic region and also two singlet peaks at the aliphatic region. The bipyridyl protons were observed as doublets at δ 9.89, 9.17, 8.55 ppm and two singlet peaks at 8.82 and 8.69 ppm. The substituted anthracene protons in the complex were found as two doublet peaks at δ 8.25 and 7.73 ppm. At the aliphatic region, the two singlet peaks at δ 2.55 and 2.08 ppm were assigned to the methyl groups. A similar pattern in the proton nmr spectrum was found in complex **C6** when compared to **C5**. The only difference could be the physical loss of one molecule of anthracene in the chemical structure of **C6**, resulting in a shielding effect of the protons chemical shift values (See Appendices 33 and 34).

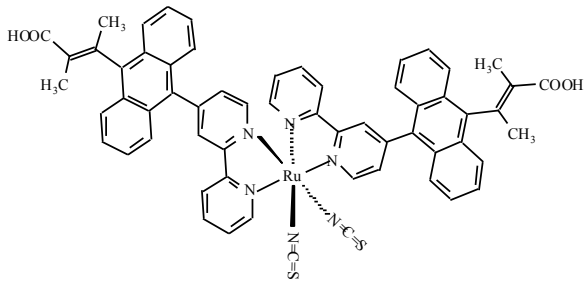

C5

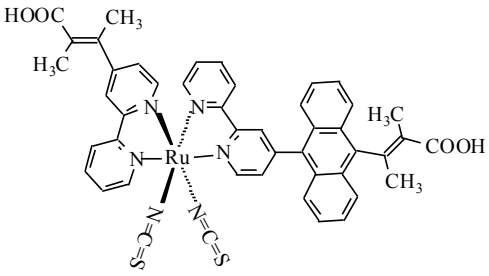

C6

The proton nmr spectrum of **C7** showed expected peaks for a 5-substituted phenanthroline ligand. In the aromatic region of the spectrum, one doublet of doublet, three doublet peaks and a singlet peak were observed. The peaks at δ 8.75, 8.06 and 6.71 ppm were assigned to H–2, 9; H–4 and H–7 protons. The doublet of doublet peak at δ 7.74 ppm was assigned to protons H–3, 8. The singlet peaks at

δ 2.06 and a multiplet peak at δ 1.71 were assigned to the methyl protons (See Appendices 35, 36).

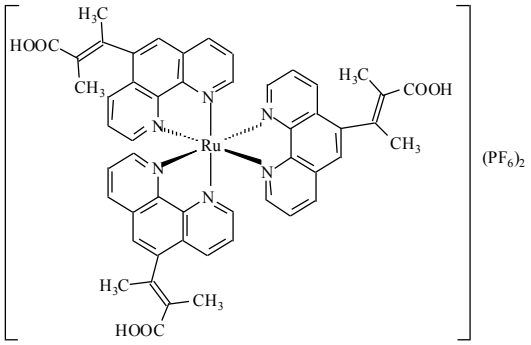

C7

The **C8** proton nmr spectrum due to chemical equivalency of the molecule show only four major coupling system in the aromatic region between proton at δ 8.77 (d, *J* = 8.0 Hz) and 7.78 (dd, *J* = 5.2, 8.0 Hz) characteristics of a 5-substituted phenanthroline. These were accounted for H–2, 9; H–3, 8; and H–4, 7. The aromatic singlet peak at δ 8.39 ppm was assigned to H–6 of the middle ring. The methyl signal was found as singlet peak at δ 2.57 ppm. The carbon 13 nmr spectrum of the complex only show five major peaks in the range of δ 153–127 ppm (See Appendices 37, 38).

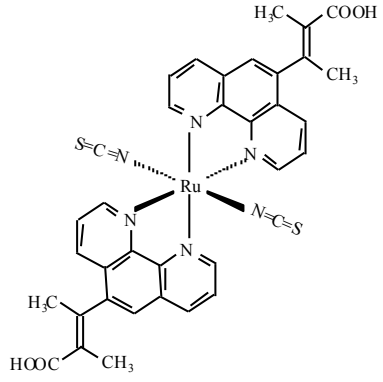

C8

The proton nmr spectrum of **C9** shows six peaks at δ 8.83 (d, *J* = 8.0 Hz), 8.56 (dd, *J* = 3.2, 6.8 Hz), 8.17 (t), 7.82 (dt, *J* = 3.2, 6.8 Hz), 7.73 (d, *J* = 5.6 Hz) and 7.53 (dd, *J* = 6.0, 6.4 Hz). The phenanthroline peak positions are very similar to that

of C8. The only difference is due to the anthracenyl peaks. The resonances were assigned to the protons that are at the 2,9 positions, 3,8 positions, 4,7 positions, 6 position and the adjacent hydrogens in the anthracene. The ^{13}C nmr spectrum shows seven peaks at δ 157.42, 152.07, 138.79, 131.26, 128.75, 125.34 and 13.94 ppm. The carbonyl peak was assigned to the peak at 157.42 ppm, the peaks at 152.07, 138.79 and 131.26 are due to the phenanthroline peaks and the two intense peaks at 128.75 and 125.34 are the anthracene peaks. The methyl group was assigned to the peak at 13.94 ppm (See Appendices 39, 40).

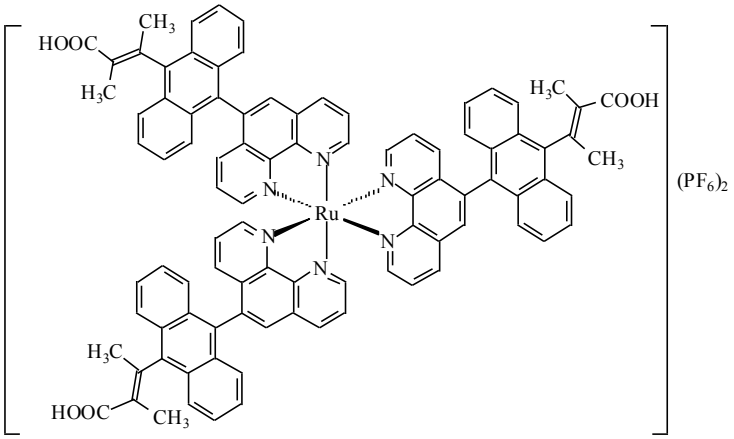

C9

The proton nmr spectrum of **C10** shows six peaks at 8.80 (s), 8.59 (dd), 8.45 (d), 8.10 (t), 7.90 (s) and 7.63 (dd) at the aromatic region and two singlet peaks at 2.17 (s) ans 2.04 (s). The observed difference in the chemical shift values as when compared to **C9** above would be due to thiocyanate substitution since both complexes contained the same type of phenanthroline ligand. A satisfactory ^{13}C nmr spectrum was not available for the complex (See Appendix 41 for ^{1}H NMR spectrum).

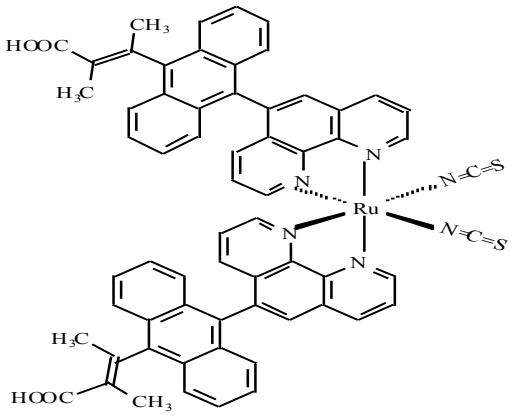

C10

The proton nmr of **C11** shows five peaks at 8.84 (d), 8.39 (s), 8.17 (t), 7.75 (d) and 7.56 (m) at the aromatic region while the upfield aliphatic region consists of two peaks at 1.73 (s) and 1.66 (d). The assignments of these peaks were difficult due to the heteronuclear nature of the ligands forming the complex. However, the ^{13}C nmr spectrum shows twenty-two carbon peaks in the range of 169-125 ppm. These peaks are for the carbonyl, bipyridine and phenanthroline ligands. The aliphatic region of the spectrum shows the two methyl peaks at 14.88 and 12.71 ppm (See Appendices 42, 43).

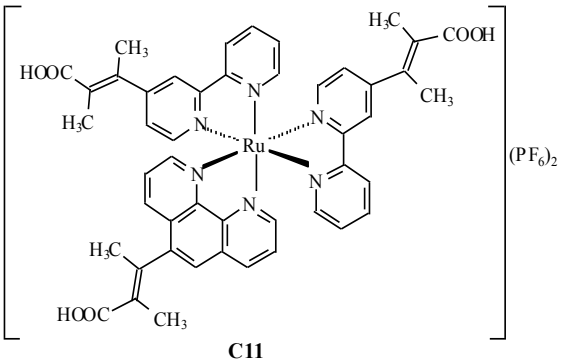

C11

The proton nmr of **C12** shows similar features as reported for **C11** above. Five distinct peaks at δ 8.81 (s), 8.43 (d, *J* = 7.2 Hz), 8.06 (s), 8.00 (d, *J* = 8.8 Hz) and 7.51 (s) were observed at the aromatic region for the bipyridine and phenanthroline ligands while the two singlet peaks at 2.17 and 1.25 were assigned to the methyl

grups in the complex. The upfield shift in resonance values may be due to the incorporation of thiocyanate ligand in the molecule. A satisfactory ^{13}C nmr spectrum could not be obtained for the complex due to poor solubility of the complex in the solvent (See Appendix 44 for ^{1}H NMR spectrum).

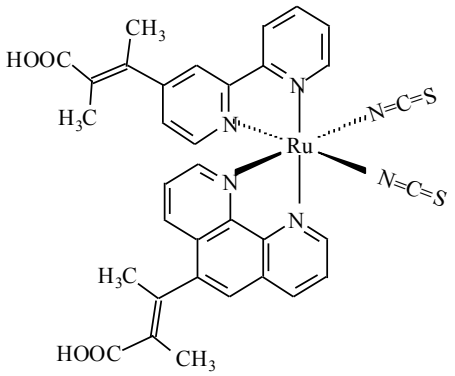

C12

The proton nmr spectrum of **C13** shows six peaks in the aromatic region at δ 8.80 (d, *J* = 7.6 Hz), 8.14 (t), 7.71 (d, *J* = 5.6 Hz), 7.50 (t), 7.21 (s), 7.09 (s), 6.96 (s), and 6.71 (d, *J* = 7.2 Hz). A slight structural variation between **C11** and **C13** are vital for comparison in that unlike **C11** with two molecules of bipyridine derivative and one phenanthroline derivative, **C13** has one molecule of bipyridine derivative and two molecule of phenanthroline derivative, thus the increase in the number of resonance peaks in **C13**. The singlet peak at 1.70 ppm was due to the methyl protons. The ^{13}C nmr spectrum shows eight peaks at δ 169.20, 156.96, 151.62, 138.36, 136.88, 135.92, 14.58, 12.36 ppm. The six peaks in the range of 135−156 ppm are due to the bipyridine and phenanthroline peaks, the resonance peak at 169.20 ppm was due to the carbonyl and the peaks at 14.58 and 12.36 ppm were assigned to the methyl groups (See Appendices 45, 46).

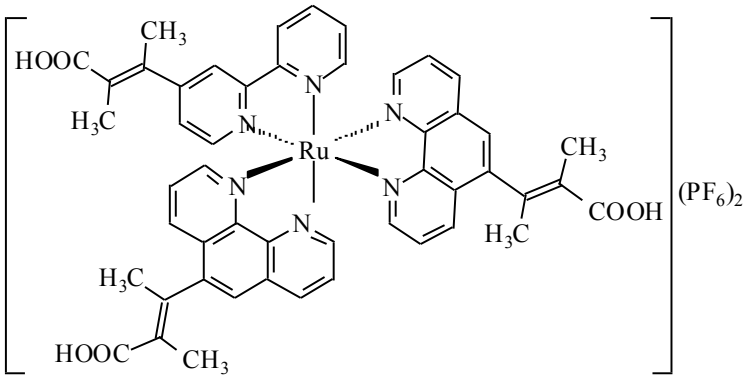

C13

A satisfactory proton nmr spectrum could not be obtained for **C14** whose ligand was **L5** due to poor solubility in the solvents such as dmso-d_6 and chlofororm-d. The spectrum only gave three resonances peaks at δ 8.60 (dd, *J* = 2.4, 6.0 Hz), 7.63 (dd, *J* = 2.0, 6.0 Hz), 7.00 (d, 2.4 Hz) which were not enough to establish correct structure for the complex. The ^{13}C nmr spectrum only shows eight peaks at δ 168.89, 135.17, 126.31, 123.52, 123.28, 122.71, 9.81, 6.81 (See Appendices 47, 48).

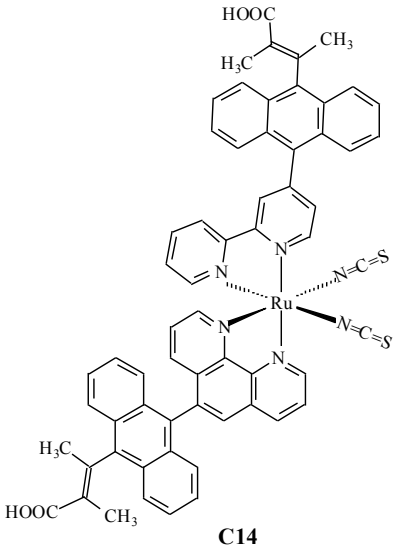

C14

The proton nmr spectrum of **C15** shows multiplet peaks in the aromatic region and the total number of hydrogens integrated for twenty-one protons due to chemical

equivalency. Compared to the two ligands **L7** and **L10** respectively, the protons in the complex shifted upfield by (ca δ 0.63, 0.48 ppm). The peaks at δ 8.53 (d, *J* = 2.8 Hz, 1H), δ 8.52 (d, *J* = 2.8 Hz, 1H), and δ 7.62 (d, *J* = 4.0 Hz, 1H) were unambiguously assigned to H–2,9, H–2',9'; H–5,6; 5',6' and 3,8, H–3',8', of the two ancillary phenanthroline ligands respectively. The different substitution patterns in **L7** of the complex gave peaks at δ 8.17 (m, 4H) and δ 7.79 (dd, *J* = 2.8, 6.8 Hz, 8H) for the anthracene protons; while the two signals at δ 7.58 (d, *J* = 11.2 Hz, 2H) and δ 7.56 (d, *J* = 8.0 Hz, 2H) were assigned to the *trans* olefinic protons of the 1,3-enyne moiety in **L10**. In the upfield aliphatic region, the eighteen methyl protons in the complex were integrated as a singlet peak for fifteen protons at δ 2.08 ppm. This could be explained in terms of the equivalency of the methyl protons of the -OCH_3 group in **L10**, unlike in **L7** where the methyl groups of the 2,3-dimethyacrylic acid were orientated in different environments on the phenanthroline ring (See Appendix 49).

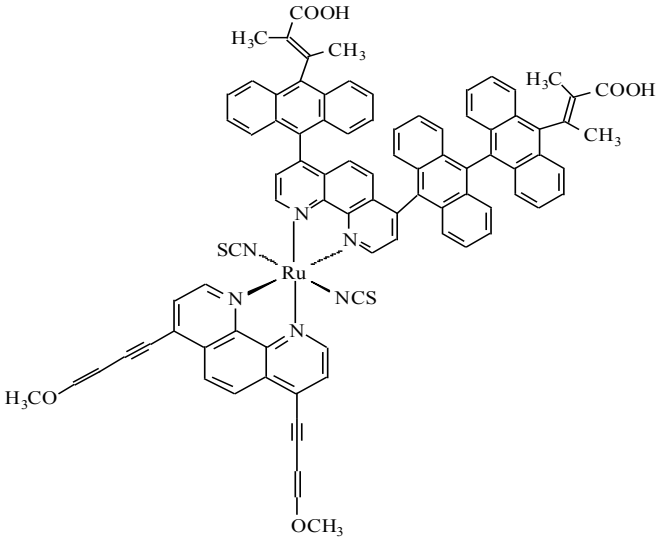

C15

The proton nmr spectrum of **C16** synthesized from ligands **L4** and **L8** is consistent with the structure shown below. Due to the presence of two different

anchoring ligand substitutions, such that all the protons are electronically found in different environments, gave complications in the proton nmr spectrum of the complex when compared to individual ligand spectrum. All the peaks were shifted downfield in the between δ 8.30 and 7.78 ppm. The deshielding pattern is ascribed to the lone pair-lone pair electron donation of the nitrogen atoms to the *d*-orbital of the ruthenium metal. The chemical shifts of the ancillary phenanthroline protons were observed as doublets at reduced intensity. In the ^{13}C nmr spectrum, the carbonyl chemical shifts was found at δ 183.2 ppm. It is interesting to note that the progressive increase toward the downfield shifts may also be partly due to extension of π-conjugation length in the molecules. The NCS peaks were found at δ 134.9 and 133.6 ppm due to *trans* orientation to other ligands. The high intensity peaks at δ 134.1 and 127.2 ppm and 128.1 and 125.3 ppm, common to both **L8** and **C16** complex, were due to the triply-linked anthracene carbon molecules (See Appendices 50, 51).

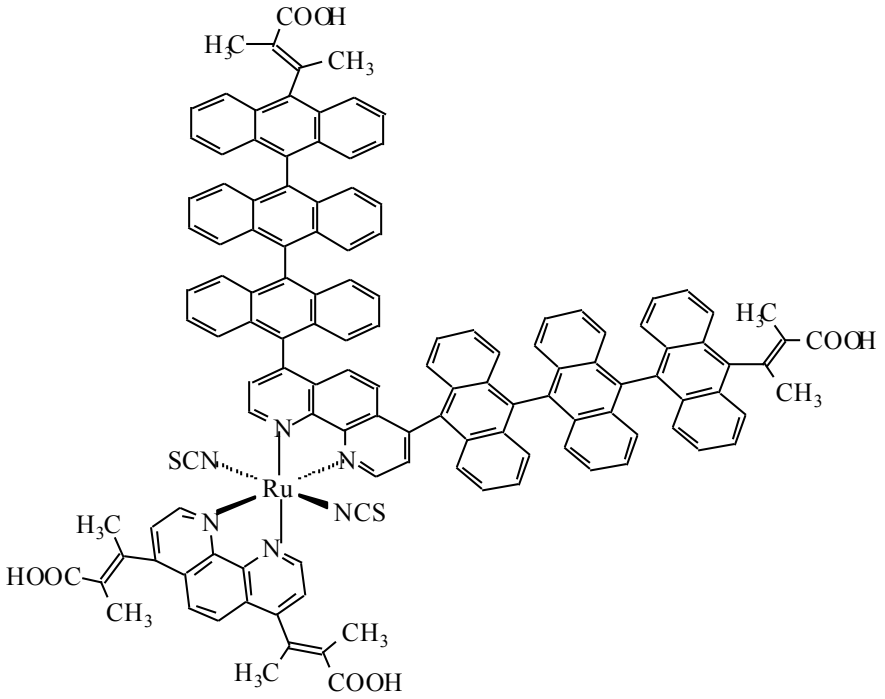

C16

2.8.5 Electrochemical study

In the potential range +1.5 to -1.5 at a scan rate 50 mV s^{-1}, the cyclic voltammograms of **L4**, **L8**, **C2**, **C4**, **C6**, **C7**, **C9**, **C10**, **C11**, **C12**, **C14** and **C16** (Figures 2.11 – 2.18), were examined using Ag|AgCl electrode in DMF solvent with 0.1 M tetrabutyl ammonium hexafluorophosphate as supporting electrolyte. The voltammograms display the Ru(III)/Ru(II) couple at positive potentials and the ligand-based reduction couples at negative potentials. The potentials are summarized in Table 2.2. The voltammograms of two phenanthroline ligands **L4** and **L8**, display irreversible oxidation peaks at +0.48 and +0.45 V respectively. Other redox waves were observed at $E_{1/2}$ = -0.41 V (for **L4**) and $E_{1/2}$ = -0.48 V and E_p = -0.94 V (for **L8**).

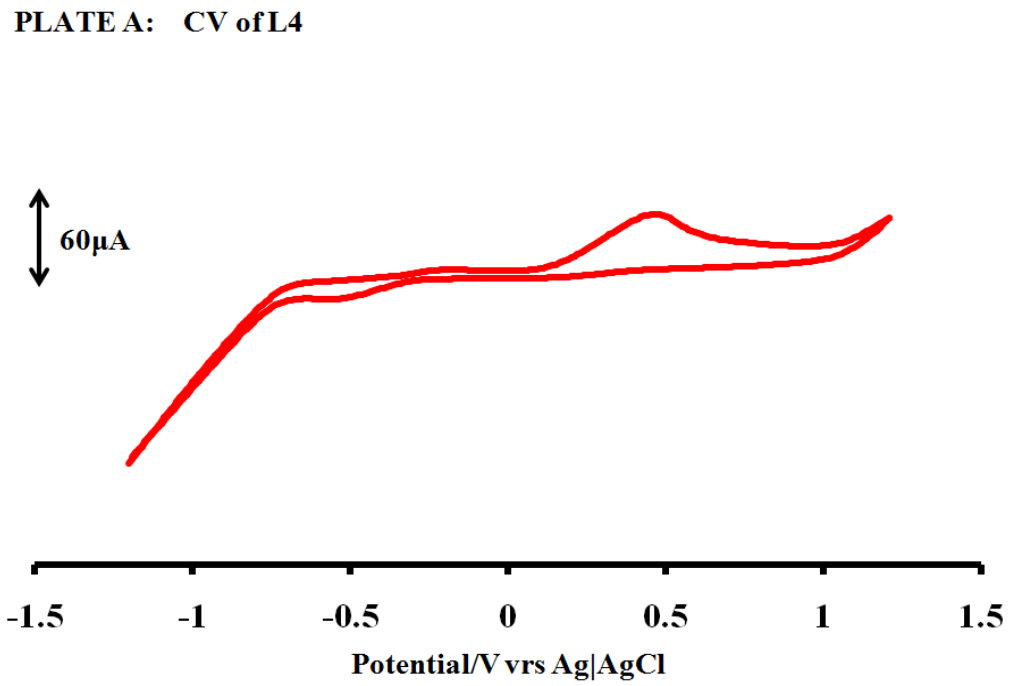

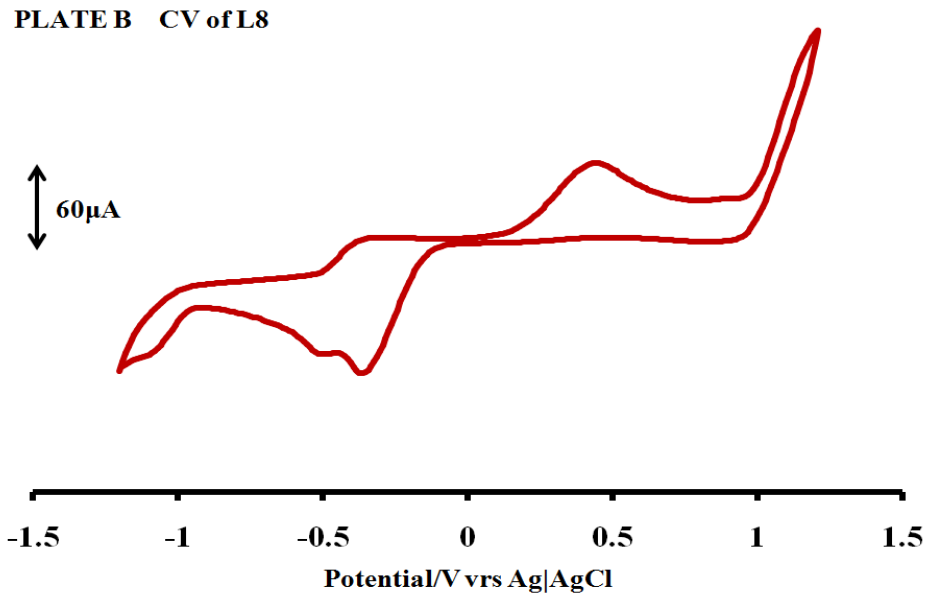

Figure 2.11 Cyclic voltammograms for phenanthroline ligands **L4 and L8** (Plates A & B) at $1x10^{-3}$ M in freshly distilled DMF containing 0.1 M $TBABF_4$ supporting electrolyte. Step potential = 5 mV, amplitude = 50 mV vs. Ag|AgCl, frequency = 10 Hz. Scan rate = 100 m Vs^{-1} vs. Ag|AgCl.

Electrochemical investigation of the 4,7-disubstituted phenanthroline ruthenium(II) complex as found for **C16** was studied in details. Five redox processes were identified and relative to the two coordinating ligands present in the complex, the oxidation potential of the metal center in **C16** is more negative, which indicate the electron-donating nature of the nitrogen to the ruthenium metal centre. As expected, the irreversible oxidation peak at 0.63 V (Process **V**) was attributed to Ru(III)/Ru(II). The redox wave of **C16** were observed at $E_{1/2}$ = -0.86, -0.45 and -0.27 V for processes **I**, **II** and **III**, respectively (See Plates C–E).

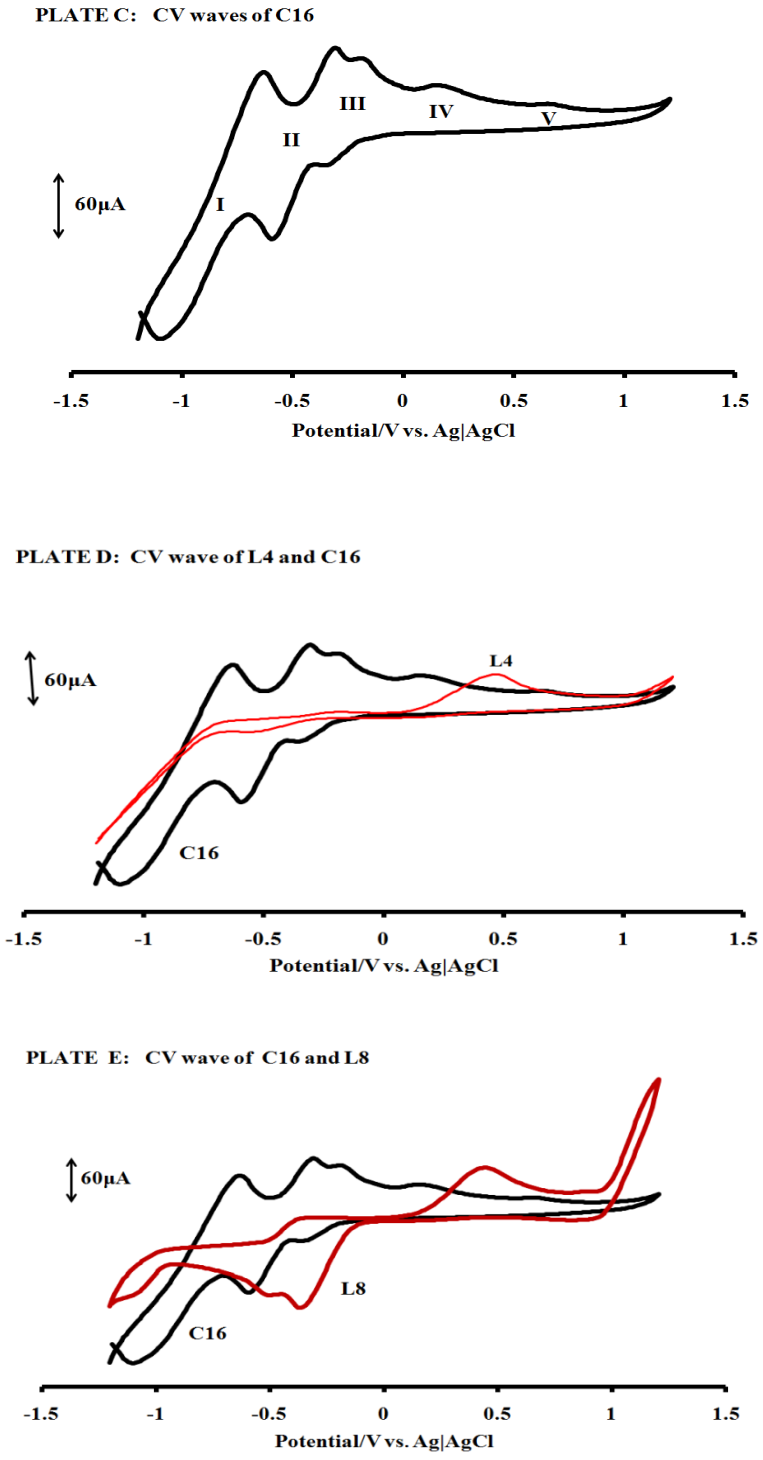

Figure 2.12: Cyclic voltammetry profiles of $1x10^{-3}$ M of **C16, L4** and **L8** in freshly distilled DMF containing 0.1 M $TBABF_4$ supporting electrolyte. Step potential = 5 mV, amplitude = 50 mV vs. Ag|AgCl, frequency = 10 Hz. Scan rate = 100 m Vs^{-1} vs. Ag|AgCl.

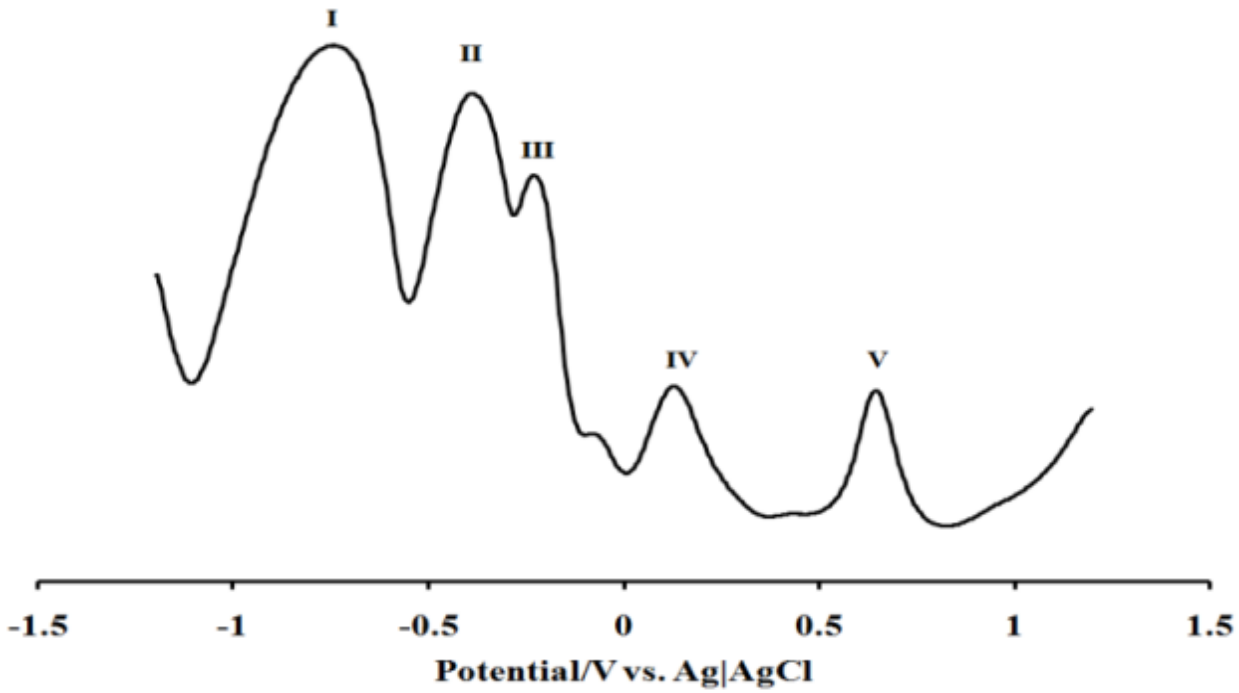

Figure 2.13 Square wave voltammetry profile of $1x10^{-3}$ M of **C16** in freshly distilled DMF containing 0.1 M $TBABF_4$ supporting electrolyte. Step potential = 5 mV, amplitude = 50 mV vs. Ag|AgCl, frequency = 10 Hz. Scan rate = 100 m Vs^{-1} vs. Ag|AgCl.

In other to obtain a more accurate measurement of redox equivalency, the three reduction processes were studied by chronocoulometry using the equation:

$$Q = \frac{2nFACD^{\frac{1}{2}}t^{\frac{1}{2}}}{\pi^{\frac{1}{2}}}$$

From the slope of the data when the quantity of electricity was plotted against square root of time (Figures 2.14 and 2.15), the number of electrons (n) for processes **I**, **II** and **III** were found to be in ratio (3:2:1), suggesting that these processes are multi-electronic in nature while process **IV** or **V** is a single-electron process. This result

indicates that different electron transfer processes are involved between the ruthenium ion, phenanthrolyl and the anthracenyl groups.

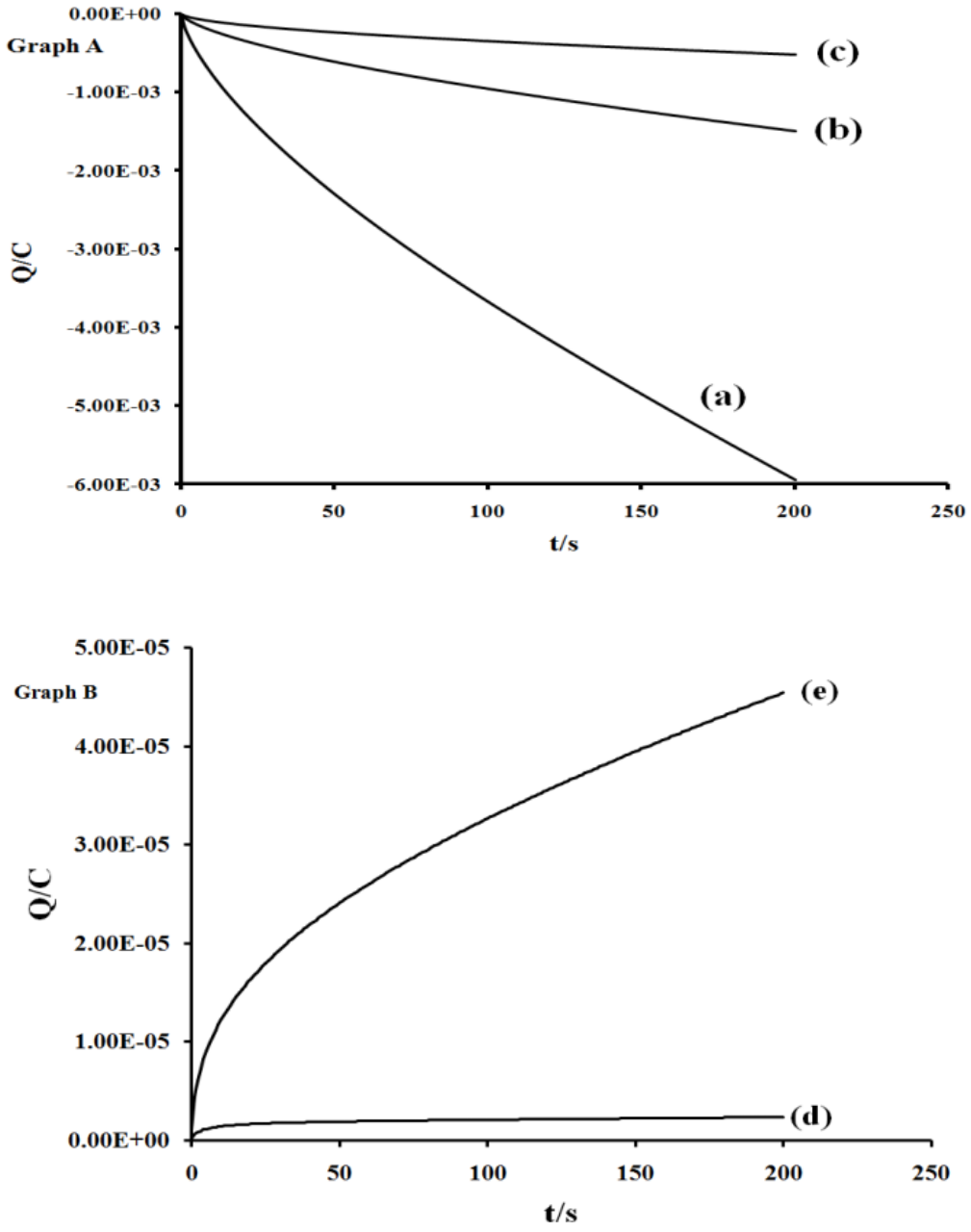

Figure 2.14 Plots of Charge-time response for processes I, II and III; and IV and V. Scan rate: 200 m Vs^{-1}

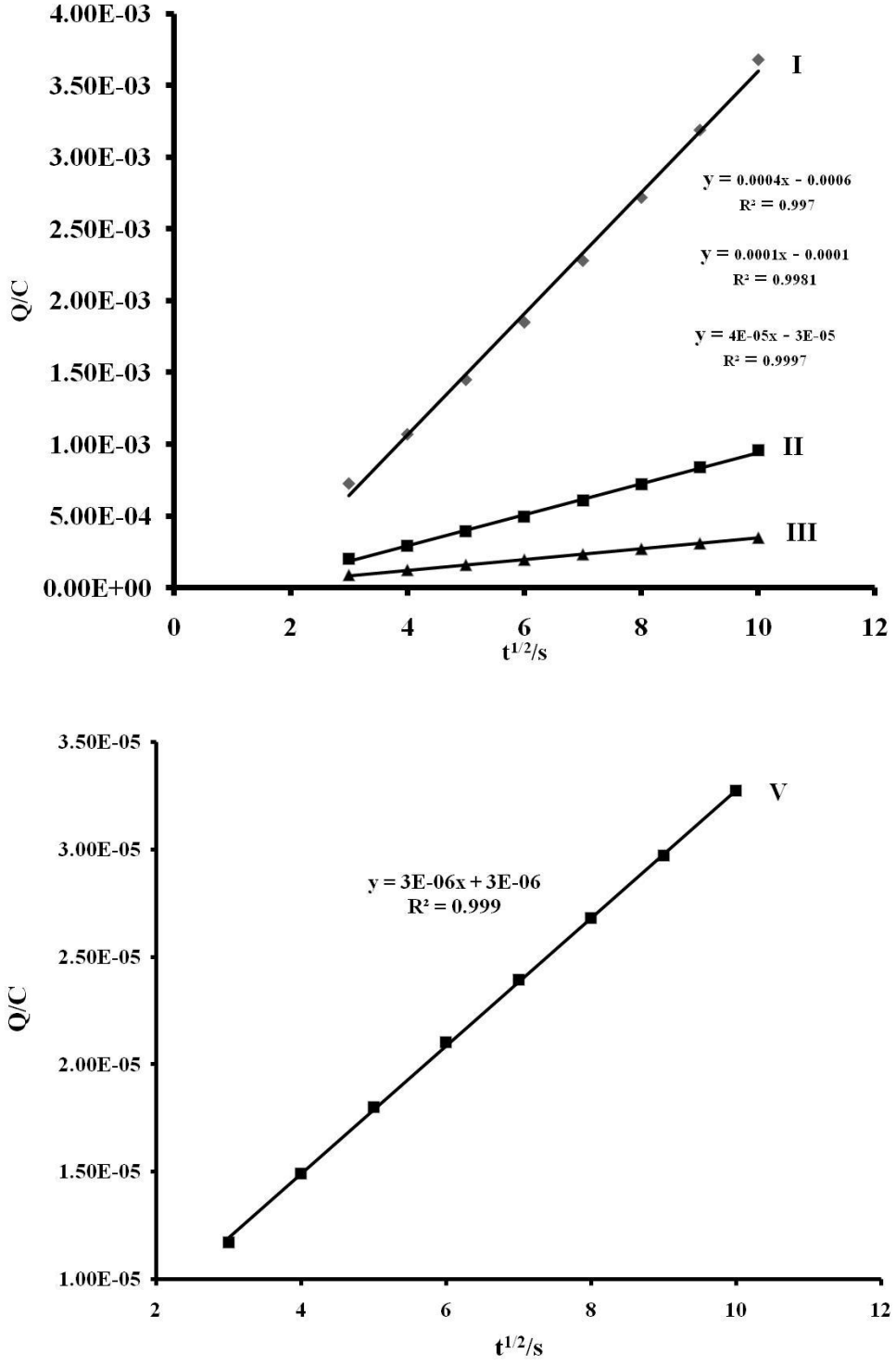

Figure 2.15 Anson plot of charge vs. square root of time (s) for processes I, II, III, and V. Scan rate: 200 m Vs^{-1}

The voltammograms of the homoleptic bipyridyl ruthenium (II) complexes as found in **C2**, **C4** and **C6** were also examined. The oxidation potentials of **C2** and **C6** show quasi-reversible and irreversible behaviour at 0.90 V and 0.47 V respectively, while a well defined reversible peak was observed for **C4** at 0.64 V. These potentials are assigned to the Ru(III)/Ru(II) couple. The redox characteristic displayed by **C2** and **C6** at these potentials is due to the fact that the oxidation potential of thiocyanate ligand is close to that of Ru^{2+} as reported by Grätzel and co-workers for other ruthenium dyes [418]. Other ligand based oxidation potentials for **C2** and **C4** were found at 0.29 and 0.42 V respectively. For the cathodic process, all the complexes show reduction potentials at -0.61V for **C2**, -0.62, -0.99 V for **C4** and -0.62, -0.91 V for **C6**. The potential in **C4** is more negative, thus giving the support to the increase in number of anthracene unit in the structure of the complex and also a corresponding increase in its electron donating ability.

Cyclic voltammetry of C2

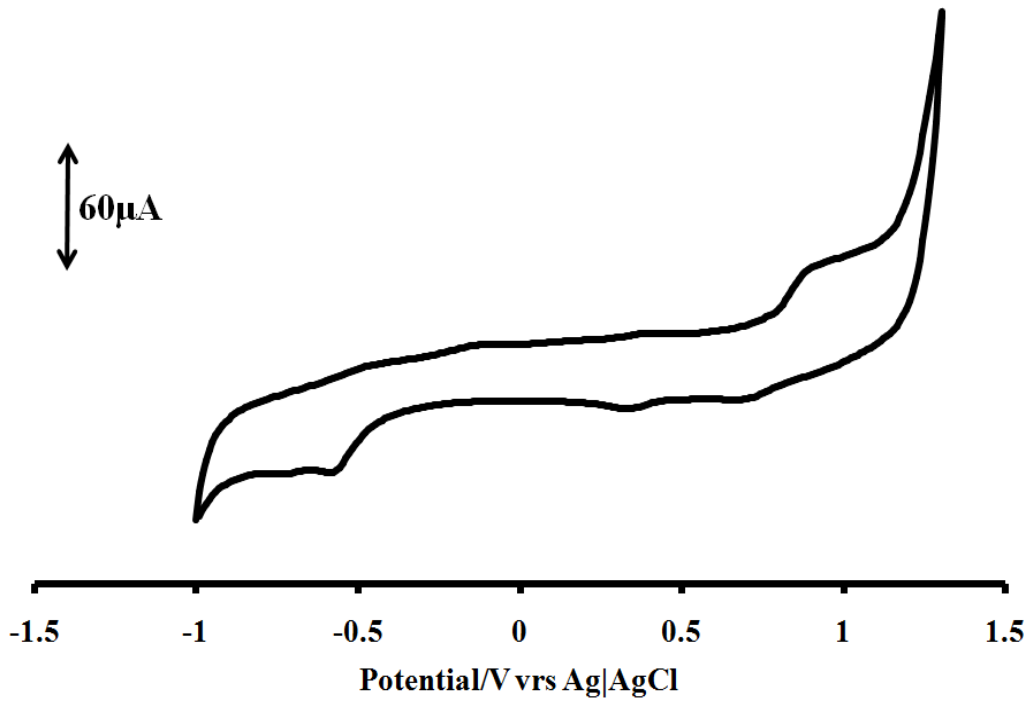

Cyclic voltammetry of complex C4

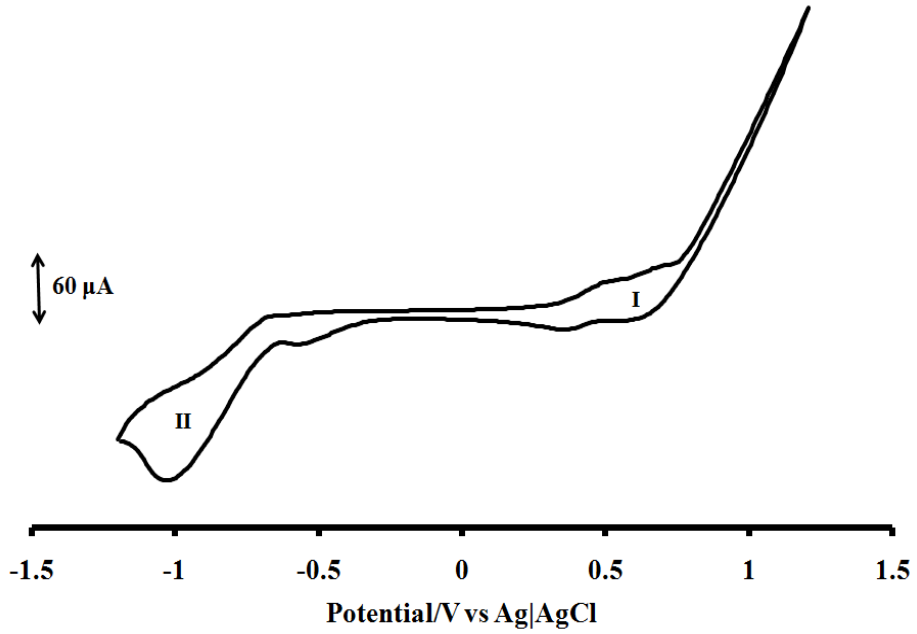

Cyclic voltammetry of C6

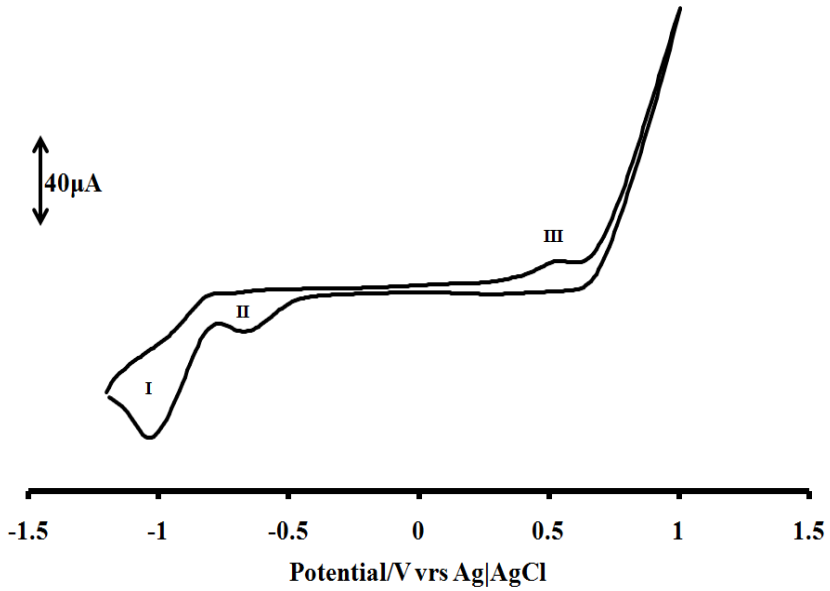

Figure 2.16 Cyclic voltammogram for bipyridine complexes **C2**, **C4** and **C6** at $1x10^{-3}$ M in freshly distilled DMF containing 0.1 M $TBABF_4$ supporting electrolyte. Step potential = 5 mV, amplitude = 50 mV vs. Ag|AgCl, frequency = 10 Hz. Scan rate = 100 m Vs^{-1} vs. Ag|AgCl.

Electrochemical measurements of **C7** reveal reversible oxidations at 0.15, 0.47 and 0.84 V; and 0.43 V for **C9** and **C10**. Only one reduction wave at -0.58 and -0.57 V were observed for **C9** and **C10** respectively. The cathodic reduction was not well-defined in **C7**. From the data, we tend to attribute the reduction waves to the substituted anthracene moiety in **C9** and **C10** since a well-defined peak potential wave was not obtainable for **C7** containing only phenanthroline ligands. However, the weak oxidation potentials at 0.15 and 0.47 V in **C7** were adduced to the phenanthroline ring oxidation potentials.

Cyclic voltammetry of complex C7

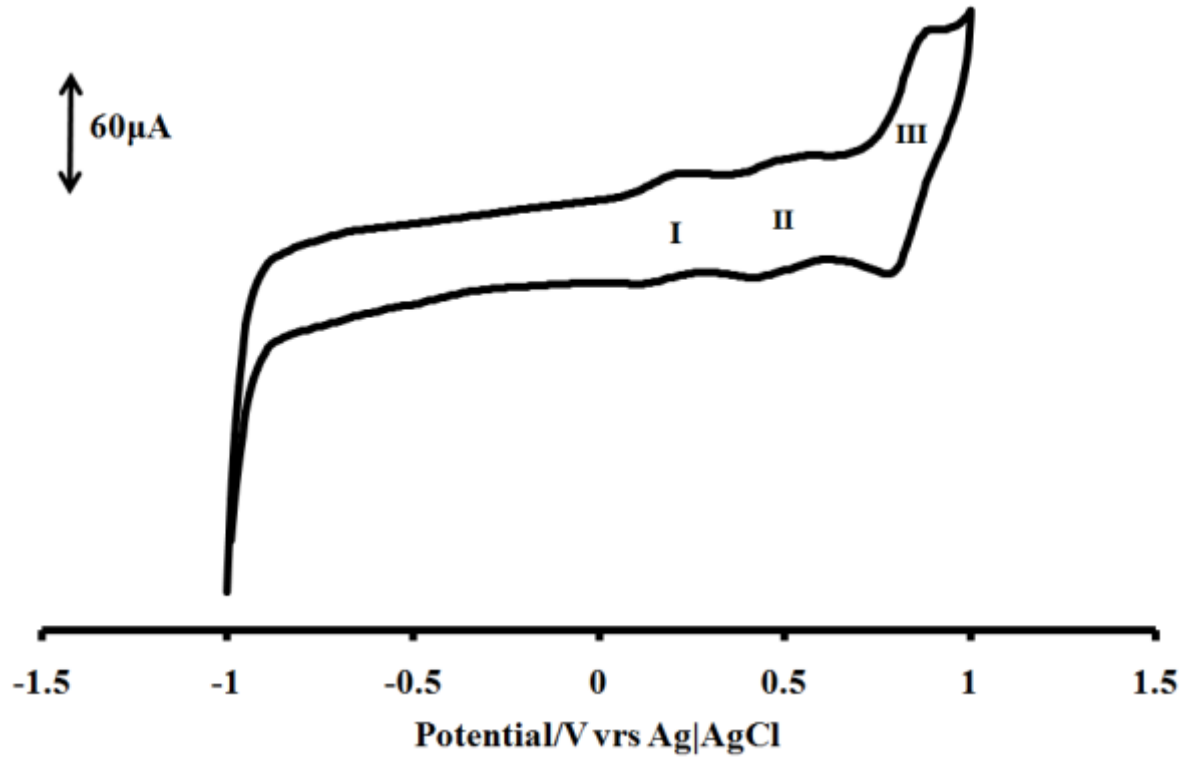

Cyclic voltammetry of complex C9

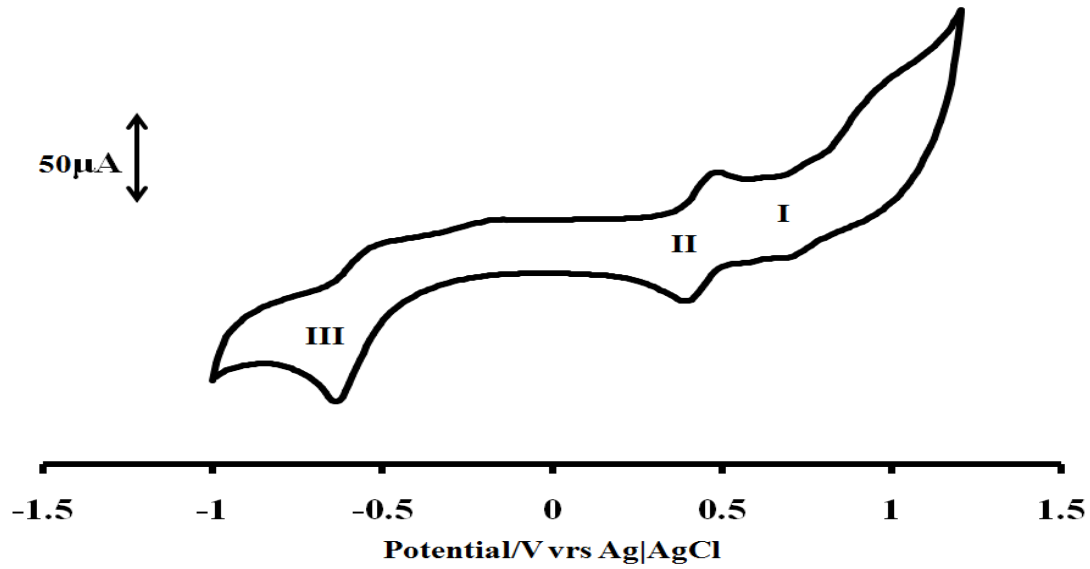

Cyclic voltammetry of complex C10

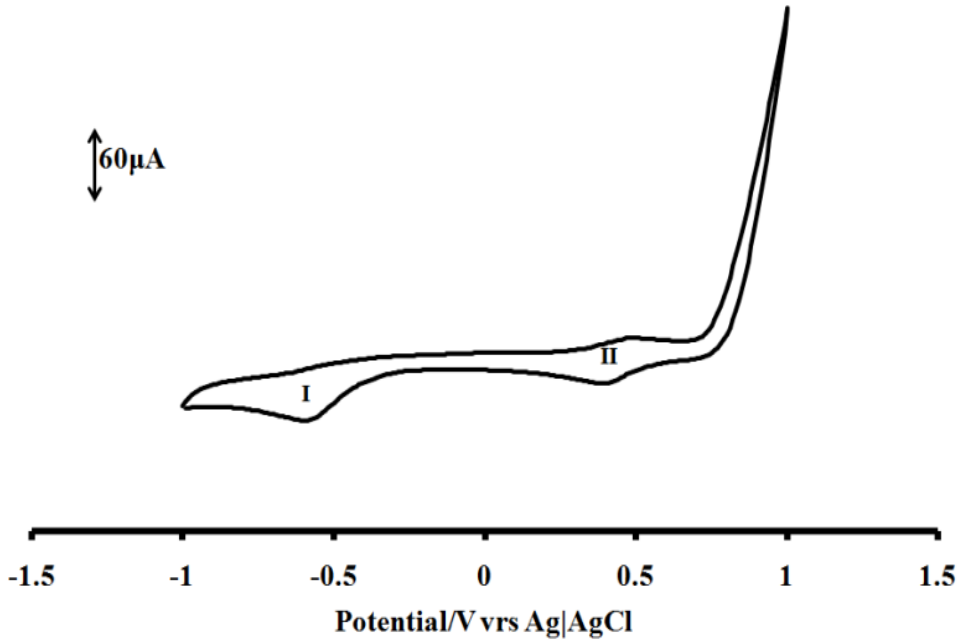

Figure 2.17 Cyclic voltammogram for bipyridine complexes **C7**, **C9** and **C10** at $1x10^{-3}$ M in freshly distilled DMF containing 0.1 M $TBABF_4$ supporting electrolyte. Step potential = 5 mV, amplitude = 50 mV vs. Ag|AgCl, frequency = 10 Hz. Scan rate = 100 m Vs^{-1} vs. Ag|AgCl.

Cyclic voltammograms of the heteronuclear ruthenium(II) complexes as found in (**C11**, **C12** and **C14**) reveal two reversible oxidation potentials at 0.43 and 0.82 V for **C11**; one irreversible oxidation at 0.45 V for **C12** and two irreversible oxidations at 0.42 and 0.93 V for **C14**. At the negative potentials, two reduction peaks were observed at -0.64 and -0.80 V for **C12**, and -0.72 V for **C14**. No reduction peak was found for **C11**. Comparison of the molecular structures of **C11**, **C12** and **C14** reveals that apart from the oxidation of the Ru(III)/Ru(II) couple at 0.82, 0.45 and 0.93 V for the respective complexes, substitution of thiocyanate ligand and the presence of anthracene units influenced the redox properties in complexes **C12** and **C14**.

Cyclic voltammetry of complex C11

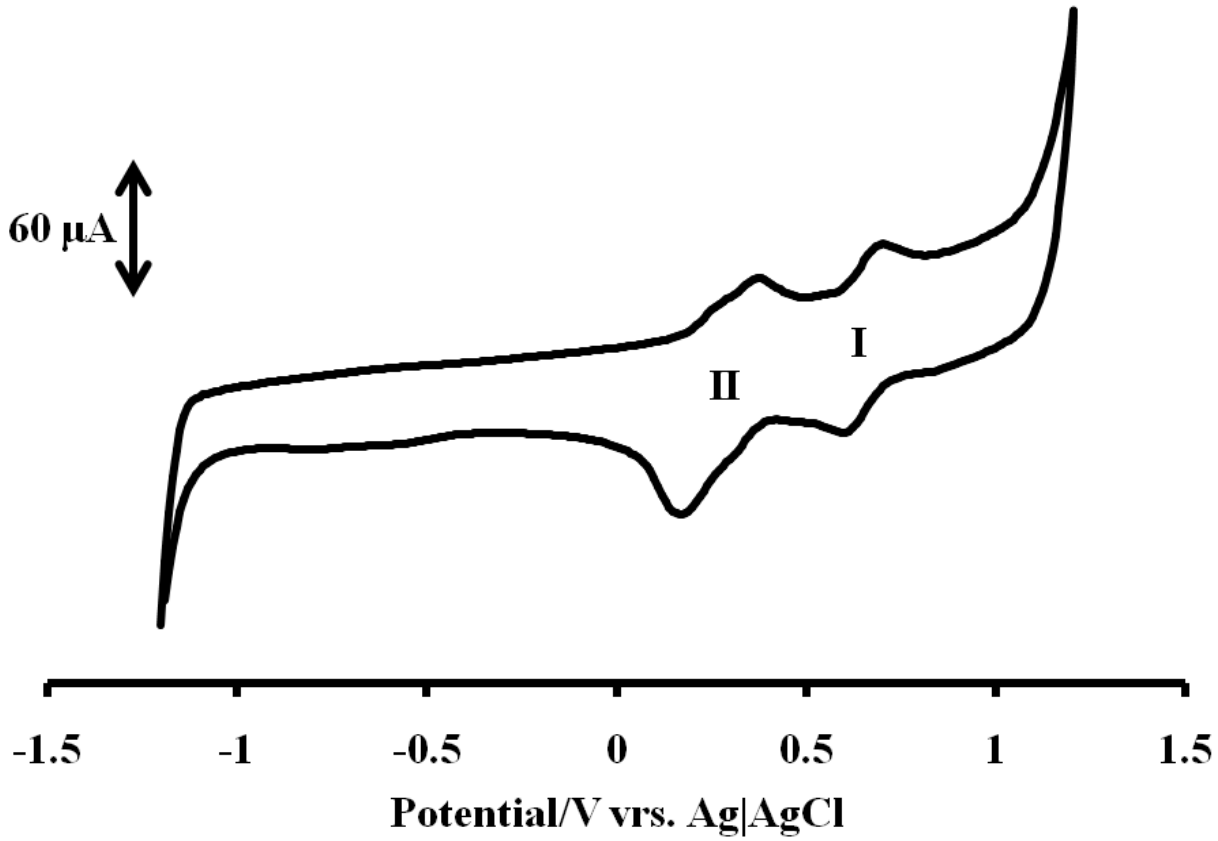

Cyclic voltammetry of complex C12

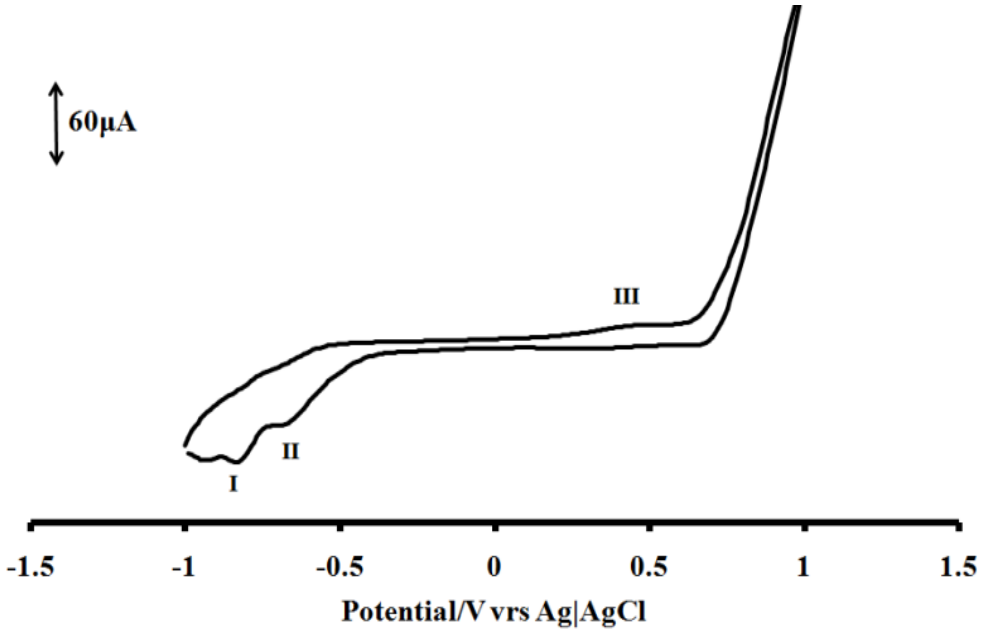

Cyclic voltammetry of complex C14

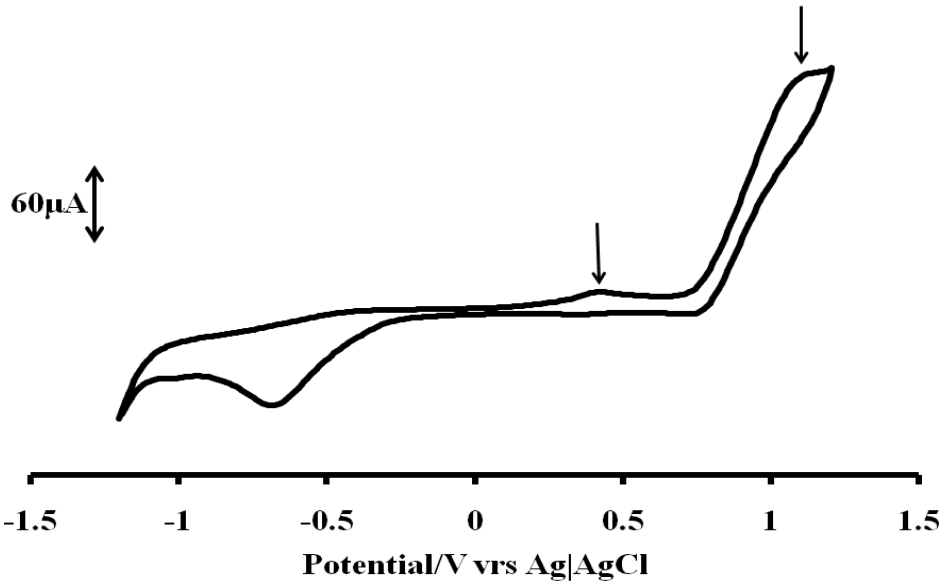

Figure 2.18 Cyclic voltammogram for bipyridine complexes **C11**, **C12** and **C14** at $1x10^{-3}$ M in freshly distilled DMF containing 0.1 M $TBABF_4$ supporting electrolyte. Step potential = 5 mV, amplitude = 50 mV vs. Ag|AgCl, frequency = 10 Hz. Scan rate = 100 m Vs^{-1} vs. Ag|AgCl.

Table 2.1 Cyclic voltammetric data E/V (ΔE_p (mV)) of bipyridyl/phenanthrolyl Ru(II) complexes

Compound	Ru(II/III)	E_{anodic}	$E_{cathodic}$	$E_{1/2}$/V
L4	–	0.45	-0.59	–
L8	–	0.48	–	-0.38, -0.57, -0.94
C1	ND	–	–	ND
C2	0.90	0.29	-0.61	–
C3	ND	–	–	ND
C4	0.64	0.42	-0.99	-0.62
C5	ND	–	–	ND
C6	0.47	–	-0.91	-0.62
C7	0.84	–	–	0.15, 0.47
C8	ND	–	–	ND
C9	0.71	0.43	–	-0.58
C10	0.43	–	-0.57	–
C11	0.82	–	-0.59	0.43
C12	0.45	–	-0.64, -0.80	–
C13	ND	–	–	ND
C14	0.93	0.42	-0.72	–
C15	ND	–	–	ND
C16	0.63	0.17	–	-0.27, -0.45, -0.86

2.9 Conclusion

Ten novel polypyridyl ligands comprising of 2,2'-bipyridine and 1,10-phenanthroline derivatives with carboxylic acid groups and their corresponding ruthenium(II) complexes have been synthesized. The photophysical, spectroscopic and electrochemical properties were studied. Five out of the ten ligands consist of anthracenyl molecular units in increasing order of one to three. Different modes of ligand substitutions were used in the coordination with ruthenium metal centre to afford both the homonuclear and heteronuclear types of complexes. All the complexes examined showed good photophysical, photoluminescence and electrochemical properties characteristics of ruthenium(II) complexes. However, the UV-Vis absorption and luminescence properties of some complexes revealed that extension of the π-bond conjugation may not be the only contributory factor responsible for the shift in absorption wavelengths of complexes to the red region and the corresponding molar absorptivity coefficient, but the types and position of substituents on ligands; and molecular weight of compounds could be as well important in the general characteristics displayed by the complexes.

This work, however, support the other works that have been reported by other workers in the use of binuclear ligands in the enhancement of absorption wavelengths to the red region. In this work, we tend to support the superiority of ruthenium (II) complexes containing bipyrydyl ligands over those of the phenanthroline ligands in terms of their better photophysical properties. All reported NMR spectroscopic data agree with the structures proposed except where other information are required to fully established the structures, most especially for the non-soluble complexes. The electrochemical properties showed that anthracene containing complexes possess good electroredox properties and that the redox

processes could be both single–and multi–electronic in nature. The result indicates that different electron transfer processes are involved between the ruthenium ion, phenathrolyl, bipyridyl and the anthracenyl groups.

CHAPTER THREE

Part of this chapter has been reported as

1. Adewale O. Adeloye and Peter A. Ajibade. Synthesis, characterization and preliminary investigation of the electro redox properties of anthracenyl-functionailzed terpyridyl ligands. *Tetrahedron Lett.* **2011**, 52, 274-277.

2. Adewale O. Adeloye and Peter A. Ajibade. (2010) "Synthesis, characterization and electrochemistry of anthracenyl-functionalized bisterpyridyl Ruthenium(II) complexes" –*IJMS* (Submitted).

CHAPTER THREE

3 SYNTHESIS OF FUNCTIONALISED 2,2':6',2"-TERPYRIDINE LIGANDS AND THEIR Ru(II) COMPLEXES

3.1 Introduction

The coordination of the polypyridyl ligand 2,2'-6',2"-terpyridine to Ru(II) affords very stable complexes and has attracted attention in recent years [387–391]. These complexes as inorganic dyes possess highly versatile luminescent and photoredox properties useful for the development of photochemistry, photophysics, photocatalysis, photoelectrochemistry, electron and energy transfer processes [5, 144, 392, 393]. One of the major important features of Ru(II) polypyridine complexes is that their ground and excited state properties can be gradually changed by adequate choice and combination of ligands having different π-accepting and σ-donating abilities [394]. In the family of Ru(II) polypyridine complexes, there are two essential complexes $[Ru(bpy)_3]^{2+}$ and $[Ru(trpy)_2]^{2+}$, which have been investigated in great detail [5, 144, 289, 301, 392 and 393]. The former has a very long excited-state lifetime and strong room temperature emission [5, 395–397], and so emission and transient characterization are readily observable. It is of interest to probe the interaction between it and other substrates. Although the latter has a shorter excited-state lifetime and a much weaker luminescence in fluid solution at room temperature [398, 399], the geometry of $[Ru(trpy)_2]^{2+}$ complexes, on the contrary, offers the possibility to design triads in which the two additional components are on opposite directions with respect to the photosensitizer.

In addition, $[Ru(trpy)_2]^{2+}$ complexes are achiral having two symmetry planes and C_2 axis, and the introduction of a single substituent at the 4'-position of each

terpyridyl ligand does not lead to isomeric mixtures. These triads are currently the object of extensive investigations [289, 400–403].

In our quest at improving the molar extinction coefficient as well as increasing the wavelength of complexes towards the near-infrared region through extension of π-bond conjugation, this chapter describes the synthesis, characterization and electrochemical properties of both anthracenyl- and non-anthracenyl functionalized terpyridines and their corresponding homonuclear ruthenium(II) complexes.

3.2 Synthesis of Terpyridyl ligands

3.2.1. Synthesis of 4'-Bromo-2,2':6',2"-Terpyridine (L11) [404]

A stirred solution of terpyridine (3.0 g, 0.013 mmol) and HBr (1.04 g, 0.7 mL, 0.013 mmol) in methanol (60 mL) was added to a 47 % aqueous solution of H_2O_2 (0.44 g, 0.4 mL, 0.013 mmol) slowly, over a period of 15 min at room temperature. The mixture was stirred for 20 h and the reaction progress monitored by TLC. After completion, the solvent was removed under reduced pressure and the residue dissolved in ethyl acetate (150 mL), and washed with brine (3 x 100 mL) and dried over anhydrous sodium bisulphate. The product was isolated by careful column chromatography on silica gel using dichloromethane–ethyl acetate (4:1, v/v, 200 mL) to give a yellow-red viscous liquid which was allowed to air dry and finally recrystallized from diethyl ether–ethanol to afford the title compound **L11**.

3.2.2 4'-(9-Bromoanthracenyl)- 2,2':6',2"-Terpyridine (L12)

A mixture of 4'-bromoterpyridine (**L11**) (1.00 g, 3.20 mmol) and 9,10-dibromoanthracene (1.08 g, 3.20 mmol) was dissolved in benzene–dichloromethane (1:1, v/v, 160 mL), and the solution stirred for 10 min until all the solid had dissolved,

followed by the addition of triethylamine (1.0 mL) and Pd/C (0.045 g). The mixture was refluxed for 8 h, concentrated under reduced pressure to remove the solvent. The organic solid was washed with distilled water (30 mL) and then extracted with chloroform (100 mL). The chloroform extract was evaporated to dryness and the solid recrystallized from ethanol to afford the title compound **L12**.

3.2.3. 4'-(9-Bromodianthracenyl)- 2,2':6',2"-Terpyridine (L13)

Ligand **L13** was synthesized as follows: Ligand **L12** (0.90 g, 1.83 mmol) and 9,10-dibromoanthracene (0.63 g, 1.83 mmol) were dissolved in benzene–dichloromethane (1:1, v/v, 160 mL), and the solution stirred for 10 min until all the solid had dissolved, followed by the addition of triethylamine (1.0 mL) and Pd/C (0.045 g). The mixture was refluxed for 8 h, concentrated under reduced pressure to remove the solvent. The organic solid was washed with distilled water (30 mL) and then extracted with chloroform (100 mL). The chloroform extract was evaporated to dryness and the solid recrystallized from ethanol to afford the title compound **L13**.

3.2.4. 4'-(9-Bromotrianthracenyl)- 2,2':6',2"-Terpyridine (L14) [405, 406].

The synthetic procedure to obtain ligand **L14** followed the same routine as reported for **L13**. A stoichiometric amount of Ligand, **L13** (0.50 g, 0.75 mmol) was reacted with 9,10-dibromoanthracene (0.25 g, 0.75 mmol) to afford the title compound as **L14**.

3.2.5. 4'-(2,3-Dimethylacrylic acid)- 2,2':6',2"-Terpyridine (L15)

In a 100 mL flask, 4'-Bromo-terpyridine (0.42 g, 1.35 mmol) and 2,3-dimethylacrylic acid (0.14 g, 1.35 mmol) were dissolved in chloroform/methanol (50 mL, 1:1, v/v). Triethylamine (1.0 mL) and palladium-carbide (0.050 g, 0.42 mmol) were added and the mixture put into reflux for 8 h at a temperature between 110-120 ^{o}C. The reaction was allowed to cool to room temperature and the solvent removed under reduced pressure. The pink residue was dissolved in degassed water and then extracted with chloroform. The chloroform extract was concentrated *in vacuo* to obtain a purple solid which was then recrystallized in diethyl ether–ethanol (1:1, v/v) to afford compound **L15**.

3.3 Synthesis of Homoleptic Ru(ll)-2,2':6',2"-Terpyridine complexes

3.3.1. Bis(4'-(2,3-dimethylacrylic acid)-2,2':6',2"-terpyridyl ruthenium(ll)bis-hexa fluorophosphate complex (C17)

Two to one equivalent molar ratio of 4'-(2,3-dimethylacrylic acid)-2,2:6,2-terpyridine (**L15**) (0.20 g, 0.61 mmol) and [$RuCl_2(dmso)_4$] (0.15 g, 0.30 mmol) were dissolved in dimethylformamide (40 mL) and refluxed for 5 h. The crude product was concentrated *in vacuo* to afford a red oil solution which on addition of 0.05 M NaOH gave red-brown precipitate. The precipitate dissolves completely with addition of 0.5 M HNO_3 (pH 3). The red solution was filtered and the filtrate was kept in the fridge for 12 h; after which the solution was concentrated and then precipitated with the addition of aqueous solution of ammonium hexafluorophosphate to afford a rusty red-brown solid. The crude solid was dissolved in minimum volume of methanol and adsorbed onto Sephadex LH-20 and was eluted using isocratic method in 250 mL of

diethyl ether-methanol (1:1, v/v). The solvent from resultant solution was removed *in vacuo* as **C17**.

3.3.2. Bis-(4-(9-anthracenyl-10-(2,3-dimethylacrylic acid)- 2,2':6',2" terpyridyl-ruthenium(II) bis-hexafluorophosphate complex (C18)

Two equivalent of 4'-(9-bromoanthracenyl)-terpyridine (**L12**) (0.50 g, 1.0 mmol) and $[RuCl_2(dmso)_4]$ (0.25 g, 0.51 mmol) in DMF (40 mL) were reflux for 1 h and to the resulting solution; 2,3-dimethylacrylic acid (0.10 g, 1.0 mmol), KOH (0.06 g, 1.0 mmol) and 1 mL triethylamine were added. The mixture was refluxed for 8 h in the dark at about 120 ^oC. The resultant solution was cooled, filtered and the solvent remove in vacuo. A 10 mL solution of NaOH (0.05 M) was added to the solid resulting in a deep orange red solution that was filtered to remove any residue. The pH of the solution was then adjusted to 3 with 0.5 M HNO_3, and the resulting solution left to stand in the fridge for 12 h. The acidic solution obtained after filtration of the insoluble precipitate was concentrated to afford a semi-solid product which was purify by column chromatography on Sephadex LH-20 in ethanol-toluene, 50 %, v/v. Column fractions were added and concentrated under reduced pressure and excess aqueous ammonium hexafluorophosphate was added to precipitate the complex as **C18** [408, 409].

3.3.3. Bis-(4-(9-dianthracenyl-10-(2,3-dimethylacrylic acid)-2,2':6',2" terpyridyl ruthenium(II) bis-hexafluorophosphate complex (C19)

Complex **C19** was prepared using the same procedure as reported for **C18** (Section 3.3.2). The reaction involved two equivalent of **L13** (0.40 g, 0.60 mmol),

$[RuCl_2(dmso)_4]$ (0.15 g, 0.30 mmol) and 2,3-dimethylacrylic acid (0.06 g, 0.60 mmol) as major reactants.

3.3.4. Bis-(4-(9-trianthracenyl-10-(2,3-dimethylacrylic acid)-2,2':6',2"-terpyridyl ruthenium(II) bis-hexafluorophosphate complex (C20)

The synthesis of complex **C20** followed the same procedure as reported for **C18** (Section 3.2.2). Two equivalent of **L14** (0.50 g, 0.60 mmol), $[RuCl_2(dmso)_4]$ (0.14 g, 0.30 mmol) and 2,3-dimethylacrylic acid (0.06 g, 0.60 mmol) were used as the major reactants.

3.4 Experimental Results and Physicochemical data on Terpyridine Ligands and Complexes

3.4.1 Characterization of compound L11

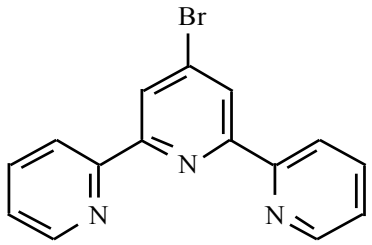

(L11)

Colour: A yellow powder.

Melting point: 209 –211 ^{o}C

IR (KBr) $\nu_{cm\text{-}1}$: 3475, 3407, 3039, 2806, 1606, 1583, 1562, 1524, 1454, 1442, 1423, 1355, 1289, 1172, 1153, 1078, 1039, 991, 857, 833, 784, 764, 547.

Elemental Analysis (%): Found: C, 57.94; H, 3.54; N, 13.27, $C_{15}H_{10}N_3Br$ requires C, 57.71; H, 3.23; N, 13.46.

Percentage yield: (2.74 g, 91 %).

3.4.2 *Characterization of compound L12*

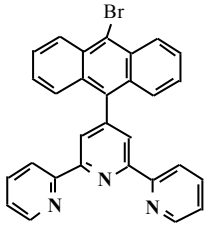

(L12)

Colour: pink-red solid

Melting point: 189 –190 ^{o}C

IR (KBr) ν_{cm-1}: 3419, 3048, 2925, 2852, 1744, 1620, 1581, 1562, 1453, 1437, 1423, 1304, 1256, 1078, 1039, 1028, 989, 926, 832, 763, 747, 675, 578.

UV-Vis (λ_{max} nm, ε = M^{-1} cm^{-1}, $CHCl_3$): 342 (36900); 361 (77000); 381 (124000); 403 (116000).

Fluorescence Data: λ_{exc} = 450 nm; λ_{em} = 745 nm (Int. 600 %).

^{1}H NMR ($CDCl_3$): δ 8.69 (d, *J* = 4.4 Hz, 2H, H-3, 3"), 8.60 (d, *J* = 8.0 Hz, 2H, H-5, 5"), 8.56 (dd, *J* = 3.2, 6.7 Hz, 4H, anthr.), 8.44 (d, *J* = 7.8 Hz, 1H, H-3'), 7.94 (t, *J* = 7.8 Hz, 2H, H-4, 4"), 7.84 (t, *J* = 7.7 Hz, 2H, H-6, 6"), 7.60 (dd, *J* = 3.1, 6.8 Hz, 4H, anthr.), 7.27 (t, *J* = 4.4 Hz, 1H, H-5'). ^{13}C NMR ($CDCl_3$): δ 156.26, 155.36, 149.14, 137.89, 136.83, 131.06, 128.28, 127.45, 123.73, 123.53, 121.16, 120.99.

Electrochemical data: E_{pa}/V = + 0.65, $E_{1/2}$ = -0.27, -0.51,-0.99 V.

Elemental Analysis (%): Found: C, 71.10; H, 3.83; N, 8.48, $C_{29}H_{18}N_3Br$ requires, C, 71.32; H, 3.71; N, 8.60.

Percentage yield: 1.36 g, 65 %.

3.4.3 *Characterization of compound L13*

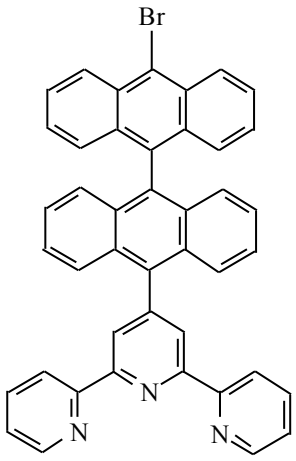

Colour: Yellow solid

Melting point: 215 –216 ^{o}C

IR (KBr) $\nu_{cm\text{-}1}$: 3473, 3409, 3035, 2926, 2851, 1929, 1620, 1606, 1582, 1561, 1523, 1437, 1423, 1350, 1304, 1289, 1256, 1150, 1077, 1027, 991, 959, 926, 838, 764, 747, 675, 578.

UV-Vis (λ_{max} nm, ε = M^{-1} cm^{-1}, $CHCl_3$): 342 (66000); 361 (118500); 381 (187500); 403 (168500).

Fluorescence Data: λ_{exc} = 450 nm; λ_{em} = 745 nm (Int. 600 %).

^{1}H NMR ($CDCl_3$): δ 8.70 (d, *J* = 4.4 Hz, 2H, H-3, 3"), 8.61 (d, *J* = 7.96 Hz, 2H, H-5, 5"), 8.56 (dd, *J* = 3.2, 6.8 Hz, 8H, anthr.), 8.44 (d, *J* = 7.8 Hz, 1H, H-3'), 7.95 (t, *J* = 7.8 Hz, 2H, H-4, 4"), 7.85 (t, *J* = 1.5, 7.7 Hz, 2H, H-6, 6"), 7.60 (dd, *J* = 3.2, 6.9 Hz, 8H, anthr.), 7.41 (t, *J* = 0.9, 5.1 Hz, 1H, H-5'). ^{13}C NMR ($CDCl_3$): δ 156.13, 155.24, 149.05, 137.95, 136.99, 131.06, 128.28, 127.46, 123.80, 123.53, 121.25, 121.09.

Electrochemical data: E_{pa}/V = + 0.73, $E_{1/2}$ = -0.36, -0.87 V.

Elemental Analysis (%): Found: C, 77.72; H, 3.64; N, 6.76, $C_{43}H_{26}N_3Br$ requires, C, 77.71; H, 3.94; N, 6.32.

Percentage yield: 0.80 g, 53 %.

3.4.4 *Characterization of compound L14*

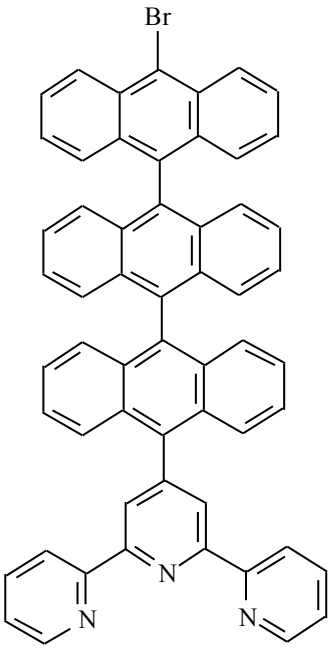

Colour: Deep yellow.

Melting point: 218 –220 ^{o}C

IR (KBr) ν_{cm-1}: 3403, 3075, 2926, 2852, 1621, 1605, 1582, 1562, 1523, 1437, 1423, 1304, 1256, 1027, 990, 960, 926, 837, 763, 746, 675, 604, 578.

UV-Vis (λ_{max} nm, ε = M^{-1} cm^{-1}, $CHCl_3$): 342 (89200); 361 (180000); 381 (274000); 403 (233500).

Fluorescence Data: λ_{exc} = 450 nm; λ_{em} = 745 nm (Int. 600 %).

^{1}H NMR ($CDCl_3$): δ 8.70 (d, *J* = 4.1 Hz, 2H, H-3, 3"), 8.61 (d, *J* = 7.92 Hz, 2H, H-5, 5"), 8.56 (dd, *J* = 3.2, 6.8 Hz, 12H, anthr.), 8.45 (d, *J* = 7.8 Hz, 1H, H-3'), 7.95 (t, *J* = 7.8 Hz, 2H, H-4, 4"), 7.86 (t, *J* = 7.7 Hz, 2H, H-6, 6"), 7.61 (dd, *J* = 3.2, 6.9 Hz, 12H, anthr.), 7.33 (t, *J* = 6.6 Hz, 1H, H-5'). ^{13}C NMR ($CDCl_3$): δ 156.03, 155.15, 148.99, 137.98, 137.09, 131.06, 128.28, 127.45, 123.83, 123.53, 121.30, 121.15.

Electrochemical data: Not visible.

Elemental Analysis (%): Found: C, 81.88; H, 4.43; N, 5.36, $C_{57}H_{34}N_3Br$ requires, C, 81.42; H, 4.08; N, 5.00.

Percentage yield: 0.59 g, 79 %.

3.4.5. Characterization of compound L15

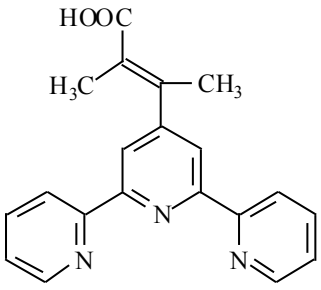

Colour: Purple crystalline solid.

Melting point: 65-67 ^{o}C.

IR (KBr) ν_{cm-1}: 3473, 3415, 3051, 1618, 1582, 1564, 1455, 1422, 1264, 1146, 1100, 1080, 1038, 989, 833, 761, 735, 622, 509, 473.

^{1}H NMR (400 MHz, DMSO-d_6): δ 8.73 (d, *J* = 4.0 Hz, 1H), 8.63 (d, *J* = 7.6 Hz, 1H), 8.45 (d, *J* = 7.6 Hz, 1H), 8.10-8.02 (m, 2H), 7.50 (d, *J* = 5.2 Hz, 1H), 2.09 (s, CH_3).

Elemental Analysis (%): Found: C, 72.15; H, 4.83; N, 12.33 $C_{20}H_{17}N_3O_2$ requires C, 72.49; H, 5.17; N, 12.68.

Percentage yield: 0.41 g, 73 %.

3.4.6. *Characterization of complex C17*

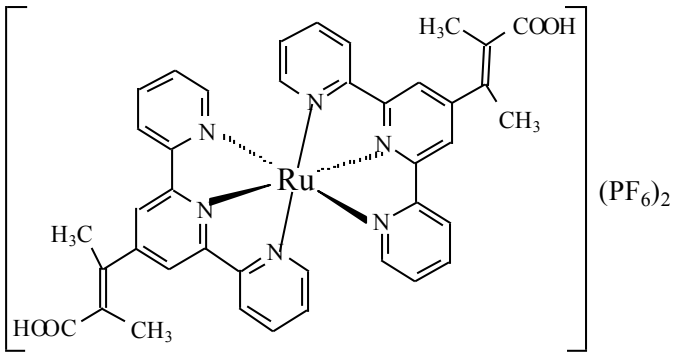

Colour: Red-brown solid.

Melting point: 210 –213 ^{o}C

IR (KBr) $\nu_{cm\text{-}1}$: 3430, 3115, 2926, 2865, 1921, 1619, 1610, 1588, 1534, 1497, 1450, 1384, 1299, 1246, 1177, 1053, 1025, 839, 779, 767, 614, 557, 399.

UV-Vis (λ_{max} nm, ε = M^{-1} cm^{-1}, $CHCl_3$-MeOH (1:1)): 310 (9090), 479 (1928), 907 (715), 1010 (660).

Fluorescence Data: (λ_{exc} = 400 nm; λ_{em} = 744 nm).

^{1}H NMR (DMSO-d_6): δ 9.25 (d, *J* = 4.4 Hz, 3H), 8.90 (d, *J* = 8.0 Hz, 3H), 8.56 (dd, *J* = 3.2, 6.8 Hz, 3H), 8.31(s, 2H), 8.25 (s, 2H), 8.10 (d, *J* = 4.4 Hz, 3H), 7.82 (t, *J* = 3.2, 6.8 Hz, 3H), 2.00 (s, CH_3).

^{13}C NMR (DMSO-d_6): δ 157.69, 154.74, 152.03, 151.78, 151.50, 146.78, 141.48, 139.64, 138.05, 135.86, 127.71, 125.90, 124.49, 123.96, 122.83, 122.77, 34.36. Elemental Analysis (%): Found: C, 45.28; H, 3.20; N, 7.49, $RuC_{40}H_{34}N_6O_4P_2F_{12}$ requires C, 45.59; H, 3.25; N, 7.98.

Percentage yield: 0.12 g, 34 %.

3.4.7 *Characterization of complex C18*

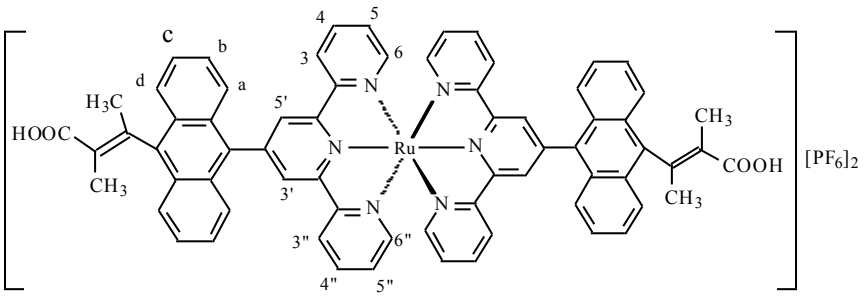

Colour: Dark brown solid

Melting point: 196 –197 ^{o}C

IR (KBr) $\nu_{cm\text{-}1}$: 3418, 3121, 2926, 2852, 2366, 1917, 1678, 1621, 1592, 1451, 1384, 1304, 1284, 1256, 1170, 1097, 1054, 1028, 926, 839, 772, 747, 694, 558, 468, 423.

UV-Vis (λ_{max}/nm, ε = M^{-1} cm^{-1}, DMF): 478 (5107), 406 (50500), 384 (52500), 363 (42800), 330 (67200).

Fluorescence Data: λ_{exc} = 400 nm; λ_{em} = 718 nm.

^{1}H NMR (400 MHz, DMSO-d_6): δ 9.08 (d, *J* = 8.1 Hz, 4H, H-3, 3"), 8.81 (d, *J* = 8.0 Hz, 4H H-5, 5"), 8.54 (dd, *J* = 3.2, 6.8 Hz, H-a), 8.21 (dd, *J* = 3.3, 5.8 Hz, H-b), 8.08 (t, *J* = 7.9, 8.1 Hz, 4H, H-4, 4"), 7.94 (dd, *J* = 3.2, 5.7 Hz, H-c), 7.80 (dd, *J* = 3.2, 6.8 Hz, H-d), 7.42 (d, *J* = 5.3 Hz, 4H, H-6, 6"), 7.26 (s, H-3', 5'), 2.73 (s, CH_3), 2.56 (s, CH_3).

^{13}C NMR (400 MHz, DMSO-d_6): δ 182.49, 157.69, 154.73, 152.01, 138.06, 135.87, 134.54, 132.99, 130.32, 130.08, 128.45, 127.73, 126.73, 124.49, 123.95, 122.75, 35.75, 34.36.

Electrochemical data: E_{anodic}/V = 0.85, Ru^{2+}/Ru^{3+} = 1.13 V, $E_{cathodic}$/V = -0.54 V.

Elemental Analysis (%): Found: C, 58.37; H, 3.65; N, 5.54, $RuC_{68}H_{50}N_6O_4P_2F_{12}$ requires C, 58.08; H, 3.58; N, 5.98.

Percentage yield: 0.18 g, 62 %

3.4.8 Characterization of complex C19

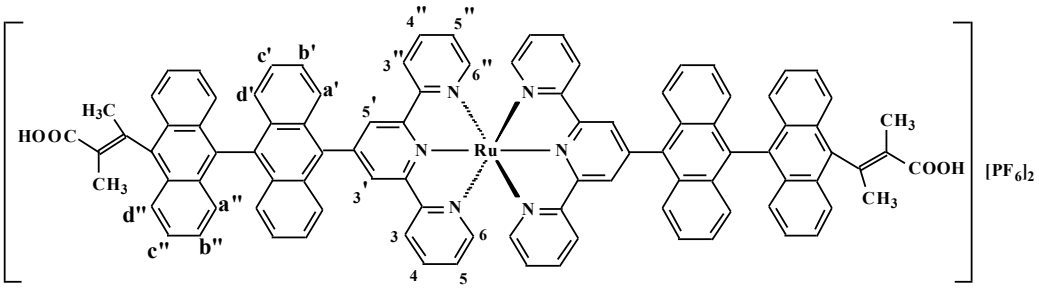

Colour: Deep orange solid

Melting point: 195 –197 ^{o}C

IR (KBr) ν_{cm-1}: 3429, 3076, 2926, 2864, 2272, 1953, 1678, 1616, 1516, 1431, 1384, 1332, 1304, 1285, 1256, 1170, 1053, 1028, 839, 776, 747, 693, 558.

UV-Vis (λ_{max}/nm, ε = M^{-1} cm^{-1}, DMF): 478 (10009), 404 (52300) 381 (58160), 360 (50300), 324 (94300).

Fluorescence Data: λ_{exc} = 400 nm; λ_{em} = 682 nm.

^{1}H NMR (400 MHz, DMSO-d_6): δ 9.08 (d, *J* = 8.2 Hz, 4H, H-3, 3"), 8.82 (d, *J* = 8.7 Hz, 4H H-5, 5"), 8.75 (dd, *J* = 4.7, 8.7 Hz, H-a'), 8.63 (d, *J* = 8.1 Hz, H-b'), 8.60 (dd, *J* = 3.8, 8.8 Hz, H-c'), 8.53 (dd, *J* = 3.4, 6.8 Hz, H-a"), 8.21 (dd, *J* = 3.4, 5.8 Hz, H-b"), 8.06 (t, *J* = 6.8, 8.0 Hz, 4H, H-4, 4"), 7.94 (dd, *J* = 3.3, 5.8 Hz, H-c"), 7.87 (dd, *J* = 6.1, 8.0 Hz, H-d'), 7.79 (dd, *J* = 3.1, 6.8 Hz, H-d"), 7.43 (d, *J* = 5.3 Hz, 4H, H-6, 6"), 7.26 (s, H-3', 5'), 2.73 (s, CH_3), 2.56 (s, CH_3). ^{13}C NMR (400 MHz, DMSO-d_6): δ 182.48, 157.69, 157.09, 156.90, 154.86, 154.74, 152.03, 138.15, 134.53, 132.99, 130.30, 130.07, 129.02, 128.44, 127.72, 127.68, 127.61, 126.72, 124.50, 124.17, 122.76, 122.49, 121.75, 121.19, 35.74, 34.35, 30.74.

Electrochemical data: E_{anodic} = 0.26 V, Ru^{2+}/Ru^{3+} = 0.71 V; $E_{cathodic}$ = -0.69 V.

Elemental analysis (%): Found: C, 65.29; H, 3.62; N, 4.46, $RuC_{96}H_{66}N_6O_4P_2F_{12}$ requires C, 65.57; H, 3.78; N, 4.78.

Percentage yield: 0.24 g, 71 %

3.4.9. Characterization of complex C20

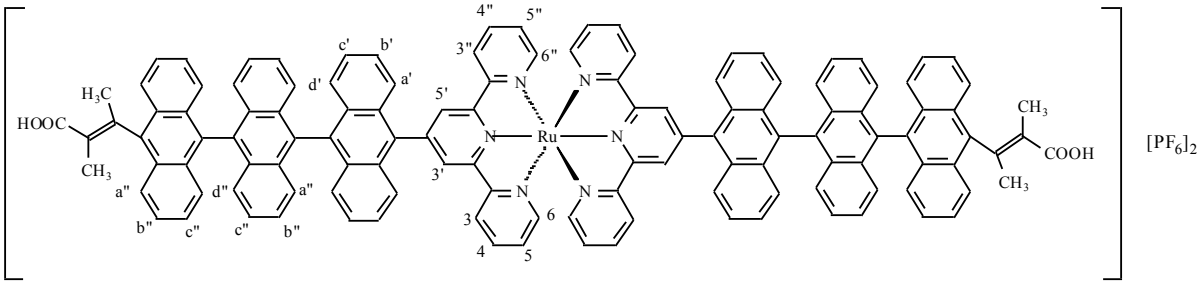

Colour: Bright orange solid.

Melting point: 205–207 ^{o}C

IR (KBr) $\nu_{cm\text{-}1}$: 3429, 3075, 3028, 2925, 2852, 1940, 1678, 1621, 1593, 1437, 1385, 1332, 1304, 1285, 1256, 1170, 1027, 926, 839, 746, 694, 578, 558.

UV-Vis (λ_{max}/nm, ε = M^{-1} cm^{-1}, DMF): 472 (10003), 405 (13880), 383 (14260), 363 (9540), 343 (6180).

Fluorescence Data: $\lambda_{exc.}$ = 400 nm; λ_{em} = 744 nm.

^{1}H NMR (400 MHz, DMSO-d_6): δ 9.08 (d, *J* = 8.2 Hz, 4H, H-3, 3"), 8.82 (d, *J* = 8.7 Hz, 4H H-5, 5"), 8.75 (dd, *J* = 4.7, 8.7 Hz, H-a'), 8.63 (d, *J* = 8.1Hz, H-b'), 8.60 (dd, *J* = 3.8, 8.8 Hz, H-c'), 8.53 (dd, *J* = 3.4, 6.8 Hz, H-a"), 8.21 (dd, *J* = 3.4, 5.8 Hz, 2H, H-b"), 8.06 (t, 4H, H-4, 4"), 7.94 (dd, *J* = 3.3, 5.8 Hz, H-c"), 7.87 (dd, *J* = 6.1, 8.0 Hz, H-d'), 7.79 (dd, *J* = 3.1, 6.8 Hz, H-d"), 7.43 (d, *J* = 5.3 Hz, 4H, H-6, 6"), 7.26 (s, H-3', 5'), 2.73 (s, CH_3), 2.56 (s, CH_3). ^{13}C NMR (400 MHz, DMSO-d_6): δ 182.48, 157.69, 157.10, 156.91, 156.82, 154.86, 152.04, 138.20, 134.53, 133.01, 130.31, 128.45, 127.73, 127.62, 126.72, 124.50, 124.17, 123.96, 122.76, 122.49.

Electrochemical data: E_{anodic} = 0.67 V, Ru^{2+}/Ru^{3+} = 0.97 V; $E_{1/2}$ = -0.92 V.

Elemental Analysis (%): Found, C, 70.33; H, 3.39; N, 3.78, requires $RuC_{124}H_{82}N_6O_4P_2F_{12}$ C, 70.55; H, 3.92; N, 3.98.

Percentage yield: 0.35 g, 69 %.

3.5 DISCUSSION OF RESULTS

3.5.1 Synthesis of terpyridyl ligands and homoleptic complexes

The traditional method of producing polymerized hydrocarbons by dehalogenation of hydrocarbons using biscyclooctadienyl nickel(0) or magnesium-diene complexes as catalysts and Sonogashira coupling of aryl bromides under palladium-catalysis are well documented [405, 407], and have been modified in this work. Scheme 3.1 shows the synthetic route for the formation of the ligands. The first step involves reaction of a stoichiometric ratio of terpyridine ligand **1a** with hydrobromic acid and hydrogen peroxide (1:1, v/v) solution in methanol at room temperature. The product, 4'-bromoterpyridine (**L11**) was subsequently reacted with 9,10-dibromoanthracene in a palladium-catalyzed cross-coupling reaction (dichloromethane–benzene, 1:1, v/v) to form ligand **L12**. Reaction of **L12** with 9,10-dibromoanthracene using the same condition afforded ligand **L13**. Ligand **L14** was obtained in a similar reaction of **L13** with 9,10-dibromoanthracene. A stoichiometric reaction in 50 % dichloromethane–benzene and the use of a higher temperature for the synthesis of **L12**, **L13** and **L14** limit the formation of mixtures of compounds as observed when milder experimental conditions and inappropriate solvents were used. For example, poor product yields and mixtures were obtained when the reactions were carried out using combination of ethanol and palladium(II) acetate as catalyst.

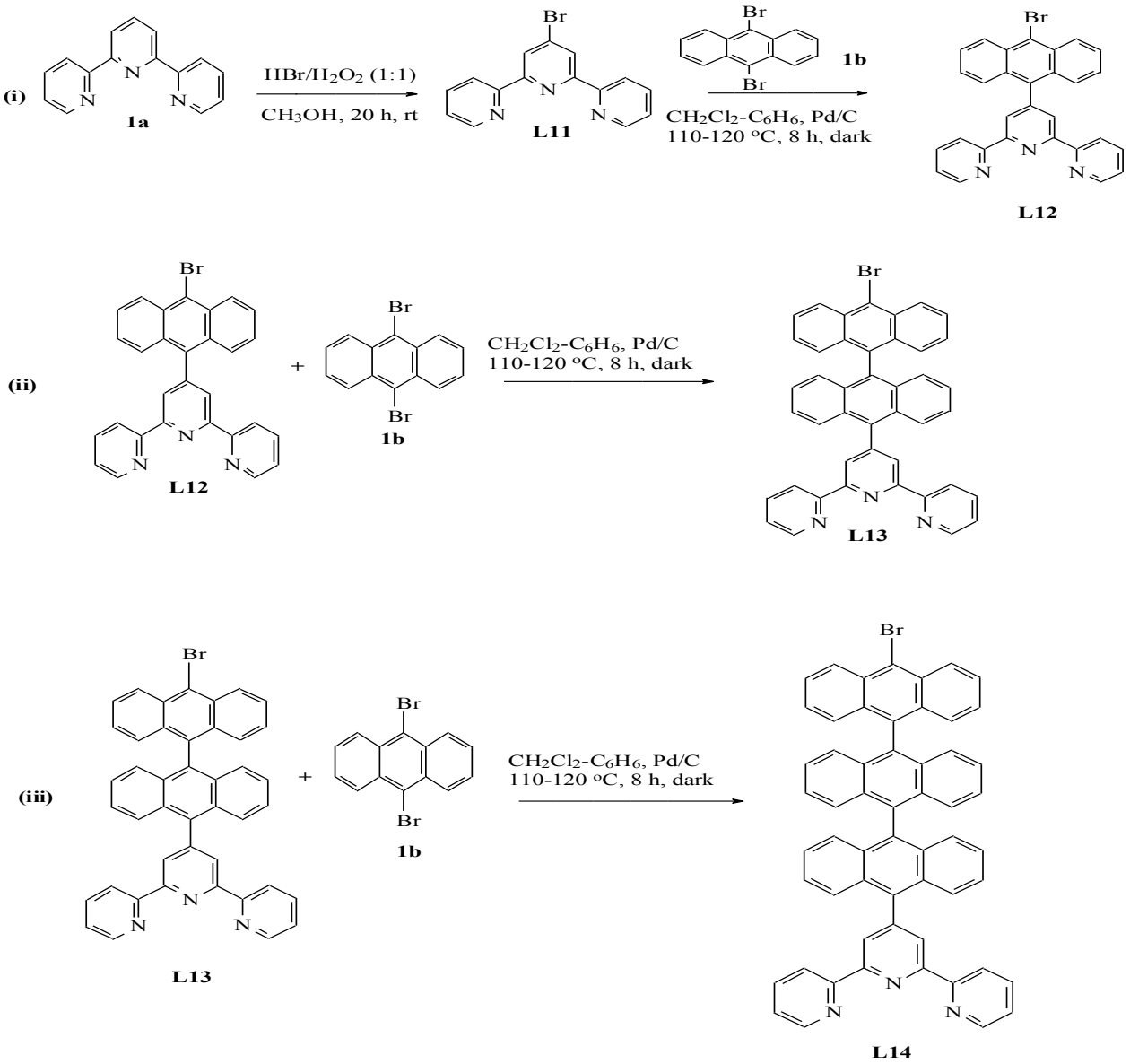

Scheme 3.1 Synthesis of bromo-, mono-, di- and trianthracenyl terpyridines.

The reaction between **L11** and 2,3-DMAA under a catalyzed palladium cross-coupling reaction using high temperature afforded the desired coupling product as **L15** (Scheme 3.2) and its complex **C17** resulted from its reaction with $[RuCl_2(dmso)_4]$ (Scheme 3.3).

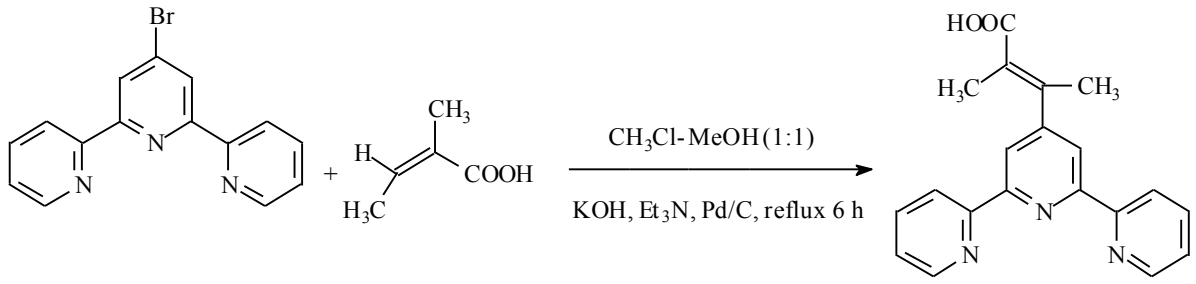

Scheme 3.2 Synthesis of **L15**: 4'-(2,3-DMAA)-terpyridine

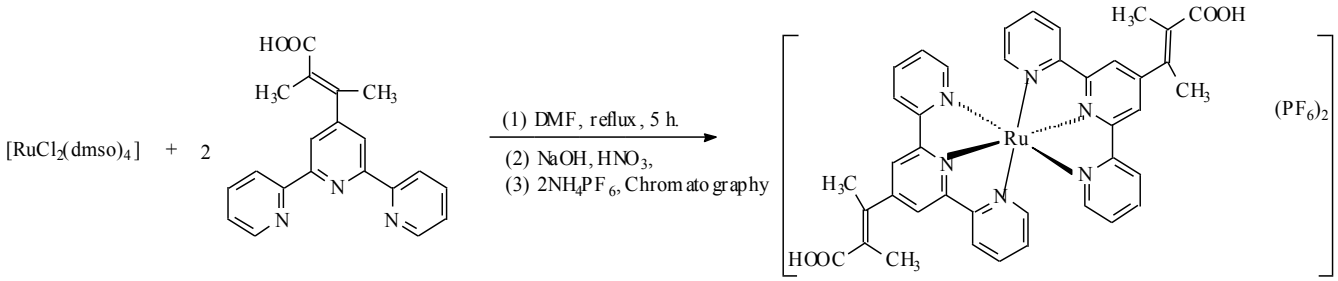

Scheme 3.3 Synthesis of Ru(II) complex of 4'-(2,3-DMAA)-terpyridine

It was observed however, in the functionalized bromoanthracenyl ligands, attempts to synthesized 2,3-dimethylacrylic acid derivatives of the ligands was not successful due to coordination with the palladium metal catalyst and undesired products were obtained. Hence, a direct reaction of the bromo ligands with the metal precursor in forming the ruthenium(II) complex first and then subsequent substitution of the bromine atoms with 2,3-dimethylacrylic acid (2,3-DMAA) to afford complexes **C18**–**C20** (Scheme 3.4).

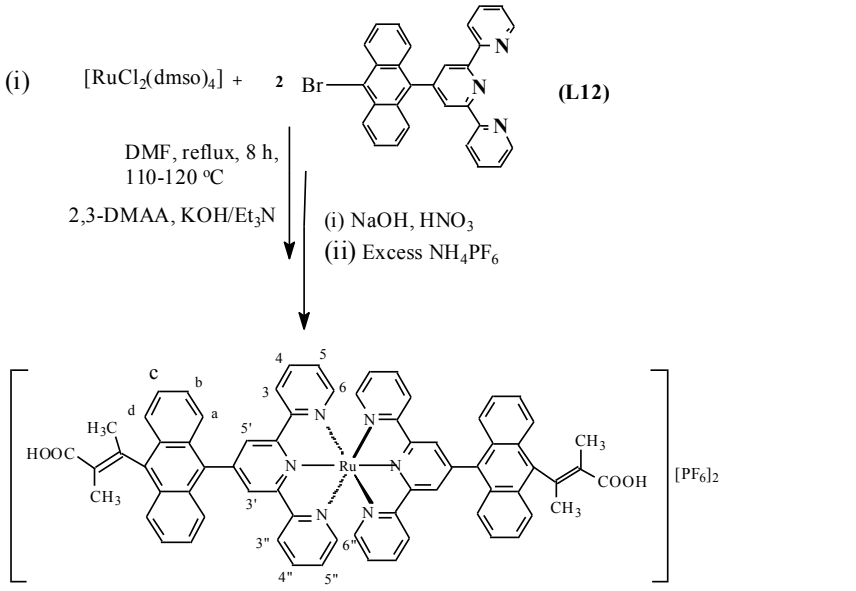
(i)
[RuCl2(dmso)4] +
2
Br
(L12)
DMF, reflux, 8 h,
110-120 °C
2,3-DMAA, KOH/Et3N
(i) NaOH, HNO3
(ii) Excess NH4PF6
HOOC
H3C
CH3
COOH
CH3
CH3
[PF6]2

C18

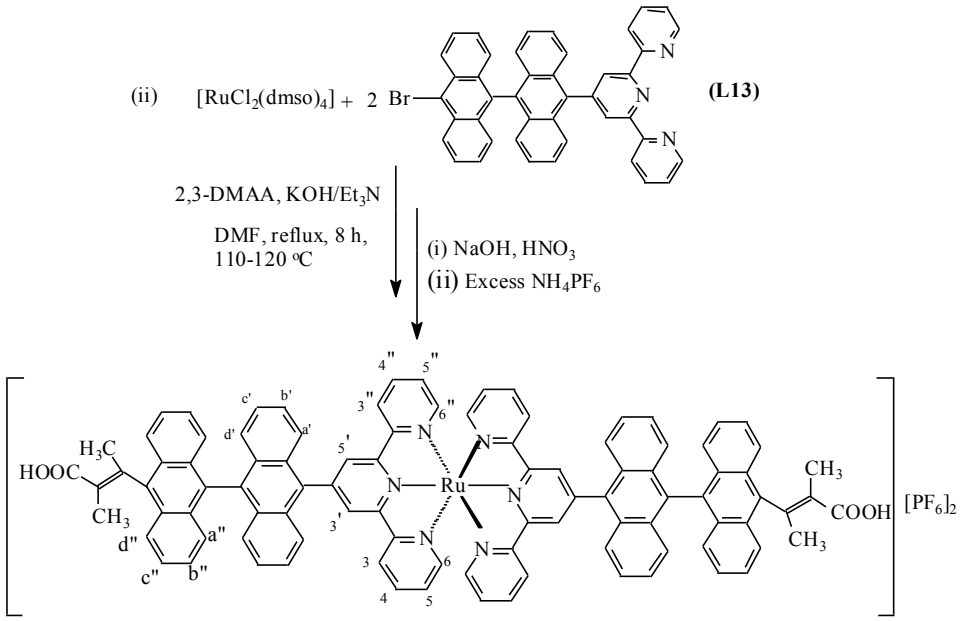
(ii)
[RuCl2(dmso)4] + 2
Br
(L13)
2,3-DMAA, KOH/Et3N
DMF, reflux, 8 h,
110-120 °C
(i) NaOH, HNO3
(ii) Excess NH4PF6
HOOC
H3C
CH3
COOH
CH3
CH3
[PF6]2

C19

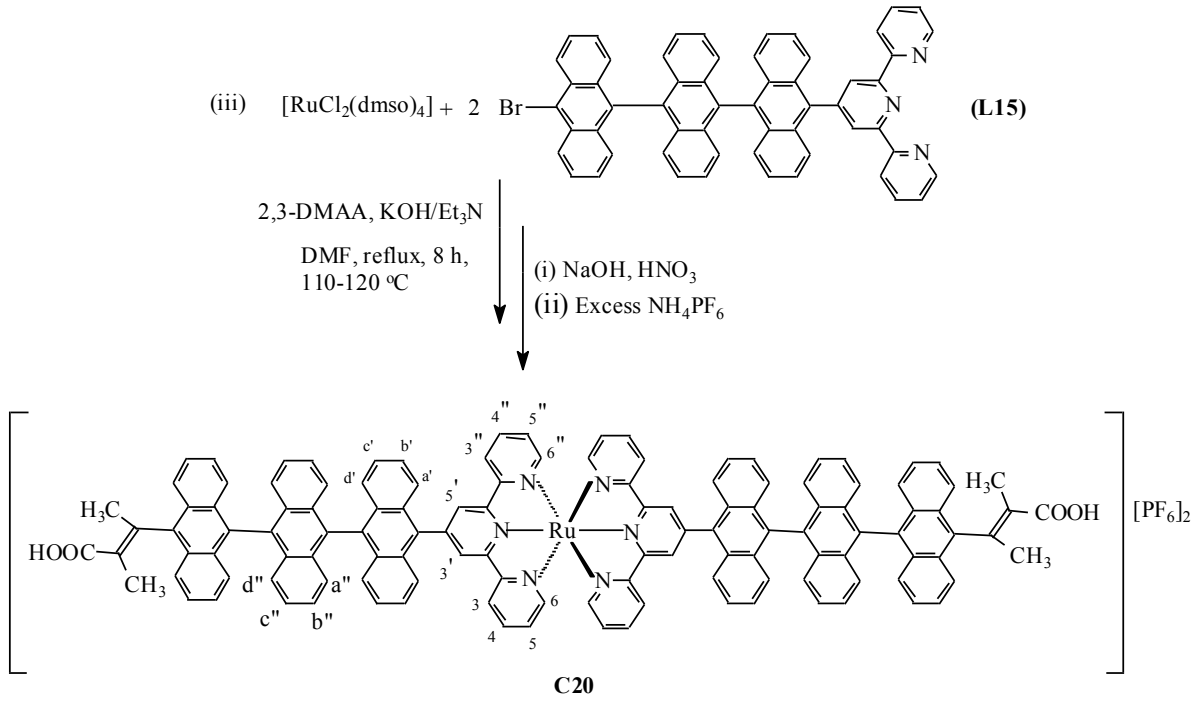

C20

Scheme 3.4 Synthesis of Ru(II) functionalized anthracenyl-bisterpyridyl bis-hexafluorophosphate complexes

3.5.2 Infrared spectra of ligands and complexes

The infrared spectra of the ligands were compared and assigned on careful comparison with the starting materials. A single broad absorption band at 3400 cm^{-1} due to an O–H vibration of the unsubstituted terpyridine ligand splits into two vibrational peaks of equal intensity at 3475 and 3407 cm^{-1} for the **L11** (4'-bromoterpyridyl derivative) and 3473 and 3415 cm^{-1} in **L15**. The IR spectra of the respective ligands showed slight shifts in the frequencies and intensities for the C=N, C=C and C–Br vibrations due to the increasing units of anthracene substitution in **L12**–**L14**.

The infrared spectra of the complexes **C17** – **C20** show strong broad bands in the region of 3430 cm^{-1} due to hydroxyl groups of the carboxylic acid moieties on the complexes. The intense peaks in the region 1950 and 1678 cm^{-1} are due to carboxylic acid groups. The presence of the carboxylate asymmetric 1593 cm^{-1} ν(-COO_{as}^{-}) and symmetric 1384 cm^{-1} ν(COO_{s}^{-}) bands together with broad ν(C=N) of the polypyridyl group at 1516 and 1451 cm^{-1} [410]. The bands in the region 1600–1400 cm^{-1} were ascribed to the stretching mode of terpyridine. A comparison of the infrared spectra of the complexes and 9,10-dibromoanthracene showed that a strong vibrational band in the former was conspicuously absent in the latter, confirming the loss of C–Br bond and the formation of C–C bond linkages of the polyanthracenyl group. Furthermore, the C–C bond linkage between anthracene and terpyridine was affirmed by the absorption frequency at 853 cm^{-1} which was shifted to lower frequency by 14 cm^{-1} in the complexes. The weak absorption frequencies at 470 and 420 cm^{-1} respectively gave indication of the coordination of nitrogen atoms of the ancillary ligands to ruthenium central metal ions. (See Appendices: 53, 56, and 59).

3.5.3 UV-Vis spectra of functionalized anthracenyl ligands and complexes

The UV-Vis absorption spectra of ligands **L12**–**L14** are shown in Figure 3.1. The π→π* intra-ligand transitions occur between 290–420 nm for the anthracene and the terpyridine conjugated couples. Maxima characteristic of anthracene derivatives are found at 342, 361, 381 and 403 nm for **L14**, these are slightly blue-shifted (*ca.*1–2 nm) for **L13** and **L12** respectively. The molar absorptivity coefficient increases with a corresponding increase in the number of anthracenes on the terpyridyl ligand is in the order **L14** > **L13** > **L12**. One interesting observation was found as the wavelength of the ligands shifted to the red. The molar absorptivity coefficient tends to favour **L13** having double-anthracenyl substitution compared to **L12** and **L14** with mono- and tri-anthracenyl substitutions. This may be indicative of an optimum number of anthracene units on the terpyridyl ligand as further increases led to aggregation thus affecting the energy transfer properties of the molecules.

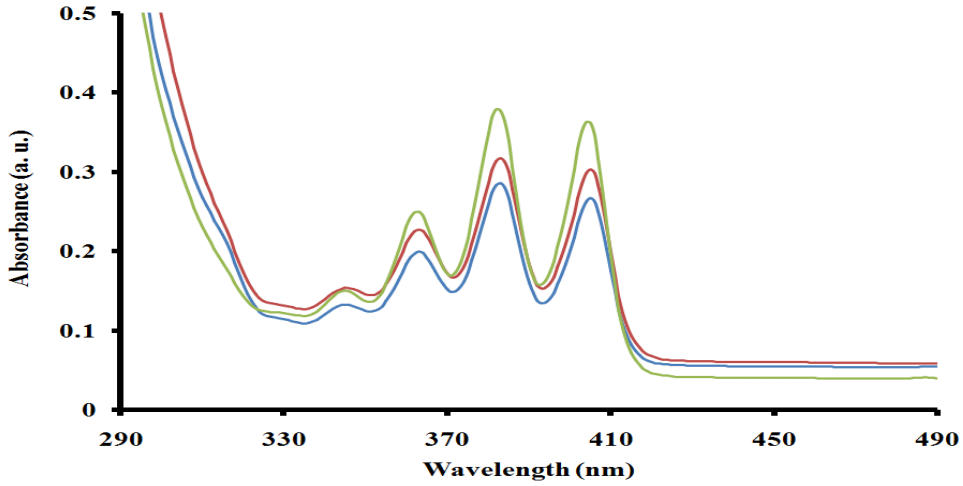

Figure 3.1 UV-Vis absorption spectra of **L12**, **L13** and **L14** in DMF (peaks in ascending mode at 350–410 nm).

The UV-Vis absorption spectrum of **C17** complex has two major parts due to the absence of anthracene unit unlike the **C18**, **C19** and **C20** complexes that are

divided into three major parts (Figure 3.2a). The first and second parts in the latter complexes show the intense and strong absorption bands in the UV region between 200 to 300 nm, and 310 to 410 nm that were assigned to the intra ligand π→π* charge-transfer transitions of terpyridine and anthracene ligands respectively. The vibronic peaks of the anthracene moiety common to the three complexes as were found in **C20** at 359, 379 and 401 nm with the highest molar extinction coefficient compared favourable with those found for **C18** and **C19**. The maxima wavelengths for **C18** and **C19** were blue-shifted (ca. 3-5 nm). In the visible region, the maximum band of the metal-to-ligand charge transfer transition (MLCT) for **C19** peaks at 476 nm (ε = 10009 M^{-1} cm^{-1}), which is blue shifted in **C18** and **C20** (473, 468 nm) respectively, with cocorminant decrease in molar extinction coefficient (Figure 3.2b). The blue shift at the visible region may be due to increase in the energy of the LUMO of the complexes, causing the dπ→π* transitions to occur at higher energies. The increase in the absorbance coefficient of **C20** in the ultra-violet region is ascribed to the increase in the length of π-bond conjugation due to progressive increase in the number of anthracene molecular units in the complex. However, it is interesting to observe that a corresponding inverse relationship was established between the molar extinction coefficient and the extension of π-bond conjugation most especially between **C19** and **C20** in the visible to the near-infrared region which may be due to molecular aggregation in **C20**. Inaddition, an optimum limit seems to be favourable to the number of anthracene units bridging the ligands to the central metal ion which is based on intra-molecular distance. The influence of anthracene in the complexes is shown when compared to **C17** with no anthracene unit. Also common to the complexes at the near-infrared region of the spectra are two important shoulder

peaks at 899 and 1007 nm. These were assigned to the ^{3}MLCT forbidden transition state of the complexes.

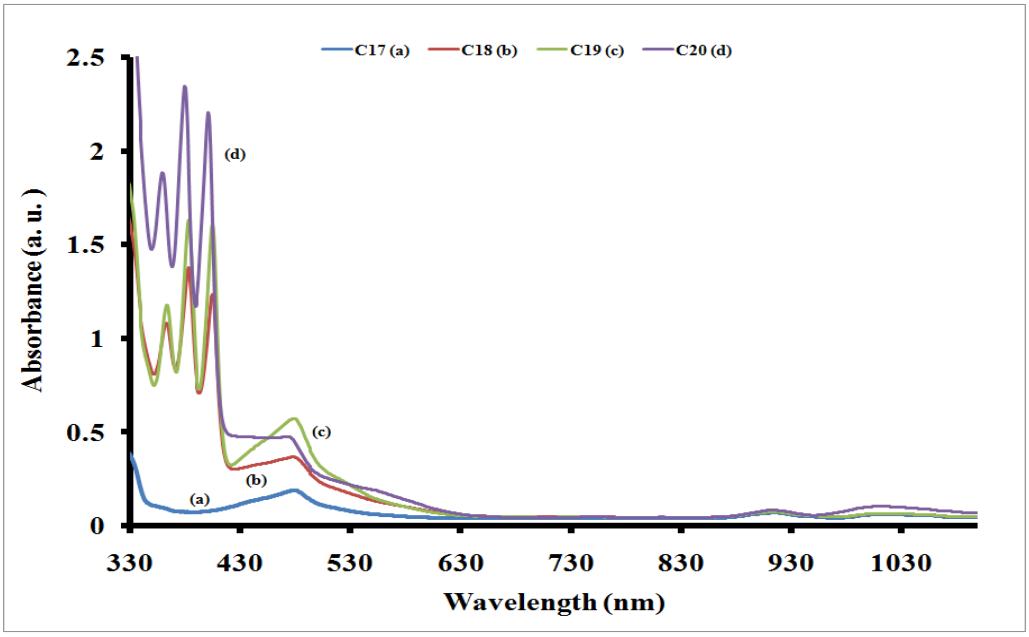

Figure 3.2a. UV-Vis absorption spectra of complexes **C17** (a), **C18** (b), **C19** (c) and **C20** (d) in DMF.

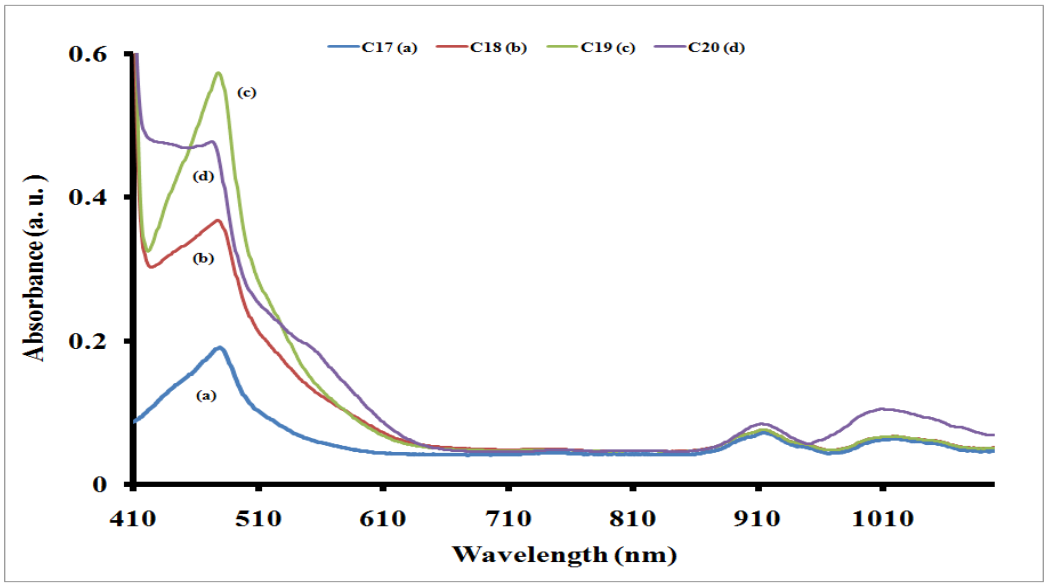

Figure 3.2b. Visible region of absorption of complexes **C17 (a)**, **C18 (b)**, **C19 (c)** and **C20 (d)**.

Table 3.1 Summary of Absorption, luminescence, and electrochemical properties of functionalized anthracenyl and non-anthracenyl bis-terpyridyl Ru(II) complexes

Complex	MLCT maximum (nm)	Abs.Coeff. (M^{-1} cm^{-1})	Emission maximum (nm)	Ru^{2+}/Ru^{3+} /(V)	E_{anodic} /(V)	$E_{cathodic}$	$E_{1/2}$
C17	479	1928	744	–	–	–	–
C18	478	5107	718	1.13	0.85	-0.54	–
C19	478	10009	682	0.71	0.26	-0.69	–
C20	472	10003	744	0.97	0.67	–	-0.92

3.5.4 Emission spectra of functionalized anthracenyl ligands and complexes

The fluorescence spectra of ligands **L11**–**L14** and **L15** are shown in Figure 3.3 and 3.4). A common strong emission wavelength band at 745 nm due to singlet-to-singlet energy transfer at an excitation wavelength of 450 nm was recorded for **L12**–**L14** which is slightly blue-shifted in **L15** (4-DMAA) ligand. The emission spectra show an inverse relationship between the bathochromic shifts in wavelength and the intensity of emission. This result is in accord with the B3LYP/6-31G theoretical calculations for substituted anthracene derivatives in which slight variations are found in the electronic structures leading to electron accepting ability, and then a decrease in the HOMO-LUMO energy gap which is believed to be the origin of the shifting in the emission wavelength to the blue-green region [411, 412]. Emission maximum wavelength was recorded for **C17** at 753 nm compared to the emission wavelength of the complex **C18** at room temperature which displayed wavelength maximum at 717 nm. The effect of the increase in the number of anthracene units was observed in the emission wavelength maxima in **C19** at 682 nm and **C20** at 744 nm (Figure 3.5). A direct relationship has been found between luminescence properties of materials and degree of aggregation. In general, aggregation in the solid state causes undesirable red shifts in the emission spectra and/or emission quenching. Thus, it is well thought that the increasing number of anthracene has resulted in the corresponding decrease in the intensity ratio of both **C19** and **C20** [406].

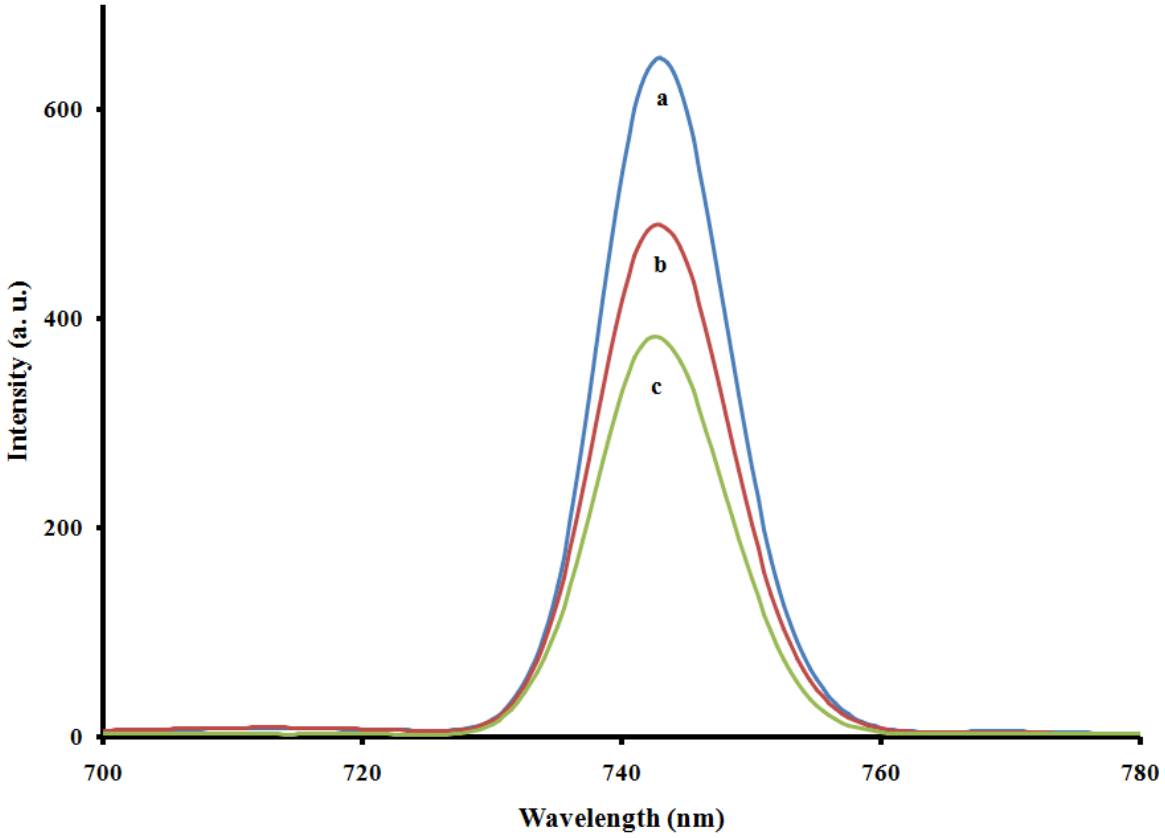

Figure 3.3 Emission spectra of Ligands **L12 (a)**, **L13 (b)** and **L14 (c)** in DMF.

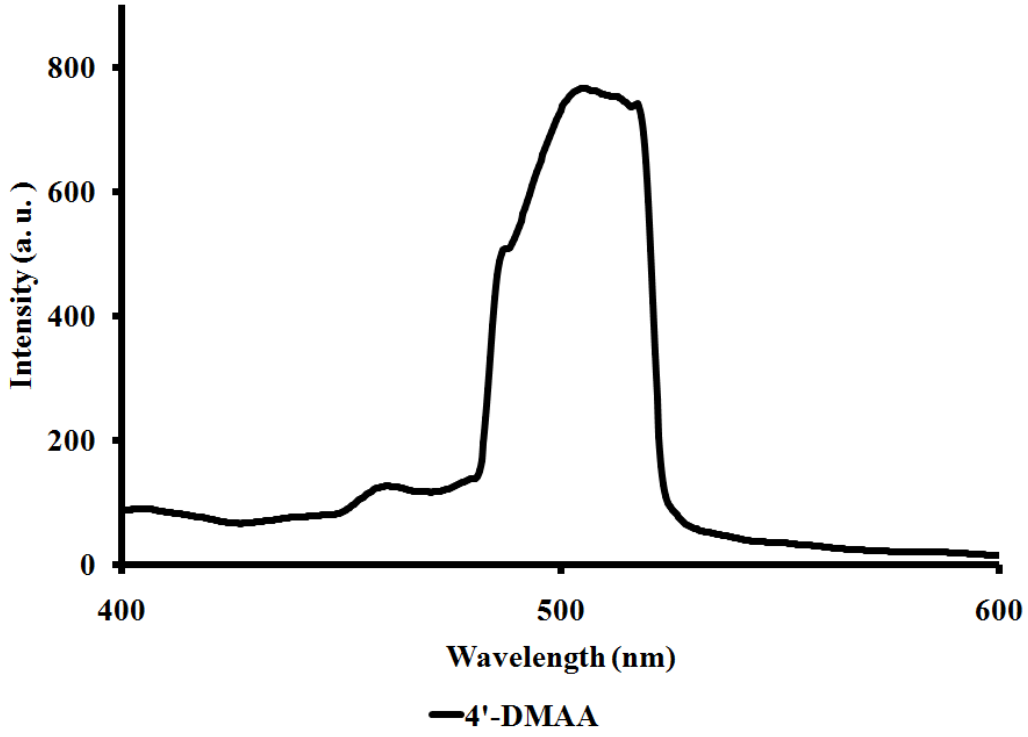

Figure 3.4 Emission spectrum of ligand **L15** (4'-DMAA) in DMF

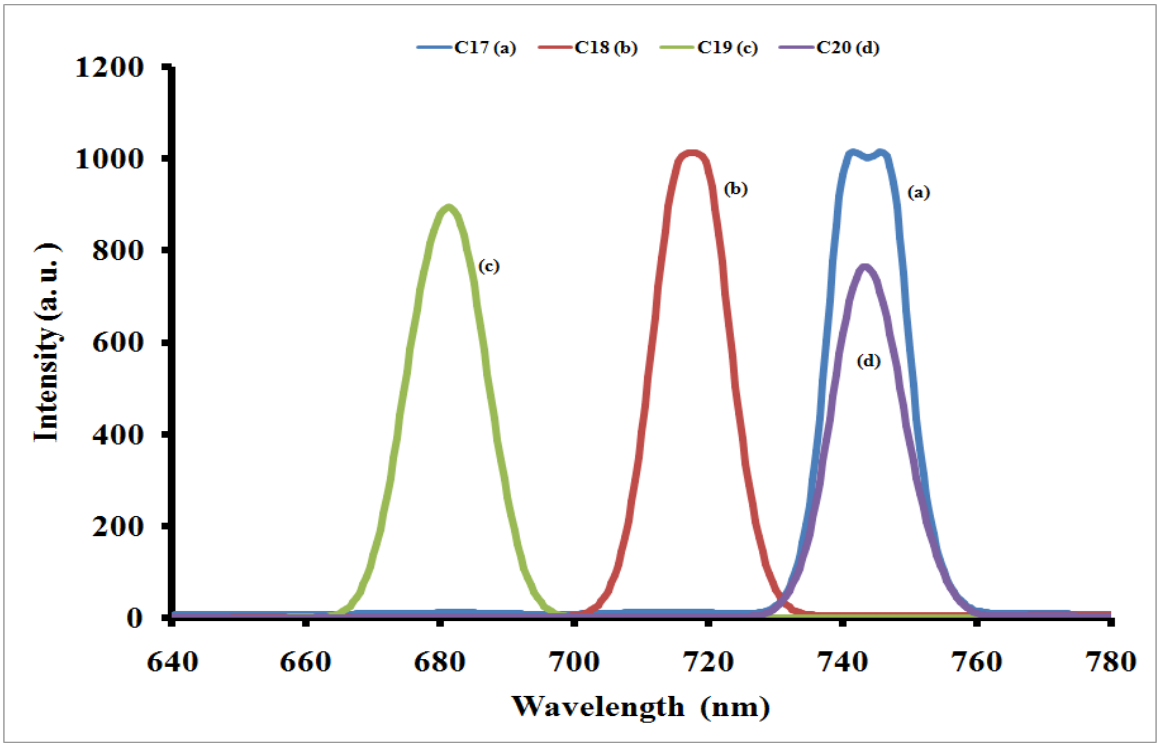

Figure 3.5 Emission spectra of complexes **C17** (a), **C18** (b), **C19** (c) and **C20** (d) in DMF.

3.5.5 NMR structure elucidation of functionalized anthracenyl ligands and complexes

The proton nmr spectra of the ligands **L12**, **L13** and **L14** are very similar. All the ligands show eight different aromatic signals with slight variations in chemical shifts (ca. 0.1–0.2 ppm). The aromatic proton doublets at δ 9.08 and 8.61 ppm (J = 4.1, 7.9 Hz) were respectively assigned to protons H–3, 3" and H–5, 5" of rings A and C for a 4'-substituted terpyridne ligands, while the signals at 8.44, 7.94, 7.84 and 7.33 ppm were assigned to other protons on the terpyridine ligands as H–3', H–4, 4", H–6, 6" and H–5' respectively. The AA'BB' coupling (doublet of doublet) system of the 9,10–disubstituted anthracene units showed two doublets of doublets signals at 8.56 and 7.61 ppm (J = 3.2, 6.8 Hz) as found in **L14**.

The proton nmr spectrum of **L15** on the other hands, showed six aromatic signals. The two broad aromatic singlet signals at δ 8.74 and 7.50 ppm were assigned to H–3' and H–5' respectively. Two doublets resonance signals at 8.63 (d, *J* = 7.6 Hz) and 8.45 (d, *J* = 7.6 Hz) were respectively assigned to H–3, 3", and H–4, 4"; while the triplet signals at 8.10 and 8.02 ppm were assigned to the H–5, 5" and H–6, 6" respectively. At the aliphatic region, the singlet peak at 2.09 ppm was unambiguously assigned to the CH_3 signal.

The proton nmr spectra of the homoleptic complexes **C18**, **C19** and **C20** display slight downfield shifts in the chemical shifts of protons for both the terpyridine ligand and the anthracene rings as found in the aromatic region. This is attributed to the coordination of the nitrogen lone-pair electron to the ruthenium ion centre of the complexes. The terpyridine protons were conspicuously found as resonance peaks at δ 9.08, 8.06 and 8.82, 7.43 ppm due to H3, H3"; H4, H4"; and H5, H5", H6, H6" respectively. The prominent singlet peaks at an upfield shift between 6.96 – 7.21 ppm common to the three complexes were assigned to the H3', H5' protons. The spectra of the complexes also display characteristic downfield shifts at δ 8.54, 8.21, 7.94 and 7.80 ppm, which is tailored towards an AA'BB' coupling patterns (doublet of doublet) characteristic of *peri* protons (resulting from ^{3}J and ^{4}J) for the anthracene molecules. Unlike in the complex **C18**, higher integral values are recorded for these protons in both complexes **C19** and **C20** which accounted for the additional anthracene units attached to the terpyridine ligands. In the aliphatic region of the proton nmr spectra of the complexes, the methyl protons are found as singlet peaks at δ 2.89, 2.73 and 1.22 ppm respectively. Similar proton signals were observed for **C17**, except that the molecule does not contain the signals accounting for the presence of anthracene moiety (See Appendices: 52, 54, 57, and 60).

Carbon 13 nmr spectra of the complexes **C18–C20** were useful in the identification of the functional groups. In the aromatic region (δ 182–120 ppm), six to eight quaternary carbon resonance signals were observed at 182.49, 157.68 and 156.90, 138.20, 130.31, 123.96, 122.49 ppm, accounting for the carbonyl and all non-hydrogenated carbon atoms in the molecule. The methine carbon resonance peaks of the terpyridyl and anthracenyl molecules are found at 154.86, 152.04, 133.00, 128.45, 127.72, 124.50 and 134.53, 126.72 ppm. (See Appendices: 55, 58 and 61).

3.5.6 Electrochemistry of functionalized anthracenyl ligands

The cyclic voltammograms of **L12**, **L13** and **L14** in DMF, containing tetrabutylammonium tetrafluoroborate as a supporting electrolyte using a Ag|AgCl reference electrode are shown in Figure 3.6 (Plates 1–4), with their electrochemical data summarized in Table 3.1. Irreversible oxidation peaks were found at +0.65 and +0.73 V, respectively for **L12** and **L13**. Other redox waves were observed at $E_{1/2}$ = -0.27, -0.51 and -0.99 V, (for **L12**) and $E_{1/2}$ = -0.36, -0.87 V (for **L13**). The cyclic voltammogram of **L14** is not well defined and did not show any appreciable electro redox properties as shown in (Plate 4). We could not rationalize a reason for this at this stage.

Plate 1: CV of **L12** (monoanthracenyl substituted terpyridine)

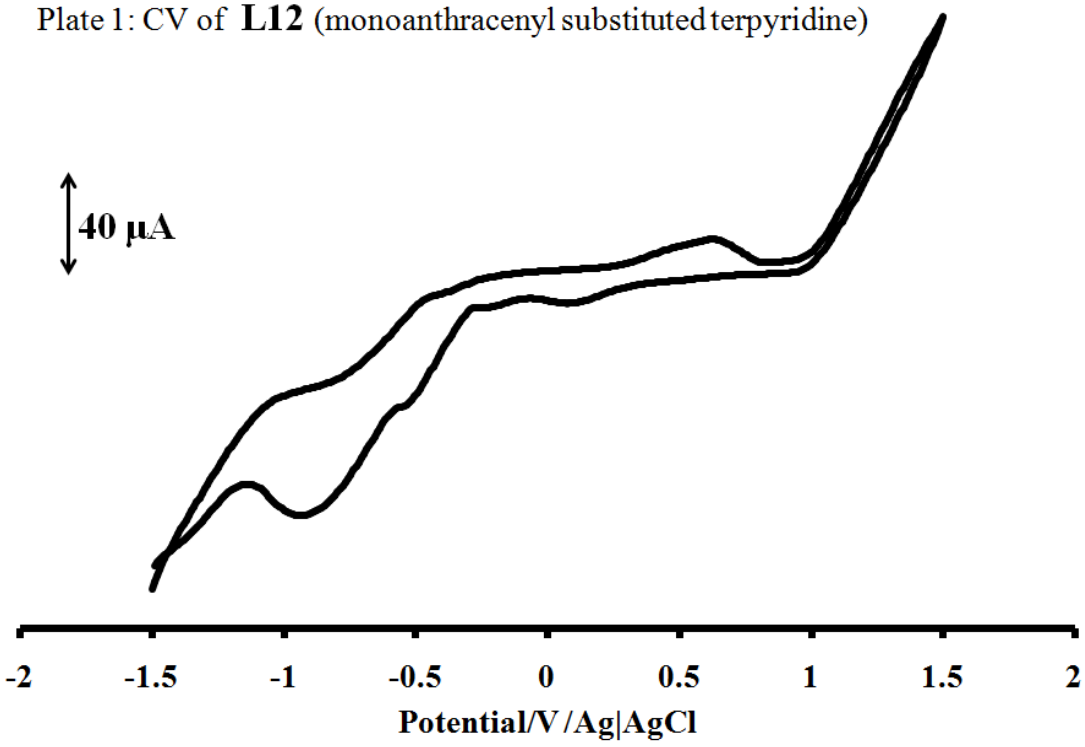

Plate 2: CV of **L13** (dianthracenyl substituted terpyridine)

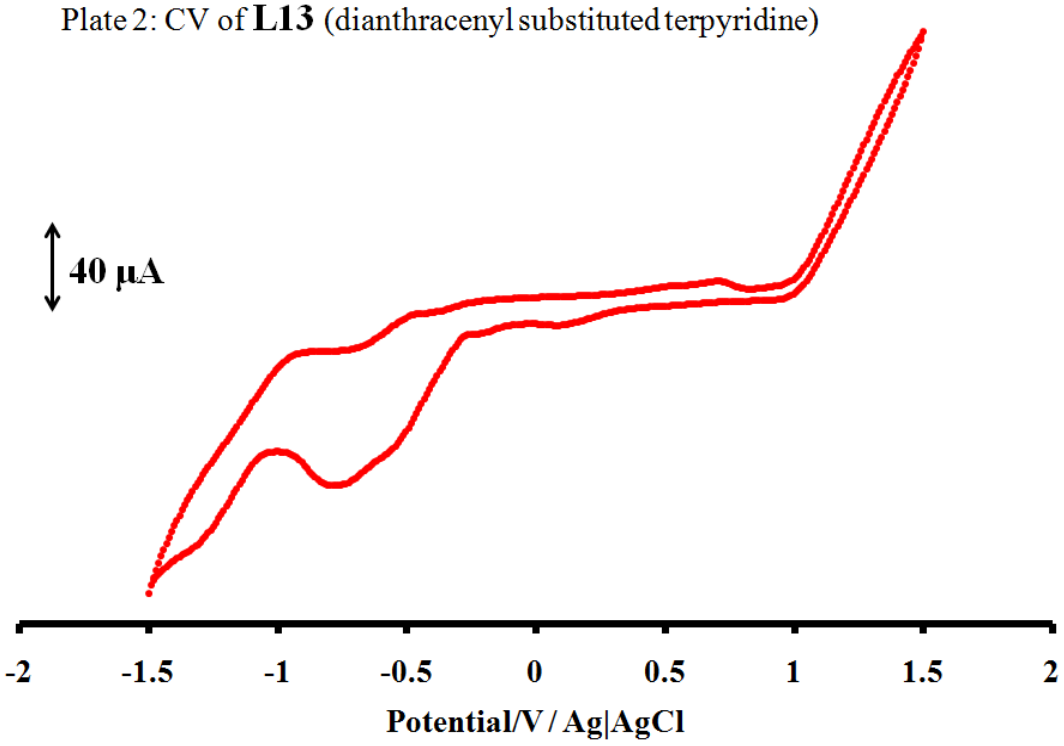

Plate 3: CVs of **L12** and **L13**

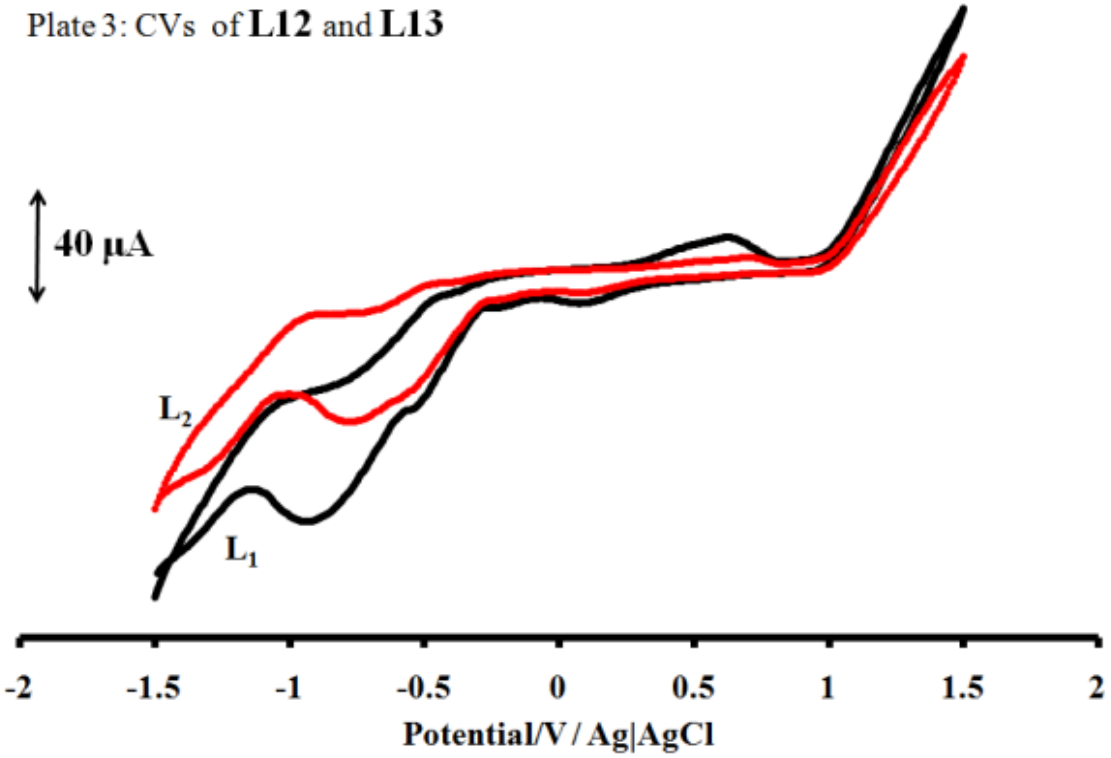

Plate 4: CV of **L14** (trianthracenyl substituted terpyridine)

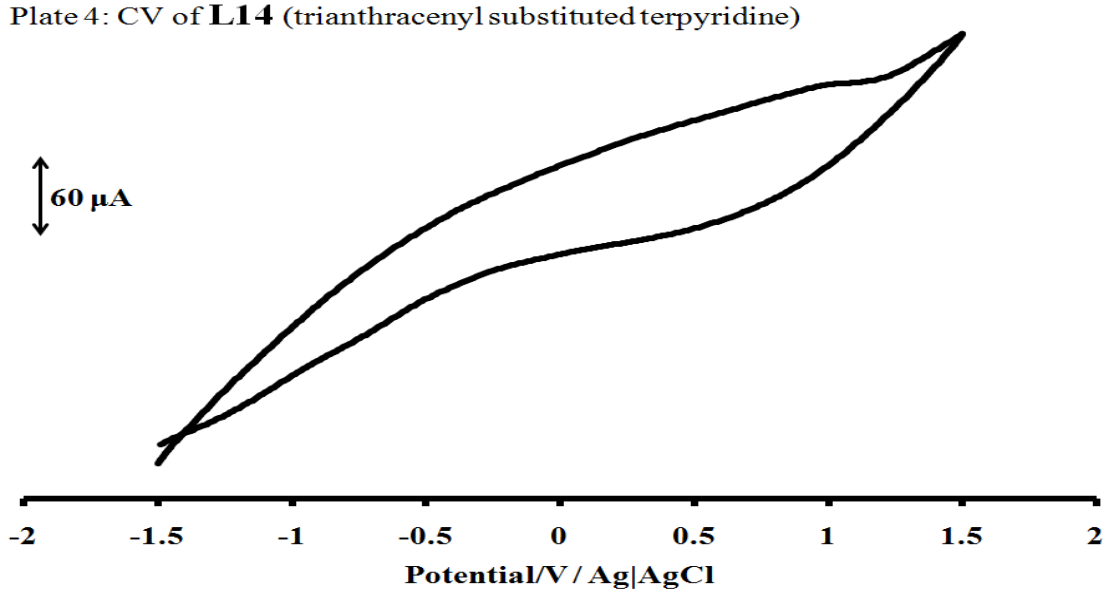

Figure 3.6. Cyclic voltammetry profiles of 1×10^{-3} M solutions of **L12**, **L13** and **L14** in freshly distilled DMF containing 0.1 M $TBABF_4$ supporting electrolyte. Step potential = 5 mV, amplitude = 50 mV vs. Ag|AgCl, frequency = 10 Hz. Scan rate = 100 m Vs^{-1} vs. Ag|AgCl.

3.5.7 Electrochemistry of functionalized terpyridine Ru(II) complexes

Cyclic and square wave voltammograms of the complexes **C18**, **C19** and **C20** are as shown in (Figures 3.7–3.9) with the data summarized in Table 3.2. The oxidation potentials of **C18**, **C19** and **C20**, were determined to be +1.18, +0.71, and +0.97 V vs. Ag|AgCl, respectively, which were derived from oxidation of Ru(II) to Ru(III). Also observed in the voltammograms are the wave characteristics of both the anthracenyl and terpyridinic ring oxidation and reduction processes. It has been established for an heteroleptic Ru(II) phenanthroline complexes with functionalized oligo-anthracenyl carboxylic acid moiety that these processes are single- and/or multi- electronic in nature [413].

A crucial observation was the well-define redox processes in the voltammogram of complex **C20** which was made from ligand **L14**, (Figure 3.6 (Plate 4)). We assert that the lone-pair lone-pair electron-donation from the nitrogen based terpyridine to the ruthenium metal centre at the coordination may be responsible for the redox wave characteristics of the complex (Figure 3.9).

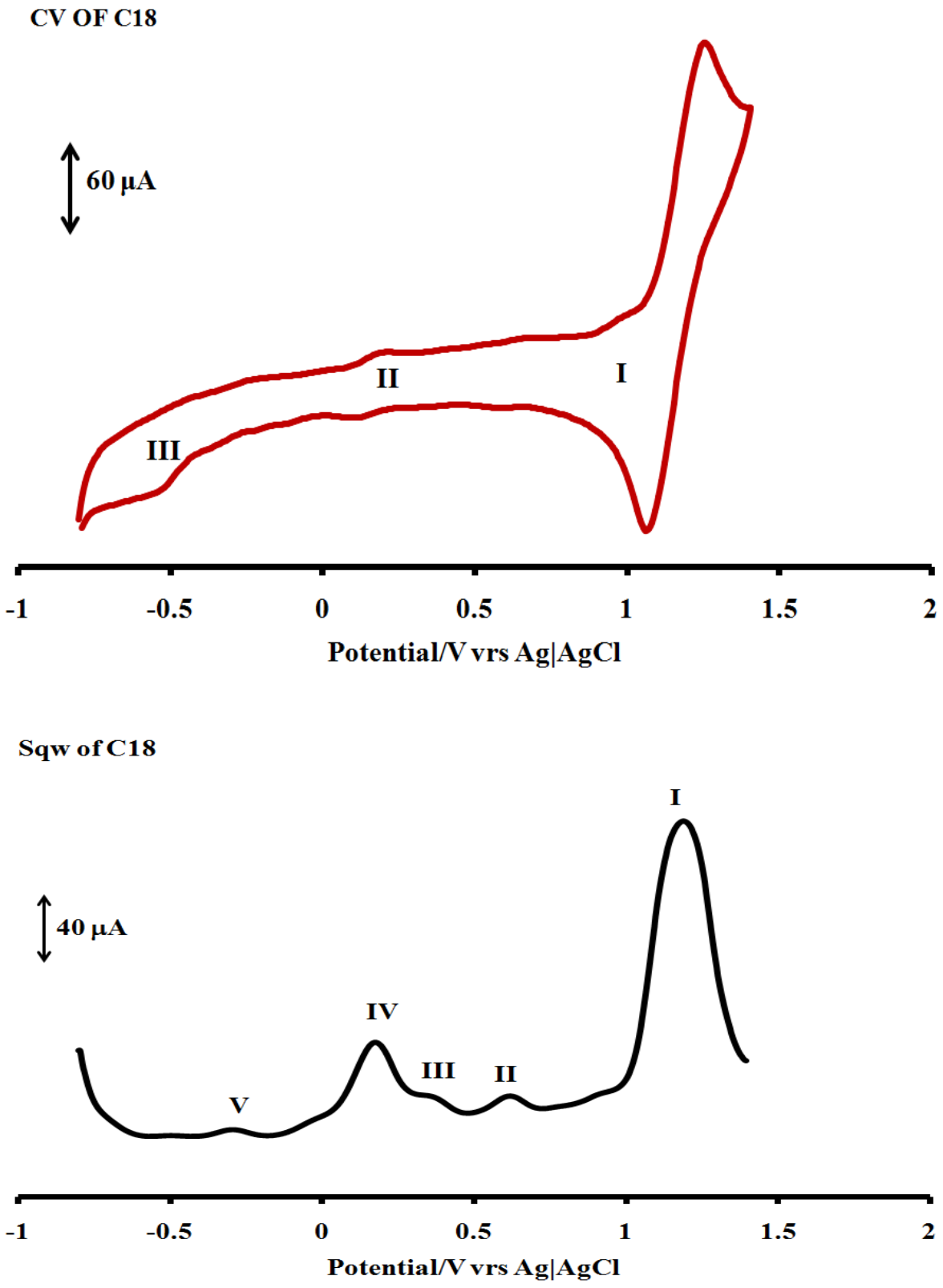

Figure 3.7 Cyclic and square wave voltammograms of **C18** in freshly distilled DMF containing 0.1 M $TBABF_4$ supporting electrolyte. Step potential = 5 mV, amplitude = 50 mV *vs*. Ag|AgCl, frequency: 10 Hz. Scan rate = 100 m Vs^{-1} *vs*. Ag|AgCl.

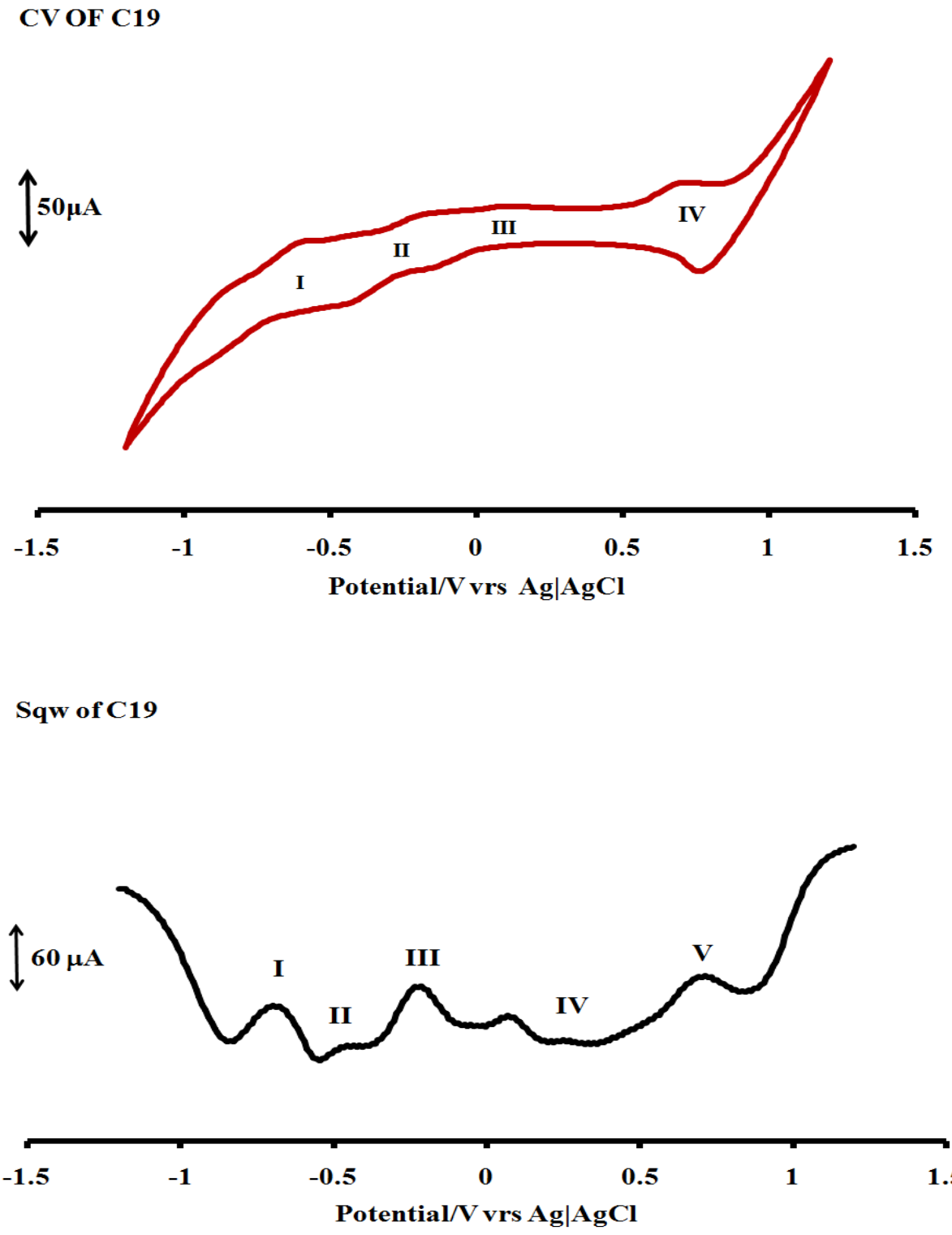

Figure 3.8 Cyclic and square wave voltammograms of **C19** in freshly distilled DMF containing 0.1 M $TBABF_4$ supporting electrolyte. Step potential = 5 mV, amplitude = 50 mV *vs*. Ag|AgCl, frequency: 10 Hz. Scan rate = 100 m Vs^{-1} *vs*. Ag|AgCl.

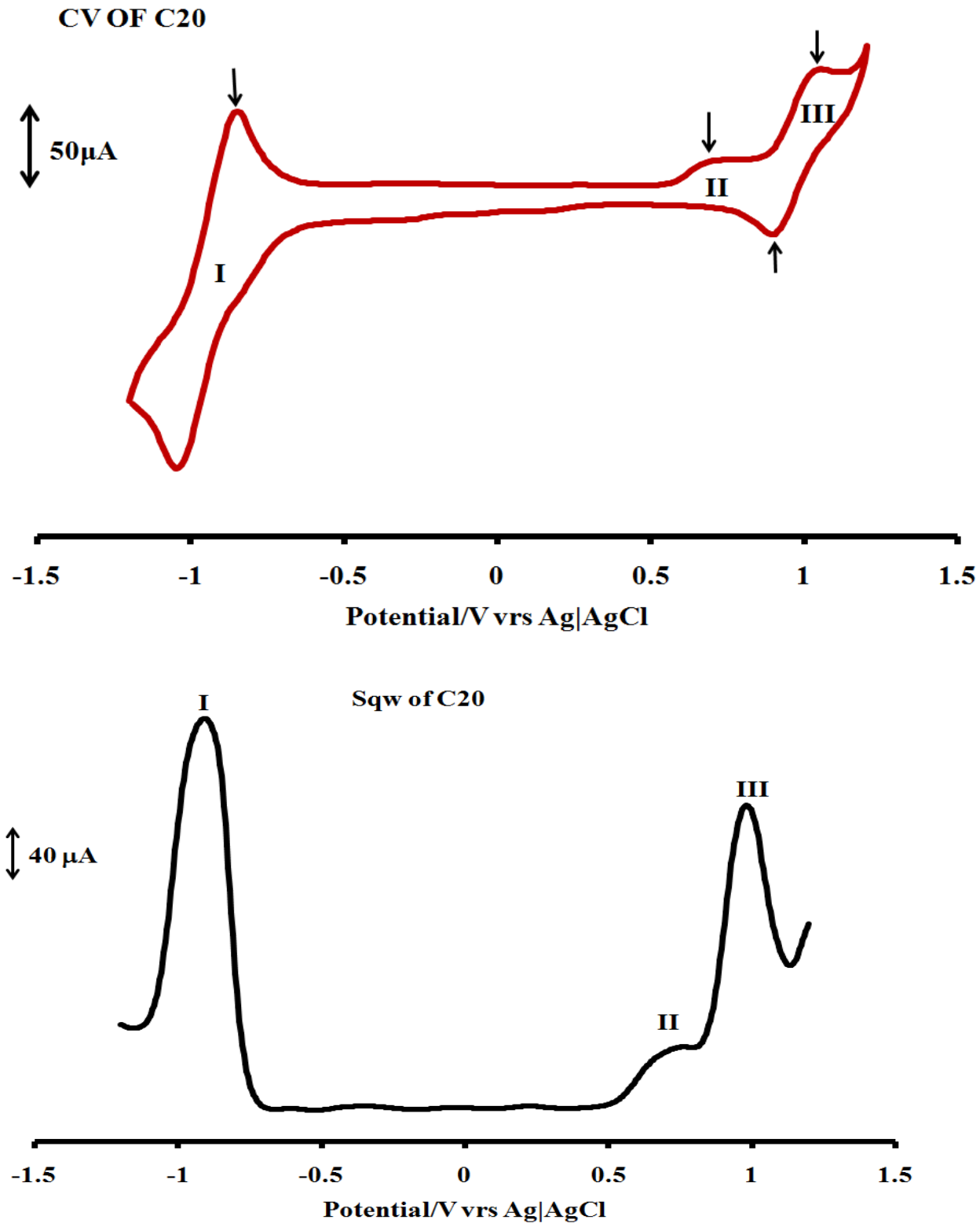

Figure 3.9 Cyclic and square wave voltammograms of **C20** in freshly distilled DMF containing 0.1 M $TBABF_4$ supporting electrolyte. Step potential = 5 mV, amplitude = 50 mV *vs*. Ag|AgCl, frequency: 10 Hz. Scan rate = 100 m Vs^{-1} *vs*. Ag|AgCl.

Table 3.2 Cyclic voltammetric data for ligands **L12**– **L14** and **C18** – **C20**

Compound	E_{anodic}/V	$E_{cathodic}$/V
L12	0.65	-0.27, -0.51, 0.99
L13	0.73	-0.36, -0.87
L14	NV	NV
C18	0.85	-0.54
C19	0.26	-0.69
C20	0.67	-0.92

Key: NV = Not visible.

Conclusion

The design, synthesis, photophysical and spectroscopic characterizations as well as the electro-redox properties of 4'-(2,3-DMAA)-terpyridine and 4'-functionalized anthracenyl terpyridine ligands and their corresponding ruthenium(II) bisterpyridyl complexes are presented in this chapter. The synthesis of all the ligands was initiated through the bromo-terpyridine ligand and further substitution reactions of the bromine with 9,10-dibromoanthracene using a palladium catalyzed cross-coupling reaction method. The one to three bromoanthracenyl terpyridine ligands so synthesized showed that highly-efficient photo-induced energy or electron transfer processes can take place over long distances. A further functionalization of the ligands through bromine substitution and their resultant coordination resulted in the synthesis of new Ru(II) terpyridine complexes bearing a controlled number of anthracene units. New information on the photophysical, photoluminescence and electro redox properties of the reported ligands has shown that other molecular architecture can be introduced to the ligands through the bromine substitution to synthesize molecules with different practical applications.

We have shown that a stepwise increase in the number of attached anthracene units anchored to an α,β-unsaturated carboxylic acid on terpyridine resulted in a better molar extinction coefficient and red shifting of the luminescence towards the near-infrared region. However, an optimum number of anthracene units may be required for a better electron- transfer processes as well as reduction in molecular aggregation. The complexes investigated show better photophysical and electro-redox properties which may endear them to be used as photosensitizers, sensors and as components in molecular assemblies for generating charge-separated states.

CHAPTER FOUR

Part of this chapter has been submitted for publication as

Adewale O. Adeloye and Peter A. Ajibade. A convenient synthesis, electrochemistry and spectroscopic properties of new series of single- and double-decked functionalized anthracenyl ruthenium(II) phthalocyanine complexes. *Dyes and Pigments* (Submitted).

CHAPTER FOUR

4 RUTHENIUM(II) PHTHALOCYANINES: SYNTHESIS, CHARACTERIZATION AND ELECTROCHEMISTRY

4.0 Introduction

The dye-sensitized solar cell (DSSC) is a sophisticated system, which is not yet understood in detail. To increase the conversion efficiency as well as the stability, almost all the elements of the solar cell device need further improvement. As for the sensitizing dye, there are strigent and several theoretical requirements that it has to comply with [415].

First, the lowest unoccupied molecular orbital (LUMO) of the dye should have a higher energy than the conduction band edge of the semiconductor and have a good orbital overlap to facilitate electron injection. Ideally, the dye should have intensive absorption in the whole solar spectrum.

Second, the dye should be attached strongly to the semiconductor surface and inject electrons into the conduction band with a quantum yield of unity, while the charge recombination between the injected electron and the oxidized dye should be slow enough for the electron transport to the external circuit.

Third, the redox potential of the dye should be sufficiently more positive than that of the redox couple in the electrolyte so that the dye can be regenerated rapidly by electron transfer from the reduced species in the electrolyte.

Finally, the dye should be chemically stable for long time exposure to natural sunlight. Another, main practical requirement is that the dye should be soluble in solvents that are compatible with the semiconductor and favourable for adsorption of a nonaggregated monolayer of the dye on the nanoparticle surface. This latter requirement is important because the dye molecules that are connected directly to

the semiconductor are more effective in injecting electrons into the semiconductor as compared to those in outer layers. For an aggregated sensitizer, the excess of dye molecules absorbs light and act as a filter. Since it is difficult to calculate all the necessary parameters and then synthesize a dye fulfilling all of them, the method of "trials and failures" is still an important approach to finding appropriate sensitizing dyes [415].

To date, ruthenium(II) polypyridyl complexes have proved to be the best sensitizers for dye-sensitized nanostructured TiO_2 solar cells [416, 417]. However, the main drawback of those sensitizers is the lack of absorption in the far-red/near-IR region of the solar spectrum [417]. To further improve the performance of these devices, it is imperative to enhance their response in the above mentioned wavelength region.

Phthalocyanines possess intensive absorption in the far-red/near-IR region; are known for their excellent chemical, light, and thermal stability; and have the appropriate redox properties for sensitization of large band-gap semiconductors, e.g., TiO_2 [334] making them attractive for DSSC. However, there are some problems to be solved for phthalocyanines to be used in solar cell applications. The typical phthalocyanines explored for sensitization of large band-gap semiconductors are free-base or metallic ones, substituted by carboxylic or sulfonic acid groups for attachment to the semiconductor surface [418]. They are poorly soluble in organic solvents, for example, ethanol and chloroform, which makes it difficult to synthesize, separate, and purify these kinds of phthalocyanines.

Another major problem with phthalocyanines is their strong tendency to aggregate on the semiconductor surface, which to some extent results in very low IPCE (typically < 4 %) of solar cells [418]. Grätzel and co-workers [419] reported a

strikingly high IPCE of 45 % in the near-infrared region for a sandwich solar cell based on a zinc tetracarboxyl phthalocyanine (ZnTcPc)-sensitized nanostructured TiO_2 electrode when surface aggregation of the sensitizer was avoided. In contrast to the typical phthalocyanines with carboxyl groups, phthalocyanines with ester groups [420] are readily synthesized and purified in good yields, as they are reasonably soluble in moderately polar solvents, for example, chloroform. However, they could not be attached to nanostructured TiO_2 film by means of ordinary methods [417]. Moreover, they were surprisingly resistant toward hydrolysis by, for example, NaOH. Research into new sensitizing dyes is increasingly focused on preparing compounds that can absorb photons with wavelengths of 600-900 nm where the solar photon flux [421] is greatest within the visible region.

Ruthenium phthalocyanine (PcRu) complexes are attractive as sensitizing dyes as they possess intense and tunable absorptions in the region of ~650 nm [422] as well as a reversible ring-based oxidation [423]. Several examples of PcRu-sensitized DSCs exist in which the dye is attached to the TiO_2 via axial ligands [424 – 426] or through anchoring groups on the macrocycle periphery [427]. Promising results were obtained with [{1,4,8,-11,15,18,22,25-Me_8Pc}Ru(3,4-pyridinedicarboxylic acid)] which returned photocurrent yields of over 50 % in the region 600-700 nm [424].

One design strategy for improved dyes involves maximizing the distance between the positive “hole” created after electron injection and the TiO_2 surface, thus creating a long lived charge separated state by reducing the rate of electron recombination. The result is a lowering of the titania quasi-Fermi level and a gain in the cell potential [245]. Sensitizers designed using this strategy can generally be classified as either acceptor-sensitizer or sensitizer-donor complexes [428].

4.1 Synthesis of Ruthenium(II) phthalocyanine complexes via electrophilic aromatic substitution reaction method

In general, metallated phthalocyanines are prepared by two methods: (i) cyclotetramerisation of a phthalic acid derivative (such as a phthalonitrile or diiminoisoindolene) in the presence of a metal salt, (ii) insertion of the desired metal ion into the preformed phthalocyanine ring either as its metal-free or dilithiated derivative [422]. The more commonly used method for the preparation of ruthenium phthalocyanine derivatives has tended to be the former and the two ruthenium reagents frequently used for the synthesis of ruthenium phthalocyanines are $RuCl_3$ and $Ru_3(CO)_{12}$. Introduction of substituents into the precursors such as phthalonitriles and final condensation to Pcs are common synthetic routes of which MPc with interesting photochemical and photophysical characteristics been made. Despite this, a precursor with specified substituents is not always readily available or, in other instances, hard to condense to Pc. In this situation, introducing substituents to Pc directly instead of to the precursor is needed. However, direct substitution of the Pc ring often results in mixtures [414]. One method to reduce position indeterminacy is displacement of a group readily introduced to a precursor which is easy to condense to Pc.

In the present work, we focused our attention on the incorporation of ruthenium as the metal centre into the cavity of non-peripheral substituted phthalocyanines using $RuCl_2(DMSO)_4$ as metal precursor [408] and functionalized anthracene [406, 413] derivatives as substituents, and most importantly, on developing an efficient, direct synthesis for these compounds. In doing so, we have identified convenient methods for preparing doubly ligated derivatives bearing either two identical or non-identical ligands. These findings have been exploited to

synthesize tetrakis-(9-anthracenyl-10-(2,3-dimethylacrylic acid)-dicarbonyl ruthenium phthalocyanine **(PC21)**, (9-dianthracenyl-10-(2,3-dimethylacrylic acid)-dicarbonyl ruthenium phthalocyanine **(PC22)**, and bis(9-dianthracenyl-10-(2,3-dimethylacrylic acid)-dicarbonyl diruthenium phthalocyanine **(PC23)** complexes by direct electrophilic aromatic substitution of the protons on the Pc ring. A direct substitution method may be useful in the syntheses of Pc most importantly where substituents are not stable in the condensation of precursor or the condensation not qualitative.

4.1.1 Synthesis of tetrakis-(9-anthracenyl-10-(2,3-dimethylacrylic acid)-dicarbonyl ruthenium (II) phthalocyanine (PC21)

The preparation of $[RuCl_2(dmso)_4]$, and the RuPc was carried out using standard methods [408, 414]. with slight modifications as follows: In a 250 mL flask, $[RuCl_2(dmso)_4]$ (0.500 g, 1.032 mmol), phthalonitrile (0.529 g, 4.128 mmol) were dissolved in 40 mL DMF and DBU 1.0 mL was added. The mixture was heated to reflux for 5 h. To the purple solution, 9-bromo-10-(2,3-dimethylacrylic acid)-anthracene **(1)** (1.462 g, 4.12 mmol), KOH (0.231 g, 4.12 mmol) and triethylamine (1.0 mL) were added and the mixture was further refluxed for 2 h. The dark blue-green solution was concentrated *in vacuo* to remove DMF. The crude product was redissolved in minimum volume of 50 % diethyl ether-MeOH (solvent system F) and chromatographed on alumina using the same solvent system (500 mL, isocratic elution), to afford a dark-green viscous liquid (R_f = 0.76). Ethanol (50 mL) was added to the dark-green viscous liquid and heated to boiling, filtered hot and concentrated *in vacuo* to afford a green liquid which was precipitated with diethyl-ether to afford the desired complex **(PC21)**.

4.1.2. Synthesis of 4-(9-dianthracenyl-10-(2,3-dimethylacrylic acid)-dicarbonyl-ruthenium(II) phthalocyanine (PC22 and PC23)

The method employed for the synthesis followed as reported in (Section 4.1.1) above. A mixture of phthalonitrile (0.53 g, 4.13 mmol), [$RuCl_2(DMSO)_4$] (0.50 g, 1.03 mmol) and DBU (1.0 mL) was refluxed for 5 h. To the resulting crude product, 9-bromo-10-(2,3-dimethylacrylic acid)-dianthracene (**2**) (0.55 g, 1.03 mmol), KOH (0.058 g, 1.03 mmol) and triethylamine (1.0 mL) were added and the mixture was further refluxed for 2 h. Two products were isolated from a careful column chromatographic elution as **PC22** and **PC23**.

4.2 Experimental Results and Physicochemical data on Ru(II) Phthalocyanine complexes

4.2.1 Tetrakis-(9-anthracenyl-10-(2,3-dimethylacrylic acid)-ruthenium(II) phthalo- cyanine (PC21)

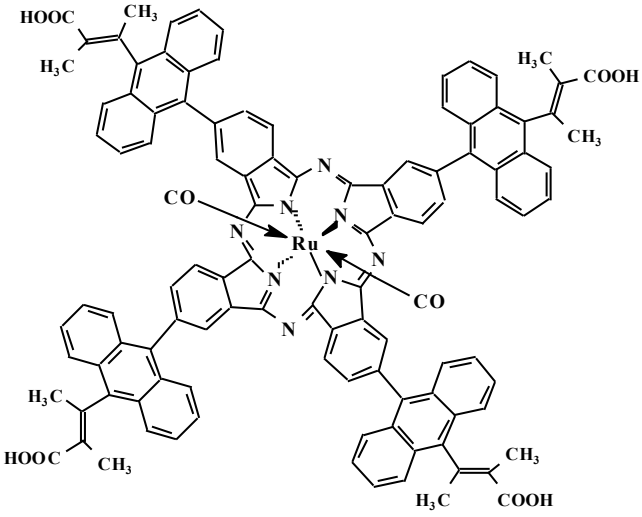

Colour: Green solid

IR (KBr) v_{max}/cm^{-1}: 3218 (OH), 3035 (OH, α, β-unsaturated acid), 2910, 2846, 1938 (C=O), 1688, 1605 (C=C), 1472 (C=N), 1461, 1432, 1311, 1281, 1165, 1117, 1059, 774, 741, 732.

UV-Vis (λ_{max}/nm, ε = M^{-1} cm^{-1}, DMF): 331 (15520), 350 (18145), 369 (21577), 388 (18000), 573 (3147), 633 (7206), 902 (1680).

Emission wavelength: ($\lambda_{exc.}$ = 640 nm, λ_{em} = 672 nm).

^{1}H NMR ($CDCl_3$): δ 8.43 (s), 8.01 (m), 7.47 (dd, *J* = 3.2, 6.4 Hz), 2.93 (s), 2.88 (s), 2.57 (s), 2.17 (s).

^{13}C NMR ($CDCl_3$): δ 166.04, 162.93, 162.74, 132.08, 129.72, 129.01, 128.54, 127.11, 126.59, 125.75, 125.56, 124.31, 39.37, 23.83, 19.56.

Cyclic voltammetry Data: Ru^{2+}/Ru^{3+} = 0.88 V; $E_{cathodic}$ = -0.71 V.

Percentage yield: 0.32 g, 16 %.

4.2.2 4-(9-dianthracenyl-10-(2,3-dimethylacrylic acid)-ruthenium(II)-phthalocya nine (monomer) (PC22)

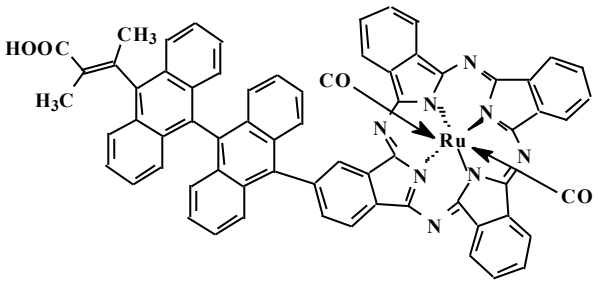

Colour: Blue-green solid,

TLC characteristic: R_f = 0.65 (Solvent system D)

IR (KBr) ν_{max}/cm^{-1}: 3392, 3194 (OH), 3081, 3024 (OH, α, β-unsaturated acid), 2929, 2859, 2803 (C-H), 1934, 1642 (C=O), 1586 (C=N), 1468, 1443, (C=C), 1321, 1288, 1245, 1204, 1121, 1089, 984, 885, 754, 690, 607.

UV-Vis (λ_{max}/nm, ε = M^{-1} cm^{-1}): 323 (43190), 343 (36160), 368 (32720), 388 (28600), 566 (1330), 618 (1907).

Emission wavelength: ($\lambda_{exc.}$ = 640 nm, λ_{em} = 682 nm).

Cyclic voltammetry Data: Ru^{2+}/Ru^{3+} = +0.88 V; $E_{cathodic}$ = -0.71 V.

Percentage yield: 0.36 g, 21 %

4.2.3. 4-(9-dianthracenyl-10-(2,3-dimethylacrylic acid)-ruthenium(II)-phthalocyanine (dimer) (PC23)

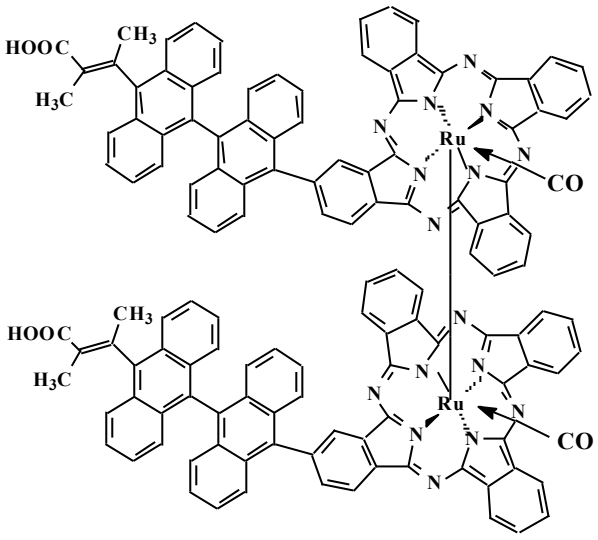

Colour: Deep Green solid.

TLC characteristic: R_f = 0.53 (Solvent system D)

IR (KBr) ν_{max}/cm^{-1}: 3307 (br), 3038, 2911, 2835, 2507 (br), 1922, 1688, 1628, 1615, 1485, 1441, 1413, 1384, 1308, 1284, 1166, 1116, 1061, 955, 882, 758, 742, 723, 719.

UV-Vis (λ_{max}/nm, $\varepsilon = M^{-1}\ cm^{-1}$): 351 (13104), 377 (11129), 561 (5132), 620 (9649), 631 (9035), 901 (1930), 1027 (5472).

Emission wavelength: ($\lambda_{exc.}$ = 640 nm, λ_{em} = 700 nm).

^{1}H NMR (DMSO-d_6): δ 1.51 (s, 3H), 2.73-3.42 (m, 11H), 7.50 (dd, *J* = 2.4, 6.8 Hz, 8H), 7.96 (s), 8.09 (dd, *J* = 3.2, 6.4 Hz), 8.33 (s, 1H), 8.55 (s, 1H), 9.12 (br, 1H).

^{13}C NMR (DMSO-d_6): δ 175.43, 166.14, 163.17, 163.13, 161.88, 143.42, 141.12, 134.90, 134.84, 132.08, 128.88, 126.86, 126.40, 121.85, 80.11, 54.19, 26.75, 24.17, 23.93, 19.71.

Cyclic voltammetry Data: E_{anodic}/V = +0.11, Ru^{2+}/Ru^{3+} = +0.71 V; $E_{cathodic}$ = -0.60 V.

Percentage yield: 1.17 g, 74 %

4.3 Discussion of results

4.3.1 Synthesis

The preparation of phthalocyanines relies on the availability of the precursor phthalonitriles which undergo cyclotetramerization to form the macrocycles. It is to be noted that a direct palladium assisted cross-coupling reaction of functionalized bromo-anthracenyl derivatives with bromo-phthalonitrile to form anthracenyl phthalonitrile prior to condensation to phthalocyanine was not successful. However, in the preparation of these compounds, we employed the method reported by Lin Mei-jin and co-workers [413], in the preparation of a substituted phthalocyanine compounds using bromo-substituted phthalonitrile as precursor followed by a nucleophilic substitution reaction of the bromo-group. In this work, we carried out a reverse synthetic procedure in which the bromo-functionalized anthracene derivatives were reacted directly in an electrophilic aromatic substitution of the protons on the free ruthenium phthalocyanine to afford the desired products (Scheme 4.1). Thus, the reaction of free ruthenium phthalocyanine (RuPc) with either 9-bromo-10-(2,3-dimethylacrylic acid)-anthracene or 9-bromo-10-(2,3-dimethyl acrylic acid)-dianthracene led to the formation of both monomer and dimer after column chromatography. However, it was found that a number of side products obtained during purification and isolation processes show no Q-band absorption characteristics of phthalocyanines in the UV-Vis spectra.

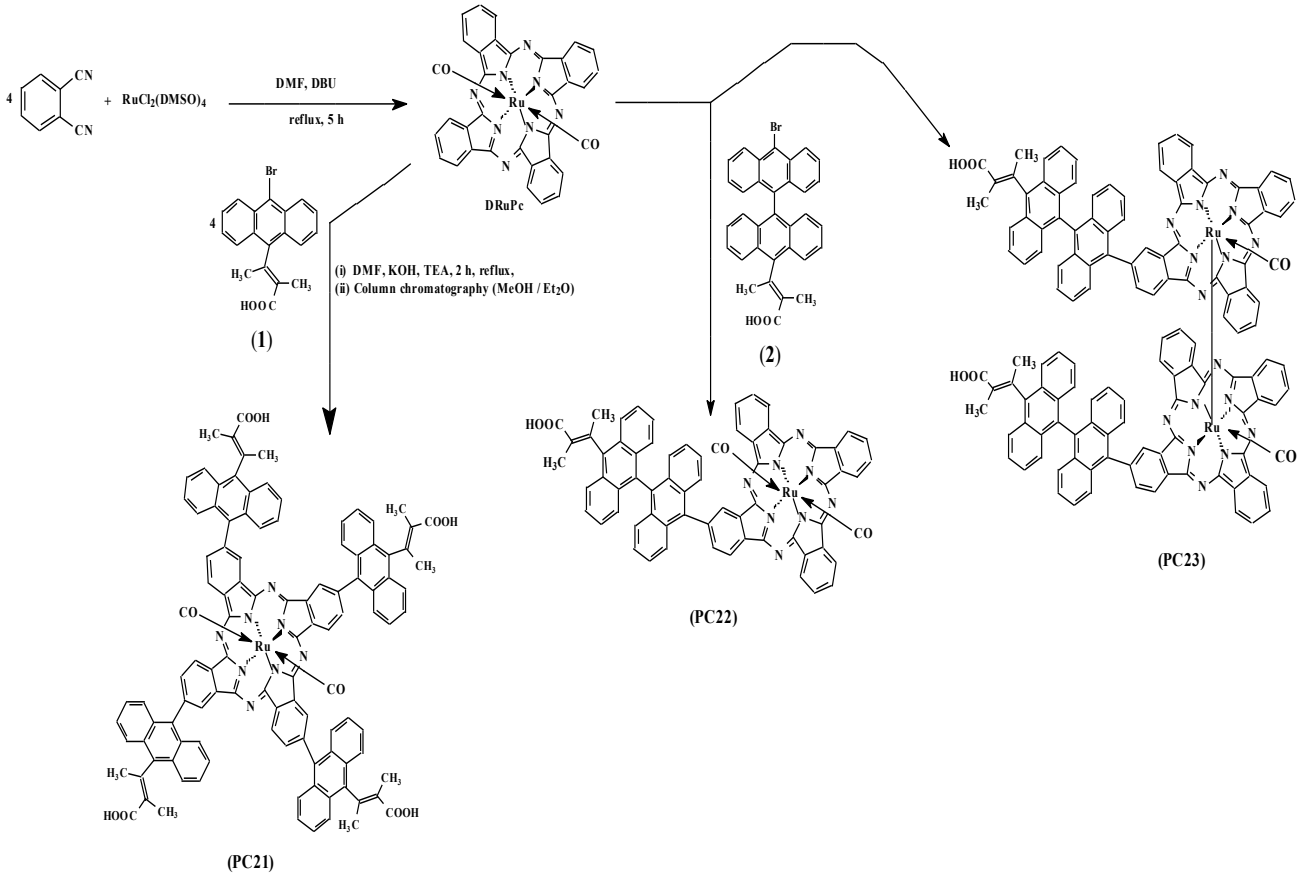

Scheme 4.1 Reaction profiles for the synthesis of Ru(II) phthalocyanine complexes

4.3.2 Infrared spectroscopy

The infrared spectra of the two functionalized anthracenyl derivatives and the ruthenium phthalocyanine compounds were studied and bands assigned on careful comparison. A strong OH vibrational stretch characteristic of α, β-unsaturated carboxylic acid was found as a broad band at 3413 cm^{-1} for both mono- and dianthracenyl derivatives. This band was shifted to lower frequencies (*ca*. 195 cm^{-1}, 21 cm^{-1} and 96 cm^{-1}) for **PC21**, **PC22** and **PC23** respectively. Both the ligands and complexes have two common stretching vibrational bands between 3081-2857 cm^{-1} which were assigned to the methyl groups in the molecules. The infrared spectra of

the complexes with axial carbonyl ligands have characteristic bands in the region 1965–1922 cm^{-1} assigned to ν(CΞO) [400]. Several authors have reported the ligand exchange reactions whereby “crude PcRu” reacted in dimethylformamide yielded the carbonyl complex [PcRu(CO)dmf], thus giving the source of axially coordinated CO in **PC21** – **PC23** complexes with the substitution of the two chloride ions in $[RuCl_2(dmso)_4]$ [400, 422]. Bands at 1688, 1642 and 1321 cm^{-1} were assigned to the ν(C=O) and ν(C–O) stretching of carboxylic acid groups in the complexes. The bands between 1642 and 1441 cm^{-1} contain contributions mostly from the atoms in the pc rings and these peaks have been found to be sensitive to the central metal atom [410]. It is well known that different polymorphic organisations of phthalocyanines also show different IR absorbance patterns which can be useful in identifying and characterizing a particular form or dimorphic transition. In particular, in the range between 800–700 cm^{-1} the out-of-plane C–H bending vibrations are expected. Due to the sensitivity of these vibrations to the molecular packing, the major differences reported so far for both metallated phthalocyanines and the free ligand of different polymorphic structures were discovered in this range [422]. All the spectra show similar characteristic frequencies in this range, but in the above mentioned region some differences can be noticed: the three band system is constituted in **PC21** (Figure 4.1) by well defined bands at 732, 741, 744 cm^{-1} while in **PC22** the first one is centred at 728 cm^{-1} with a pronounced shoulder at 754 cm^{-1} and in the third **PC23** is found at 742, 723, 758 cm^{-1} with a shoulder at 719 cm^{-1} [401]. In the neighbourhood of 900-960 cm^{-1}, a strong sharp peak was observed in **PC23** which was conspicuously absent in **PC21** and **PC22**. At this region, one can notice the disappearance and/or a low absorbance in the latter complexes, which can be attributed to different molecular packing in the molecules. These small

differences in the infrared spectra could well support the differences attributed to the complexes in the optical spectra reported below (Figure 4.1).

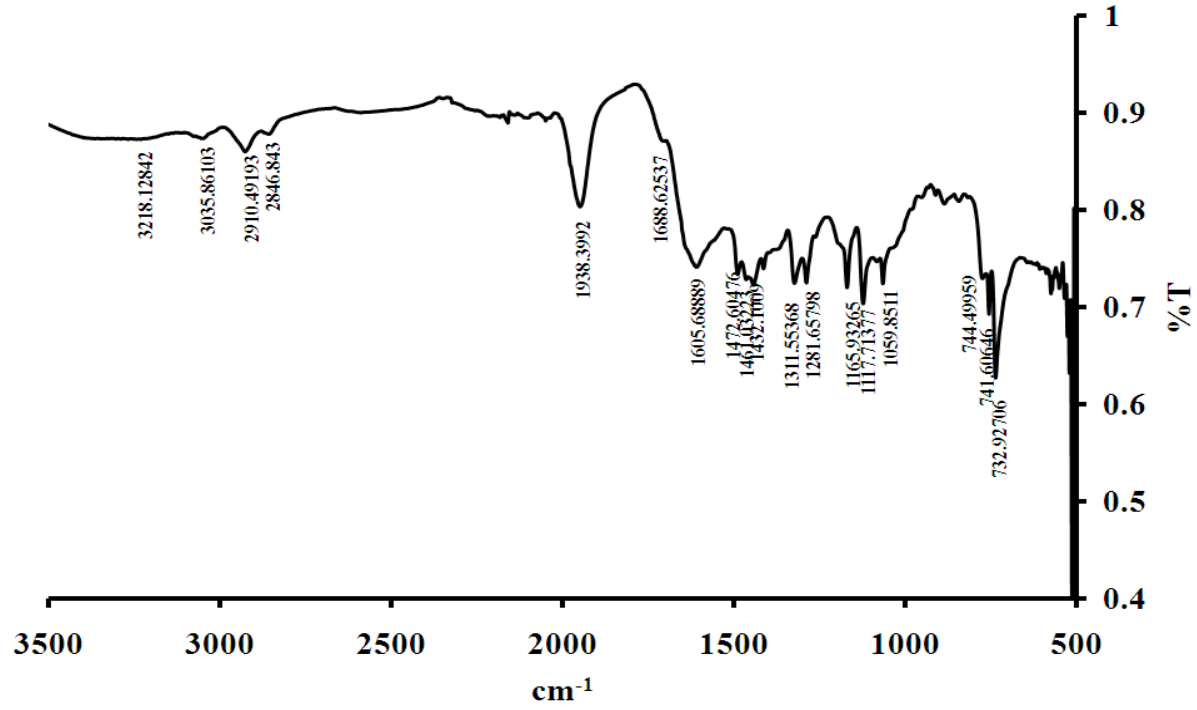

Figure 4.1 Infrared spectrum of Tetrakis-(9-anthracenyl-10-(2,3-dimethylacrylic acid)-dicarboxyl ruthenium(II) phthalocyanine (**PC21**)

4.3.3. UV-Vis absorbance spectroscopy

The electronic spectra of ruthenium phthalocyanines complexes **PC21**, **PC22** and **PC23** show the Q bands of a typical macrocycle substituted Pcs. The energy level location corresponding to this band is illustrated in (Figure 4.2). In the UV-region, anthracene displays strong absorptions between 300-400 nm in the solution, with pronounced vibronic peaks at 331, 350, 369 and 388 nm. The highest molar absorptivity coefficient is recorded for **PC21**. The presence of these bands is thought to have overlapped the weak Soret band which normally appears in the region 340-385 nm and attributed to a charge transfer (CT) transition. In the visible region, **PC21** and **PC22** showed single-broad Q-bands (633, 618 nm) with accompanied weak

shoulder bands at (573, 566 nm) respectively. The Q-band, splits to two bands at 620 and 631 nm in **PC23** with corresponding weak shoulder band at 561 nm. These absorptions were assigned to π→π* transition within the macrocycle. Coordination of a carbonyl ligand induces a bathchromic shift of 300 – 500 cm^{-1} and a significant increase in the molar absorptivity. The splitting of the Q-band as found in **PC23** may be adduced to the new steric and symmetrical properties imposed on the complex by solvation of the phthalocyanine and axial ligands; and the polar electronic influence of the solvents on the ligands. Peripheral substitution of the macrocycle has only a weak influence on the position of the Q-band. Hanack group [429] reported that peripheral substitution with an electron-donating group causes a weak bathochromic shift of the Q-band. The high prominent near infrared absorption peak at 1027 nm (ε = 5472 M^{-1} cm^{-1}) in **PC23** was attributed to a better π-bond conjugation indicative of the synergy effect of the Ru-Ru metal bond linkage of the dimeric complex.

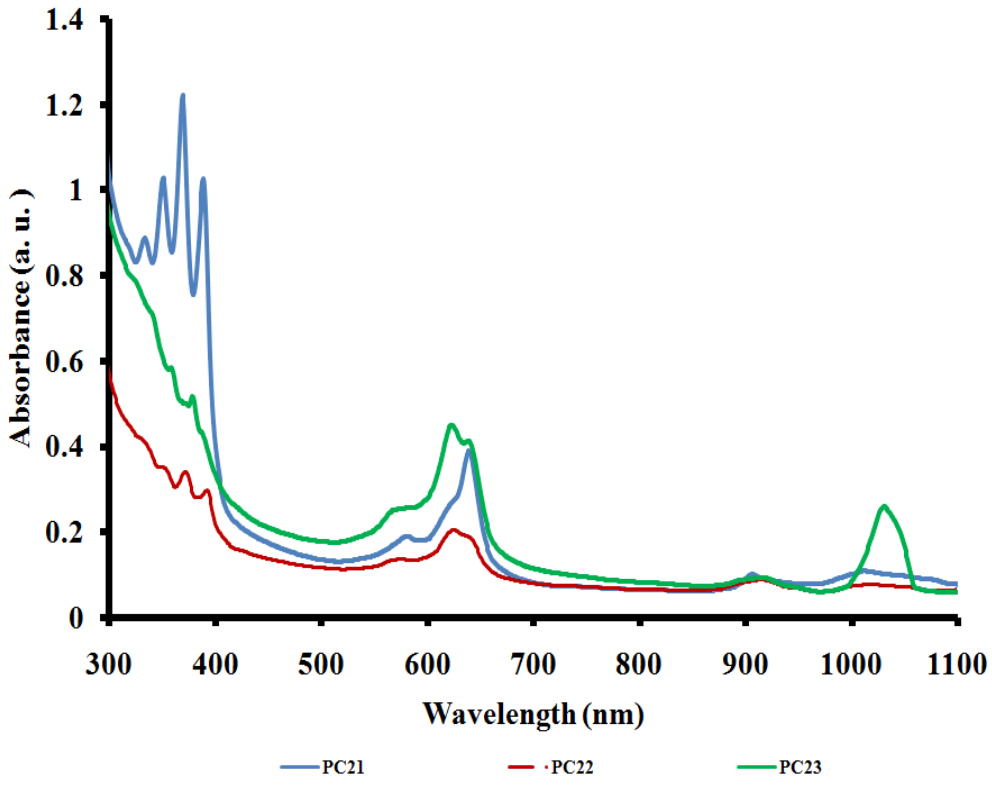

Fig. 4.2 UV-Vis absorption spectra of **PC21**, **PC22** and **PC23** in DMF.

4.3.4. Emission spectroscopy

The **PC21**, **PC22** and **PC23** complexes exhibit intense and long-lived orange-red luminescence upon irradiation in fluid solutions at 298 K (λ_{exc} = 400 nm). The emission spectra are shown in (Figure 4.3). The emission maxima of the complexes **PC21**, **PC22** and **PC23** occur at 672, 682, 700 nm respectively. The emission is likely to originate from an excited state of ^{3}MLCT dπ(Ru) → π* (macrocycle) and (anthracene) characters. An extended π system in the complexes has allowed a greater delocalization of the excited electron, which reduces the adjustments in local bond displacements and modulates the vibrational overlap between states.

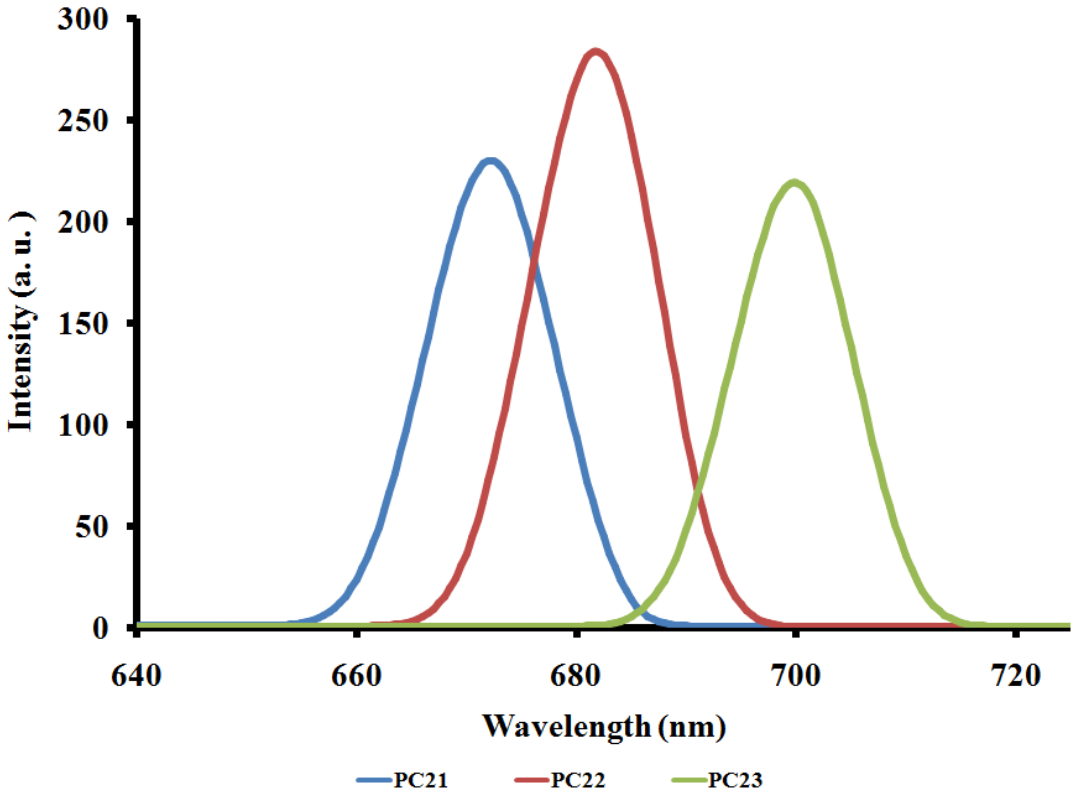

Fig. 4.3 Emission spectra of **PC21**, **PC22** and **PC23** in DMF

4.3.5 Nuclear Magnetic Resonance spectroscopy

The proton nmr spectra for **PC21** and **PC23** show the expected aggregation and broadening of the signals. The AA'BB' signals of the anthracene units in the aromatic region are well resolved and appear as doublet of doublet peaks at chemical shift values at δ 7.47, 7.50 and 8.09 ppm respectively. In addition, the macrocyclic Pc ring protons were found as doublet at δ 8.01 ppm and a singlet at δ 8.43 ppm for **PC21** typical of AAAA-type coupling pattern, while an ABBB-type in **PC23** could be ascribed to the proton singlet peaks at 9.12, 8.55, 8.33 and 7.96 ppm. The aliphatic region of the complexes **PC21** and **PC23**, rather presents an unstructured signals between 2.93-2.17 ppm. However, the methyl groups of the 2,3-dimethylacrylic acid moiety are strong and well resolved.

In the ^{13}C nmr spectra of **PC21** and **PC23**, there are characteristic signals for the axial coordinated carbonyl groups which appear at 166.04 ppm for **PC21** and 175.43 ppm for **PC23**. The downfield shift may be ascribed to the steric hindrance in the dimer molecule. The extension of the π-conjugated bond as a result of the doubly linked anthracene and the dimeric nature of **PC23** complex appeared to have synergistic effects when compared to a monomeric anthracenyl substitution in **PC21**. The carboxylic acid (C=O) functionalities are found as signals between δ 166.16-161.88 ppm for the two complexes. Also present in the spectra are two different peaks with high intensity at δ 128.88 and 126.86 ppm for **PC21** and δ 129.01 and 125.75 ppm for **PC23**. These signals were unambiguously assigned to the anthracene units in the complexes. The macrocyclic ring signals were found between δ 143.42-132.84 ppm. The methyl groups were found as signals at δ 23.93 and 19.56 ppm. A satisfactory ^{1}H and/or ^{13}C nmr spectrum could not be obtained for **PC22** due to poor solubility.

4.3.6 Electrochemistry

Cyclic voltammograms were measured for the functionalized anthracenyl ruthenium(II) phthalocyanine complexes in 0.05 M TBAH-DMF solution. Similar electro-redox properties were observed for **PC21** and **PC22** (Figure 4.4). The two complexes show a reversible one-electron oxidation process at + 0.88 V, this process involves the oxidation of the phthalocyanine macrocycle to give $[Pc^{0}Ru^{II}(CO)_2]^{2+}$ species. One-electron reduction process was observed in the two complexes at -0.71 V and was assigned to reduction of the macrocycle and/or the anthracene unit. When compared to complexes of the type $[Pc^{0}Ru^{II}L_2]^{2+}$ (where L = N-donor ligands), the presence of CO always show only one oxidation process at more positive potentials which may be expected due to greater π-backbonding of the ligated CO complexes.

The dimeric complex **PC23** displays somewhat different redox behaviour to monomeric complexes in that it undergoes two quasi-reversible oxidations at 0.11 and 0.71 V, and one reversible reduction process at –0.60 V (vs. Ag|AgCl) (Figure 4.5). The two oxidation processes may be due to involve metal-centred oxidation or ring-based oxidation. The reduction process is attributed to either the addition of electrons into metal d(π*) orbitals giving $Ru^{1} - Ru^{1}$ species or the electron reduction of the phthalocyanine macrocycle. The possibility of this to the electron-donor nature of the anthracene molecular unit is not excluded.

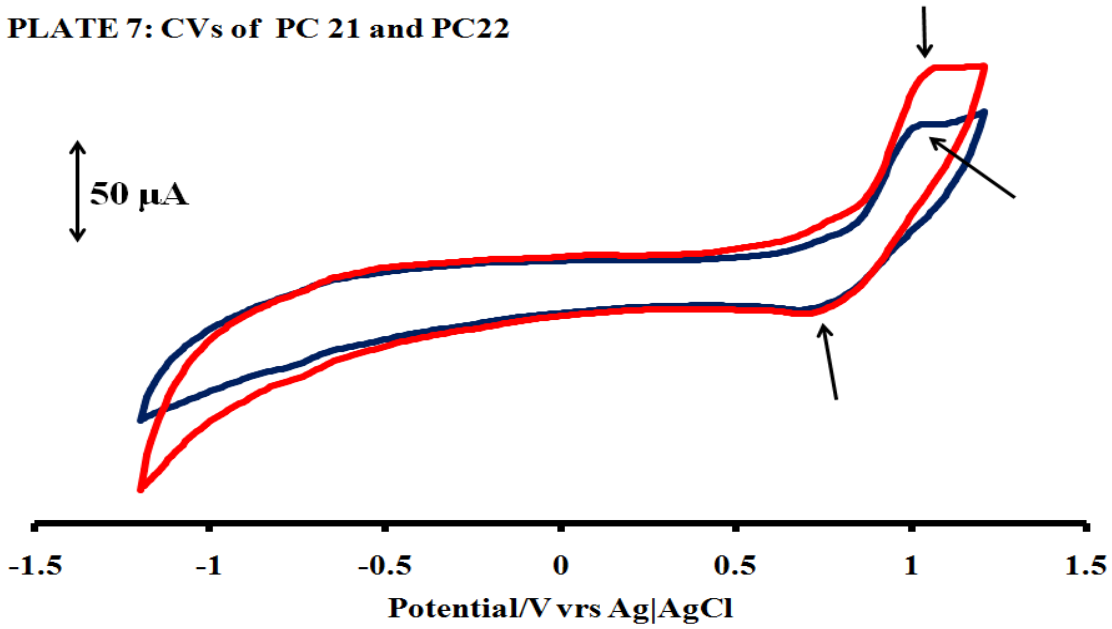

Fig. 4.4 Cyclic voltammetry of **PC21** and **PC22**

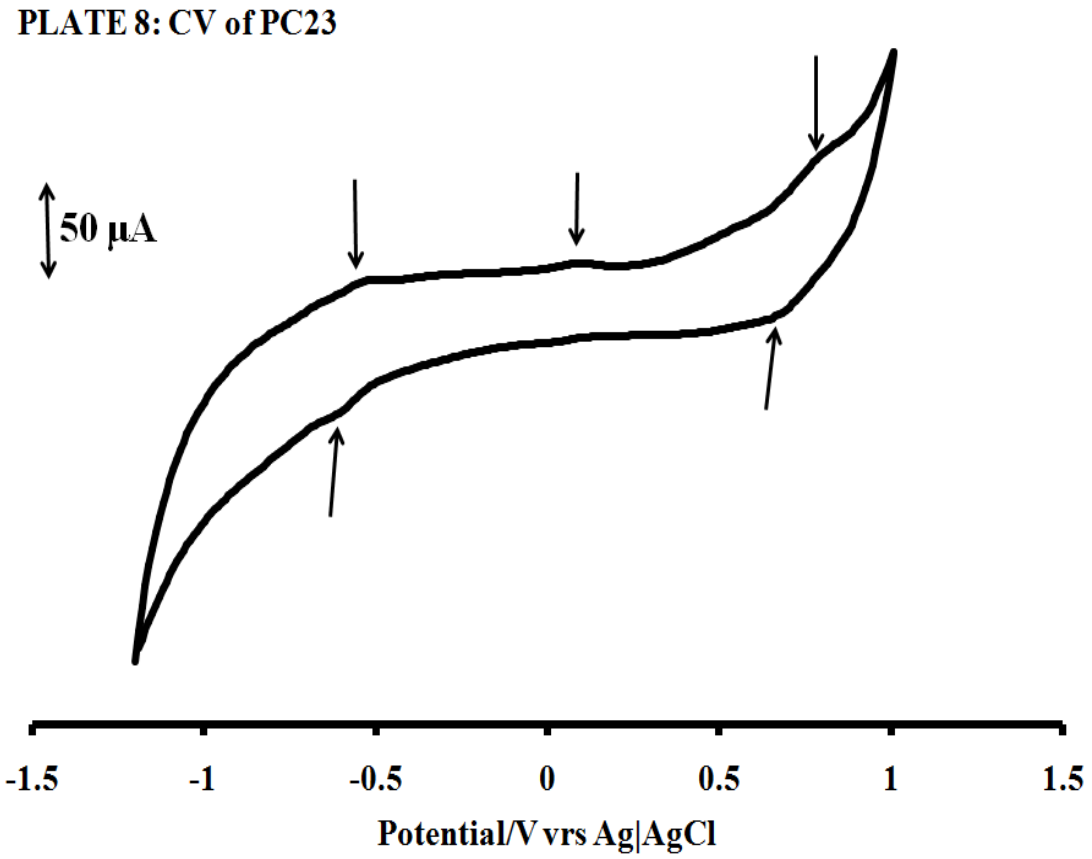

Figure 4.5 Cyclic voltammetry of **PC23**

Conclusion

In summary, 9-bromo-10-(2,3-dimethylacrylic acid) anthracene and 9-bromo-10-(2,3-dimethylacrylic acid) dianthracene reacted conveniently with a non-substituted ruthenium phthalocyanine in an electrophilic aromatic substitution reaction. This route may be useful in the synthesis of substituted metal phthalocyanines where the condensation reaction of the precursors bearing the target group substitution is difficult. The photophysical and electrochemical properties exhibited by **PC21**, **PC22** and **PC23** complexes makes them suitable as potential materials for molecular electronic devices, most especially their use as sensitizers for dye-sensitized solar cells (DSSCs). The dimeric **PC23** complex due to its near infra red absorption property could also serve as carrier generation material.

CHAPTER FIVE

CHAPTER FIVE

5 PRELIMINARY INVESTIGATION OF Ru(II) POLYPYRIDYL COMPLEXES IN THE DYE-SENSITIZED SOLAR CELLS

5.1 Introduction

The dye-sensitized solar cell (DSSC) is one of the recent possibilities of harvesting solar energy by converting it into electricity. The heart of this cell is a photoanode, which is based on a nanoporous nanocrystalline, commonly called nanostructured, TiO_2 film covered by a monolayer of a sensitizing dye [416–418] Upon light excitation, the adsorbed dye molecules inject electrons from their excited states into the conduction band of the semiconductor. The electrons are brought back to the oxidized dye through an external circuit, a platinum counter electrode, and a redox system (typically I^-/I_3^-). The use of a nanostructured TiO_2 film together with the $Ru(dcbpy)_2(NCS)_2$ [dcbpy = 4,4'-dicarboxy-2,2'-bipyridine] (RuN3 for short) dye introduced by Grätzel and co-workers [416] was a breakthrough in terms of a commercial application. An overall conversion efficiency of ~10 % has been achieved. Since then, extensive attention has been paid to this research field [430].

5.2 Dye-sensitized solar cell fabrication

The preparation and I–V curves of sandwiched solar cells based on three series of sensitizers grouped by structures are reported. The dye solutions were prepared in the concentration range of 2-3 x 10^{-4} M in dimethylformamide and a commercially made TiO_2 nanocrystalline from Solaronix was dipped into the dye solution for 14–16 h at room temperature. The dye-coated electrodes were rinsed quickly with ethanol and used as such for photovoltaic measurements. The dye

deposited film is used as a working electrode. A sandwich cell was prepared with a second conducting glass coated with chemically deposited platinum from 0.05 M hexachloroplatinic acid. The platinum coated counter electrode and the dye coated TiO_2 film of surlyn polymer frame (Dupont). The sandwiched electrodes were tightly held using a pressure hot filler to seal the two electrodes. A thin layer of electrolyte consisting of 0.6 M BMII; 0.05 M I_2; 0.1 M LiI; 0.5 M tert-butyl pyridine in 1:1 acetonitrile and valeronitrile was introduced into inter electrode space from the counter electrode side through pre-drilled holes. The drilled holes were sealed with cellophane to avoid leakage of the electrolyte solution (Figure 5.1).

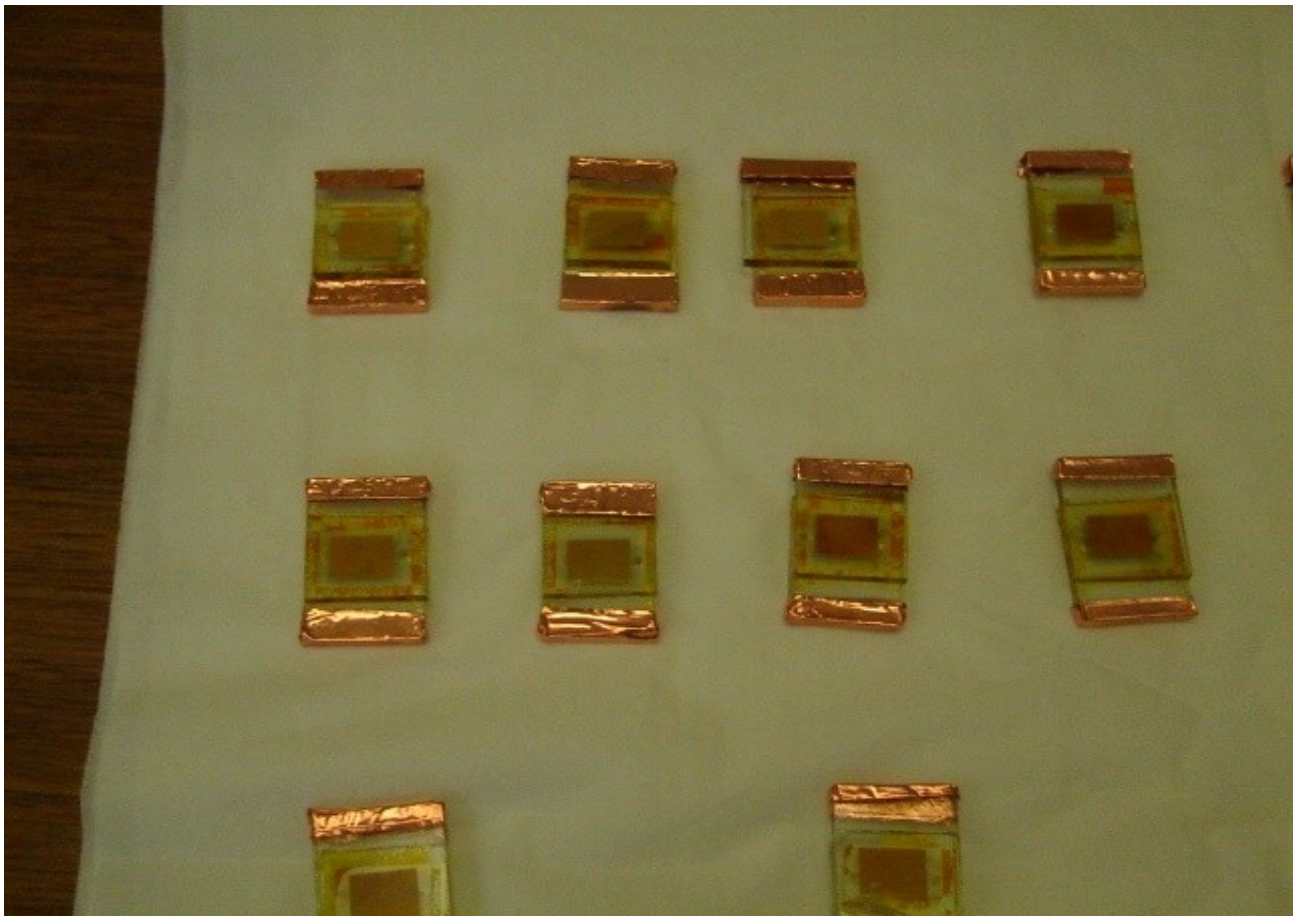

Figure 5.1 Photographic picture of solar cells made from synthesized dyes.

5.3 Photoelectrochemical measurements

Photoelectrochemical data were measured using a 450 W Xenon light source that was focused to give 1000 W/m^2 (the equivalent of one sun at air mass 1.5) at the surface of the test cell. The applied potential and measured cell current were measured using a Keithley model 2400 digital sources meter. The photoelectrochemical properties were investigated by measuring the current and voltage (I–V) characteristics (Figures 5.2– 5.7).

5.4 Results and Discussion

The I–V curves for the evaluated complexes **C2, C6, C9, C11, C12** and **C14** are displayed in (Figures 5.2-5.7) for the shunt and series resistance (R_{sh} and R_s). The short circuit currents (J_{sc}), open circuit potentials (V_{oc}), fill factors (FF) and the conversion efficiencies are listed in Table 5.1. The solar conversion efficiency (n) was calculated using the equation:

$$n = J_{sc} \times V_{oc} \times FF/P_{input},$$

where, P_{input} = 0.088 W

Based on the data generated from the I–V curve, the DSSCs efficiencies of the dyes show very low overall performance. The difference between the performances of the dyes may be attributed to various factors among which include the surface concentrations. The low absorption of the dyes may also be interpreted to be due to presence of a bulky anthracenyl groups. The bulky sensitizers require more space on the TiO_2 surface and penetrate less easily in the small cavities of the nanocrystalline TiO_2 than the sterically less hindered complexes. The effects can be compared with the corresponding ratios of J_{sc} values, which range from 4 % – 21 % in the dyes. Here, it is clear that J_{sc} depends on the dye surface concentration. Though, it has been reported that ratios are significantly higher than what would be expected if the surface concentration were the only determining factor [432, 433]. V_{oc} is also observed to decrease with decrease in surface concentration. In our cells, the low dye coverage had led to lower current output values, as could be observed in various I–V curves. Indeed the fitting of the cells I–V characteristics revealed a low R_{sh}, indicative of a high recombination rate at the photoanode surface and a high R_s, indicative of the ohmic losses at the counter electrode and at the contacts. Although,

the tested dyes have appreciable absorption wavelengths in the visible region of absorption for metal-to-ligand charge transfer (MLCT) transitions, the energy difference between the LUMO levels and the TiO_2 conduction band could affect the electron injection from the excited dyes. This could be a significant factor in the overall performance of the DSSCs. Another, important factor that may be responsible for the low efficiency values of the dye was the electrolyte leakage during preparation of the solar cells. It is well known that electrode must be able to transport the charge carrier between photoanode and counterelectrode. After the complex injects electrons into the conduction band of TiO_2, the oxidized dye must be reduced to its ground state rapidly. The leakage of the electrolyte from the cells may have blocked the smooth transport of the electrons from the complexes to the semiconductor band gap.

Figure 5.2 DSC I–V curves over the positive and negative voltage range for **C2**

(a) Series (Resistance)

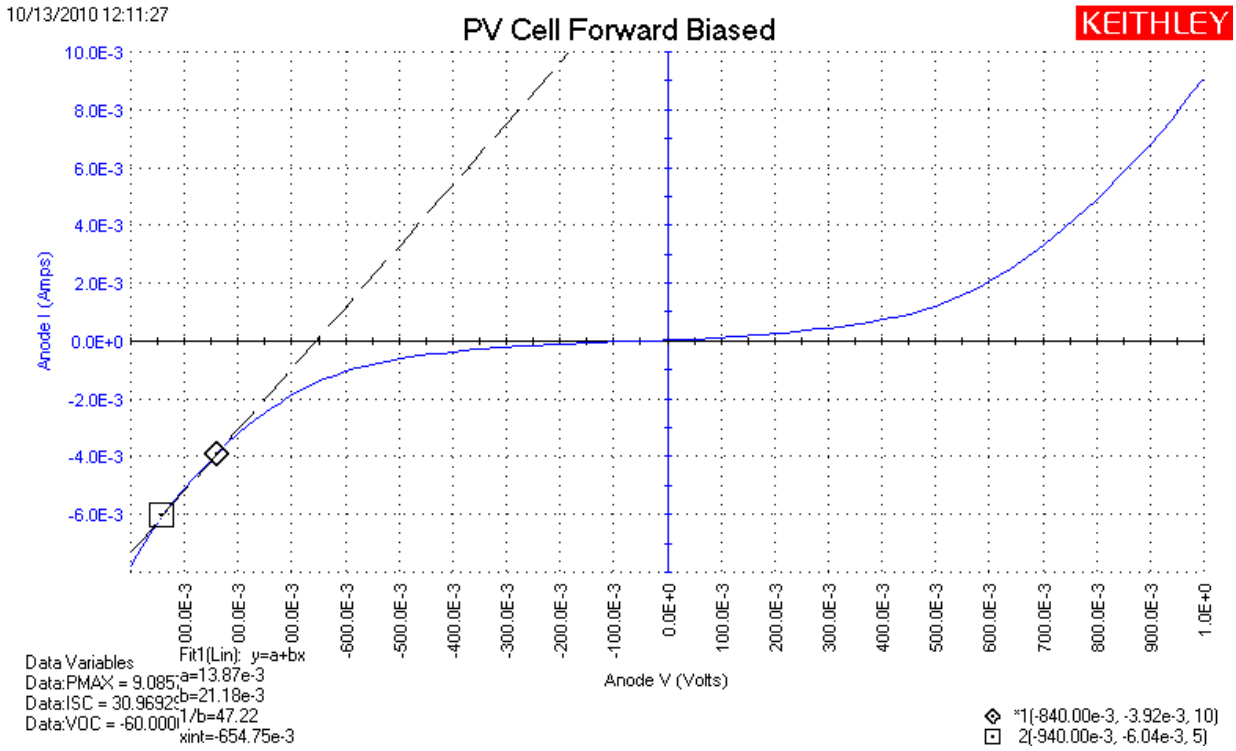

(b) Shunt (Resistance)

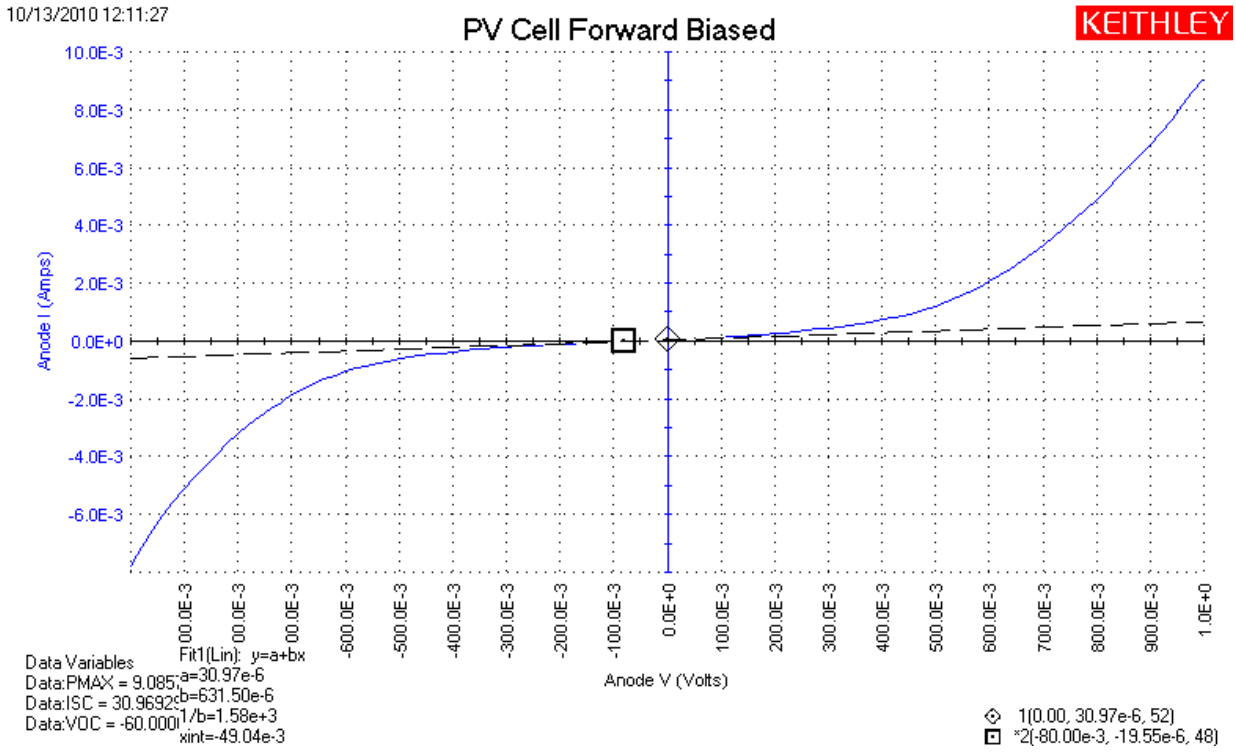

Figure 5.3 DSC I–V curves over the positive and negative voltage range for **C6**

(a) Series Resistance

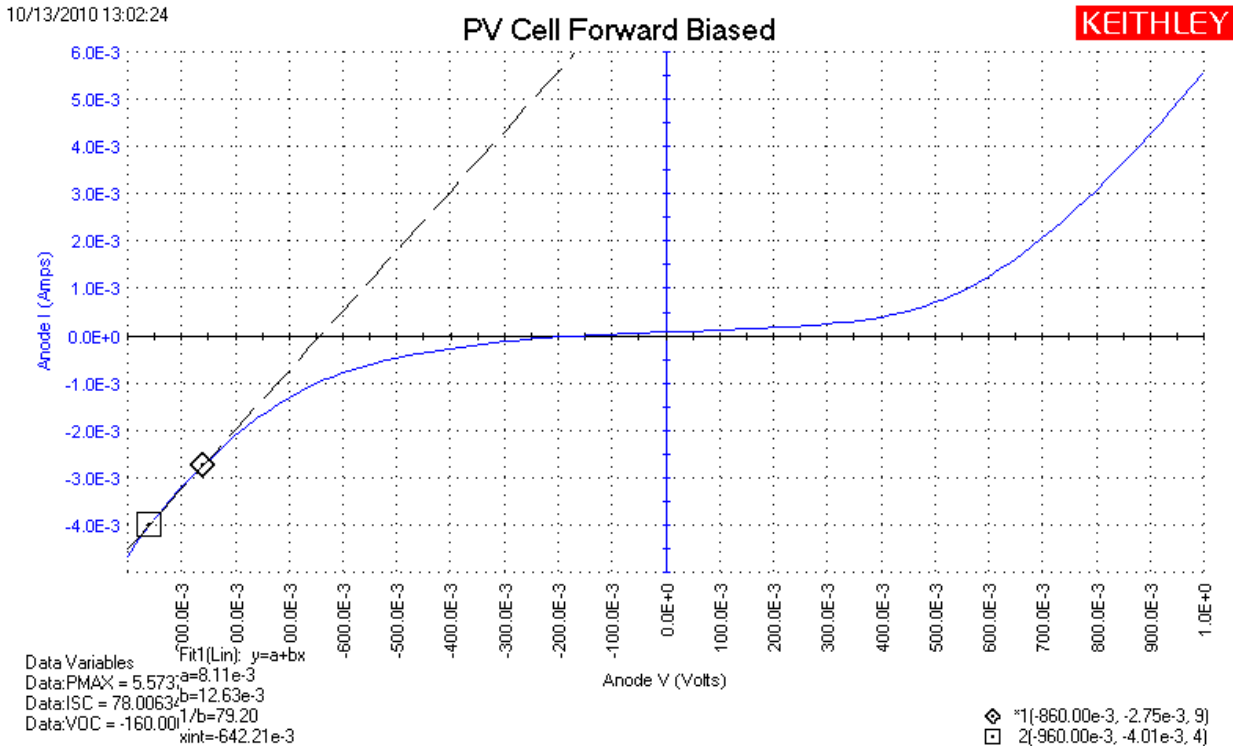

(b) Shunt Resistance

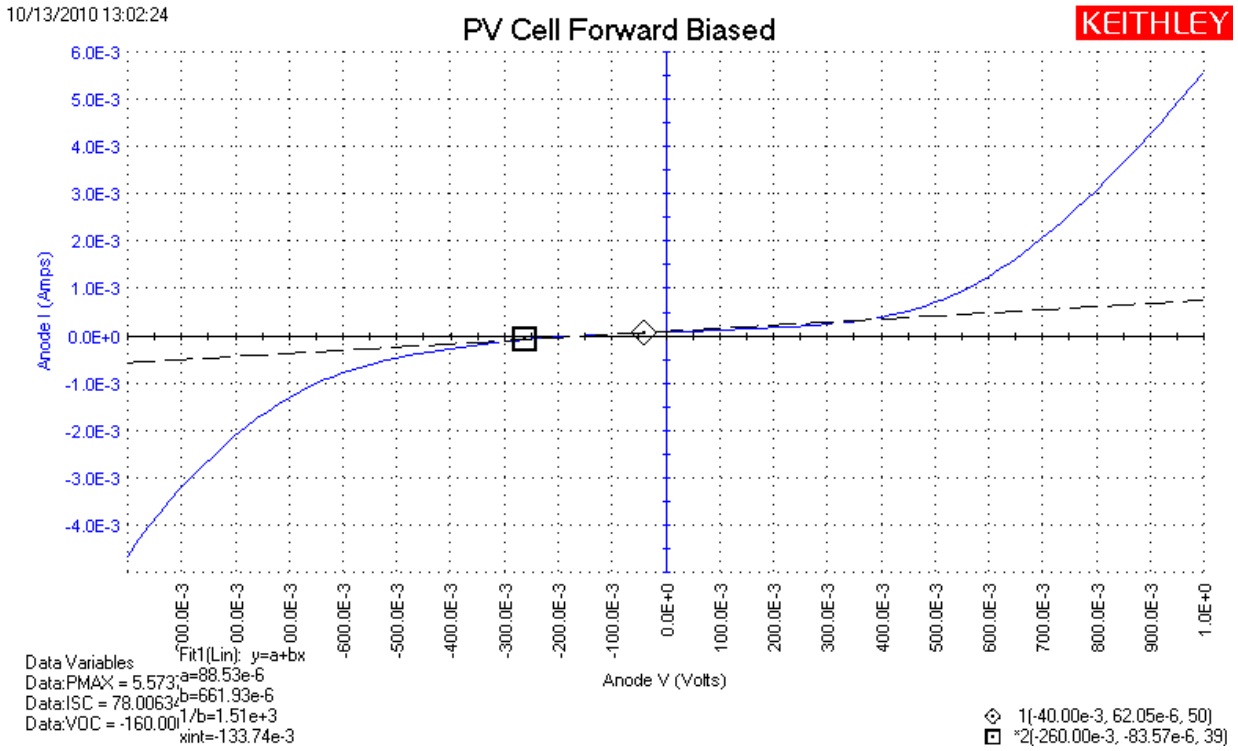

Figure 5.4 DSC I–V curves over the positive and negative voltage range for **C9**

(a) Series Resistance

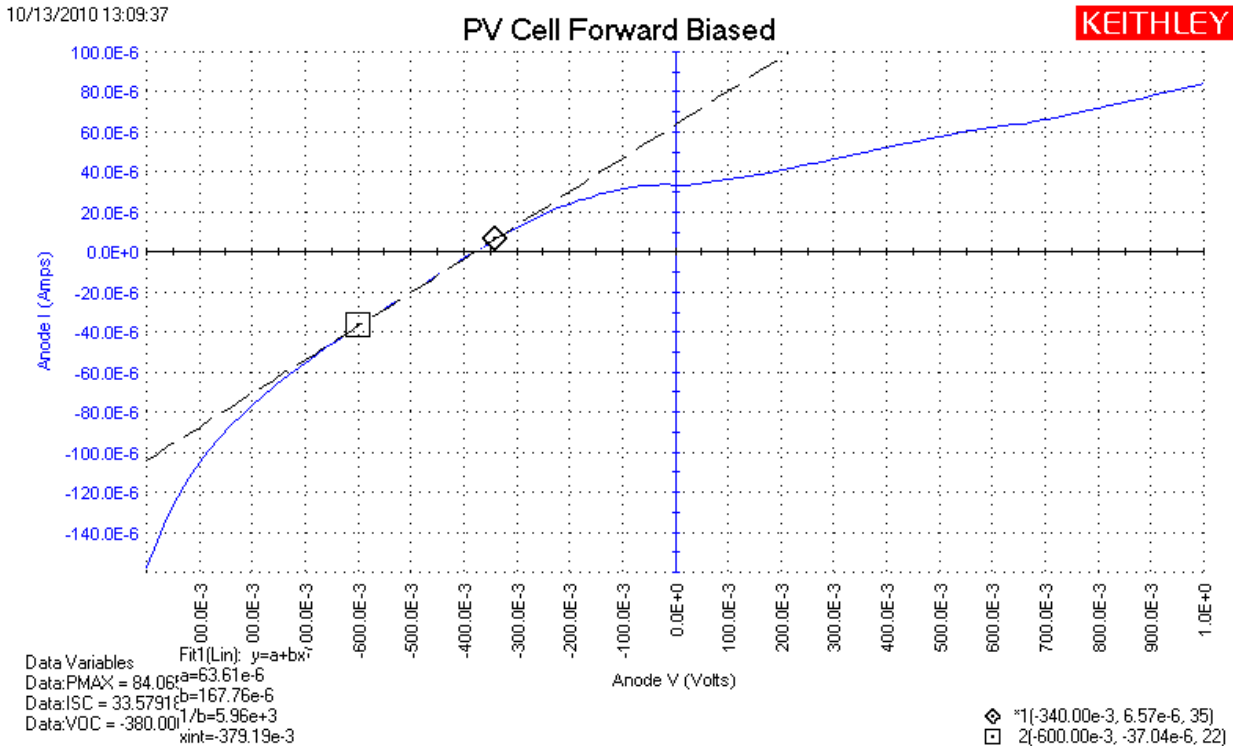

(b) Shunt Resistance

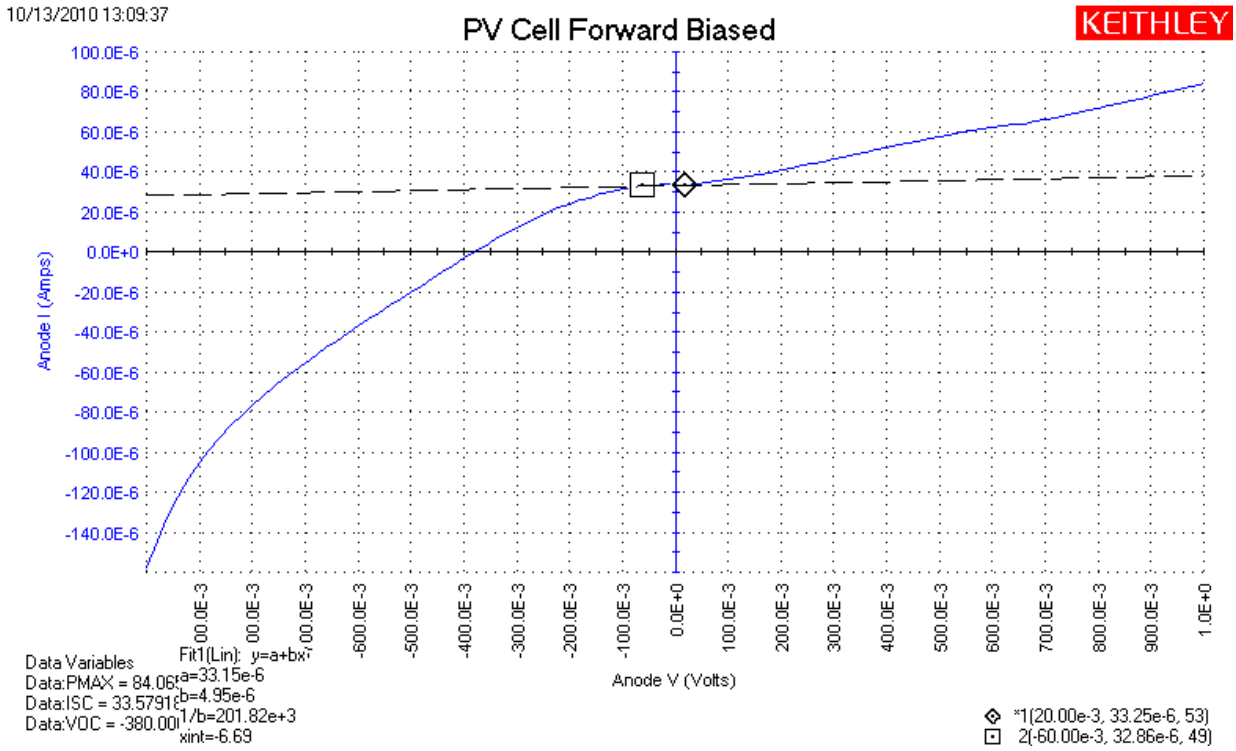

Figure 5.5 DSC I–V curves over the positive and negative voltage range for **C11**

(a) Series Resistance

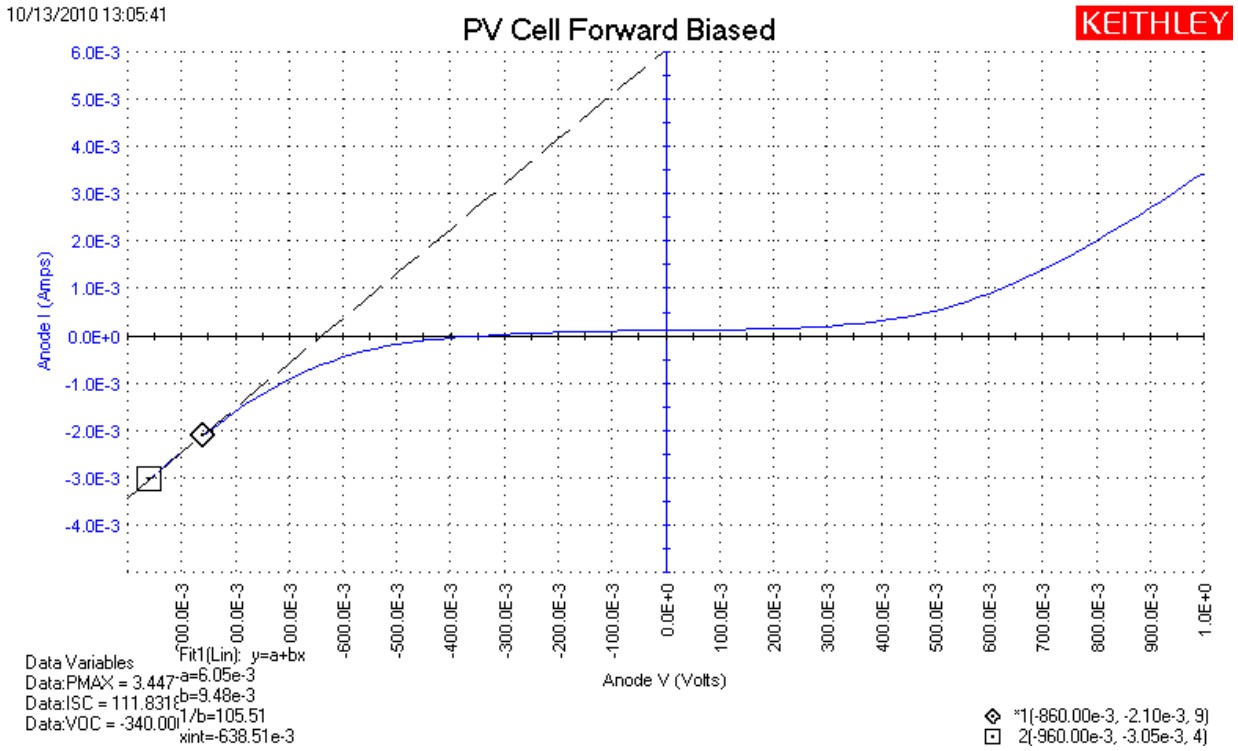

(b) Shunt Resistance

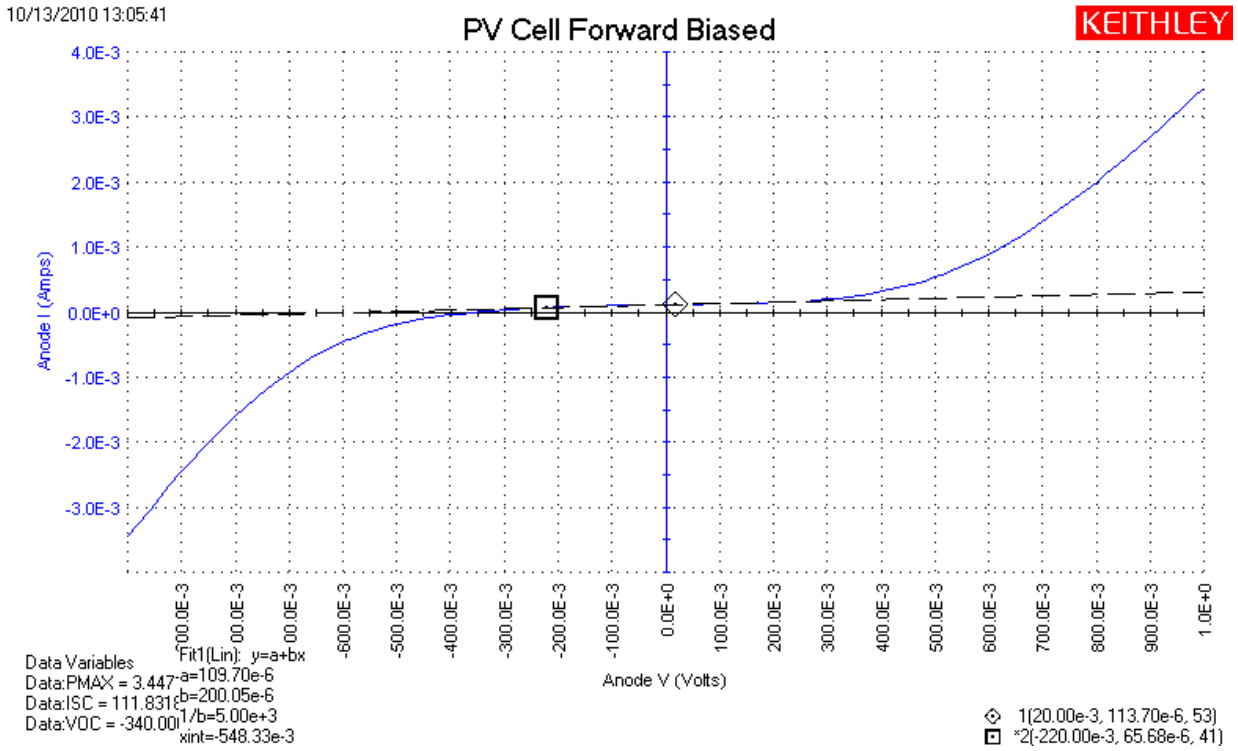

Figure 5.6 DSC I–V curves over the positive and negative voltage range for **C12**

(a) Series Resistance

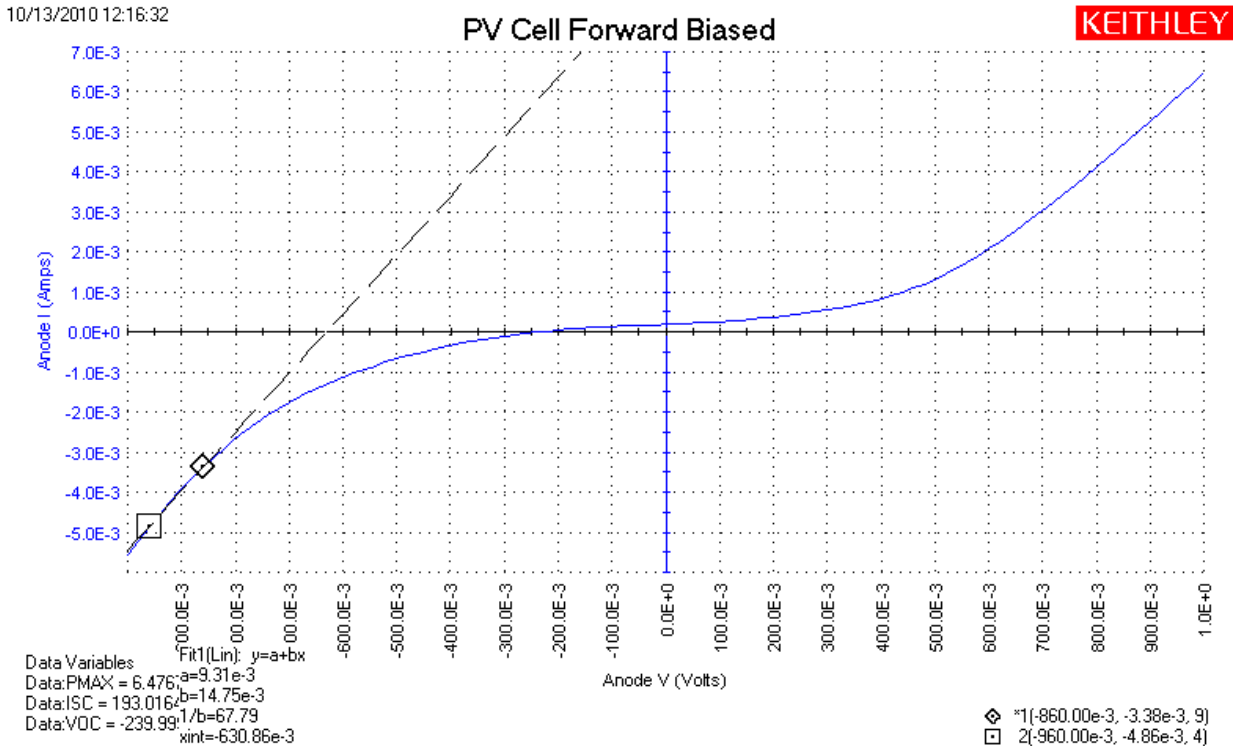

(b) Shunt Resistance

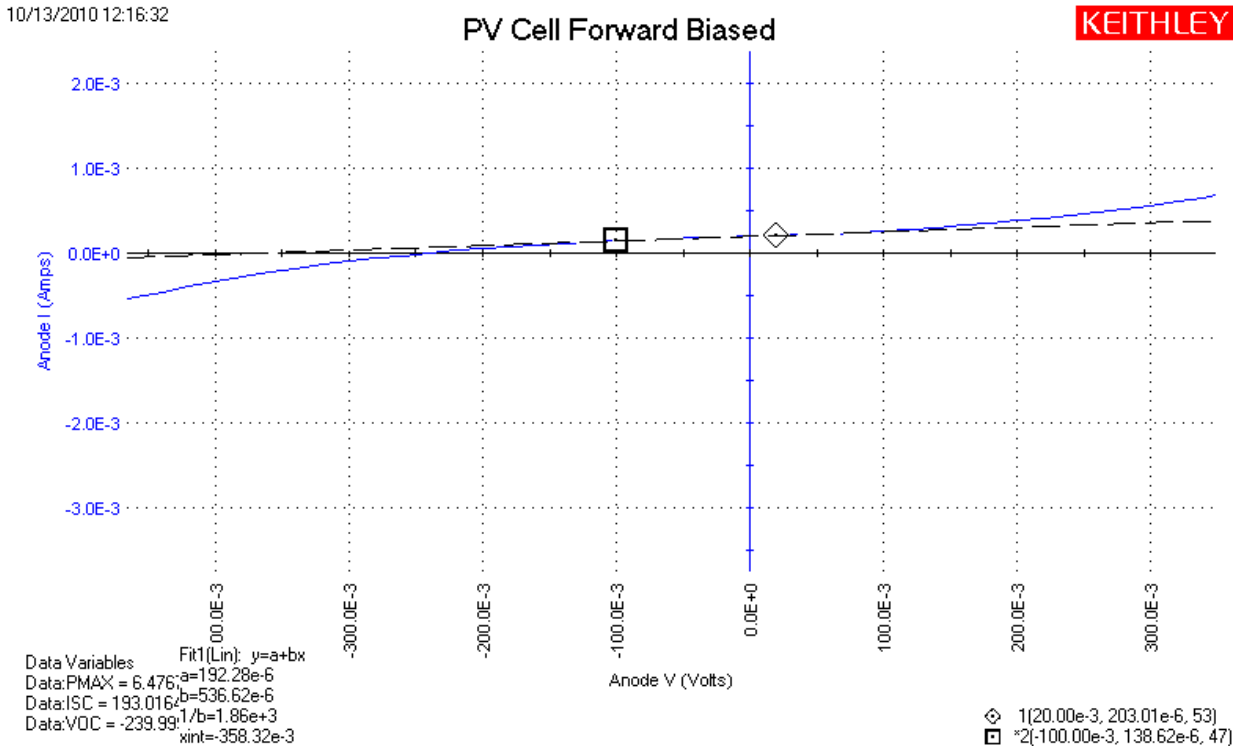

Figure 5.7 DSC I–V curves over the positive and negative voltage range for **C14**

(a) Series Resistance

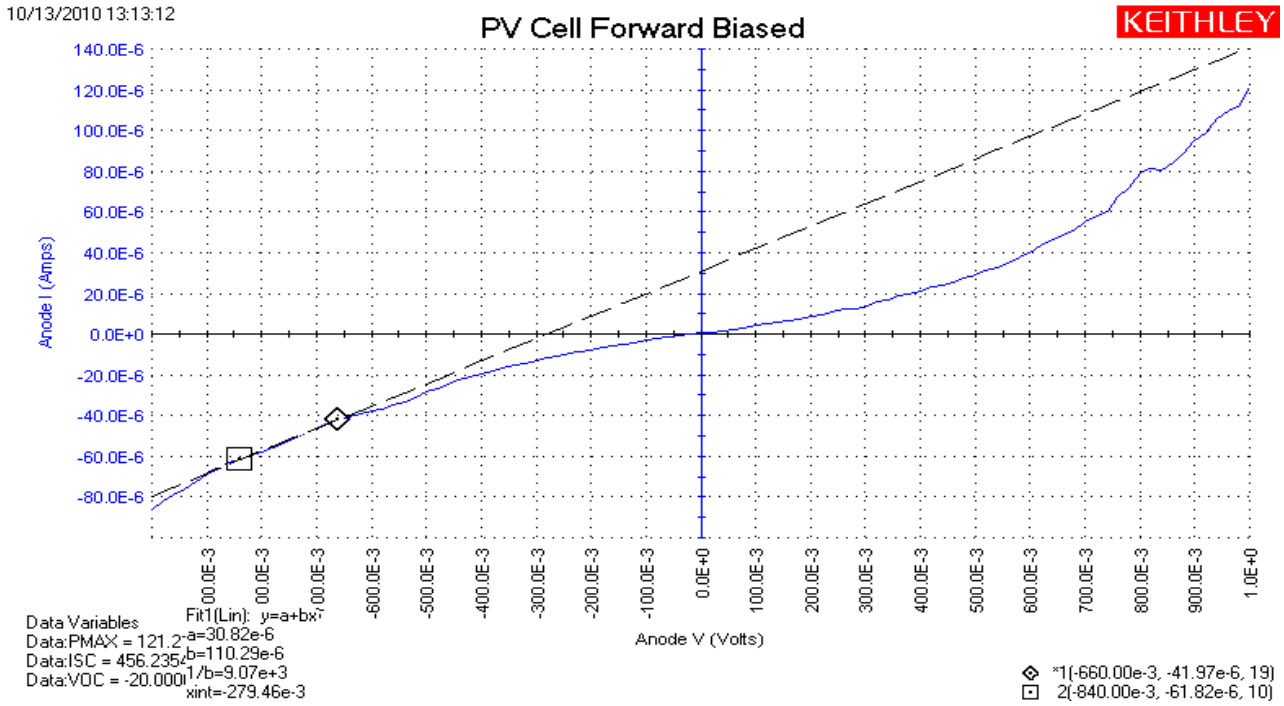

(b) Shunt Resistance

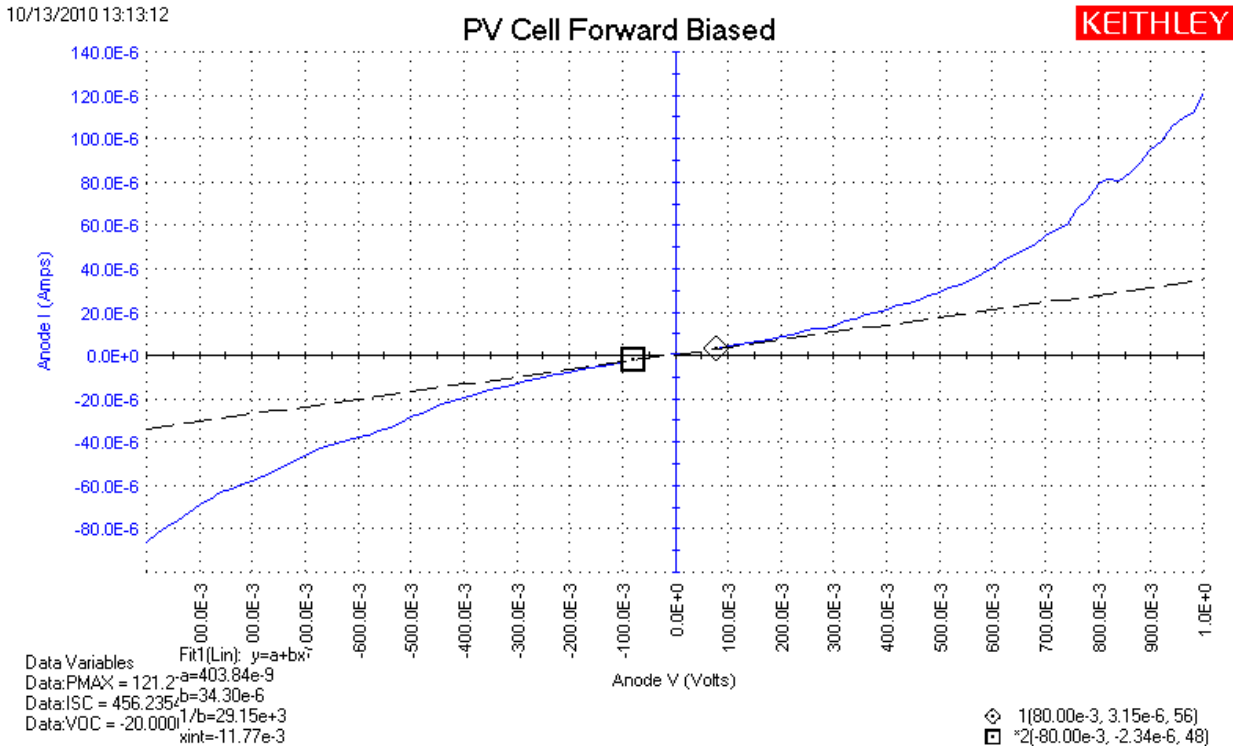

Table 5.1 Optical and DSSC performance parameters of Ru(II) bipyridine/ phenanthroline complexes

Dye	**λ_{abs}[a]/ nm ($\varepsilon/M^{-1}cm^{-1}$)**	**J_{sc} (mA/cm^2)**	**V_{oc} x10^{-3} (V)**	**P_{max}**	**Fill Factor (FF)**	**(η) %**
C2	665 (1090)	35.2 x 10^{-3}	-60	9.09 x 10^{-3}	-4.9 x 10^{3}	0.103
C6	512 (4543)	78.0 x 10^{-3}	-160	5.57 x 10^{-3}	-446.6*	0.063
C9	452 (11556)	33.6 x 10^{-3}	-380	84.1 x 10^{-6}	-6.6*	0.00096
C11	452 (21160)	111.8 x 10^{-3}	-340	3.45 x 10^{-3}	-90.7*	0.04
C12	501 (6970)	193.0 x 10^{-3}	-240	6.48 x 10^{-3}	-139.8 x 10^{3}	0.074
C14	513 (3874)	9.1 x 10^{-3}	-20	121.2 x 10^{-6}	-13.3 x 10^{3}	0.001

[a] Absorption spectra were measured in DMF solution.

* Values may not be taken as true reflection of Fill factor (FF) for the complexes.

CHAPTER SIX

6.0 Summary of the work

This thesis details the synthesis of a series of 4-substituted-2,2-bipyridine, 4,7-disubstituted and 5-substituted-1,10-phenanthroline, and 4′-substituted terpyridine ligands and their corresponding homonuclear, homoleptic and heteroleptic ruthenium(II) complexes containing both simple conjugated substituents such as 2,3-dimethylacrylic acid, 1-methoxy-1-buten-3yne, and a series of mono- to oligo-anthracenyl conjugated substituents as anchoring ligands. Anthracenyl functionalized ruthenium(II) phthalocyanine complexes were synthesized.

The first step involved the bromination of the polypyridine ligands using a simple environmentally benign brominated method as reported by Vyas group [404]. The bromination of the aromatic compounds was used in order to be able to introduce the functional group containing anchoring ligands. The anthracenyl polypyridine derivatives were obtained as a result of a good solvent system developed in our laboratory using 50 % dichloromethane-benzene (V/V) to overcome the poor solubility of anthracene derivatives in common organic solvents such as ethanol or chloroform [406, 413]. This represents a significant advancement in synthetic ability with regards to polypyridine substitutions at the various positions. Moreover, the possibility for a variety of conjugated-extended polymers containing different metal units is made opened. The method of synthesis of new carbon-carbon formation following a modified method as reported by Yamamoto group [405] using a zero-valent palladium catalyzed cross-coupling of aryl halides work best in the overall build-up of the large molecules unlike our initial use of palladium acetate as core catalyst which involved many purification processes and overall lower yield of

products. We also used the method as reported by the Venkataraman group [407] to successfully synthesized a phenanthroline ligand substituted with a 1,3-enyne group. The π-bond elongation of the polypyridine ligands was employed specifically to enhance the absorption properties in the visible region and the molar extinction coefficient of the corresponding complexes. The 2,3-dimethylacrylic acid group was added to the polypyridine ligands to serve, firstly as anchoring agent to semiconductor, secondly, to enhance the stability properties of the complexes due to the presence of two methyl groups in *trans*-spatial orientation and lastly, to suppress or prevent surface aggregation of the sensitizers.

Anthracene derivative was chosen for this work due to their photophysical and photochemical properties most especially for the light harvesting capacity of the complexes. Anthracene family compounds show both hole and electron transport properties and they have been employed as hole transfer materials. Information on the synthetic use of 1-methoxy-1-buten-3-yne is very limited, but this compound was employed for its conjugative property in this work. The influence of the double-to-triple bond linkage was observed in the enhancement of the molar absorptivity coefficient.

The ruthenium(II) complexes of the different substituted polypyridine ligands were obtained first by making the ruthenium(II) complex precursor when ruthenium(III) trichloride monohydrate was refluxed in dimethylsulphoxide following a reaction methodology as reported by Evans group [408]. The procedures as reported by Mitsopoulou group [409] were employed in the overall synthesis of various complexes. The ruthenium(II) phthalocyanine complexes were obtained using direct electrophilic aromatic substitution method. All reported polypyridine ligands, ruthenium(II) polypyridine complexes and ruthenium(II) phthalocyanine complexes

were characterized using available spectroscopic techniques such as infrared, UV-Vis, ^{1}H and ^{13}C NMR and photoluminescence. The elemental analytical compositions and some electrochemical properties of the complexes were also reported.

Due to poor solubility in deuterated solvents, the ^{1}H and ^{13}C of some of the complexes were either poorly resolved or unable to be recorded irrespective of their good absorption and photolumininescent properties. The UV-Vis and luminescence spectra of anthracenyl and thiocyanate containing substituted complexes exhibited red shift compared to the bis-hexafluorophosphate containing complexes. This feature is also observed in the luminescence properties of the complexes, presumably due to the thiocyanate ligand turning the spectra and redox properties of the sensitizers by destabilization of the metal t_2g orbital.

Most of the complexes exhibit a distinctive MLCT (metal-to-ligand charge transfer) absorption band (450-690 nm). The UV-Vis spectra display a gradual red shift of the MLCT band as the conjugation increases. The presence of anthracene groups reduces the energy of the π* state in the d→π* MLCT transition, allowing for the red shift. On the other hand, the molar extinction coefficient was also found to increase in terpyridine complexes as the number of anthracenyl units on the ligand increases from one to three, most especially in the UV region of absorption. This was not so in the visible region for the MLCT transitions as optimum number of anthracene units may be require, this we assumed to be due to molecular aggregation and or steric hindrance. Ru(II) phthalocyanine complexes showed good near-infrared Q-band absorptions (640 nm, 1027 nm), with the Soret band at the near-visible regions (380-405 nm) which were overlap with the vibronic peaks of the anthracene derivatives.

All the polypyridine complexes display bright luminescence in solution between 650-750 nm. A general trend in the photoluminescence properties of various compounds could not be established; however, the bromoanthracenyl terpyridyl ligands gave insight into the correlation between the increase in the number of anthracene molecular units and the luminescent properties in which an inverse relationship was found in the mono-, di-, and trianthracenyl bromo-terpyridine at a common emission wavelength. The results may also be explained to be due to aggregation and/or steric factors in the compounds.

The electrochemical redox properties of two phenanthroline ligands were recorded to show the influence of ruthenium metal substitution on complexation. The results also showed that the various complexes possess good electrochemical properties. The number of electrons involved in each of the redox process was determined by chronocoulometry and was found to be both single and multi-electronic in nature. This was assumed to be general for those complexes containing multi-anthracenyl unit groups. It was also observed that for most complexes with thiocyanate substitution, the oxidation potential overlaps with that of Ru^{3+}/Ru^{2+} redox couple when compared to the complexes having bis-hexafluorophophate ions.

The solar cell parameters and the global efficiency (η) of only six complexes were reported in this work. The highest efficiency (0.103 %) was recorded for complex **C2**. The complexes were chosen based on their visible absorption and molar extinction coefficient properties. The lower efficient may be due to poor adsorption of the tested complexes on the active surface layer of the nanocrystalline TiO_2 semiconductor and/or the incompatibility of the solvent used in the dissolution of the material in relation to the semiconductor and the counter electrode.

6.1 Conclusion

The aims and objectives of the present work involve the design, synthesis, spectroscopic and electrochemical characterization of a number of new functionalized polypyridine ligands and their corresponding Ru(II) homonuclear, heteroleptic, and heteronuclear complexes, as well as Ru(II) phthalocyanine complexes and then carry out their evaluation as potential sensitizers in the dye-sensitized solar cells. It has been established through various studies the importance of visible and or near-infrared absorption, as well as a high molar extinction coefficient to be one of the important way to increase solar efficiency of sensitizers, the main idea in this work focused on the extension of the π→π conjugation bonds of both the ligands and their corresponding complexes.

The ligands and complexes synthesized showed good photophysical, photoluminescence at the visible and near-infrared region of absorption. The electroredox properties of the ligands and complexes showed that they might be useful in the design of chemosensors, photoemitters and other photoelectrochemical processes.

The results obtained in the present study showed that the extension of conjugative π-bonds through tailored ligand synthesis improves the photophysical and electroredox properties especially those of Ru(II) polypyridyl and phthalocyanine complexes. Further work is however, necessary to fine-tune the surface morphology of the complexes and the semiconductor to bring about strong adsorption at the interface which would enhance the photon conversion efficiency of the compounds.

6.2 Recommendations

The objective of this research was to develop a new ruthenium(II) polypyridyl and phthalocyanine complexes as sensitizers for dye-sensitized solar cells, and based on the results obtained so far, the future work would be to investigate apart from the modifications to be made on the chemical structures of the synthesized complexes, further probe into the various parameters affecting the performance of the dye solar cells filled with iodine electrolyte and prepared from as-received, non-purified starting materials resembling cleanness level typical of hypothetical industrial conditions is recommended.

The low surface coverage and adsorption of the tested dyes and other dyes yet to be tested on TiO_2 nanocrystalline semiconductor could be enhanced if the adsorption of the dyes on nanocrystalline TiO_2 semiconductor is carried out at optimum elevated temperature. It has been established by various authors that physical parameters of the dye solar cells such as the electron quasi-Fermi level [435], electron diffusion coefficient [436], electron transport time [437] and conduction and mobility of the electrons in the nanostructure TiO_2 [438] has direct temperature dependence. Studies of these parameters could invariably lead to chemical modifications of the structures of dyes to accommodate the large anthracenyl molecular units into the small cavity pores of the TiO_2 semiconductor. This viewpoint is valid considering a slight increase in the temperature leading to more efficient electron diffusion in the TiO_2 film. According to the trapping/detrapping model for the electron transport in the nanocrystalline TiO_2, Peter et al. [436] have shown that the apparent electron diffusion coefficient increases with temperature as more electrons are released from trap states to the conduction band. On the other

hand, the rate constant for the recombination reaction for the conduction band electrons in the I_3^- in the electrolyte also increases with temperature [435].

Moreover, there is a need to eliminate unwanted side reactions in the electrolyte or reactions of the electrolyte species and/or TiO_2 with possible impurities present in the cell (water, oxygen). This we adduced to be responsible for the lower cell performance. In this study, it may be possible that the short-circuit currents and efficiencies are lowered by impurities in the electrolyte (and possible dye degradation caused by them). As all chemicals used for the evaluation were not of analytical quality, and stored at room temperature instead of oxygen, and water vapour free atmosphere, the purity of the electrolyte was probably lower than if carefully pretreated such as distillation or re-crystallization of its ingredients had been performed. For example, LiI is hygroscopic and water molecules may have been transported into the cell, especially if the electrolyte is prepared during high relative humidity [439].

Disadvantageous changes in the TiO_2 film structure include loosening of the interparticle connections or the contact between the film and the substrate (unlikely for the sintered films, though), which may have led to the overall resistance of the cell. The sealing method used in this study gave room for electrolyte leakage and /or evaporation which had caused cell deterioration and poor transport of the generated electrons from the dyes into the conduction band of the TiO_2 nanocrystalline semiconductor leading to overall poor performance of the cells. Therefore, better sealing method to minimize or totally eliminate this problem is recommended.

It would also be of interest to re-examine these complexes using other standard semiconductor materials such as zinc oxide (ZnO) and/or nobium

pentoxide (Nb_2O_5), having lower band gaps perhaps to cater for the poor electron injection of the complexes into TiO_2 semiconductor wide band gap.

Lastly, impedance spectroscopic analysis (EIS) would be necessary with the clear objective to investigate the overall internal resistance of the cell which in turn influences the cell performance. Nyquist and Bode plots determination would give valuable information regarding the charge transfer resistance and the mechanisms involved in the electrodeposition, electrodissolution and passivity of the dye molecules. Most importantly, since EIS analysis would help in the study of semiconductor interfaces, EIS spectra correlation as a function of temperature is recommended to exactly identify the temperature-induced changes in the charge transport.

REFERENCES

1. Wong, W. Y. *J.Organomet. Chem.* 2009, 694, 2644–2647.
2. Shaheen, S. E.; Ginley, D. S.; Jabbour, G. E. *MRS Bull*. 2005, 30, 10.
3. Barnham, K. W. J.; Mazze, M.; Clive, B. *Nature*, 2006, 5, 161.
4. Maria Abrahamsson. PhD Thesis: ACTA Universitatis Upsaliensis Uppsala 2006. ISBN 91-554–6707-5.
5. Robertson, T. *Angew. Chem., Int. Ed. Engl*. 2006, 45, 2338.
6. Grätzel, M. *Inorg. Chem*. 2005, 44, 6841.
7. Nazeeruddin, M. K.; Gratzel, M. 2007, *Struct. Bond*, 123, 113.
8. Thompson, B. C.; Frechet, J. M. J. 2008, *Angew. Chem., Int. Ed. Engl.* 47, 58.
9. Goncalves, L. M.; de Zea Bermudex, V.; Riberio, H. A.; Mendes, A. M. 2008, *Energy Environ. Sci*. 1, 655.
10. M. Grätzel, *Nature* 414 (2001) 338–344.
11. Wong, W. Y. 2008, *Macromol. Chem. Phys*. 209, 14.
12. Staniszewski, A.; Ardo, S.; Sun, Y., Castellano, F., N.; Meyer, G. J. 2008, *J. Am. Chem. Soc.*, 130, 11586-11587.
13. Sun, Y. PhD Thesis (2009). Bowlin Green State University, USA.
14. Blau, F. *Monatsh. Chem.* 1889, *10*, 375-388.
15. Schumacher, J. N.; Green, C. R.; Best, F. W.; Newell, M. P. *J. Agric. Food Chem.* 1977, *25*, 310-320.
16. Foder, G. B.; Colasanti, B. In *Alkaloids*: *Chemical and Biological Perspectives*; Pelletier, S. W. Ed.; Wiley: New York, 1985; Vol. 3, Chapter 1.
17. Ziessel, R.; Toupet, L.; Chardon-Noblat, S.; Deronzier, A.; Matt, D. *J. Chem. Soc. Dalton Trans.* 1997, 3777-3784.

18. Juris, A.; Balzani, V.; Barigelletti, F.; Campagna, S.; Belser, P.; von Zelewsky, A. *Coord. Chem. Rev.* 1988, *84*, 85–277.

19. Lindoy, L. F.; Livingstone, S. E. *Coord. Chem. Rev.* 1967, *2*, 173–193.

20. Balzani, V.; Juris, A. *Coord. Chem. Rev.* 2001, *211*, 97–115.

21. Hui, J. W. S.; Wong, W. T. *Coord. Chem. Rev.* 1998, *172*, 389–436.

22. Sun, L. C.; Hammarstrom, L. Akermark, B.; Styring, S. *Chem. Soc. Rev.* 2001, *30*, 36–49.

23. Dürr, H.; Bossmann, S. *Acc. Chem. Res.* 2001, *34*, 905–917.

24. Burstall, F. H. *J. Chem. Soc.* 1938, 1662–1672.

25. Case, F. H.; Kasper, T. J. *J. Am. Chem. Soc.* 1956, *78*, 5842–5844.

26. MacBride, J. A. H.; Wright, P. M.; Wakefield, B. J. *Tetrahedron Lett.* 1981, *22*, 4545–4548.

27. Sasse, W. H. F. *Org. Synth.* 1966, *46*, 5–10.

28. Badger, G. M.; Sasse, W. H. F. *Adv. Heterocycl. Chem.* 1963, *2*, 179–202.

29. Krö hnke, F. *Synthesis* 1976, 1–24.

30. Undheim, K.; Benneche, T. *Adv. Heterocycl. Chem.* 1995, *62*, 305–418.

31. Ito, K.; Yoshitake, M.; Katsuki, T. *Tetrahedron* 1996, *52*, 3905–3920.

32. Wang, Z.; Reibenspies, J.; Motekaitis, R. J.; Martell, A. E. *J. Chem. Soc. Dalton Trans.* 1995, 1511–1518.

33. Neuman, U.; Vö gtle, F. *Chem. Ber.* 1989, *122*, 589–591.

34. Constable, E. C.; Morris, D.; Carr, S. *New J. Chem.* 1998, 287–294.

35. Attias, A. J.; Cavalli, C.; Bloch, B.; Guillou, N.; Noél, C. *Chem. Mater.* 1999, *11*, 2057–2068.

36. Trécourt, F.; Mallet, M.; Mongin, O.; Gervais, B.; Quéguiner, G. *Tetrahedron* 1993, *49*, 8373–8380.

37. Onggo, D.; Goodwin, H. A. *Aust. J. Chem.* 1991, *44*, 1539–1551.

38. Yoo, J.; Kim, J.-H.; Sohn, Y. S.; Do, Y. *Inorg. Chim. Acta* 1997, *263*, 53–60.

39. Shan, B.-Z.; Zhao, Z.; Goswami, N.; Eichhorn, D. M.; Rillema, D. P. *Coord. Chem. Rev.* 2001, *211*, 117–144.

40. Schubert, U. S.; Eschbaumer, C.; Hochwimmer, G. *Tetrahedron Lett.* 1998, *39*, 8643–8644.

41. Ulrich, G.; Bedel, S.; Picard, C.; Tisnés, P. *Tetrahedron Lett.* 2001, *42*, 6113–6115.

42. Yamamoto, Y.; Tanaka, T.; Yagi, M.; Inamoto, M. *Heterocycles* 1996, *42*, 189–194.

43. Fallahpour, R. A.; Neuburger, M. *Eur. J. Org. Chem.* 2001, 1853–1856.

44. Echavarren, A. M.; Stille, J. K. *J. Am. Chem. Soc.* 1987, *109*, 5478–5486.

45. Godard, A.; Rovera, J. C.; Marsais, F.; Plé , N.; Quéquiner, G. *Tetrahedron* 1992, *48*, 4123–4134.

46. Nshimyumukiza, P.; Cahard, D.; Rouden, J.; Lasne, M.-C.; Plaquevent, J. C. *Tetrahedron Lett.* 2001, *42*, 7787–7790.

47. Savage, S. A.; Smith, A. P.; Fraser, C. L. *J. Org. Chem.* 1998, *63*, 10048–10051.

48. Smith, A. P.; Savage, S. A.; Love, J. C.; Fraser, C. L. *Org. Synth.* 2001, *78*, 51–62.

49. Wang, Z.; Xiong, R.-G.; Naggar, E.; Foxman, B. M.; Lin, W. *Inorg. Chim. Acta* 1999, *288*, 215–219.

50. Siegel, J. S.; Loren, J. C. *Angew. Chem., Int. Ed. Engl*. 2001, *40*, 754–757.

51. Ishikura, M.; Kamada, M.; Terashima, M. *Synthesis* 1984, 936–938.

52. Fernando, S. R. L.; Maharoof, U. S. M.; Deshayes, K. D.; Kinstle, T. H.; Ogawa, M. Y. *J. Am. Chem. Soc.* 1996, *118*, 5783–5790.

53. Cruskie, M. P.; Zoltewicz, J. A.; Abboud, K. A. *J. Org. Chem.* 1995, *60*, 7491–7495.

54. Furukawa, N.; Shibutani, T.; Fujihara, H. *Tetrahedron Lett.* 1989, *30*, 7091–7094.

55. Uenishi, J.; Ueno, T.; Hata, S.; Nishiwaki, K.; Tanaka, T.; Wakabayashi, S.; Yonemitsu, O.; Oae, S. *Heterocycles,* 1999, *50*, 341–351.

56. Zhang, N.; Thomas, L.; Wu, B. *J. Org. Chem.* 2001, *66*, 1500–1502.

57. Hitchcock, S. A.; Mayhugh, D. R.; Gregory, G. S. *Tetrahedron Lett.* 1995, *36*, 9085–9088.

58. Charbonniére, L. J.; Weibel, N.; Ziessel, R. F. *Tetrahedron Lett.* 2001, *42*, 659–662.

59. Potts, K. T.; Winslow, P. A. *J. Org. Chem.* 1985, *50*, 5405–5409.

60. Potts, K. T.; Gheysen Raiford, K. A.; Keshavarz, M. K. *J. Am. Chem. Soc.* 1993, *115*, 2793–2807.

61. Sauer, J.; Heldmann, D. K.; Pabst, G. R. *Eur. J. Org. Chem.* 1999, 313–321.

62. Varela, J. A.; Castedo, L.; Saá, C. *J. Org. Chem.* 1997, *62*, 4189–4192.

63. Varela, J. A.; Castedo, L.; Saá, C. *J. Am. Chem. Soc.* 1998, *120*, 12147–12148.

64. Jones, G.; Pitman, M. A.; Lunt, E.; Lythgoe, D. J.; Abarca, B.; Ballesteros, R.; Elmasnaouy, M. *Tetrahedron* 1997, *53*, 8257–8268.

65. Abarca, B.; Ballesteros, R.; Elmasnaouy, M. *Tetrahedron* 1998, *54*, 15287–15292.

66. Tadesse, S.; Bhandari, A.; Gallop, M. A. *J. Comb. Chem.* 1999, *1*, 184–187.

67. Haginiwa, J. *Jpn. J. Pharmacol.* 1955, *75*, 731–733.

68. Krumholz, P. *J. Am. Chem. Soc.* 1953, *75*, 2163–2166.

69. Khandelwal, G. D.; Swan, G. A.; Roy, R. B. *J. Chem. Soc. Perkin Trans.* 1 1974, 891–896.

70. Maerker, G.; Case, F. H. *J. Am. Chem. Soc.* 1958, *80*, 2745–2748.

71. Hadda, T. B.; Zidane, I.; Moya, S. A.; Le Bozec, H. *Polyhedron* 1996, *15*, 1571–1573.

72. Zoltewicz, J. A.; Cruskie, M. P., Jr. *Tetrahedron* 1995, *51*, 11401–11410.

73. Downard, A. J.; Honey, G. E.; Steel, P. *J. Inorg. Chem.* 1991, *30*, 3733–3737.

74. Wenkert, D.; Woodward, R. B. *J. Org. Chem*. 1983, *48*, 283–289.

75. Oae, S.; Kawai, T.; Furukawa, N. *Phosphorus Sulfur* 1987, *34*, 123–132.

76. Kelly, T. R.; Lee, Y.-J.; Mears, R. J. *J. Org. Chem.* 1997, *62*, 2774–2781.

77. Nakashima, K.; Shinkai, S. *Chem. Lett.* 1994, 1267–1270.

78. Romero, F. M.; Ziessel, R. *Tetrahedron Lett.* 1995, *36*, 6471–6474.

79. Garber, T.; Rillema, D. P. *Synth. Comm. 1990*, *20*, 1223–1239.

80. Penicaud, V.; Odobel, F.; Bujoli, B. *Tetrahedron Lett.* 1998, *39*, 3689–3692.

81. Corcoran, R. C.; Bang, S. H. *Tetrahedron Lett.* 1990, *31*, 6757–6758.

82. Uenishi, J.; Tanaka, T.; Nishiwaki, K.; Wakabayashi, S.; Oae, S.; Tsukube, H. *J. Org. Chem.* 1993, *58*, 4382–4388.

83. Uenishi, J.; Tanaka, T.; Wakabayashi, S.; Oae, S. *Tetrahedron Lett.* 1990, *31*, 4625–4628.

84. Choppin, S.; Gros, P.; Fort, Y. *Org. Lett.* 2000, *2*, 803–805.

85. Masood, M. A.; Sullivan, B. P.; Hodgson, D. *J. Inorg. Chem.* 1999, *38*, 5425–5430.

86. Antonini, I.; Claudi, F.; Cristalli, G.; Franchetti, P.; Grifantini, M.; Martelli, S. *J. Med. Chem.* 1981, *24*, 1181–1184.

87. Schneider, J. P.; Topgi, R. S.; Kelly, J. W. *Synth. Comm.* 1992, *22*, 1033–1037.

88. Janiak, C.; Deblon, S.; Wu, H.-P.; Kolm, M. J.; Klüfers, P.; Piotrowski, H.; Mayer, P. *Eur. J. Inorg. Chem.* 1999, 1507–1521.

89. Ellison, D. K.; Iwamoto, R. T. *Tetrahedron Lett.* 1983, *24*, 31–32.

90. Kitamura, N.; Rajagopal, S.; Tazuke, S. *J. Phys. Chem.* 1987, *91*, 3767–3771.

91. Damrauer, N. H.; Boussie, T. R.; Devenney, M.; McCusker, J. K. *J. Am. Chem. Soc.* 1997, *119*, 8253–8268.

92. Rodriguez, A. L.; Peron, G.; Duprat, C.; Vallier, M.; Fouquet, E.; Fages, F. *Tetrahedron Lett.* 1998, *39*, 1179–1182.

93. Kocian, O.; Mortimer, R. J.; Beer, P. D. *Tetrahedron Lett.* 1990, *31*, 5069–5072.

94. Oki, A. R.; Morgan, R. J. *Synth. Commun*. 1995, *25*, 4093–4098.

95. Crooker, J. C.; Murray, R. W. *Anal. Chem*. 2000, *72*, 3245–3252.

96. Veriot, G.; Dutasta, J.-P.; Matouzenko, G.; Collet, A. *Tetrahedron* 1995, *51*, 389–400.

97. Dholakia, S.; Gillard, R. D.; Wimmer, F. L. *Polyhedron* 1985, *4*, 791–795.

98. Hadda, T. B.; Sam, N.; Le Bozec, H.; Dixneuf, P. H. *Inorg. Chem. Commun.* 1999, *2*, 460–462.

99. Dupau, P.; Renouard, T.; Le Bozec, H. *Tetrahedron Lett.* 1996, *37*, 7503–7506.

100. Hwang, K. O.; Sasaki, T. *J. Mater. Chem.* 1998, *8*, 2153–2156.

101. Hirao, T.; Koichiro, I. *Chem. Commun*. 2001, 431–432.

102. Mines, G. A.; Bjerrum, M. J.; Hill, M. G.; Casimiro, D. R.; Chang, I. J.; Winkler, J. R.; Gray, H. B. *J. Am. Chem. Soc.* 1996, *118*, 1961–1965.

103. Rowe, K. E.; Bruce, D. W. *J. Mater. Chem.* 1998, *8*, 331–341.

104. El-ghayoury, A.; Ziessel, R. *J. Org. Chem.* 2000, *65*, 7757–7763.

105. Smith, A. P.; Corbin, P. S.; Fraser, C. L. *Tetrahedron Lett.* 2000, *41*, 2787–2789.

106. Harding, M. M.; Koert, U.; Lehn, J. M.; Marquis-Rigault, A.; Piguet, C.; Siegel, J. *Helv. Chim. Acta* 1991, *74*, 594–610.

107. Lee, J. K.; Yoo, D.; Rubner, M. F. *Chem. Mater.* 1997, *9*, 1710–1712.

108. Eisenbach, C. D.; Schubert, U. S.; Baker, G. R.; Newkome, G. R. *J. Chem. Soc., Chem. Commun.* 1995, 69–70.

109. Della Ciana, L.; Hamachi, I.; Meyer, T. J. *J. Org. Chem.* 1989, *54*, 1731–1735.

110. Smith, A. P.; Fraser, C. L. *Macromolecules* 2002, *35*, 594–596.

111. Newkome, G. R.; Gross, J.; Patri, A. K. *J. Org. Chem.* 1997, *62*, 3013–3014.

112. Albrecht, M.; Riether, C. *Synlett* 1995, 309–312.

113. Nocentini, G.; Barzi, A. *Gen. Pharmacol*. 1997, *29*, 701–706.

114. Jenkins, I. H.; Rees, N. G.; Pickup, P. G. *Chem. Mater.* 1997, *9*, 1213–1216.

115. Alcock, N. W.; McLaren, F.; Moore, P.; Pike, G. A.; Roe, S. M. *J. Chem. Soc. Chem. Commun.* 1989, 629–632.

116. Couchman, S. M.; Jeffery, J. C.; Ward, M. D. *Polyhedron* 1999, *18*, 2633–2640.

117. Holligan, B. M.; Jeffery, J. C.; Norgett, M. K.; Schatz, E.; Ward, M. D. *J. Chem. Soc., Dalton Trans.* 1992, 3345–3351.

118. Fraser, C. L.; Smith, A. P. *J. Polym. Sci, Part A: Polym. Chem.* 2000, *38*, 4704–4716.

119. Schubert, U. S.; Nuyken, O.; Hochwimmer, G. *J. Macromol. Sci. Pure* 2000, *37*, 645–658.

120. Williams, M. E.; Masui, H.; Long, J. W.; Malik, J.; Murray, R. W. *J. Am. Chem. Soc.* 1997, *119*, 1997–2005.

121. Naka, K.; Yaguchi, M.; Chujo, Y. *Chem. Mater.* 1999, *11*, 849–851.

122. Chujo, Y.; Naka, A.; Krämer, M.; Sada, K.; Saegusa, T. *J. Macromol. Sci. Pure* 1995, *32*, 1213–1223.

123. Vö gtle, F.; Plevoets, M.; Nieger, M.; Azzellini, G. C.; Credi, A.; De Cola, L.; De Marchis, V.; Venturi, M.; Balzani, V. *J. Am. Chem. Soc.* 1999, *121*, 6290–6298.

124. Schubert, U. S.; Weidl, C. H.; Rapta, P.; Harth, E.; Müllen, K. *Chem. Lett.* 1999, 949–950.

125. Choi, B.-K.; Takahashi, H.; Kanbara, T.; Yamamoto, T. *Polym. J.* 2000, *32*, 991–994.

126. Bouachrine, M.; Lére-Porte, J. P.; Moreau, J. J. E.; Serein-Spirau, F.; Torreilles, C. *J. Mater. Chem.* 2000, *10*, 263–268.

127. Yamamoto, T.; Maruyama, T.; Zhou, Z. H.; Ito, T.; Fukuda, T.; Yoneda, Y.; Begum, F.; Ikeda, T.; Sasaki, S.; Takezoe, H.; Fukuda, A.; Kubota, K. *J. Am. Chem. Soc.* 1994, *116*, 4832–4845.

128. Wang, Q.; Yu, L. *J. Am. Chem. Soc.* 2000, *122*, 11806–11811.

129. Yu, S. C.; Gong, X.; Chan, W. K. *Macromolecules* 1998, *31*, 5639–5646.

130. Tan, L. S.; Burkett, J. L.; Simko, S. R.; Alexander, M. D., Jr. *Macromol. Rapid Commun.* 1999, *20*, 16–20.

131. Osaheni, J. A.; Jenekhe, S. A. *J. Am. Chem. Soc.* 1995, *117*, 7389–7398.

132. Tan, L. S.; Srinivasan, K. R.; Bai, S. J. *J. Polym. Sci. Polym. Chem.* 1997, *35*, 1909–1924.

133. Yagi, K.; De Loudres Rivera-Castro, M. *Inorg. Chim. Acta* 1987, *131*, 273–275.

134. Yu, S. C.; Hou, S.; Chan, W. K. *Macromolecules* 2000, *33*, 3259–3273.

135. Wang, B.; Wasielewski, M. R. *J. Am. Chem. Soc.* 1997, *119*, 12–21.

136. Park, H. W.; Sung, S. M.; Min, K. S.; Bang, H.; Suh, M. P. *Eur. J. Inorg. Chem.* 2001, 2857–2863.

137. Lu, J.; Yu, C.; Niu, T.; Paliwala, T.; Crisci, G.; Somosa, F.; Jacobson, A. *J. Inorg. Chem.* 1998, *37*, 4637–4640.

138. Lu, J.; Paliwala, T.; Lim, S. C.; Yu, C.; Niu, T.; Jacobson, A. *J. Inorg. Chem.* 1997, *36*, 923–929.

139. Lu, J. Y.; Cabrera, B. R.; Wang, R. J.; Li, J. *J. Inorg. Chem.* 1999, *38*, 4608–4611.

140. Carlucci, L.; Ciani, G.; Proserpio, D. M.; Sironi, A. *J. Am. Chem. Soc.* 1995, *117*, 4562–4569.

141. Keller, S. W. *Angew. Chem., Int. Ed. Engl.* 1997, *36*, 247–248.

142. Zhu, S. S.; Swager, T. M. *J. Am. Chem. Soc.* 1997, *119*, 12568–12577.

143. Storrier, G. D.; Colbran, S. B. *Polyhedron* 1997, *16*, 2705–2710.

144. Aranyos, V.; Hjelm, J.; Hagfeldt, A.; Grennberg, H. *J. Chem. Soc. Dalton Trans.* 2001, 1319–1325.

145. Walters, K. A.; Trouillet, L.; Guillerez, S.; Schanze, K. S. *Inorg. Chem.* 2000, *39*, 5496–5509.

146. Wang, L. H.; Kang, E. T.; Huang, W. *Polymer* 2001, *42*, 3949–3952.

147. Gerdeissen, Ber. 1889, *22*, 244–254.

148. Walden, Jr., G. H.; Hammett, L. P.; Chapman, R. P. *J. Am. Chem. Soc.* 1931, *53*, 3908.

149. Richter, F.; Smith, G. F. *J. Am. Chem. Soc.* 1944, *66*, 396–398.

150. Smith, G. F.; Cagle, F. W., Jr. *J. Am. Chem. Soc.* 1947, *69*, 781–784.

151. Smith, G. F.; Richter, F. P. Phenanthroline and Substituted Phenanthroline Indicators, their Preparation, Properties, and Applications to Analysis; G. F. Smith Chemical Co, Columbus, OH, 1944.

152. Diehl, H.; Smith, G. F. The Copper Reagents: Cuproine, Neocuproine, Bathocuproine; G. F. Smith Chemical Co, Columbus, OH, 1958.

153. Case, F. H. *J. Org. Chem.* 1951, *16*, 941–945.

154. Case, F. H.; Sasin, R. *J. Org. Chem.* 1955, *20*, 1330–1336.

155. Case, F. H.; Catino, S.; Scholnick, F. *J. Org. Chem.* 1953, *19*, 31–36.

156. Schilt, A. A. Analytical Applications of 1,10-Phenanthroline and Related Compounds; Pergamon Press, New York, 1969.

157. Kalyanasundaram, K. Photochemistry of Polypyridine and Porphyrin Complexes; Academic Press: New York, 1992, 339-369.

158. Buckingham, D. A.; Dwyer, F. P.; Goodwin, H. A.; Sargeson, A. M. *Aust. J. Chem.* 1964, *17*, 325–336.

159. Lindoy, L. F.; Livingstone, S. E. *Coord. Chem. Rev.* 1967, *2*, 173–193.

160. Armaroli, N. Chem. Soc. Rev. 2001, *30*, 113–124.

161. Kohjiro, H.; Hideki, S.; Lok, P. S.; Ashlaful, I.; Ryuzi, K.; Masatoshi, Y.; Kazuhiro, S.; Shigeo, M.; Hironori, A. *J. Photochem. Photobiol. A: Chem.* 2001, *145*, 117-122.

162. Smith, C. R. *J. Am. Chem. Soc.* 1930, *52*, 397–403.

163. Gladiali, S.; Pinna, L.; Delogu, G.; De Martin, S.; Zassinovich, G.; Mestroni, G. *Tetrahedron: Asymmetry* 1990, *1*, 635–648.

164. Thummel, R. P. *Synlett*, 1992, 1–12.

165. Riesgo, E. C.; Jin, X.; Thummel, R. P. *J. Org. Chem.* 1996, *61*, 3017–3022.

166. Hung, C.-Y.; Wang, T.-L.; Shi, Z.; Thummel, R. P. *Tetrahedron*, 1994, *50*, 10685–10692.

167. Gladiali, S.; Chelucci, G.; Soccolini, F.; Delogu, G.; Chessa, G. *J. Organomet. Chem.* 1989, *370*, 285–294.

168. Wu, F.; Thummel, R. P. *Inorg. Chim. Acta* 2002, *327*, 26–30.

169. Thummel, R. P. *Tetrahedron* 1991, *47*, 6851–6886.

170. Snyder, H. R.; Freier, H. E. *J. Am. Chem. Soc.* 1946, *68*, 1320–1322.

171. Hyungsock Suh, M. S.; Synthesis and Properties of Conjugation-Extended Phenanthroline. PhD Thesis 2010.

172. Connors, P. J., Jr.; Tzalis, D.; Dunnick, A. L.; Tor, Y. *Inorg. Chem*. 1998, *37*, 1121–1123.

173. Tzalis, D.; Tor, Y.; Failla, S.; Siegel, J. S. *Tetrahedron Lett.* 1995, *36*, 3489–3490.

174. Hissler, M.; Connick, W. B.; Geiger, D. K.; McGarrah, J. E.; Lipa, D.; Lachicotte, R. J.; Eisenberg, R. *Inorg. Chem*. 2000, *39*, 447–457.

175. Schmittel, M.; Ammon, H. *Synlett* 1997, 1096–1098.

176. Antkowiak, R.; Antkowiak, W. *Heterocycles* 1998, *47*, 893–909.

177. Yamada, M.; Nakamura, Y.; Hasegawa, T.; Itoh, A.; Kuroda, S.; Shimao, I. *Bull. Chem. Soc. Jpn.* 1992, *65*, 2007–2009.

178. Mathis, J. M.; Pallenberg, A. *J. Synth. Comm.* 1997, *27*, 2943–2951.

179. Okada, E.; Tsukushi, N. *Synthesis*, 2000, 499–501.

180. Beer, R. H.; Jimenez, J.; Drago, R. S. *J. Org. Chem.* 1993, *58*, 1746–1747.

181. Miller, M. T.; Gantzel, P. K.; Karpishin, T. B. *Angew. Chem. Int. Ed.* 1998, *37*, 1556–1558.

182. Newkome, G. R.; Theriot, K. J.; Gupta, V. K.; Fronczek, F. R.; Baker, G. R. *J. Org. Chem.* 1989, *54*, 1766–1769.

183. Chandler, C. J.; Deady, L. W.; Reiss, J. A. *J. Heterocycl. Chem.* 1981, *18*, 599–601.

184. Torres, A. S.; Maloney, D. J.; Tate, D.; Saad, Y.; MacDonnell, F. M. *Inorg. Chim. Acta* 1999, *293*, 37–43.

185. Gillard, R. D.; Hill, R. E. E. *J. Chem. Soc., Dalton Trans.* 1974, 1217–1236.

186. Yamada, M.; Tanaka, Y.; Yoshimoto, Y.; Kuroda, S.; Shimao, I. *Bull. Chem. Soc. Jpn*. 1992, *65*, 1006–1011.

187. Bodige, S.; MacDonnell, F. M. *Tetrahedron Lett.* 1997, *38*, 8159–8160.

188. De Zwart, M. A. H.; Bastiaans, H. M. M.; Van der Goot, H.; Timmerman, H. *J. Med. Chem.* 1991, *34*, 1193–1201.

189. Krishnan, S.; Kuhn, D. G.; Hamilton, G. A. *J. Am. Chem. Soc.* 1977, *99*, 8121–8123.

190. Moody, C. J.; Rees, C. W.; Thomas, R. *Tetrahedron*, 1992, *48*, 3589–3602.

191. Shen, Y.; Sullivan, B. P. *Inorg. Chem.* 1995, *34*, 6235–6236.

192. Lö pez, R. B.; Loeb, B. L.; Boussie, T.; Meyer, T. J. *Tetrahedron Lett.* 1996, *37*, 5437–5440.

193. Yanagida,M.; Singh, L. P.; Sayama, K.; Hara, K.; Katoh, R.; Islam, A.; Sugihara, H.; Arakawa, H.; Nazeeruddin, M. K.; Grätzel, M. *J. Chem. Soc., Dalton Trans.* 2000, 2817–2822.

194. Angeloff, A.; Daran, J. C.; Bernadou, J.; Meunier, B. *Eur. J. Inorg. Chem.* 2000, 1985–1996.

195. Pallenberg, A. J.; Koenig, K. S.; Barnhart, D. M. *Inorg. Chem.* 1995, *34*, 2833–2840.

196. Dietrich-Buchecker, C. O.; Marnot, P. A.; Sauvage, J. P. *Tetrahedron Lett.* 1982, *23*, 5291–5294.

197. Masood, M. A.; Zacharias, P. S. *J. Chem. Soc., Dalton Trans.* 1991, 111–114.

198. Alonso-Vante, N.; Nierengarten, J.-F.; Sauvage, J. P. *J. Chem. Soc., Dalton Trans.* 1994, 1649–1654.

199. Katritzky, A. R.; Long, Q. H.; Malhotra, N.; Ramanarayanan, T. A.; Vedage, H. *Synthesis* 1992, 911–913.

200. Ziessel, R.; Suffert, J.; Youinou, M. T. *J. Org. Chem.* 1996, *61*, 6535–6546.

201. Suffert, J.; Ziessel, R. *Tetrahedron Lett.* 1991, *32*, 757–760.

202 Harriman, A.; Ziessel, R. *Chem. Commun.* 1996, 1707–1716.

203. Tzalis, D.; Tor, Y. *Chem. Commun.* 1996, 1043–1044.

204. Tzalis, D.; Tor, Y. *J. Am. Chem. Soc.* 1997, *119*, 852–853.

205. Guo, W.; Galoppini, E.; Rydja, G.; Pardi, G. *Tetrahedron Lett.* 2000, *41*, 7419–7421.

206. Schmittel, M.; Michel, C.; Wiegrefe, A.; Kalsani, V. *Synthesis* 2001, 1561–1567.

207. Liu, S. X.; Michel, C.; Schmittel, M. *Org. Lett.* 2000, *2*, 3959–3962.

208. Dietrich-Buchecker, C.; Jimenez, M. C.; Sauvage, J. P. *Tetrahedron Lett.* 1999, *40*, 3395–3396.

209. Shiotsuki, M.; Yamamoto, Y.; Okuno, S.; Kitou, M.; Nozaki, K.; Onaka, S. *Chem. Commun.* 2002, 590–591.

210. Miyaura, N.; Suzuki, A. *Chem. Rev.* 1995, *95*, 2457–2483.

211. Beer, P. D.; Danks, J. P.; Drew, M. G. B.; McAleer, J. F. *J. Organomet. Chem.* 1994, *476*, 63–72.

212. Sugihara, H.; Hiratani, K. *Coord. Chem. Rev.* 1996, *148*, 285–299.

213. Obare, S. O.; Murphy, C. J. *Inorg. Chem.* 2001, *40*, 6080–6082.

214. Yam, V. W. W.; Lee, V. W. M.; Ke, F.; Siu, K. W. M. *Inorg. Chem.* 1997, *36*, 2124–2129.

215. Shen, Y.; Sullivan, B. P. *J. Chem. Educ.* 1997, *74*, 685–689.

216. Bacon, J. R.; Demas, J. N. *Anal. Chem.* 1987, *59*, 2780–2785.

217. Demas, J. N.; Harris, E. W.; McBride, R. P. *J. Am. Chem. Soc.* 1977, *99*, 3547–3551.

218. Xu, W.; Kneas, K. A.; Demas, J. N.; DeGraff, B. A. *Anal. Chem.* 1996, *68*, 2605–2609.

219. Xu, W.; McDonough, I.; Clayton, R.; Langsdorf, B.; Demas, J. N.; DeGraff, B. A. *Anal. Chem.* 1994, *66*, 4133–4141.

220. Carraway, E. R.; Demas, J. N.; DeGraff, B. A.; Bacon, J. R. *Anal. Chem.* 1991, *63*, 337–342.

221. Demas, J. N.; DeGraff, B. A. *Coord. Chem. Rev*. 2001, *211*, 317–351.

222. Zipp, A. P.; Sacksteder, L.; Streich, J.; Cook, A.; Demas, J. N.; DeGraff, B. A. *Inorg. Chem.* 1993, *32*, 5629–5632.

223. Carraway, E. R.; Demas, J. N.; DeGraff, B. A. *Anal. Chem.* 1991, *63*, 332–336.

224. Jain, A.; Xu, W.; Demas, J. N.; DeGraff, B. A. *Inorg. Chem.* 1998, *37*, 1876–1879.

225. Price, J. M.; Xu, W.; Demas, J. N.; DeGraff, B. A. *Anal. Chem.* 1998, *70*, 265–270.

226. Giordano, P. J.; Bock, C. R.; Wrighton, M. S. *J. Am. Chem. Soc.* 1978, *100*, 6960–6965.

227. Mizuno, T.; Wei, W.-H.; Eller, L. R.; Sessler, J. L. *J. Am. Chem. Soc.* 2002, *124*, 1134–1135.

228. Anzenbacher, P. Jr.; Tyson, D. S.; Jurisková , K.; Castellano, F. N. *J. Am. Chem. Soc.* 2002, *124*, 6232–6233.

229. Tyson, D. S.; Luman, C. R.; Zhou, X.; Castellano, F. N. *Inorg. Chem.* 2001, *40*, 4063–4071.

230. Tyson, D. S.; Castellano, F. N. *Inorg. Chem.* 1999, *38*, 4382–4383.

231. Tyson, D. S.; Gryczynski, I.; Castellano, F. N. *J. Phys. Chem. A*, 2000, *104*, 2919–2924.

232. Tyson, D. S.; Castellano. F. N., J. Phys. Chem. A, 1993, 103, 10955-10960.

233. Ford, W. E.; Rodgers, M. A. J. *J. Phys. Chem.* 1992, *96*, 2917–2920.

234. Simon, J. A.; Curry, S. L.; Schmehl, R. H.; Schatz, T. R.; Piotrowiak, P.; Jin, X.; Thummel, R. P. *J. Am. Chem. Soc.* 1997, *119*, 11012–11022.

235. Bonnefous, C.; Bellec, N.; Thummel, R. P. *Chem. Commun.* 1999, 1243–1244.

236. Bonnefous, C.; Chouai, A.; Thummel, R. P. *Inorg. Chem.* 2001, *40*, 5851–5859.

237. Tyson, D. S.; Bialecki, J.; Castellano, F. N. *Chem. Commun.* 2000, 2355–2356.

238. Tyson, D. S.; Henbest, K. B.; Bialecki, J.; Castellano, F. N. *J. Phys. Chem. A* 2001, *105*, 8154–8161.

239. Schanze, K. S.; Sauer, K. *J. Am. Chem. Soc.* 1988, *110*, 1180–1186.

240. Kim, M. J.; Konduri, R.; Ye, H.; MacDonnell, F. M.; Puntoriero, F.; Serroni, S.; Campagna, S.; Holder, T.; Kinsel, G.; Rajeshwar, K. *Inorg. Chem.* 2002, *41*, 2471–2476.

241. Berg-Brennan, C.; Subramanian, P.; Absi, M.; Stern, C.; Hupp, J. T. *Inorg. Chem.* 1996, *35*, 3719–3722.

242. Panunzi, B.; Roviello, A.; Ruffo, F.; Vivo, A. *Inorg. Chim. Acta* 1998, *281*, 141–147.

243. Surridge, N. A.; McClanahan, S. F.; Hupp, J. T.; Danielson, E.; Gould, S.; Meyer, T. J. *J. Phys. Chem.* 1989, *93*, 294–304.

244. Surridge, N. A.; Hupp, J. T.; McClanahan, S. F.; Gould, S.; Meyer, T. J. *J. Phys. Chem.* 1989, *93*, 304–313.

245. Bergstedt, T. S.; Hauser, B. T.; Schanze, K. S. *J. Am. Chem. Soc.* 1994, *116*, 8380–8381.

246. Fussa-Rydel, O.; Zhang, H.-T.; Hupp, J. T.; Leidner, C. R. *Inorg. Chem.* 1989, *28*, 1533–1537.

247. Zhang, H.-T.; Yan, S. G.; Subramanian, P.; Skeen-Jones, L. M.; Stern, C.; Hupp, J. T. *J. Electroanal. Chem.* 1996, *414*, 23–29.

248. Williams, M. E.; Stevenson, K. J.; Massari, A. M.; Hupp, J. T. *Anal. Chem.* 2000, *72*, 3122–3128.

249. Bidan, G.; Divisia-Blohorn, B.; Lapkowski, M.; Kern, J. M.; Sauvage, J. P. *J. Am. Chem. Soc.* 1992, *114*, 5986–5994.

250. Chamchoumis, C.; Potvin, P. G. *J. Chem. Res., Synop.* 1998, *4*, 180–181, 870–875

251. Spahni, W.; Calzaferri, G. *Helv. Chim. Acta* 1984, *67*, 450–454.

252. Korall, P.; Bö erje, A.; Norrby, P. O.; Akermark, B. *Acta Chem. Scand.* 1997, *51*, 760–766.

253. Sun, S. S.; Lees, A. J. *Inorg. Chem*. 2001, 3154–3160.

254. Licini, M.; Williams, J. A. G. *Chem. Commun.* 1999, 1943–1944.

255. Whittle, B.; Everest, N. S.; Howard, C.; Ward, M. D. *Inorg. Chem*. 1995, *34*, 2095–2032.

256. Grosche, P.; Hö ltzel, A.; Walk, T. B.; Trautwein, A. W.; Jung, G. *Synthesis* 1999, *11*, 1961–1970.

257. Kalyanam, N.; Likhate, M. A.; Manjunatha, S. G. *Indian J. Chem., Sect. B.* 1992, *31B*, 555–556.

258. Bonhö te, P.; Moser, J. E.; Humphry-Baker, R.; Vlachopoulos, N.; Zakeeruddin, S. M.; Walder, L.; Grätzel, M. *J. Am. Chem. Soc.* 1999, *121*, 1324–1336.

259. Kimura, M.; Shiba, T.; Muto, T.; Hanabusa, K.; Shirai, H. *Chem. Commun*. 2000, 11–12.

260. Nagata, T.; Tanaka, K. *Inorg. Chem*. 2000, *39*, 3915–3521.

261. Constable, E. C.; Meier, W.; Nardin, C.; Mundwiler, S. *Chem. Commun*. 1999, 1483–1484.

262. Lainé, P.; Bedioui, F.; Ochsenbein, P.; Marvaud, V.; Bonin, M.; Amouya, E. *J. Am. Chem. Soc.* 2002, *124*, 1364–1377.

263. Constable, E. C.; Ward, M. D. *J. Chem. Soc. Dalton Trans.* 1990, *4*, 1405–1409.

264. Schubert, U. S.; Eschbaumer, C.; Hien, O.; Andres, P. R. *Tetrahedron Lett.* 2001, *42*, 4705–4707.

265. Inoue, H.; Furukawa, T.; Shimizu, M.; Tamura, T.; Matsui, M.; Ohtsuka, E. *Chem. Commun. (Cambridge)* 1999, *1*, 45 –46.

266. Zakeeruddin, S. M.; Nazeeruddin, M. K.; Pechy, P.; Rotzinger, F. P.; Humphry-Baker, R.; Kalyanasundaram, K.; Grätzel, M.; Shklover, V.; Haibach, T. *Inorg. Chem.* 1997, *36*, 5937–5946.

267. Cuenoud, B.; Schepartz, A. *Tetrahedron Lett.* 1991, *32*, 3325–3328.

268. Potts, K. T.; Konwar, D. *J. Org. Chem.* 1991, *56*, 4815–4816.

269. Khatyr, A.; Ziessel, R. *J. Org. Chem.* 2000, *65*, 3126–3134.

270. Bell, T. W.; Hu, L. Y. *Tetrahedron Lett.* 1988, *29*, 4819–4822.

271. Constable, E. C.; Edwards, A. J.; Martínez-Máñez, R.; Raithby, P. R.; Thompson, A. M. W. C. *J. Chem. Soc. Dalton Trans.* 1994, *5*, 645–650.

272. Butler, I. R.; McDonald, S. J.; Hursthouse, M. B.; Malik, K. M. A. *Polyhedron* 1995, *14*, 529–539.

273. Constable, E. C.; Edwards, A. J.; Marcos, M. D.; Raitby, P. R.; Martínez-Máñez, R.; Tendero, M. J. L. *Inorg. Chim. Acta* 1994, *224*, 11–14.

274. Padilla-Tosta, M. E.; Martínez-Máñez, R.; Soto, J.; Lloris, J. M. *Tetrahedron* 1998, *54*, 12039–12046.

275. Siemeling, U.; Vorfeld, U.; Neumann, B.; Stammler, H. G.; Zanello, P.; Fabrizi De Biani, F. *Eur. J. Inorg. Chem.* 1999, *1*, 1–5.

276. Sauer, J.; Heldmann, D. K.; Pabst, G. R. *Eur. J. Org. Chem.* 1999, *1*, 313–321.

277. Mitsunobu, O.; Yamada, Y. *Bull. Chem. Soc. Japan* 1967, *40*, 2380-2382.

278. Pabst, G. R.; Pfüller, O. C.; Sauer, J. *Tetrahedron Lett.* 1998, *39*, 8825–8828.

279. Tingoli, M.; Tiecco, M.; Testaferri, L.; Andrenacci, R.; Balducci, R. *J. Org. Chem.* 1993, *58*, 6097–6102.

280. Cuperly, D.; Gros, P.; Fort, Y. *J. Org. Chem.* 2002, *67*, 238–241.

281. Schubert, U. S.; Eschbaumer, C. *Org. Lett.* 1999, *1*, 1027–1029.

282. Dietrich-Buchecker, C. O.; Marnot, P. A.; Sauvage, J. P. *Tetrahedron Lett.* 1982, *23*, 5291–5294.

283. Newkome, G. R.; Hager, D. C.; Kiefer, G. E. *J. Org. Chem.* 1986, *51*, 850–853.

284. El-ghayoury, A.; Ziessel, R. *J. Org. Chem.* 2000, *65*, 7757–7763.

285. Yamaguchi, Y.; Katsuyama, I.; Funabiki, K.; Matsui, M.; Shibata, K. *J. Heterocycl. Chem.* 1998, *35*, 805–810.

286. Raboin, J.-C.; Kirsch, G.; Beley, M. *J. Heterocycl. Chem.* 2000, *37*, 1077–1080.

287. Ulrich, G.; Bedel, S.; Picard, C.; Tisnés, P. *Tetrahedron Lett.* 2001, *42*, 6113–6115.

288. Ziessel, R. *Tetrahedron Lett.* 1989, *30*, 463–466.

289. Constable, E. C.; Khan, F. K.; Lewis, J.; Liptrot, M. C.; Raithby, P. R. *J. Chem. Soc. Dalton Trans.* 1985, *2*, 333–335.

290. Fallahpour, R. A.; Neuburger, M.; Zehnder, M. *Synthesis* 1999, *6*, 1051–1055.

291. Sasaki, I.; Daran, J. C.; Balavoine, G. G. A. *Synthesis* 1999, *5*, 815–820.

292. Thummel, R. P.; Jahng, Y. *J. Org. Chem.* 1985, *50*, 2407–2412.

293. Riesgo, E. C.; Jin, X.; Thummel, R. P. *J. Org. Chem.* 1996, *61*, 3017–3022.

294. Mamo, A. *J. Heterocyclic Chem.* 2000, *37*, 1225–1231.

295. Ferguson, J.; Reeves, L. W.; Schneider, W. G. *Can. J. Chem*; 1957, *35*, 1117-1123.

296. Masayoshi N. The Science of Colour, Baifukan, 2002, 108. www.shimadzu-france.com/enews/September 09/...shimadzu_UV2550.pdf data.

297. Ahmed, I.; Jing ping, Z.; Yingfei, C. *Theor. Chem. Acc*; 2010, 1-8.

298. Tamaki, T.; Kokubu, T.; Ichimura, K. *Tetrahedron*, 1987, *43*: 7, 1485-1494.

299. de Bony, J.; Tocanne, J. F. *Eur. J. Biochem*. 1984, *143*, 373-379.

300. Donati, D.; Guarini, G. G. T.; Santi-Fantoni, P. *J.Therm. Anal.* 1991, *37*: 1917-1922.

301. Raghunath, P.; Ananth R. M.; Gouri, C.; Bhanuprakash, K.; Jayathirtha R. V. *J. Phys Chem. A*, 2006, *110*, 1152-1162.

302. Sauvage, J.-P.; Collin, J.-P.; Chambron, J.-C.; Guillerez, S.; Coudret, C.; Balzani, V.; Barigelletti, F.; De Cola, L.; Flamigni, L. *Chem. Rev.* 1994, *94,* 993-1019.

303. Baranoff, E.; Collin, J.P.; Flamigni, L.; Sauvage, J.P. *Chemical Society Reviews,* 2004, *33,* 147-155.

304. Murov, S.L.; Carmichael, I.; Hug, G.L., *Handbook of photochemistry*. 2 ed. 1993, New York: Marcel Dekker.

305. Pomeranc, D.; Heitz, V.; Chambron, J.-C.; Sauvage, J.-P. *J. Am. Chem.Soc.* 2001, *123,* 12215-12221.

306. Medlycott, E.A.; Hanan, G.S. *Coord. Chem. Rev.* 2006, *250,* 1763–1782.

307. Medlycott, E.A.; Hanan, G.S. *Chem. Soc. Rev.* 2005, *34,* 133-142.

308. Duati, M.; Fanni, S.; Vos, J.G. *Inorg. Chem. Commun.* 2000, *3,* 68-70.

309. Duati, M.; Tasca, S.; Lynch, F.C.; Bohlen, H.; Vos, J.G.; Stagni, S.; Ward, M.D. *Inorg. Chem.* 2003, *42,* 8377-8384.

310. Constable, E.C.; Cargill Thompson, A.M.W.; Armaroli, N.; Balzani, V.; Maestri, M. *Polyhedron* 1992, *11,* 2707-2709.

311. Maestri, M.; Armaroli, N.; Balzani, V.; Constable, E.C.; Cargill Thompson, A.M.W. *Inorg. Chem.* 1995, *34,* 2759-2767.

312. Wang, J.H.; Fang, Y.Q.; Hanan, G.S.; Loiseau, F.; Campagna, S. *Inorg. Chem.* 2005, *44,* 5-7.

313. Indelli, M.T.; Bignozzi, C.A.; Scandola, F.; Collin, J.P. *Inorg. Chem.* 1998, *37,* 6084-6089.

314. Son, S.U.; Park, K.H.; Lee, Y.S.; Kim, B.Y.; Choi, C.H.; Lah, M.S.; Jang, Y.H.; Jang, D.J.; Chung, Y.K. *Inorg. Chem.* 2004, *43,* 6896-6898.

315. Constable, E.C.; Thompson, A.M.W.; Cherryman, J.; Liddiment, T. *Inorg.Chim. Acta* 1995, *235,* 165-171.

316. Baba, A. I.; Shaw, J. R.; Simon, J. A.; Thummel, R. P.; Schmehl, R. H. *Coord. Chem. Rev*. 1998, 171, 43-59.

317. Passalacqua, R.; Loiseau, F.; Campagna, S.; Fang, Y.-Q.; Hanan, G.S. *Angew. Chem. Int. Ed.* 2003, *42,* 1608-1611.

318. Wang, J.H.; Hanan, G.S.; Loiseau, F.; Campagna, S. *Chem. Commun.* 2004, 2068-2069.

319. McClenaghan, N.D.; Leydet, Y.; Maubert, B.; Indelli, M.T.; Campagna, S. *Coord. Chem. Rev.* 2005, *249,* 1336-1350.

320. Hissler, M.; Harriman, A.; Khatyr, A.; Ziessel, R. *Chem. Eur. J.* 1999, *5,* 3366-3381.

321. Simon, J.A.; Curry, S.L.; Schmehl, R.H.; Schatz, T.R.; Piotrowiak, P.; Jin, X.Q.; Thummel, R.P. *J. Am. Chem. Soc.* 1997, *119,* 11012-11022.

322. Harriman, A.; Hissler, M.; Khatyr, A.; Ziessel, R. *Chem. Commun.* 1999, 735-736.

323. Ford, W.E.; Rodgers, M.A.J. *J. Phys. Chem.* 1992, *96,* 2917-2920.

324. Tyson, D.S.; Henbest, K.B.; Bialecki, J.; Castellano, F.N. *J. Phys. Chem. A* 2001, *105,* 8154-8161.

325. Crosby, G. A. *Acc. Chem. Res*., 1975, *8*, 231-238.

326. Crosby, G. A. *Adv. Chem. Ser*., 1976, *150*, 149.

327. Crosby, G. A.; Watts, R. J.; Carstens, D. H. W. *Science*, 1970, *170*, 3963, 1195-1196.

328. Balzani, V.; Juris, A.; Barigelletti, F.; Belser, P.; von Zelewsky, A. *Riken Q.,* 1984, *78*, 78-85.

329. Henderson Jr., L. J.; Fronczek, F. R.; Cherry, W. R. *J. Am. Chem. Soc.*, 1984, *106*, 5876-5879.

330. Nalwa, H. S.; Shirk, J. S. In *Phthalocyanines, Properties and Applications* Eds: (C. C. Leznoff, A. B. P. Lever), VCH, New York, 1996, vol. 4, pp 79-182, and cited therein.

331. Moser, F. H.; Thomas, A. L. *The Phthalocyanines*, CRC: Boca Raton, FL, 1983.

332. *Phthalocyanines, Properties and Applications,* (Eds: C. C. Leznoff, A. B. P. Lever), VCH, New York, 1989 – 1996, vol 1– 4.

333. Baumann, F.; Bienert, B.; Rösch, G.; Vollmann, H.; Wolf, W. *Angew. Chem.*, 1956, *68*, 133-168.

334. Hanack, M.; Lang, M. *Adv. Mater*., 1994, *6*, 819-833.

335. Hanack, M.; Lang, M. *Chemtracts*, *Org. Chem*., 1995, *8*, 131-165.

336. Hanack, M.; Datz, A.; Fay, R., Fischer, K.; Kepeler, U.; Koch, J.; Metz, J.; Metzger, M.; Schneider, O.; Schulze, H..J. In *Handbook of Conducting Polymers*, vol 1 (Ed.: T. A. Skotheim) M. Dekker Inc., New York, 1986, 133.

337. Schultz, H.; Lehman, H.; Rein, M.; Hanack, M. *Structure and Bonding 74*, Springer-Verlag, Heidelberg, 1991, 41.

338. Drechsler, U.; Hanack, M. In *Comprehensive Supramolecular Chemistry*, J. L. Atwood, J. E. D. Davies, D. D. McNicol, F. Vögtle Eds., Pergamon: Oxford, 1996, Vol 9, 283-311.

339. van der Pol, J. F.; Neelman, E.; Zwikker, J. W.; Nolte, R. J. M.; Drenth, W.; Aerts, J.; Visser, R.; Picken, S. J. *Liq. Cryst.*, 1989, *6*, 577-592.

340. Simon, J.; Sirlin, C. *Pure Appl. Chem.*, 1989, *61*, 1625-1629.

341. Engel, M. K.; Bassoul, P.; Bossio, L.; Lehmann, H.; Hanack, M.; Simon, J. *Liq. Cryst.*, 1993, *15*, 709-722.

342. Roberts, G. G.; Petty, M. C.; Baker, S.; Fowler, M. T.; Thomas, N. J. *Thin Solid Films,* 1985, *132*,113-123.

343. Cook, M. J.; Dunn, A. J.; Daniel, F. M.; Hart, R. C. O.; Richardson, R. M.; Roser, S. J. *Thin Solid Films*, 1988, *159*, 395-404.

344. Palacin, S.; Lesieur, P.; Stefanelli, I.; Barraud, A. *Thin Solid Films*, 1988, *159*, 83-90.

345. Burghard, M.; Schmelzer, M.; Roth, S.; Haisch, P.; Hanack, M. *Langmuir*, 1994, *10*, 4265-4269.

346. Cook, M. J. *J. Mater. Chem*, 1996, *6*, 677-689.

347. Simon, J.; André, J. J. In *Molecular Semiconductors*, Lehn, J. M., Rees, C. W. Eds., Springer: Berlin, 1985, 73-84.

348. Gregory, P. *High-Technology Applications of Organic Colorants*, Plenum: New York, 1991, 59-65.

349. Takano, S.; Enokida, T.; Kambata, A. *Chem. Lett*., 1984, 2037.

350. Loutfy, R. O.; Hsiao, C. K.; Hor, A. M.; Di Paola-Baranyl, G. J. *Imaging Sci*., 1985, *29*, 148-153.

351. Law, K. Y. *Chem. Rev*., 1993, *93*, 449-486.

352. Kuder, J. E. *Imaging Sci*., 1988, *32*, 51-56.

353. Kobayashi, S.; Iwasaki, K.; Sasaki, H.; Ohhara, S.; Nishizawa, M.; Katayose, M. *Jpn. J. Appl. Phys*., 1991, *30*, 114.

354. Ao, R.; Kümmert, L.; Haarer, D. *Adv. Mater*., 1995, *5*, 495.

355. Wohrl, D.; Shopova, M.; Muller, S.; Milev, A. D.; Mantareva, V. N.; Krastev, K. K. *J. Photochem. Photobiol. B*, 1993, *21*,155.

356. Bonnett, R. *Chem. Soc. Rev*., 1995, *95*, 19-33.

357. Brown, S. B.; Truscott, T. G. *Chem. Ber*., 1993, *29*, 955-959.

358. Lever, A. B. P.; Hempstead, M. R.; Leznoff, C. C.; Liu, W.; Melnik, M.; Nevin, W. A.; Seymour, P. *Pure Appl. Chem.*, 1986, *58*, 1467-1476.

359. Schlettwein, D.; Wöhrle, D.; Karmann, E.; Melville, U. *Chem. Mater*; 1994, *6,* 1, 3-6.

360. Wöhrle, D.; Meissner, D. *Adv. Mater*., 1991, *3*, 129-138.

361. Battenberg, A.; Breidt, V. F.; Vahrenkamp, H. *Sensor and Actuators B*, 1996, *30*, 29-34.

362. Collins, R. A.; Mohamed, K. A. *J. Phys. D*, 1988, *21*, 154-161.

363. Temofonte, T. A.; Schoch, K. F. *J. Appl. Phys.*, 1989, *65*, 1350.

364. Sadaoka, Y.; Jones, T. A.; Göpel, W. *Sensors* and *Actuators B*, 1990, *1*, 148-153.

365. Wright, J. D. *Prog. Surf. Sci*., 1989, *31*, 1.

366. Dogo, S.; Germani, J. P.; Maleysson, C.; Pauly, A. *Thin Solid Films*, 1992, *219*, 244-250.

367. Mukhopadhyay, S.; Hogarth, C. A.; Thorpe, S. C.; Cook, M. J. *J. Mater. Sci., Mater. Electron*, 1994, *5*, 321-323.

368. Schierbaum, K. D.; Zhou, R.; Knecht, S.; Dieing, R.; Hanack, M.; Göpel, W. *Sensors and Actuators B*, 1995, *24/25*, 69-71.

369. Marks, T. J. *Science*, 1985, *227*, 881-889.

370. Marks, T. J. *Angew. Chem. Int. Ed. Engl.*, 1990, *29*, 857-879.

371. Kato, M.; Nishioka, Y.; Kaifu, K.; Kawamura, K.; Ohno, S. *Appl. Phys Lett.*, 1985, *86*, 196-197.

372. Casstevens, M. K.; Samoc, M.; Pfleger, J.; Prasad, P. N. *J. Chem. Phys.*, 1990, *92*, 2019-2025.

373. Simon, J.; Bassoul, P.; Norvez, S. *New J. Chem.*, 1989, *13*, 13-31.

374. Weiss, C.; Kobayashi, H.; Gouterman, M. *J. Mol. Spectrosc*. 1965, *16*, 415-450

375. Orti, E.; Bredas J. L.; Clarisse, C. *J. Chem. Phys*., 1990, *92*, 1228-1235

376. Leznoff, C. C. In Phthalocyanines, Properties and Applications, (Eds: C. C. Leznoff, A. B. P. Lever) VCH, New York, 1989, Vol. 1, Chapter 1.

377. Kalz, W.; Homborg, H.; Kuppers, H.; Kennedy, B. J.; Murray, M. S. *Z. Naturforsch; Teil B,* 1984, *39*, 1478-1489.

378. Kennedy, B. J.; Murray, K. S.; Zwack, P. R.; Homborg, H.; Kalz, W. *Inorg. Chem.* 1986, *25*, 2539-2545.

379. Kepeler, U.; Hanack, M. *Chem. Ber*. 1986, *119*, 3636.

380. Pawlowski, G.; Hanack, M. *Synthesis*, 1980, 287-289.

381. Eberhardt, W.; Hanack, M. *Synthesis*, 1997, 95-100.

382. Calvete, M. PhD Thesis. Tobias-lib.unituebingen.de/volltexte/2004/1094/.../dissertation_calvete.pdf

383. Sommerauer, M.; Rager, C.; Hanack, M. *J. Am. Chem. Soc.,* 1996, *118*, 10085-10093.

384. Schmid, G.; Sommerauer, M.; Geyer, M.; Hanack, M. in Phthalocyanines, Properties and Applications, (Eds: C. C. Leznoff, A. B. P. Lever), VCH, New York, 1996, vol. 4, 1-18.

385. Kobayashi, N.; Nakajima, S.; Osa, T. *Inorg. Chim. Acta*, 1993, *210*, 131-133.

386. Orti, E.; Bredas, J. L., in Conjugated Polymeric Materials: Opportunities in Electronics, Optoelectronics and Molecular Electronic J. L. Bredas, R. R. Chance, Eds; Kluwer Acaedmic Publisher: The Netherlands, 1990, 517-530.

387. Meyer, T.J.; Huynh, M.H.V. *Inorg. Chem.* 2003, *42*, 8140-8160.

388. Bonnet, S.; Collin, J.P.; Sauvage, J.P. *Inorg. Chem.* 2006, *45*, 4024-4034.

389. Karidi, K.; Garoufis, A.; Tsipis, A.; Hadjiliadis, N.; Dulk, H.; Reedijk, J.J. *Chem. Soc., Dalton Trans*. 2005, 1176-1187.

390. Ott, C.; Schubert, U.S. *Polymer Preprints*, 2007, *48*, 712.

391. Moore, J.A.; Acquaye, H.J. *Polyhedron*, 2009, *28*, 386-392.

392. Horva'th, O.; Stevenson, K.L. Charge Transfer Photochemistry of Coordination Compounds. VCH Publisher, Inc, 1993, 230-250.

393. Balzani, V.; Juris, A.; Venturi, M. *Chem. Rev*., 1996, *96*, 759-833.

394. Kawanishi, Y.; Kitamura, N.; Tazuke, S. *Inorg. Chem*., 1989, *28*, 2968-2975.

395. Kirchhoff, J.R.; McMillin, D.R.; Marot, P.A.; Sauvage, J.P. *J. Am. Chem. Soc.,* 1985, *107*, 1138-1141.

396. Creutz, C.; Chou, M.; Netzel, T.L.; Okumura, M., Sutin, N. *J. Am. Chem. Soc.,* 1980, *102*, 1309-1319.

397. Milder, S.J. *Inorg. Chem*., 1989, *28*, 868-872.

398. Winkler, J.R.; Netzel, T.L.; Creutz, C. *J. Am. Chem. Soc.*, 1991, *109*, 2381-2392.

399. Hecker, C.R.; Gushurst, A.I.; McMillin, D.R. *Inorg. Chem.*, 1994, *30*, 538-544.

400. Coronada, E.; Gavina, P.; Tatay, S.; Groarke, R.; Vos, J.G. *Inorg. Chem.,* 2010, *49*, 6897-6903.

401. Collin, J.P.; Guillerez, S.; Sauvage, J.P.; Barigelleti, F.; De Cola, L.; Flamigni, L.; Balzani. *Inorg. Chem*., 1991, *30*, 4230-4238.

402. Constable, E.C.; Cargill Thompson, A.M.W. *J. Chem. Soc. Dalton Trans*., 1992, 3467-3475.

403. Holbrey, J.D.; Tiddy, G.T.J.; Bruce, D.W. *J. Chem. Soc. Dalton Trans*., 1995, 1769-1774.

404. Vyas, P.; Bhatt, A. K.; Ramachandraiah, G.; Bedeka, A. V. *Tetrahedron Lett*. 2003, 44, 4085-4088.

405. Yamamoto, T.; Morita, A.; Miyazaki, Y.; Maruyama, T.; Wakayama, H.; Zhou, Z. H.; Nakamura, Y.; Kanbara, T.; Sasaki, S.; Kubota, K. *Macromolecules*, 1992, 25, 1214-1223.

406. Adeloye, A. O.; Ajibade, P. A. *Tetrahedron Lett*. 2011, 52, 274-277.

407. Venkataraman, D.; Bates, C. G.; Saejueng, P. US Patent No 7,473,797 B2, January, 2009.

408. Evans, I. P.; Spencer, A.; Wilkinson, G. *J. Chem. Soc. Dalton*, 1973, 204-208.

409. Mitsopoulou, C. A.; Veroni, I.; Philippopoulos, A. I.; Falaras, P. *J. Photochem. Photobiol. A: Chem*. 2007, 191, 6-12.

410. Gunzler, H.; Gremlich, H. IR spectroscopy – An Introduction; WILEY-VCH Verlag GmbA: Weinheim, Germany, 2002.

411. Zhang, P.; Xia, B.; Sun, Y.; Yang, B.; Tian, W.; Wang, Y.; Zhang, G. *Chin. Sci. Bull*. 2006, 51, 2444-2450.

412. Zhang, J.; Lee, J. K.; Wu, Y.; Royce, W. M. *Nano. Lett*. 2003, 3, 403-407.

413. Adeloye, A. O.; Ajibade, P. A. *Int. J. Mol. Sci*., 2010, 11, 3158-3176.

414. Lin, M. J.; Wang, J. D.; Chen, N. S.; Huang, J. L. *J. Coord Chem*. 2006, 59, 6, 607–11.

415. Nazeeruddin, M. K.; Péchy, P.; Renouard, T.; Zakeeruddin, S. M.; Humphry-Baker, R.; Comte, P.; Liska, P.; Cevey, L.; Costa, E.; Shklover, V.; Spiccia, L.; Deacon, G. B.; Bignozzi, C. A.; Grätzel, M. *J. Am. Chem. Soc.* 2001, 123, 1613.

416. He, J.; Benko, G.; Korodi, F.; Polívka, T.; Lomoth, R.; Ǻkermark, B.; Sun, L.; Hagfeldt, A.; Sundströ m. *J. Am. Chem. Soc*. 2002, 124, 4922-4932.

417. O'Regan, B.; Grätzel, M. *Nature* 1991, *353*, 737-740.

418. Nazeeruddin, M. K.; Kay, A.; Rodicio, I.; Humphry-Baker, R.; Müller, E.; Liska, P.; Vlachopoulos, N.; Grätzel, M. *J. Am. Chem. Soc.* 1993, *115*, 6382-6390.

419. Nazeeruddin, M. K.; Humphry-Baker, R.; Grätzel, M.; Wö hrle, D.; Schnurpfeil, G.; Schneider, G.; Hirth, A.; Trombach, N. *J. Porphyrins Phthalocyanines* 1999, *3*, 230.

420. Aranyos, V.; Hjelm, J.; Hagfeldt, A.; Grennberg, H. *J. Porphyrins and Phthalocyanines*. 2001, 5, 8, 609-616.

421. American Society for Testing and Materials, ASTM G 159-98, 2000, 14.04

422. Rawling, T.; McDonagh, A. *Coord. Chem. Rev.* 2007, *25,* 1128-1157.

423. Rawling, T.; Xiao, H.; Lee, S.-T.; Colbran, S. B.; McDonagh, A. M. *Inorg. Chem.* 2007, *46*, 2805-2813.

424 Nazeeruddin, M. K.; Humphry-Baker, R.; Grätzel, M.; Murrer, B. A. *Chem. Commun.* 1998, 719-720.

425. Yanagisawa, M.; Korodi, F.; He, J.; Sun, L.; Sundstrom, V.; Akermark, B. *J. Porphyrins Phthalocyanines* 2002, *6*, 217-224.

426. O'Regan, B. C.; Lopez-Duarte, I.; Martinez-Diaz, M. V.; Forneli, A.; Albero, J.; Morandeira, A.; Palomares, E.; Torres, T.; Durrant, J. R. *J. Am. Chem. Soc.*, *130*, 2906-2907.

427. Yanagisawa, M.; Korodi, F.; Bergquist, J.; Holmberg, A.; Hagfeldt, A.; Akermark, B.; Sun, L. *J. Porphyrins Phthalocyanines,* 2004, *8*, 1228-1235.

428. Kleverlaan, C. J.; Indelli, M. T.; Bignozzi, C. A.; Pavanin, L.; Scandola, F.; Hasselman, G. M.; Meyer, G. J. *J. Am. Chem. Soc.* 2000, *122*, 2840-2849.

429. Hanack, M. Kang, Y. G. *Chem. Ber*. 1991, 124, 1607-1612.

430. Kelly, C. A.; Meyer, G. J. *Coord. Chem. Rev.* 2001, *211*, 295-314.

431. Alagna, L.; Capobianchi, A.; Casaletto, M. P.; Mattogno, G.; Paolleti, A. M.; Pennesi, G.; Rossi, G. *J. Mater. Chem*. 2001, 11, 1928-1935.

432. Ali, S.; Arta, S.; Sina, H.; Siguang, C.; Pierre, G. P.; Sylvie, M. *J. New Mat. Electrochem. Systems*, 2008, 11, 281-285.

433. Ruhle, S.; Greenshtein, M.; Chen, S. G.; Merson, A.; Pizen, H.; Sukenik, S.; Cahen, D.; Zaban, A. *J. Phys. Chem. B,* 2005, 109, 18907.

434. Calvete, M. PhD Thesis, 2004. Eberhard – Karls – Universität Tubingen.

435. Lobato, K.; Peter, L. M. *J. Phys. Chem. B*, 2006, 110, 21920−21923.

436. Peter, L. M.; Walker, A. B.; Boschloo, G.; Hagfeldt, A. *J. Phys. Chem. B* 2006, 110, 13694−13699.

437. Boschloo, G.; Hagfeldt, A. *J. Phys. Chem. B* 2005, 109, 12093−12098.

438. Greijer-Agrelll, H.; Boschloo, G.; Hagfeldt, A. *J. Phys. Chem. B* 2004, 108, 12388−12396.

439. Toivola, M.; Peltokorpi, L.; Halme, J.; Lund P. *Solar Energy Materials & Solar Cells*, 2007, 91, 1733 − 1742.

440. Goze, C.; Kozlov, D. V.; Castellano, F. N.; Suffert, J.; Ziessel, R. *Tetrahedron Lett.* 2003, 44, 8713–8716.

Appendices

Appendix 1: ^{1}H NMR spectrum of **L1**

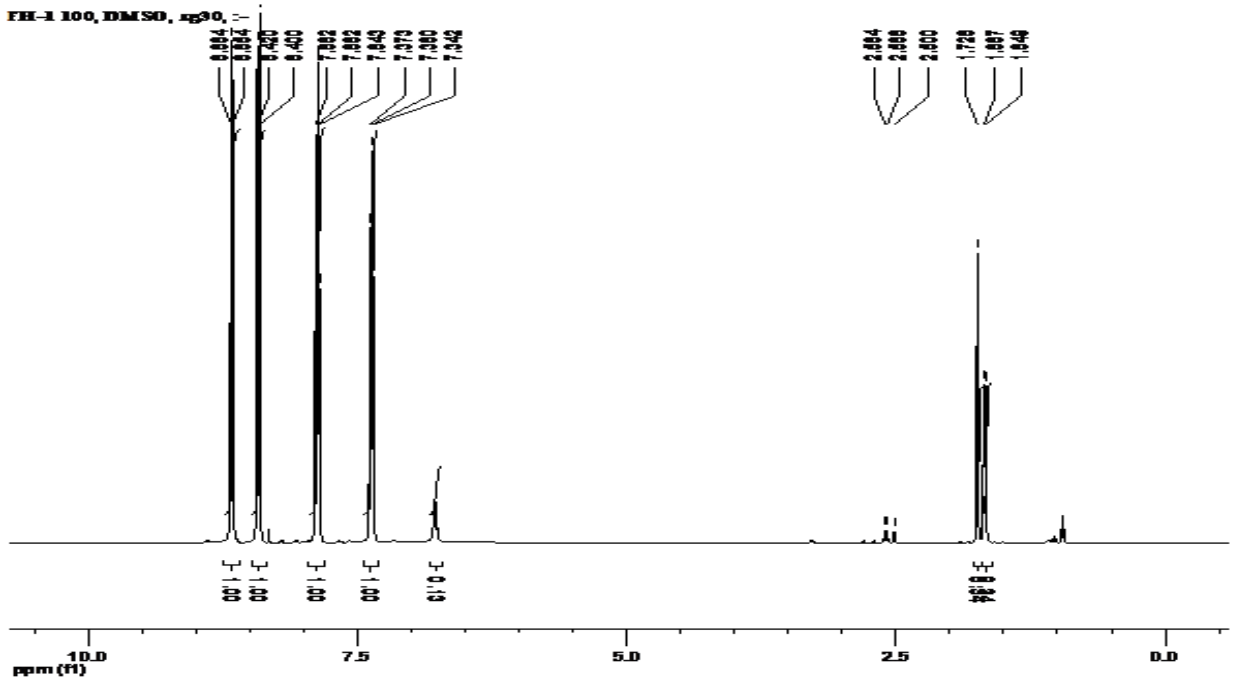

Appendix 2: ^{13}C NMR spectrum of **L1**

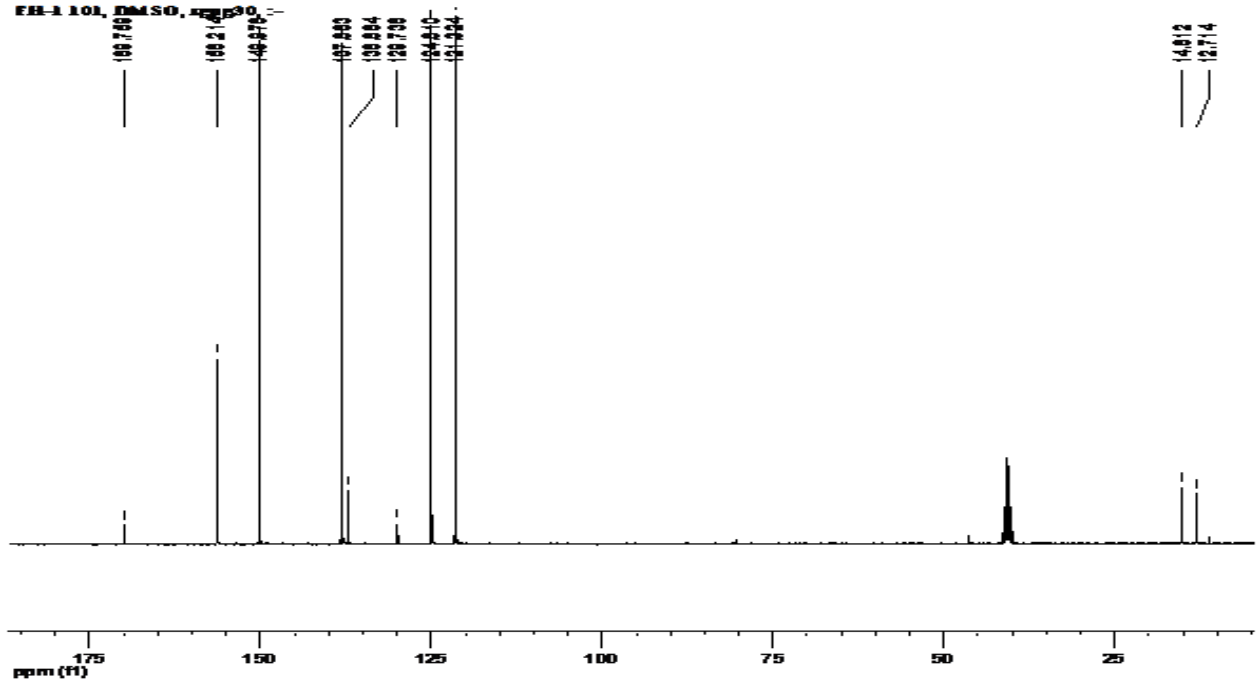

Appendix 3: ^{1}H NMR spectrum of **L2**

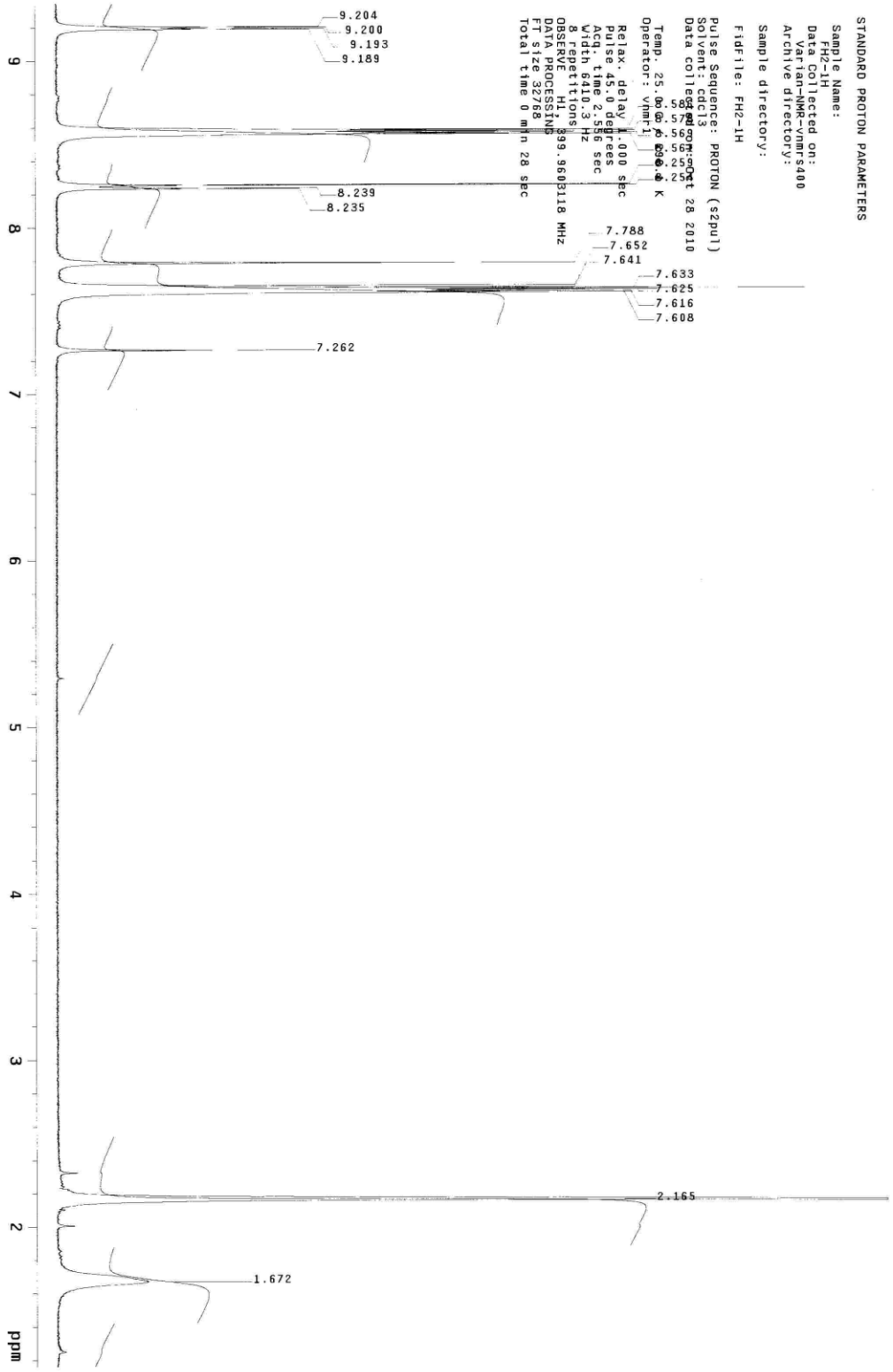

Appendix 4: Expanded Aromatic Region of ^{1}H NMR spectrum of **L2**

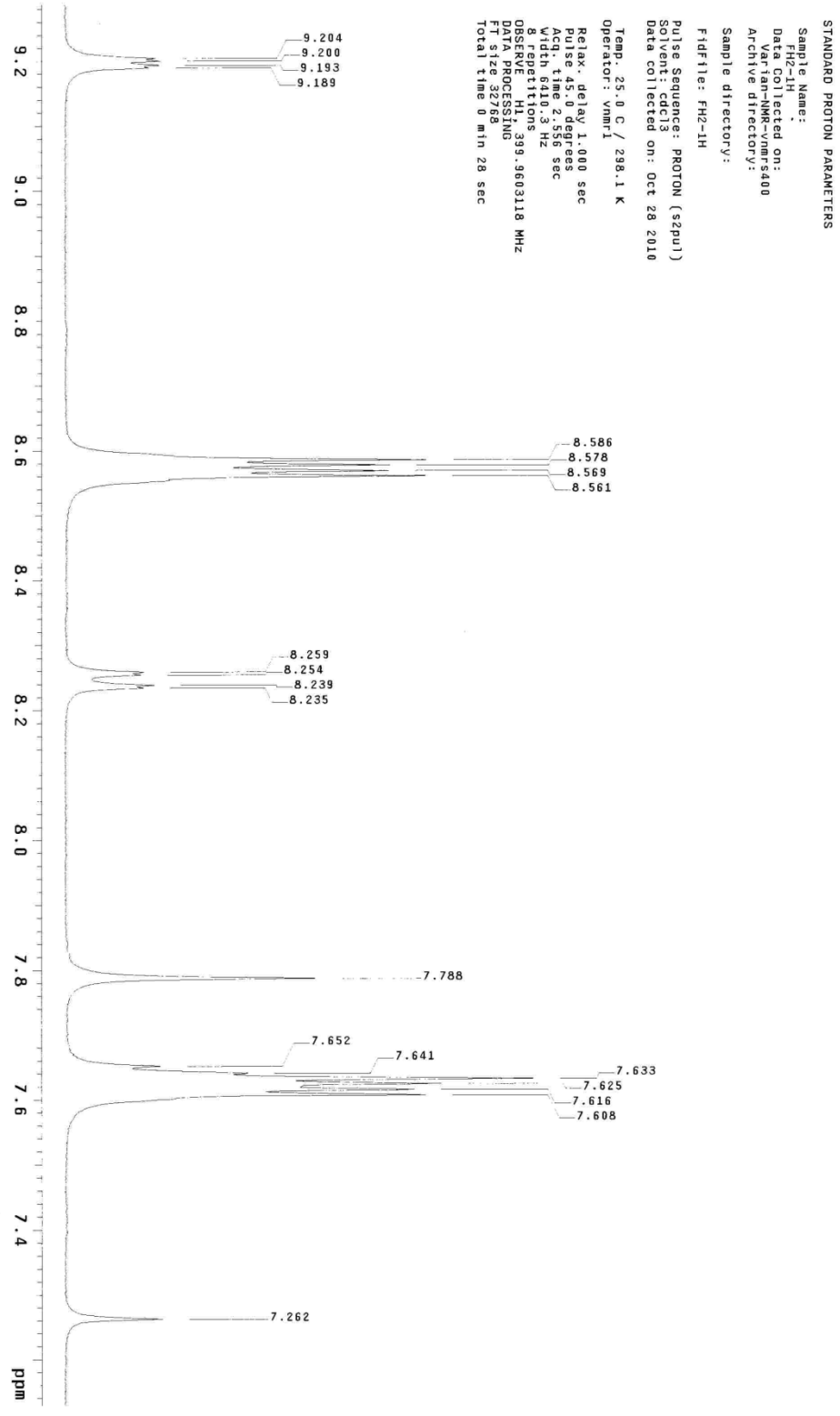

Appendix 5: ^{13}C NMR spectrum of **L2**

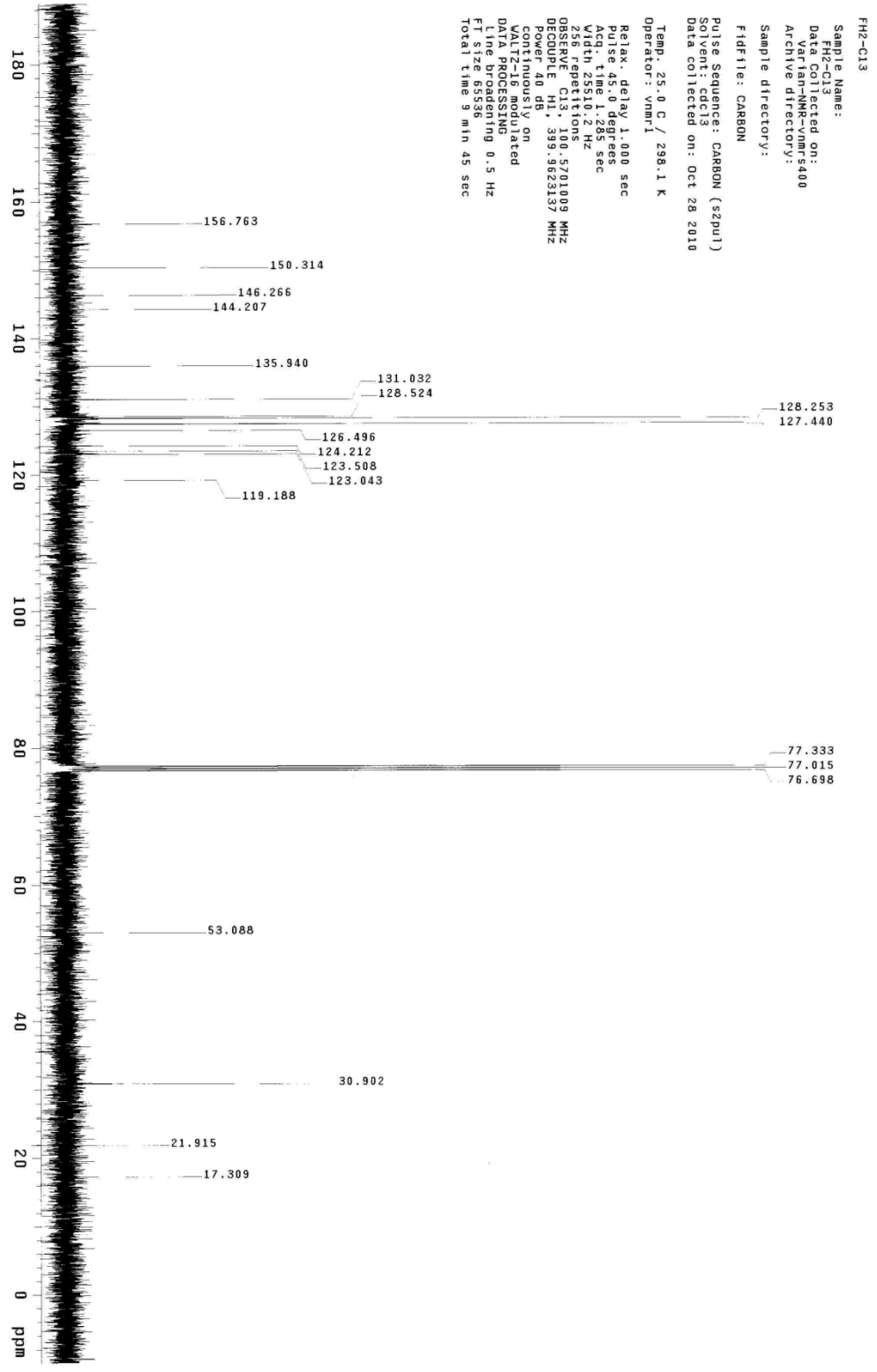

Appendix 6: ^{1}H NMR spectrum of **L3**

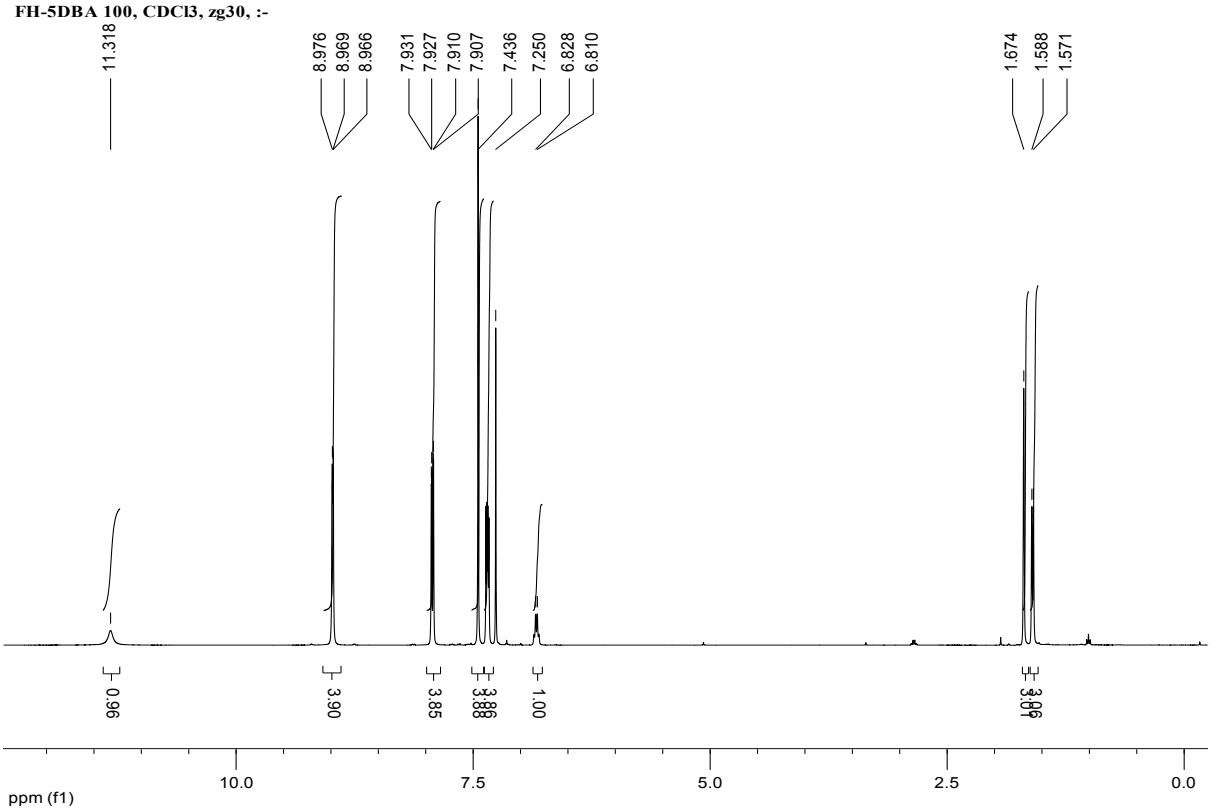

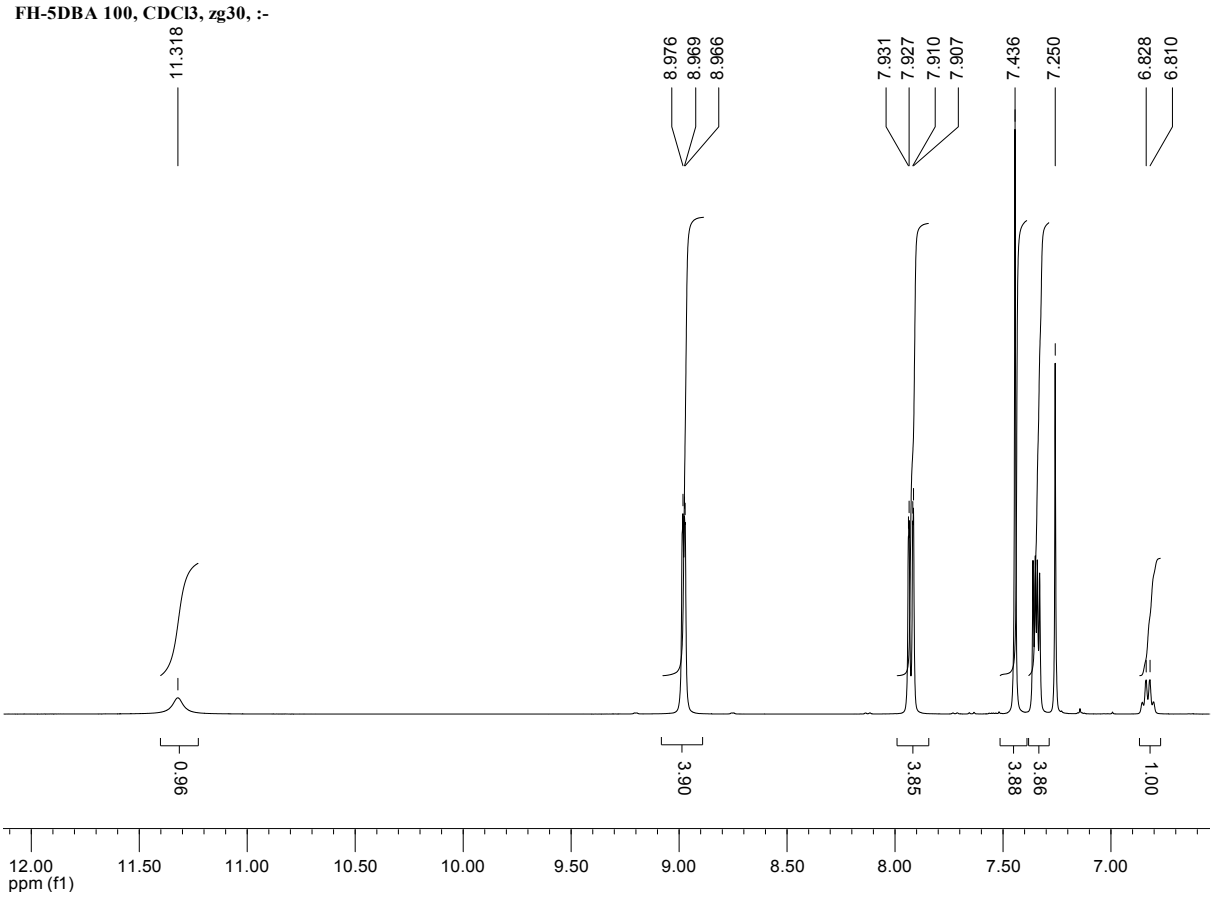

Appendix 7: ^{13}C NMR spectrum of **L3**

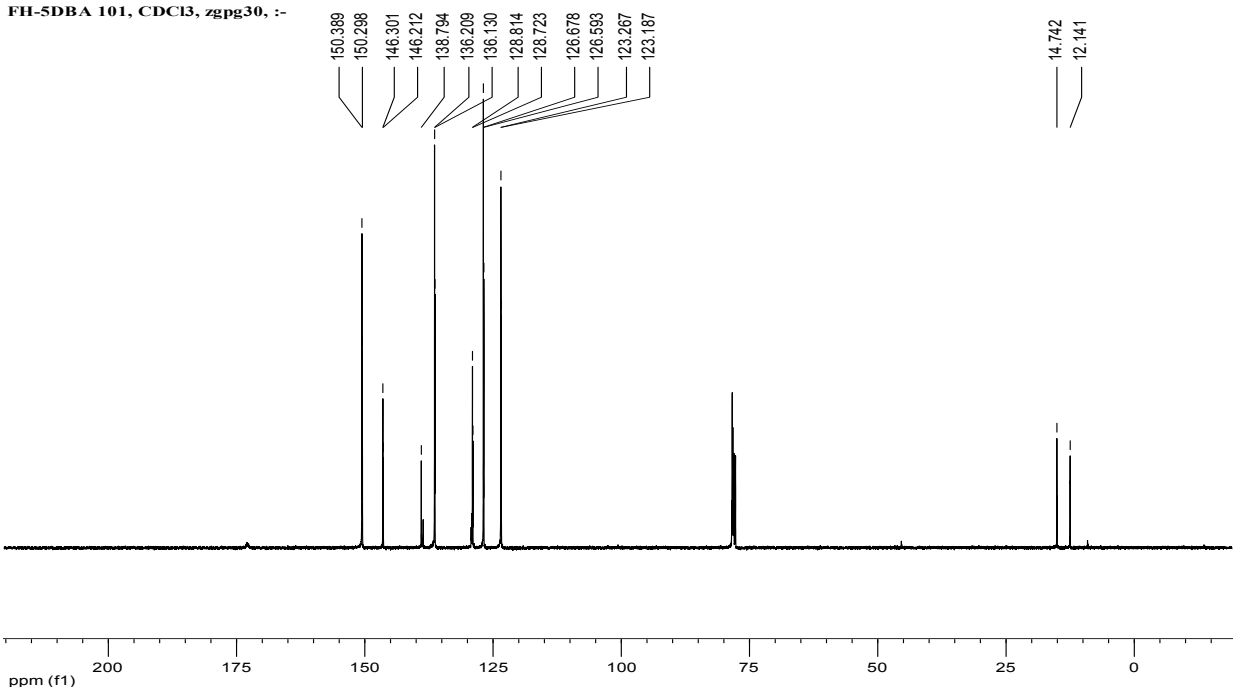

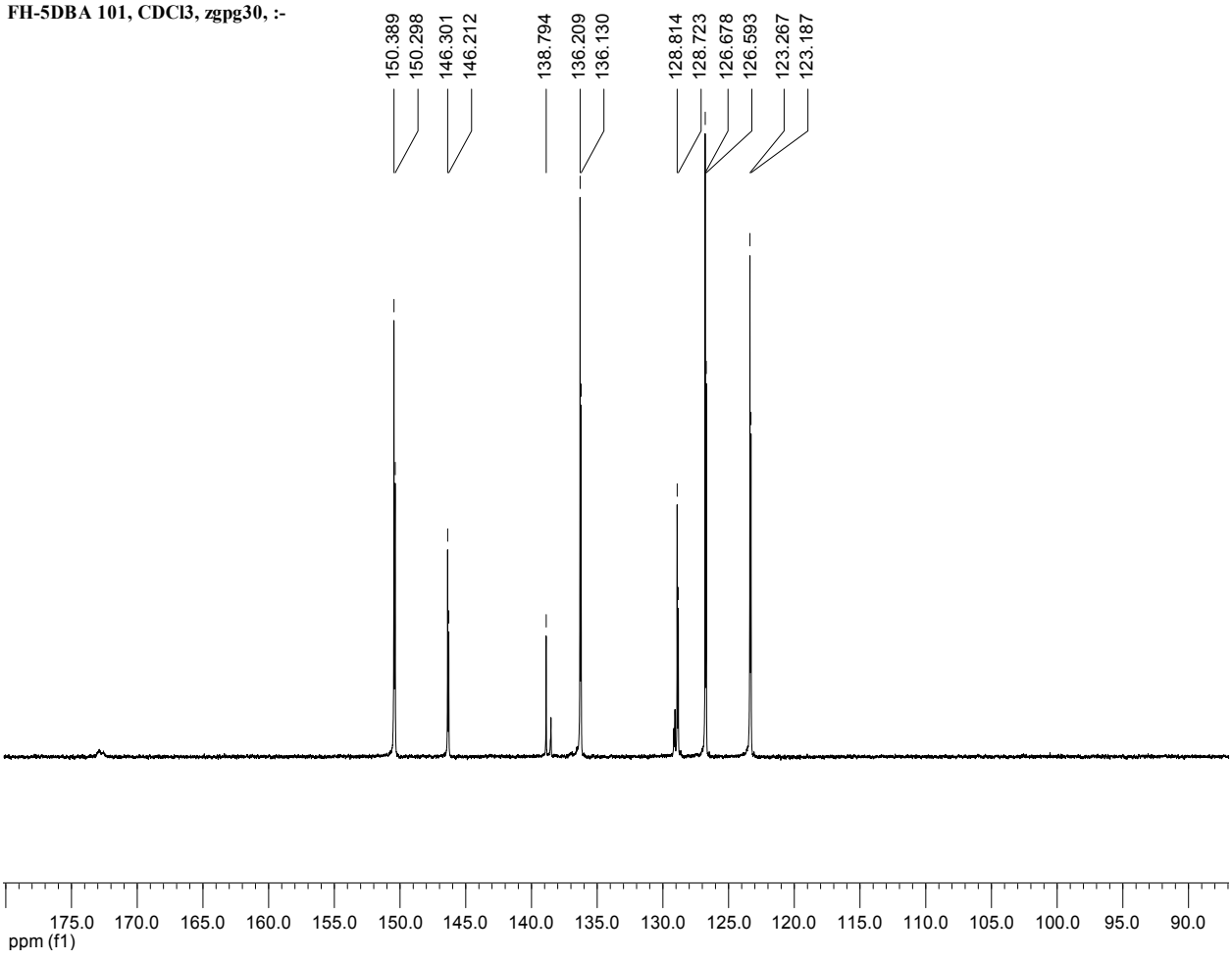

Appendix 8: ^{1}H NMR spectrum of **L4**

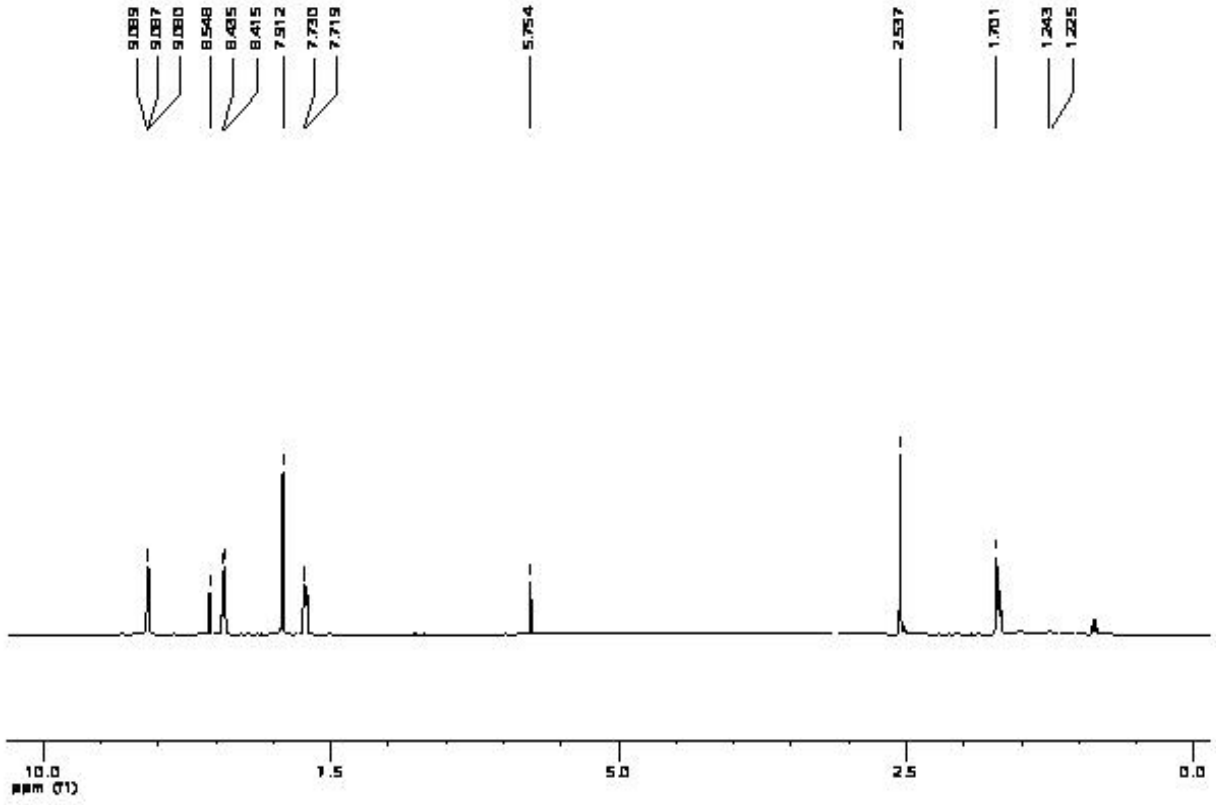

Appendix 9: ^{13}C NMR spectrum of **L4**

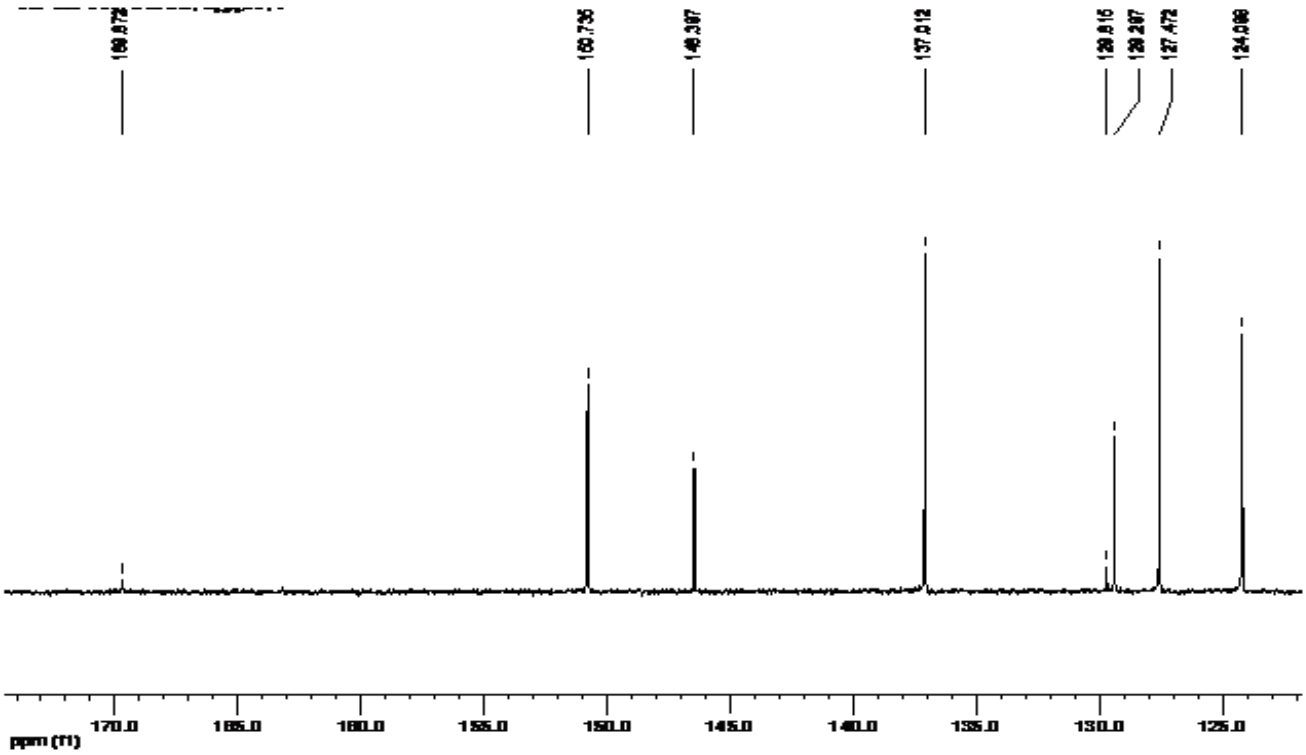

Appendix 10: ^{1}H NMR spectrum of **L5**

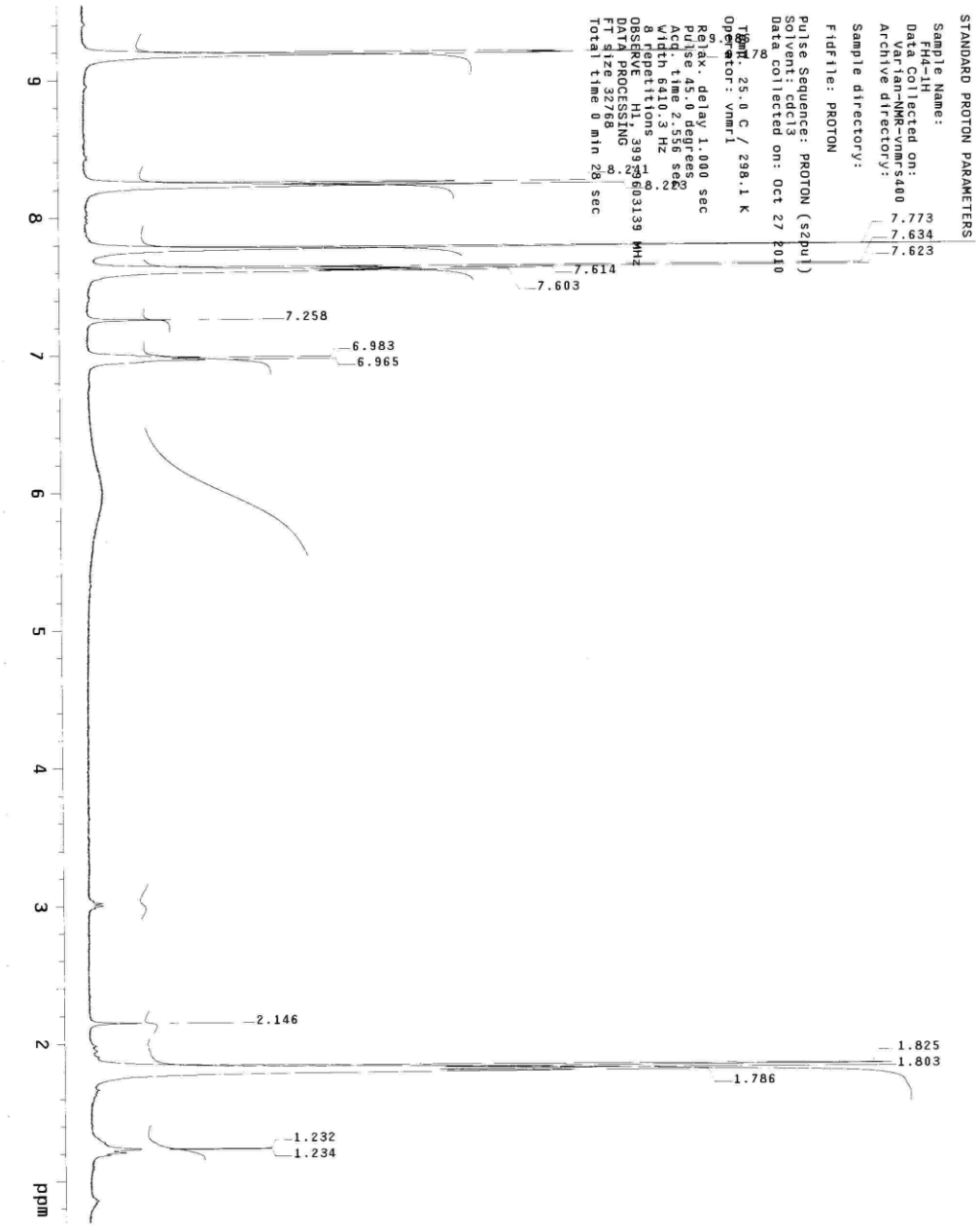

Appendix 11: ^{13}C NMR spectrum of **L5**

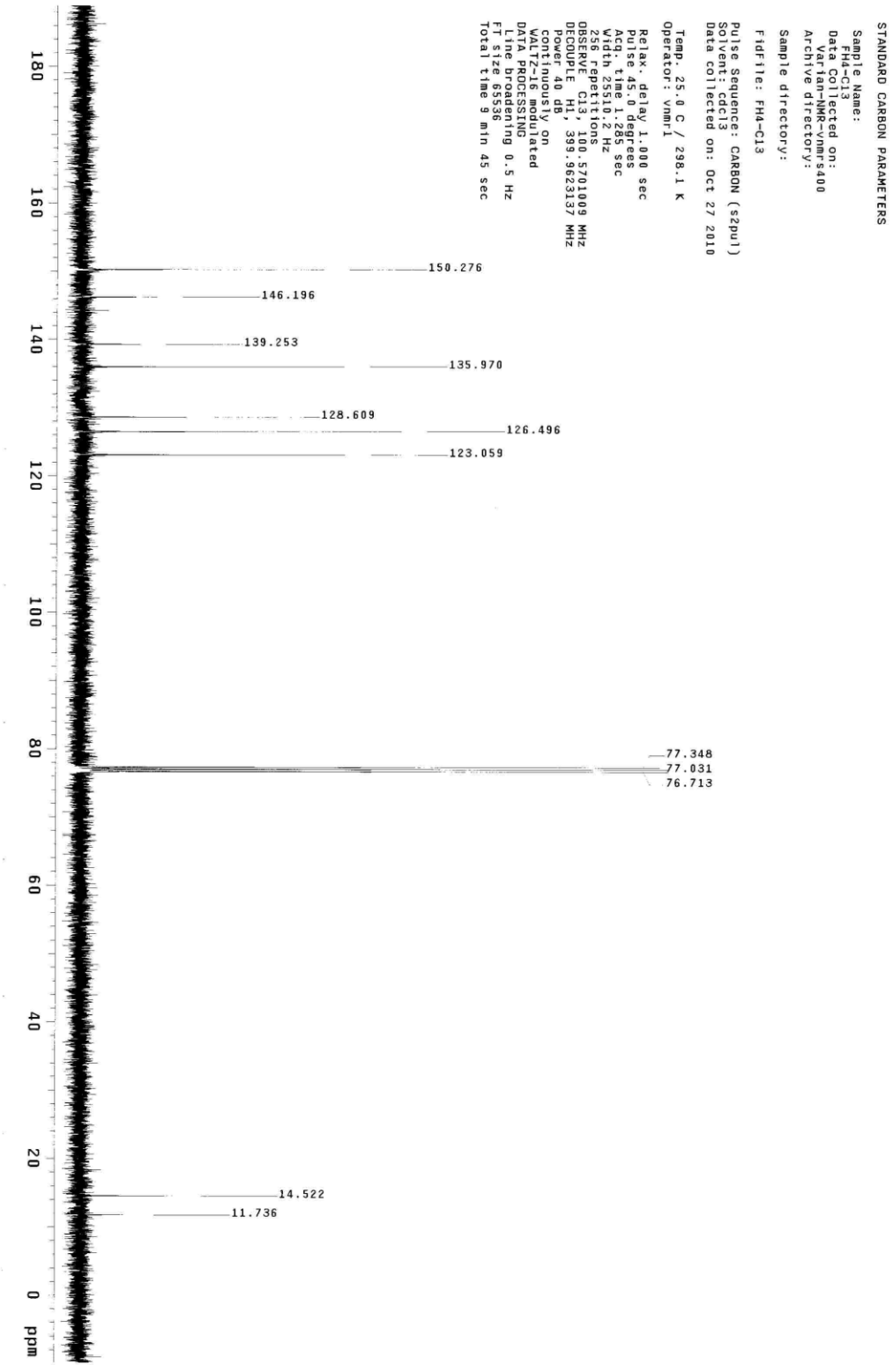

Appendix 12: ^{1}H NMR spectrum of **L6**

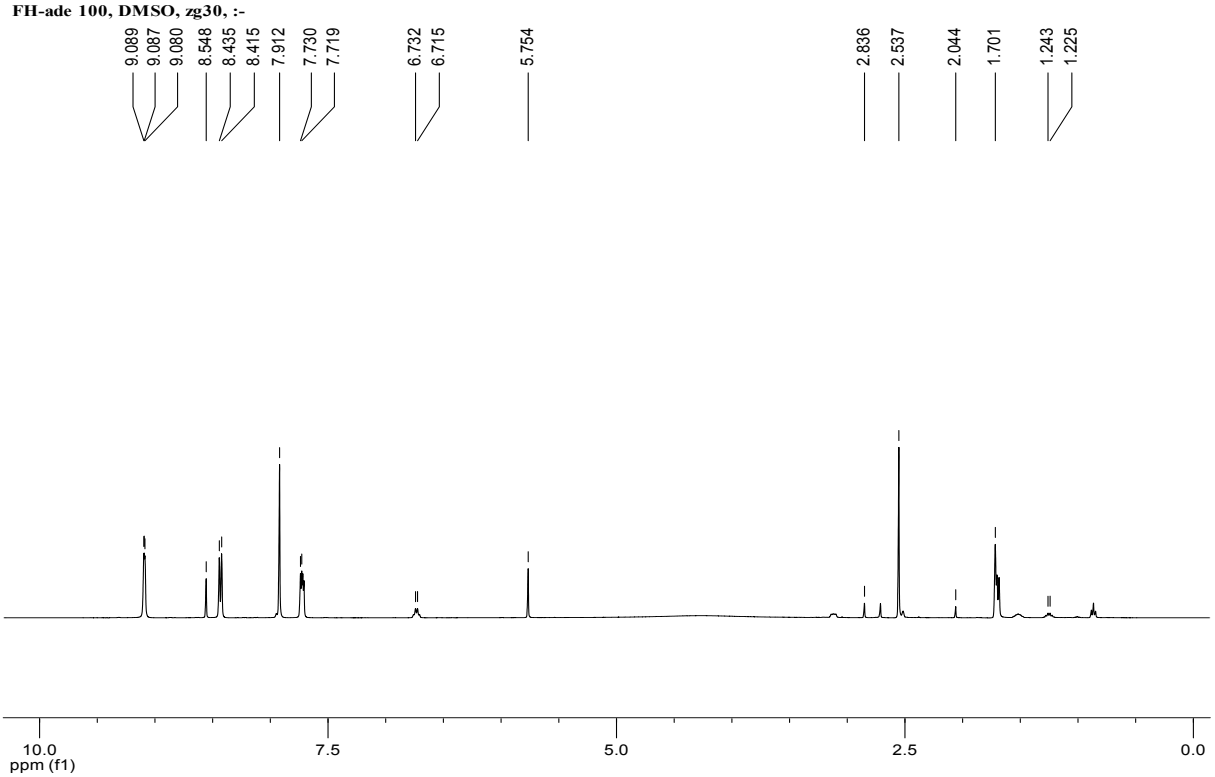

Appendix 13: ^{13}C NMR spectrum of **L6**

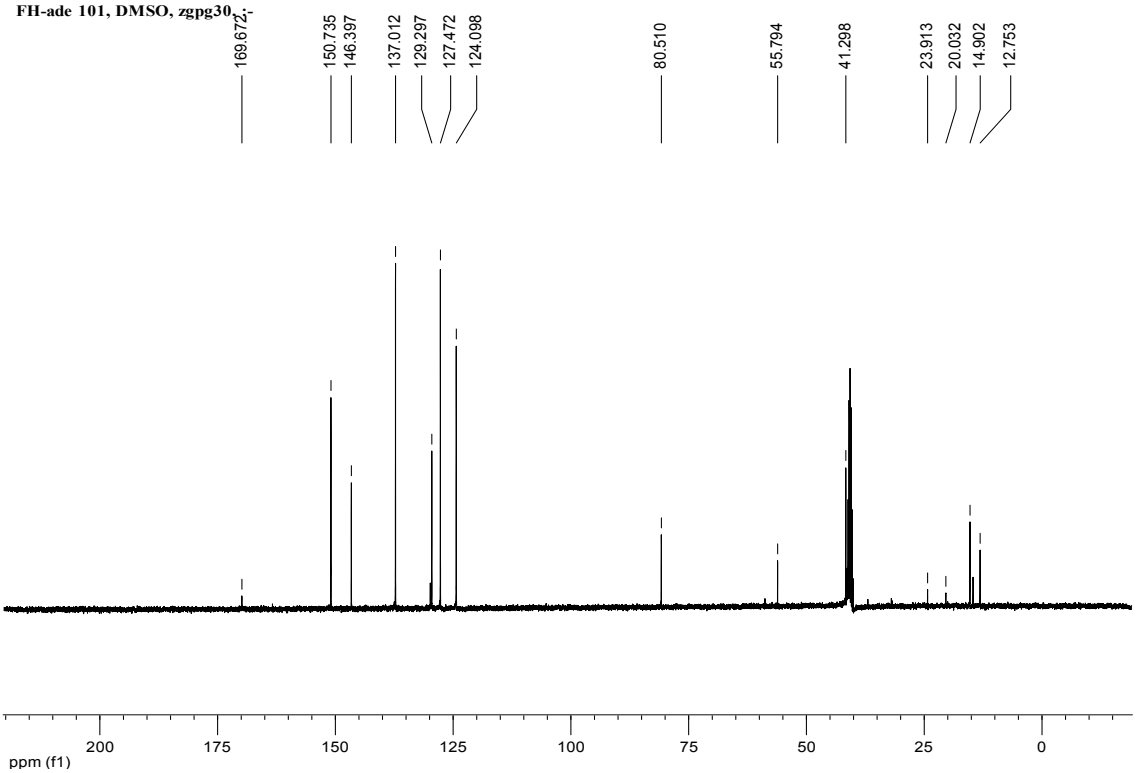

Appendix 14: ^{1}H NMR spectrum of **L7**

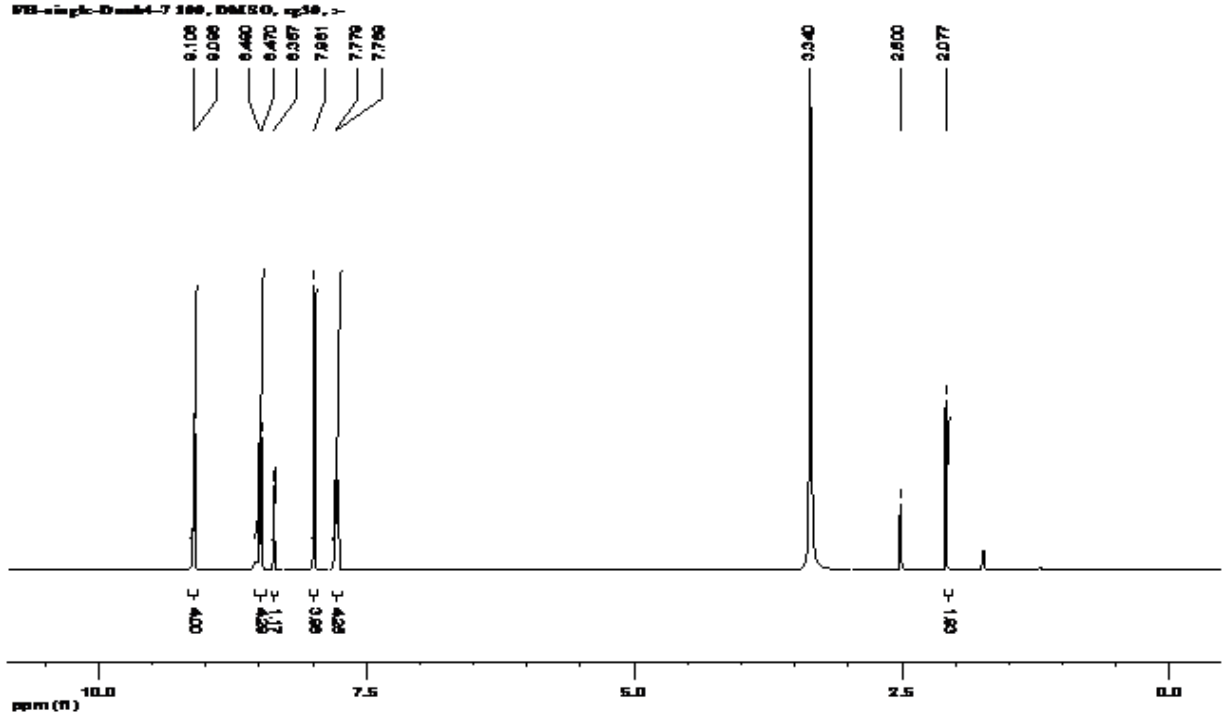

Appendix 15: ^{13}C NMR spectrum of **L7**

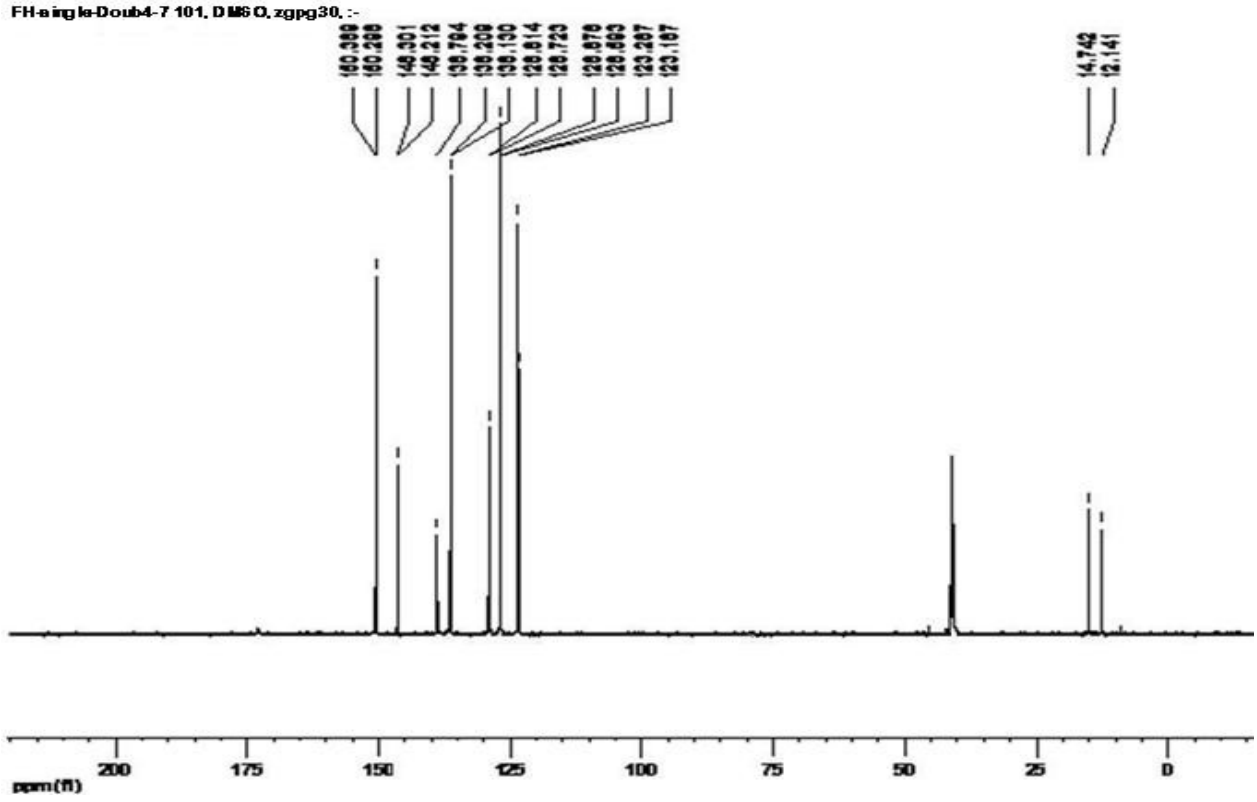

Appendix 16: ^{1}H NMR spectrum of **L8**

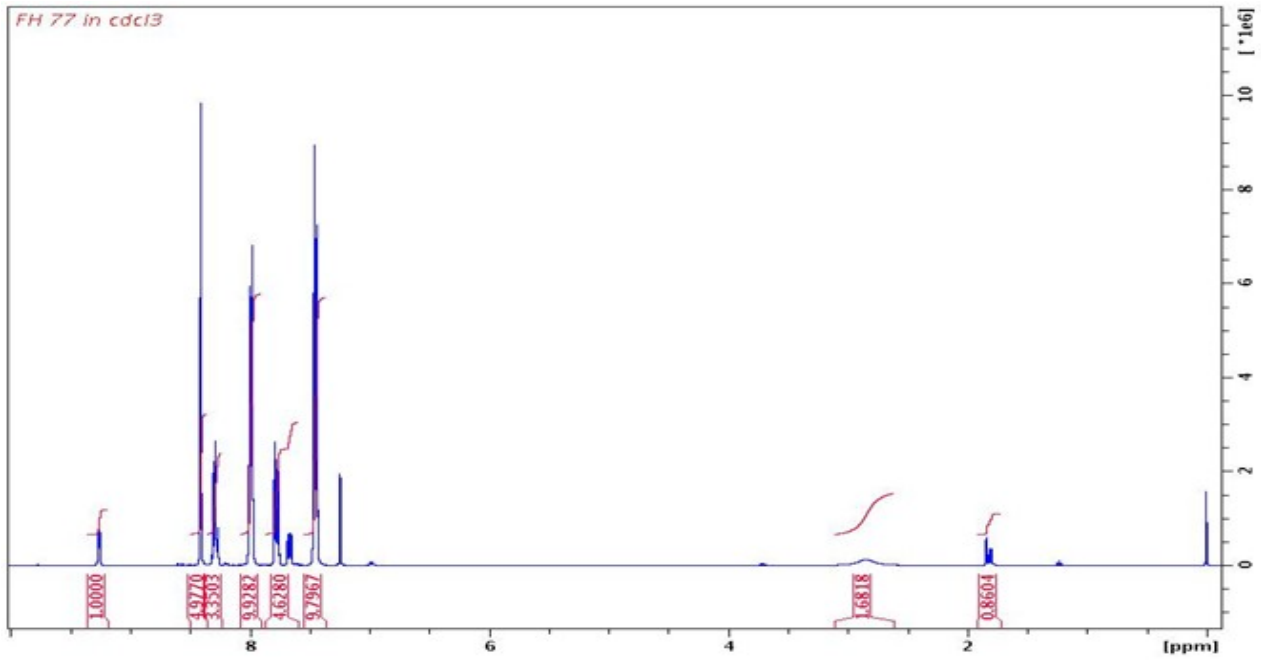

Appendix 17: ^{13}C NMR spectrum of **L8**

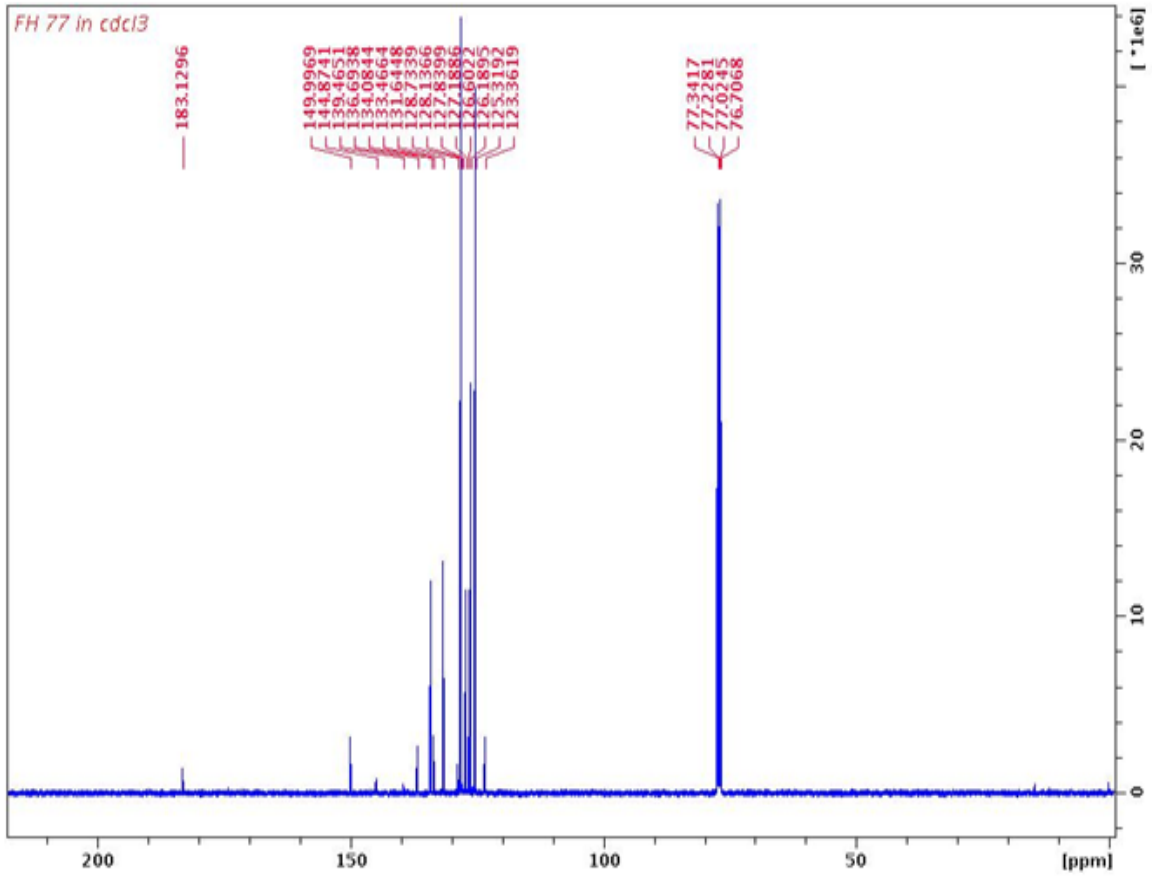

Appendix 18: ^{1}H NMR spectrum of **L9**

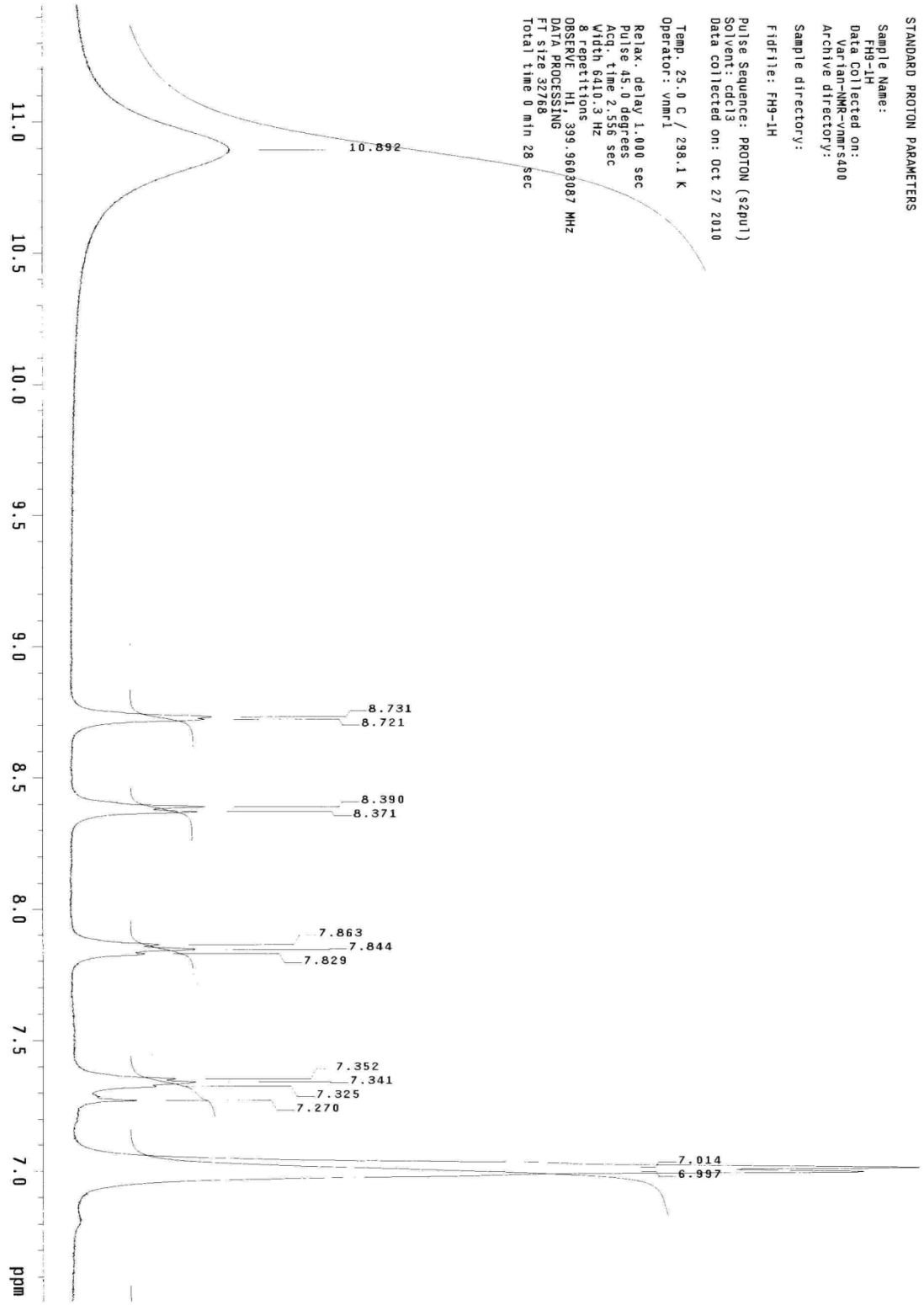

Appendix 19: ^{13}C NMR spectrum of **L9**

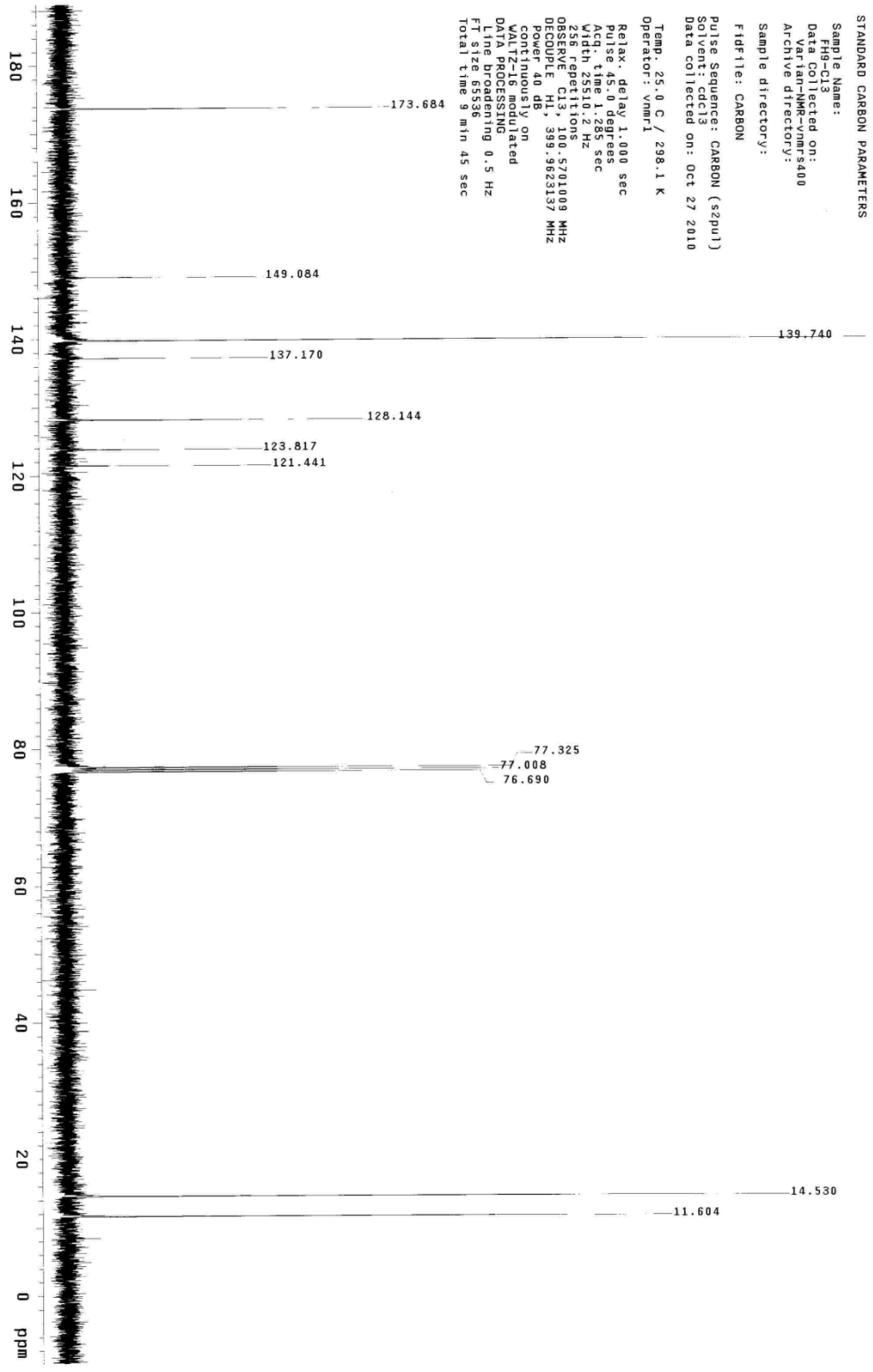

Appendix 20: ^{1}H NMR spectrum of **L10**

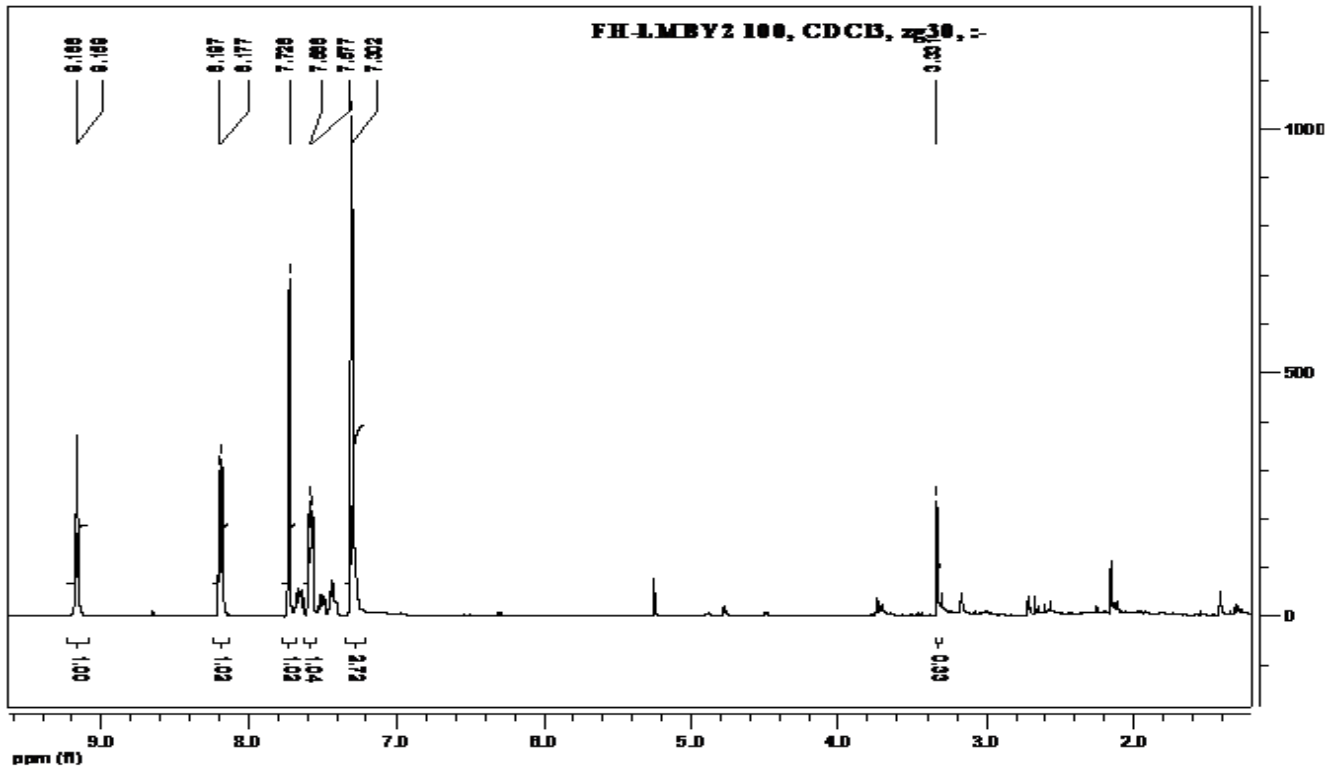

Appendix 21: ^{13}C NMR spectrum of **L10**

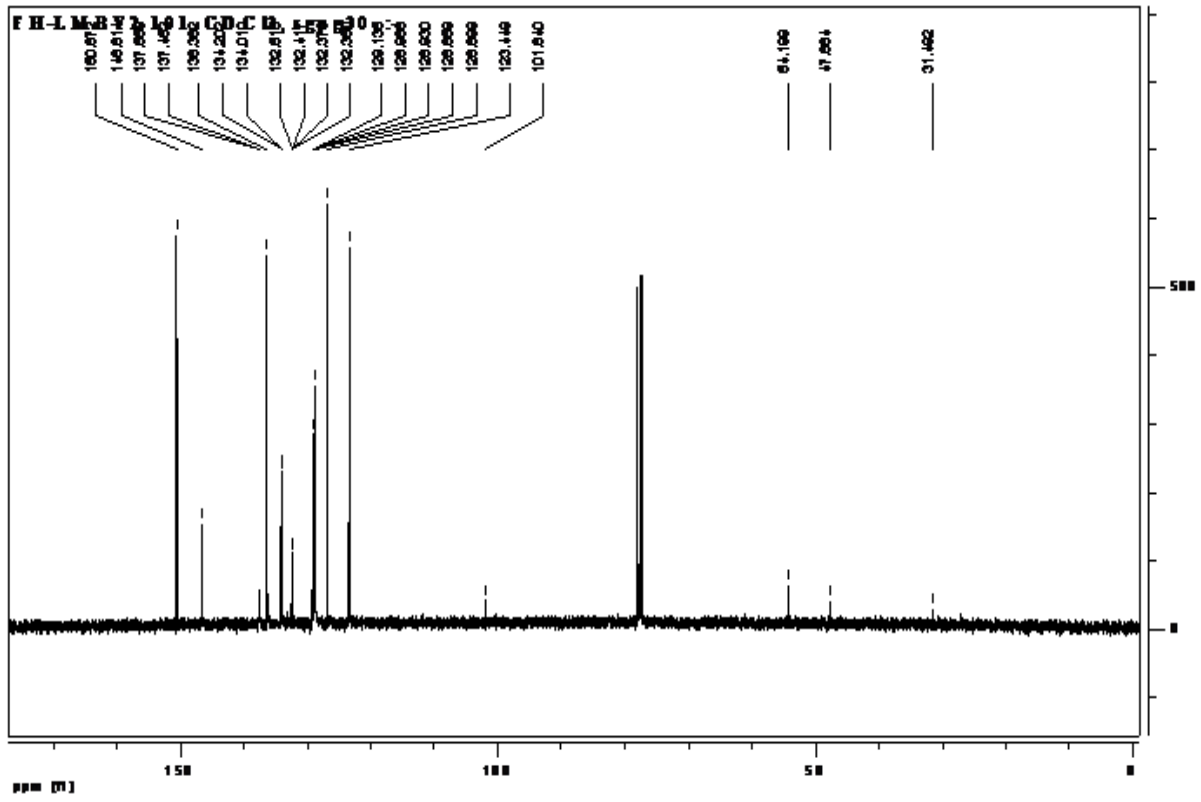

Appendix 22: ^{1}H NMR spectrum of **L12**

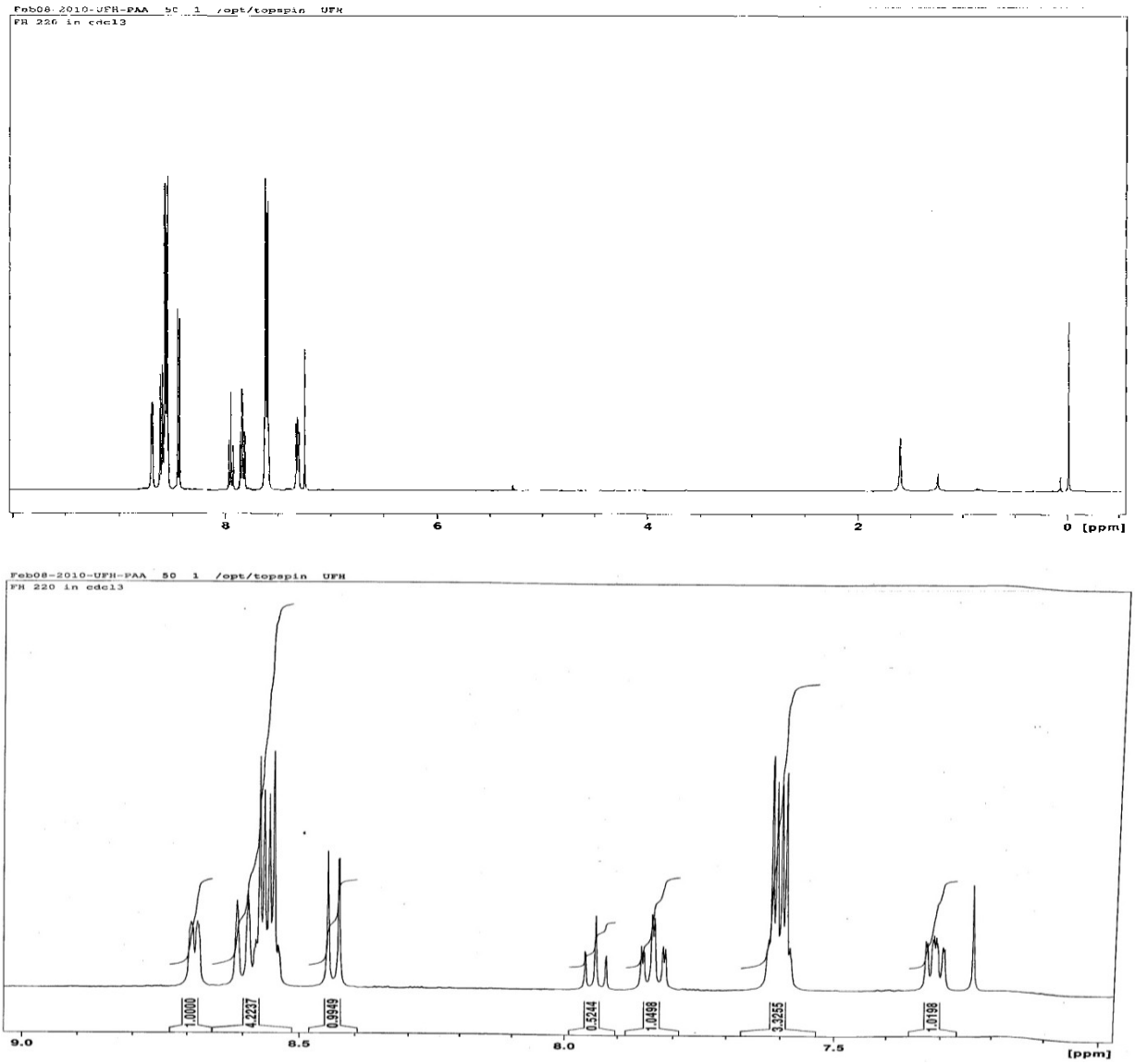

Appendix 23: ^{13}C NMR spectrum of **L12**

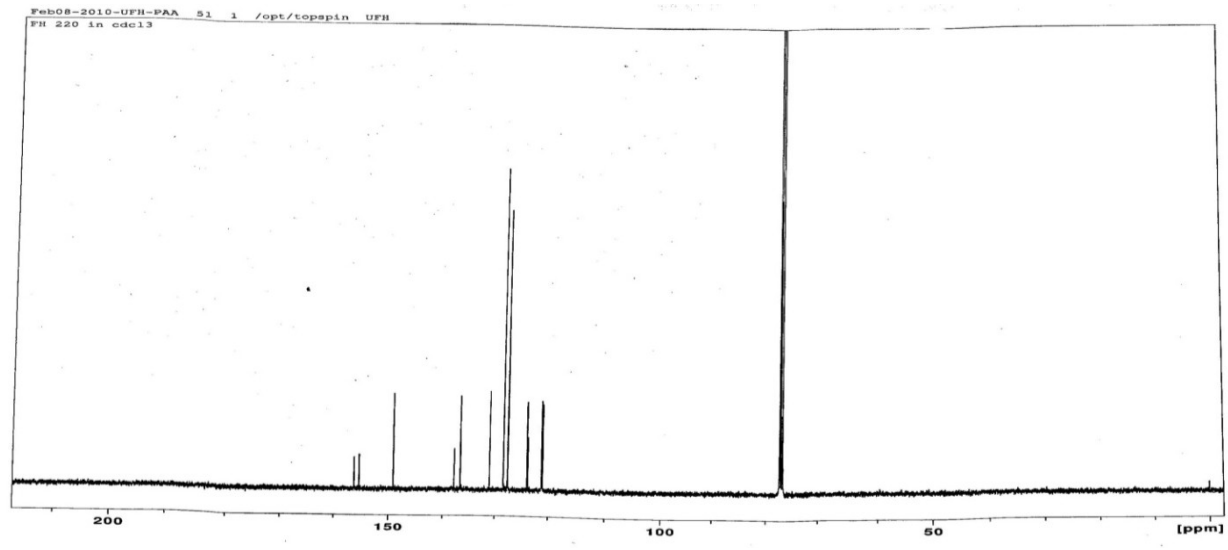

Appendix 24: ^{1}H NMR spectrum of **L13**

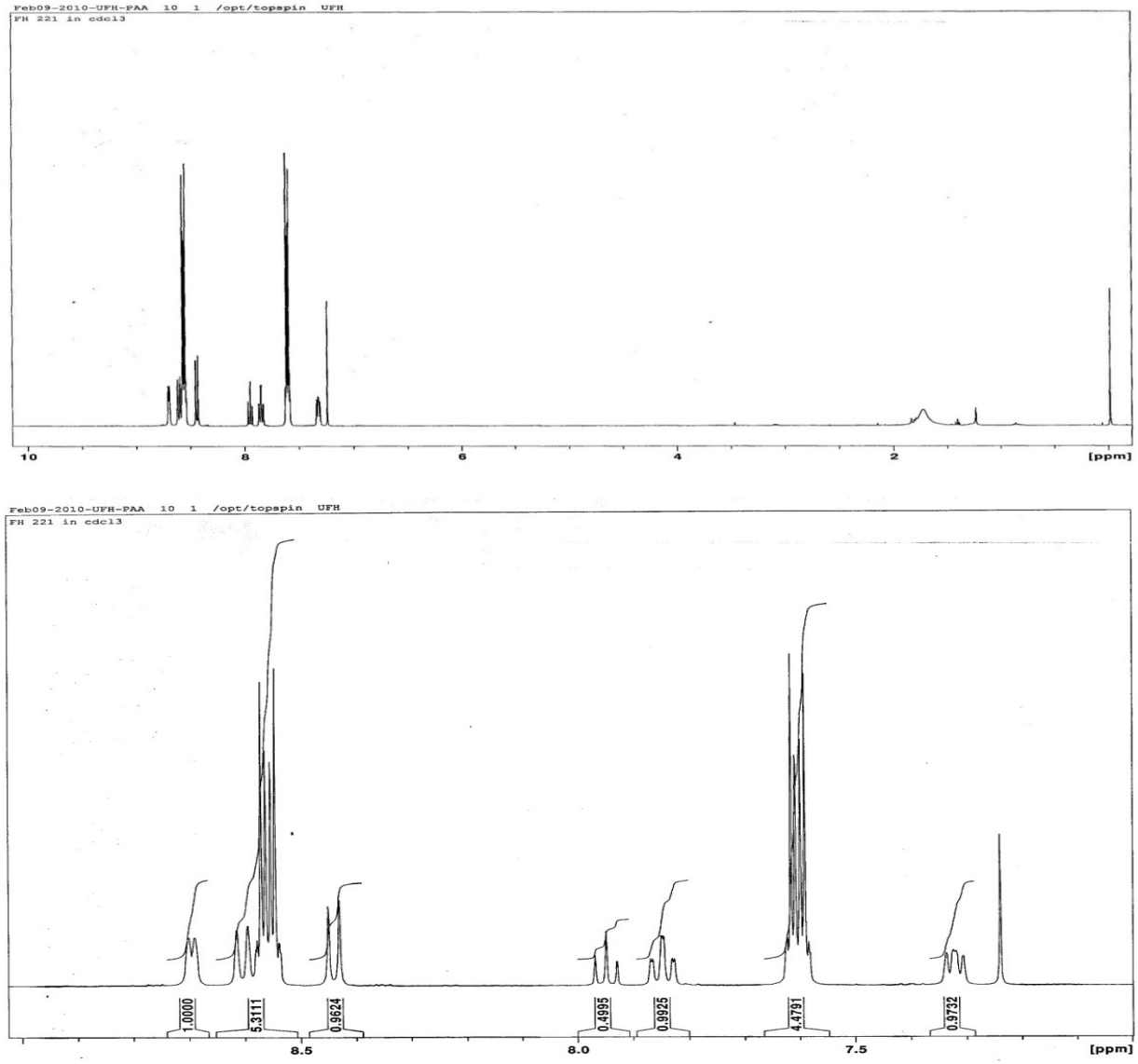

Appendix 25: ^{13}C NMR spectrum of **L13**

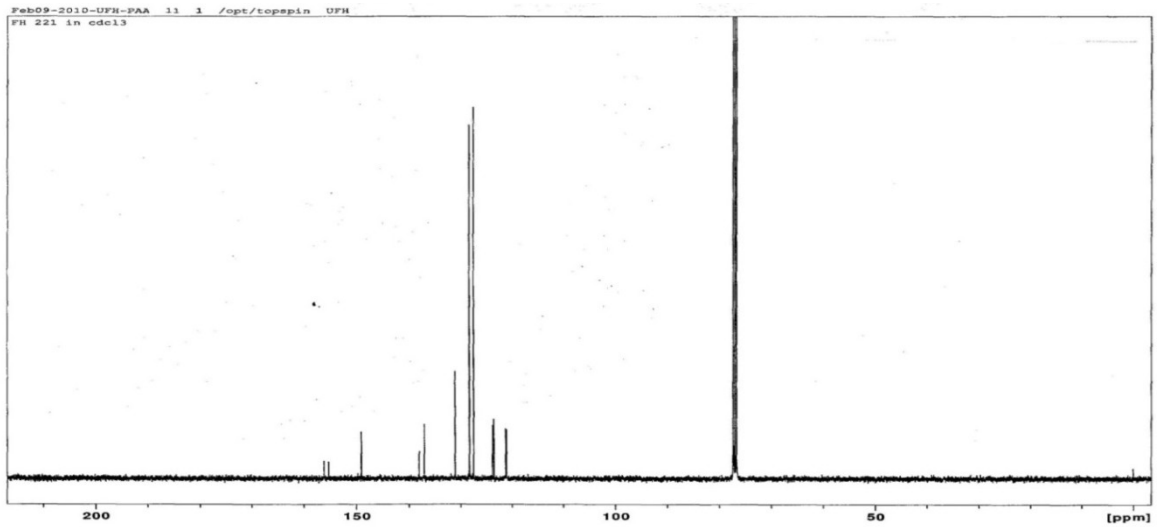

Appendix 26: ^{1}H NMR spectrum of **L14**

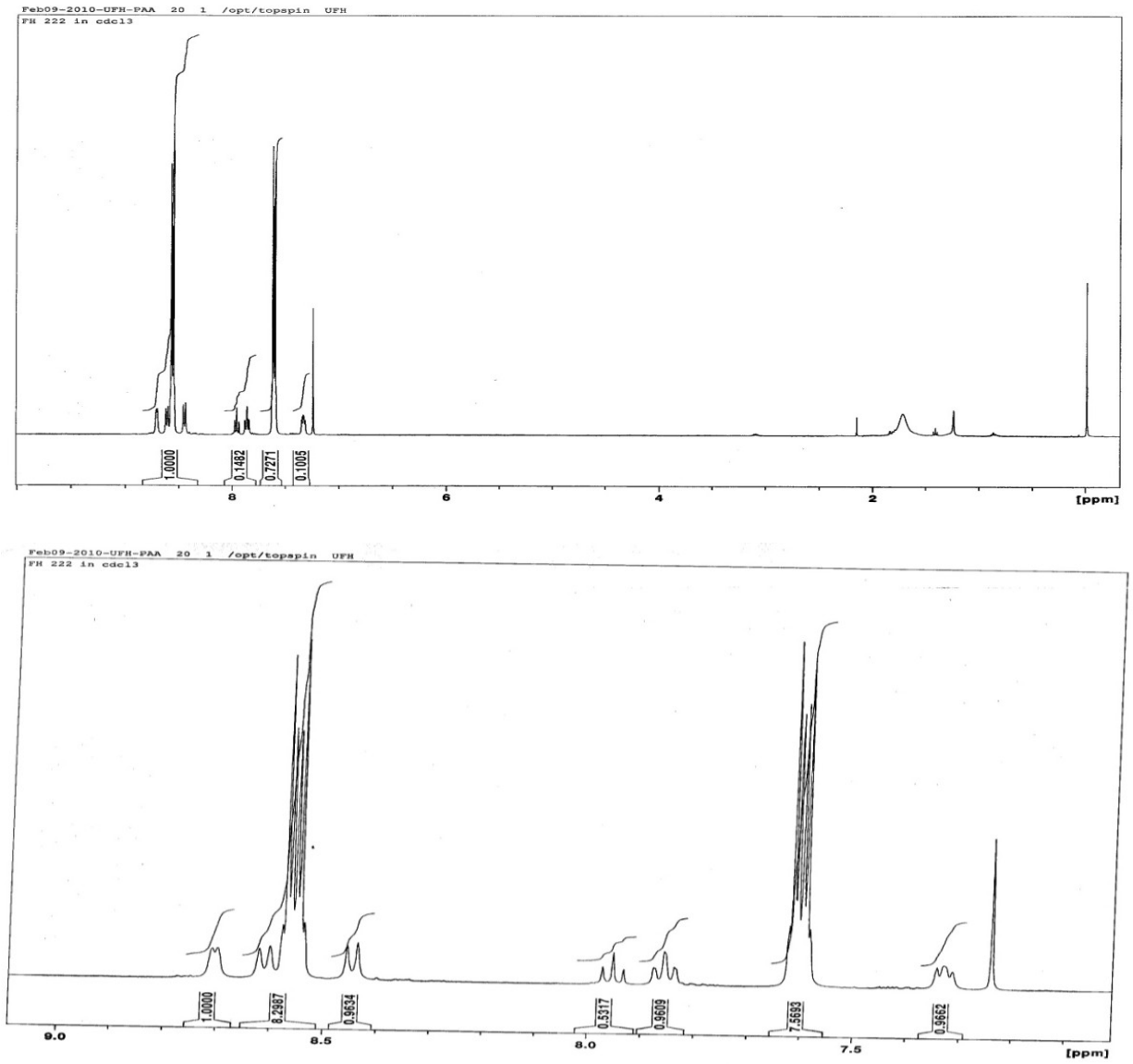

Appendix 27: ^{13}C NMR spectrum of **L14**

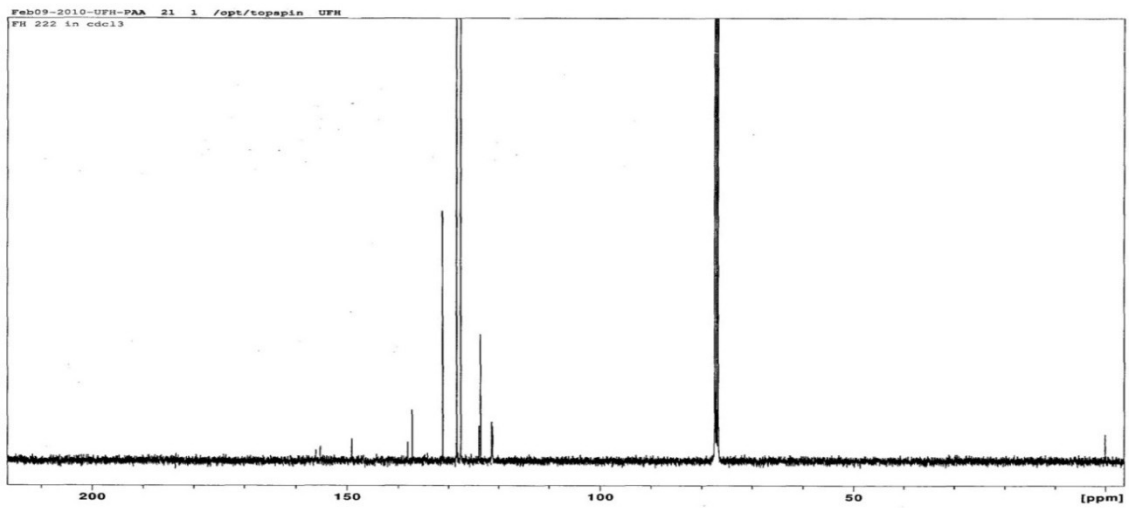

Appendix 28: ^{1}H NMR spectrum of **L15**

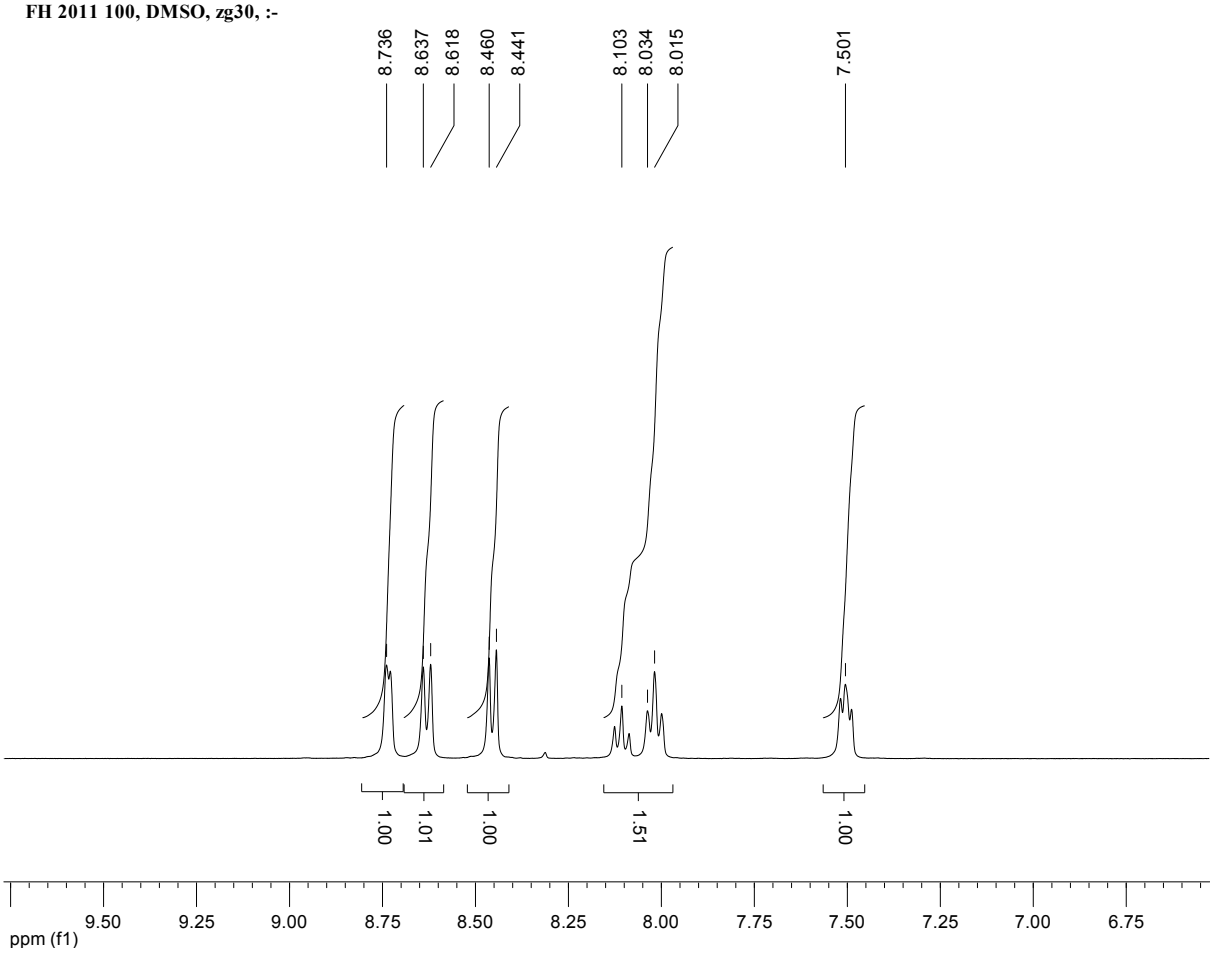

Appendix 29: ^{1}H NMR spectrum of **C1**

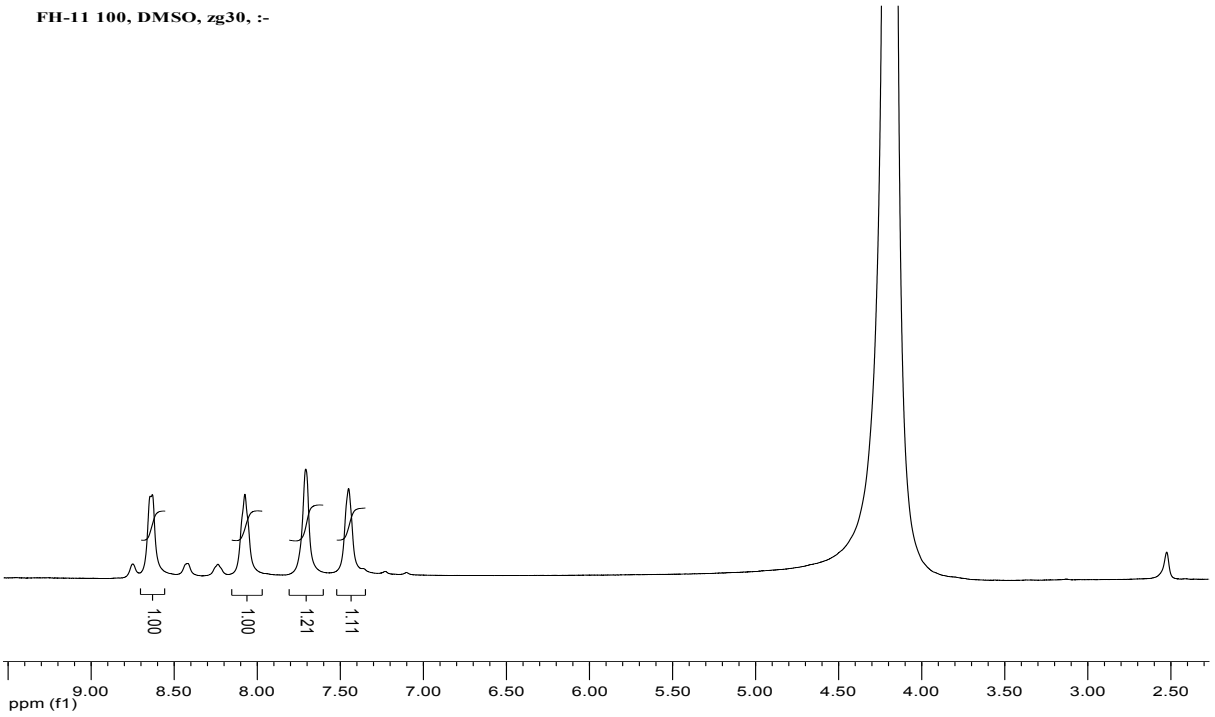

Appendix 30: Aromatic region of ^{13}C NMR spectrum of **C1**

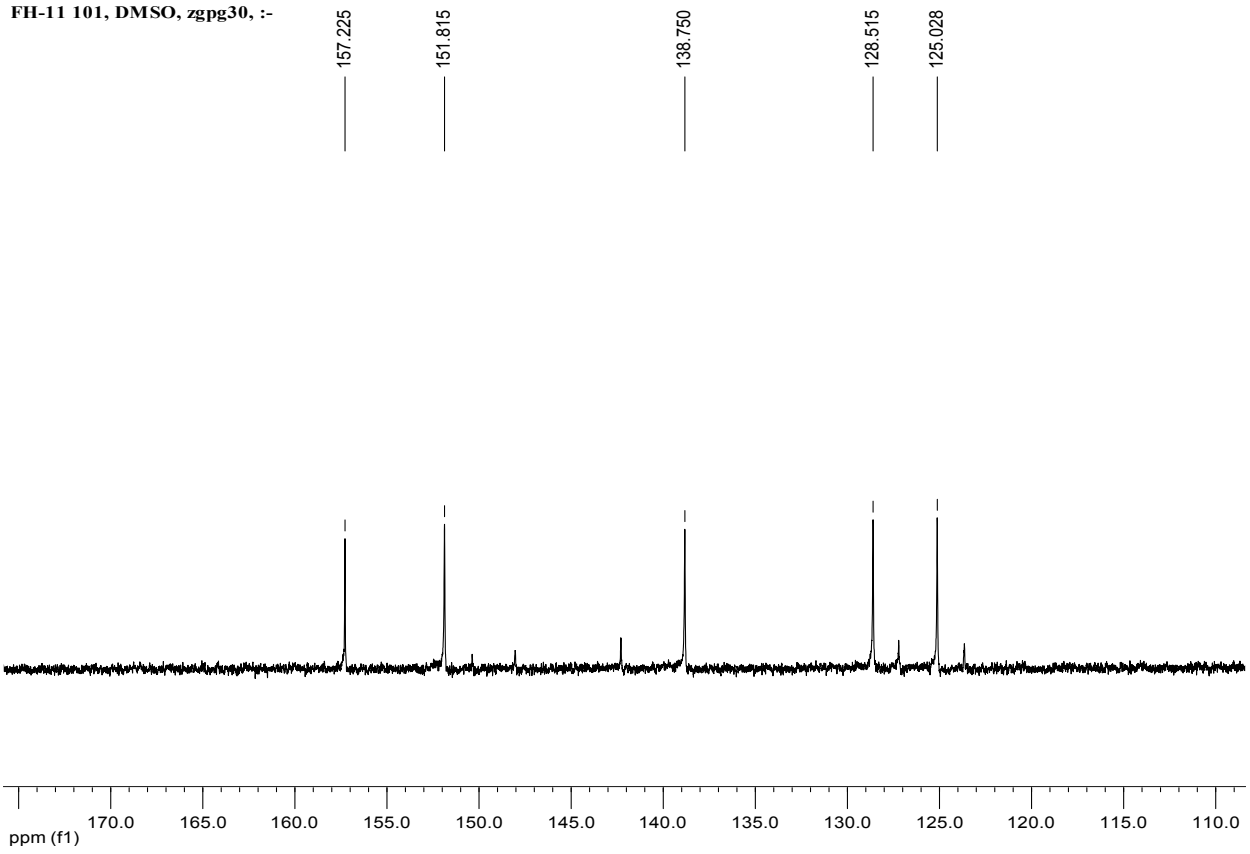

Appendix 31: ^{1}H NMR spectrum of **C2**

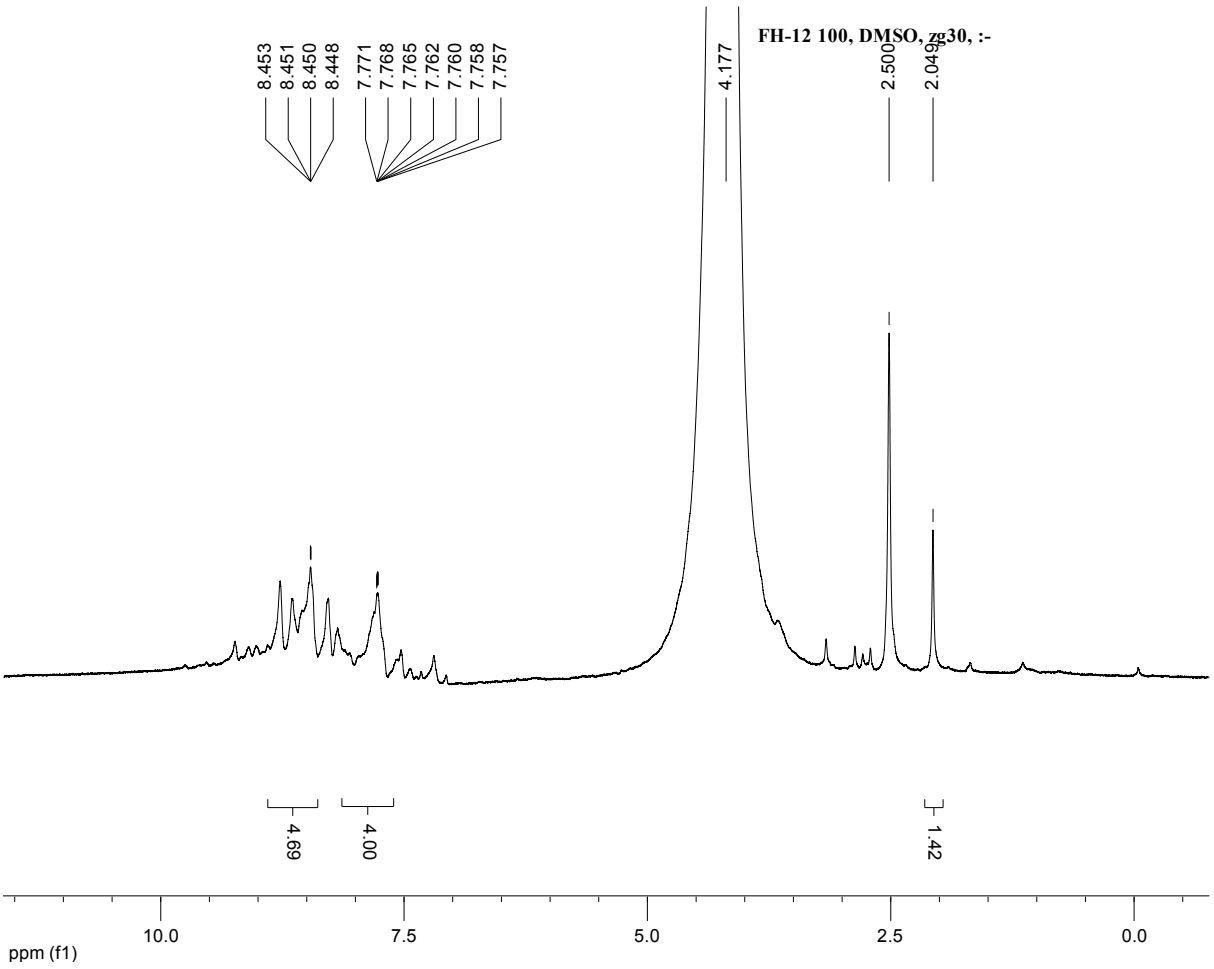

Appendix 32: ^{1}H NMR spectrum of **C4**

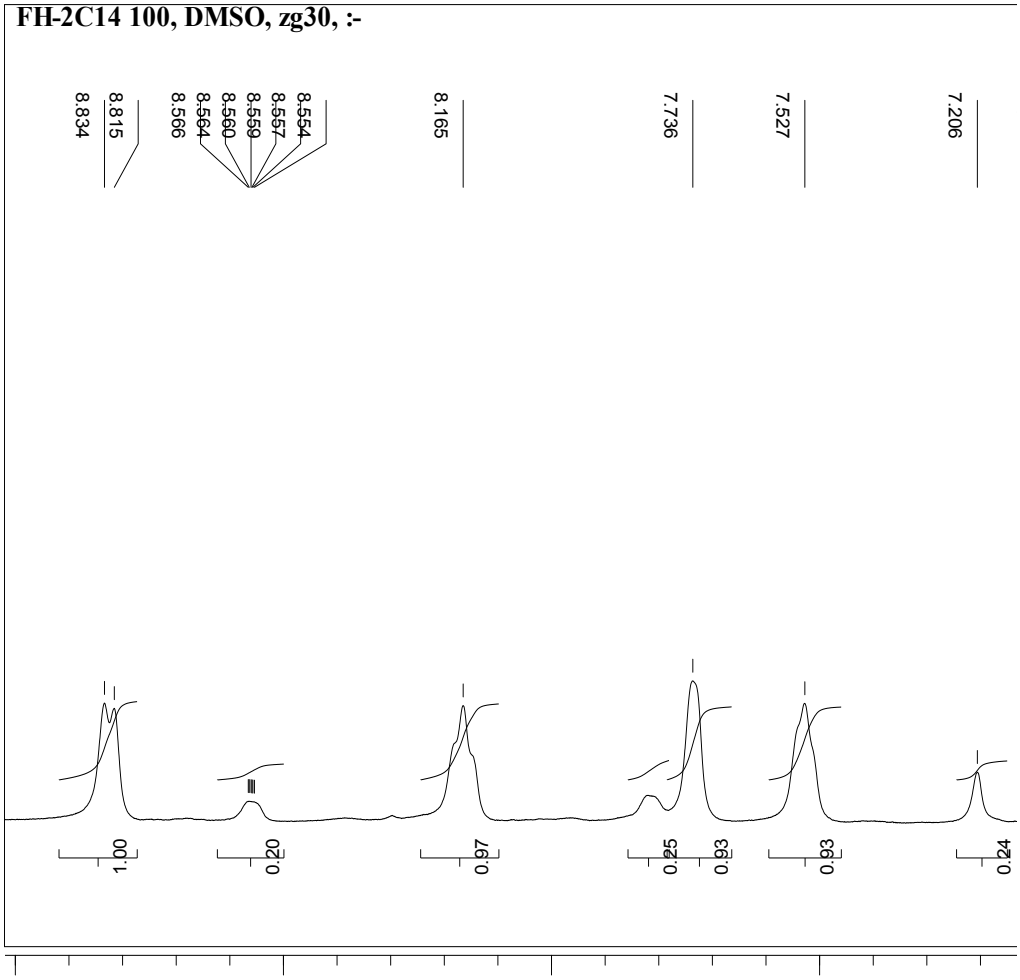

Appendix 33: ^{1}H NMR spectrum of **C5**

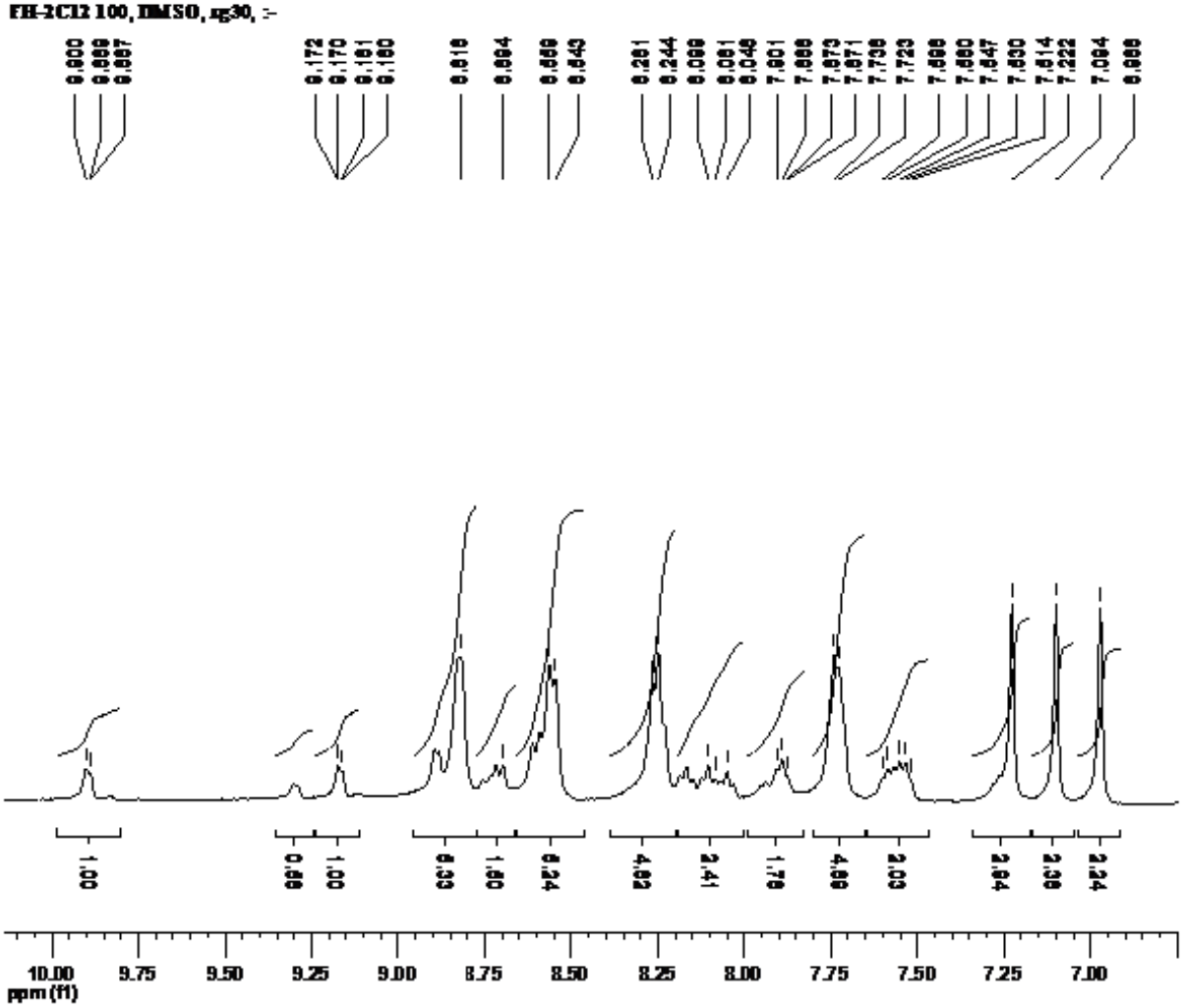

Appendix 34: ^{1}H NMR spectrum of **C6**

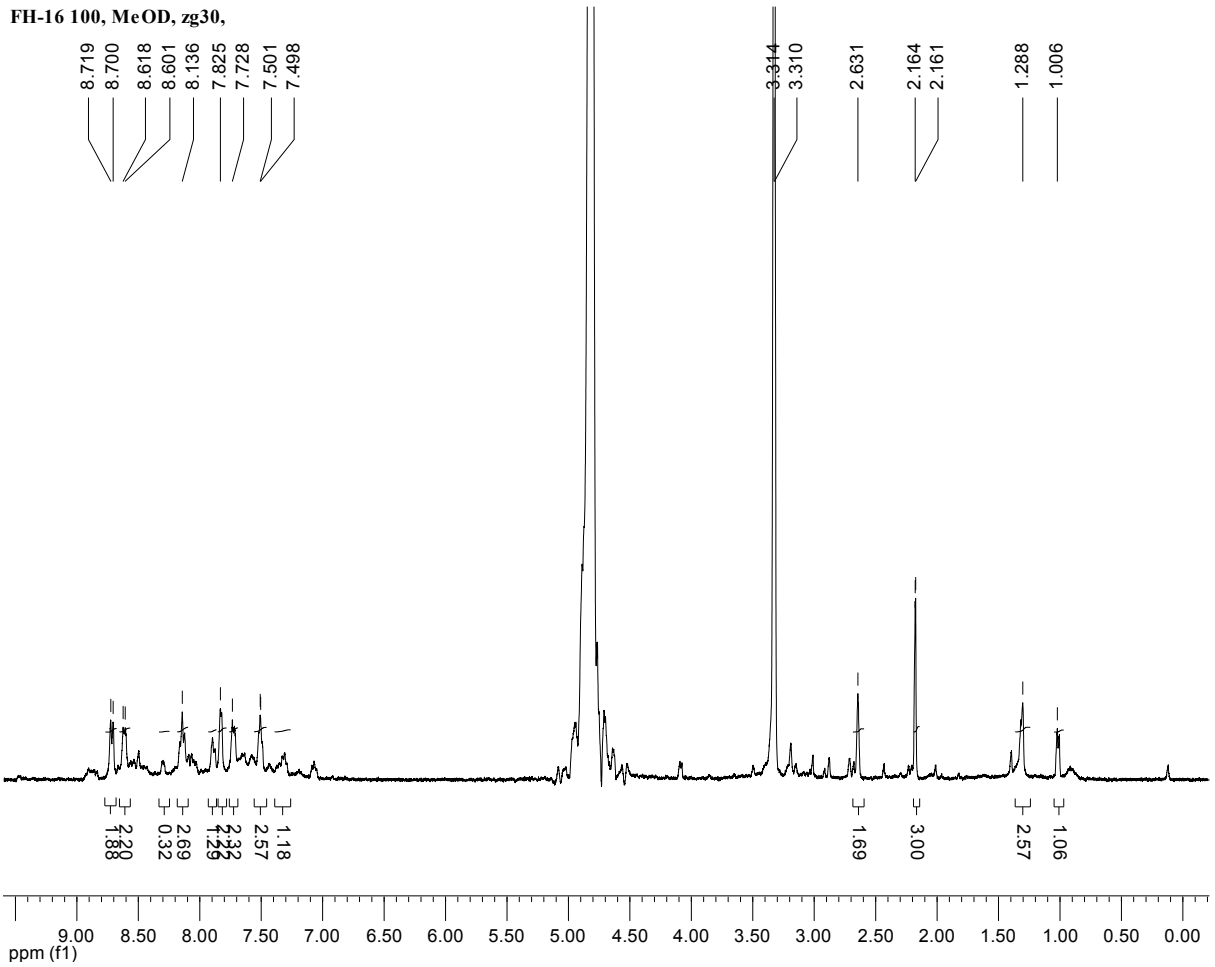

Appendix 35: ^{1}H NMR spectrum of **C7**

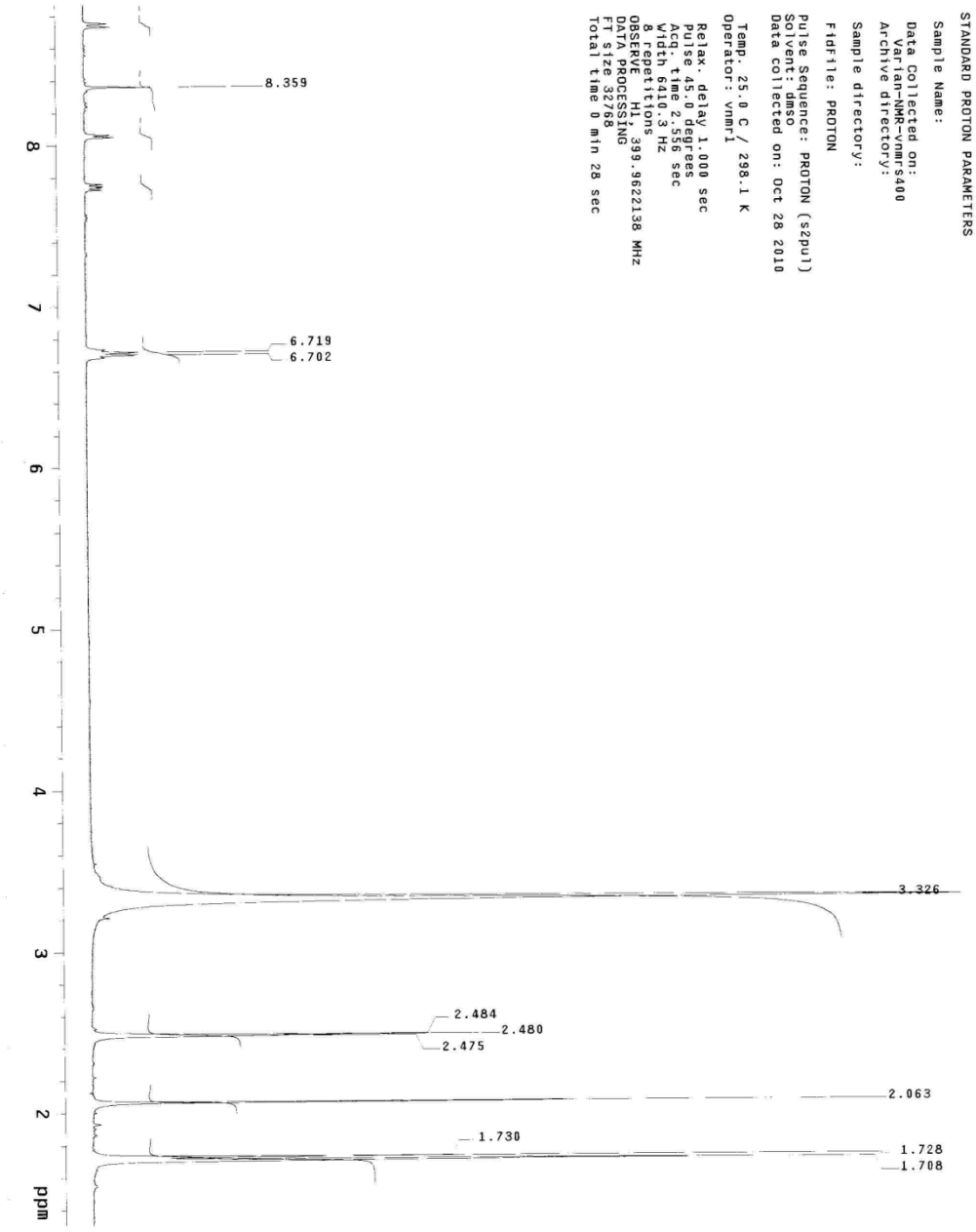

Appendix 36: Expanded ^{1}H NMR spectrum of **C7**

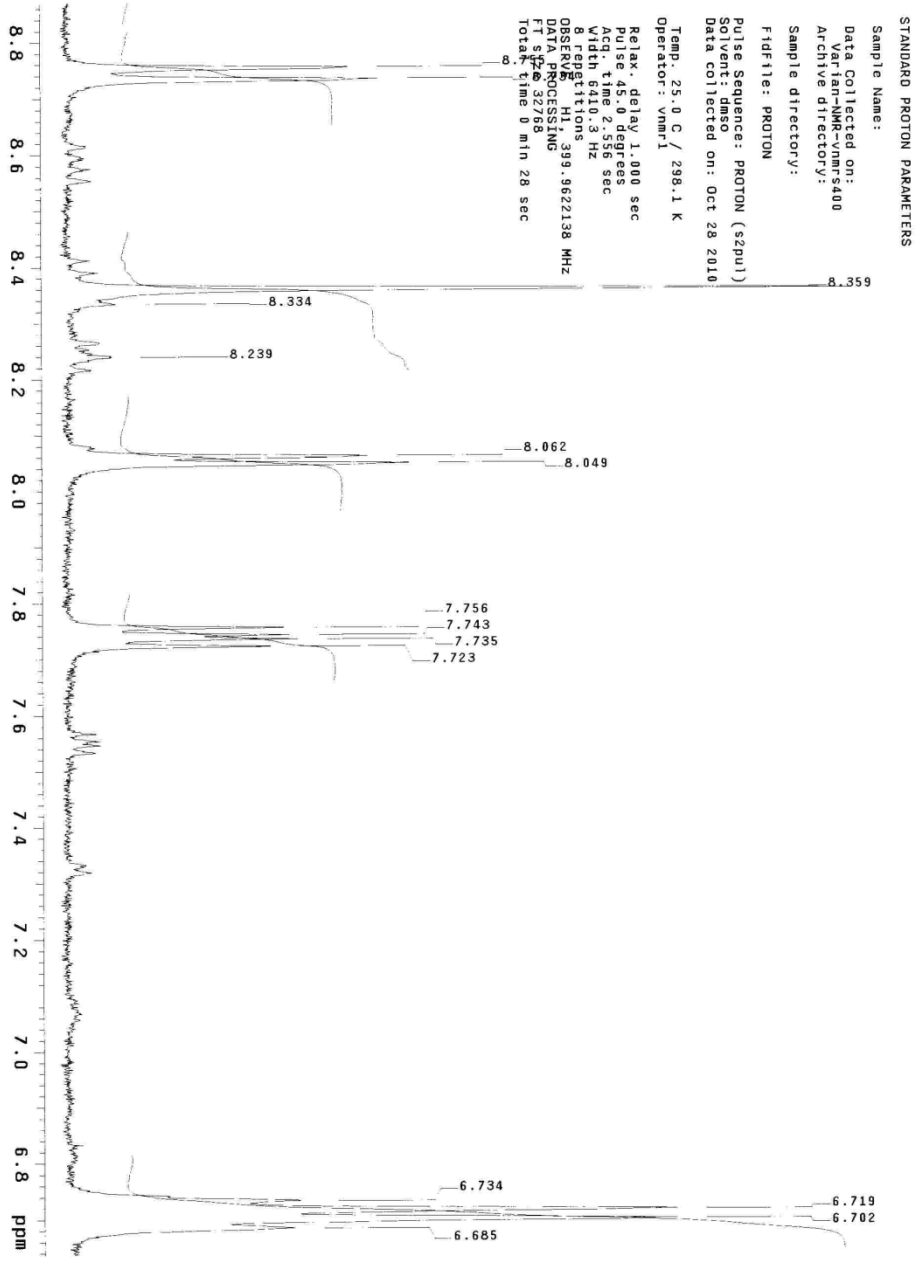

Appendix 37: ^{1}H NMR spectrum of **C8**

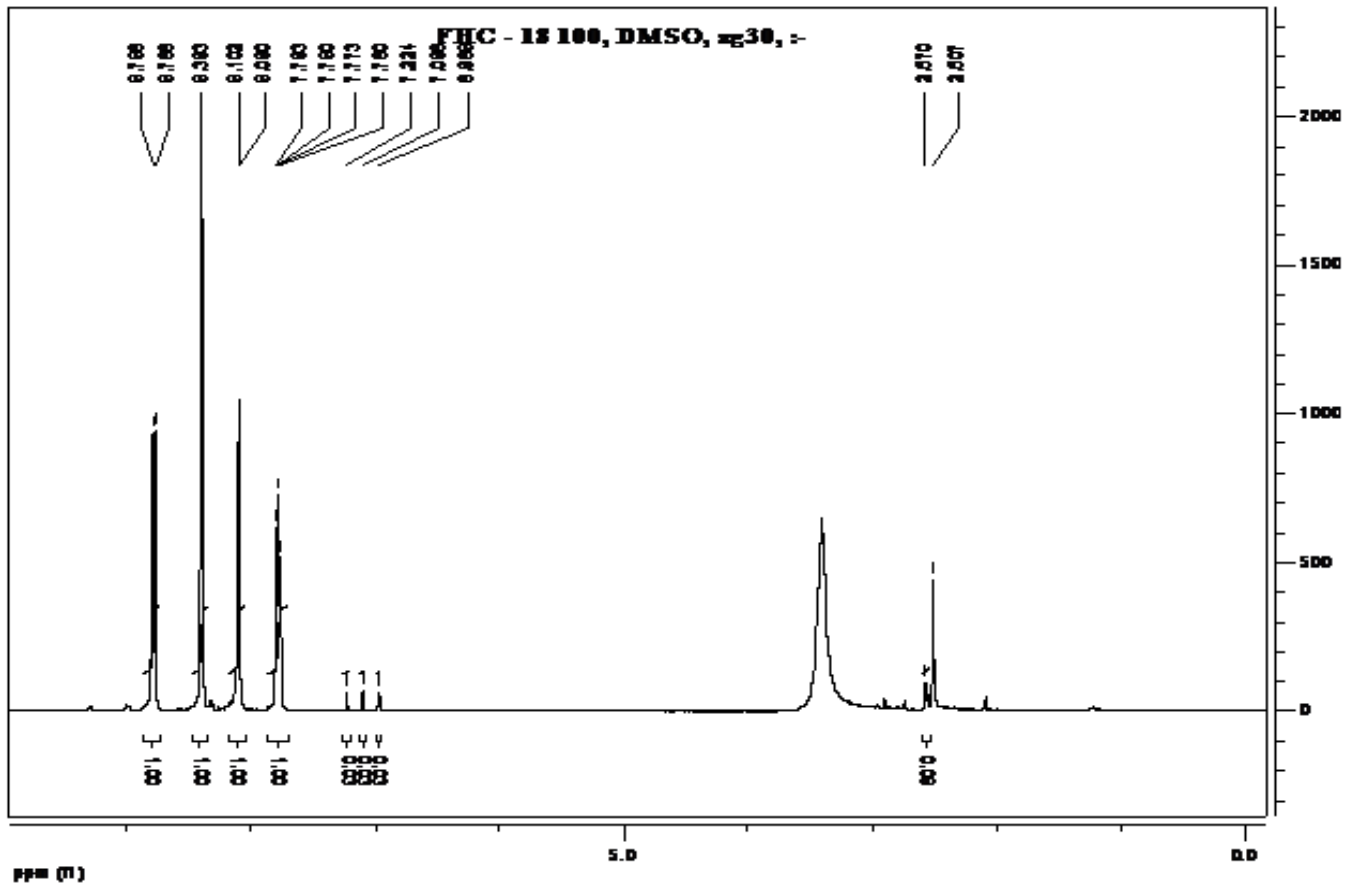

Appendix 38: ^{13}C NMR spectrum of **C8**

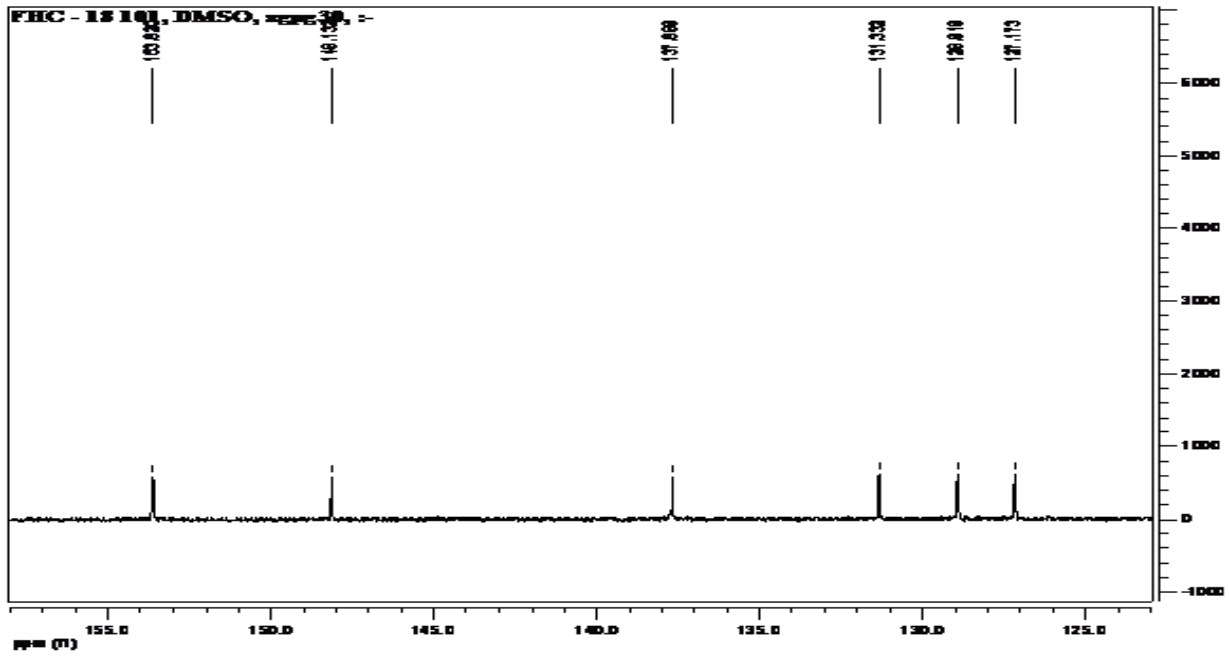

Appendix 39: ^{1}H NMR spectrum of **C9**

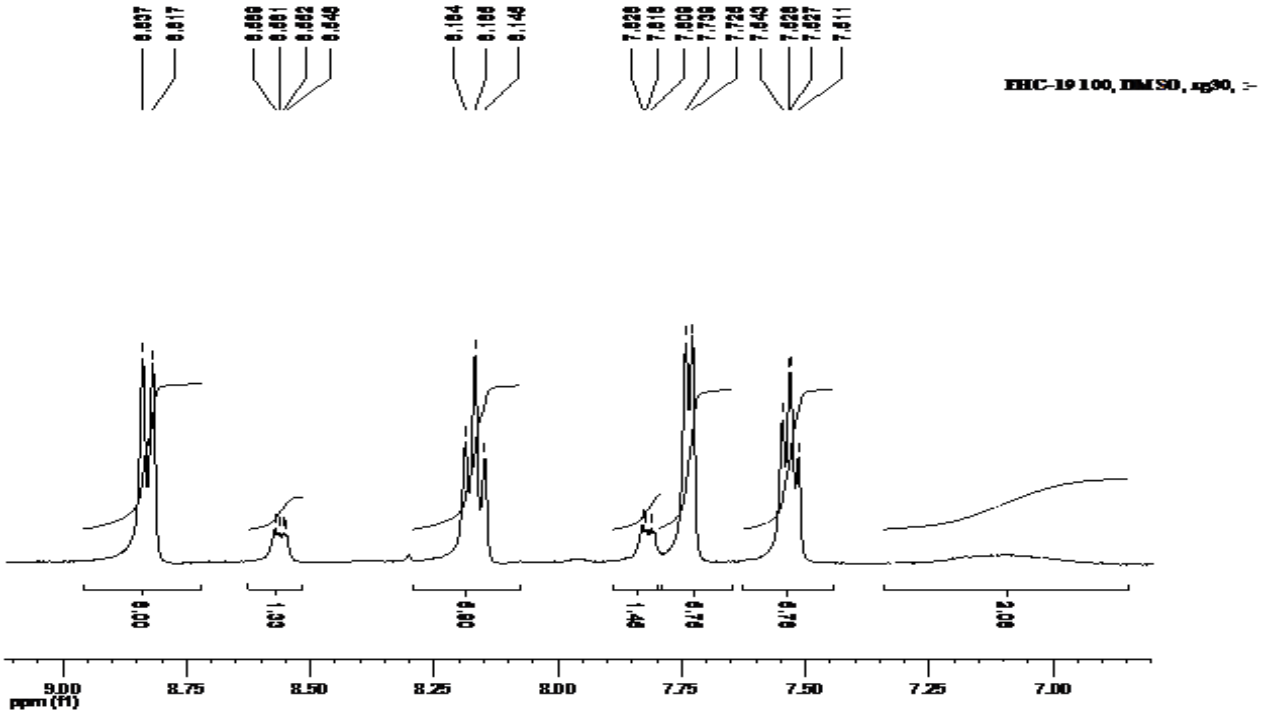

Appendix 40: ^{13}C NMR spectrum of **C9**

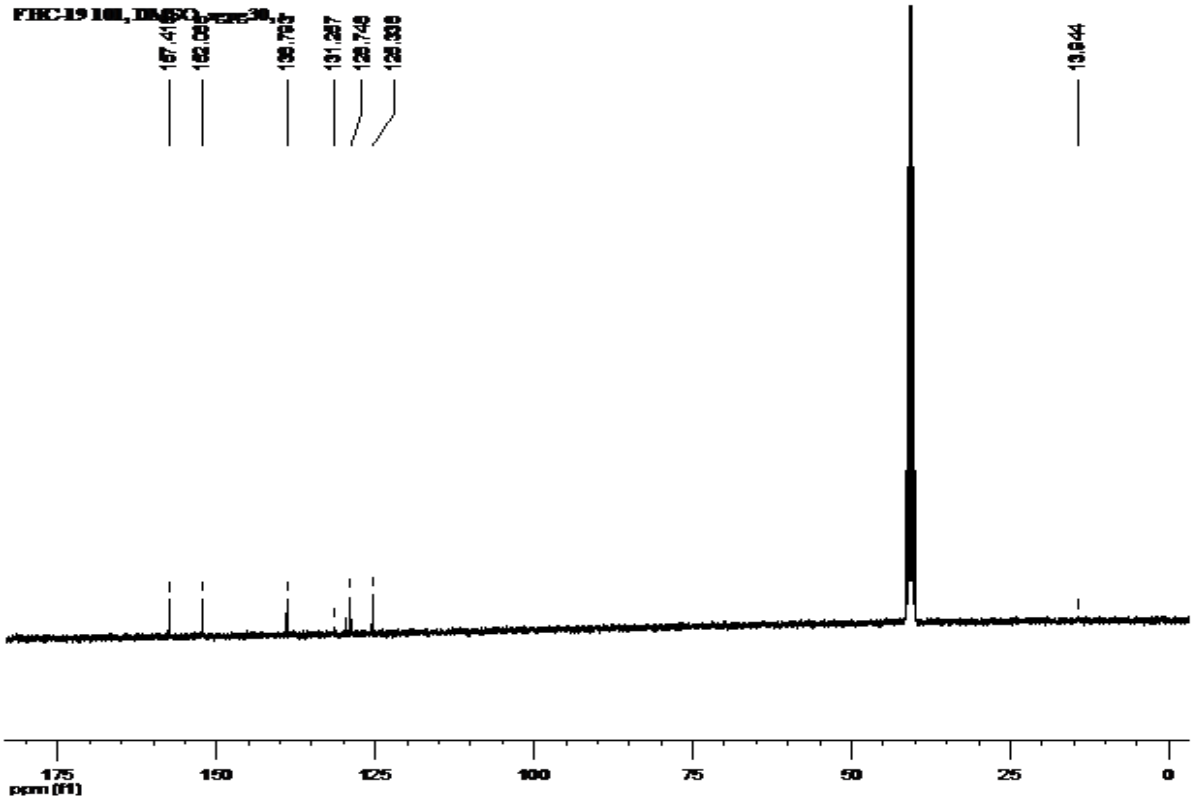

Appendix 41: ^{1}H NMR spectrum of **C10**

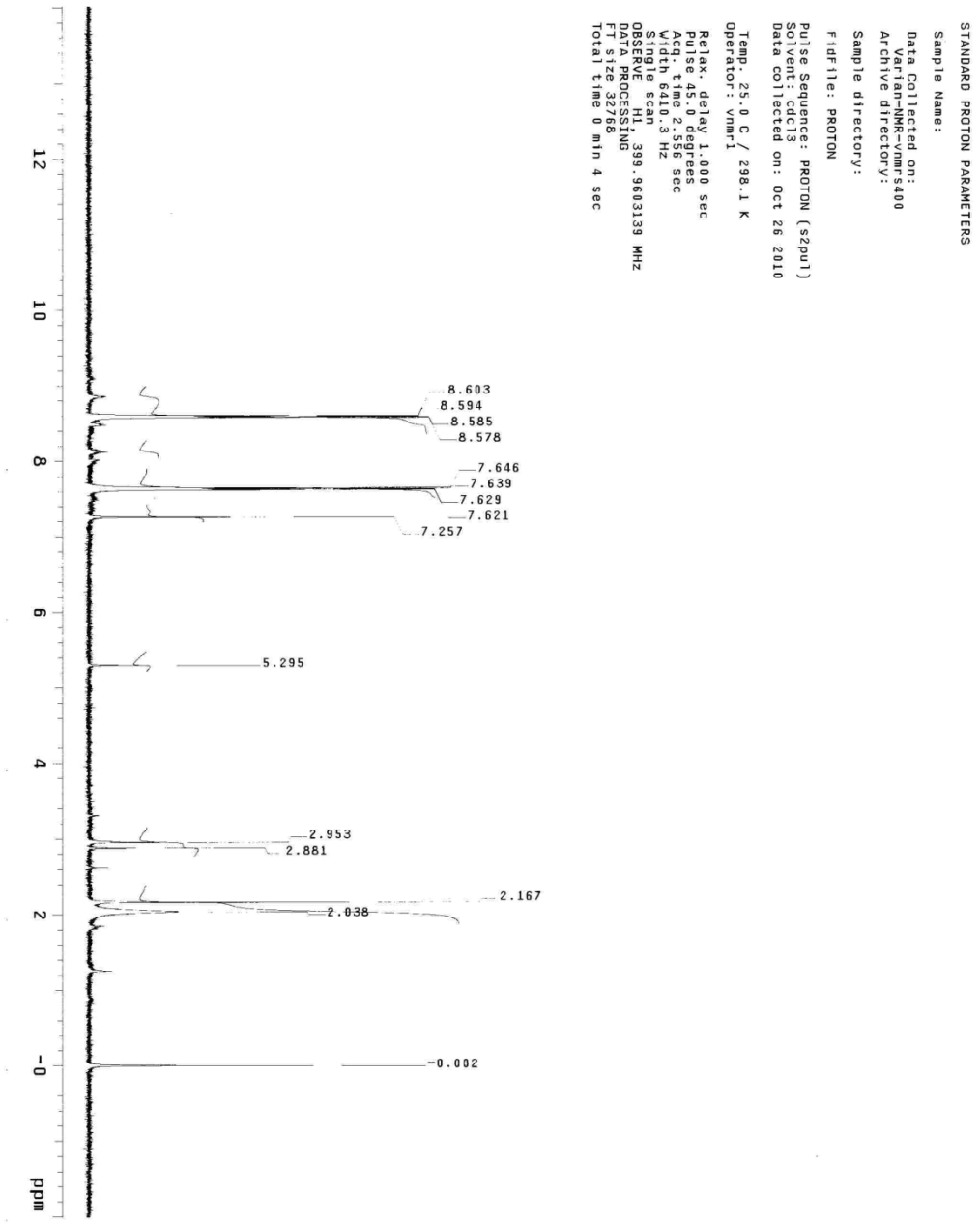

Appendix 42: ^{1}H NMR spectrum of **C11**

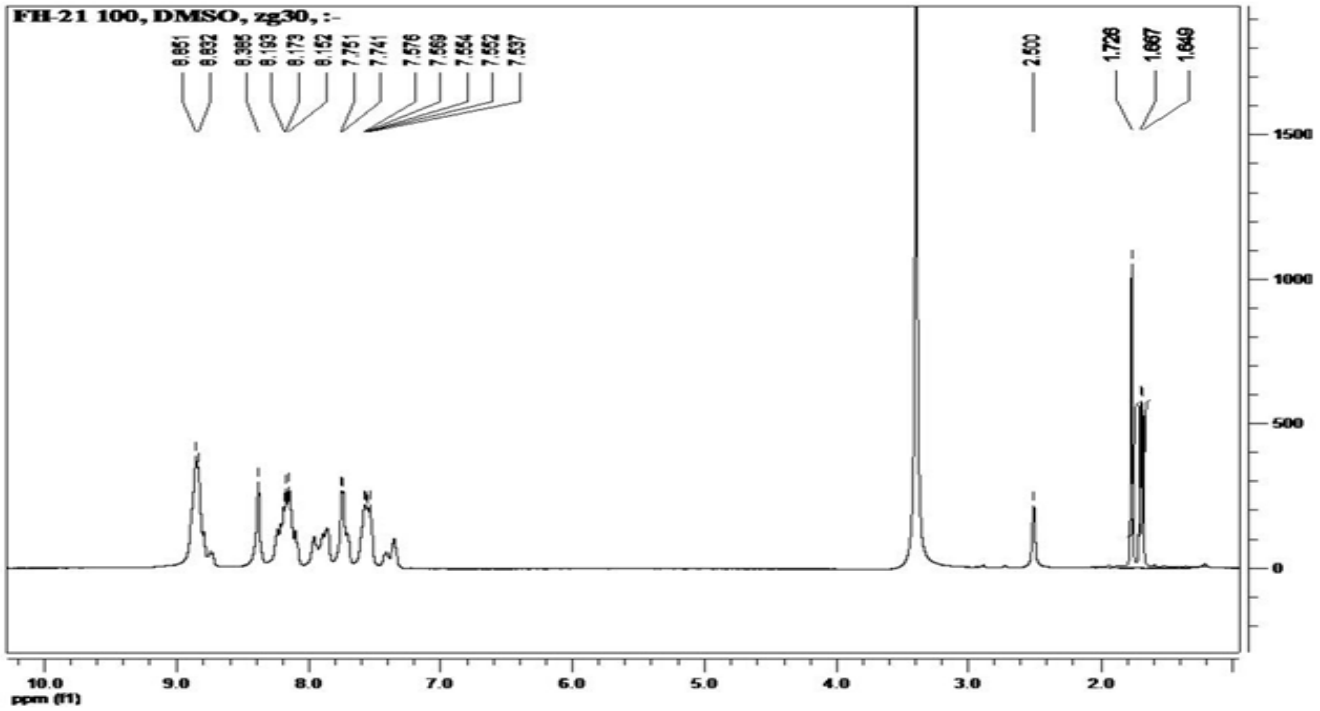

Appendix 43: ^{13}C NMR spectrum of **C11**

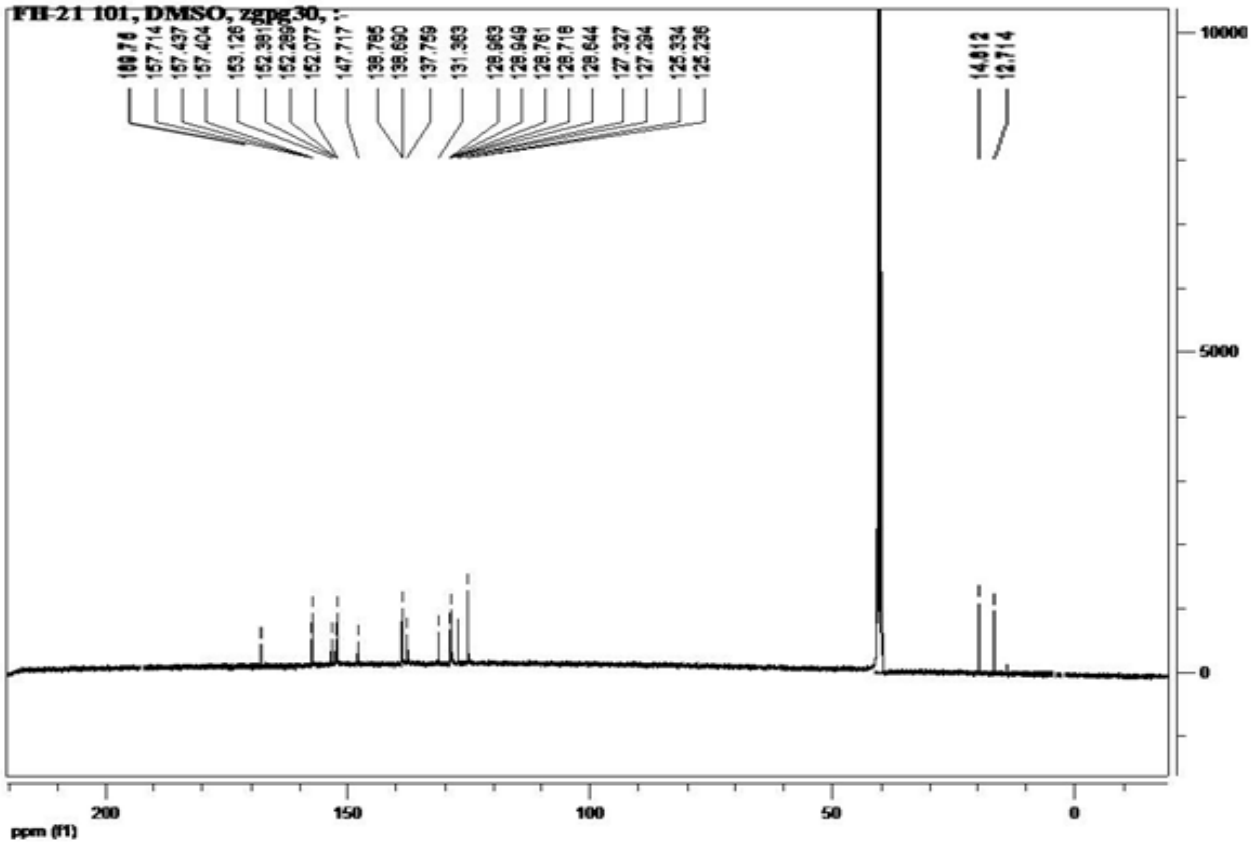

Appendix 44: ^{1}H NMR spectrum of **C12**

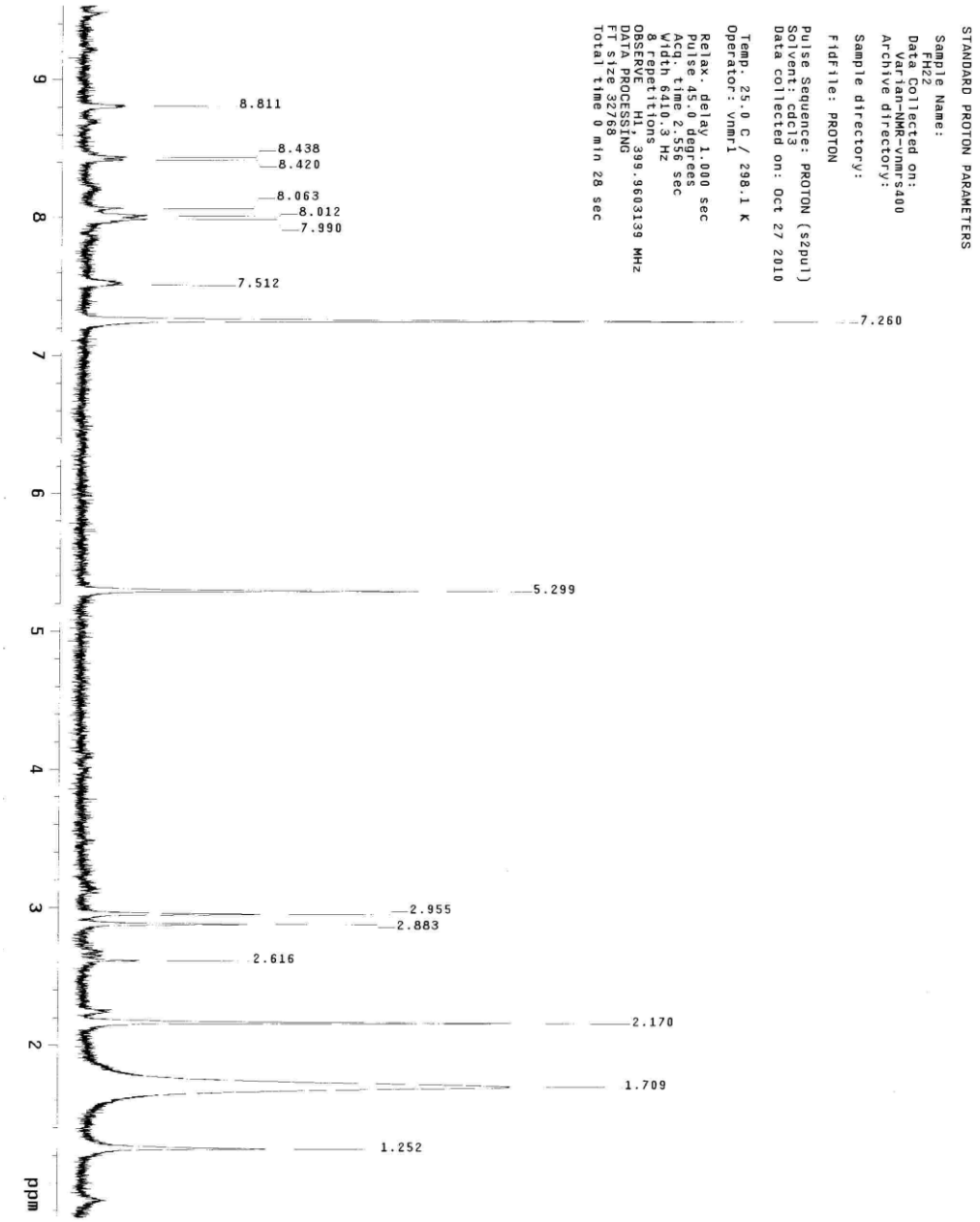

Appendix 45: ^{1}H NMR spectrum of **C13**

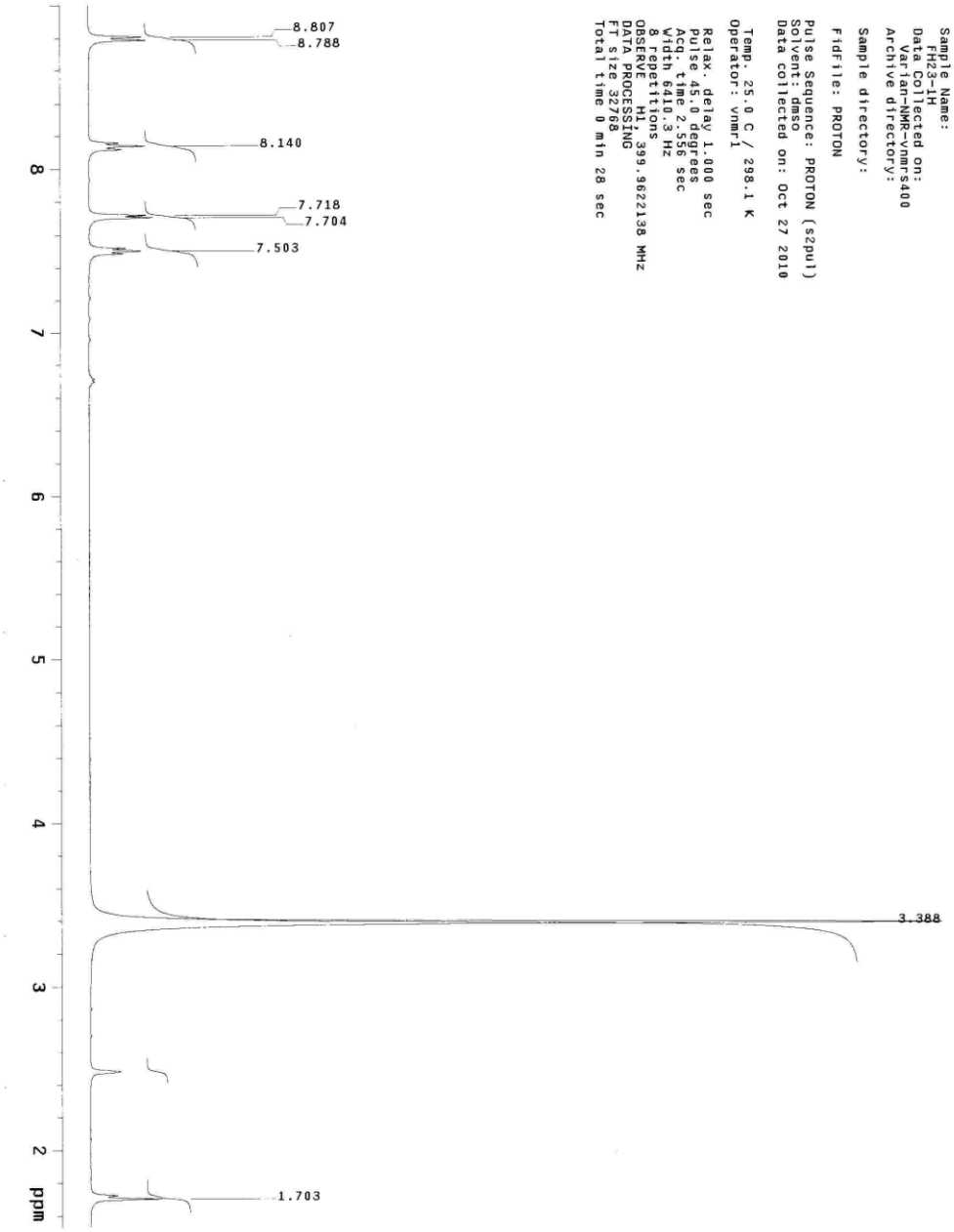

Appendix 46: ^{13}C NMR spectrum of **C13**

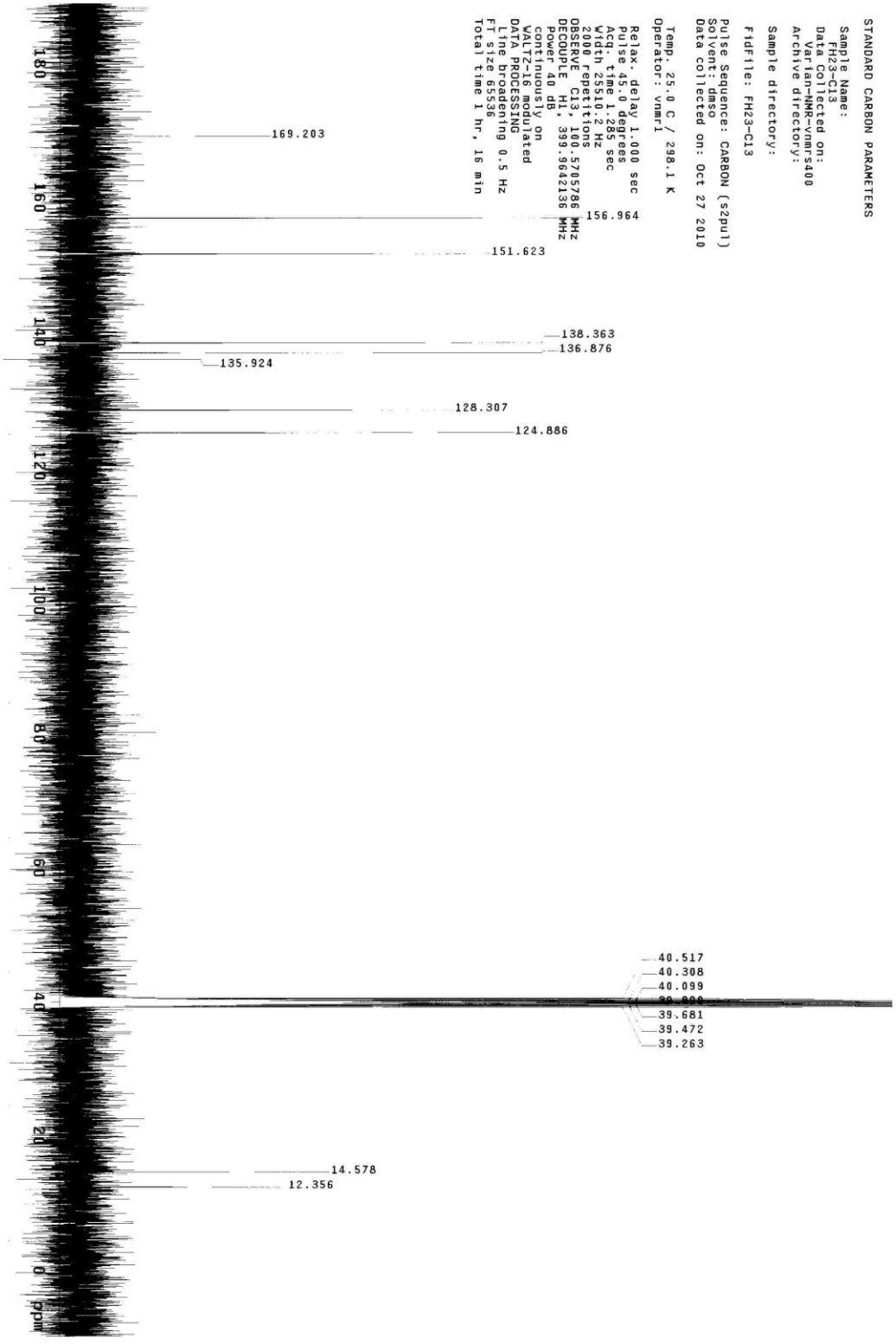

Appendix 47: ^{1}H NMR spectrum of **C14**

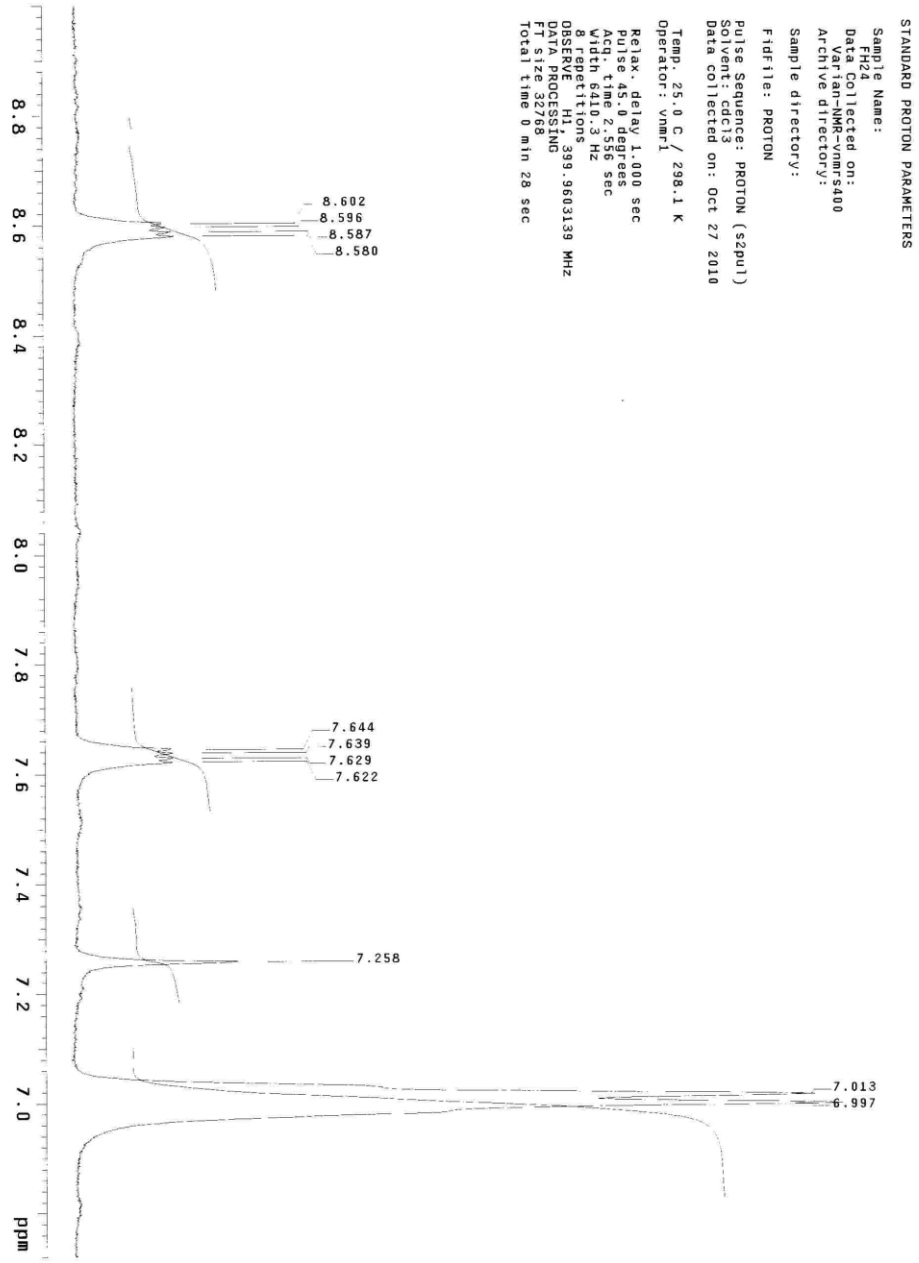

Appendix 48: ^{13}C NMR spectrum of **C14**

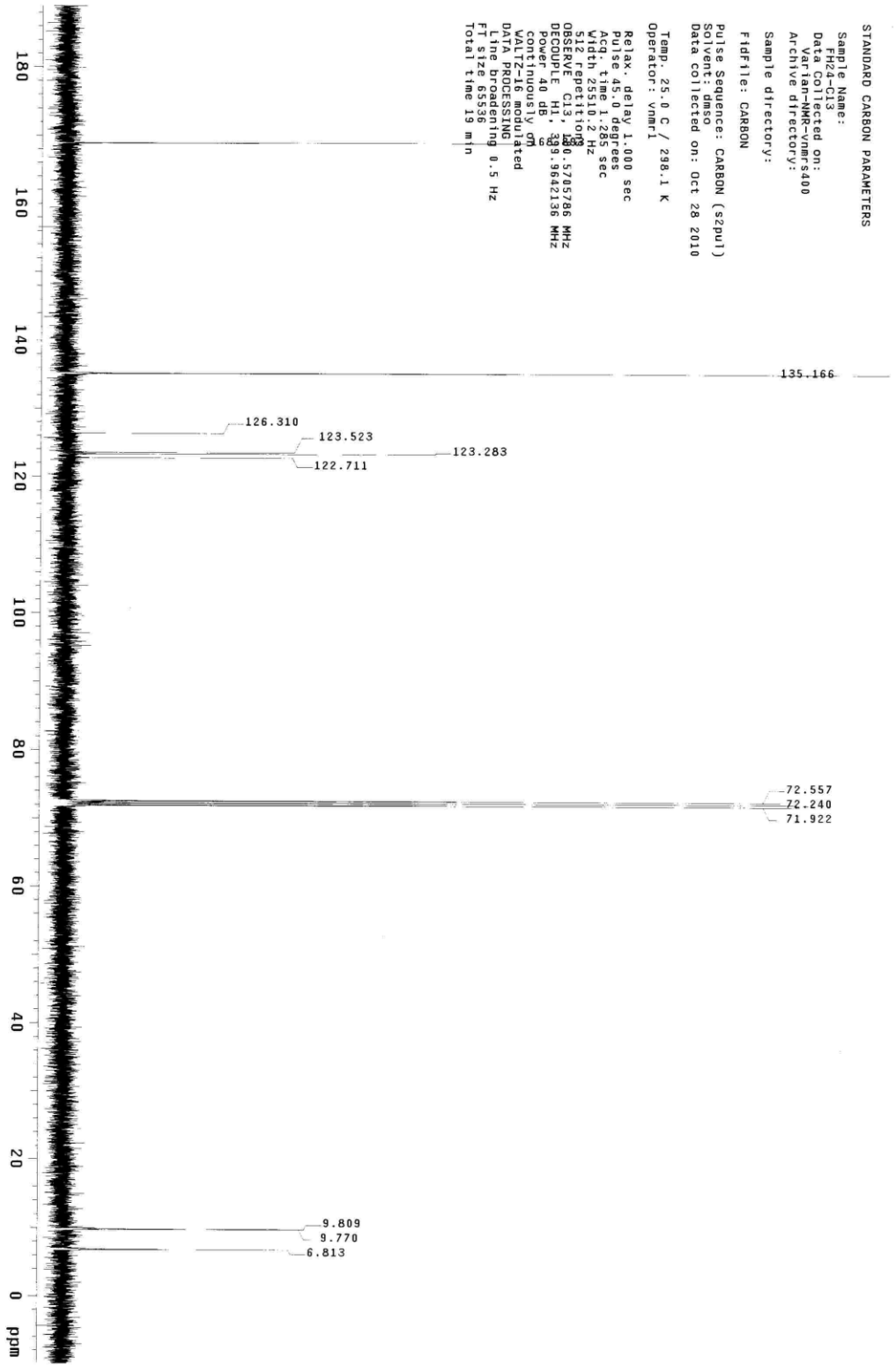

Appendix 49: ^{1}H NMR spectrum of **C15**

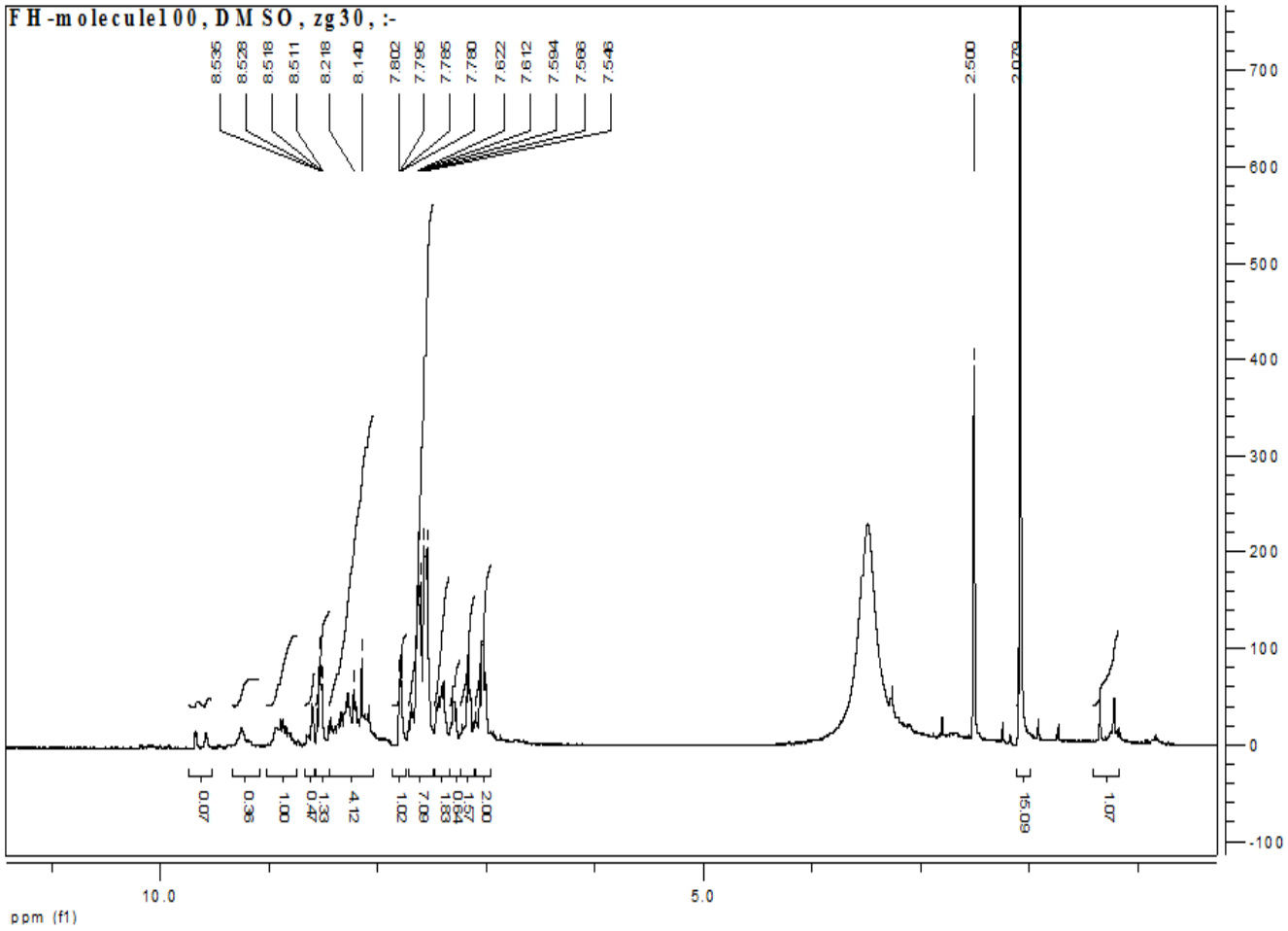

Appendix 50: Aromatic region of ^{1}H NMR spectrum of **C16**

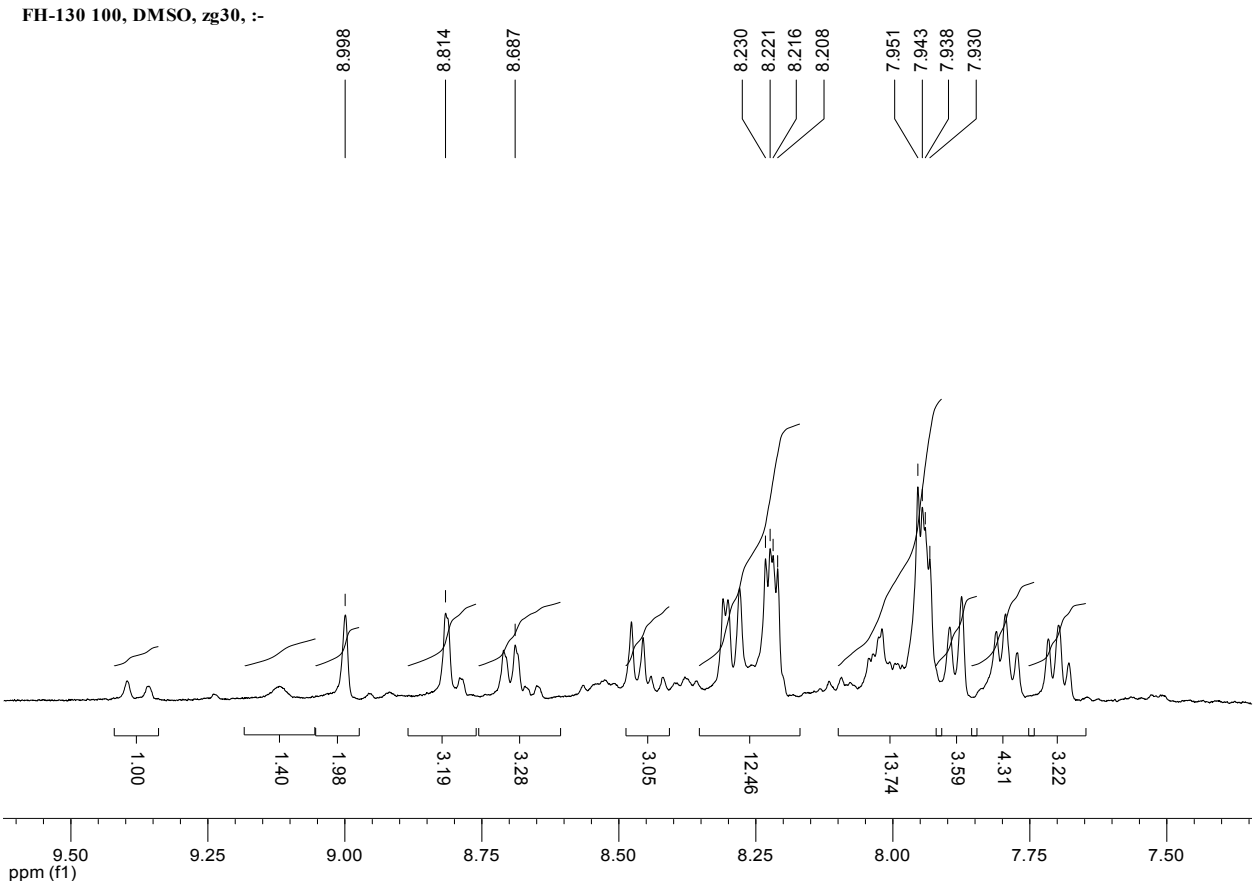

Appendix 51: ^{13}C NMR spectrum of **C16**

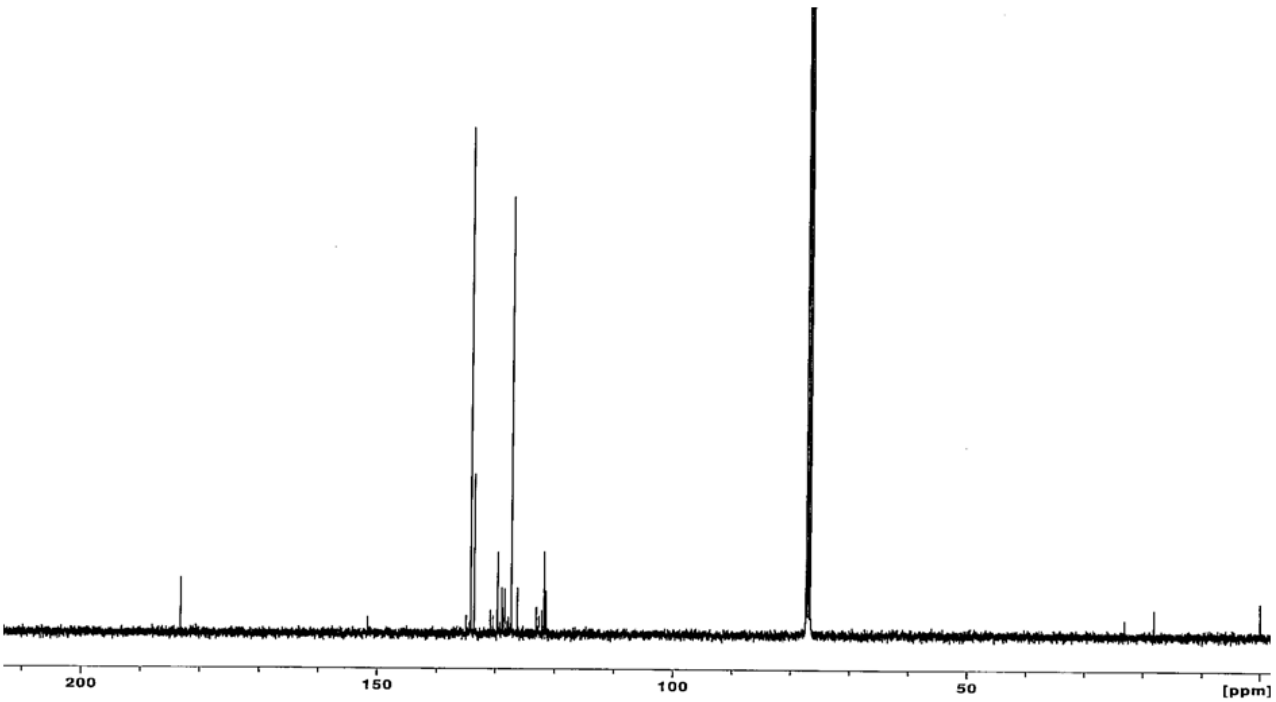

Appendix 52: ^{1}H NMR spectrum of **C17**

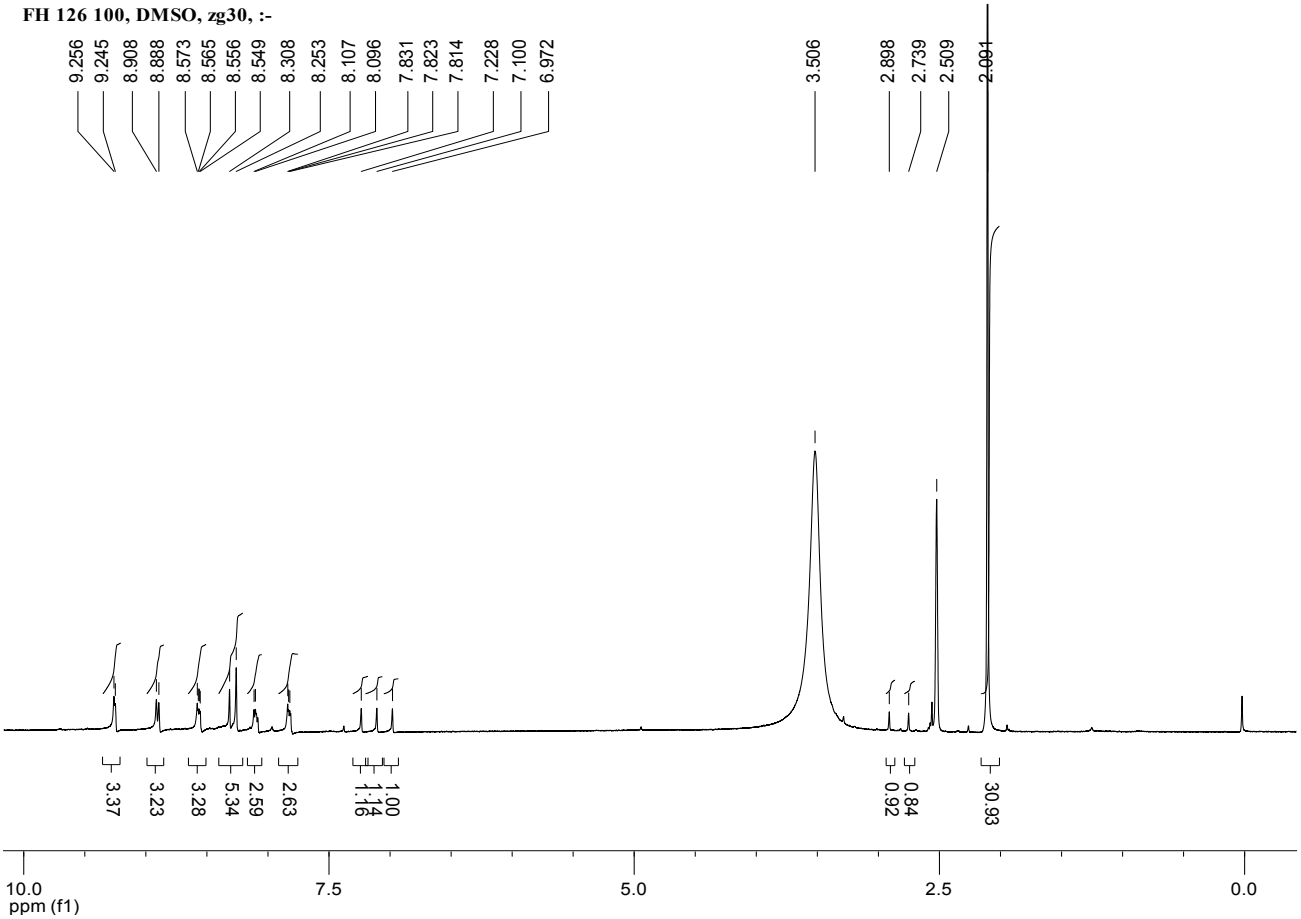

Appendix 53: IR spectrum of **C18** in KBr

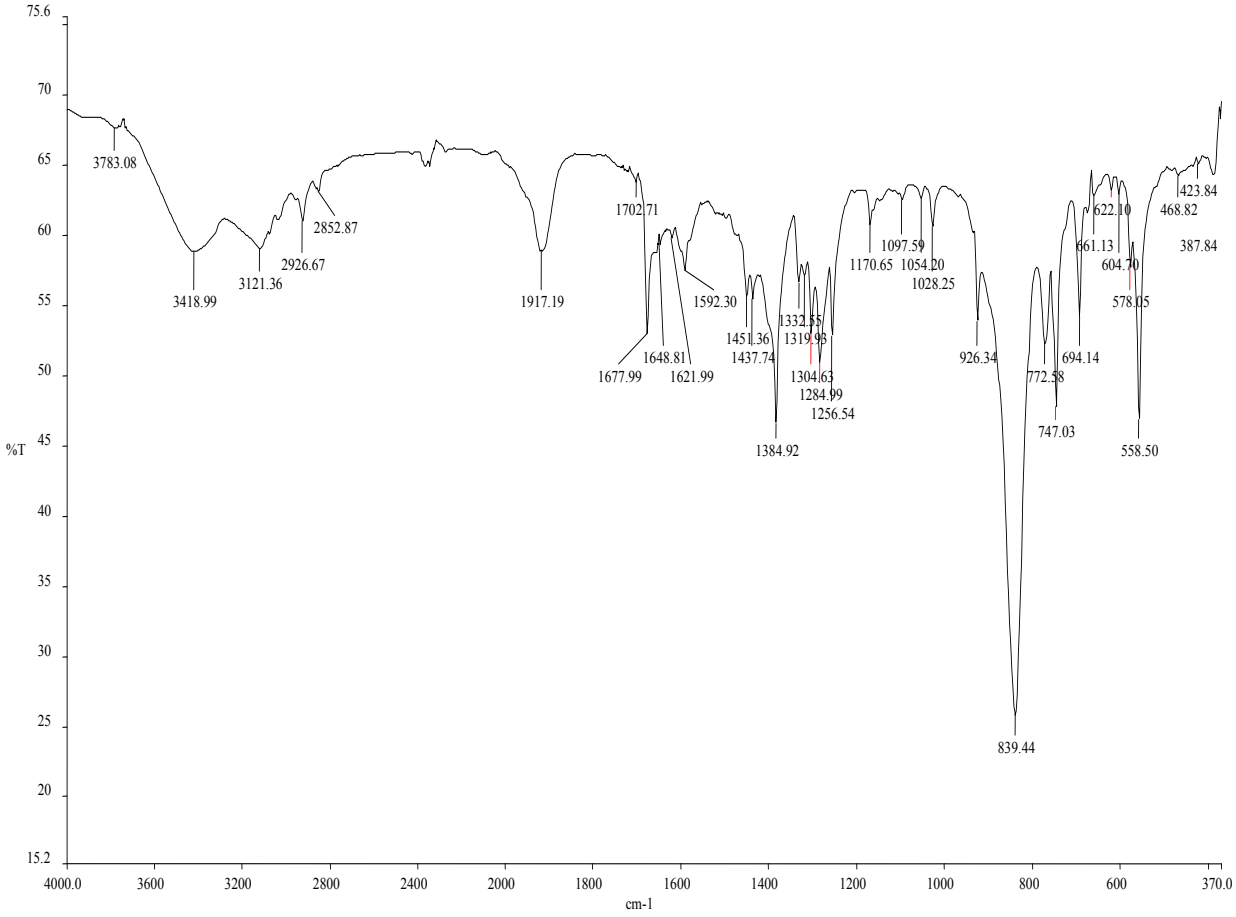

Appendix 54: ^{1}H NMR spectrum of **C18**

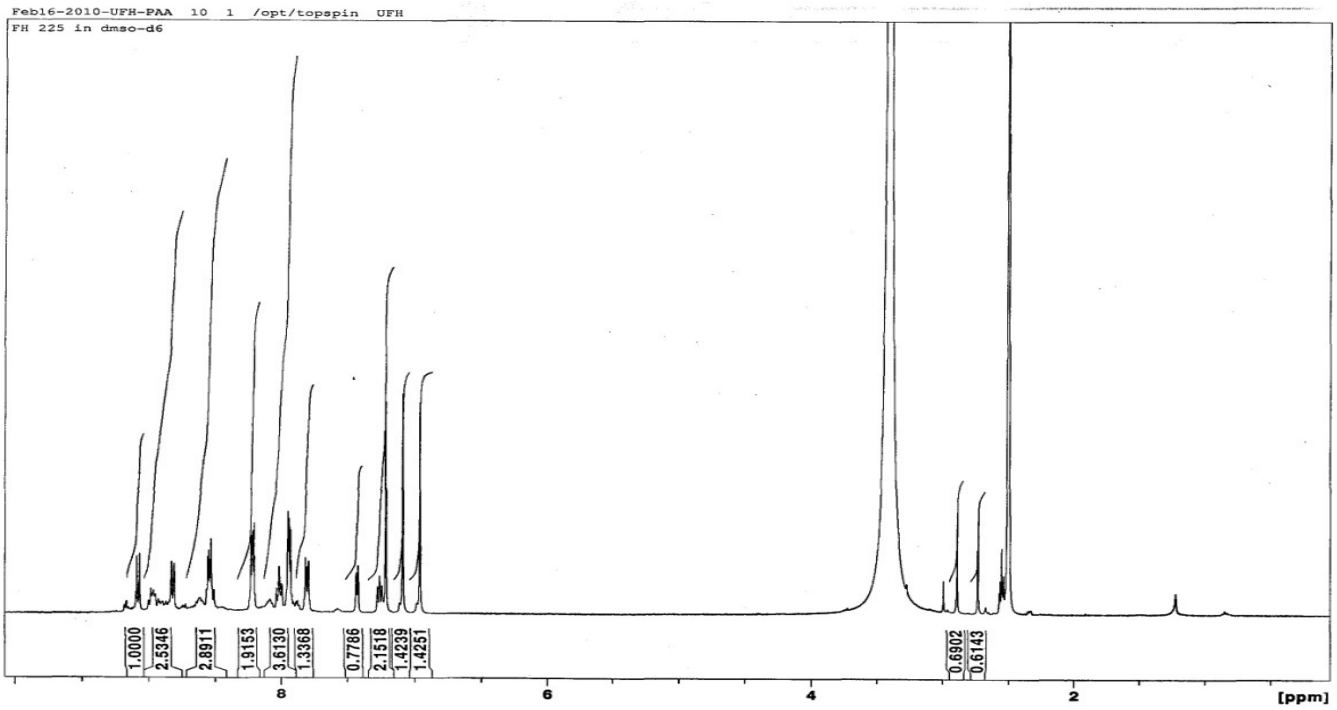

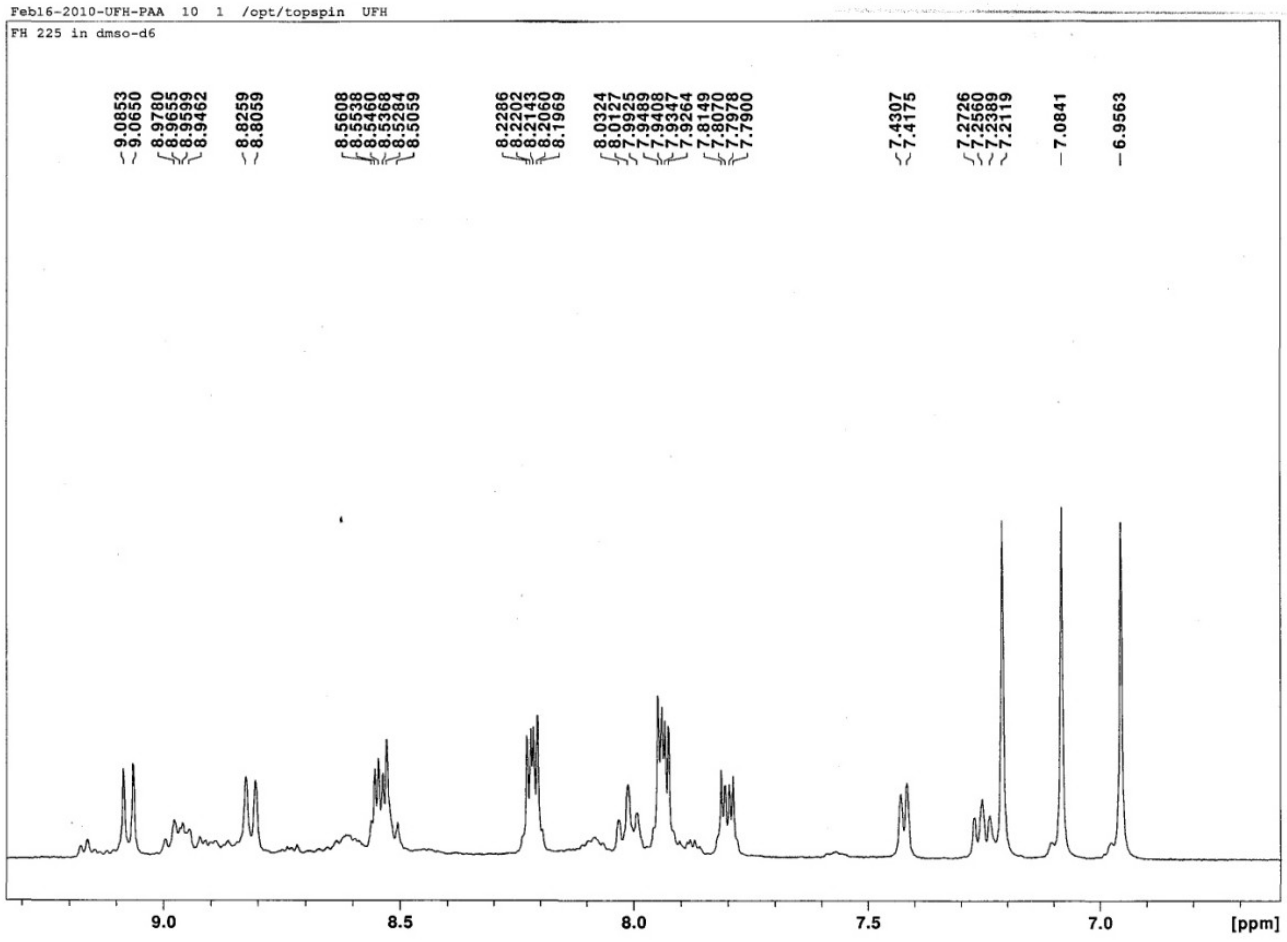

Appendix 55: ^{13}C NMR spectrum of **C18**

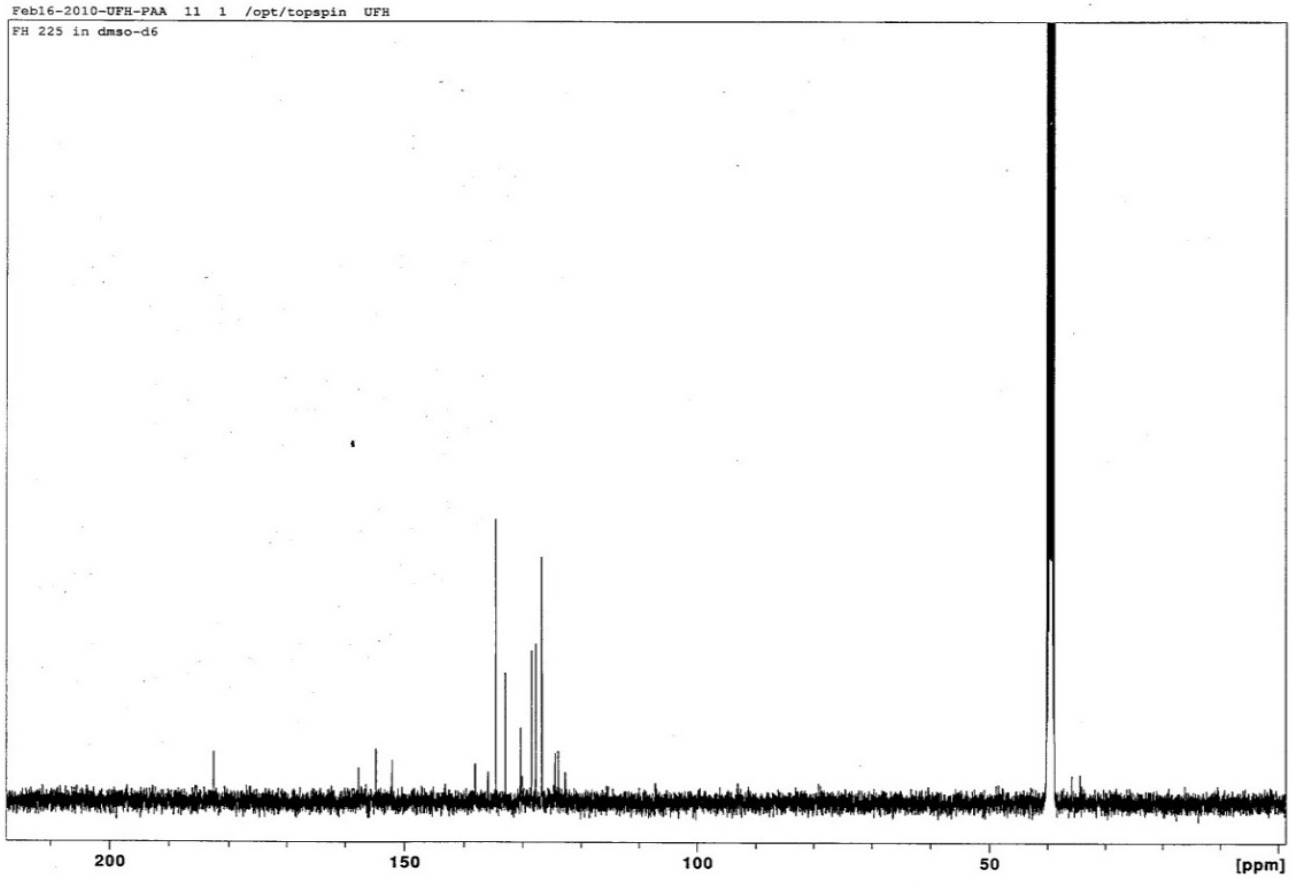

Appendix 56: IR spectrum of **C19** in KBr

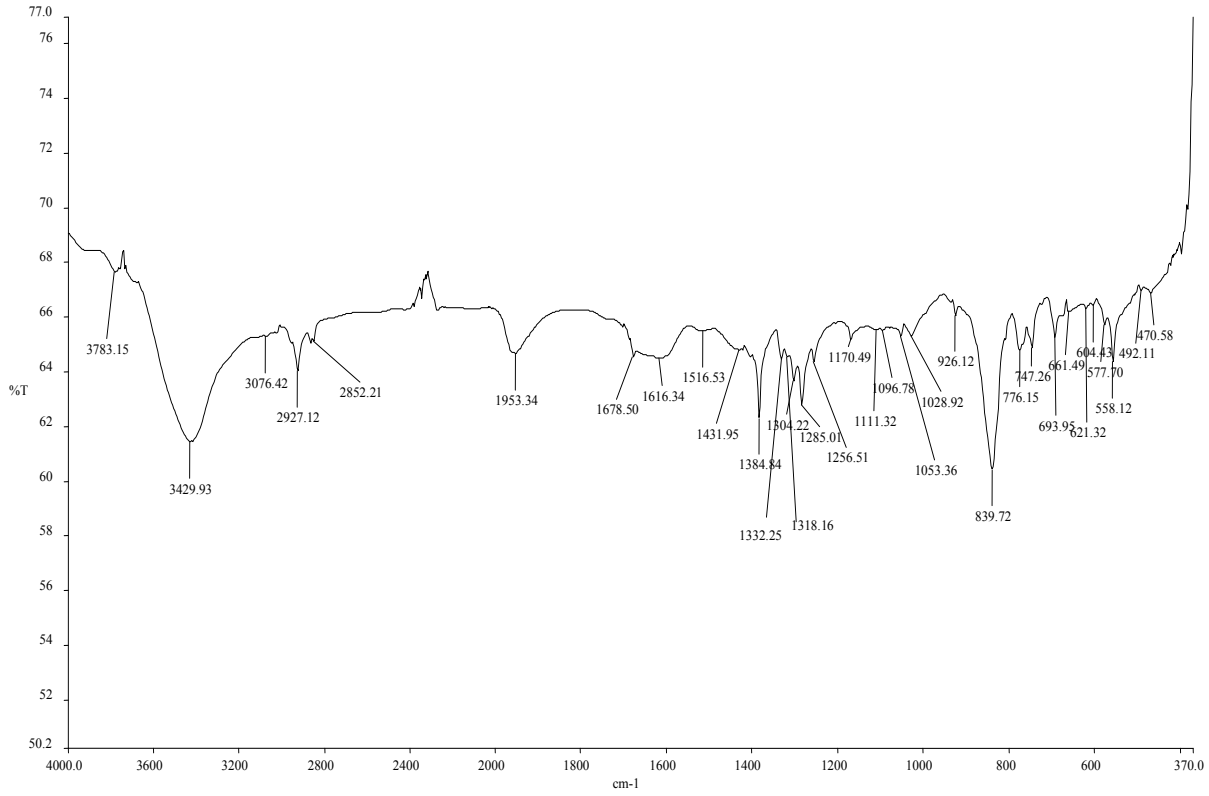

Appendix 57: ^{1}H NMR spectrum of **C19**

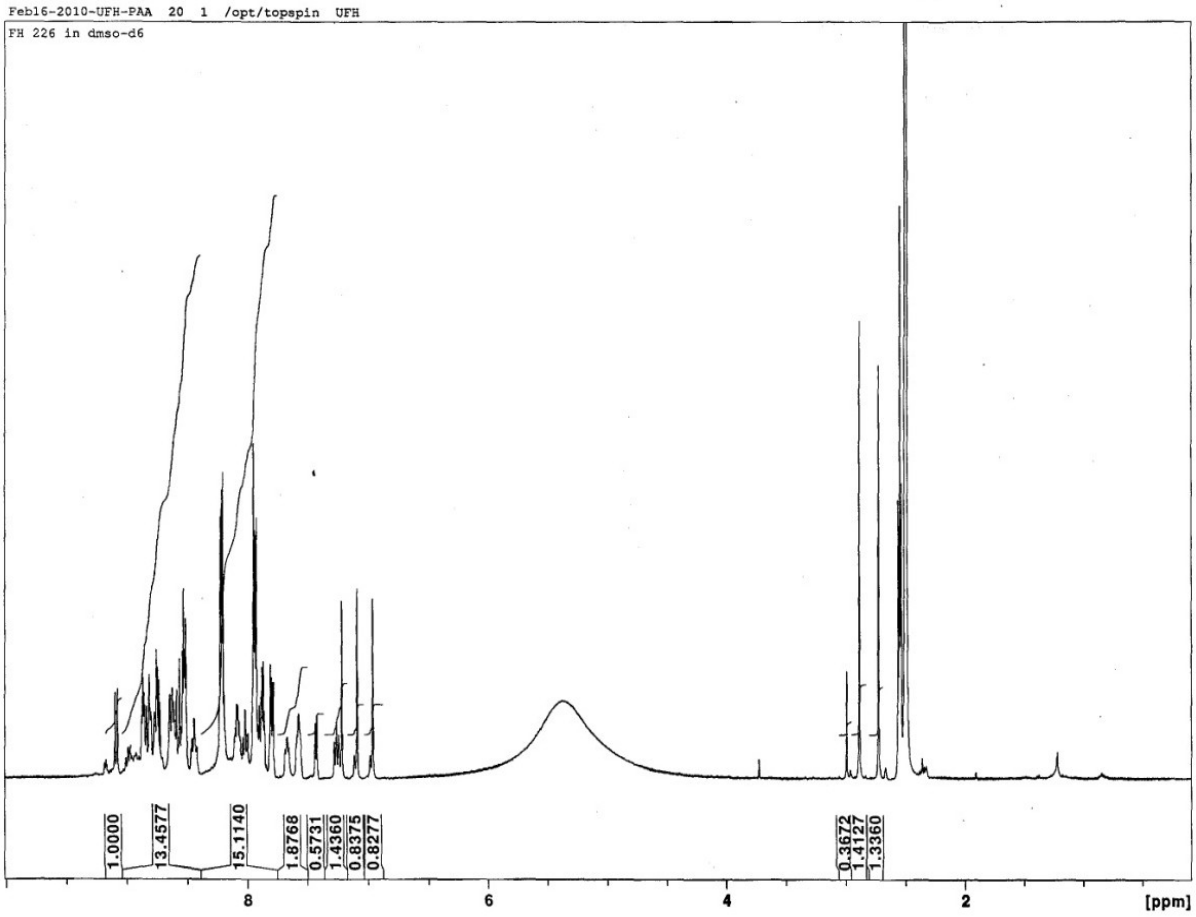

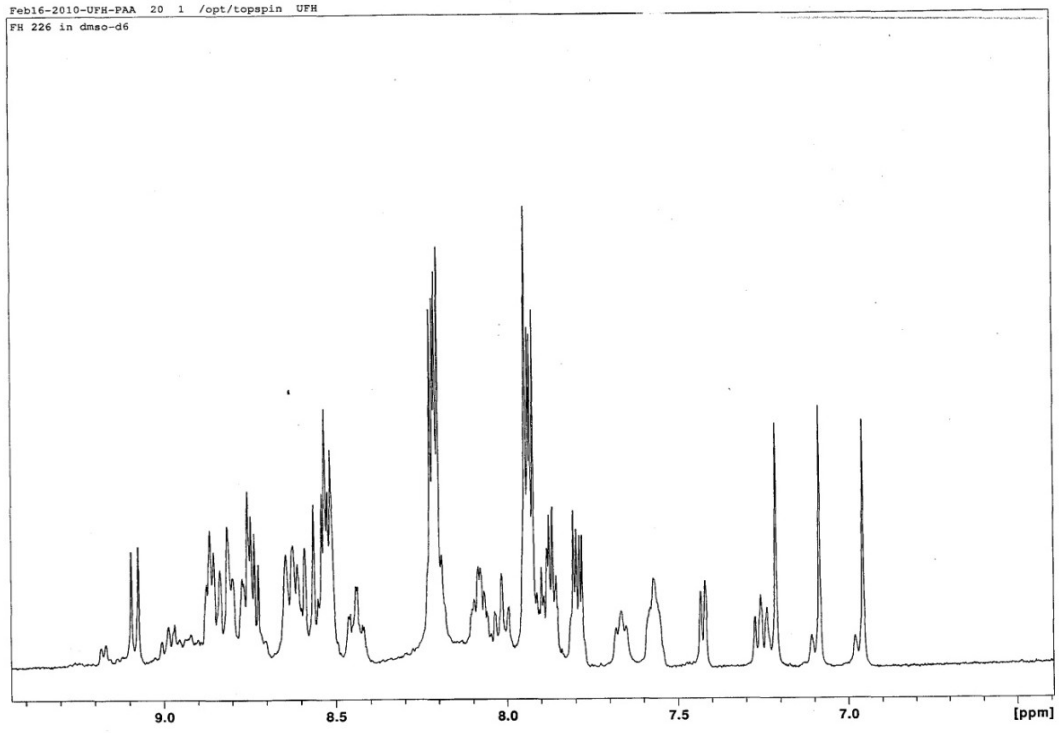

Appendix 58: ^{13}C NMR spectrum of **C19**

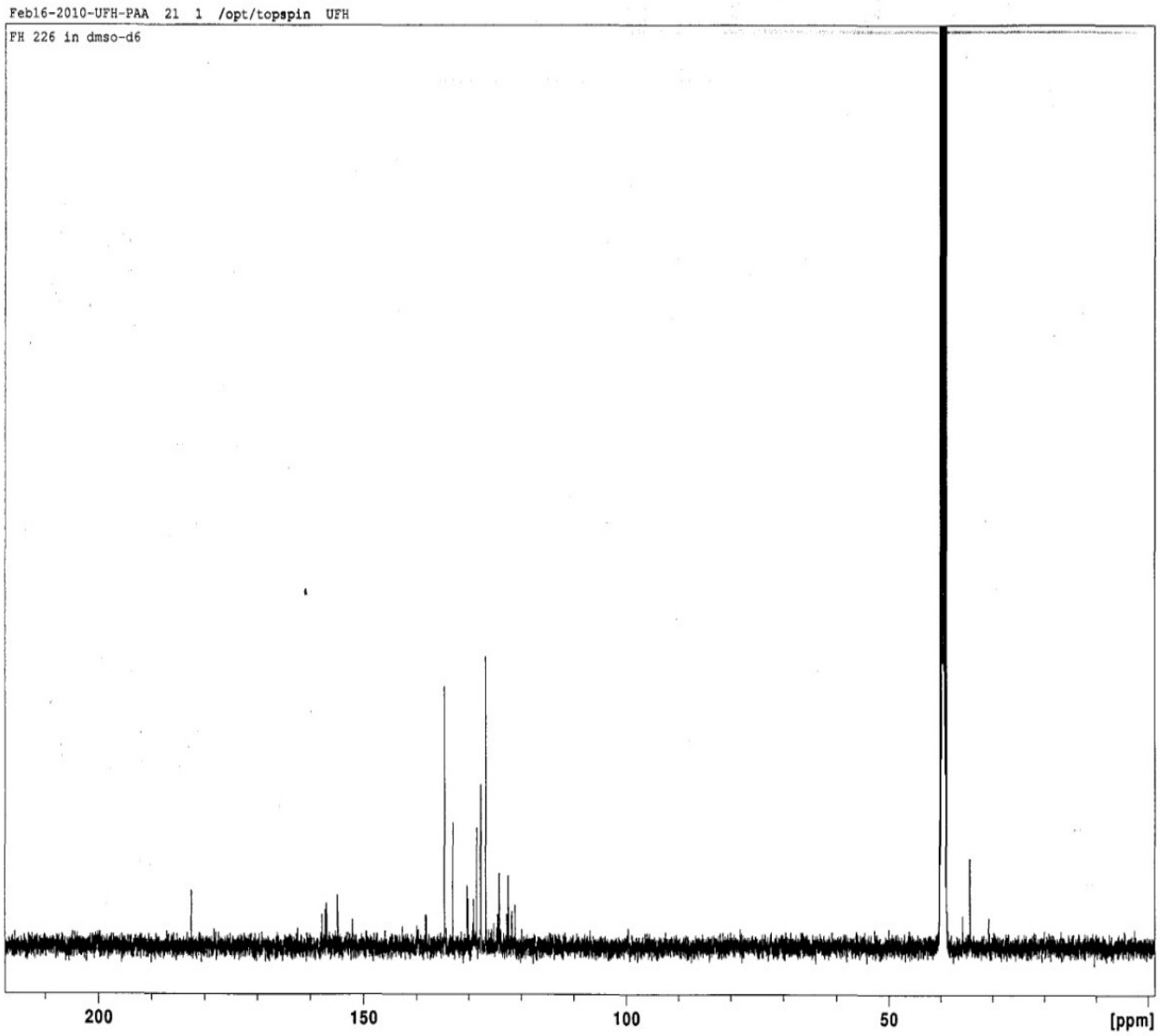

Appendix 59: IR spectrum of **C20** in KBr

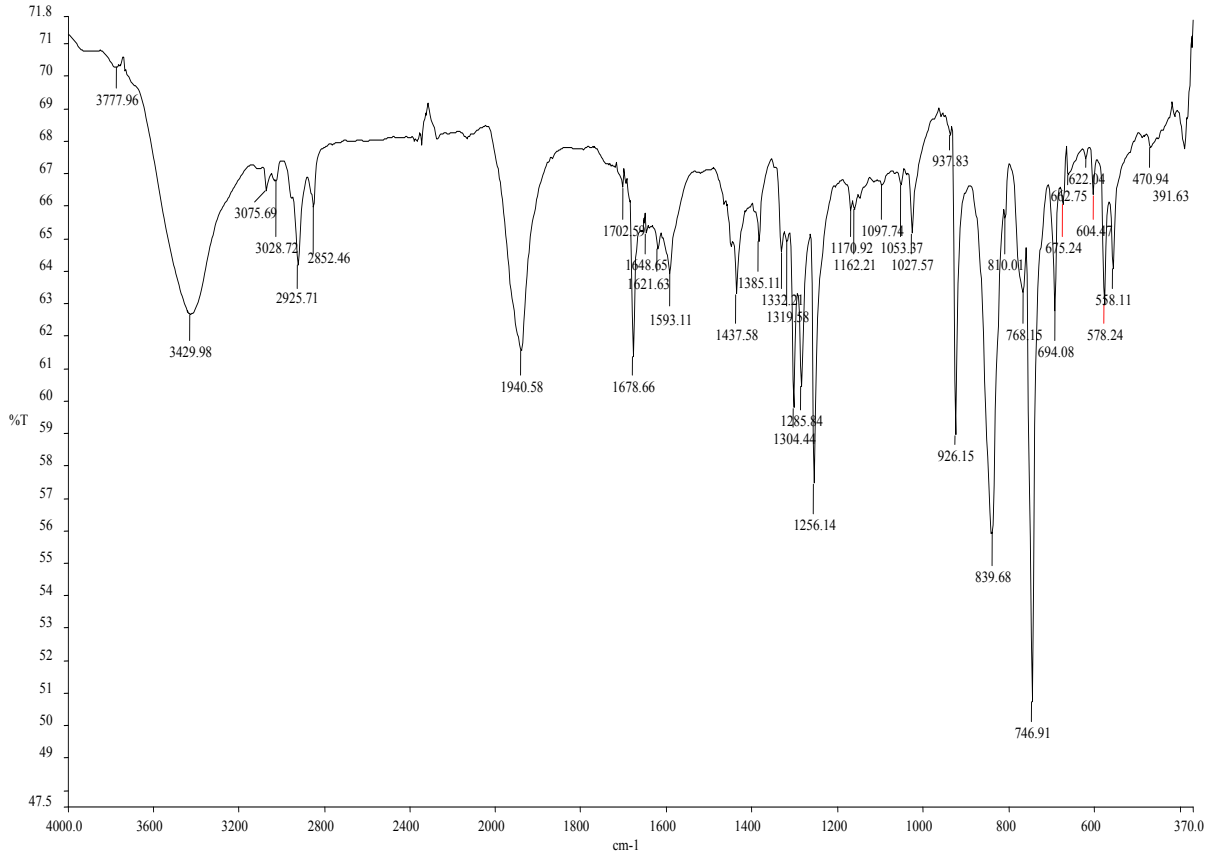

Appendix 60: ^{1}H NMR spectrum of **C20**

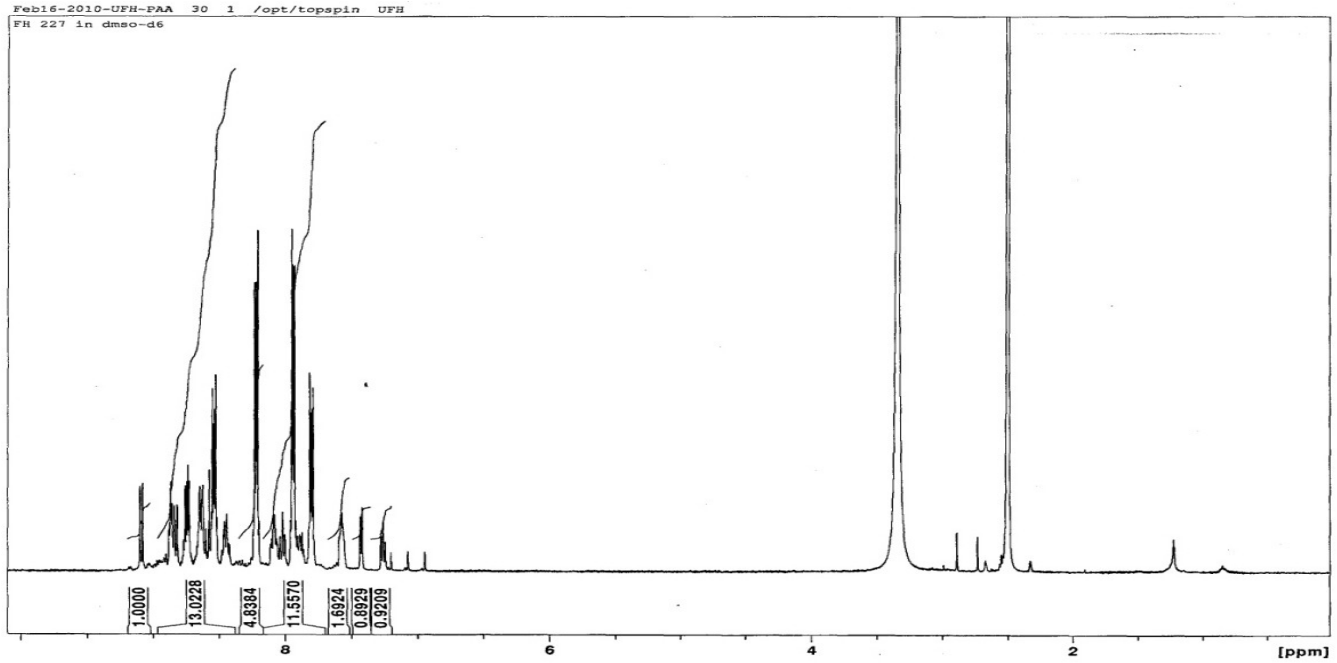

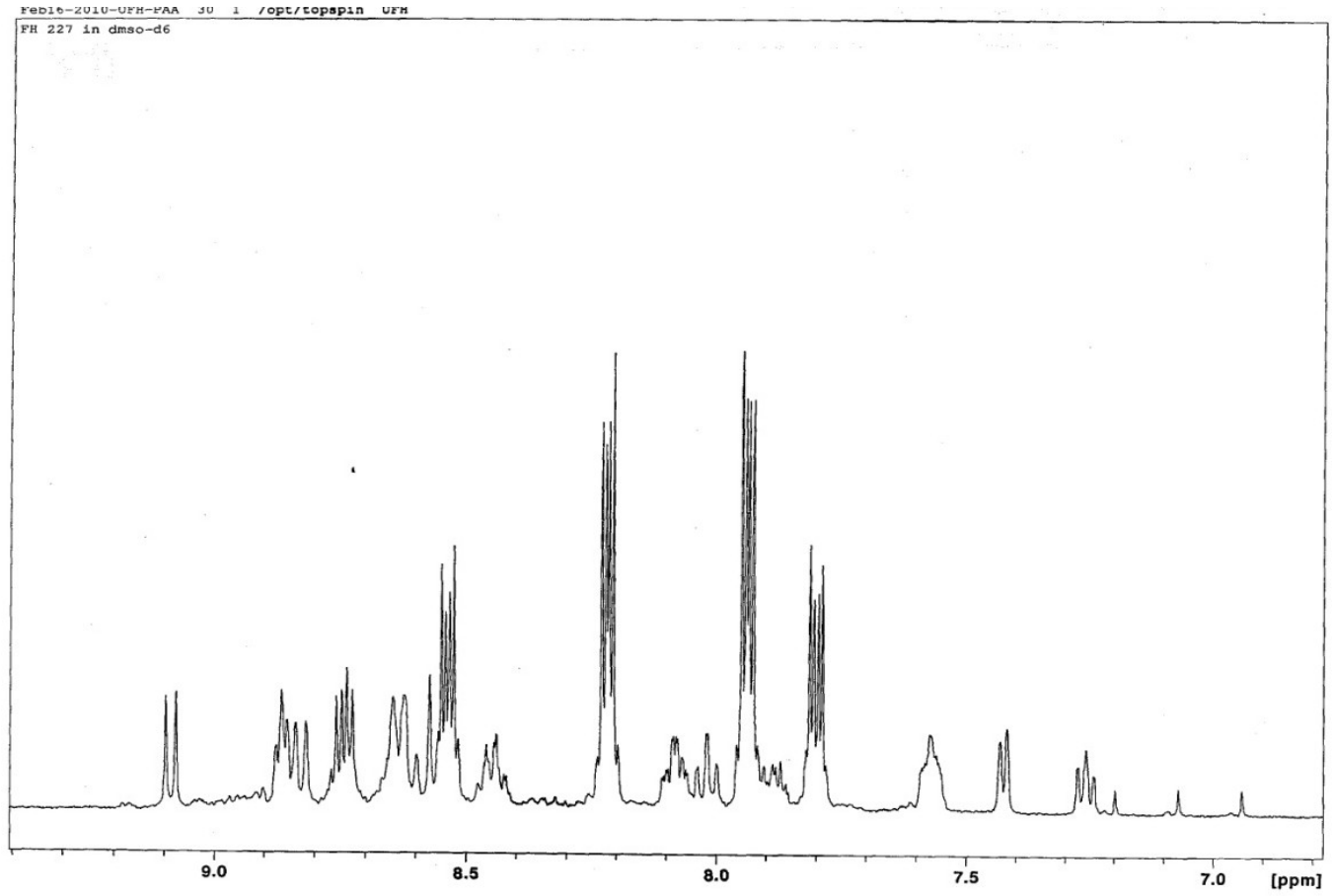

Appendix 61: ^{13}C NMR spectrum of **C20**

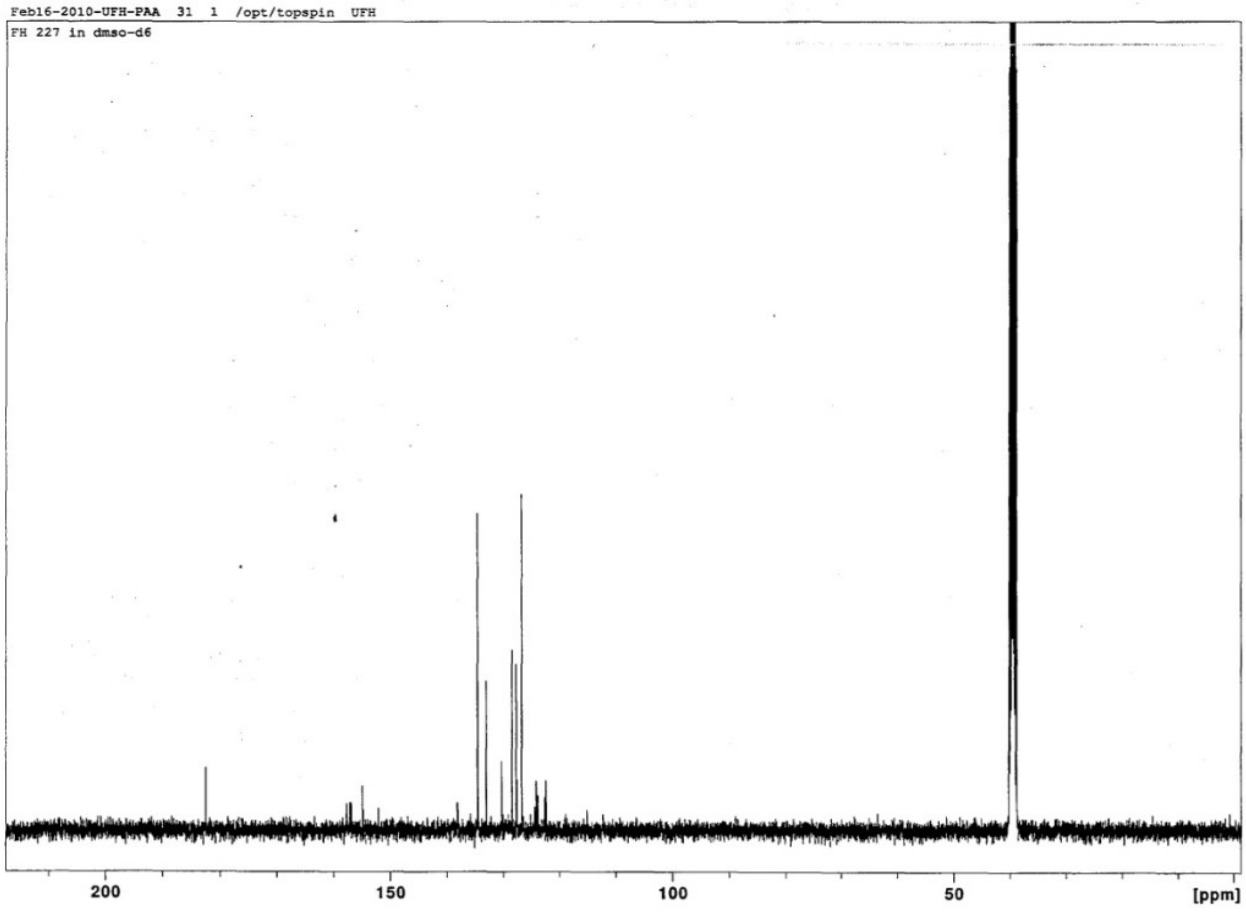

Appendix 62: IR spectrum of **PC21** in KBr

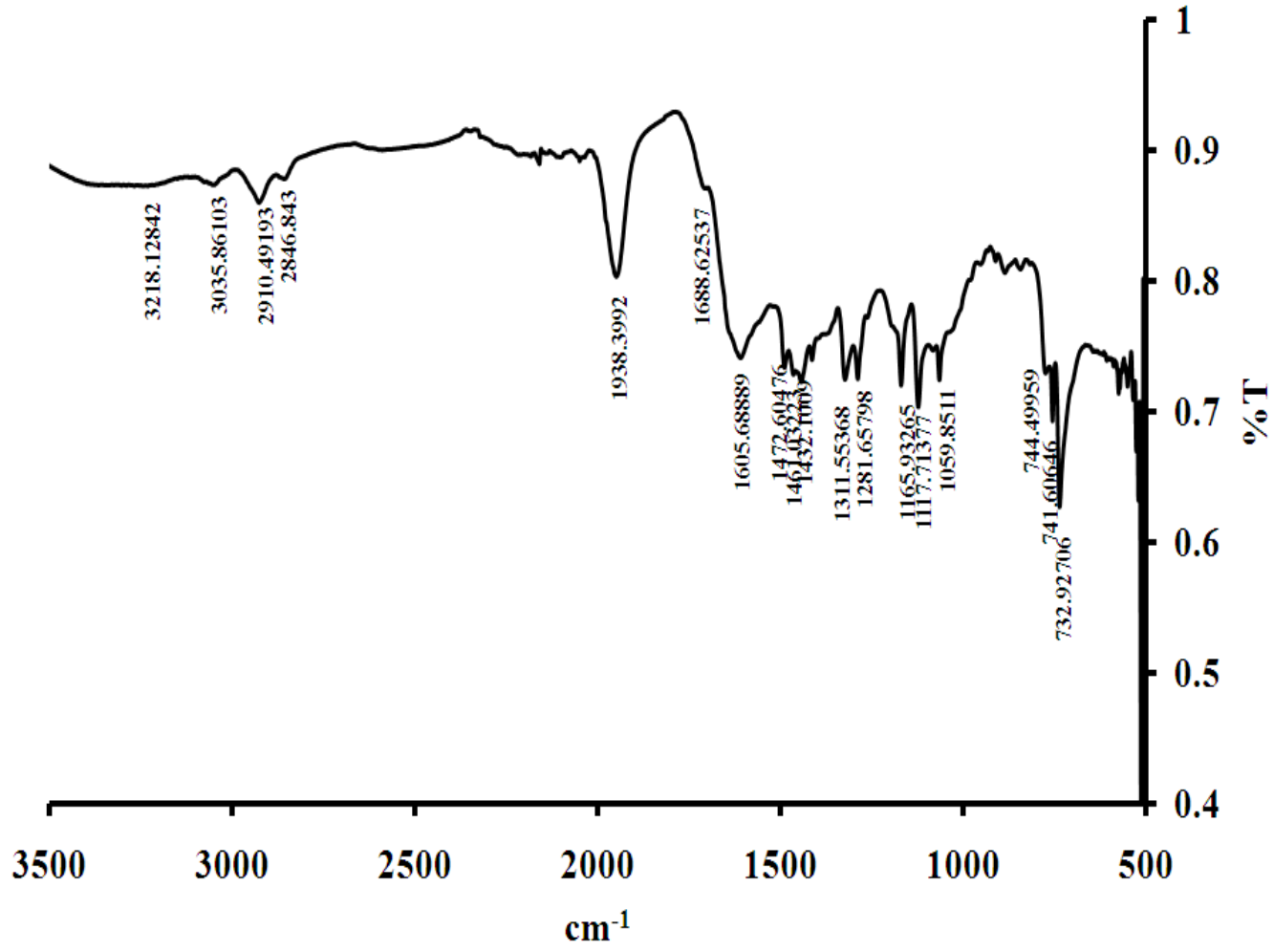

Appendix 63: ^{1}H NMR spectrum of **PC21**

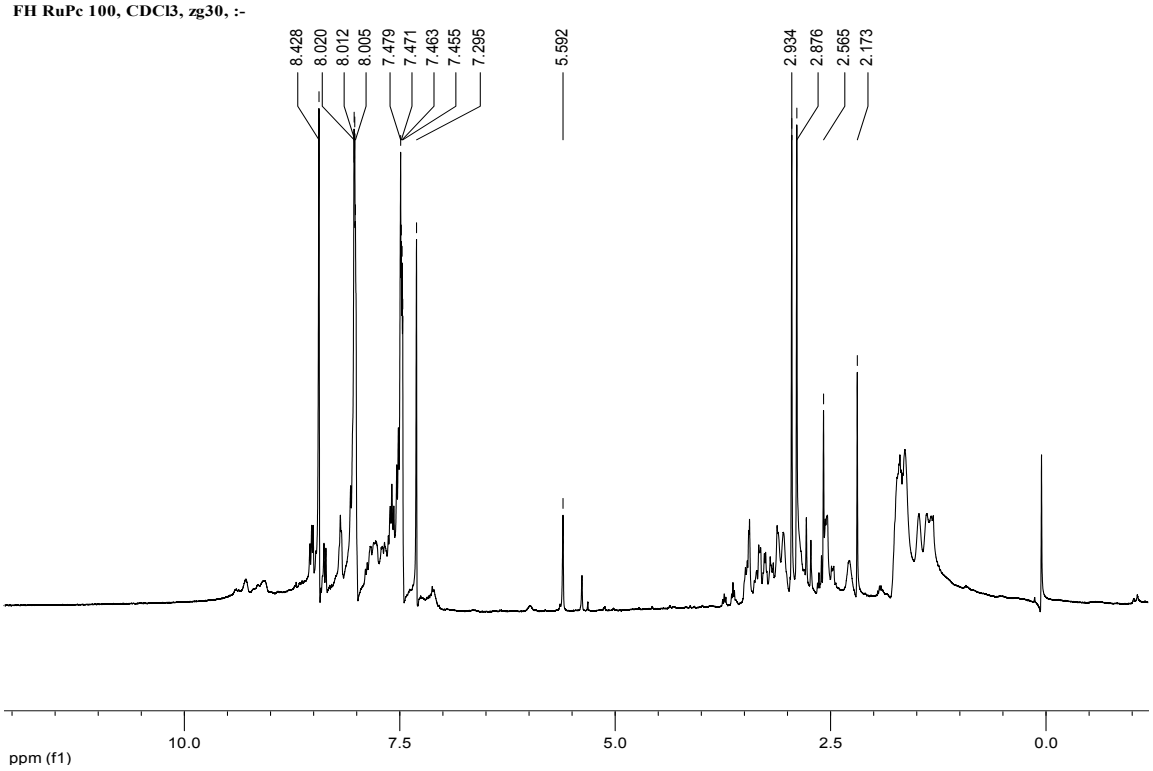

Appendix 64: ^{13}C nmr spectrum of **PC21**

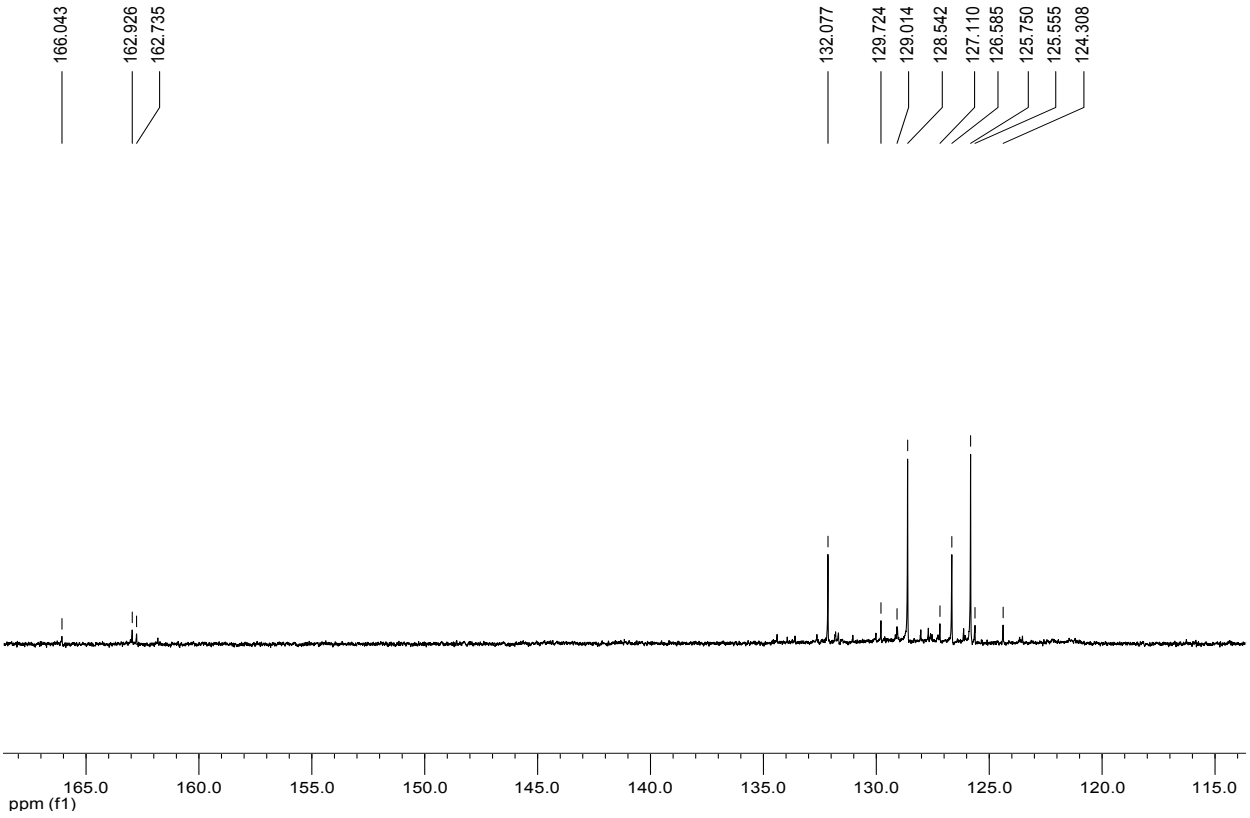

Appendix 65: IR spectrum of **C23** in KBr

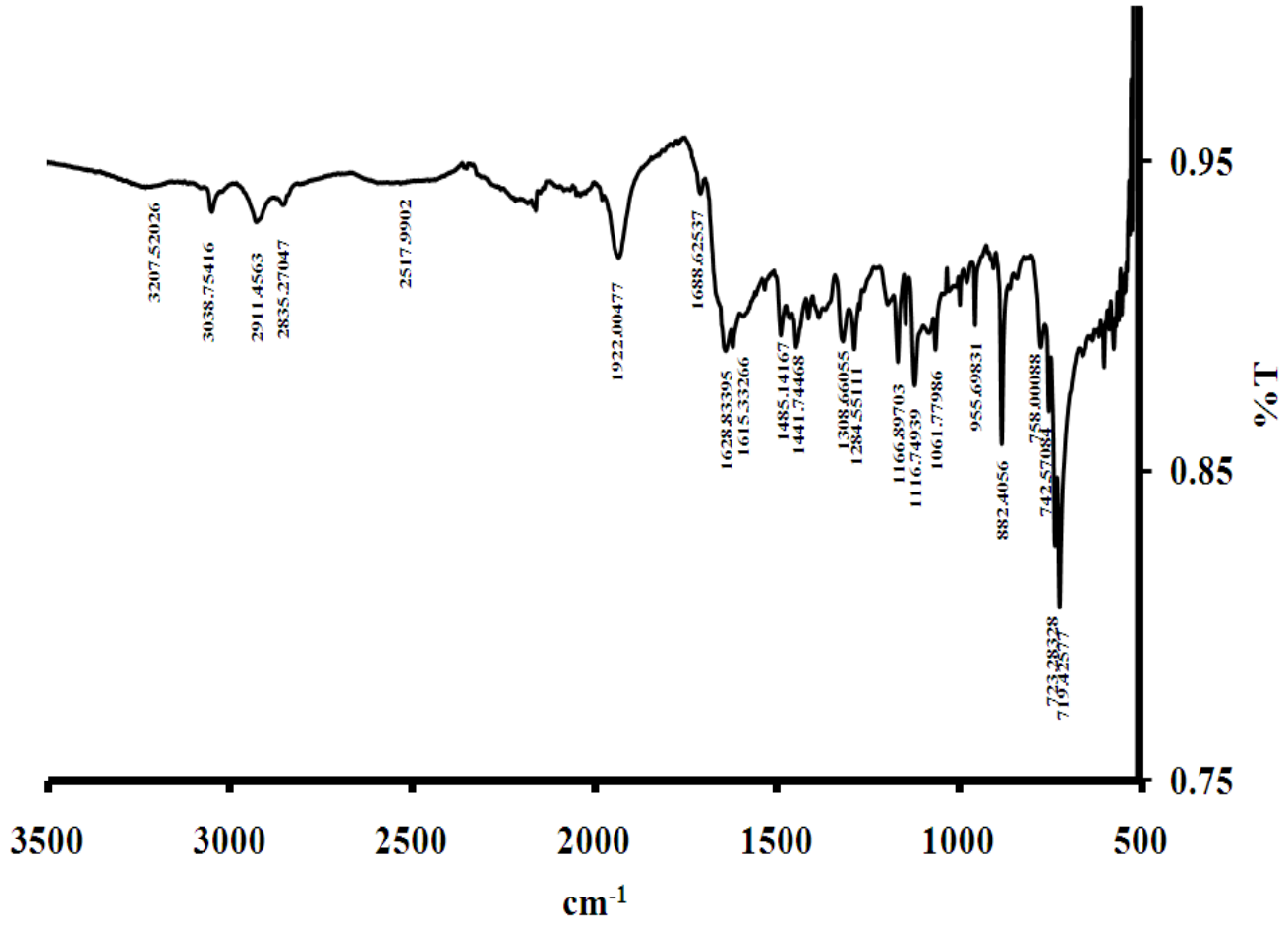

Appendix 66: ^{1}H NMR spectrum of **PC23**

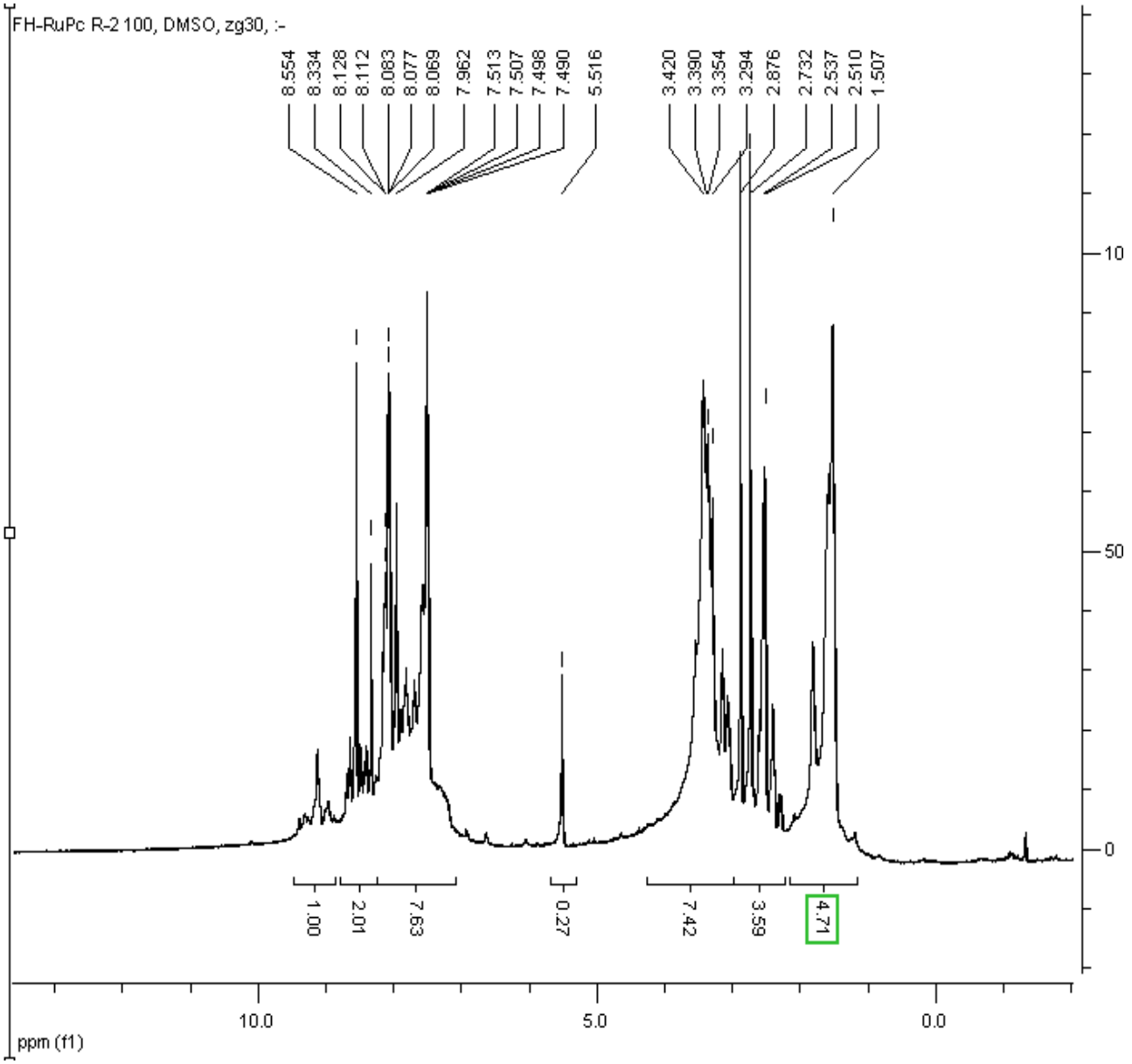

Appendix 67: ^{13}C NMR spectrum of **PC23**

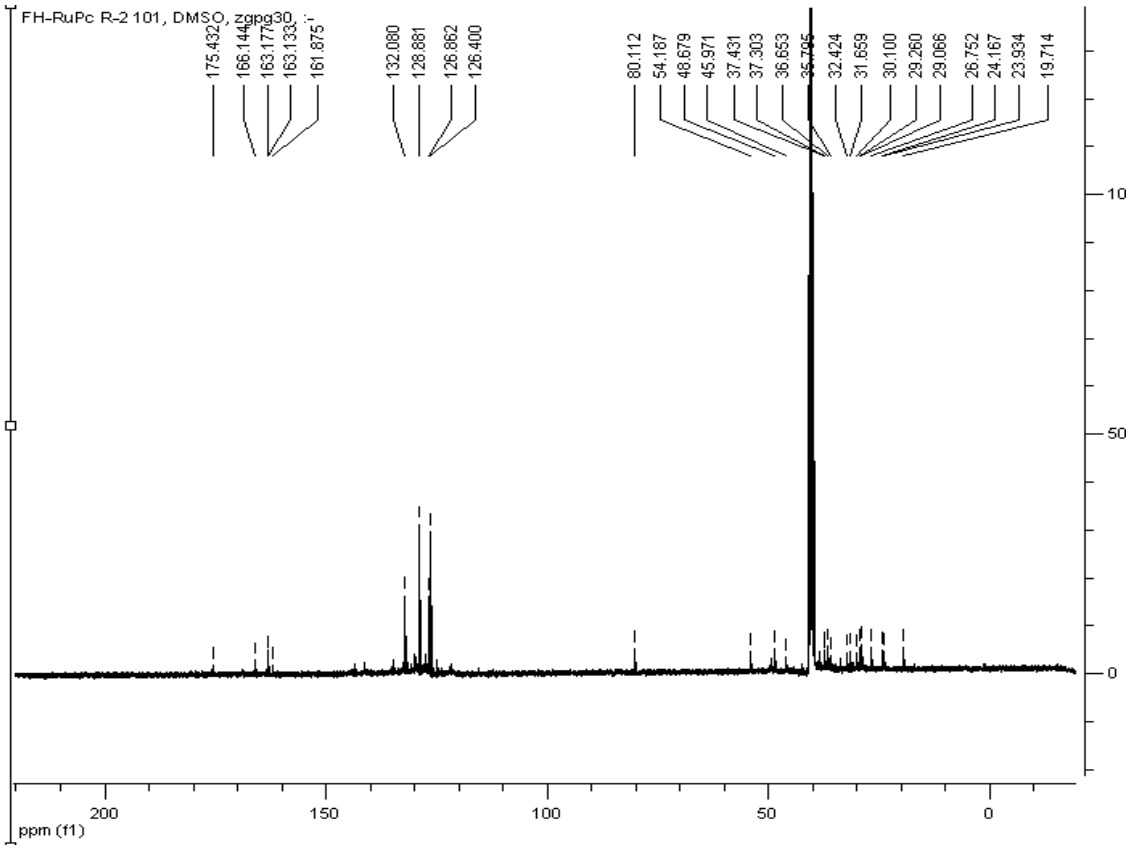

Appendix 67: Expanded aromatic region of ^{13}C NMR spectrum of **PC23**